

University of Bradford eThesis

This thesis is hosted in Bradford Scholars – The University of Bradford Open Access repository. Visit the repository for full metadata or to contact the repository team

© University of Bradford.

This work is licenced for reuse under a Creative Commons Licence.

L-L

IN-LINE PROCESS MEASUREMENTS FOR INJECTION MOULDING CONTROL

In-line rheology and primary injection phase process measurements for injection moulding of semi-crystalline thermoplastics, using instrumented computer monitored injection moulding machines, for potential use in closed loop process control.

Russell Gordon SPEIGHT B.Eng (Hons)

submitted for the degree
of Doctor of Philosophy

Department in Mechanical and Manufacturing Engineering
University of Bradford

1993

DEDICATION

In loving memory of my father Gordon Speight

To my family and friends

ABSTRACT

IN-LINE PROCESS MEASUREMENTS FOR INJECTION MOULDING CONTROL

Russell Gordon SPEIGHT

KEYWORDS: Injection Moulding Control
 In-line Nozzle Rheometry
 In-line Capillary Rheometry
 In-line Process Measurements
 Polymer Melt Rheology
 Intelligent Process Control
 Closed Loop Process Control
 Statistical Process Control
 Accurate Process Measurements
 Computer Monitoring

In-line rheological and process measurements are studied, during the primary injection phase, as a potential aid to closed loop process control for injection moulding. The feasibilities of attaining rheological and process measurements of sufficient accuracy and precision for use in process control are investigated. The influence of rheological and process measurements on product quality are investigated for semi-crystalline thermoplastic materials. A computer based process and machine parameter monitoring system is utilised to provide accurate and precise process data for analysis.

ACKNOWLEDGEMENTS

Professor Phil Coates for his enthusiastic support and guidance throughout the course of this work

Polymer Engineering Group (PEG) of Science and Engineering Research Council (SERC)

BASF plc

Birkbys Plastics Ltd

BP Chemicals Ltd

Du Pont (UK) Ltd

Dynisco (UK) Ltd and Dynisco (US) Inc

Ford Motor Company (UK) Ltd

NANMAC Corporation

Sandretto Industries (UK) Ltd

Terwin Instruments Ltd

Friends and Colleagues:

Dr R M Rose, Wolfson Research Fellow

D Chavda, G Clay, M F Fellows, A R Haynes, R Jowett, B Neen, C Parminter, C Roberts, G Speight, G Sullivan, J Whitworth and M Woodhead

Photographic Studio, University of Bradford: D Berryman, S Davis and A Sutton

Secretarial Staff: M Cooper, E D Ellis, A Hall and S C Hill

	Page
ABSTRACT - KEYWORDS	i
ACKNOWLEDGEMENTS	ii
LIST OF CONTENTS	iii
APPENDICES	ix
LIST OF FIGURES	xi
LIST OF TABLES	xviii
NOMENCLATURE	xxi

LIST OF CONTENTS

CHAPTER 1	Introduction, Aims and Scope of Research	
1.1	Introduction	1
	1.1.1 Recent Machine Parameter Sequence Control Developments	1
	1.1.2 Closed Loop Process Control for Injection Moulding	2
	1.1.3 Material Variation Through Recycling	5
1.2	Aims	8
1.3	Scope of Research	8
CHAPTER 2	Review and Critical Assessment of Injection Moulding	
2.1	Introduction	10
2.2	Brief History of Injection Moulding	12
2.3	Stages of the Injection Moulding Process	15
2.4	Thermoplastic Injection Moulding Materials	20
2.5	Process Control Technology	27
	2.5.1 Summary of Material Variation Through Recycling	28
	2.5.2 In-line Rheometry of Injection Moulding Control	29
	2.5.3 Development of Closed Loop Process Control for Injection Moulding	30
	2.5.4 Modelling and Simulation of the Injection Moulding Process	31
	2.5.5 Model Reference Injection Moulding Process Control Systems	32
	2.5.6 Statistical Process Control for Injection Moulding	32
	2.5.7 Cincinnati Milacron In-line Closed Loop Process Control	33
2.6	In-line Process Measurement Technology	35
	2.6.1 In-line Pressure Transducer Technology	35
	2.6.2 In-line Temperature Transducer Technology	36
CHAPTER 3	Polymer Melt Rheology	
3.1	Introduction	39

3.2	Off-line, On-line and In-line Rheometry	42
3.3	Capillary Rheometry	44
3.3.1	Poiseuille Law for Capillary Flow	44
3.3.2	Extensional Viscosity from Flow Through an Orifice Die	45
3.3.3	Corrections for Apparent Viscosity	45
3.3.3.1	Bagley Correction (Ends Pressure Drop)	46
3.3.3.2	Rabinowitsch Correction (Non-Velocity Profile)	46
3.3.3.3	Influence of Pressure on Viscosity	46
3.3.3.4	Influence of Temperature on Viscosity	47
3.4	Converging Flows	47
3.4.1	Cogswell Model	48
3.4.2	Spherical Velocity Field Model (Gibson)	49
3.4.3	Binding Model	50
3.4.4	Machine Nozzle Geometry	51
3.5	Power Law Model	51
CHAPTER 4 Design and Modification of Experimental Equipment		
4.1	Introduction	53
4.2	Modular Nozzle Rheometer Design and Construction	58
4.3	Beaker Tool Design and Construction	63
4.4	Container Tool Configuration	70
4.5	High Temperature Pressure Transducer Calibration and Test Facility	74
4.6	Modification of Screw Velocity Controller Performance of Sandretto 60 tonne Injection Moulding Machine	78
CHAPTER 5 Instrumentation for Accurate Process Measurements		
5.1	Introduction	79
5.2	Transducers for Machine and Process Monitoring	82
5.2.1	Nozzle Melt Pressure Transducers	82
5.2.2	Nozzle Melt Temperature Transducers	88
5.2.3	Screw Displacement and Velocity Transducers	88
5.3	Melt Pressure Transducer Assessment	89
5.4	Transducer Signal Conditioning	93
5.5	Transducer Calibration	95
5.5.1	Pressure Transducers (Static Calibration)	95
5.5.2	Displacement Transducers (Static/Dynamic Calibration)	96
5.5.3	Temperature Transducers (Static/Dynamic Calibration)	99
5.5.4	Velocity Transducer (Static Calibration)	102
5.5.5	Screw Rotational Speed (Static Calibration)	102

CHAPTER 6 Machine and Process Variable Monitoring Technique		
6.1	Introduction	103
6.2	Machine and Process Variable Monitoring Initiation Triggers	106
6.3	Machine and Process Variable Monitoring System Hardware	108
	6.3.1 Computer Specification	108
	6.3.2 Modular Interface Unit	110
6.4	Machine and Process Variable Monitoring System Software	112
	6.4.1 Software for Injection Moulding Process	112
	6.4.2 Software for Transducer Static Calibration and Performance Assessment	113
6.5	Data Processing and Analysis	115
 CHAPTER 7 In-line Capillary Rheometry		
7.1	Introduction	116
	7.1.1 Scope of this Chapter	117
	7.1.2 In-line Capillary Rheometry	118
	7.1.3 Off-line Capillary Rheometry	121
7.2	Materials Investigated	122
	7.2.1 High Density Polyethylene (HDPE)	122
	7.2.2 Polyoxymethylene (POM)	123
7.3	Experimental Comparison of In-line and Off-line Capillary Rheometry	124
	7.3.1 Configuration of In-line Modular Nozzle Rheometer	127
	7.3.2 Configuration of Rosand RH7-2 Twin Bore Off-line Capillary Rheometer	134
7.4	Extrapolation of In-line Die Entrance Pressure	138
	7.4.1 Calculation of In-line Die Entrance Pressure	139
	7.4.2 Accuracy of Corrected Capillary Die Entrance Pressure	140
7.5	Comparison of In-line and Off-line Capillary Rheometry	
	Experimental results for High Density Polyethylene	143
	7.5.1 Comparison of Wall Shear Stress Versus Apparent Wall Shear Rate Data	143
	7.5.2 Influence of Melt Temperature on Wall Shear Stress	150
	7.5.3 Effect of Bagley Correction	154
	7.5.4 Effect of Rabinowitsch Correction	157
7.6	Comparison of In-line and Off-line Capillary Rheometry	
	Experimental Results for Polyoxymethylene	159
	7.6.1 Comparison of Wall Shear Stress Versus Apparent Wall Shear Rate Data	159
	7.6.2 Effect of Bagley Correction	165
	7.6.3 Effect of Rabinowitsch Correction	169
7.7	Discussion of Results	171
	7.7.1 High Density Polyethylene (HDPE) Data	171

7.7.2	Polyoxymethylene (POM) Data	173
7.7.3	Corrected In-line Capillary Die Entrance Pressure (CDEP)	175
7.8	Concluding Comments	179

CHAPTER 8 In-line Nozzle Rheometry and Process Measurements for Injection Moulding

8.1	Introduction	181
8.1.1	Scope of this Chapter	183
8.1.2	Experimental Moulding Tests Analysed	183
8.2	Experimental Configuration	185
8.2.1	In-line Modular Nozzle Rheometer Configuration	185
8.2.2	Monitored Parameters	188
8.2.3	Machine Parameters	191
8.3	Beaker Tool Experimental Results	193
8.3.1	Introduction	193
8.3.2	Initial Experimental Observations	193
8.3.3	Integration of Full Pressure Profiles During Primary Injection	193
8.3.4	Integration of Specific Area of Pressure Profiles	195
8.3.5	Summary of Results	198
8.3.6	Comparison of Nozzle Melt Pressure and Hydraulic Injection Pressure Integrals During Primary Injection	199
8.4	Container Tool Experimental Results	202
8.4.1	Introduction	202
8.4.2	Initial Experimental Observations	202
8.4.3	Integration of Full Pressure Profiles During Primary Injection	202
8.4.4	Integration of Specific Area of Pressure Profiles	204
8.4.5	Summary of Results	207
8.4.6	Comparison of Nozzle Melt Pressure and Hydraulic Injection Pressure Integrals During Primary Injection	208
8.5	Measurement of Specific Nozzle Melt Pressure Integrals for Material Batch to Batch Variation Identification	211
8.6	Influence of Screw Injection Velocity Control Performance for In-line Rheological and Process Measurements	220
8.6.1	Introduction	220
8.6.2	Theoretical Considerations of In-line Nozzle Rheometry	220
8.6.3	Experimental Results	222
8.6.4	Changing the Performance of the Screw Injection Velocity Control	227
8.7	Relationship Between In-line Nozzle Melt Pressure and Hydraulic Injection Pressure Measurements During Primary Injection	234

8.7.1	Introduction	234
8.7.2	Comparison of Nozzle Melt Pressure and Hydraulic Injection Pressure Measurements During Primary Injection	234
8.7.3	Theoretical Considerations for the Relationship Between Nozzle Melt Pressure and Hydraulic Injection Pressure Measurements	235
8.7.4	Experimental Results	236
8.8	Industrial Process Monitoring	246
8.8.1	Introduction	246
8.8.2	Experimental Configuration	246
8.8.3	Experimental Results	249
8.8.4	Summary of Experimental Results	251
8.8.5	Comparison of Nozzle Melt Pressure and Hydraulic Injection Pressure Integrals During Primary Injection	252
8.8.6	Identification of Specific Pressure Integral Time Periods	252
8.9	Discussion of Results	266
8.9.1	Determination of an Optimum Assessment of Polymer Melt Viscosity During Primary Injection	266
8.9.2	Importance of Screw Injection Velocity Control	270
8.10	Concluding Comments	271
CHAPTER 9 Influence of Process Variation on Product Quality		
9.1	Introduction	272
9.1.1	Scope of this Chapter	273
9.1.2	Experimental Moulding Tests	275
9.2	Influence of Tool and Melt Temperature on Heat Transfer Rate from Polymer Melt in the Cavity to Adjacent Tool	276
9.2.1	Influence of Tool Temperature on Heat Transfer Rate	276
9.2.2	Transient Response of Tool Temperature Controller	277
9.2.3	Influence of Tool Temperature on Product Quality	277
9.2.4	Product Density Distribution	282
9.3	Influence of Molecular Weight on Polymer Melt Viscosity	283
9.3.1	Initial Experimental Observations	283
9.3.2	Primary Injection Screw Velocity Profile	286
9.3.3	Relationship Between Nozzle Melt Pressure and Nozzle Melt Temperature During Primary Injection	286
9.3.4	Comparison of Theoretical and Practical Nozzle Melt Temperature Differentials	294
9.3.5	Process Sensitivity	295
9.4	Influence of Screw Injection Velocity on Melt Viscosity	296

9.4.1	Initial Experimental Observations	297
9.4.2	Relationship Between Nozzle Melt Pressure and Nozzle Melt Temperature During Primary Injection	302
9.4.3	Relationship Between Nozzle Melt Temperature and Product Quality	310
9.4.4	Comparison of Theoretical and Practical Nozzle Melt Temperature Differentials	317
9.4.5	Process Sensitivity	317
9.5	Discussion of Results	319
9.5.1	Influence of Tool Temperature on Product Quality	319
9.5.2	Influence of Melt Viscosity on Product Quality	320
9.5.3	Process Sensitivity	323
9.6	Concluding Comments	324
CHAPTER 10 Global Discussion of Results		
10.1	Introduction	325
10.2	In-line Capillary Rheometry	325
10.3	Optimum Accuracy and Precision of Polymer Melt Viscosity Measurements	326
10.3.1	Determination of an Optimum Assessment of Polymer Melt Viscosity	326
10.3.2	Importance of Screw Injection Velocity Control	327
10.4	Influence of Polymer Melt Viscosity on Product Quality	327
10.5	Influence of Packing Phase on Product Quality	328
10.6	Injection Moulding Closed Loop Process Control	329
CHAPTER 11 Conclusions and Recommendation for Future Work		
11.1	Conclusions	335
11.1.1	In-line Capillary Rheometry	335
11.1.2	In-line Nozzle Rheometry and Process Measurements in Injection Moulding	335
11.1.3	Influence of Process Variation on Product Quality	336
11.2	Recommendations for Future Work	338
11.2.1	Implementation of Closed Loop Process Control	338
11.2.2	Modular Nozzle Rheometer Design	339
11.2.3	In-line Capillary Rheometry	341
11.2.4	Utilisation of Instrumented Beaker Tool	341
11.2.5	Design of a Flexible Insert Tool	341
11.2.6	Influence of Process variation on Product Quality for Amorphous Materials	343
REFERENCES		344

APPENDICES

		Page
Appendix A	Sandretto Series Seven 60 Tonne Injection Moulding Machine	
(i)	Technical specification	A1
(ii)	Details of Sandretto series seven 60 tonne injection unit	A2
(iii)	Sandretto viscosity index calculation	A3
(iv)	Original Sandretto series seven 60 tonne nozzle design	A4
(v)	40 mm diameter screw tip	A5
(vi)	Serial communication, connections and protocol	A6
Appendix B	Rosand RH7-2 Off-line Twin Bore Capillary Rheometer	
(i)	Technical specification and selection guide	B1
Appendix C	Experimental Procedures	
(i)	Off-line capillary rheometry	C1
(ii)	In-line capillary rheometry and experimental moulding tests	C2
Appendix D	Modular Nozzle Rheometer Design	
(i)	Modular nozzle rheometer assembly	D1
(ii)	Details of modular nozzle rheometer	D2
(iii)	Capillary rheometry front nozzle section	D3
(iv)	Long capillary die (L= 16.0 mm, R= 0.5 mm, L/R= 32.0)	D4
(v)	Short capillary die (L= 3.0 mm, R= 0.5 mm, L/R= 6.0)	D5
Appendix E	Temperature Controllers	
(i)	Modular nozzle heater bands (elements)	E1
(ii)	Tool temperature	E1

Appendix F	Instrumented Beaker Tool	
(i)	Single impression beaker design	F1
(ii)	Initial beaker tool design	F2
(iii)	Beaker tool general assembly (Complexa Tools)	F3
(iv)	Beaker tool temperature control zones	F4
(v)	Hot sprue bushing ('hot tip') technical specification	F5
(vi)	Hot sprue bushing ('hot tip') mounting	F6
Appendix G	Instrumented Container Tool	
(i)	Container design	G1
(ii)	Container tool general assembly	G2
(iii)	Container tool temperature control zones	G3
Appendix H	Materials Processed	
	BP Rigidex high density polyethylene (HDPE)	
(i)	Grade HD5226EA, BP technical information sheet T211/1	H1
(ii)	Grade HD5050EA, BP technical information sheet T206/1	H2
(iii)	Du Pont Delrin II polyoxymethylene (POM)	H3
Appendix I	Experimental Moulding Tests	
(i)	Sandretto series seven 60 tonne	I1
(ii)	Stork 440 tonne, Birkbys Plastics Limited	I3
(iii)	Cincinnati Milacron ACT30 30 tonne	I3
Appendix J	Statistic Analysis	J1
Appendix K	Nozzle Thermocouple Mounting	
(i)	Design considerations of nozzle thermocouple mounting	K1
(ii)	Design for thermocouple mounting	K2

LIST OF FIGURES

Figure	Title	Page
1.1	Closed loop process control of the injection moulding process, Coates (1989a)	3
1.2	Accurate measurement of process variables is at the heart of process analysis, control and understanding of how molecular features influence processing, Coates (1991)	4
2.1	Relationship between service properties and ease of processing: a common sense experience, not a law of physics, Cogswell (1981 p71)	11
2.2	Stages of a typical injection moulding process cycle	19
2.3	The end use of plastic products in Western Europe in 1978, McCrum et al (1988 p 6)	21
2.4	European consumption of polymeric materials 1987 to 1988, European Plastics News (1989)	22
2.5	Molecular symmetry (stereoregularity), isotactic, syndiotactic and atactic, Morton-Jones (1989 p 10)	23
2.6	Storage modulus E' - temperature diagram for polymers, Morton-Jones (1989 p 14)	24
2.7	Cincinnati Milacron in-line viscometer for closed loop process control	34
2.8	Typical VDU display screen for Cincinnati Milacron in-line viscometer	34
3.1	Simple shear: area A and distance h remain constant during deformation	39
3.2	Simple extensional: cross-sectional area A and sample length l both vary during deformation	41
3.3	Off-line, on-line and in-line rheometry, Coates (1991)	43
3.4	Sandretto series seven 60 tonne injection nozzle geometry	51
4.1	General view of Sandretto 60 tonne injection moulding machine	55
4.2	General view of Rosand RH7-2 off-line twin bore capillary rheometer	56
4.3	Crosshead and pistons of Rosand RH7-2 off-line twin bore capillary rheometer	57
4.4	Pressure transducer locations for Rosand RH7-2 off-line twin bore capillary rheometer	57
4.5	Modular nozzle rheometer configured for injection moulding experimental tests	60
4.6	Nozzle front section for injection moulding experimental tests	60
4.7	Modular nozzle front section spigot location ring	61
4.8	Modular nozzle instrumentation sections	61
4.9	Modular nozzle back section for location with machine barrel	62
4.10	Modular nozzle front section and dies for in-line capillary rheometry	62
4.11	Schematic diagram of instrumented beaker tool (single impression)	65
4.12	Beaker tool core and cavity plates	66
4.13	Beaker tool core plates showing core	66

4.14	Instrumentation flat on side of beaker cavity	67
4.15	Hot sprue bushing ('hot tip') for beaker tool	67
4.16	Closed beaker tool located between machine platens	68
4.17	Open beaker tool showing stripper plate	68
4.18 a	Example of injection moulded beaker component	69
4.18 b	Example of injection moulded beaker component showing instrumentation location flats	69
4.19	Schematic diagram of instrumented container tool (two impression 'family' tool)	71
4.20	Container tool core plate showing ejector pins	72
4.21	Container tool cavity plate	72
4.22 a	Example of injection moulded container component (external view) and sprue	73
4.22 b	Example of injection moulded container component (internal view) and sprue	73
4.23	Schematic diagram of high temperature pressure transducer calibration and test facility	75
4.24	High temperature pressure transducer calibration and test facility	76
4.25	Six pressure transducers located in temperature controlled manifold	76
4.26	Schematic diagram of improved pressure transducer high temperature pressure transducer calibration and test facility	77
4.27	Improved high temperature pressure transducer calibration and test facility	77
5.1	Schematic diagram of instrumented injection unit of Sandretto 60 tonne injection moulding machine	80
5.2	General view of instrumented injection unit of Sandretto 60 tonne injection moulding machine	81
5.3	Screw linear displacement and velocity transducers located on injection unit	84
5.4	Screw rotational speed transducer	84
5.5	Schematic diagram of beaker tool instrumentation for cavity pressure and temperature measurements	86
5.6	Schematic diagram of container tool instrumentation for cavity pressure and temperature measurements	87
5.7	Maximum linearity errors for full pressure range of three different technology pressure transducers	91
5.8	Influence of step temperature change on zero pressure values for three different technology pressure transducers	92
5.9	Schematic diagram of linear screw displacement and velocity transducers located on the injection unit	96
5.10	Steady state dynamic error lag of LVDT measurements referenced to linear potentiometer measurements	97
5.11	Dynamic response of LVDT and linear potentiometer transducers for an injection screw velocity of 97 mm/s	98
5.12	Dynamic response of 1 mm diameter thermocouple to temperature Step change	100

5.13	Dynamic response of industrial nozzle thermocouple to temperature step change	101
6.1	Schematic diagram of machine and process variable monitoring system	104
6.2	Synoptic cycle indication VDU display screen for Selec machine controller	107
6.3	Machine and process variable monitoring system hardware	109
6.4	Biodata Microlink modular interface unit	111
6.5	Typical nozzle melt pressure profiles during injection and packing phase	114
7.1	Schematic diagram of modular nozzle configuration for in-line capillary rheometry	119
7.2	Modular nozzle rheometer configured for in-line capillary rheometry	120
7.3	Schematic diagram of in-line capillary rheometer installation	128
7.4	General view of Sandretto 60 tonne injection moulding machine Configured for in-line capillary rheometry	129
7.5	Short capillary die located on modular nozzle rheometer	129
7.6	Short capillary die sealed by moving platen during plasticisation phase	132
7.7	In-line capillary rheometry 'airshot', POM Delrin II 500, long capillary die, 5 mm/s screw injection velocity	132
7.8	In-line corrected long capillary die entrance pressure and screw displacement for Du Pont Delrin II 500 at 5 mm/s screw injection velocity during a typical 'airshot'	133
7.9	Schematic diagram of Rosand RH7-2 twin bore capillary rheometer	135
7.10 a	Pressure transducer location for in-line capillary rheometry	138
7.10 b	Pressure transducer location for off-line capillary rheometry	139
7.11	Influence of correction factor on in-line nozzle melt pressure	142
7.12	In-line and off-line capillary rheometry (uncorrected HDPE data)	144
7.13	Comparison of in-line and off-line capillary rheometry (uncorrected HDPE data)	146
7.14	Influence of apparent wall shear rate on power law index n (uncorrected HDPE data)	149
7.15	Influence of temperature on wall shear stress (uncorrected HDPE data)	151
7.16	Influence of shear heating on polymer melt temperature	152
7.17	In-line and off-line capillary rheometry (Bagley corrected HDPE data)	155
7.18	In-line and off-line capillary rheometry (Bagley and Rabinowitsch corrected HDPE data)	158
7.19	In-line and off-line capillary rheometry (uncorrected POM data)	160
7.20	Two non-Newtonian linear flow regions for three molecular weight grades of POM(uncorrected data)	161
7.21	Comparison of in-line and off-line capillary rheometry (uncorrected POM data)	162
7.22	Velocity profiles in capillary dies	165
7.23	In-line and off-line capillary rheometry (Bagley corrected POM data)	166
7.24	In-line and off-line capillary rheometry (Bagley and Rabinowitsch corrected POM data)	170

7.25	In-line and off-line capillary rheometry extrudate surface appearance	178
8.1	Schematic diagram of in-line modular nozzle rheometer configured for injection moulding experimental tests	186
8.2	In-line modular nozzle rheometer configured for injection moulding experimental tests	187
8.3	Mean nozzle melt pressure, mean hydraulic injection pressure and mean screw displacement during primary injection	194
8.4	Mean nozzle melt pressure and coefficient of variation during primary injection	196
8.5	Mean hydraulic injection pressure and coefficient of variation during primary injection	197
8.6	Relationship between nozzle melt pressure and hydraulic injection pressure integrals for the full period of primary injection	200
8.7	Relationship between nozzle melt pressure and hydraulic injection pressure integrals for a specific period of primary injection	201
8.8	Mean nozzle melt pressure, mean hydraulic injection pressure and mean screw displacement during primary injection	203
8.9	Mean nozzle melt pressure and coefficient of variation during primary injection	205
8.10	Mean hydraulic injection pressure and coefficient of variation during primary injection	206
8.11	Relationship between nozzle melt pressure and hydraulic injection pressure integrals for the full period of primary injection	209
8.12	Relationship between nozzle melt pressure and hydraulic injection pressure integrals for a specific period of primary injection	210
8.13	Mean nozzle melt pressure and mean screw displacement during primary injection for Batch 1	213
8.14	Mean nozzle melt pressure and mean screw displacement during primary injection for Batch 2	214
8.15	Nozzle melt pressure integrals for full period of primary injection	215
8.16	Nozzle melt pressure integral based on the Sandretto viscosity index calculation	216
8.17	Mean nozzle melt pressure and coefficient of variation during primary injection for Batch 1	217
8.18	Mean nozzle melt pressure and coefficient of variation during primary injection for Batch 2	218
8.19	Nozzle melt pressure integrals for a specific period of primary injection	219
8.20	Mean screw injection velocity and coefficient of variation during primary injection, Test P30%20B	223
8.21	Mean screw injection velocity and mean screw acceleration during primary injection, Test P30%20B	224
8.22	Mean screw injection velocity and coefficient of variation during primary injection, Test 3-D500	225
8.23	Mean screw injection velocity and mean screw acceleration during primary injection, Test 3-D500	226

8.24	Mean screw injection velocity and coefficient of variation for level A screw displacement accuracy, Test L40%20B	229
8.25	Mean nozzle melt pressure and coefficient of variation for level A screw displacement accuracy, Test L40%20B	230
8.26	Mean screw injection velocity and coefficient of variation for level B screw displacement accuracy, Test I40%20B	231
8.27	Mean nozzle melt pressure and coefficient of variation for level B screw displacement accuracy, Test I40%20B	232
8.28	Product weight distribution for level A and B screw displacement accuracy	233
8.29	Relationship between maximum nozzle melt pressure and hydraulic injection pressure, during primary injection	238
8.30	Hydraulic oil temperature distribution for increasing screw injection velocity	239
8.31	Mean screw injection velocity and mean ratio of nozzle melt pressure to hydraulic injection pressure during primary injection	240
8.32	Differential of mean ratio of nozzle melt pressure to hydraulic injection pressure compared to coefficient of variation of nozzle melt pressure	241
8.33	Differential of mean ratio of nozzle melt pressure to hydraulic injection pressure compared to coefficient of variation of nozzle melt pressure	242
8.34	Mean screw injection velocity and mean ratio of nozzle melt pressure to hydraulic injection pressure during primary injection	243
8.35	Differential of mean ratio of nozzle melt pressure to hydraulic injection pressure compared to coefficient of variation of nozzle melt pressure	244
8.36	Differential of mean ratio of nozzle melt pressure to hydraulic injection pressure compared to coefficient of variation of nozzle melt pressure	245
8.37	Stork 440 tonne injection moulding machine	253
8.38	Moulded product, sprue and runner system	254
8.39	Industrial nozzle rheometer	255
8.40	In-line nozzle rheometer during industrial process monitoring	256
8.41	Mean nozzle melt pressure and mean screw displacement during a typical industrial monitored injection moulding cycle	257
8.42	Mean nozzle melt pressure, mean hydraulic injection pressure and mean screw displacement during primary injection	258
8.43	Mean nozzle melt pressure and coefficient of variation during primary injection	259
8.44	Mean injection hydraulic pressure and coefficient of variation during primary injection	260
8.45	Relationship between nozzle melt pressure and hydraulic injection pressure integrals for the full period of primary injection	261
8.46	Relationship between nozzle melt pressure and hydraulic injection pressure integrals for a specific period of primary injection	262
8.47	Mean ratio of nozzle melt pressure to hydraulic injection pressure and differential of ratio during primary injection	263
8.48	Differential of mean ratio of nozzle melt pressure to hydraulic injection pressure and coefficient of variation of nozzle melt pressure during primary injection	264

8.49	Differential of mean ratio of nozzle melt pressure to hydraulic injection pressure and coefficient of variation of nozzle melt pressure during primary injection	265
8.50	Mean nozzle melt pressure and coefficient of variation during primary injection - Cincinnati Milacron ACT30	269
8.51	Relationship between screw velocity and pressure variation	270
9.1	Closed loop process control for injection moulding	274
9.2	Set tool temperature and mean measured tool temperature	278
9.3	Mean measured tool temperature and product weight	279
9.4	Mean measured tool temperature and product height dimension	280
9.5	Relationship between product weight and product height dimension	281
9.6	Measurement of beaker height dimension	282
9.7	Mean nozzle melt pressure and mean screw displacement during primary injection for HDPE grade HD5226EA	284
9.8	Mean nozzle melt pressure and mean screw displacement during primary injection for HDPE grade HD5050EA	285
9.9	Mean screw injection velocity during primary injection for two different molecular weight grades of HDPE (HD5226EA and HD5050EA)	287
9.10	Mean nozzle melt pressure and mean nozzle melt temperature during primary injection for HDPE grade HD5226EA	288
9.11	Mean screw acceleration and mean nozzle melt temperature during primary injection	289
9.12	Differential of mean ratio of nozzle melt pressure to hydraulic injection pressure and mean nozzle melt temperature during primary injection	290
9.13	Mean nozzle melt pressure and mean nozzle melt temperature during primary injection for HDPE grade HD5050EA	291
9.14	Mean screw acceleration and mean nozzle melt temperature during primary injection	292
9.15	Differential of mean ratio of nozzle melt pressure to hydraulic injection pressure and mean nozzle melt temperature during primary injection	293
9.16	Influence of screw injection velocity on product quality (weight and height dimension)	296
9.17	Mean nozzle melt pressure for screw injection velocity range	298
9.18	Mean screw displacement for screw injection velocity range	299
9.19	Mean screw injection velocity range	300
9.20	Mean nozzle melt temperature for screw injection velocity range	301
9.21	Mean nozzle melt pressure and mean nozzle melt temperature during primary injection for set screw injection velocity of 20 mm/s	303
9.22	Mean screw acceleration and mean nozzle melt temperature during primary injection for set screw injection velocity of 20 mm/s	304
9.23	Differential of mean ratio of nozzle melt pressure to hydraulic injection pressure and mean nozzle melt temperature during primary injection for set screw injection velocity of 20 mm/s	305
9.24	Mean nozzle melt pressure and mean nozzle melt temperature during primary injection for set screw injection velocity of 50 mm/s	306

9.25	Mean screw acceleration and mean nozzle melt temperature during primary injection for set screw injection velocity of 50 mm/s	307
9.26	Differential of ratio nozzle melt pressure to hydraulic injection pressure and mean nozzle melt temperature during primary injection for set screw injection velocity of 50 mm/s	308
9.27	Relationship between nozzle melt pressure and nozzle melt temperature for final screw acceleration point	309
9.28	Relationship between product weight and product height dimension	311
9.29	Influence of nozzle melt temperature on product quality (weight and dimension)	312
9.30	Mean nozzle melt pressure and coefficient of correlation between nozzle melt pressure with product weight during primary injection	313
9.31	Mean screw displacement and coefficient of correlation between screw displacement with product weight during primary injection	314
9.32	Mean screw velocity and coefficient of correlation between screw velocity with product weight during primary injection	315
9.33	Mean nozzle melt temperature and coefficient of correlation between nozzle melt temperature with product weight during primary injection	316
9.34	Influence of nozzle melt temperature on product quality	319
9.35	Mean nozzle melt pressure and mean nozzle melt temperature during primary injection, industrial process monitoring data	322
10.1	Mean screw displacement and coefficient of correlation between screw displacement and product weight for periods of screw relaxation	331
10.2	Mean nozzle melt pressure and coefficient of correlation between nozzle melt pressure and product weight for periods of screw relaxation	332
10.3	Correlation between screw packing displacement and product weight	333
10.4	Polymer melt viscosity assessment techniques for injection moulding closed loop process control	334
11.1	Proposed cross section of reservoir bore using optical melt pressure and temperature transducers	340
11.2	Dependence of apparent wall shear rate on secondary capillary die radius	342

LIST OF TABLES

Figure	Title	Page
2.1	Machine parameter settings for typical injection moulding cycle shown in figure 2.2	18
5.1	List of injection unit transducers	83
5.2	List of beaker tool transducers	85
5.3	List of container tool transducers	85
5.4	Performance of different pressure transducer technologies at 200C	90
5.5	Signal conditioning of machine and process monitoring transducers	93
5.6	Signal conditioning of Sandretto injection moulding machine	94
5.7	Pressure transducer calibration information	95
6.1 a	Personal computer specification for injection monitoring	108
6.1 b	Personal computer specification for plasticisation monitoring	108
7.1 a	Specification of high density polyethylene (HDPE)	122
7.1 b	Specification of polyoxymethylene (POM)	123
7.2	Apparent wall shear rate for in-line and off-line capillary rheometry	126
7.3 a	In-line capillary rheometer injection monitored parameters	130
7.3 b	In-line capillary rheometry plasticisation monitored parameters	130
7.4	In-line nozzle rheometer machine parameter settings	131
7.5	Off-line capillary rheometer monitored parameters	134
7.6 a	Off-line capillary rheometer machine parameter settings (HDPE)	136
7.6 b	Off-line capillary rheometer machine parameter settings (POM)	137
7.7	Nozzle melt pressure accuracy data for typical 'airshot'	140
7.8 a	Summary of power law results for HDPE grade HD5226EA (uncorrected data)	145
7.8 b	Summary of power law results for HDPE grade HD5050EA (uncorrected data)	147
7.9	Second order polynomial curve fit data for HDPE grades HD5226EA and HD5050EA	148
7.10 a	Summary of power law results for HDPE grade HD5226EA (Bagley corrected data)	154
7.10 b	Summary of power law results for HDPE grade HD5050EA (Bagley corrected data)	154
7.11	Summary of n values for uncorrected and Bagley corrected HDPE data	156
7.12	Off-line capillary rheometry power law results for POM	159
7.13 a	Summary of power law results for POM grade 900F (uncorrected data)	163
7.13 b	Summary of power law results for POM grade 500 (uncorrected data)	163
7.13 c	Summary of power law results for POM grade 100	

	(uncorrected data)	163
7.14 a	Summary of power law results for POM grade 900F data (Bagley corrected data)	167
7.14 b	Summary of power law results for POM grade 500 data (Bagley corrected data)	167
7.14 c	Summary of power law results for POM grade 100 data (Bagley corrected data)	167
7.15	Summary of n values for uncorrected and Bagley corrected POM data	168
7.16	Summary of HDPE power law n values (uncorrected data)	172
7.17	Summary of HDPE power law n values (Bagley corrected data)	172
7.18	Summary of POM power law n values (uncorrected data)	174
7.19	Summary of POM power law n values (Bagley corrected data)	174
7.20	Nozzle melt pressure correction factors	175
7.21	Power law index n values for Bagley corrected in-line capillary rheometry data	176
7.22	Nozzle melt pressure values for long and short capillary dies	176
8.1 a	Beaker tool injection monitored parameters	188
8.1 b	Beaker tool plasticisation monitored parameters	189
8.2	Container tool injection monitored parameters (Test 3-D500)	189
8.3 a	Container tool injection monitored parameters	190
8.3 b	Container tool plasticisation monitored parameters	190
8.4	Machine parameter settings for polyoxymethylene (POM)	191
8.5	Machine parameter settings for high density polyethylene (HDPE)	192
8.6	Summary of coefficient of variation results for test P30%20B	198
8.7	Summary of measurement accuracy results for test P30%20B	198
8.8	Summary of coefficient of variation results for test 3-D500	207
8.9	Summary of measurement accuracy results for test 3-D500	207
8.10	Material batch information	211
8.11	Coefficients of variation results for material batch 1 and 2	212
8.12	Coefficient of variation results for level A and B screw displacement accuracy	228
8.13	Injection and plasticisation monitored parameters	247
8.14	Processing properties (BASF Campus Database)	248
8.15	Machine parameter settings for Stork machine	249
8.16	Summary of coefficient of variation results for industrial process monitored data	251
8.17	Summary of measurement accuracy results for industrial process monitored data	252
8.18	Summary of coefficient of variation results for beaker tool	266
8.19	Summary of coefficient of variation results for container tool	267
8.20	Summary coefficient of variation results for industrially monitored data	267
9.1	Comparison of coefficients of correlation for tool temperature and	

	product quality (weight and height dimension)	277
9.2	Summary of periods of screw acceleration	302
9.3	Product quality assessment, weight and dimension (height)	310
9.4	Melt temperature and pressure measurement accuracy for typical injection moulding process conditions	321

NOMENCLATURE

t	Time
P	Pressure
T	Temperature
ΔT	Temperature Differential
ΔP	Pressure Differential
ρ	Density
C_p	Specific Heat
T_g	Glass Transition Temperature
T_m	Polymer Melting Point Temperature
E'	Storage Modulus
P_l	Pressure Drop Through Long Die
P_s	Pressure Drop Through Short Die
P_o	Orifice Pressure Drop
L/D	Length to Diameter Aspect Ratio
L/R	Length to Radius Aspect Ratio
$\dot{\gamma}$	Shear Strain Rate (Shear Rate)
$\dot{\gamma}_a$	Apparent Shear Strain Rate (Shear Rate)
τ_s	Shear Stress
η	Absolute Shear Viscosity
η_a	Apparent Shear Viscosity
λ	Extensional Viscosity
σ_E	Extensional Stress
$\dot{\epsilon}$	Extensional Strain Rate (Extensional Rate)
n	Power Law Index
K	Consistency Index

ABBREVIATIONS

CAD	Computer Aided Design	MB	Mega Byte
CDEP	Corrected Die Entrance Pressure	RAM	Random Access Memory
CPU	Central Processing Unit	RAW	Uncalibrated Data File
CSV	Comma Separated Variable	RPM	Revolutions Per Minute
DEN	Digital equivalent Number	VGA	Virtual Graphics Adapter
FEA	Finite Element Analysis	FSR	Full Scale Range
LVDT	Linear Variable Differential Transformer		

CHAPTER 1

Introduction, Aims and Scope of Research

1.1 Introduction

Injection moulding is one of the most important and efficient manufacturing techniques for polymeric materials, with the capability to manufacture high value added products. Injection moulding machines have benefited from advances in microprocessor based machine parameter control, since the late 1970's, resulting in enhanced, flexible control systems that provide improved injection and sequence control.

1.1.1 Recent Machine Parameter and Sequence Control Developments

Injection moulding machine design is continually improving, Whelan and Craft (1978) describe developments in injection moulding and Whelan and Craft (1981) describe improvements to machine efficiency. Canovi (1989) describes injection unit developments that improve machine productivity, aspects of the injection unit described are, hopper, barrel heaters, screw, nozzle and machine maintenance.

Improvements to machine design have been complemented by developments to microprocessor based machine parameter and sequence control. A report of developments at Kunststoffe 1979, Science Research Council (1979), describes the application of microprocessors to the injection moulding process. The report includes work from three separate contributors, P Farrar, University College Cardiff, P D Coates, University of Bradford and J Parnarby, University of Bradford. Coates reported that many machine manufacturers had developed their own systems 'in house' and that only one major manufacturer, Buhler, were not displaying a microprocessor system, but would shortly be introducing one. Ames (1984) describes the potential

use of microprocessors for improving hydraulic circuit design, with three aims (i) versatility of machine functions, (ii) simplicity, and (iii) energy efficiency. It is suggested by Sandretto (1988) that microcomputers for injection moulding machines have reached their practical limits for mechanical and hydraulic evolution and that further performance enhancement depends on software development.

1.1.2 Closed Loop Process Control for Injection Moulding

Material, machine and process variations are convolved in this complex process. Modern day microprocessor based machines operate with a high degree of repeatability, but often lack the measurement capability to interpret real time process variations, allowing raw material variations to influence the injection moulding process. As machine parameter control continues to improve, the significance of material variation will become a pronounced processing problem. Long term lot variations, variations in regrind level, drying conditions and additive concentration can change a polymer's flow behaviour and hence product quality, Ross et al (1990).

Implementation of process control will be a much more demanding step than that of closed loop machine control, since there is a need to develop viable process control strategies, based upon accurate, precise and reliable data. Coates (1989a) discusses in-line rheological measurements as a potential aid to closed loop process control and describes issues relating to the development of intelligent polymer processing machinery. Coates et al (1989b) propose that measurement of polymer melt 'state' at the nozzle is most attractive from an industrial view point, where a single transducer (most likely pressure or temperature) would provide useful information independent of the type of tool being used. Speight and Coates (1991) report that mean nozzle melt pressure measurements during in-line capillary rheometry, typically achieve coefficients of variation of 0.2%, representing a measurement accuracy of $\pm 0.6\%$, based on a ± 3 standard deviation distribution about the mean (assuming a normal distribution). This

work emphasises that for closed loop process control it will be necessary to deconvolve machine and process parameters, allowing accurate and precise measurement of process variations.

Foresight for the injection moulding process predicts a machine that maintains repeatable product quality for: (i) material variation, i.e. for batch to batch variation, use of regrind or recycled materials, (ii) the first to the last machine cycle, producing no scrap, and (iii) interruptions to production, where the machine has been stopped for an indefinite time period. Process control is required to compensate for process variations brought about by changes in the feed material, due to batch differences, or the use of regrind. This will result in reduced scrap material, increased product quality, and promote recycling of non-virgin materials, this latter point will have significant bearing in future years if Earth's natural resources are to be conserved.

Figure 1.1 shows a block diagram of a proposed closed loop process control system for injection moulding.

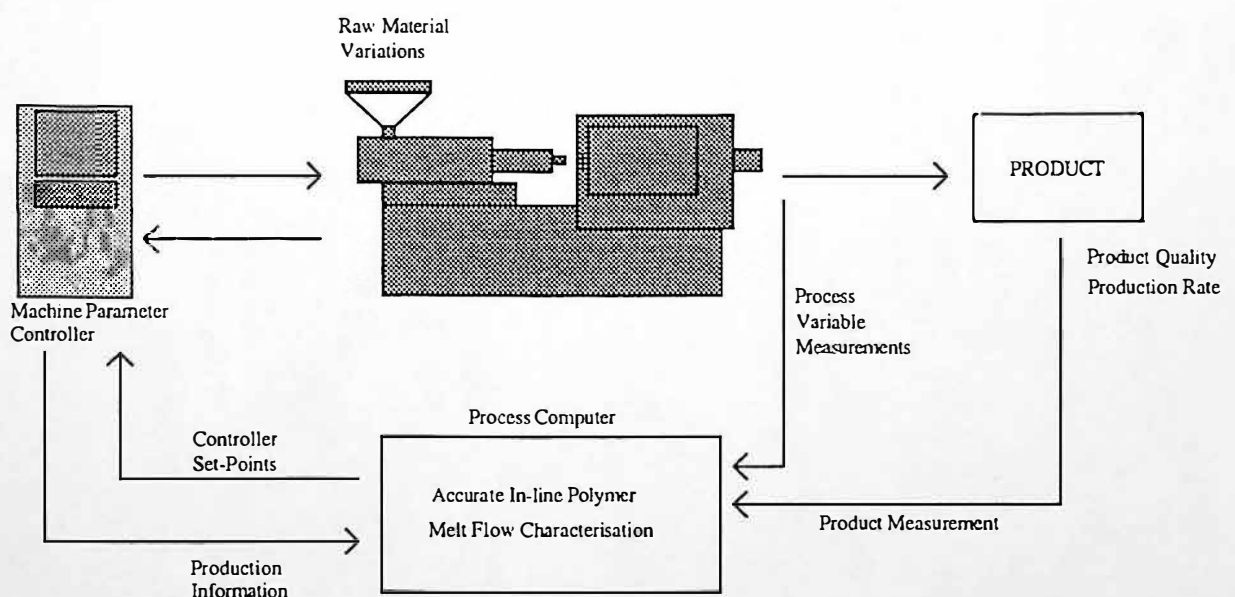


Figure 1.1 Closed loop process control of the injection moulding process, Coates (1989a)

Analysis and control of polymer processing operations requires high quality information concerning the polymer being processed. Figure 1.2 shows the uses of accurate polymer melt flow characterisation. Accurate characterisation of polymer melt rheology is required to:

- (i) provide the necessary data for analysis of tool design, using either physical modelling or Computer Aided Design (CAD), Finite Element Analysis (FEA) approaches;
- (ii) develop, using the raw data, a real time closed loop feedback control strategy, feed forward control strategies, or enhanced statistical process control;
- (iii) study processing-structure-property interactions, to gain understanding of molecular or compositional effects which influence processing or product properties, Coates (1991).

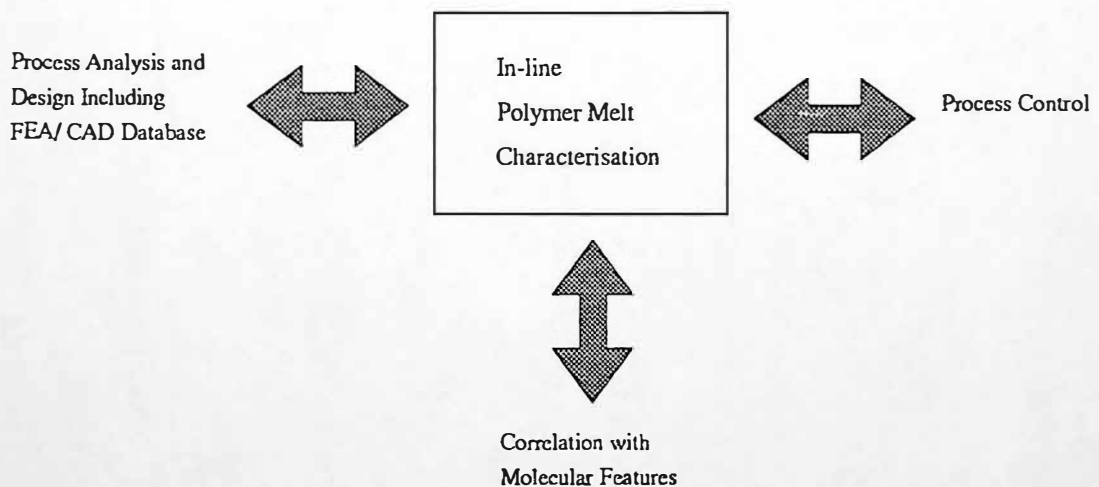


Figure 1.2 Accurate measurement of process variables is at the heart of process analysis, control and understanding of how molecular features influence processing, Coates (1991)

Statistical process control is currently used to maintain control of product quality in the industrial environment, whereby moulded products are sampled and statistically analysed. Product quality is commonly quantified by; weight, specific dimensions and surface appearance. Product weight has been shown by Harry (1991) to be a reasonable predictor of other product properties particularly dimensions. In tests where the process was perturbed to permit variations, linear regression calculations show a coefficient of correlation of 0.97 between product weight and length. Weight measurement devices (electronic scales) are capable of greater repeatability than typical dimensional measurement devices (digital micrometers) and therefore product weight measurements offer significant benefits in the industrial environment. The assessment of other product features such as surface appearance and roughness may require optical quality control systems, Fornfeld and Suchanek (1984), such systems may be used to identify contamination of translucent products, such as poly(methyl-methacrylate) lenses.

1.1.3 Material Variation Through Recycling

In recent years there has been a growing awareness for research to investigate the aspects of recovering value from scrap polymeric materials. Menges et al (1992) reports that as a result of pressure from the public, a powerful movement has begun to fight the 'throw-away mentality' of the past decades. The recycling of polymeric materials has been the subject of considerable research in recent years. European Plastics News (1979) describes what is claimed to be the first, and highly successful, method for complete recycling of moulded expanded polystyrene (XPS) scrap, by Kjeld Bentzen Maskiner APS of Hillerod, Denmark. Menges et al (1992) reports new and unconventional methods for recycling mixed plastic scrap and proposes that waste polymeric material, whether filled or unfilled, extremely pure or mixed can be divided more or less into their molecular components by chemical means. An article in European Plastics News (1993a) describes the competition to recycled materials from

virgin materials in the US market, in recent years, whereby the cost of virgin materials is the same, or even less than the recycled equivalent.

Polymer processors and distributors are positively identifying component materials, for example, The Body Shop HDPE bottles, The Body Shop International Plc (1991). Ultrasonic polymeric material identification techniques have been developed by Hull and Langton (1992), Hull et al (1992), which have potential use at reclamation centres, for the automatic identification and sorting of components/materials. Hull et al (1993) concludes that ultrasound attenuation analysis is a cheap and reliable method of identifying recycle in the polymer waste reclamation industry.

Recycled materials will hopefully form an important part of polymer processing in the near future. The German law says manufacturers must ensure that by 1st July 1995, 80% of all packaging is collected and that 80% of this amount is recycled, Genillard (1993). There is a phase-in period: since 1st January 1993 60% of glass packaging, 40% of tin-plate packaging and 30% of aluminium, card board, paper and polymeric packaging has to be collected, Genillard (1993). Today 44% of the feedstock into the German paper industry is waste paper, and a similar percentage applies to glass production. The recycling of polymeric materials is less profitable due to the complications of polymer processing, Genillard (1993). According to Frank Annighofer (German based head of Arthur D Little's European environment department) polymeric materials are recycled for political reasons. Environmentalists claim that inspection is not enough to ensure that viable ecological processes are maintained. Claims are made that waste exported to developing countries is dumped or incinerated. Norbert Bohm, a director of TK Umweltdienste, the DSD waste disposal contractor for Bonn, says "It takes know-how and large capital investment, which cannot be acquired overnight".

European Plastics News (1978) ^{shows that} thermoset scrap runners, purgings and flashed mouldings can be recycled, and used as a filler. The scrap is pulverised and then atomised into a powder. This recycled material is then mixed with virgin material to form a blend, of which the ratio of recycled material may vary between 0 to 40%.

The effect of processing operations on rheological, molecular characteristics and mechanical properties of injection moulded components is an area of detailed research. Crawford (1980) reported that the use of regrind material decreases impact strength of a moulded component. Polypropylene copolymer (ICI type GWM 201) was processed at 230C, using a six gated frame tool, results showed impact strength reduced by 17% and 25% for re-granulation passes one and two, respectively. Bernardo et al (1993) reports the effect of fibre degradation on the properties of recycled polycarbonate. It is stated that reprocessing does not significantly affect the tensile strength for MFI grades 2.66 and 6.27 (g/600s) polycarbonate, contrarily impact strength shows a marked drop after 4 to 6 reprocessing cycles.

Nolley et al (1980) describe a strategy for recovering some value from scrap polymeric materials. It is reported that reprocessing materials that are a generic mix, results in a product that is a blend, unless a method of segregation is used. The mechanical properties of blends from incompatible components are frequently poor, but in some cases may be improved by the addition of a 'compatiliser'. Fellahi et al (1991) conclude that a mixture of polymeric waste exhibits some strength, despite being composed of incompatible polymers, and should be useful for low grade applications. The incorporation of titanate coupling agents, CPE, peroxide and Novolak in polymeric mixtures, improves polymer melt rheology and mechanical properties and provides the possibility of having a range of materials that can compete on an equal basis with virgin materials. Baker et al (1993) describes the influence of processing history on LDPE viscoelastic response. Transient modification of entanglement networks is the most likely explanation for modified viscosity and elastic results.

The influence of processing operations on polymer melt is necessary to determine the rheological behaviour of recycled and regrind materials

1.2 Aims

To ascertain the feasibility of using rheological and process measurements for eventual closed loop process control of injection moulding, it is aimed in particular to:

1. Design, build and use rheometers in both the machine injection unit and tool;
2. Computer monitor major injection moulding in-line rheological, machine and process variables;
3. Analyse the trends of variation in selected process variables and rheological measurements on a shot by shot basis, in order to study correlations between these quantities;
4. Assess if the rheological measurements provide adequate resolution for eventual control purposes.

The work reported uses semi-crystalline thermoplastic materials, high density polyethylene (HDPE) and polyoxymethylene (POM). Amorphous material, Acrylonit- Butadiene Styrene (ABS) is utilised during industrial process monitoring.
rile

1.3 Scope of Research

A review and critical assessment of injection moulding is outlined in chapter 2, including a brief history of injection moulding, stages of the process, thermoplastic injection moulding materials, process control technology and in-line process

measurement technology. Chapter 3 describes polymer melt rheology regarding the injection moulding process.

Chapter 4 describes the design and modification of experimental equipment used, namely, an instrumented Sandretto 60 tonne injection moulding machine, an in-line modular nozzle rheometer, instrumented beaker and container tools and high temperature pressure transducer test and calibration facility. Chapter 5 describes the instrumentation used for accurate process measurements. Dynamic assessment of displacement and temperature transducers shows the importance of time response of transducers, during the primary injection phase. Detailed pressure transducer assessments are used to verify transducer performance. Chapter 6 describes machine and process variable monitoring techniques, for precision monitoring of the injection moulding process. Injection and plasticisation initiation triggers, computer hardware, modular interface unit, software and data processing and analysis are described.

Chapters 7, 8 and 9 outline the reported experimental work. Chapter 7 compares in-line and off-line capillary rheometry, for 'absolute' property measurements. In-line capillary rheometry has a potential use in CAD and FEA, determining polymer melt rheology for true process conditions. In-line and off-line capillary rheometry results are compared to assess the usefulness and accuracy of in-line capillary rheometry. Chapter 8 investigates the methodology for determining an optimum accuracy and precision of polymer melt rheology, for true process conditions. Chapter 9 describes the influence of nozzle melt pressure and temperature on product quality (weight, dimension), during the primary injection phase, for semi-crystalline polymers.

Chapter 10 is a global discussion of the experimental results of chapters 7, 8 and 9. Detailed discussions are also included in chapters 7, 8 and 9. Experimental work is discussed regarding scientific and technological aims. Concluding comments and recommendations for future work are described in chapter 11.

CHAPTER 2

Review and Critical Assessment of Injection Moulding

2.1 Introduction

Injection moulding is used extensively for the manufacture of plastic products and is essentially a cyclic process characterised by several phases: (i) plasticisation phase, heating and mixing polymeric material to a uniform state of fluidity (ii) injection phase, injecting melt under pressure into a mould (iii) cooling phase, cooling and solidification in the mould, and (iv) product recovery (ejection). The injection moulding process is described by Han (1976 p 284), Fenner (1979 p 9), Crawford (1985a p 168), Johannaber (1985), Morton-Jones (1989 p 146) and Whelan and Goff (1991).

Thermoplastic materials flow as a viscous fluid when heated, on cooling they solidify to form amorphous/crystalline structures. These materials can be reversibly heated and cooled, to form moulded products. Thermoset materials form an infusible cross-linked structure, which inhibits viscous flow when re-heated. The physical shape of the moulded cross-linked product can be altered by application of heat, force and sufficient cooling time, but re-heating allows the original shape to return, described as thermoset 'memory'. The cross-linked structure can only be changed by degradation. It is apparent that thermoplastic materials have a significant processing advantage, allowing the use of 'regrind' and recycled materials.

The injection moulding process has three interacting domains for research and development; (i) material technology, the introduction of new and improved materials; (ii) machine technology, development of injection and sequence control; and (iii) processing technology, analysis of the complex interactions of machine and process parameters. Important advances in recent years have been made to machine

technology, with the introduction of microprocessor based machine parameter and sequence controllers, Whelan and Craft (1978) and (1981), Science Research Council (1979), Ames (1984), Sandretto (1988) and Canovi (1989). These improvements have been to such an extent that material variations are becoming a significant processing problem. The work reported concerns processing technology and the requirements necessary for closed loop process control, to compensate for material variation.

As demands for increased product quality and mechanical properties are made of polymeric materials, processing becomes increasingly difficult. Figure 2.1 shows that as service properties increase processability decreases. Therefore, one approach to compensate for material viscosity variation and increase process performance, is to develop a closed loop process control strategy.

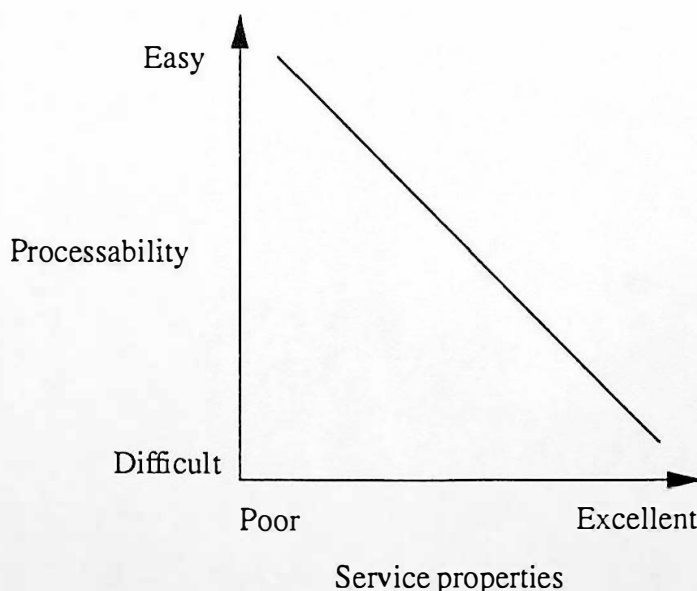


Figure 2.1 Relationship between service properties and ease of processing: a common experience, not a law of physics, Cogswell (1981 p 71)

2.2 Brief History of Injection Moulding

Injection moulding originally developed from research into substitution products for ivory and hard rubber, Crawford (1985b). Late 19th century developments were slow, as an explosive mixture of cellulose nitrate and camphor was the only available process material. A single action hydraulic injection moulding machine was patented by the Hyatt brothers, Hyatt (1872). The Hyatt machine undoubtedly borrowed technology from pressure die-casting of metals, which in turn borrowed ideas from a machine invented in 1863 for the automatic casting of printing type. Advances in injection moulding technology were limited at first as there was no alternative to cellulose nitrate. Cellulose acetate became available in the mid 1890's, but was predominantly used in compression moulding until the potential of injection moulding was realised, with the first products manufactured in the early 1920's. Horizontal injection moulding machines started to reduce the dominance of compression moulding in early 1930's, heating-cylinder design, Gaston (1932). The appearance of poly(methyl-methacrylate) (acrylic) and polystyrene stimulated further advances in technology with faster cycle times and closer moulding tolerances.

Until the late 1930's injection moulding had been carried out on a small scale, but during the Second World War injection moulding became established as a large scale engineering process. The addition of polyethylene and later nylon, to the range of injection moulding materials, showed the need for improved processing technology. In the early 1950's a reciprocating screw design superseded the simple ram, giving a more predictable polymer melt and very large plasticising shot capacity. The first reciprocating screws had relatively low length to barrel diameter aspect ratios (L/D). In the mid 1950's to mid 1960's L/D aspect ratios were in the order of 10 to 1, by the late 1970's L/D aspect ratios were 18 or 20 to 1. The longer screw lengths gave greater melting and mixing capacity, with improved melt quality. The reciprocating screw design is predominantly used by modern day injection moulding machines.

Machine parameter control has advanced since the late 1930's, from mechanical cam operated machines. Machines of the 1940's introduced thermionic valves for timer control, superseded by solid state electronics in the 1950's, to present day fully integrated computer control systems.

The majority of modern day injection moulding machines are hydraulically actuated, with the recent introduction of electrical actuation by alternating current servo motors, Winninger and Effmann (1989) and Plank (1991). Modern injection moulding machines have the facility to operate remotely, controlled by a centralised computer system. Communication between machine and computer control system is most commonly implemented by serial data transmission. Remote machine operation significantly reduces the number of machine operators and setters, promoting an efficient factory environment. Materials are fed to the machine hoppers by conveyer systems, incorporating dehumidification where necessary, Litherland (1989).

In recent years a novel technology has been developed, shear controlled orientation technology (SCORTEC), comprising of shear controlled orientation in injection moulding (SCORIM), British Technology Group (1984) and shear controlled orientation in extrusion (SCOREX). The process is based on the use of controlled melt pressure sources at a multiplicity of gates to a cavity, to influence fibre and molecular orientation in the final component. The process can be used with any commodity or engineering grade thermoplastics (reinforced or unreinforced). The process provides improvements in component mechanical strength (50 to 100% improvements are typical, but 2000% has been achieved in some applications), particularly where weld lines would normally occur, Wang et al (1993) and European Plastics News (1993c). Multi live-feed moulding (MLFM) provides a method for the management of fibres in complex shaped moulded parts. The control of the microstructure results from the imposition of a controlled shearing action on the solidifying melt, Allen and Bevis (1989).

Heasman (1989) and Shah and Hlavaty (1991) report that gas injection moulding combines many of the advantages of conventional high pressure injection moulding with those of structural foam moulding. Gas injection moulding is a low pressure process, i.e. hydraulic clamp and screw injection pressures, and therefore equipment costs are lower. Gas injection moulding machines are now readily available, for example the Sandretto Logigas system, of which thirty machines have been sold, world-wide, to date. Lower cavity melt pressure results in lower moulded-in stress, producing dimensional stability and low distortion. The first gas injection moulding attempts were made in the early 1970's. There are basically two types of gas injection moulding machines: (i) gas through nozzle and (ii) gas through runner or cavity, the inert gas usually used is nitrogen.

The injection moulding industry is improving machine productivity by the application of Computer Aided Engineering (CAE). This new technology allows an efficient transition from initial component design conception to full production, Bernhardt and Bertacchi (1984). CAE ranges over all phases of the development process: (i) computer aided design (CAD) and drafting, (ii) structural analysis of parts and tools, (iii) simulation of polymer melt flow and heat transfer, cooling and shrinkage and (iv) computer aided manufacture (CAM) utilising Computer Numerical Control (CNC) facilities, Hoven-Nielvelstein (1985) and Hauck (1988). The cavity filling stage of the injection moulding process has been the subject of extensive research, whereby proper tool design yields increased production efficiency. Polymer melt flow algorithms based on a finite difference scheme provide the easiest and most direct method of analysing the pressure drop through a defined geometry, Austin (1987). Hieber et al (1981) describes a finite element/finite difference numerical program for the simulation of filling thin cavities of variable gap thickness.

2.3 Stages of the Injection Moulding Process

The main objective of any moulding operation should be the manufacture of component products, to a specific quality level, in the shortest time, Manizone (1984), in a repeatable and fully automatic cycle, Wolf (1989). The typical injection moulding sequence is as follows:

Plasticisation Phase: Plasticisation occurs as the screw rotates, pressure develops against the 'closed-off' nozzle and the screw moves backwards to accumulate a fresh shot of melt in front of the screw tip. Back pressure determines the amount of work done on the polymer melt during plasticisation. Polymer melt is forced through the screw non-return valve.

Injection Phase: (i) *Primary Injection*, the empty mould is closed, a shot of polymer melt is ready in the injection unit. Primary injection occurs, polymer melt is forced through the nozzle into the mould. The screw non-return valve closes and prevents back-flow of polymer melt. This is the mould filling part of the injection moulding cycle, often high pressures are needed to achieve the required injection velocity.

(ii) *Packing Phase*, a secondary packing pressure occurs at a specified switch-over point (velocity-pressure-transfer-point) and is necessary during the early stages of cooling to counteract polymer contraction. Switch-over should occur when the tool cavity is approximately 95% to 98% full, Goff (1993), to promote an efficient packing phase. This phase compensates for material shrinkage, by forcing more material into the mould. After packing a lower holding pressure is sometimes used until the mould gate freezes, the injection pressure can then be released. Typical industrial machine settings use one secondary pressure, combining packing and holding phases. The switch-over from primary to secondary injection is typically initiated by screw position. Switch-over can be initiated by pressure i.e. hydraulic or nozzle melt injection

pressures or cavity melt pressure. A study of injection to holding pressure switch-over techniques based on time, position and pressure is reported by Malloy et al (1987).

Work by Nguyen and Kamal (1991) shows that under packing results in premature shrinkage, which may lead to dimensional variation and sink marks. Over packing may cause premature tool opening (flashing), difficulties in part removal (sticking) and excessive residual stresses resulting in warpage. Analysis of the packing phase is therefore an essential step in predicting the final product quality. Fritch (1987) reports that the portion of filling after switch-over can be more important than the velocity controlled primary injection stage. Speight and Coates (1991) and Speight et al (1993) report that for periods screw relaxation during the packing phase of injection, screw displacement and nozzle melt pressure correlate to product quality to a high degree. Calculation of packing displacement is used as a product quality indicator, with typical coefficient of correlation to product weight = - 0.97.

Cooling Phase: This phase starts as soon as polymer melt is injected into the cavity. The polymer melt begins to solidify when in contact, with the cavity surface. The estimation of cooling time is becoming increasingly important, especially when large quantities of components are being moulded. In order to calculate cooling time component ejection temperature should be known. To date there is no easy way of determining component ejection temperature, even though material selected and part thickness are known, Yu and Sunderland (1992). Cooling an injection moulded product uniformly may mean cooling the mould at different rates, in different areas. The aim must be to cool the product as quickly as possible, while ensuring that faults such as poor surface appearance^{and} changes in physical properties are not encountered. Opolski and Kwon (1987) describe an interactive CAD system for tool cooling system design, to manage core and cavity parts of the tool simultaneously. The design aims for a cooling system are: (i) minimum cooling time, (ii) even cooling on part surfaces, and (iii) balanced cooling between a core and a cavity part of two-plate tool system.

Tool temperature control is required to maintain a temperature differential ΔT between the tool and the polymer melt, for example typical polyoxymethylene melt temperature is 215C, Tool temperature is 70C, therefore $\Delta T = 145C$. Freil (1985) reports the importance of tool temperature control and suggests typical tool temperatures for materials. Adverse effects to product quality must be expected for no or poor temperature control. Freil (1986) reports the influence of tool surface temperature control on processing and on the quality of injection mouldings. Brito et al (1991 p 373) state that tool temperature is one of the process parameters that has the most influence on properties of a moulded component. The cooling phase enables the polymer melt to solidify in the impression, due to the heat transfer from the moulded product to the tool. Tool temperature influences the rate at which heat is transferred from the polymer melt to the tool. The differences in heat transfer rate influence polymer melt shrinkage, which in turn influences product density. This effect influences product weight, dimensions, micro-structure and surface finish. The tool cavity surface temperature is critical to processing and quality of injection moulded components, Friel (1986).

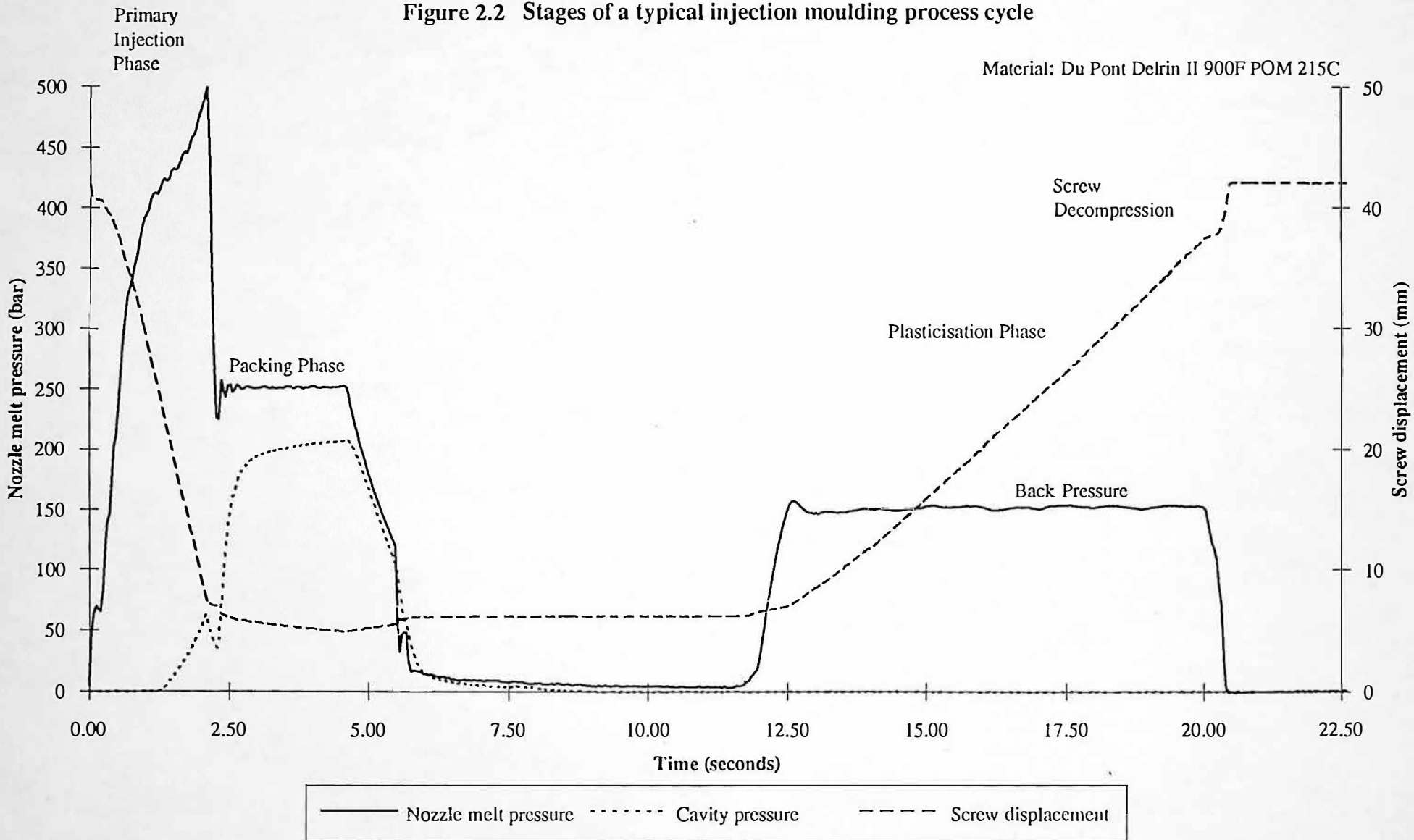
Each part of the product should be cooled at the same rate, this often means that non-uniform cooling must be applied to the tool, for example, cool water should be fed into the inner parts of the tool cooling system (particularly in the area of the gate) and warmer water should be fed into the outer parts. This technique is essential when moulding flat components to close tolerances, or large components that include long melt flow lengths from the gating position. Tool design has to incorporate adequate temperature control zones (flow ways), to provide the desired tool temperature. Tool temperature control zones commonly use water for temperatures up to 100C, above this temperature oil or electrical heating is used.

Figure 2.2 shows screw displacement, nozzle melt pressure and cavity pressure for a typical moulding cycle, processing polyoxymethylene, Du Pont Delrin II 900F. The primary injection, packing and plasticisation phases are shown. Table 2.1 shows the machine parameter settings for the typical injection moulding cycle shown in figure 2.2.

Machine Parameter Settings	Beaker Tool
Plasticising Screw Rotation Speed (RPM)	80
Plasticising Back Pressure (bar)	3
Plasticising End Position (%)	38.0
Decompression Stroke at Plasticisation end (%)	3
Total Injection Time, Primary and Packing (seconds)	5.50
Primary Injection Velocity (%)	30
Maximum Hydraulic Injection Pressure (bar)	115
Switch Over Position to Packing Phase (%)	7.00
Secondary Packing Hydraulic Injection (bar)	20
Secondary Packing Time (seconds)	3.00
Decompression Stroke at Injection End (%)	0
Cooling Time (seconds)	35
Nozzle Temperature Control Zone 1 (C)	215
Nozzle Temperature Control Zone 2 (C)	215
Barrel Temperature Control Zone A (C)	215
Barrel Temperature Control Zone B (C)	210
Barrel Temperature Control Zone C (C)	205
'Hot Tip' Temperature (C)	215
Feed Zone Cooling, (YES/NO)	YES
Tool Temperature, Polymer Melt Feed Zone (C)	60
Tool Temperature, Fixed Platen (C)	60
Tool Temperature, Moving Platen (C)	60

Table 2.1 Machine parameter settings for the typical injection moulding cycle shown in figure 2.2

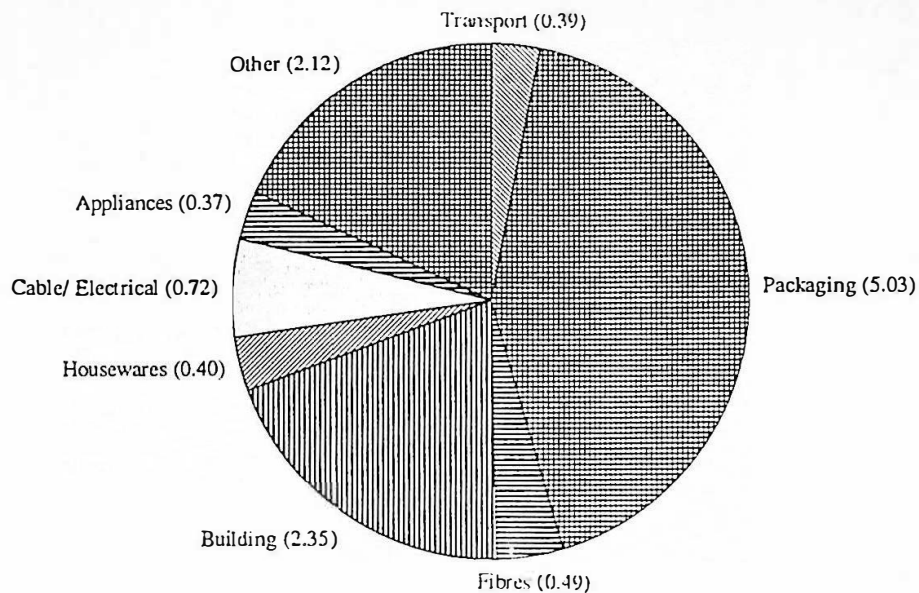
Figure 2.2 Stages of a typical injection moulding process cycle



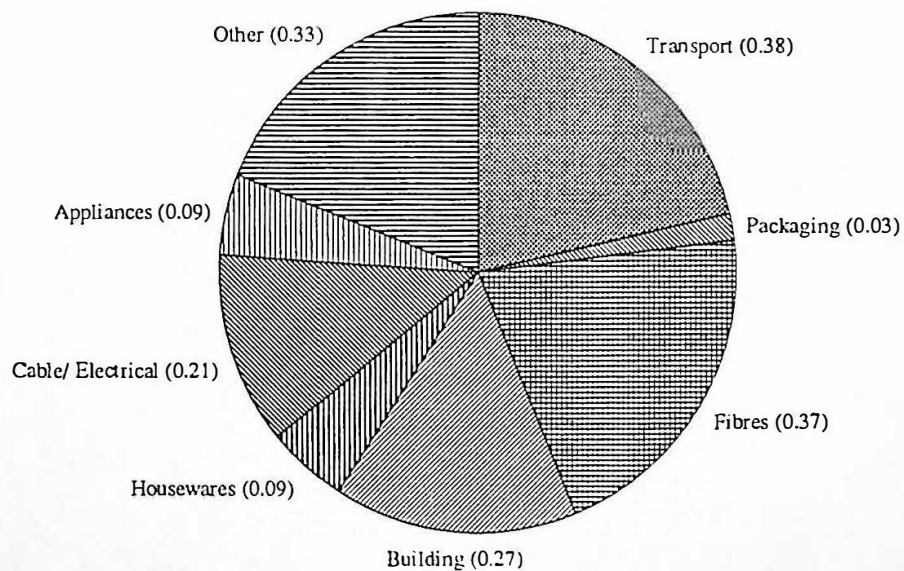
2.4 Thermoplastic Injection Moulding Materials

Thermoplastic polymers flow as a highly viscous liquid when heated, and do so reversibly, when re-heated and cooled. The difference between thermoplastic and thermoset materials are described in chapter 2.1. In 1978, 13.6 million tonnes of polymeric materials were produced in Western Europe, 87.5% of which were thermoplastics and 12.5% thermosets. The major applications of these materials are shown in figure 2.3. In 1988 18.3 million tonnes of thermoplastic polymeric materials were consumed in Western Europe, of which 93.25% were commodity thermoplastics and 6.75% engineering thermoplastics. The consumption of commodity thermoplastic materials showed an average increase of 9% during 1988, and engineering thermoplastics an average increase of 11%. Figure 2.4 shows the consumption of thermoplastic polymer types for 1987 and 1988. In 1992, 21.04 million tonnes of thermoplastic materials were consumed in Western Europe, showing an average increase of 3.5%.

On a molecular level the polymeric molecules form amorphous/crystalline structures: Amorphous polymers are hard and brittle, often described as glassy. On heating they eventually soften and become rubbery, this occurs over a well defined temperature band, the central point being the glass transition temperature T_g . Crystalline polymers are invariably partly crystalline (semi-crystalline) and partly amorphous, the term crystalline always implies partially crystalline. Crystalline polymers have molecular regularity, an irregular molecular structure prevents crystallisation. Crystalline polymers have distinct advantages over amorphous polymers in terms of stiffness and ductility, being able to form useful fibres. The crystals are extremely thin and form lamellae, sandwiching the amorphous portions. It is this two phase structure, with a high-modulus crystalline fraction and low-modulus amorphous fraction, that leads to good stiffness and ductility.



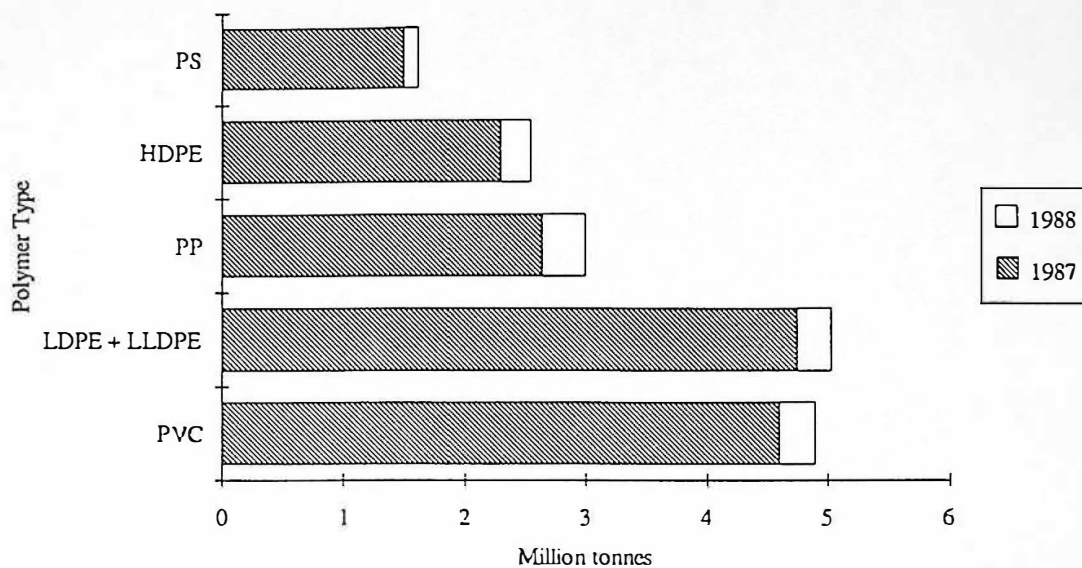
Thermoplastics total 11.9 million tonnes



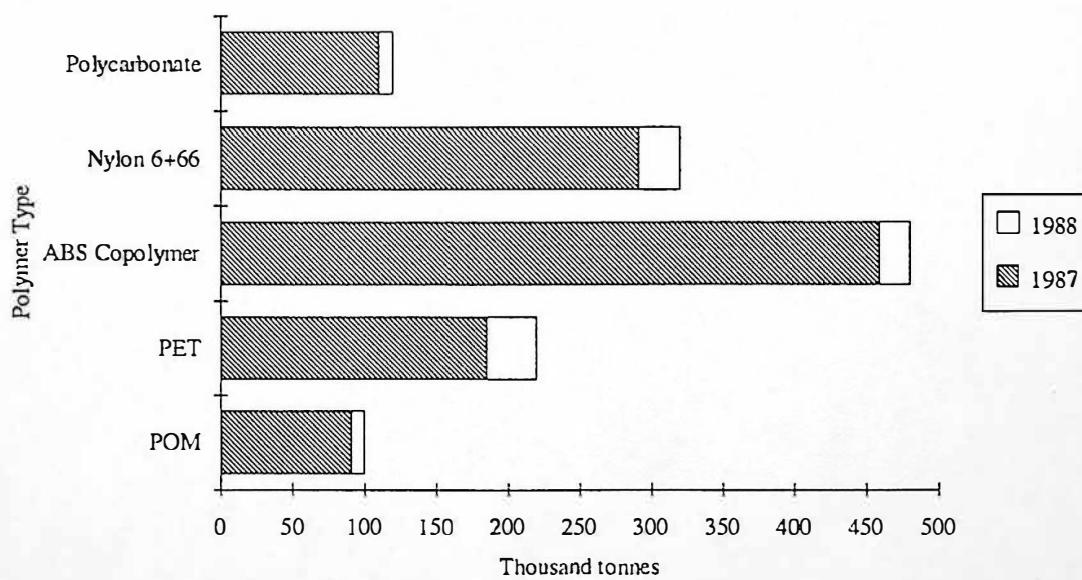
Thermosets total 1.7 million tonnes

(figures in parenthesis are millions of tonnes)

Figure 2.3 The end use of plastic products in Western Europe in 1978, McCrum et al (1988 p 6)



European consumption of commodity thermoplastics (million tonnes)

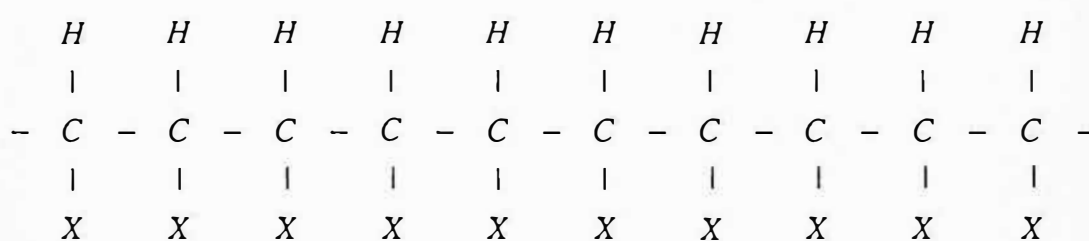


European consumption of engineering thermoplastics (thousand tonnes)

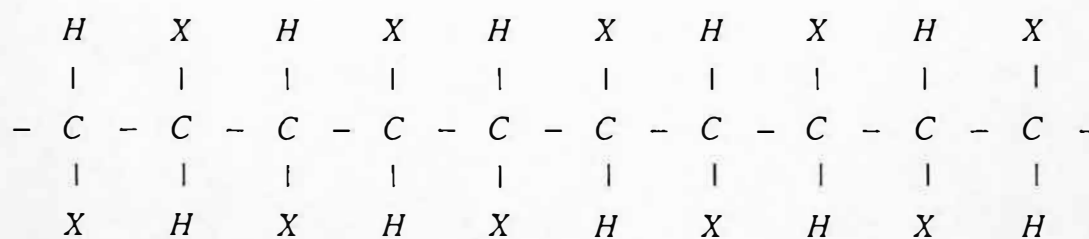
Figure 2.4 European consumption of polymeric materials 1987 to 1988, European Plastics News (1989)

There are three forms of molecular symmetry, or stereo-regularity, that determine a polymers structure, isotactic, syndiotactic and atactic, as shown in figure 2.5.

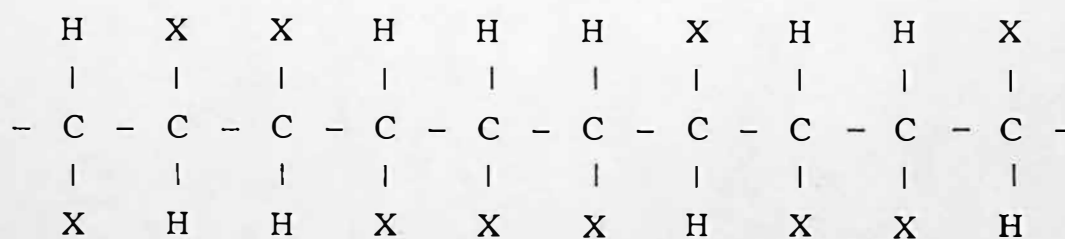
Crystalline structures are always formed from isotactic polymers, they are sometimes formed from syndiotactic polymers and never formed from atactic polymers. Figure 2.6 shows the storage modulus E' for amorphous and semi-crystalline polymers at different temperatures. The glass transition region can be seen for the amorphous polymer, and also the rubbery plateau region.



Isotactic



Syndiotactic



Atactic

Figure 2.5 Molecular symmetry (stereoregularity), isotactic, syndiotactic and atactic, Morton-Jones (1989 p 10)

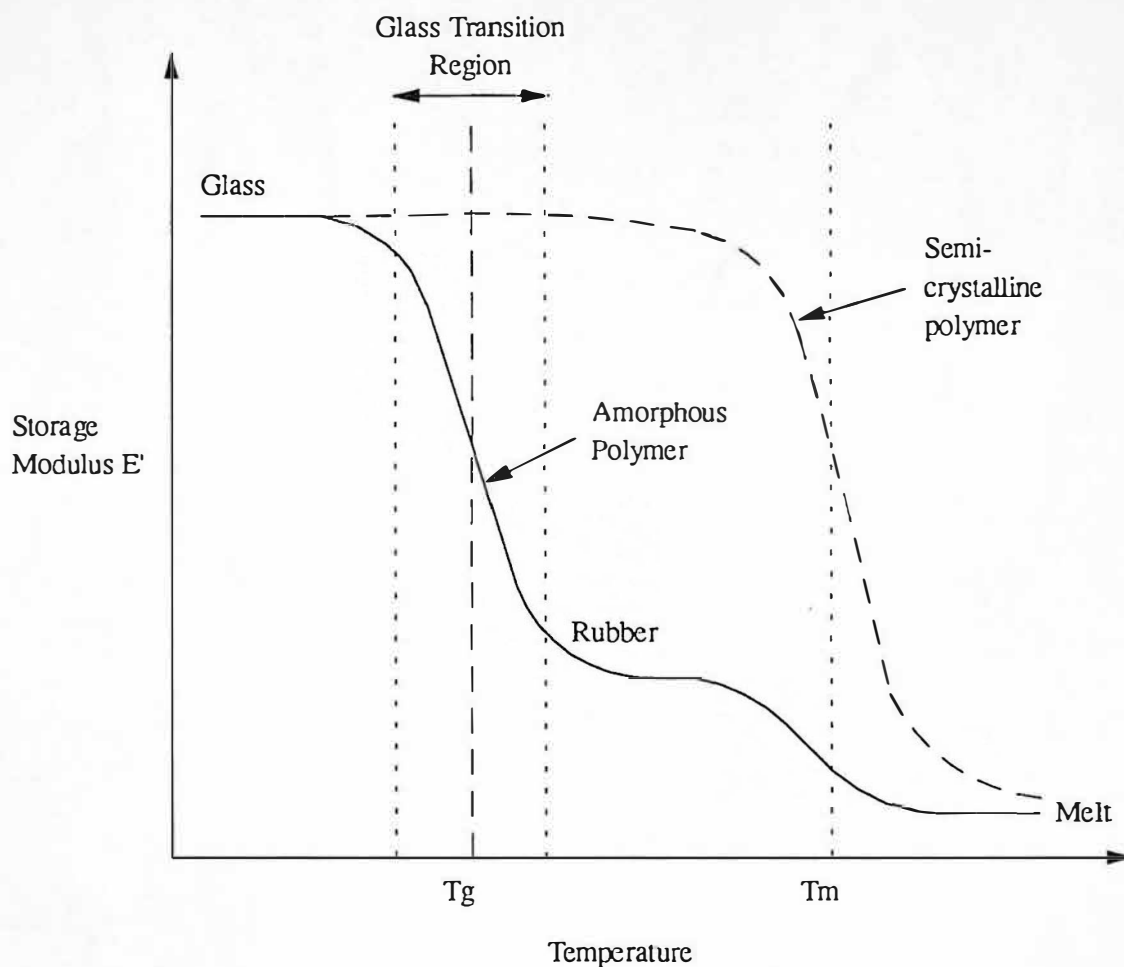


Figure 2.6 Storage modulus E' - temperature diagram for polymers, Morton-Jones (1989 p 14)

Where: T_g = Glass transition temperature and T_m = Melting point temperature

Molecular orientation in injection moulded components and its influence on mechanical properties is the subject of considerable research: Haworth et al (1980) describe the analysis and control of residual stresses and the evaluation of their effect on properties in polystyrene injection moulded bars. Harland et al (1980) observed that the pattern of orientation along the direction of filling of a thin, square, polystyrene plaque, has been explained in terms of die swell, radial and extensional flow, and shear flow. A review of mathematical design methods for thermoplastic machine parts is described,

BASF materials data sheet (1982). The influence of molecular orientation, moulded-in stresses and filler orientation are discussed. White and Spruiell (1983) present a critical review of the specification of orientation and its development in polymer processing operations. Orientation may in general be specified by orientation distribution functions, but is most conveniently expressed as orientation factors. It is stated that the performance of moulded products is determined by internal structure, i.e. level of crystallinity and polymer chain orientation. Isayev (1983) shows for an amorphous polymer (polystyrene) that the simplest way of defining the state of orientation in a moulded part is to measure the three mutually independent components of birefringence, namely, Δn , $n_{11}-n_{33}$, and $n_{22}-n_{33}$, corresponding to the mutually perpendicular planes (with 1, 2 and 3 corresponding to flow, gapwise and width directions of the cavity). In general it is concluded that increasing melt temperature significantly reduces all of the gapwise averaged components of birefringence. Flaman (1993a) described a numerical model for predicting the build-up of flow-induced molecular orientation in amorphous injection moulded products of simple geometry. Flaman (1993b) describes experimental studies for the verification of the numerical model, Flaman (1993a). Predicted pressure profiles agree well with experimental values, the packing phase model results were less satisfying. It is concluded that the model can be used to optimise processing conditions for high quality products with minimum frozen-in orientation.

Process conditions are shown to have a strong influence on moulded component microstructure and skin formation. Bakir and Marshal (1980) report that skin thickness of a PVC injection moulded plaque is significantly affected by tool temperature, melt temperature and injection velocity. Skin thickness is shown to decrease with increased tool temperature, melt temperature and injection velocity, due to reduced shrinkage. Simple tensile tests demonstrate that the tensile behaviour is dependent on the core morphology. Brito et al (1991) report that the skin-core boundary location has a major affect on the mechanical properties of moulded

polypropylene copolymers. Injection velocity is shown to control skin formation, and is dependent on shear stress and temperature. Finite difference is used to predict the onset of skin formation and hence the skin thickness. Component microstructure is commonly described by a five layer model, with a spherulitic core, two intermediate crystalline and oriented layers and two highly oriented skins, Fujiyama and Wakino (1988). Wu and White (1992) examine the crystalline orientation in injection high density polyethylene (HDPE) moulded components. Orientation was well developed in the wall region and decreased towards the core. Processing conditions such as high melt temperature and high tool temperature are shown to limit orientation at the wall region. Fujiyama and Wakino (1992) report that skin thickness for injection mould polypropylene copolymers with ethylene decreases with increased melt temperature. A positive relationship exists between properties such as flexural modulus, flexural strength, heat distortion temperature, impact strength, component shrinkage and thickness of the skin layer.

The influence of microstructure on component failure has been the subject of considerable research. Schultz (1984) investigates the microstructure of failure in semi-crystalline polymers. Failure development in semi-crystalline polymers can be expressed in terms of a temperature-strain rate failure map. Development of such a map should become increasingly important as more demands are made of filled and unfilled polymers for engineering applications. Wagner and Kaylon (1991) conclude that the frequency and location of cracking of an engineering polymer, poly (2,6-dimethyl-1,4-phenylene Ether) is related to operating conditions, tool geometry and surface irregularities. Results suggest that cracking can be minimised by using higher tool temperatures and higher injection velocities. The use of sharp corners, rapidly changing tool cavity geometry and surface irregularities should be avoided in tool design. The presence of cracks in moulded components intimately relate to microstructure, where discontinuities in birefringence distributions may act as precursors to crack initiation sites.

2.5 Process Control Technology

In recent years, injection moulding machine manufacturers have concentrated on improvements to machine parameter and sequence control. Improvements are continually being made, in 1979 the Krupp-Reinfehauser KR90 injection machine control system was one of the more sophisticated devices utilising three Motorola M6800 microprocessors for machine and sequence control, Science Research Council (1979). The Battenfeld Unilog TC 40 control system currently uses transputer technology for machine and sequence control, Battenfeld (1991). Cincinnati Milacron are using AC servo motors for accurate and precise position and velocity control. As machine parameter control continues to improve material variation will become a more significant processing problem, as increasingly higher standards of product quality are demanded. The increase in the use of recycled materials will add to process variation. Presently the economics of using virgin materials are more attractive to polymer processors, than the economics of using recycled polymers. This is illustrated by the following worked example:

Worked example to show present day economics of polymer processing

Processor A, this polymer processor moulds 10,000 computer cabinets using virgin material. The sprue and runner system are used as 'regrind', to the material suppliers specification. The virgin material costs £1500 per tonne, and 10 tonnes are required, therefore the total material cost £15,000. During typical production conditions a scrap rate of 5% resulted, incurring an extra cost of £750. Therefore the total cost to produce 10,000 computer cabinets was £15,750, using virgin material and excluding overheads.

Processor B, this polymer processor moulds 10,000 computer cabinets using a recycled material. The sprue and runner system are used as 'regrind', to material

suppliers specification. The recycled polymer costs £1200 per tonne, for 10 tonnes of material the cost is £12,000, an apparent saving of £3000 compared to processor A. During typical production conditions a scrap rate of 40% resulted, incurring an extra cost of £4,800. Therefore the total cost to produce 10,000 computer cabinets was £16,480, using recycled material and excluding overheads.

This example shows the present problems of using recycled materials. The economics for not using recycled materials are emphasised as processor A moulded 10,000 computer cabinets in, 75% of the time of processor B. Considering overheads, this may be more significant than the extra cost of material.

2.5.1 Summary of Material Variation Through Recycling

During the period 1991 to 1992 the average cost of virgin materials, in the USA was reduced from 53 to 31 Cents per pound, where the estimated cost of efficient recycled materials was 31 Cents per pound, European Plastics News (1993a). Polymer processors were able to purchase virgin materials for the same or less cost than recycled materials, during the last quarter of 1991 to the first half of 1992, European Plastics News (1993a). Clearly, polymer processors utilise the most cost effective materials available, therefore, recycling of materials may have to be promoted for political reasons, until such a time, that processing technology reduces the efficient cost of recycling.

In the near future Government legislation will most likely demand recycling of polymeric materials. The German law says manufacturers must ensure that by 1st July 1995 80 per cent of all packaging is collected and that 80 per cent of this amount is recycled, Genillard (1993). Therefore, injection moulding machine manufacturers are recognising that true process control is required, to compensate for material variations.

2.5.2 In-line Rheometry for Injection Moulding Control

The basis of closed loop injection moulding process control is most likely to be, an accurate and precise assessment of polymer melt viscosity. Considerable research has investigated the use of in-line nozzle rheometers and rheometers associated with the tool, for study of polymer melt rheology and polymer melt processing.

Hayashi (1984) reports of the use of infra-red melt temperature transducers, located in a modified machine nozzle and tool cavity. Proposals were made for closed loop process control strategies, based on (i) infra-red melt temperature transducer located in the nozzle, controlling the machines barrel temperature control zones, and (ii) infra-red melt temperature transducer located in the tool cavity. Sharp (1986) utilised nozzle, runner, gate and two pressure transducers for analysis of thermoset injection moulding. Gibson, Collyer and Clegg (1988 p 57) utilises a single melt pressure transducer in a modified nozzle for in-line capillary rheometry. Malloy (1988), Malloy et al (1989), Ross et al (1990) and Wu and Chen (1990) describes two rheological nozzle configurations; (i) a single melt pressure and temperature transducer rheometer, and (ii) a nozzle rheometer with three melt pressure and two melt temperature transducers. Sukanek and Campbell (1990) utilised a nozzle melt pressure transducer and infra-red melt temperature transducer at the nozzle inlet, located 30 degrees apart. Dontula et al (1991) show a schematic diagram of the modified machine nozzles utilised by Sukanek and Campbell (1990). Bader et al (1991) utilise two piezoelectric nozzle melt pressure transducers. Hastenburg et al (1992) utilises four cavity pressure transducers to measure time and place pressure behaviour. Yu and Sunderland (1992) utilised a flat plate tool with three melt pressure and temperature transducers. An in-line nozzle rheometer utilising two melt pressure transducers, shown at (Kunststoffe 92) was installed on a Krauss Maffei recycling injection moulding machine R-SGM.

2.5.3 Development of Closed Loop Process Control for Injection Moulding

Development of closed loop process control has been the subject of considerable research. Control strategies based on in-line nozzle melt pressure measurements currently make no attempt to optimise nozzle melt pressure measurements. European Plastics News (1979) reports developments in closed loop process control, with the ultimate purpose of improving production efficiency, the Syntrol closed loop control systems are described, where by injection and packing pressures are controlled, no statistical process control is applied on a cycle to cycles basis. Pandelidis and Agrawal (1987) describe a self tuning control algorithm for screw injection velocity control. Coates (1989a) discusses in-line rheological measurements as a potential aid to closed loop process control and describes issues relating to the development of intelligent polymer processing machinery. Coates et al (1989b) propose that measurement of polymer melt 'state' at the nozzle is most attractive from an industrial view point, where a single transducer (most likely pressure or temperature) would provide useful information independent of the type of tool being used. Coates (1991) describes the global aspects of analysis and control of polymer processing. Smud et al (1991) investigates the application of advanced control strategies to the injection moulding process. The objective was to control cavity pressure during the packing and holding phases of the moulding cycle, a variable volume cavity is used which relies on the manipulation of clamping force.

Bernhardt and Bertacchi (1991) describe an expert system for injection moulding trouble shooting. Jan and O'Brien (1991) describe the architecture of such an expert system. The five elements are; user, user interface, explanation facility, knowledge base and inference engine. Wu et al (1991) reports on the development of an In-line cavity pressure based expert system for injection moulding process control. Measuring the cavity pressure is an effective way to 'see' inside the tool cavity and enables detection of process variations and abnormal cavity pressure patterns.

2.5.4 Modelling and Simulation of the Injection Moulding Process

Accurate process modelling allows simulation of injection moulding, enabling results from process parameter perturbations to be achieved. Injection moulding process simulation is extremely useful for tool design, allowing cavity filling prediction. Byam and Colbert (1980) report that the majority of trial and error factory operations, can be eliminated by simulating the operation with a computer. Bullen (1983) investigates the effect of gate area of a tool cavity upon the overall pressure drop during primary injection. Theoretical pressure drop calculations for capillary, tab and converging gates are compared to practical pressure drop measurements derived from hydraulic injection pressure, processing LDPE on a barrel and plunger type machine. Chen and Liu (1989) describe a two phase model for simulating the primary injection phase and including the effect of transient melt solidification, i.e. the phase change effect. Chiu et al (1991b) describes a dynamic model of the primary injection phase formulated by the Reynolds transport theorem, which is applied to describe the polymer flow dynamics. Hsiung and Cakmak (1991) describes a model developed to simulate the crystallinity gradients developed in injection moulding of slowly crystallising polymers. Hieber et al (1981) describes a finite element/finite difference numerical program for the simulation of filling thin cavities of variable gap thickness. Singh (1984) describes a finite difference simulation program to solve mass, momentum and energy conservation equations. Bernhardt and Bertacchi (1987) describe computer integrated injection moulding (CIIM) linking process simulation with machine settings. Computer process simulations are translated by post-processors to machine parameter settings. The use of CIIM may in the future replace the traditional trial and error methods of process optimisation. Yu and Sunderland (1992) describes a combination of experimental, analytical and statistical methods to establish equations for calculating ejection temperature according to material properties, component thickness and process conditions, such as melt and tool temperatures. Knowledge of component ejection temperature allows cooling time to be estimated in the early design stages.

2.5.5 Model Reference Injection Moulding Process Control Systems

Control strategies have been developed that incorporate models and simulations of the injection moulding process. Chiu et al (1991a) describes an adaptive model following control (ASFC) system applied to the primary injection phase and packing phases. Stoll et al (1991) describe the modelling and control of a typical cyclic polymer process, such as injection moulding or thermoforming. The model developed is used for evaluation of conventional proportional controllers and statistical process controllers. For batch-to-batch processes, statistical process controllers are shown to give superior performance to step and ramp load disturbances and improved performance for sinusoidal load disturbances. Ricketson and Wang (1987) describe injection moulding process control based on an empirical model. Statistical experimental designs were used to establish a steady state process model.

2.5.6 Statistical Process Control for Injection Moulding

The development of a closed loop process control algorithm will incorporate aspects of statistical process control (SPC). Hunkar (1987) describes the benefits of SPC of the injection moulding process. The following parameters are monitored; plasticising pressure, screw rotational speed, holding pressure and screw injection velocity. Financial savings were made due to increased production efficiency and process documentation was available for customers to analyse. Windsor Shaw (1989) describes a practical experience of SPC for injection moulding using an 'intelligent terminal' for data analysis. Sercer (1989) describes a computer check program controlling the trend of the thermoplastics injection moulding process for the optimisation of product quality. Woodhead (1990) investigates the use of SPC for injection moulding statistical process control. Experimental tests processing HDPE data show that increasing tool temperature reduces product weight and dimensions, these product quality changes reflect in maximum hydraulic pressure and total screw

displacement measurements. Wu and Chen (1990) use statistical analysis techniques to examine the correlation between peak cavity pressure and product weight, on a cycle-to-cycle basis to identify the pattern characteristics of process parameters.

2.5.7 Cincinnati Milacron In-line Nozzle Rheometer for Closed Loop Process Control

In-line nozzle rheometer closed loop process control systems are being developed by machine manufacturers, in an attempt to compensate for material variation. The Cincinnati Milacron in-line nozzle rheometer utilises two Dynisco pressure transducers, located in the nozzle reservoir bore. This in-line nozzle rheometer is used for closed loop process control system, and is based on a hydraulic injection moulding machine, with velocity controlled screw injection. The system is based on nozzle rheometer technology developed at Lowell University, Massachusetts, USA, Malloy (1988), Malloy et al (1989), Ross et al (1990) and Wu and Chen (1990). The pressure differential between two melt pressure transducers is used to calculate melt viscosity, for the primary injection phase. This assessment of polymer melt viscosity includes variation resulting from machine parameter variations, depending on material, tool and machine parameters. A schematic diagram of the process control system is shown in figure 2.7. The polymer melt viscosity assessment is used to control the two barrel heater bands, as shown. Figure 2.8 shows a typical display from the Cincinnati Milacron in-line viscometer, where injection velocity and polymer melt viscosity are plotted against screw position.

It is apparent from published work that no significant attempts have been made to optimise the assessment of nozzle melt pressure and hydraulic injection pressure during primary injection. Machine manufacturers calculate a viscosity index from hydraulic injection pressure, for example, the method used by Sandretto is described in appendix A(iii), whereby sections of the hydraulic injection pressure profile are simply ignored,

at the start and finish of primary injection. Work reported (see chapter 8.5) has shown that the viscosity index algorithm applied to nozzle melt pressure, has a detrimental influence on measurement accuracy.

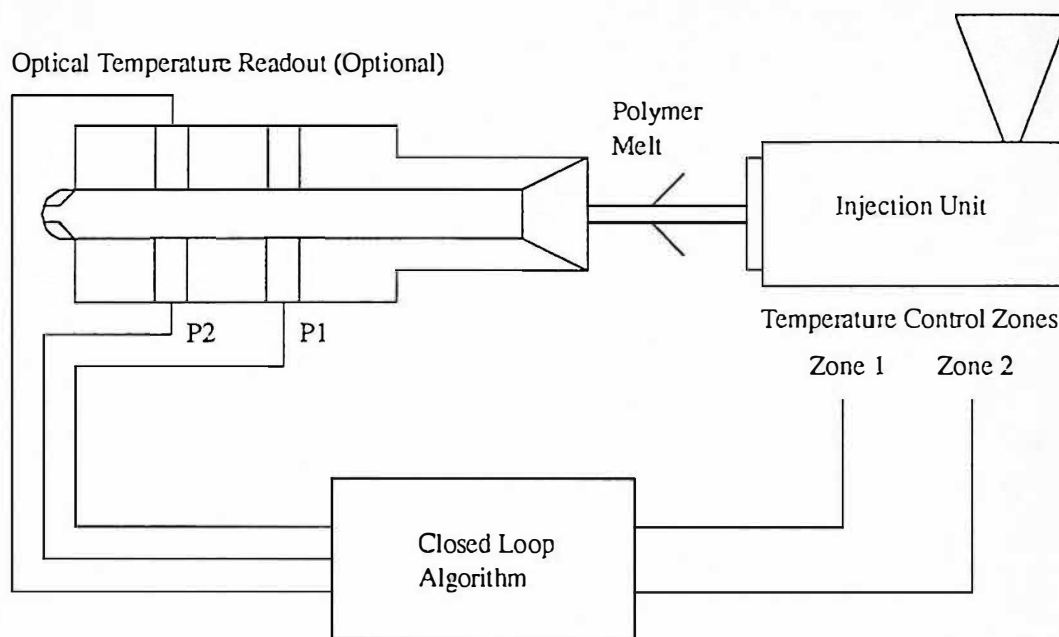


Figure 2.7 Cincinnati Milacron in-line viscometer developed at Lowell University, Massachusetts, USA

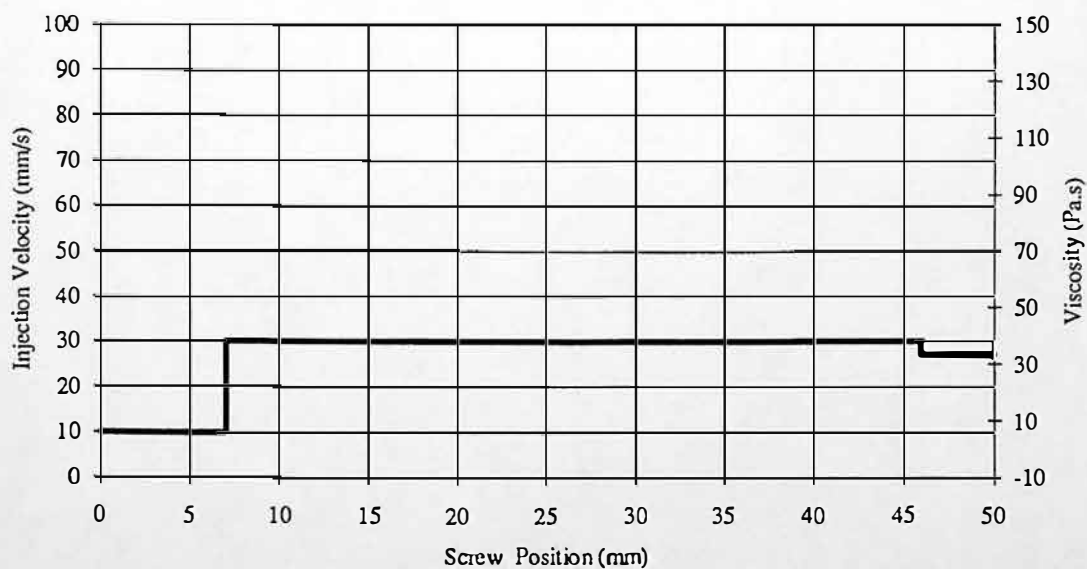


Figure 2.8 Typical VDU display screen for Cincinnati Milacron in-line viscometer

2.6 In-line Process Measurement Technology

Accurate, precise and reliable process measurements are obtained by careful transducer selection. A transducer must have an adequate dynamic response to measure process variations. Transducer linearity, repeatability, hysteresis and resolution are also important parameters to consider.

2.6.1 In-line Pressure Transducer Technology

Liquid filled, Dynisco (1989b) to Dynisco (1990b), force tube, Terwin (1986) and push rod, Dynisco (1990a) and Dynisco (1990b) devices were assessed for measuring nozzle melt pressure, during the injection moulding process. The three technologies assessed, were chosen due to their robustness, against high temperatures (300 C) and pressures (1409 bar). The liquid filled device showed a best performance in all categories, but more importantly was the only flexible device, suitable for an in-line nozzle rheometer. The assessment of liquid filled, force tube and push rod devices are described in chapter 5.3. The typical response time of a liquid filled pressure transducer is 17 ms. Push rod devices have a typical dynamic response of 5 ms, but suffer from hysteresis and linearity effects.

Piezoelectric (quartz device), Kistler (1990) and piezoresistive, Kistler (1990) and Endveco(1992) pressure transducers were not considered for assessment due to the high pressure and temperatures experienced in the nozzle rheometer. These piezoelectric and piezoresistive devices have excellent dynamic responses, with natural frequencies up to 180 kHz.

The recent introduction of the Dynisco (OPT 700) fibre optic melt pressure transducer, Dynisco (1990b) to Dynisco (1993) is an important development for pressure transducer technology. The patented optical system provides an electrical output

signal proportional to the change in light intensity generated by diaphragm deflection. The device: (i) has improved thermal stability and temperature compensation, (ii) uses a thicker diaphragm than liquid filled, force tube and push rod devices, and is therefore less susceptible to damage from over pressuring, (iii) an improved response time of 500 μ s and (iv) eliminates the need for a liquid filled capillary during food processing.

2.6.2 In-line Temperature Transducer Technology

The first reported infra-red temperature measurement techniques are documented, Mullard Ltd (1971), Vanzetti (1972) and Wright (1973). Application of these techniques to the development of infra-red melt temperature transducers, has allowed a dynamic non-intrusive measurement of nozzle melt temperature, during primary injection.

Maher and Plant (1974) utilise an infra-red sensing unit and fibre optic probe installed at the transition zone between barrel and nozzle, of an injection moulding machine. The infra-red melt temperature transducer measured the highly transient polymer melt temperatures and cycle to cycle temperature variations that otherwise went unnoticed by a similarly located thermocouple. The work of Maher and Plant (1974) needs to be built on, using present day microprocessor technology for accurate and precise data monitoring. Galskoy and Wang (1978) report that thin-film thermocouples mounted on glass rods are more accurate transducers of tool melt temperatures than are infra-red melt temperature transducers, while the reverse is true for runner temperatures. Hansbery and Vanzetti (1981) report on fibre optics as a new approach to monitoring and control of process temperatures. Hayashi (1984), investigate nozzle and cavity melt temperature measurements, using a MOBAC MBC 700 infra-red melt temperature transducer, time response for this device ranges from 20 to 50 milliseconds. Proposals were made for closed loop process control strategies, based on (i) infra-red melt temperature transducer located in the nozzle, controlling the

machines barrel temperature control zones, and (ii) infra-red melt temperature transducer located in the tool cavity. Barron (1990) reports that an understanding of fibre-optic cables, probes and sensor configurations is essential for optimising fibre optic melt temperature measurements.

The experimental tests reported in this work, use the Dynisco MTT935A infra-red temperature transducer, this device was originally based on the Vanzetti linearised infra-red temperature transducer, model 4121, Vanzetti Systems Inc (1984) and Vanzetti Systems Inc (1989).

The infra-red melt temperature transducer has a response time of approximately 10 ms compared to 2.30 s of a typical industrial thermocouple (see chapter 5.5.3). The infra-red device also has the advantage of a non-intrusive measurement of melt temperature. Current research has shown the infra-red device to measure an average melt temperature between 3 and 6 mm into the melt, over a 60 degree arc, unless the polymer solidifies then it becomes the surface temperature Shen et al (1992) and Davies (1993).

Research by Rieveld and Lai (1993) are currently investigating measured and predicted polymer melt temperatures for an infra-red temperature transducer viewing a linear temperature gradient.

Research by Sukanek and Campbell (1990) investigates the influence of back pressure and screw speed on an infra-red melt temperature measurement. Results show that screw speed have minimal influence on melt temperature at low back pressures. However at higher back pressures (greater than 10^7 Pa) screw speeds above 150 RPM have a significant effect on melt temperature. Experimental tests on a Boy 50 tonne injection moulding machine using high impact polystyrene investigated the influence of screw speed (50 to 350 RPM) and melt back pressures (0 to 2.4×10^7 Pa) on melt

temperature, maximum rise of 42C was possible for these experimental conditions. It was reported that injection pressure has minimal influence on melt temperature.

Further research by Dontula et al (1991) conclusively shows the importance of back pressure and screw speed. This work also shows the importance of shot size, injection pressure and polymer type being processed.

A second type of melt temperature transducer with the required response time was assessed. A Nanmac fast response thermocouple Type J calibration, operating with a typical time response of 10 ms, Nanmac (1992). Results from this transducer are not reported in this work. A comparison between infra-red, fast response thermocouple and typical industrial thermocouple are described, Speight (1993b). Current work is evaluating the response of a Nanmac fast response thermocouple Type E calibration (chromel constantan). The thermocouple has a fixed immersion tip of dimensions 4.8 mm outside diameter by 3.2 mm long, Nanigian (1993).

CHAPTER 3

Polymer Melt Rheology

3.1 Introduction

Rheology is the study of flow or deformation behaviour of materials, and is concerned with the relationship between stress (force per unit area), strain (change in dimension per unit dimension), and time. Rheometry is the measurement of flow or deformation of materials. Polymer melt rheology is measured by use of off-line, on-line and in-line rheometry techniques, as described in chapter 3.2. During simple shear the stress is applied tangentially, and in simple extension the stress is applied normal to the material. Molecular weight of a material influences shear viscosity, and molecular weight distribution influences extensional viscosity. Figures 3.1 and 3.2 illustrate simple shear and extensional deformation. In bulk deformation the stress is applied normal to all faces, whereby, stress is the applied pressure and the strain is the change in volume per unit volume, $\delta V/V$. The practical rheology of polymer melts is a complex interaction of shear, extension and bulk deformations.

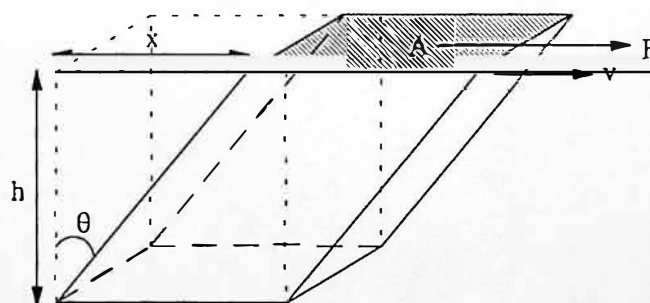


Figure 3.1 Simple shear: area A and distance h remain constant during deformation

where	$F =$ Applied Force	(N)
	$A =$ Area	(m ²)
	$h =$ height	(m)
	$x =$ shear displacement	(m)

$$v = \frac{\delta x}{\delta t} \quad (\text{m/s})$$

$$\theta = \text{angle of shear deformation} \quad (\text{degrees})$$

In practical processes there are two major classes of shear flow: (i) flow between relatively moving surfaces, and (ii) flow induced by a pressure gradient. Injection moulding and capillary rheometry are described by a pressure driven flow. In a pressure driven flow the pressure to promote adhesion between the melt and die wall is present, if this adhesion breaks, certain classes of non-laminar flow may occur, i.e. melt fracture. Heat generation occurs close to the die walls, where heat is transferred away from the melt. The important quantities involved in measuring shear viscosity may be defined as follows:

$$\text{Shear stress } \tau_s = \frac{\text{Shear force } F}{\text{Area } A \text{ of shear face}} \quad \text{Eq. 3.1}$$

$$\text{Shear strain (unity) } \gamma = \frac{\text{Amount of shear displacement } x}{\text{Height between shearing surfaces } h} = \tan \theta \quad \text{Eq. 3.2}$$

$$\text{Rate of shear strain (sec}^{-1}\text{) } \dot{\gamma} = \frac{1}{h} \frac{dx}{dt} = \frac{v}{h} \quad \text{Eq. 3.3}$$

$$\text{Shear viscosity } \eta = \frac{\text{Shear stress}}{\text{Rate of shear strain}} = \frac{\tau_s}{d\gamma/dt} = \frac{\tau_s}{\dot{\gamma}} \quad \text{Eq. 3.4}$$

Polymer melts are deformed by tensile stresses as well as shear stresses. An extensional viscosity is calculated from the tensile forces, during deformation of polymer melt from one cross-sectional area to another. The rheology in extensional flow is different from that in simple shear flow. In shear flow, the greater the shear stress, the lower the shear viscosity. During extensional flows the extensional stress

causes the material to tension thin, but not to the same extent as shear thinning behaviour and may result in a tension stiffening behaviour.

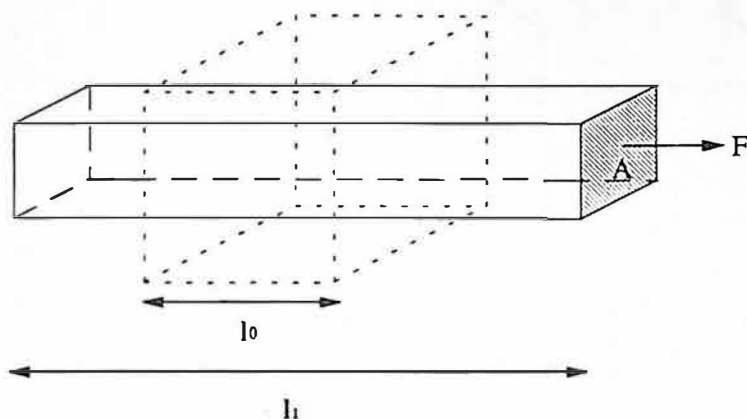


Figure 3.2 Simple extension: cross-sectional area A and sample length l both vary during deformation

where l_0 = Original length before deformation (m)

l_1 = Extended length (m)

The important quantities involved in measuring extensional viscosity may be defined as follows:

$$\text{Extensional stress } \sigma_E = \frac{F}{A} \quad \text{Eq. 3.5}$$

$$\text{Extensional Strain } \epsilon = \int_{l_0}^{l_1} \frac{dl}{l} = \ln \frac{l_1}{l_0} \quad \text{Eq. 3.6}$$

$$\text{Rate of extensional strain } \dot{\epsilon} = \frac{v}{l} \quad \text{Eq. 3.7}$$

$$\text{Extensional viscosity } \lambda = \frac{\sigma_E}{\dot{\epsilon}} \quad \text{Eq. 3.8}$$

3.2 Off-line, On-line and In-line Rheometry

Polymer melt rheology can be measured using off-line, on-line and in-line rheometry, as shown in figure 3.3. The work reported presents off-line and in-line rheometry.

Off-line rheometry is the measurement of polymer melt rheology away from the process, using specialised testing equipment. Off-line rheometry allows accurate and precise measurement of polymer melt rheology, but under non-typical shear and temperature histories. Typical off-line rheometry tests are, capillary rheometry, coaxial cylinder, cone and plate and melt flow index (MFI). Off-line rheometry is extremely important for scientific research, but for polymer processing operations is a slow method of polymer melt assessment.

On-line rheometry involves the extraction of a continuous stream of material from the process, this stream is then processed using specialised testing equipment. This measurement technique may effect the process history of the polymer melt, during transfer from the process to the testing equipment. An on-line rheometer functions in either a continuous or batch mode of operation. In a continuous mode of operation, polymer melt is tested at a constant shear rate, this is useful for statistical process control, where process trends are analysed. In a batch mode of operation polymer melt is tested over a range of shear rates.

In-line rheometry involves direct process measurement of polymer melt rheology. This measurement technique allows a real-time assessment of polymer melt, for true process conditions. In-line rheometry is least likely to change the polymer melt shear and process history, compared to off-line and on-line techniques. This real time assessment of polymer melt rheology is likely to form an essential basis for closed loop process control, where control actions compensate for polymer melt viscosity

variation. In-line rheometry will increase in important in future years when recycled materials are used.

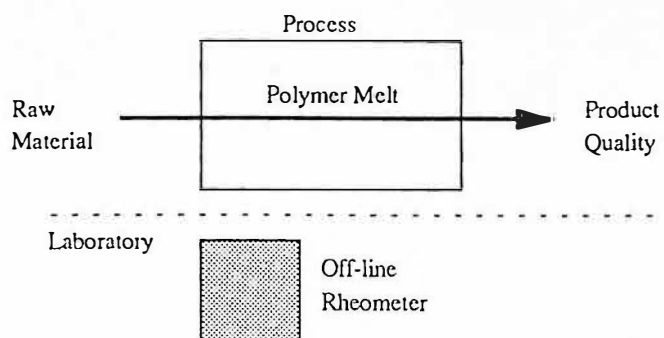


Figure 3.3 a Off-line rheometry

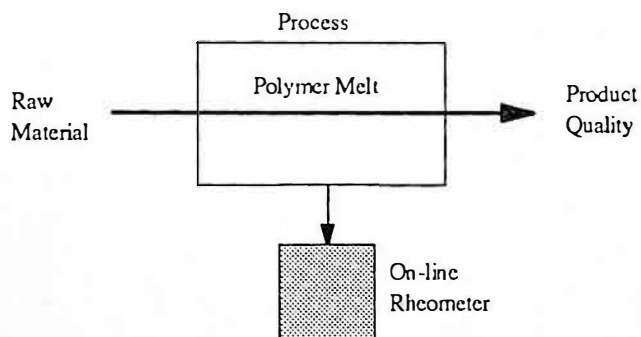


Figure 3.3 b On-line rheometry

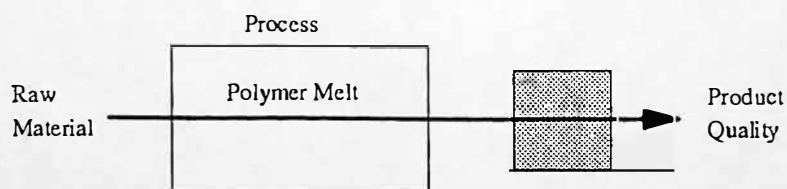


Figure 3.3 c In-line rheometry

Figure 3.3 Off-line, on-line and in-line rheometry, Coates (1991)

3.3 Capillary Rheometry

Capillary rheometry is an off-line test, usually performed in the laboratory environment, for measurement of polymer melt rheology, Patel (1980) and LeBlanc (1980). Polymer melt is forced by a piston from a reservoir bore through a capillary die. The quantity of polymer melt extruded from the capillary die per unit time, for a specific pressure drop is the basic measurement used to calculate viscosity, Nielsen (1977).

3.3.1 Poiseuille Law for Capillary Flow

The derivation of the Poiseuille law for capillary flow yields the following equations for Newtonian fluids, Whorlow (1979) and Brydson (1981 p 18):

$$\text{wall shear stress,} \quad \tau_s = \frac{PR}{2L} \quad (\text{Pa}) \quad \text{Eq. 3.4a}$$

$$\text{wall shear rate,} \quad \dot{\gamma} = \frac{4Q}{\pi R^3} \quad (\text{sec}^{-1}) \quad \text{Eq. 3.5a}$$

$$\text{shear viscosity,} \quad \eta = \frac{\tau_s}{\dot{\gamma}} \quad (\text{Pa.s}) \quad \text{Eq. 3.6a}$$

The Poiseuille equation for capillary flow yields an apparent measure of viscosity.

where

- P is the pressure drop (Pa)
- Q is the volumetric flow rate (m³/s)
- R is the capillary radius (m)
- L is the capillary length (m)

3.3.2 Extensional Viscosity from Flow Through an Orifice Die (Cogswell Model)

Polymer melt forms streamlines when flowing from the reservoir of a capillary rheometer into a die, the convergence and acceleration, produces a strong extensional viscosity. The interpretation assumes that the elastic deformation response of polymer melt is infinite, Cogswell (1981 p 60).

$$\text{extensional viscosity, } \lambda = \frac{9}{32} \frac{(n+1)^2}{\eta} \left(\frac{P_0}{\dot{\gamma}} \right)^2 \quad (\text{Pa.s}) \quad \text{Eq. 3.7a}$$

$$\text{extensional stress, } \sigma_E = \frac{3}{8} (n+1) P_0 \quad (\text{Pa}) \quad \text{Eq. 3.8a}$$

$$\text{extensional rate, } \dot{\epsilon} = \frac{\sigma_E}{\lambda} \quad (\text{sec}^{-1}) \quad \text{Eq. 3.9}$$

3.3.3 Corrections for Apparent Viscosity

Interpretation of capillary rheometry data using the Poiseuille equation for capillary flow, yields an apparent rather than a true measure of viscosity. True viscosity is derived by a series of mathematical corrections, described in chapters 3.3.3.1 to 3.3.3.4. Chapters 3.3.3.3 and 3.3.3.4 describe the influence of pressure and temperature on melt viscosity. It should be noted that for pressure driven flows the effect on viscosity of a pressure difference ΔP and temperature rise ΔT may balance, Fenner (1979 p 149), eliminating the need for these corrections.

3.3.3.1 Bagley Correction (Ends pressure drop)

The Poiseuille equation for capillary flow calculates shear stress from the pressure drop through a capillary die. Associated with the pressure drop are die entrance and exit pressure drops. The Bagley correction compensates for these pressure drops, by use of two different die lengths. The greatest sensitivity is obtained by combining a long die (aspect ratio $L/R = 32$) with an orifice die ($L/R = 0$), producing pressure drops P_L and P_0 respectively. In practice it may be necessary to use a short length die ($L/R = 6$) instead of an orifice die ($L/R = 0$).

wall shear stress,
$$\tau_s = \frac{(P_L - P_0)R}{2L} \quad (\text{Pa}) \quad \text{Eq. 3.10}$$

3.3.3.2 Rabinowitsch Correction (Non-velocity profile)

The Rabinowitsch correction is used to compensate for the fact that the assumed velocity profile is more 'plug-like' because of non-Newtonian behaviour.

true wall shear rate,
$$\dot{\gamma}_{\text{true}} = \left(\frac{3n+1}{4n} \right) \frac{4Q}{\pi R^3} \quad (\text{sec}^{-1}) \quad \text{Eq. 3.11}$$

3.3.3.3 Influence of Pressure on Viscosity

The pressure dependence of viscosity is more difficult to measure, Fenner (1979 p 31), it is best described by:

$$\eta = \eta_0 \exp(\alpha P) \quad (\text{Pa}) \quad \text{Eq. 3.12}$$

Where η_0 is the viscosity of zero pressure and α is the pressure coefficient of viscosity at constant shear rate. Typical values of α are 5 m²/GN for polyethylenes, 10 m²/GN for polypropylenes and 50 m²/GN for polystyrenes, Fenner (1979 p 31).

3.3.3.4 Influence of Temperature on Viscosity

Polymer melt viscosities are sensitive to changes in temperature. If flow curves are produced at different temperatures, the resulting curves are similar, but off-set. As temperature increases viscosity is reduced. This effect implies that the power law (see chapter 3.5) is not significantly dependent on melt temperature, Fenner (1979 p 31).

$$\eta = \eta_0 \exp[-b(T - T_0)] \quad (\text{Pa}) \quad \text{Eq. 3.13}$$

Where η_0 is the reference viscosity at the reference temperature T_0 , b is the temperature coefficient of viscosity at constant shear rate (for material obeying the power law, it is b/n), b is typically 0.01 - 0.02 C⁻¹, implying a reduction in viscosity of between about 10 to 20 per cent for a 10C rise in temperature, Fenner (1979 p 31), Mavridis and Shroff (1992).

3.4 Converging Flows

In a converging flow, such as that in an extrusion die or injection moulding nozzle, an extensional flow is superimposed on a shear flow. Research has shown that two superimposed shearing flows strongly interact, Cogswell (1981). Therefore an extensional flow superimposed on a shear flow is likely to form complex interactions.

At the wall of the die where velocity is zero, the shear strain rate (shear rate) is a maximum and extensional strain rate (extensional rate) is zero. The maximum

extensional rate occurs along the die centre line, where velocity is a maximum and shear rate is zero.

3.4.1 Cogswell Model

Cogswell (1981), for narrow convergence angles (less than 10 degrees), shear is the dominant flow mechanism and the extensional flow may be ignored. At convergence angles of 45 degrees it is likely that shear and extensional components are approximately equal. For convergence angles above 45 degrees the polymer melt is likely to form its own convergence pattern by establishing recirculating regions in the corners of the die. The Cogswell equations are claimed to be accurate at low die angles, they in fact describe the extensional contribution reasonably accurately up to about 45 degrees.

A pragmatic view allows the interactions between shear and extensional flows to be ignored, yielding the following relationships:

$$\text{Pressure Drop } P_{E_{nt}} = P_{S_{Enl}} + P_{E_{Enl}} \quad \text{Eq. 3.14}$$

$$P_S = 2\tau_{sl} \left[1 - (R_1 / R_0)^{3n} \right] / 3n \tan \alpha \quad \text{Eq. 3.15}$$

$$P_E = 2\sigma_{E1} \left[1 - (R_1 / R_0)^3 \right] / 3 \quad \text{Eq. 3.16}$$

$$P_{S_{Enl}} = \frac{2K}{3n \tan \alpha} \left(\frac{3n+1}{4n} \right)^n \dot{\gamma}_a^n \left(1 - \left(\frac{R_1}{R_0} \right)^{3n} \right) \quad \text{Eq. 3.17}$$

$$P_{E_{Enl}} = \frac{\lambda_a \tan \alpha}{3} \dot{\gamma}_a \left(1 - \frac{R_1^3}{R_0^3} \right) \quad \text{Eq. 3.18}$$

- where R_0 is the die entry radius (m)
- R_1 is the die exit radius (m)
- α is the half angle of convergence (degrees)
- τ_{s1} is the shear stress corresponding to the shear rate at die wall at the exit, $\dot{\gamma} = 4Q / \pi r_1^3$ (Q being the volumetric flow rate)
- n is the power law index (see chapter 3.5)
- σ_{E1} is the extensional stress corresponding to the average extensional strain rate, $\dot{\epsilon}_1 = (\dot{\gamma}_1 \tan \alpha) / 2$
- $P_{S_{En}}$ contribution of shear dissipation towards P_{En}
- $P_{E_{En}}$ contribution of extensional dissipation towards P_{En}

3.4.2 Spherical Velocity Field (Gibson)

The shear and extensional flow contributions to entry pressure are described by the equilibrium model, equations 3.19 and 3.20 respectively. The shear components derived from the Cogswell and equilibrium models, equation 9.17 and 9.19, respectively, have a high degree of agreement. At low die angles, both become asymptotic to the same expression, Collyer and Clegg (1988 p 77), giving:

$$\lim_{\alpha \rightarrow 0} P_{S_{En}} = \frac{2\eta\dot{\gamma}_a}{3\alpha} \quad \text{for} \quad \frac{R_1^3}{R_0^3} \ll 1$$

The extensional components derived from Cogswell model, with $n=1$, and equilibrium model both agree at low die angles. Equation 3.20 has the advantage that it gives a finite value of pressure for a flat entry die, however it gives poor agreement with experimental results above die angles of about 40 degrees and shows a maximum at 60 degrees, which is unlikely to be exhibited by a polymer melt. The reason for this inaccuracy at large die angles, is that no allowance has been made for the pressure

drop (P'_{Ent}) between the spherical exit boundary and the entrance to the capillary. The discrepancy which results, is greatest at large die angles where the convergent regime continues for some distance beyond the spherical exit boundary, Collyer and Clegg (1988). The equilibrium model can be corrected by determining the extra pressure (P'_{Ent}) between the spherical exit boundary and the entrance to the capillary, as shown in equation 3.21.

$$P_{S_{Ent}} = \frac{\eta \dot{\gamma}_a \sin \alpha \cos \alpha (1 + \cos \alpha)^2}{4(1 - \cos \alpha)(1 + 2 \cos \alpha)} \left(1 - \frac{R_1^3}{R_0^3} \right) \quad \text{Eq. 3.19}$$

$$P_{E_{Ent}} = \frac{\lambda \dot{\gamma}_a \sin \alpha (1 + \cos \alpha)}{6} \left(1 - \frac{R_1^3}{R_0^3} \right) \quad \text{Eq. 3.20}$$

The corrected equilibrium model for the extra pressure drop between the exit boundary and the capillary entrance is described by equation 3.22.

$$P'_{Ent} = \frac{\lambda \dot{\gamma}_a}{8} \left(\alpha - \frac{\sin 2\alpha}{2} \right) \quad \text{Eq. 3.21}$$

$$\text{Corrected } P_{E_{Ent}} = P_{E_{Ent}} + P'_{Ent} \quad \text{Eq. 3.22}$$

3.4.3 Binding Model

Energy principles are employed to relate the entry pressure drop to flow rate and fundamental rheological properties. One of the aims of the analysis is to investigate the influence of extensional viscosity on such flows, particularly with regard to the occurrence and enhancement of vortex motion in the entry corners, Binding (1988).

The analysis for contraction flows may readily be extended to converging flows where for example fluid is forced through a profiled nozzle.

3.4.4 Machine Nozzle Geometry

Figure 3.4 shows a schematic diagram of the Sandretto series seven 60 tonne injection nozzle for use with a screw of diameter 40 mm. Appendix A (iv) shows a detail drawing of the machines original nozzle. Appendix D shows details of the modular nozzle design.

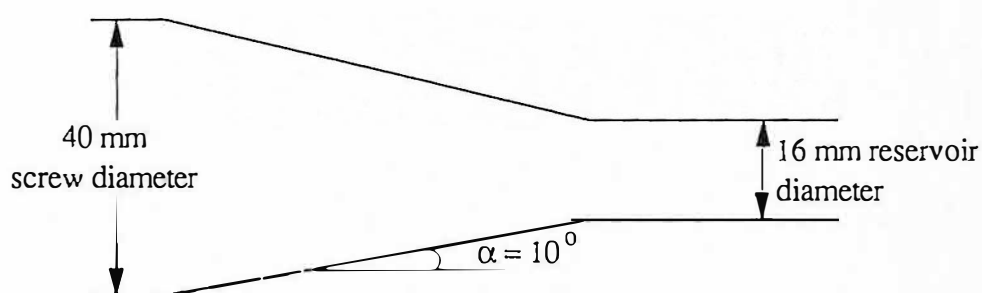


Figure 3.4 Sandretto series seven 60 tonne injection nozzle geometry

For the 10 degree convergence angle of the nozzle, shear flow is likely to be the dominant flow mechanism, this is in agreement with the Cogswell and Gibson models. At the 90 degree capillary die entrance the pressure drops associated with shear and extensional flows may be approximately equal, Cogswell (1981), or the shear contribution may be a small percentage of the total pressure drop, Gibson (1988). It is apparent that shear and extensional viscosity models and theories are the subject of on-going research, Groves et al (1993).

* i.e. depends on the established convergent flow regime.

3.5 Power Law Model

Most polymer melts exhibit non-Newtonian behaviour, whereby apparent viscosity (η_a) decreases as shear rate ($\dot{\gamma}$) increases. This viscosity decrease may occur over many decades of shear rate, and the viscosity at high shear rates may be several orders of magnitude smaller than at lower shear rates, Nielsen (1977 p 47). This

phenomenon is extremely important for efficient polymer processing operations, injection moulding and extrusion.

This pseudoplastic behaviour may be described by a power law model, whereby a flow curve of $\log(\tau)$ versus $\log(\dot{\gamma})$, is a straight line, for a specific shear rate range, Lenk (1968), Nielsen (1977) and Cogswell (1981). The development of this empirical constitutive relationship is essentially no more than a curve fitting process and as such generally does not hold for more than two decades of shear rate.

$$\text{Shear stress } \tau = K \dot{\gamma}^n \quad \text{Eq. 3.23}$$

The dimensionless term 'n' is frequently referred to as the power law index and indicates the degree of non-Newtonian behaviour, where 1 indicates Newtonian and $0 < n < 1$ indicates non-Newtonian behaviour. The constant K has the unit of $\text{Pa}\cdot\text{s}^n$ and is termed the consistency index.

A typical polymer melt exhibits pseudoplastic behaviour, whereby n is less than unity and decreases with increasing shear rate. For most linear polymer melts, there is a critical value of shear stress, at which there is a change of flow curve gradient. This flow curve discontinuity has been identified with oscillatory flow regimes and slip at the capillary die wall, Cogswell (1981 p 98), Hatzikiriakos and Dealy (1992b) and Dobbie (1993).

CHAPTER 4

Design and Modification of Experimental Equipment

4.1 Introduction

The subject matters described in this chapter are: (i) design and construction of a modular nozzle rheometer, for flexible nozzle configuration, (ii) design and construction of an instrumented beaker tool (single impression tool), (iii) configuration of an instrumented container tool (two impression 'family' tool), (iv) design and construction of a high temperature pressure transducer test and calibration facility, and (v) modification to the screw velocity control performance of the 60 tonne Sandretto injection moulding machine.

A 60 tonne Sandretto series seven hydraulic injection moulding machine was utilised for this research (see appendix A(i) for technical specification). Injection and plasticisation phases were accurately monitored, using a sophisticated machine and process variable monitoring system. An in-line modular nozzle rheometer was used to measure polymer melt rheology for true process conditions. The machine was utilised for injection moulding experimental tests and in-line capillary rheometry. Figure 4.1 shows a general view of the instrumented Sandretto 60 tonne injection moulding machine configured with a Haynes and Fordham beam robot for product recovery. Experimental test parameters are stored after each test, the full machine parameter set (10 pages) is transmitted by serial communication to a personal computer.

A computer controlled Rosand twin bore capillary rheometer was used for off-line measurement of polymer melt rheology (see appendix B for technical specification). Figure 4.2 shows a general view of the Rosand twin bore capillary rheometer. The computer system is used for (i) sequence and machine parameter control and (ii)

analysis and graphical display of results. The computer system uses two visual display units (VDU), one for sequence monitoring and the other for graphical display of results. Installed on the Rosand off-line capillary rheometer is a haul off test, to study elastic deformation of polymer melt. Figures 4.3 and 4.4 show the crosshead and pistons, and the pressure transducer locations in the barrel, for the Rosand off-line twin bore capillary rheometer.

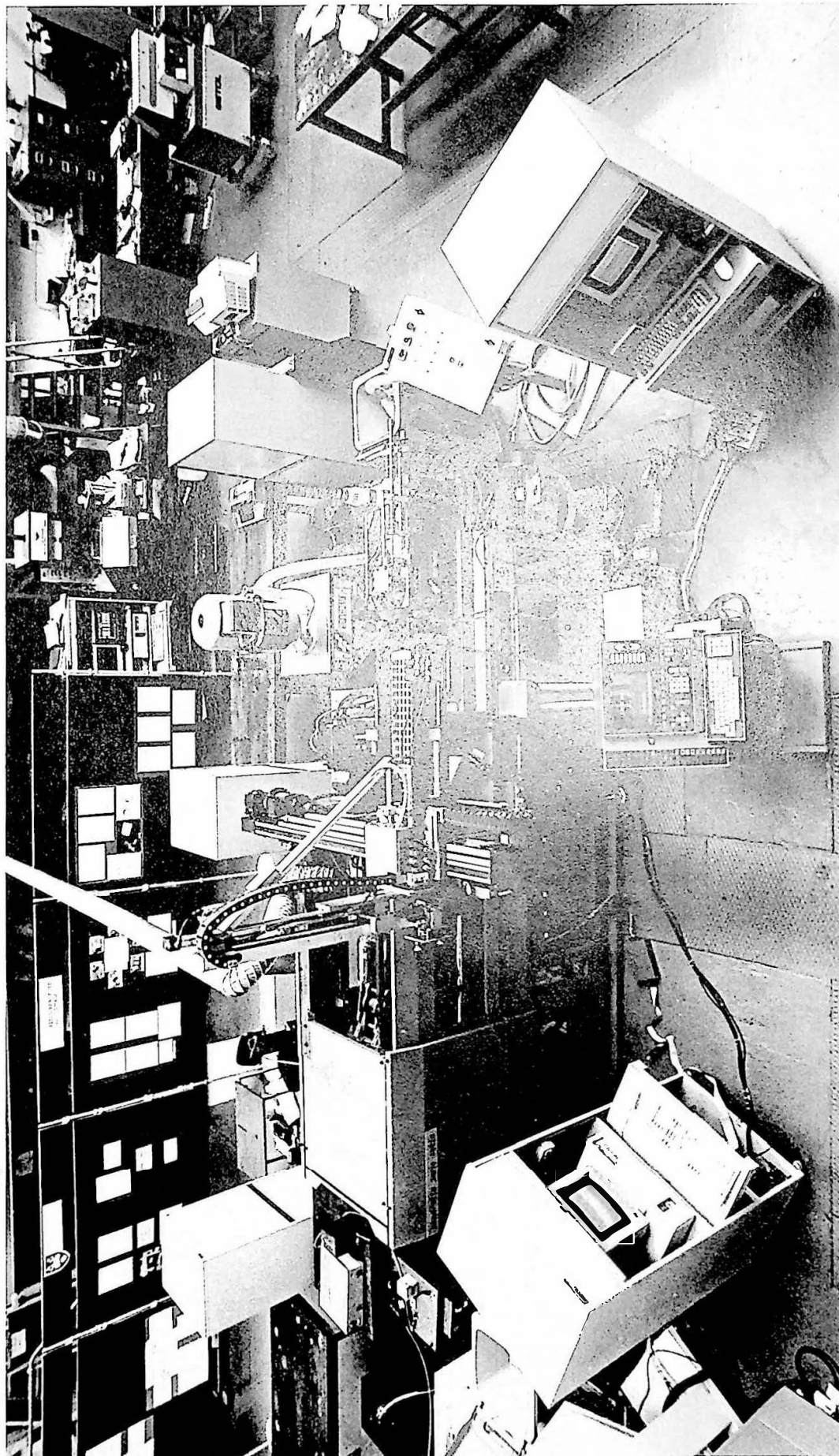


Figure 4.1 General view of Sandretto 60 tonne injection moulding machine



Figure 4.2 General view of Rosand RH7-2 off-line twin bore capillary rheometer

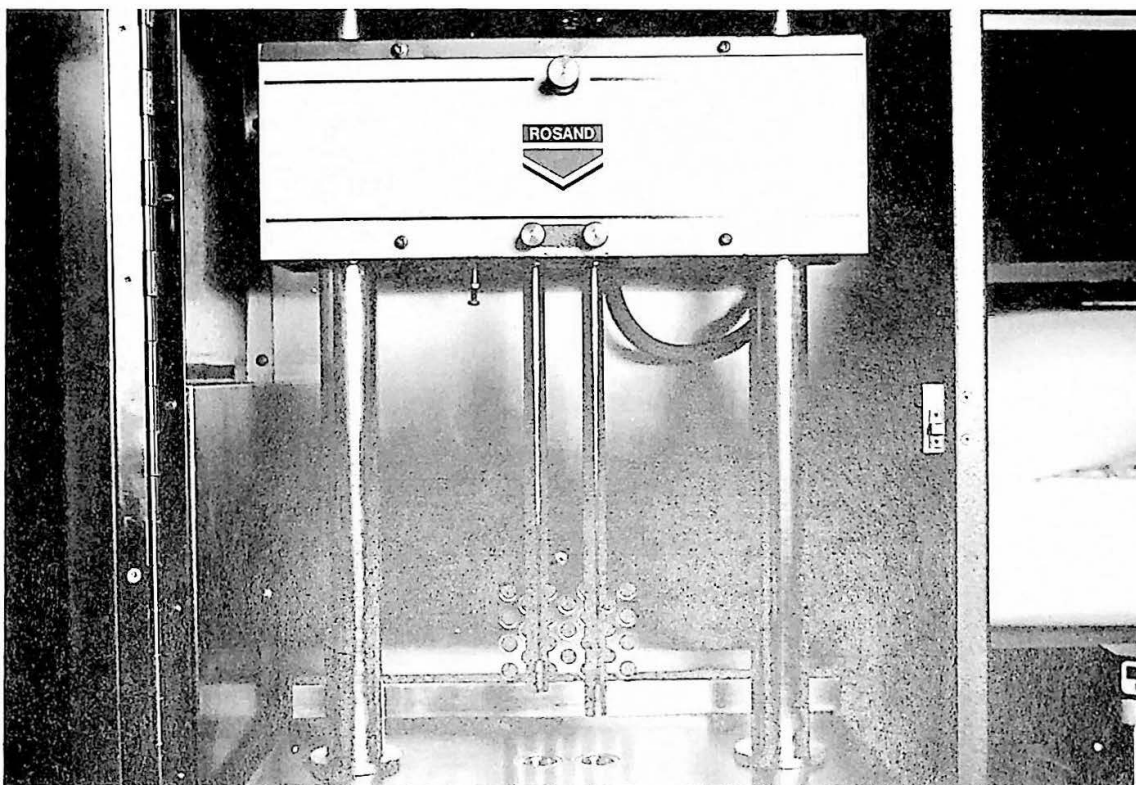


Figure 4.3 Crosshead and pistons of Rosand RH7-2 off-line twin bore capillary rheometer

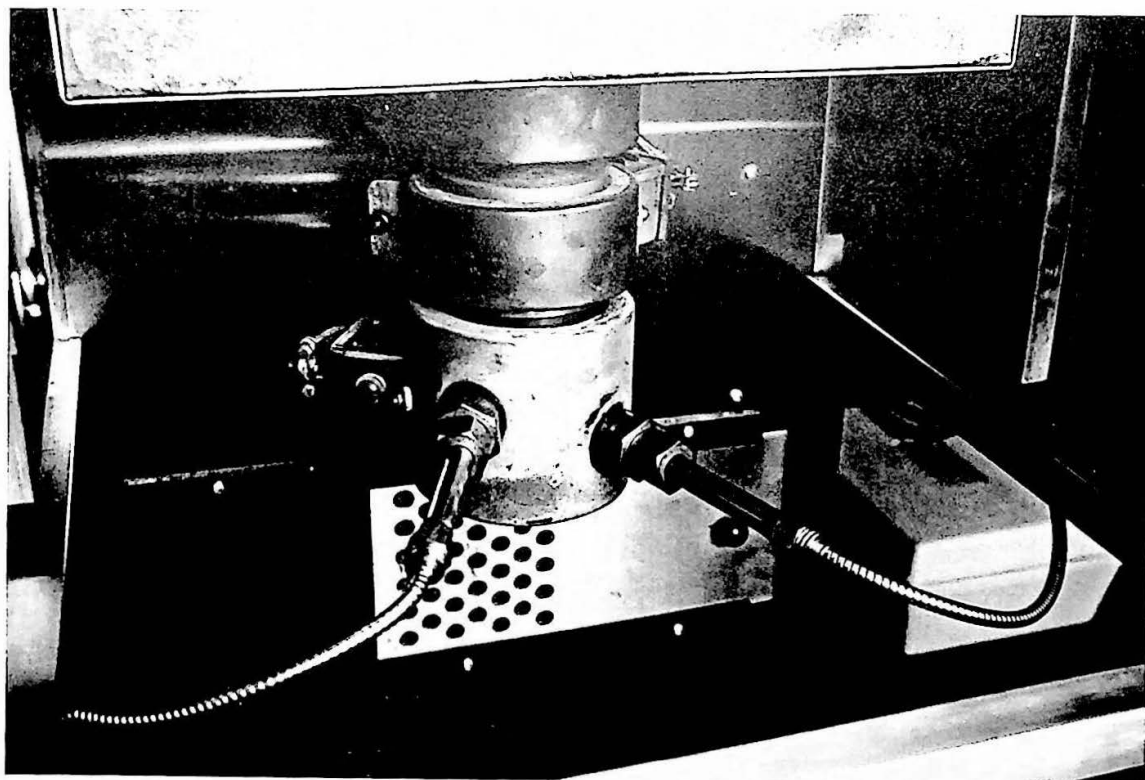


Figure 4.4 Pressure transducer locations for Rosand RH7-2 off-line twin bore capillary rheometer

4.2 Modular Nozzle Rheometer Design and Construction

A flexible function rheological nozzle was designed for operation at injection moulding pressures, allowing instrumented sections, spacer sections and different front end sections to be configured, therefore removing the need to construct separate nozzles for different experimental test configurations. The existing machine nozzle geometries were utilised as a basis for design of the nozzle rheometer, details of the original nozzle are shown in appendix A(iv). Melt pressure and temperature transducers are located on a 16 mm diameter step on the taper of the original nozzle, described as the reservoir bore. The instrumentation modules accommodate melt pressure and melt temperature transducers, 180 degrees apart. Details of the modular nozzle rheometer design are shown in appendix D, Table 4.1 describes the nozzle modules used, the internal convergence geometries for the modular nozzle rheometer were highly polished.

Module Number	Nozzle Module Description	Figure
1	Front section. experimental moulding tests	4.6 and 4.7
2	30 mm wide Instrumentation section	4.8
3	40 mm wide Instrumentation section	4.8
4	15 mm wide spacer section	-
5	Back section	4.9
6	Front section. in-line capillary rheometry	4.10

Table 4.1 Nozzle rheometer modules

The modular nozzle rheometer configurations for in-line capillary rheometer and injection moulding experimental tests are shown in chapters 7 and 8 respectively. Figure 4.5 shows the modular nozzle rheometer configured using sections 1, 3, 4, 2, 5. Figures 4.6 to 4.10 show features of the modular nozzle rheometer for moulding and in-line capillary rheometry.

Type T calibration thermocouples are used for nozzle body temperature control, with Eurotherm controllers, Eurotherm (1975), see appendix E(i). The location of the temperature controller thermocouples are shown in appendix D(i) and figure 8.1. The temperature control thermocouple for the capillary dies was located between the heater band and die. This proved the simplest and most practical method of die thermocouple location, problems of poor temperature control were not encountered, due to the small mass of the dies. Care has been taken, when connecting more than one heater to a controller (in parallel), to ensure that the heaters are of the same power, to avoid the occurrence of 'hot spots' along the nozzle, Wilkinson (1991).



Figure 4.5 Modular nozzle rheometer configured for injection moulding experimental tests

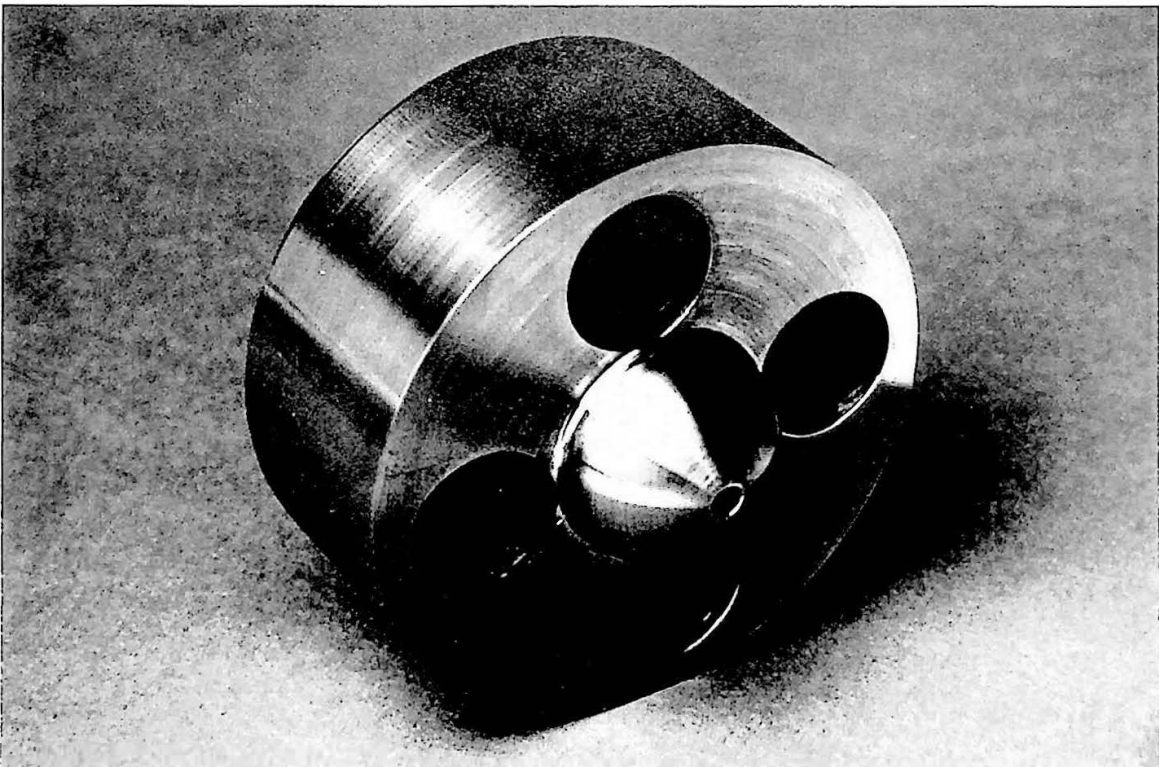


Figure 4.6 Nozzle front section for injection moulding experimental tests

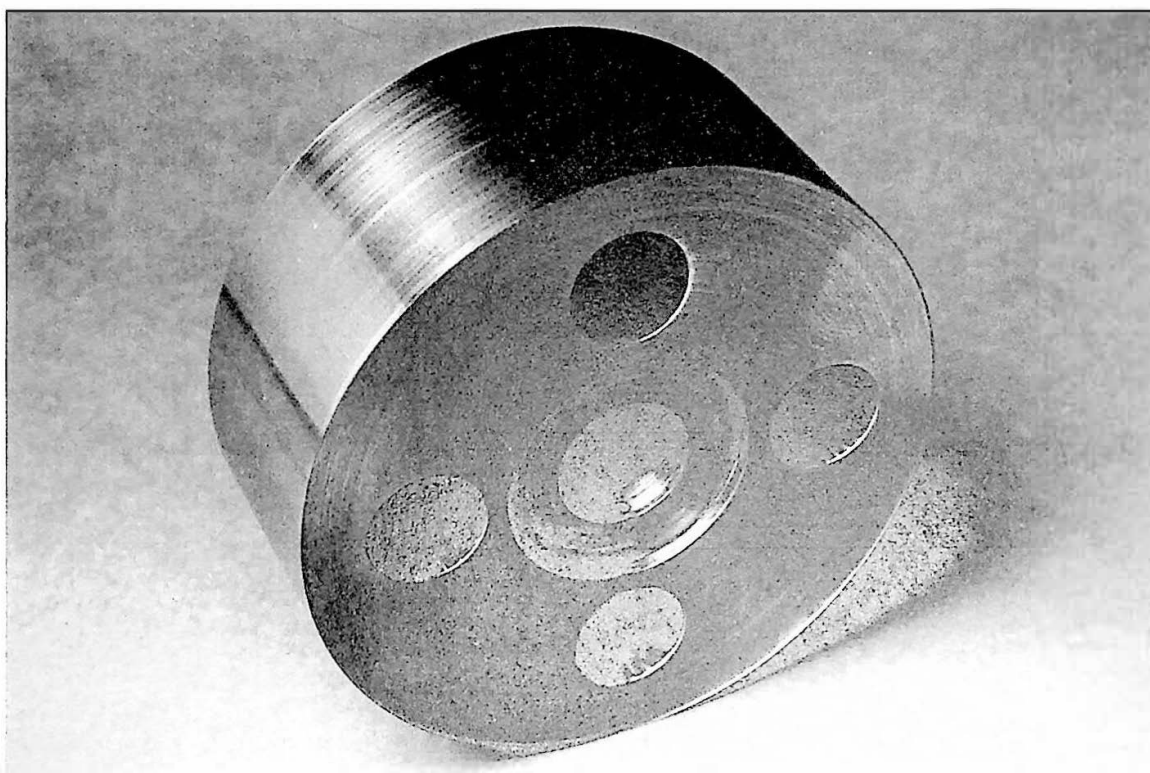


Figure 4.7 Modular nozzle front section spigot location ring

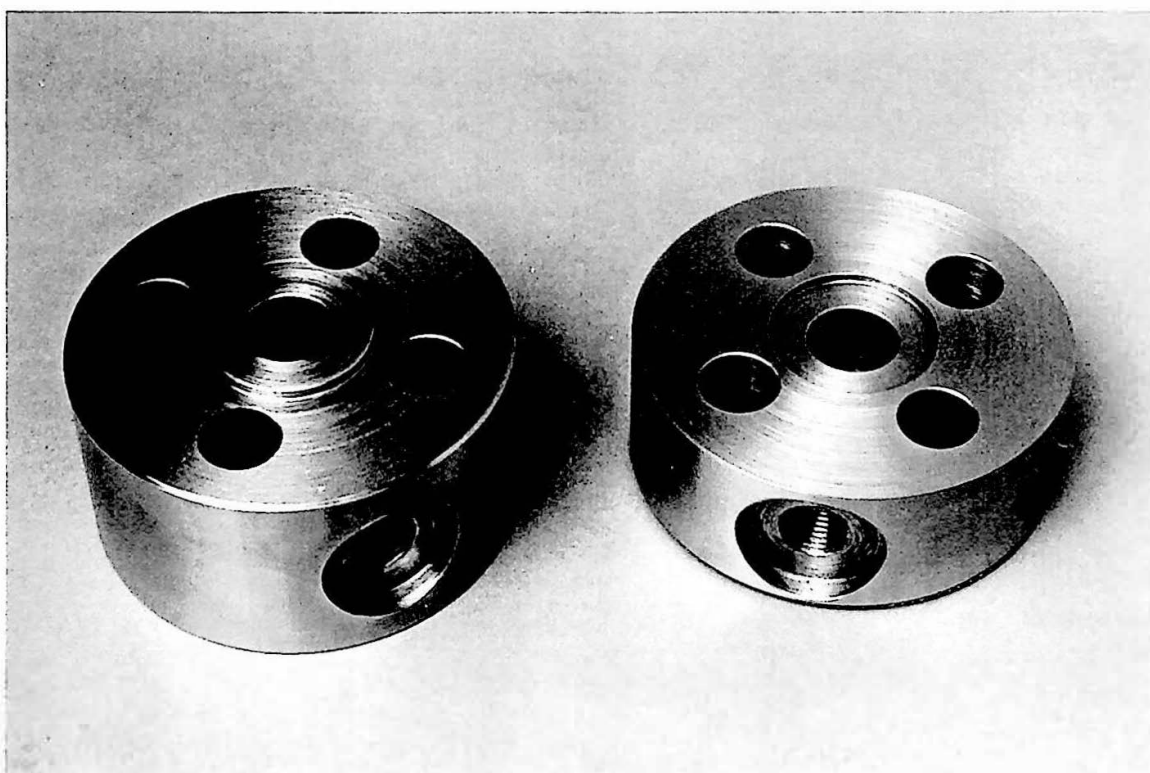


Figure 4.8 Modular nozzle instrumentation sections



Figure 4.9 Modular nozzle back section for location with machine barrel

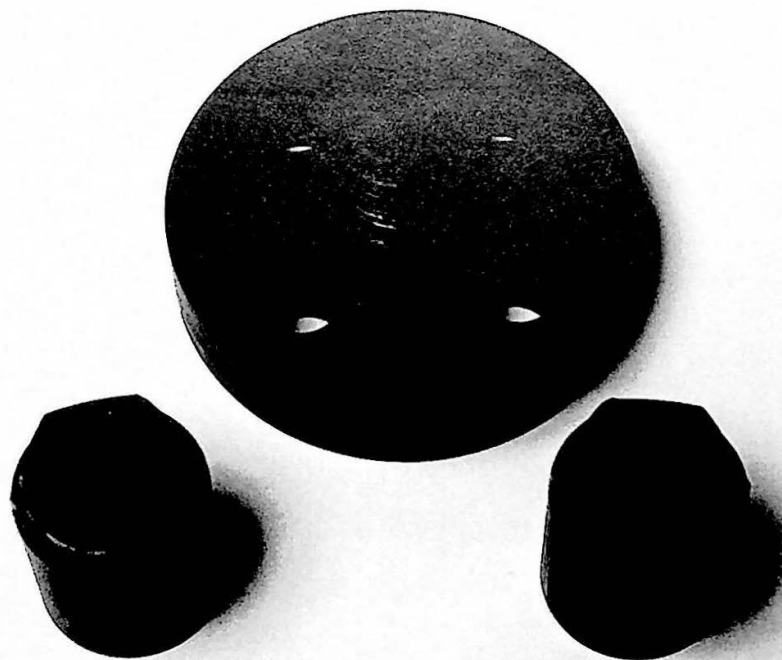


Figure 4.10 Modular nozzle front section and dies for in-line capillary rheometry

4.3 Beaker Tool Design and Construction

An instrumented beaker tool has been designed, constructed and successfully utilised for experimental moulding tests. The tool design incorporates the following features: (i) single impression, (ii) centre gated by hot or cold sprue bushing, (iii) an average wall thickness of 2 mm, (iv) an allowance of 1.2% for material shrinkage in the cavity, (v) location for three melt pressure and three melt temperature transducers, (vi) core, cavity and feed zone temperature control zones, and (vii) location for tool temperature transducers. The beaker design is shown in appendix F(i), measuring 80 mm in height and 65 mm base diameter, allowing a shallow angle to help facilitate component ejection. Appendix F(ii) shows the initial tool design, whereby a stripper ring actuated by a conventional ejection plate was utilised, Pye (1983 p 107). Appendix F(iii) shows the final general assembly drawing (Complex Tools, Glossop, UK) of the beaker tool. The final design utilised a stripper plate utilising length-bolt actuation, Pye (1983 p 104). To prevent the tool from being damaged, both software and physical hardware protections are used to limit the tool opening distance. Figure 4.11 shows a schematic diagram of the instrumented beaker tool, figures 4.12 to 4.17 show features of the instrumented beaker tool and figures 4.18 a and 4.18 b show examples of the moulded beaker component.

The tool was designed for measurement of in-line cavity melt pressure and melt temperatures. Two flats on the outside diameter of the beaker at 180 degrees apart provide a location for tool instrumentation. The melt pressure and temperature transducers are located at 20 mm regular intervals along the two instrumentation flats. Further details of tool instrumentation, melt pressure and temperature transducers, are described in chapter 5. During installation of the pressure transducers, copper shims were necessary to ensure the pressure transducer diaphragms were flush mounted. It was possible to machine the temperature transducers, to ensure flush mounting. The tool design includes a thermocouple location directly into the core.

The tool was designed for either a hot sprue bushing 'hot -tip' or conventional cold sprue bush, see appendix F(v) for the 'hot tip' technical specification. The tool was originally designed for a Hasco 'hot tip', as shown on the assembly drawing, see appendix F(iii). The final tool configuration used a Kona heat pipe hot tip design (see appendix F(v)), the mounting for this is shown in appendix F(vi). Dynamic behaviour of heat pipes has been studied by Ali (1979) for use in plastics extruder applications, where step and frequency response tests have been performed to determine expressions for the system transfer functions and transient response. The heat pipe 'hot tip' should provide a more uniform temperature distribution, compared to electrically heated 'hot tips', which may suffer from localised temperature 'hot spots'.

Three temperature control zones were incorporated in to the tool design, core, cavity and feed zones. The tool temperature control zones are apparent from the general assembly drawing, see Appendix F(iii). Appendix F(iv) shows a schematic diagram of the tool temperature control zones. Piping connections to the tool were quick release self sealing connectors (Swagelok Ltd), allowing quick tool changes, or removal for in-line capillary rheometry. The three zones were independently controlled by Churchill tool temperature control units, Churchill (1978), see appendix E(ii) for technical specification.

The final tool design was assessed by BASF Engineers, M D Smith and I Hyland BASF Cheadle, UK and R Kabus BASF Aktiengesellschaft, Ludwigshafen, Germany. The following comments were made: (i) cavity cooling channels would perform more efficiently closer to the cavity, (ii) cooling channels should be positioned uniformly around the cavity, (iii) diameter of the cooling channels should be increased to increase cooling efficiency, (iv) use of air ejection may assist product ejection if sticking occurs, (v) cavity ventilation may need modifying if regular cleaning is necessary, to remove blockages.

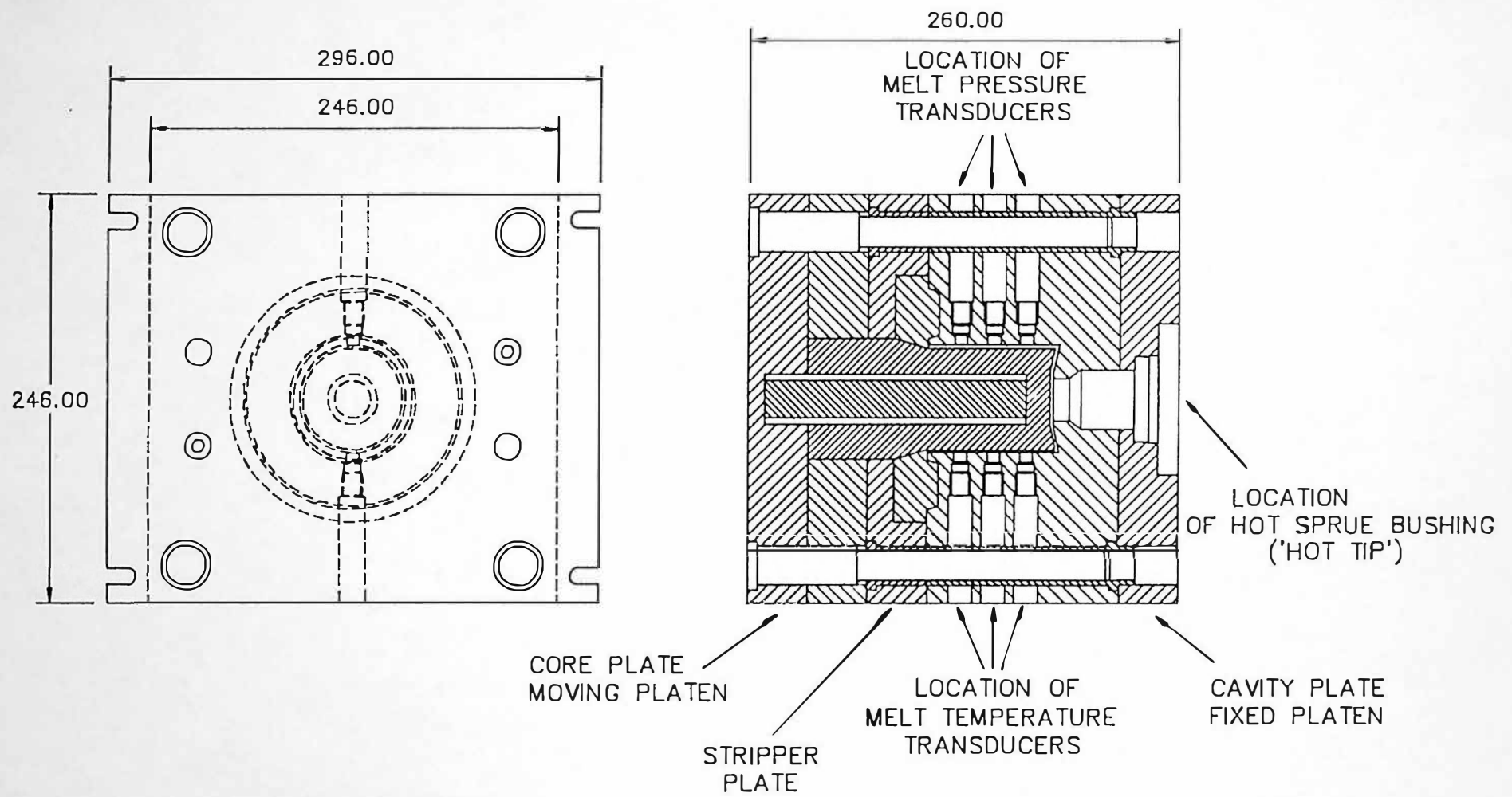


Figure 4.11 Schematic diagram of instrumented beaker tool (single impression)

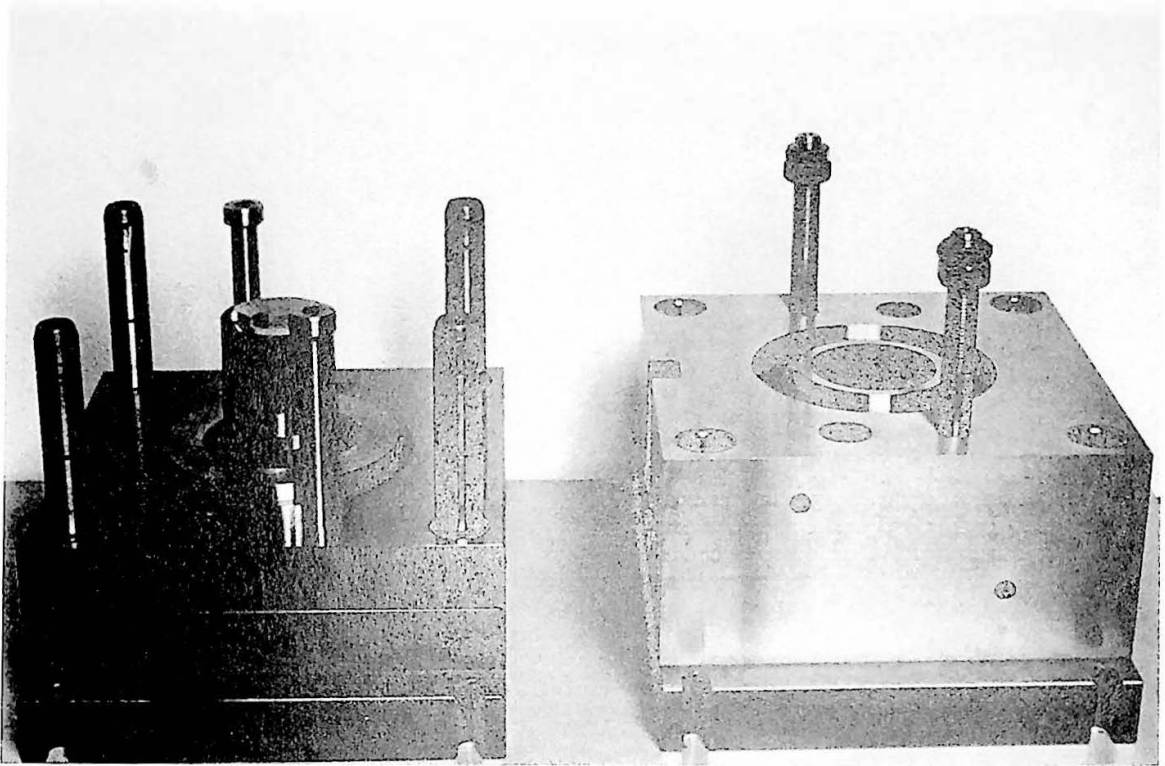


Figure 4.12 Beaker tool core and cavity plates



Figure 4.13 Beaker tool core plate showing the core

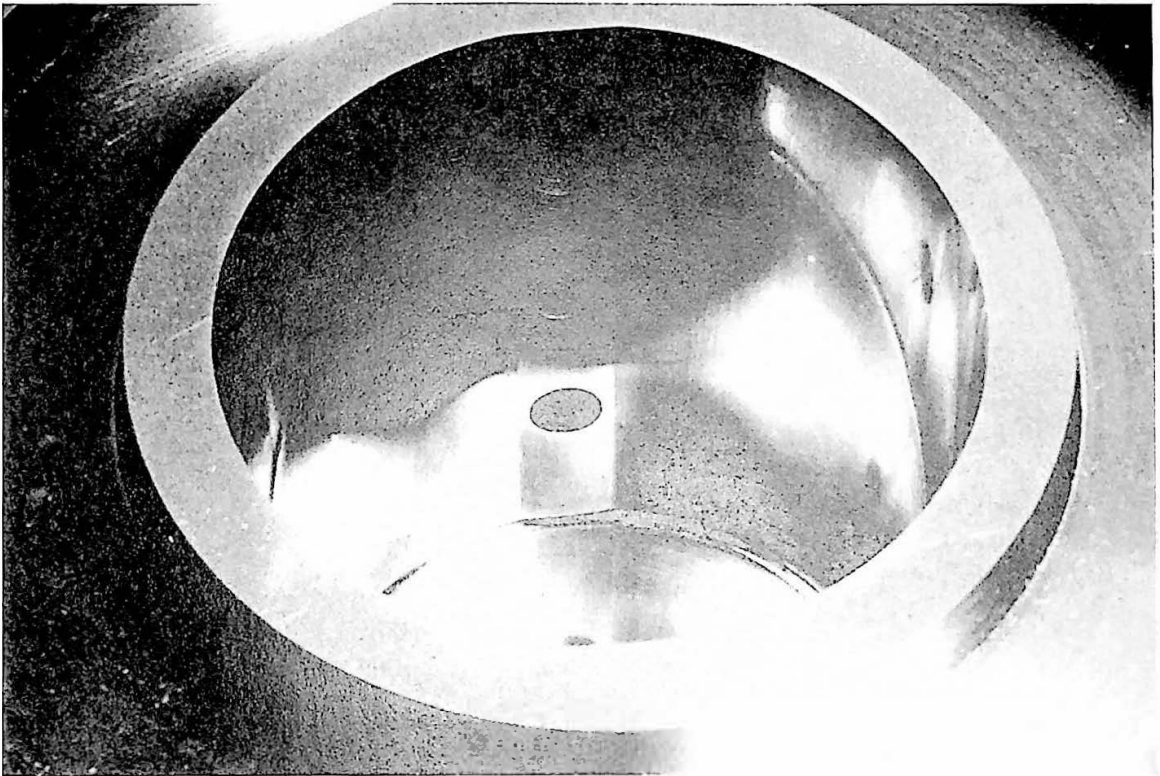


Figure 4.14 Instrumentation flat on side of beaker cavity

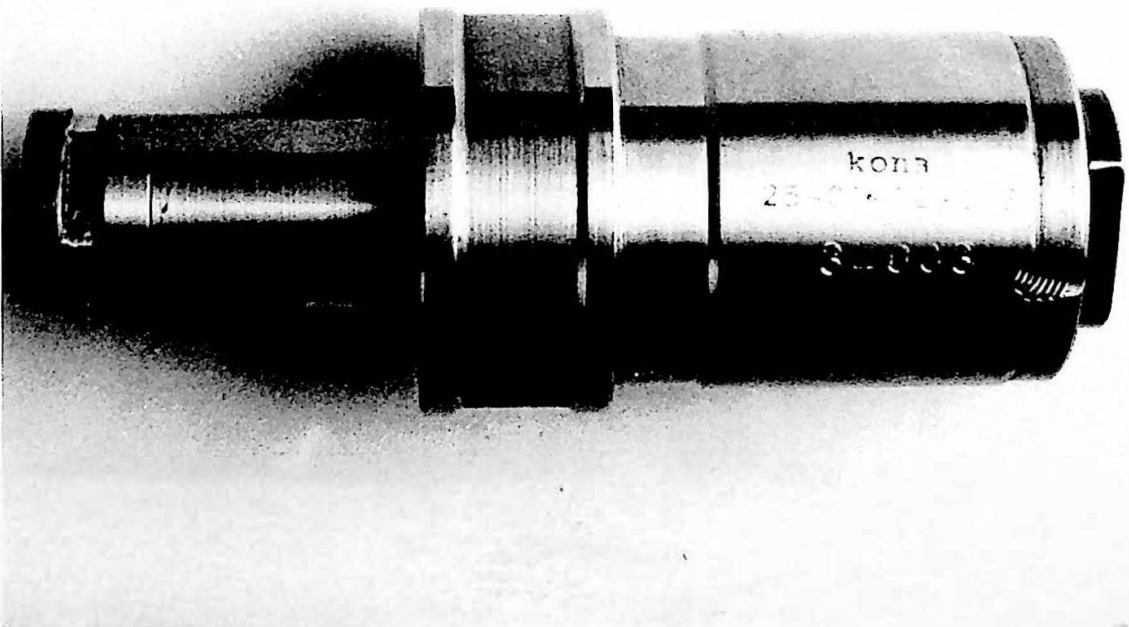


Figure 4.15 Hot sprue bushing ('hot tip') for beaker tool

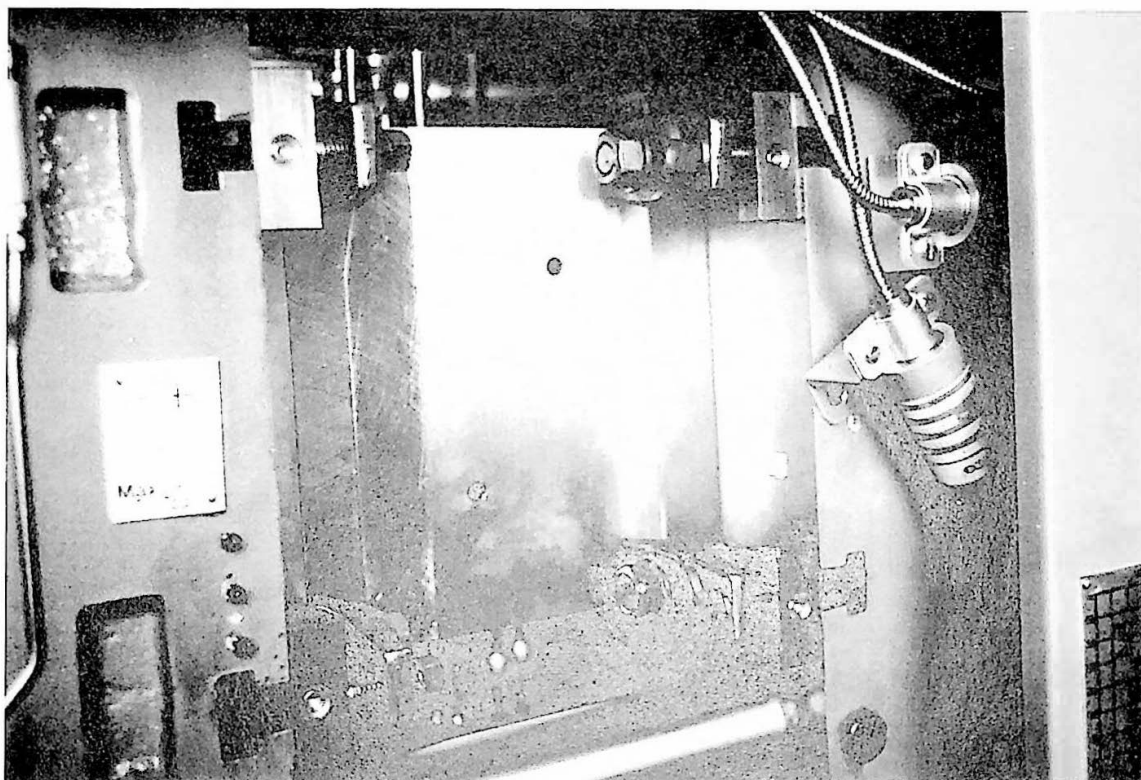


Figure 4.16 Closed beaker tool located between machine platens

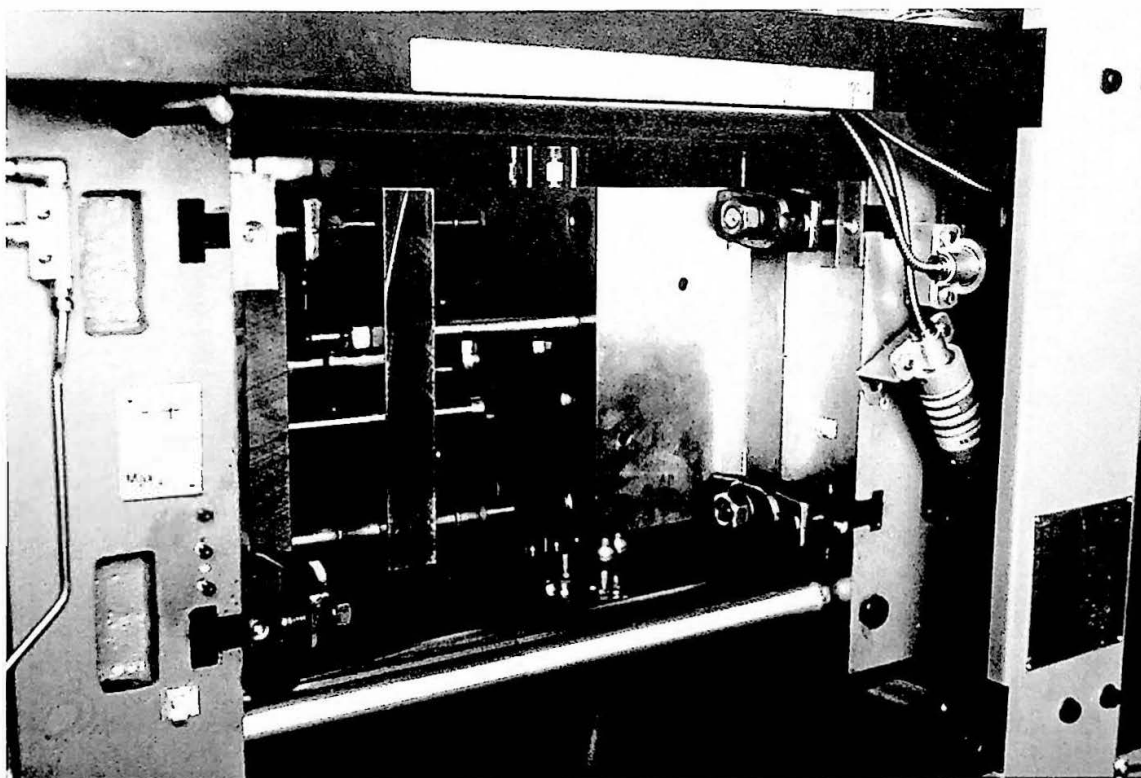


Figure 4.17 Open beaker tool showing stripper plate

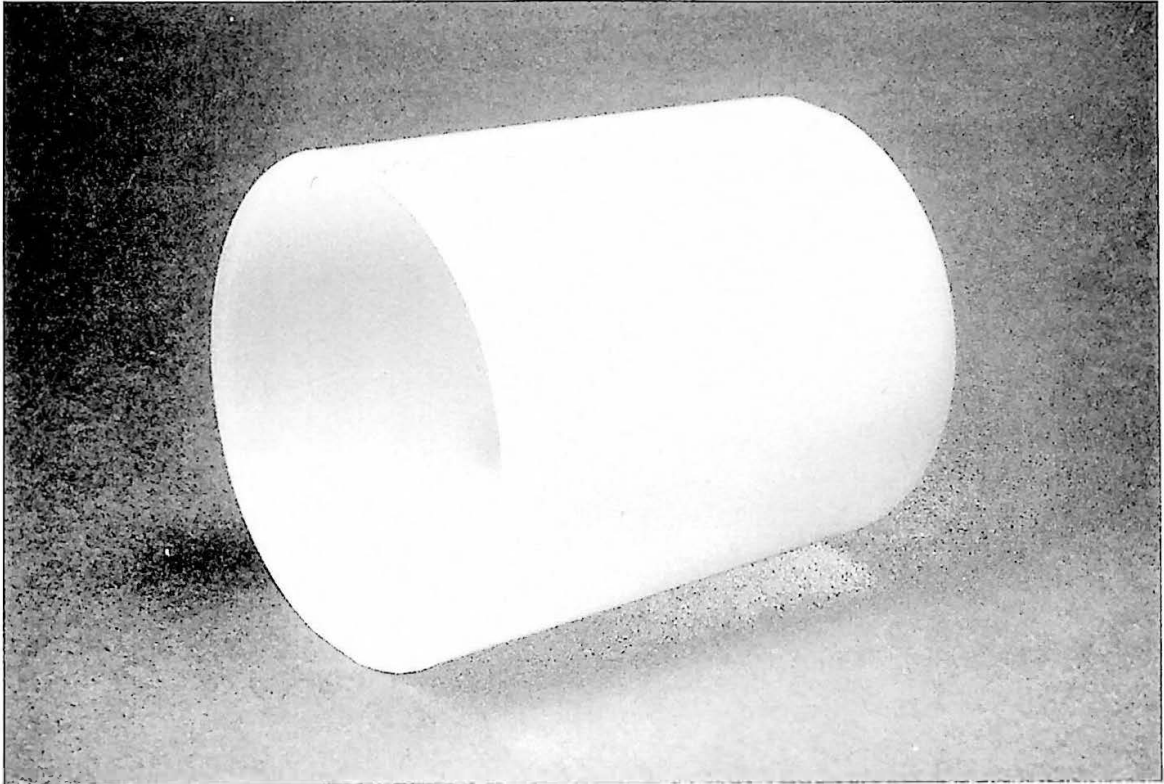


Figure 4.18 a Example of injection moulded beaker component

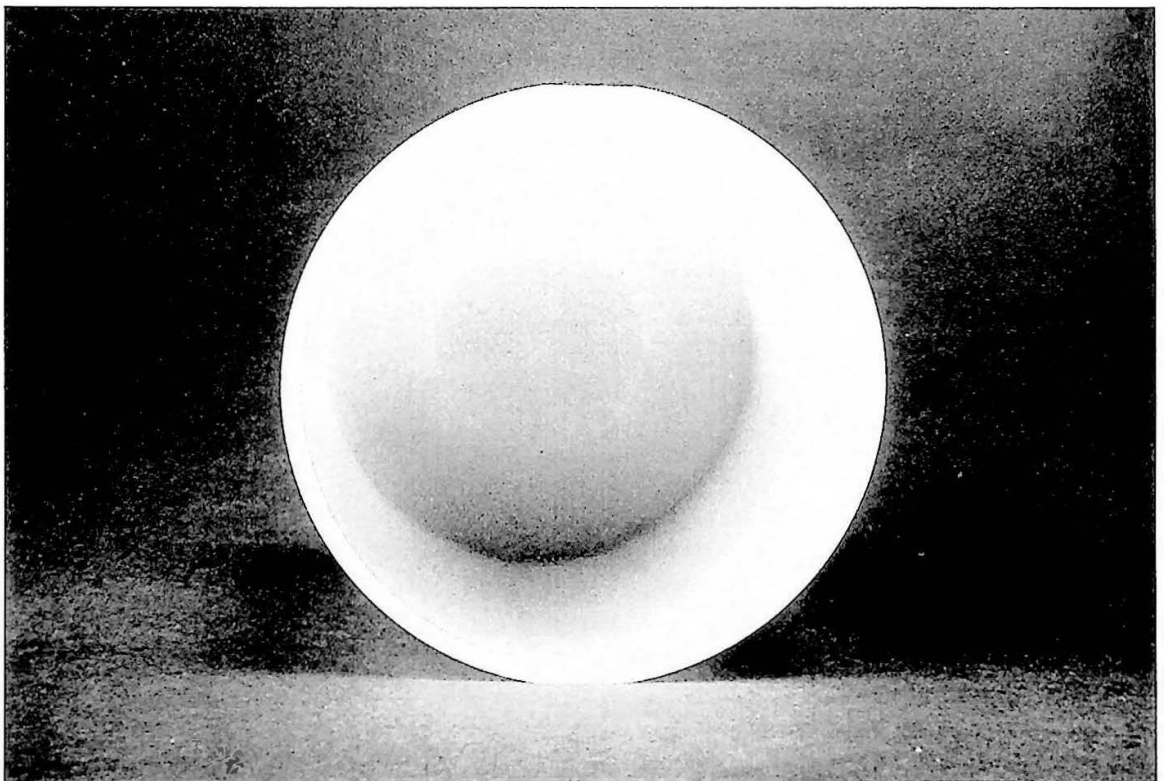


Figure 4.18 b Example of injection moulded beaker component showing instrumentation location flats

4.4 Container Tool Configuration

An existing instrumented two impression 'family' tool was utilised for experimental moulding tests, Harrison (1977), the container base (female half) and lid (male half) had an average wall thickness of 2 mm. Figure 4.19 shows a schematic diagram of the instrumented (temperature measurement only) container tool. Figures 4.20 and 4.21 show the core and cavity plates, respectively, the ejector pins are shown in figure 4.20. Figures 4.22 a and 4.22 b show an example of a moulded container and sprue, external and internal views are shown.

Figure 5.6 shows a schematic diagram of the thermocouple locations, approximately 4 mm from the cavity surface. Three type T calibration thermocouples were installed in purpose designed thermocouple location points, in both core and cavity plates. The thermocouple tips were welded in position, by a capacitive discharge technique.

Moulded products were ejected by means of six ejector pins for each impression, with a single pin for the sprue. The core and cavity tool plates were separately controlled by two Churchill tool temperature controllers, Churchill (1978), see appendix E(ii) for technical specification. Tool temperature control zones are apparent from the assembly drawing shown in appendix G(ii). Appendix G(iii) shows a schematic diagram of the tool temperature control zones. The polymer melt was injection through pin gates, located on the edge of the moulded products.

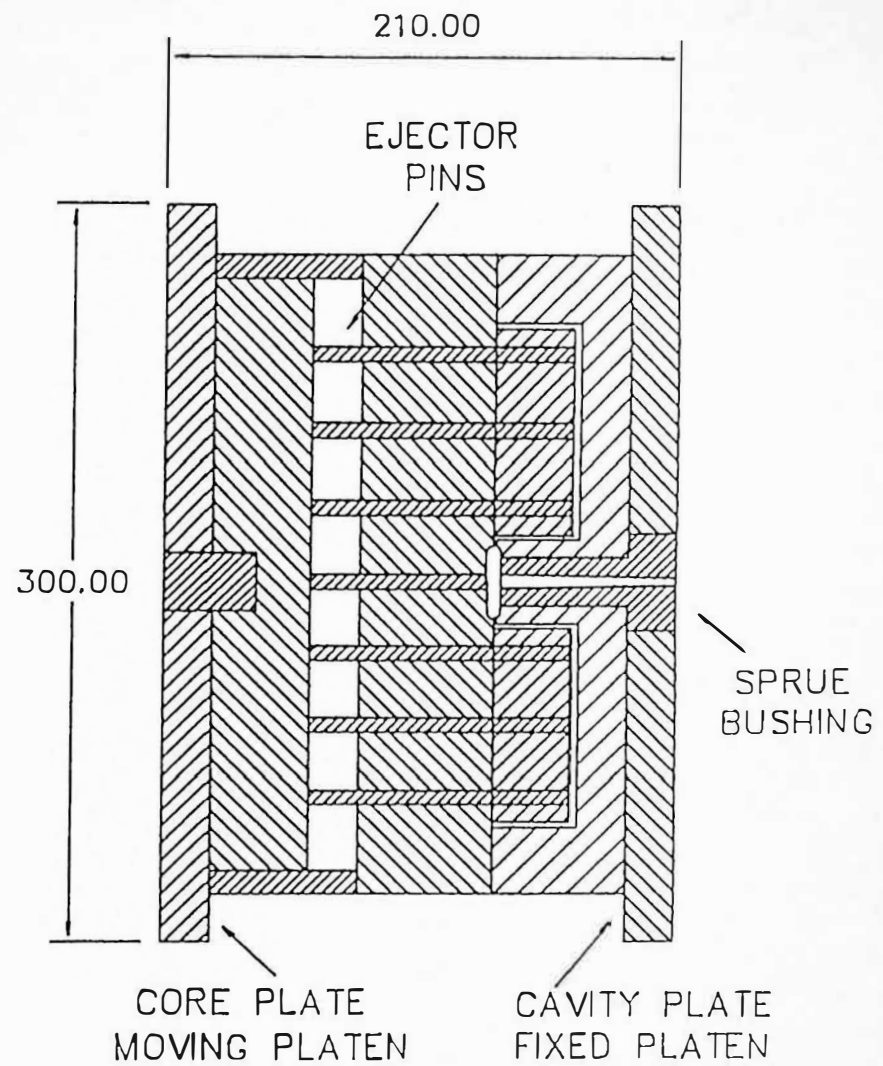
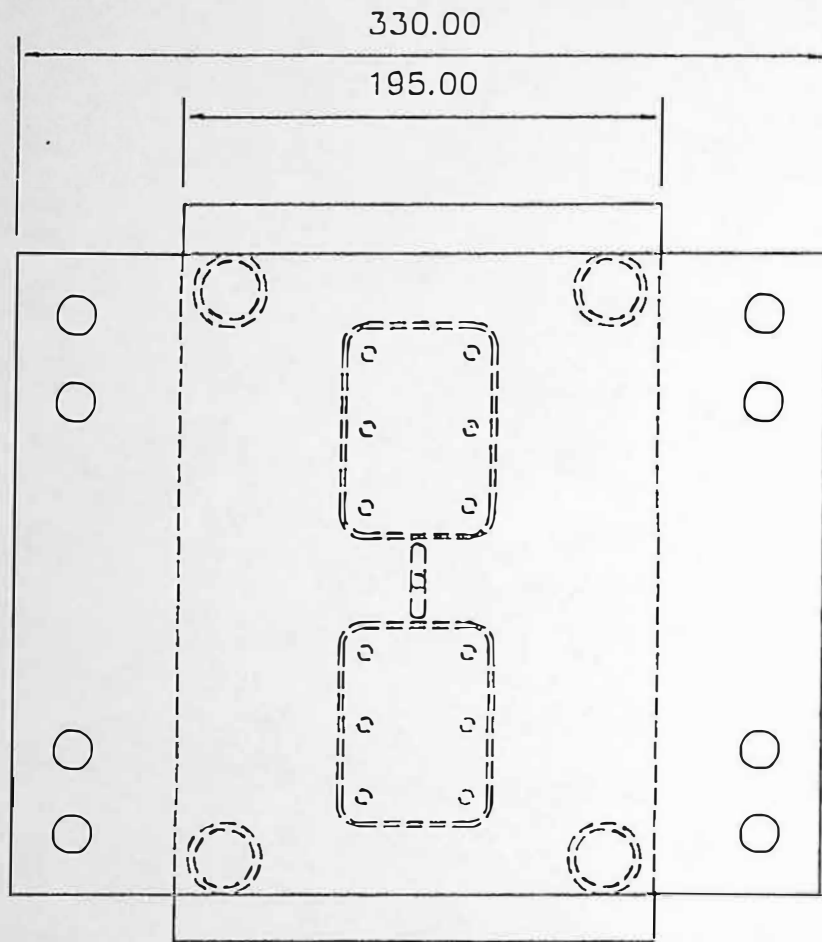


Figure 4.19 Schematic diagram of instrumented container tool (two impression 'family' tool)

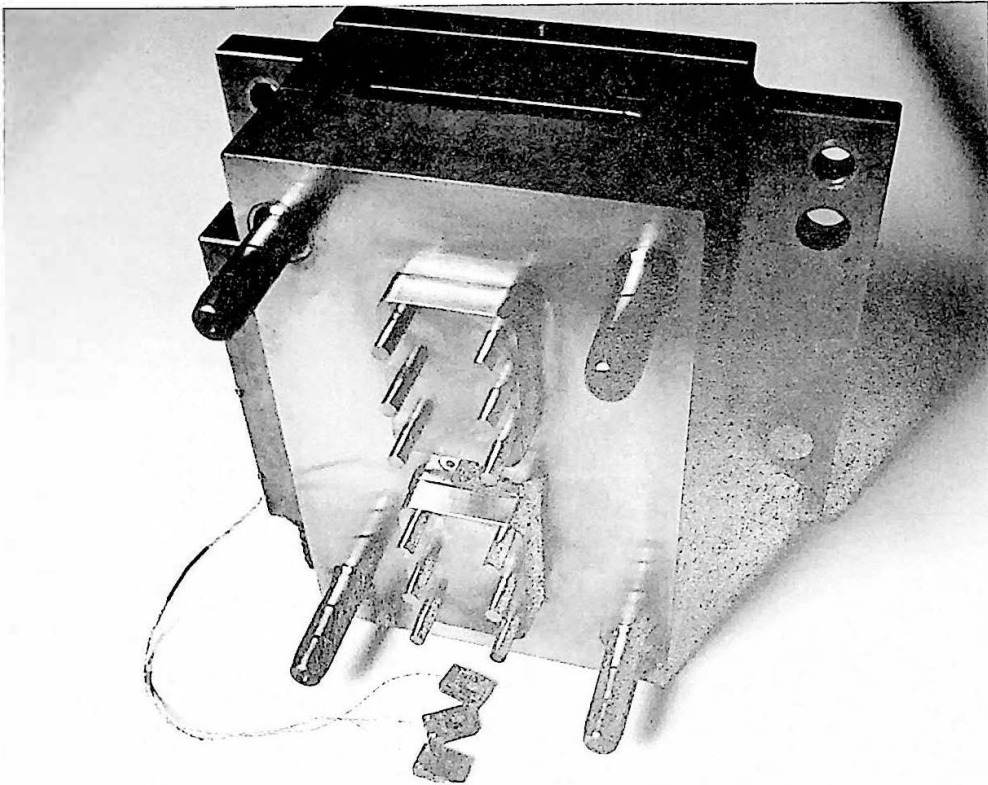


Figure 4.20 Container tool core plate showing ejector pins

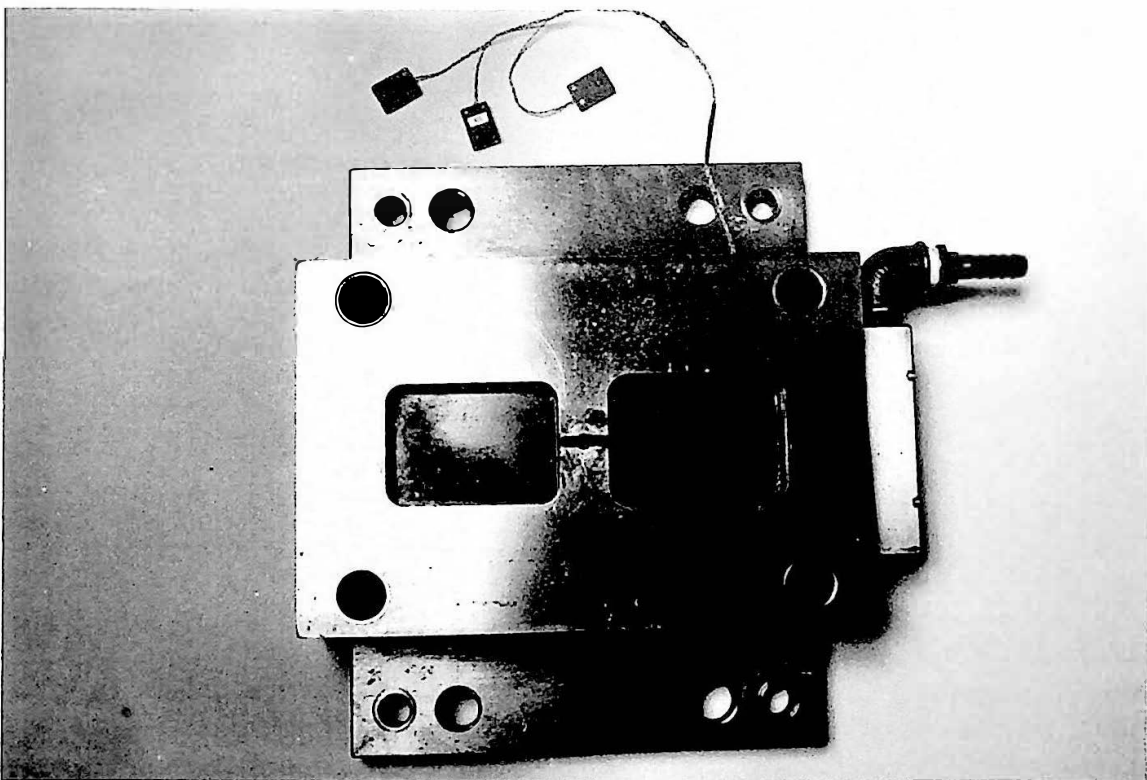


Figure 4.21 Container tool cavity plate

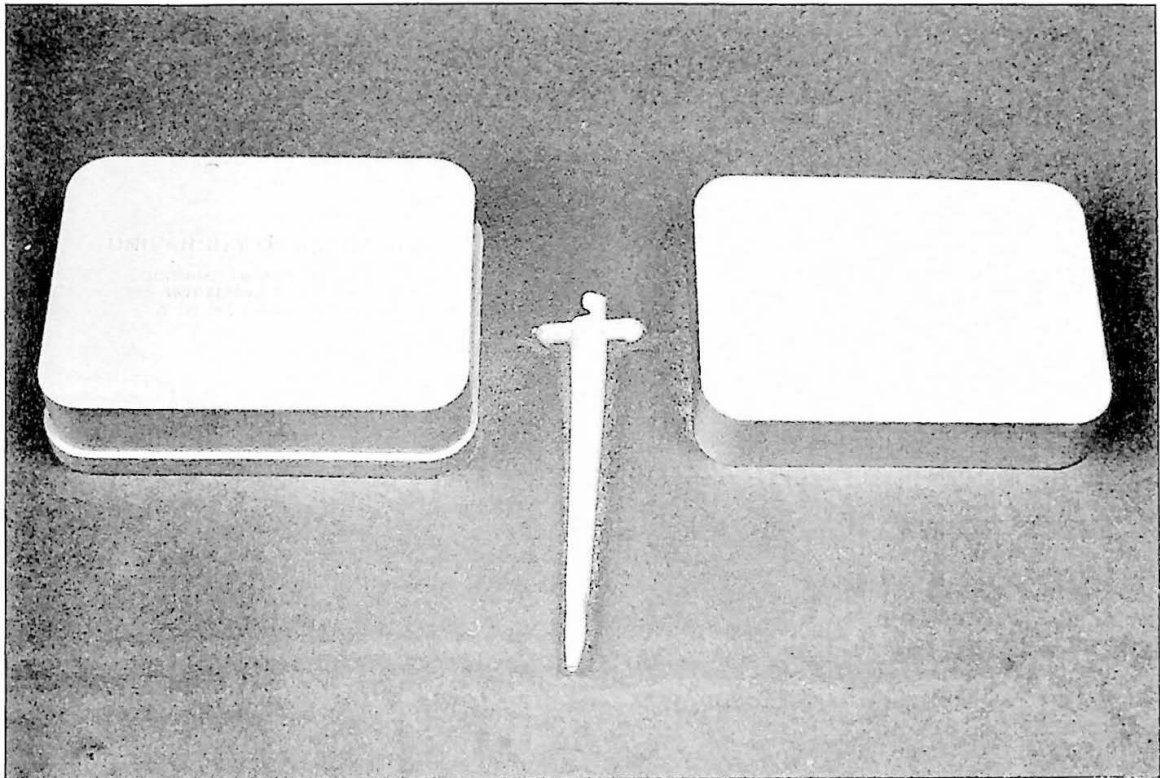


Figure 4.22 a Example of injection moulded container component (external view) and sprue

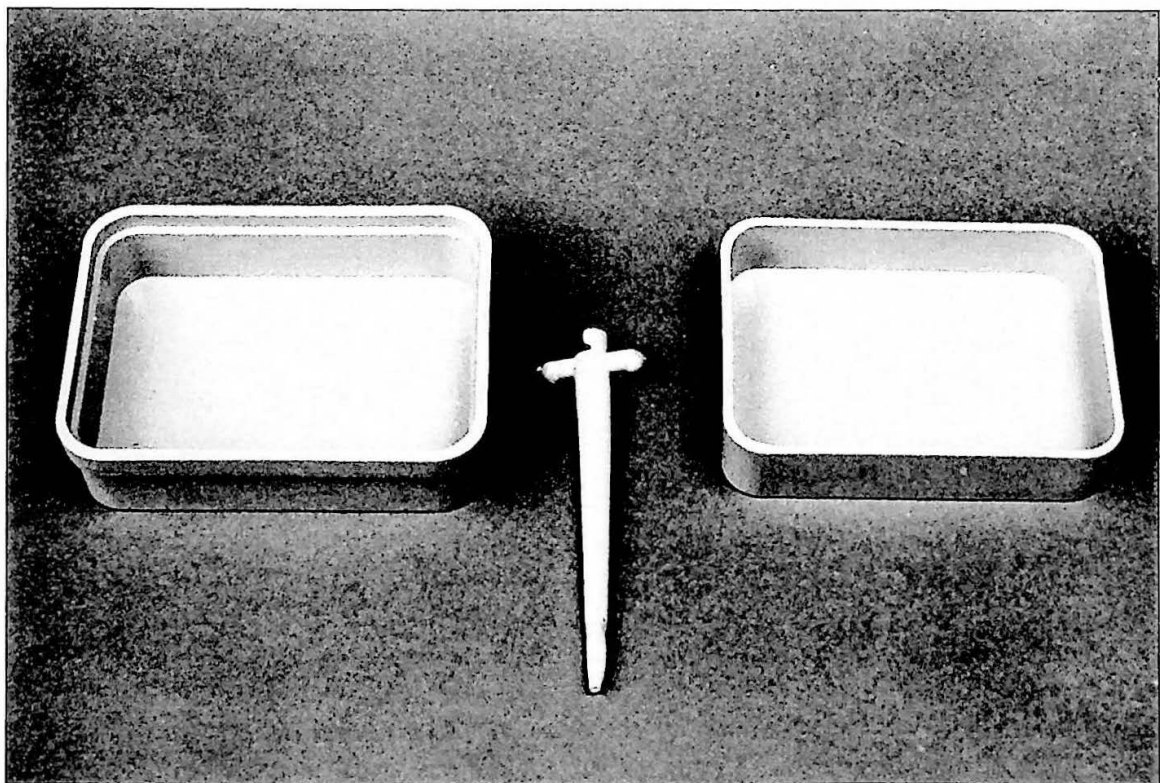


Figure 4.22 b Example of injection moulded container component (internal view) and sprue

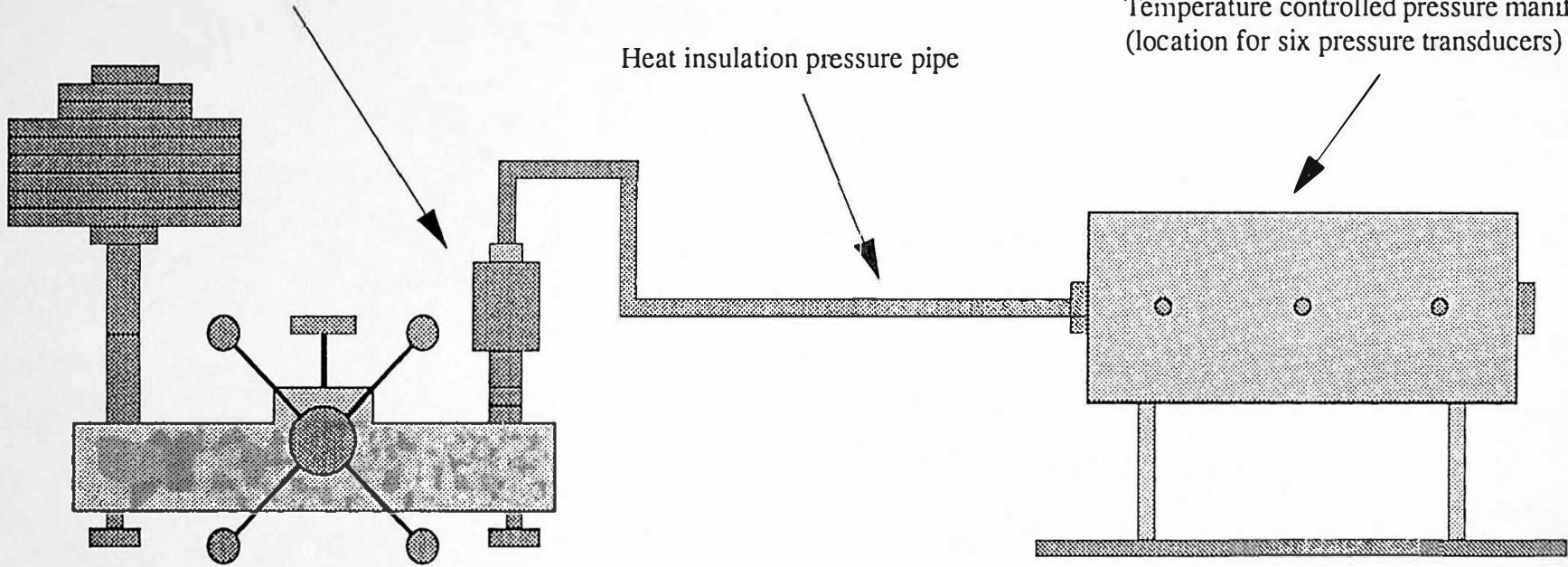
4.5 High Temperature Pressure Transducer Test and Calibration Facility

Pressure transducer assessment and calibration requires pressure testing at operating temperatures. Pressure transducers calibrated at ambient temperature using a Budenburg dead weight tester, are accurate for measuring pressures at ambient temperature, but at operating temperatures the calibration is subject to a constant error (see chapter 5.3) melt pressure transducer assessment for further information. The calibration of pressure transducers at operating temperatures is essential if an absolute measurement of polymer melt pressure is necessary.

The basis of the high temperature test facility was a Budenburg Gauge Company Ltd (Budenburg) dead weight tester model 380HX (N.A.M.A.S. certificate number: T03724 Lab. Ref: 0134, maximum error 0.03%), capable of generating a maximum pressure of 1200 bar \pm 0.36 bar. A manifold block that accommodates six melt pressure transducers was used. Silicon hydraulic fluid was used for the heated manifold block, the silicon fluid had a quoted minimum flash point of 260C, supplied by Century Oils Ltd. The maximum temperature that the oil was heated to was 300C. To prevent contamination between the silicon fluid and the hydraulic oil of the Budenburg dead weight tester a Budenburg diaphragm seal model (3/25) was utilised. The pressure loss due to the seal (Viton sac) is quoted at 0.028 bar maximum. At high operating temperatures leakage from the transducer ports was apparent for some pressure transducers, therefore, Polytetrafluoroethylene (PTFE) tape, melting point $T_m = 327C$, Crawford (1985a p 55) was utilised to reduce the leakage.

The configuration shown in figure 4.23 proved difficult to prime between tests, due to the long capillaries. An improved configuration was then implemented, whereby the manifold block was located directly on the pressure seal. This design proved more successful regarding priming operations.

Diaphragm seal
(prevents contamination between hydraulic fluids)



Budenburg dead weight tester (0 to 1200 bar)

Figure 4.23 Schematic diagram of high temperature pressure transducer calibration and test facility

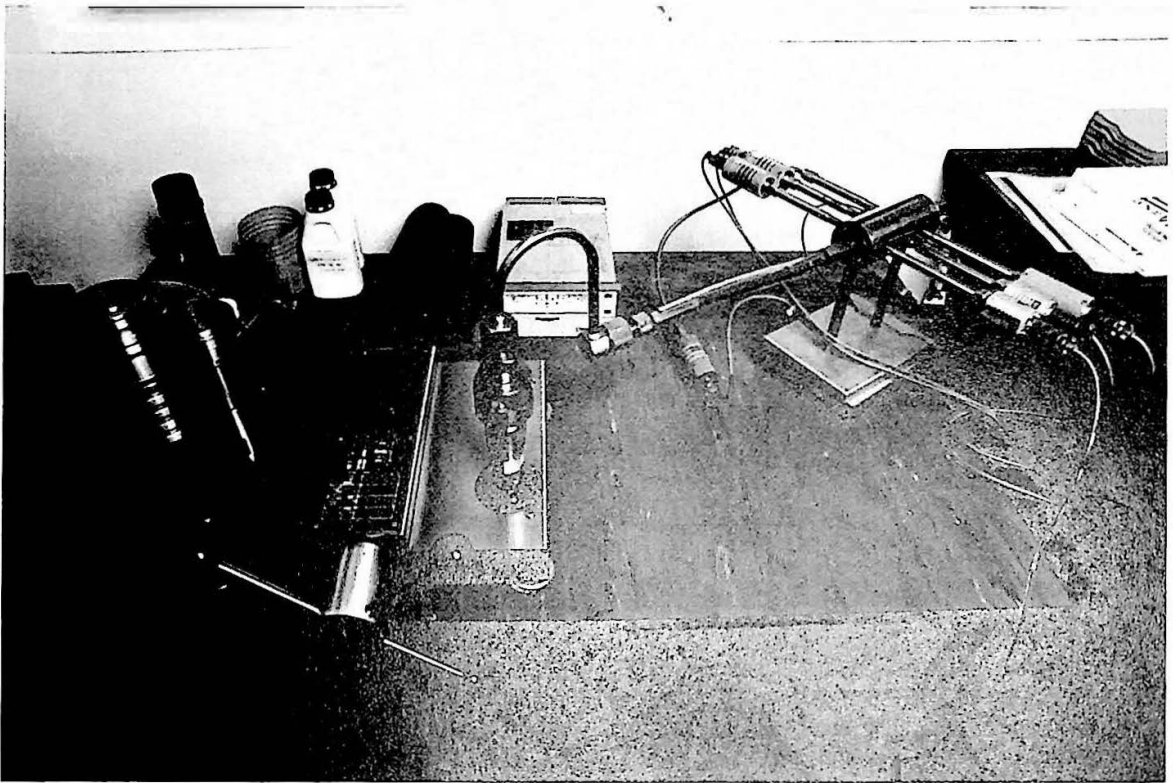


Figure 4.24 High temperature pressure transducer calibration and test facility

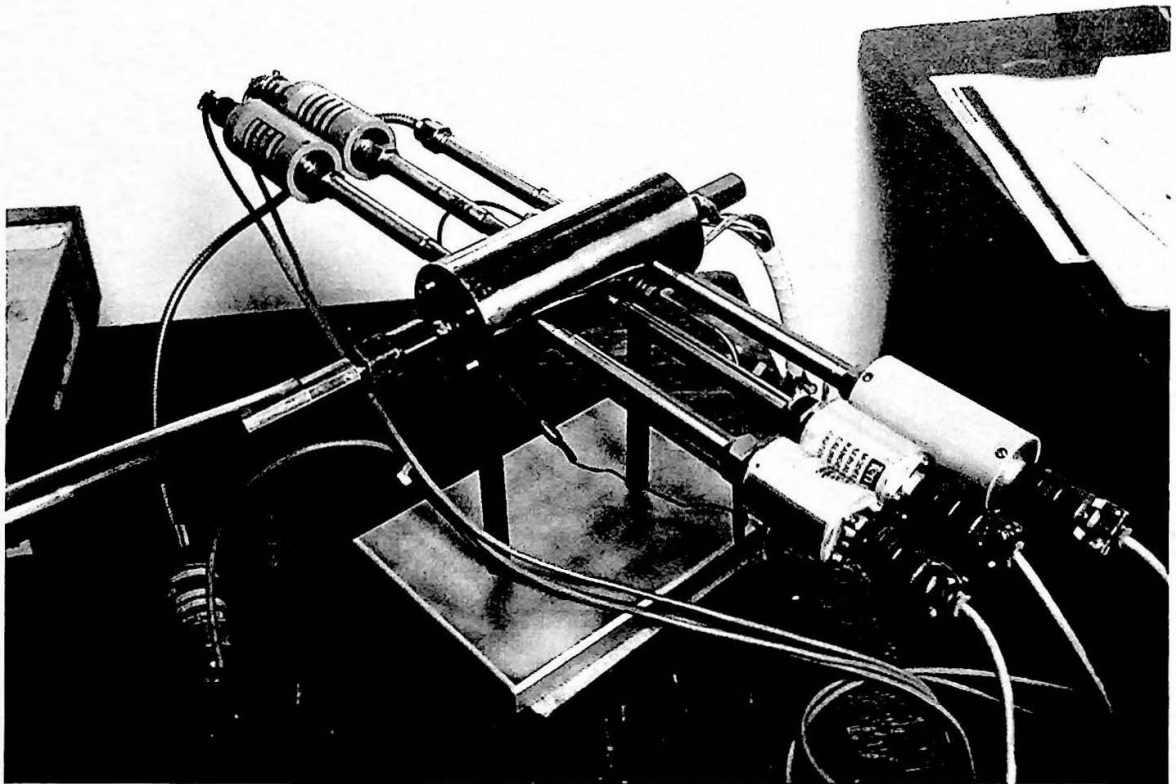


Figure 4.25 Six pressure transducers located in temperature controlled manifold

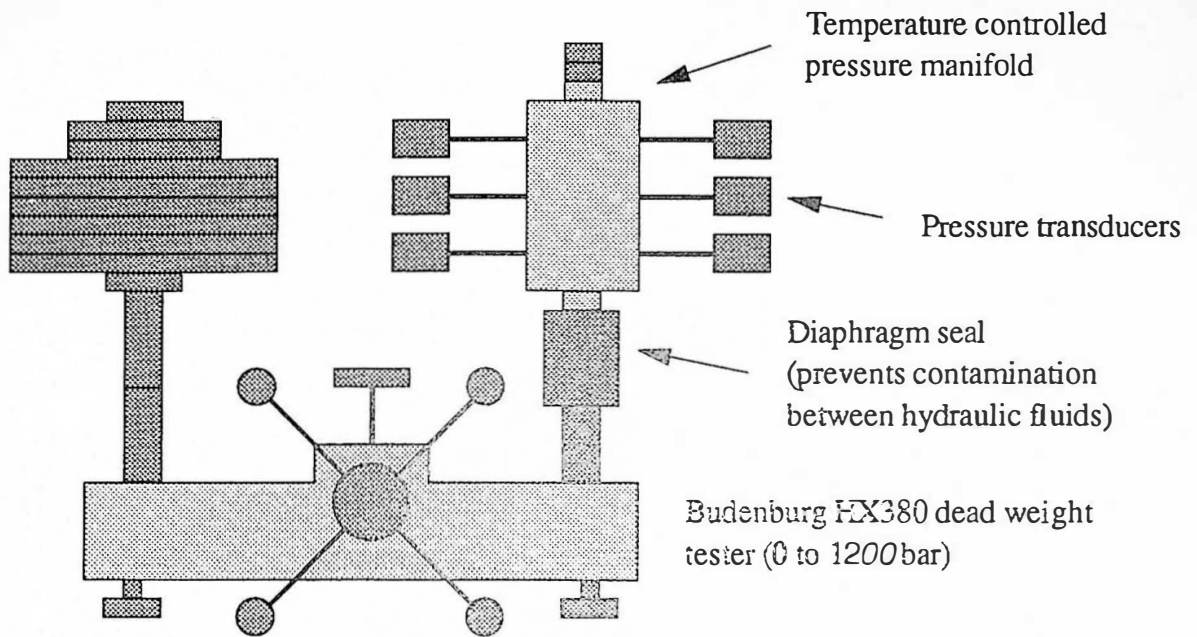


Figure 4.26 Schematic diagram of improved pressure transducer high temperature pressure transducer calibration and test facility

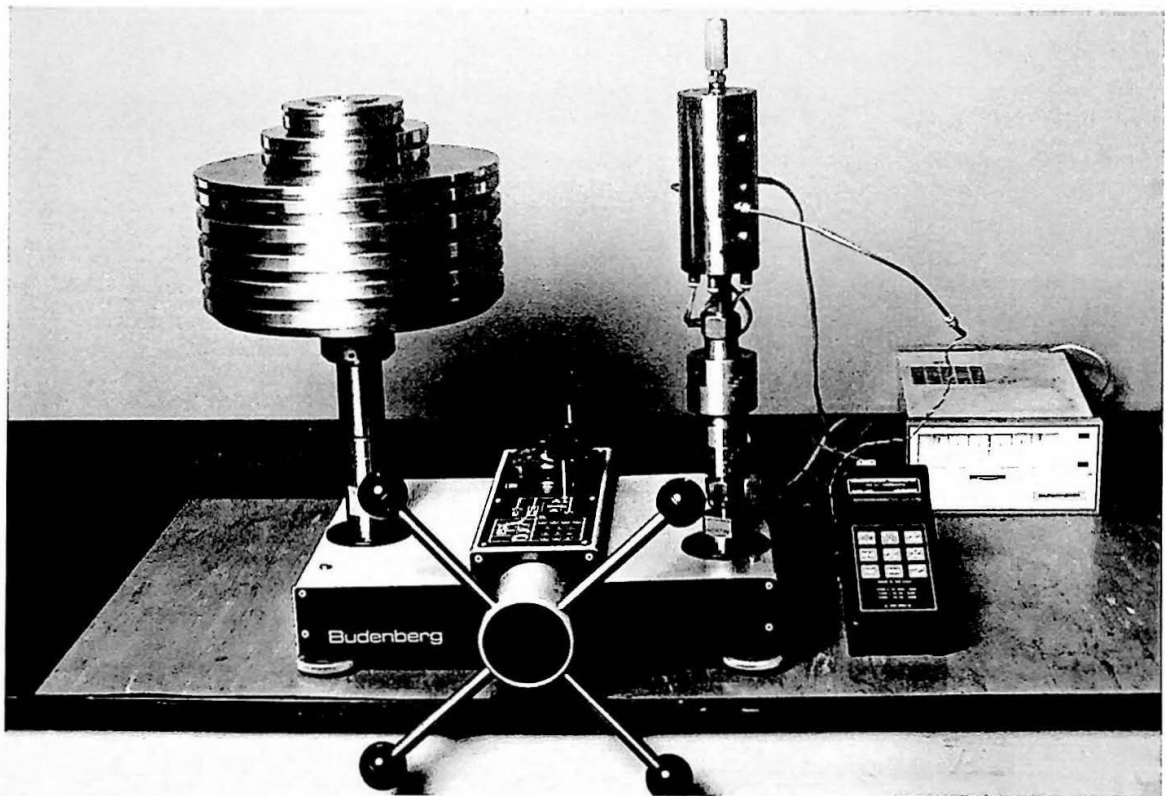


Figure 4.27 Improved high temperature pressure transducer calibration and test facility

4.6 Modification of Screw Velocity Controller Performance of Sandretto 60 Tonne Injection Moulding Machine

The primary injection phase of the injection moulding process is of extreme importance, for in-line process measurements and polymer melt rheology. The primary injection phase is velocity controlled, therefore the quality of this control influences the accuracy and precision of process measurements. The quality of screw velocity control on in-line process measurements was investigated by comparison of two levels of velocity control.

The two levels of velocity control were achieved by modification of the machine velocity controller. Injection screw velocity is controlled by a microprocessor control algorithm called 'Logiflux', patent pending. Hydraulic injection pressure is provided by two variable displacement hydraulic pumps, a large capacity pump providing fast response to large load demands and a small capacity pump providing accurate pressure control. The feedback velocity signal for the control algorithm is achieved by differentiation of the machine's screw position linear variable displacement transducer (LVDT) signal. The accuracy of the machine LVDT signal = ± 0.22 mm (Level A screw displacement accuracy). For the process monitoring this signal was conditioned to an accuracy of ± 0.03 mm, therefore it was possible to use this signal as the feedback control signal. The accuracy of the modified feedback control signal = ± 0.06 mm, (Level B screw displacement accuracy) slightly higher than the process monitored variable, due to instrumentation noise introduced by the machine parameter controller.

CHAPTER 5

Instrumentation for Accurate Process Measurements

5.1 Introduction

Detailed study of the injection moulding process requires the ability to accurately and precisely monitor all relevant machine and process parameters. Instrumentation forms an extremely important part of this monitoring process. Selection of a transducer for a specific process, requires knowledge of the process system dynamics, usually modelled as first or second order systems. The transient response of a transducer is usually reported as a first order time constant for convenience. This selection procedure must also consider process conditions, such as pressure, temperature and environment. Transducer signal conditioning electronic circuitry design must also take in to account system dynamics. This chapter describes the instrumentation used for process monitoring a Sandretto 60 tonne hydraulic injection moulding machine, during experimental moulding tests. Figures 5.1 and 5.2 show a schematic diagram and general view of the instrumented Sandretto 60 tonne injection unit, respectively.

Instrumentation is described for the machine injection unit, beaker tool and container tool. The transducer types, specification and location are described. The reasons for using specific instrumentation are discussed, with an extensive assessment of melt pressure transducers. The practical implications of transducer dynamic response are investigated for displacement and temperature transducers.

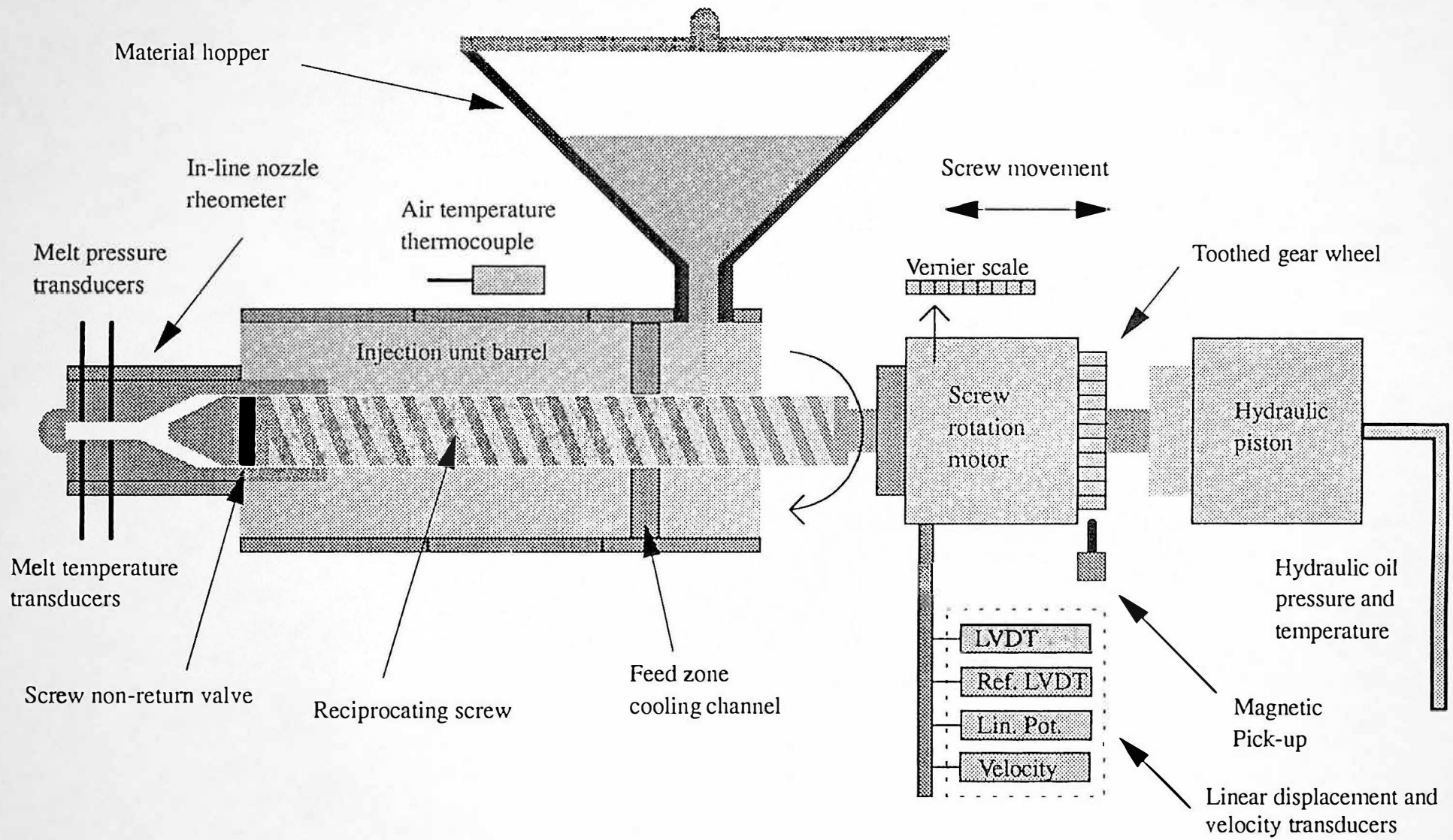


Figure 5.1 Schematic diagram of instrumented injection unit of Sandretto 60 tonne injection moulding machine

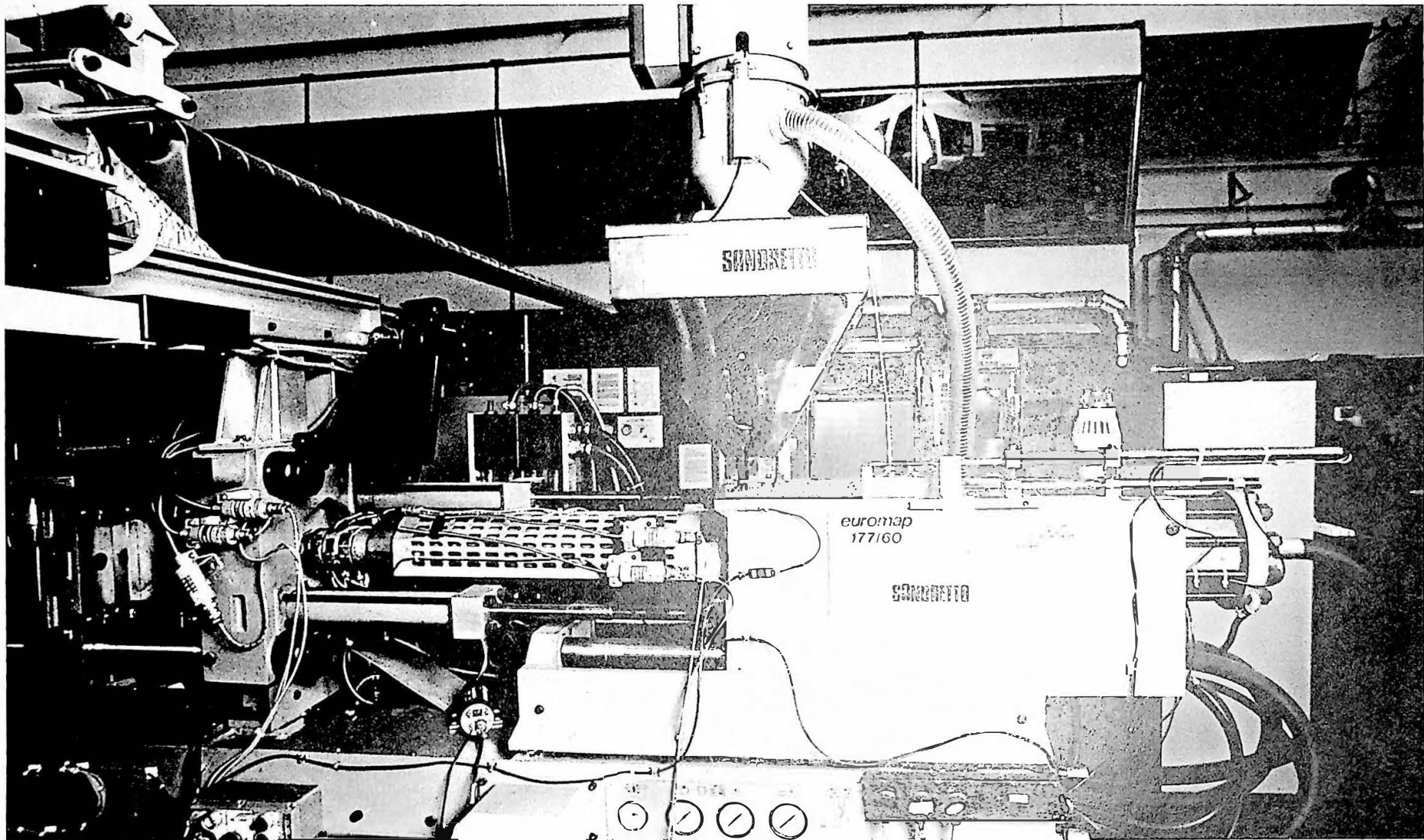


Figure 5.2 General view of instrumented injection unit of Sandretto 60 tonne injection moulding machine

5.2 Transducers for the Process Monitoring System

Table 5.1 describes the process and machine parameter monitoring transducers, for the injection unit of the Sandretto machine. Existing transducers were used in conjunction with additional machine and process transducers. Figures 5.3 and 5.4 show the screw linear displacement and velocity transducers located on the injection unit and screw rotational speed transducer, respectively. Tables 5.2 and 5.3 describe the process and machine parameters for the beaker and container tools, respectively. Figures 5.5 and 5.6 show the transducer locations for the beaker and container tool, respectively. Appendix F and G include details of the beaker and container tool instrumentation locations.

5.2.1 Nozzle Melt Pressure Transducers

The range of commercially available melt pressure transducers is extensive. Diaphragm melt pressure transducers that are capable of functioning reliably in the nozzle of an injection moulding machine. Three main types of diaphragm devices were available during the selection process (1989), liquid filled, force tube and push rod. Since 1992 optical pressure transducers have been available, (see chapter 2.6.1), Dynisco (1992). The presence of melt pressure transducers in the nozzle reservoir bore: (i) may necessitate the nozzle reservoir bore to be modified, allowing accommodation of the melt pressure transducers, which may introduce associated residence time problems, and (ii) increases the possibility of disturbance to polymer melt rheology (flow vortices). During machine process operations, it is not practical to have a range of melt pressure transducers, in the nozzle of an injection moulding machine. Therefore, it was necessary to assess the different melt pressure transducer devices, to determine the most appropriate for processing operations. The pressure transducer assessments are described in chapter 5.3. The Dynisco liquid filled range of melt pressure transducers were chosen, as a result of consistent high accuracy and

precision performance. The Dynisco liquid filled melt pressure transducers have a stated time response of 10 ms.

Description of Transducer (* = existing machine transducer)	Symbolic Name	Location
- Nozzle melt Pressure 1, 0-1379 bar, S/N 270792 Dynisco PT435A, Diaphragm device	NMP 1	Modular Nozzle Rheometer
- Nozzle melt pressure 1, 0-1379 bar, S/N 270790 Dynisco PT435A, Diaphragm device	NMP 2	Modular Nozzle Rheometer
- Nozzle melt temperature, 135-371C, Type J Dynisco MTT935A, Infra-red device	NMT 1	Modular Nozzle Rheometer
- Nozzle melt temperature, -20-500C, Type J Nanmac fast response thermocouple	NMT 2	Modular Nozzle Rheometer
- Nozzle melt temperature, -20-500C, Type J Control Techniques industrial insulated thermocouple	NMT 3	Modular Nozzle Rheometer
* Hydraulic injection pressure, 103 bar Schaevitz P723-001, Diaphragm device	HYDP	Hydraulic Line to Piston
* Injection screw displacement, 0-110 mm CEI, Linear variable differential transformer (LVDT)	SDISP 1	Injection unit
- Reference injection screw displacement, 0 - 150 mm RDP DCT3000C, LVDT	SDISP 2	Injection unit
- Injection screw displacement, 0-200 mm Penny and Giles HLP190, Linear potentiometer	SDISP 3	Injection unit
- Injection screw velocity, 0-100 mm/s RDP, Inductive device, filtered	SVEL 1	Injection unit
- Injection screw velocity, 0-100 mm/s RDP, Inductive device, unfiltered	SVEL 2	Injection unit
* Plasticising screw rotational speed, 0-200 RPM Sandretto, Magnetic pickup	SRPM	Screw rotation motor
- Hydraulic oil temperature Type J thermocouple, -20-500 C	OILT	Hydraulic oil sump
- Air temperature Type J thermocouple, -20-500 C	AIRT	Injection unit

Table 5.1 List of injection unit transducers

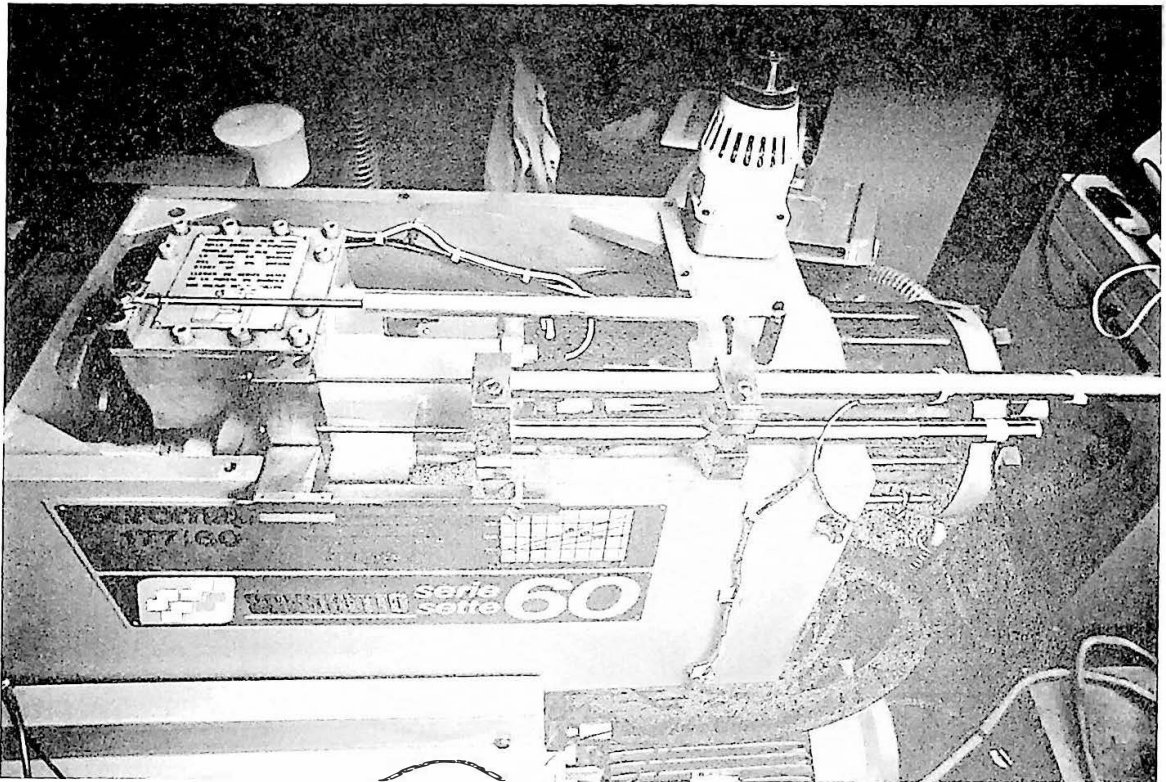


Figure 5.3 Screw linear displacement and velocity transducers located on injection unit

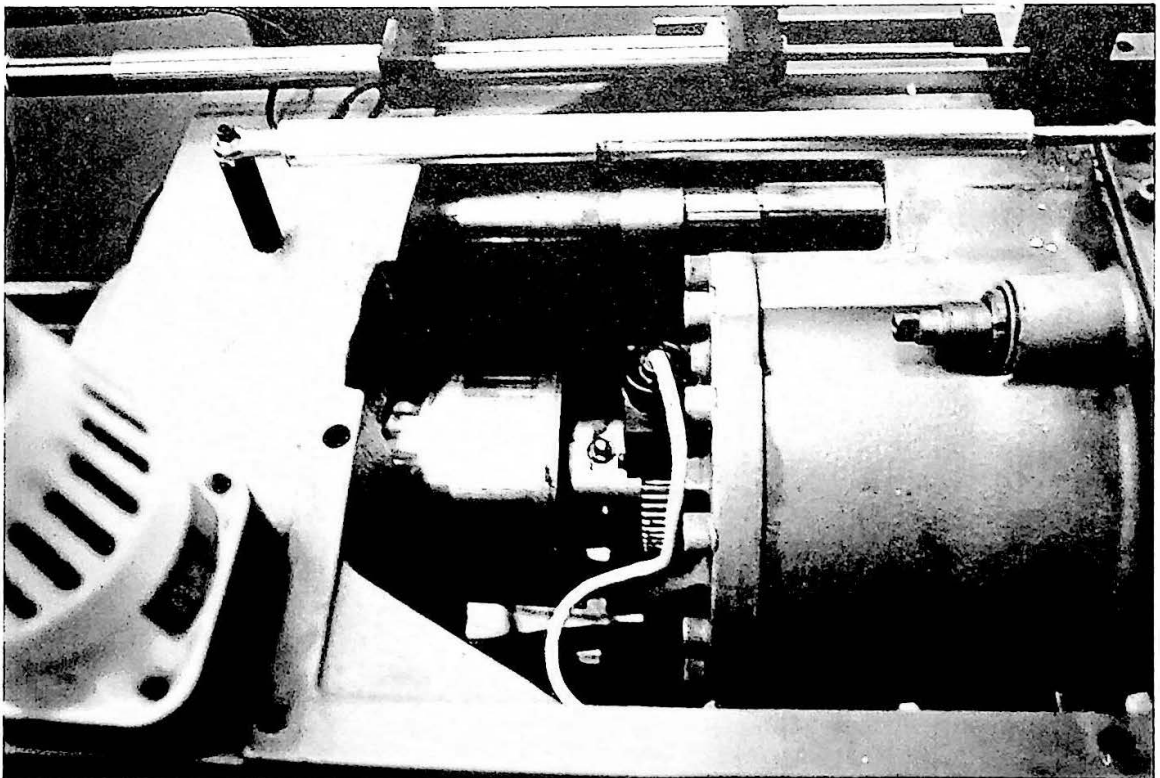


Figure 5.4 Screw rotational speed transducer

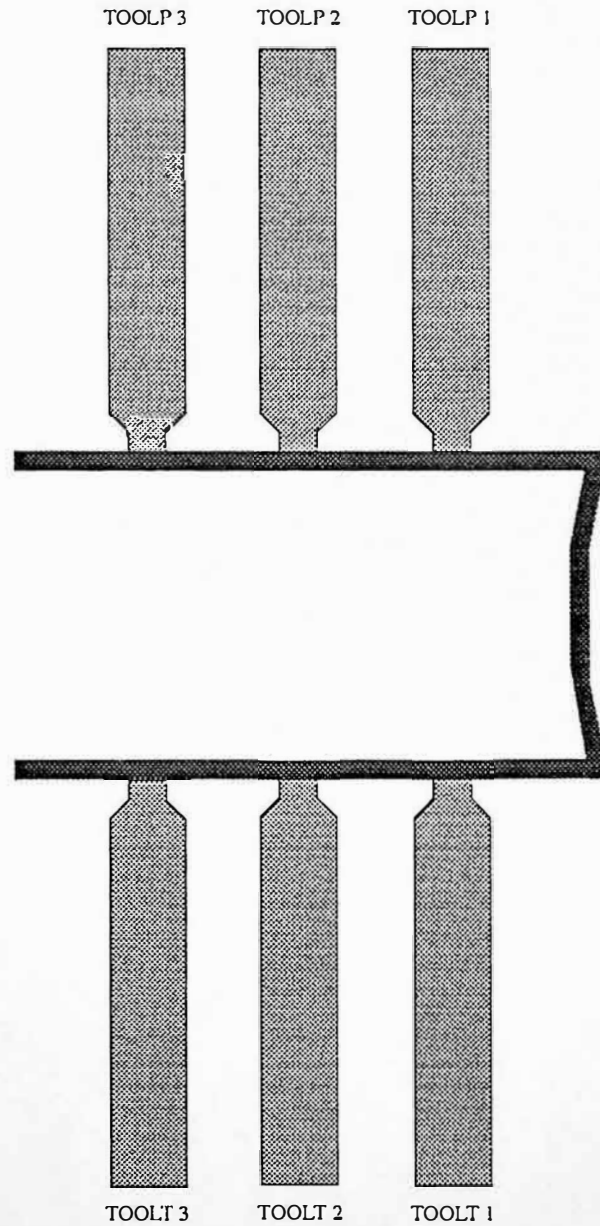
Description of Transducer	Symbolic Name	Location
Tool pressure 1, 0-690 bar, S/N 461333 Dynisco PT422A, Diaphragm device	TOOLP 1	Located 20 mm from beaker base on top flat
Tool pressure 2, 0-690 bar, S/N 461331 Dynisco PT422A, Diaphragm device	TOOLP 2	Located 40 mm from beaker base on top flat
Tool pressure 3, 0-690 bar, S/N 462293 Dynisco PT422A, Diaphragm device	TOOLP 3	Located 60 mm from beaker base on top flat
Tool temperature 1, -20-500 C Dynisco, Type J Thermocouple	TOOLT 1	Located 20 mm from beaker base on bottom flat
Tool temperature 2, -20-500 C Dynisco, Type J Thermocouple	TOOLT 2	Located 40 mm from beaker base on bottom flat
Tool temperature 3, -20-500 C Dynisco, Type J Thermocouple	TOOLT 3	Located 60 mm from beaker base on bottom flat

Table 5.2 List of beaker tool transducers

Description of Transducer	Symbolic Name	Location
Tool temperature 1 Type T Thermocouple, 0-400 C	TOOLT 1	Bottom of cavity Plate
Tool temperature 2 Type T Thermocouple, 0-400 C	TOOLT 2	Middle of cavity Plate
Tool temperature 3 Type T Thermocouple, 0-400 C	TOOLT 3	Top of cavity Plate
Tool temperature 4 Type T Thermocouple, 0-400 C	TOOLT 4	Bottom of core plate
Tool temperature 5 Type T Thermocouple, 0-400 C	TOOLT 5	Middle of core plate
Tool temperature 6 Type T Thermocouple, 0-400 C	TOOLT 6	Top of core plate
Tool temperature 7 Type T Thermocouple, 0-400 C	TOOLT 7	Cavity plate feed

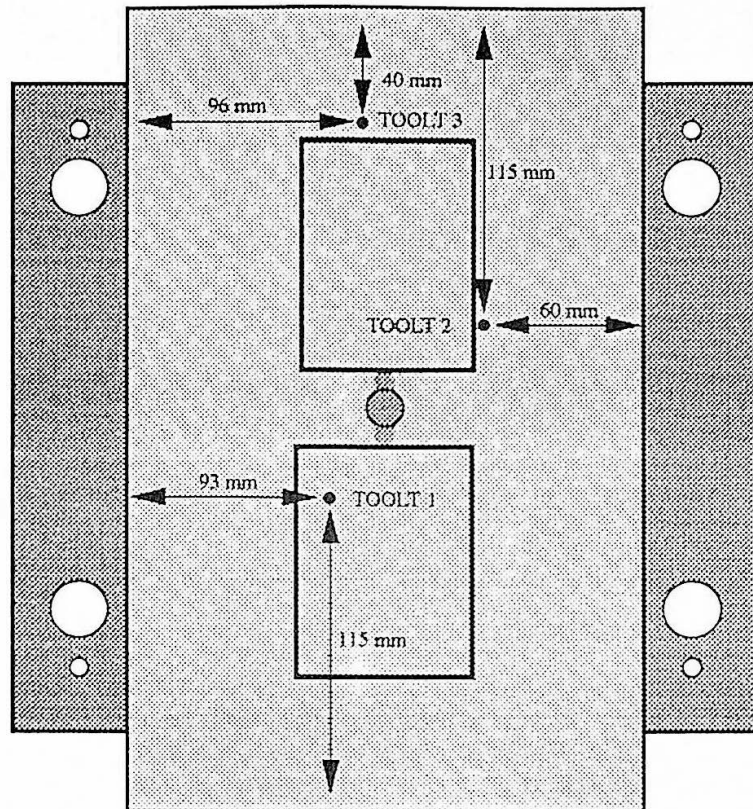
Table 5.3 List of container tool transducers

Tool Cavity Melt Pressure Transducers

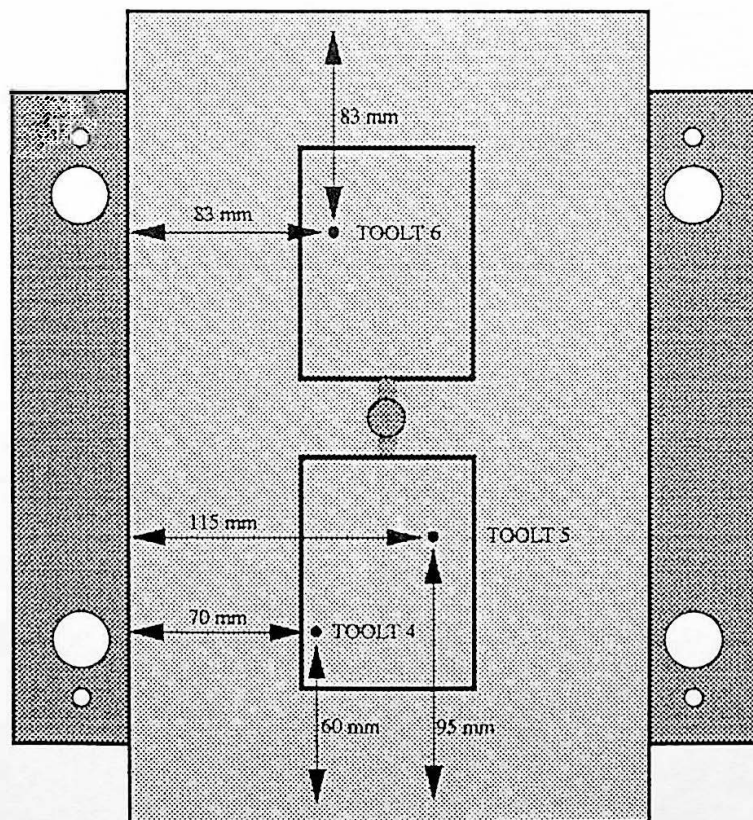


Tool Cavity Melt Temperature Transducers

Figure 5.5 Schematic diagram of beaker tool instrumentation for cavity pressure and temperature measurements



Core Plate - Moving Platen



Cavity Plate - Fixed Platen

Thermocouples located approximately 4 mm below tool surface
 Impression corners are shown square for convenience
 Impression (corners are radii of 10 mm), Water Cooling Manifolds are not shown

Figure 5.6 Schematic diagram of container tool instrumentation for cavity and core plates

5.2.2 Nozzle Melt Temperature Transducers

The measurement of nozzle melt temperature requires a transducer with an adequate dynamic response. Chapter 5.3.3. describes the dynamic calibration of a 1 mm diameter insulated thermocouple and typical industrial nozzle thermocouple, the first order response times for these thermocouples were 0.21 and 2.30 seconds respectively. Appendix K describes a design that accommodates a 1 mm diameter insulated thermocouple in the nozzle rheometer bore, Speight and Coates (1990). A dynamic response time constant of 0.21 seconds is not adequate for monitoring the injection moulding process, therefore a Dynisco infra-red temperature transducer and Nanmac fast response thermocouple were utilised. The Nanmac thermocouple is currently being assessed. The Dynisco infra-red temperature transducer was utilised for the reported work. The infra-red temperature transducer has the following advantages over conventional devices: (i) non-intrusive, (ii) not affected by the surrounding nozzle temperature, (iii) first order time constant of 10 ms, (iv) gives an accurate and repeatable measurement of actual melt temperature beyond the reservoir wall, (v) robust for industrial environments.

5.2.3 Screw Linear Displacement and Velocity Transducers

The measurement of screw displacement is not restricted by the number of usable transducers, as linear displacement transducers have negligible coefficients of friction, compared to the screw injection unit. Direct comparisons can be made between linear displacement transducer technologies simultaneously, during the experimental tests. The number of melt pressure transducers is restricted during experimental tests, due to the nozzle geometry and possible disturbances to polymer melt rheology. Therefore, pressure transducer technologies need to be assessed off-line, see chapter 5.3.

5.3 Melt Pressure Transducer Assessment

The Dynisco range of liquid filled (mercury) pressure transducers were utilised, as performance was combined with flexible mounting. Transducer performance was investigated using the original configuration of the high temperature pressure transducer test and calibration facility (see chapter 4.5). Liquid filled, force tube and push rod pressure transducers were assessed, these three technologies are diaphragm devices, due to their robustness and ability to operate at typical nozzle melt pressures and temperatures. Piezoelectric and piezoresistive pressure transducers are presently more suited to measure cavity melt pressures. Research by Baker et al (1990) assesses the performance of liquid filled, force tube and push rod pressure transducers. The conclusions state that the push rod pressure transducer (Gentran GT76/6D8-10M) performance fell far short of the liquid filled and force tube devices and that the force tube device has a performance equal to or even better than the liquid filled devices. The performance of pressure transducer technologies was not definite, therefore an independent assessment was necessary.

The transducers tested were a Dynisco PT422A (liquid filled), Terwin 1076 (force tube) and Dynisco PT411 (push rod), each with an operating pressure range of 0 - 690 bar. The transducers were tested for linearity, hysteresis, repeatability, zero shift with temperature change and zero sensitivity shift with temperature change. The results of the pressure transducer assessments are shown in table 5.4. The values reported are the maximum errors that occurred, for the full pressure range of the transducers (0 - 680 bar) at 200C. Repeatability was assessed by successively increasing pressure to 340 bar from zero bar, for ten measurements. The Dynisco PT422A liquid filled pressure transducer resulted in the highest performance for each category, as shown in table 5.4. The liquid filled devices also offered the best mounting flexibility, with the ability to locate in a limited space, Dynisco PT435A nozzle melt pressure transducer.

Transducer Technology	Linearity (% FSR)	Hysteresis (% FSR)	Repeatability (\pm % FSR)	Zero Shift (% FSR / C)	Sensitivity Shift (% FSR / C)
Liquid Filled	-1.18	-0.16	0.04	1.02×10^{-3}	0.03
Force Tube	4.31	0.22	0.06	9.45×10^{-3}	0.06
Push rod	3.72	0.44	0.23	2.04×10^{-2}	0.32

(FSR = Full Scale Range)

Table 5.4 Performance of different pressure transducer technologies at 200C

Table 5.4 shows maximum linearity error as a percentage of full scale range (FSR). The assessments of linearity are referenced to the internal calibration of the individual pressure transducers (R-CAL, internal shunt calibration resistor, for the fully active strain gauge bridge), at ambient temperature. Figure 5.7 shows the maximum percentage linearity errors of the full scale pressure range (FSR), versus manifold temperature, for the three pressure transducer technologies. The maximum percentage linearity error correction, at 200C, is 0.32% for the liquid filled pressure transducer, compared to 1.73 and 4.92 %, for the push rod and force tube pressure transducers, respectively. The linearity results for the liquid filled device show that the internal calibration or the calibration of the dead weight tester may be the reason for the -1.18 % FSR error. Figure 5.8 shows the influence of a step temperature change, ambient temperature to 250C, on the pressure transducers zero values. The liquid filled pressure transducer shows the best performance.

Calibration of melt pressure transducers at ambient temperature using a Budenburg dead weight tester, reduces errors resulting from the influence of temperature and the pressure transducer internal calibration. The percentage linearity errors for the liquid filled pressure transducer is low compared to the percentage linearity errors for the push rod and force tube pressure transducers. Figure 5.7 shows that calibration at actual operating temperature is required for an absolute assessment of nozzle melt pressure.

Figure 5.7 Maximum linearity error for full pressure range of three pressure transducer technologies

Pressures 0, 100, 200, 300, 400, 500, 600 and 680 bar

Calculation based on pressure transducer internal calibration facility (R-CAL)

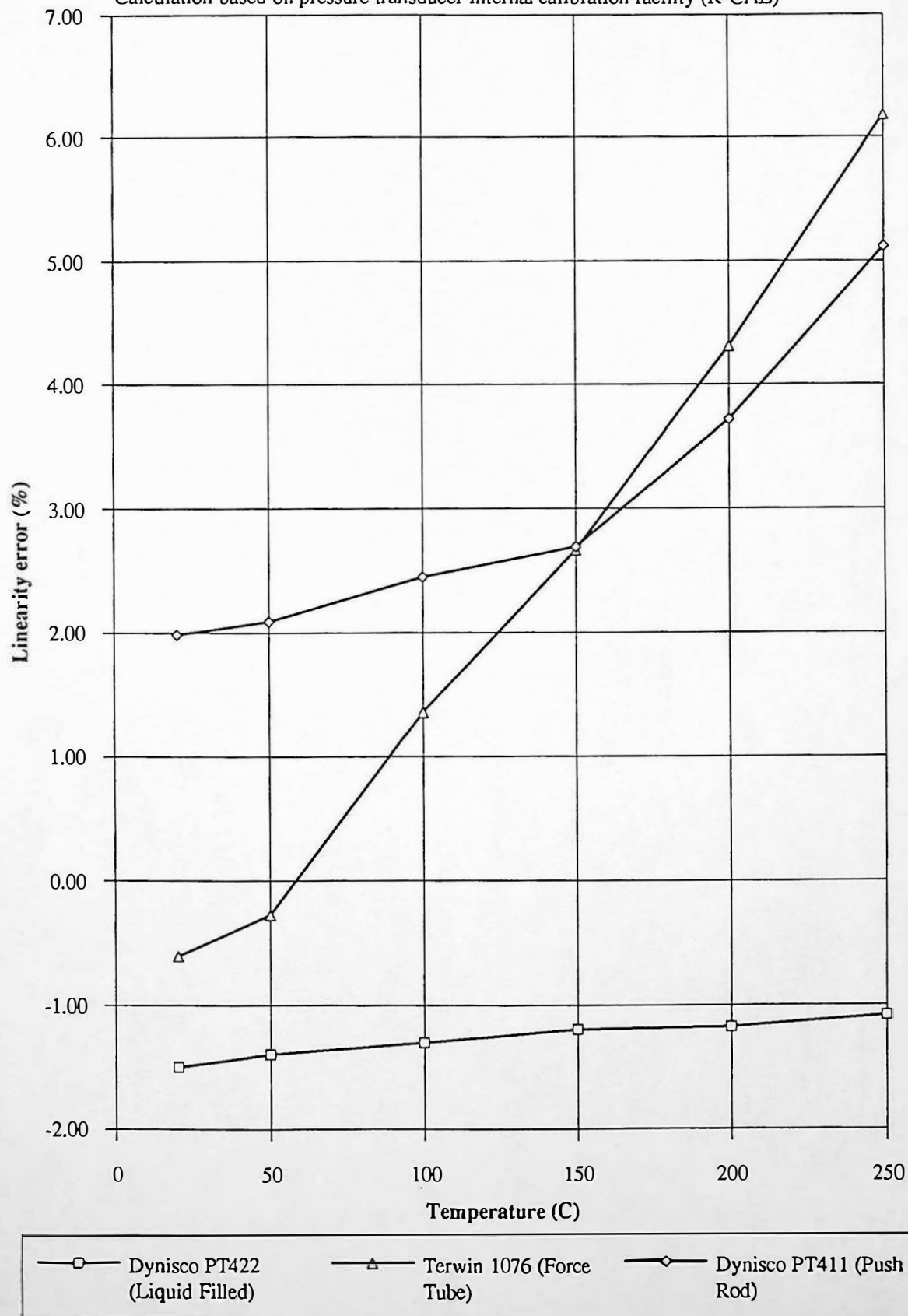
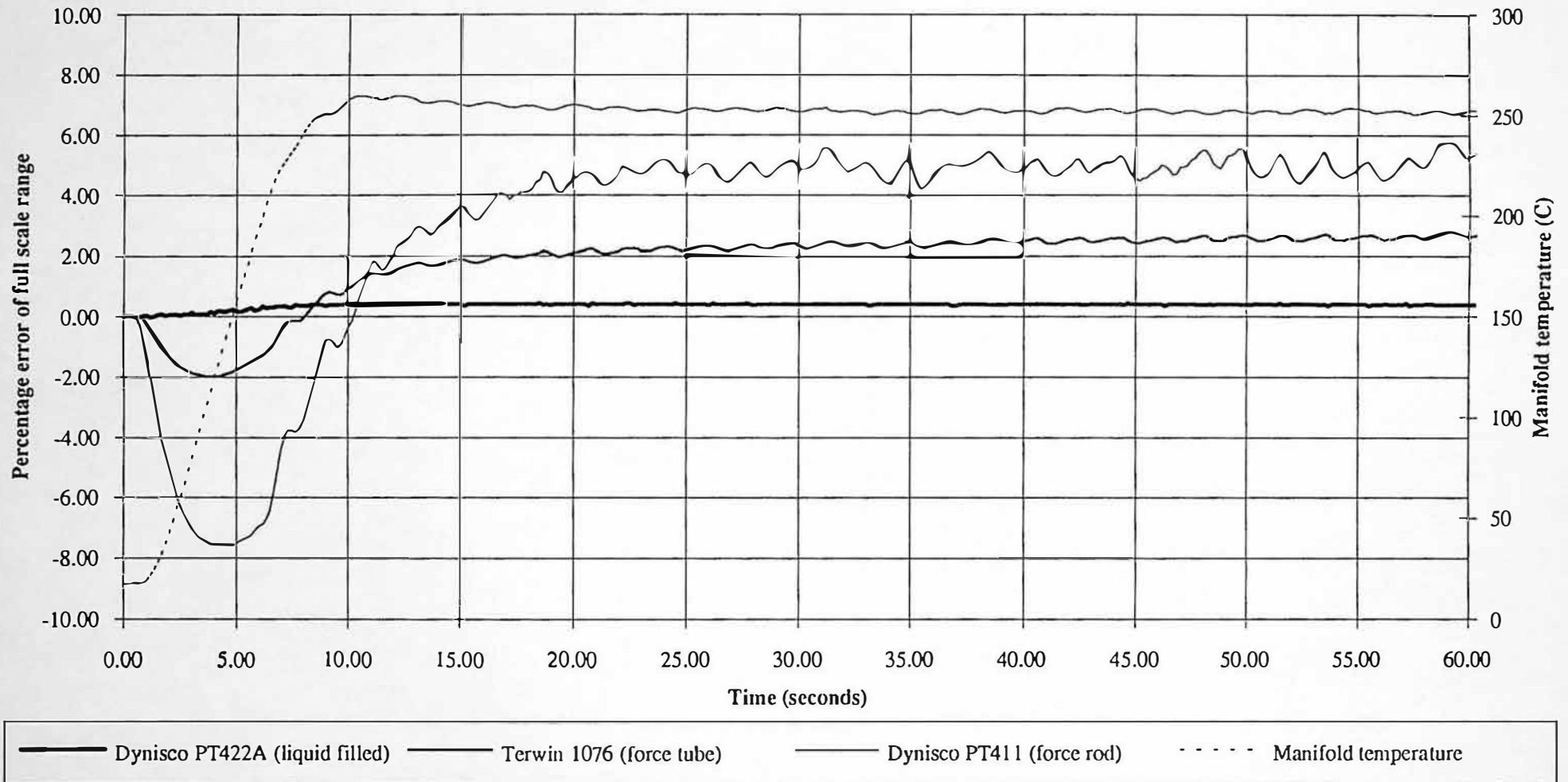


Figure 5.8 Influence of step temperature change on zero pressure values for three different technology pressure transducers



5.4 Transducer Signal Conditioning

Transducer signal conditioning is extremely important for accurate and precise process monitoring, Carr (1991) and Fulcher (1991). The level of signal noise influences measurement precision, and should therefore be minimised. The reduction of signal noise must be accomplished by proper frequency analysis of the transducer output, using an oscilloscope. The specific frequencies that signal noise occurs were identified. The signal conditioning electronic circuitry should filter signal noise at these specific frequencies, unless they conflict with the system dynamic frequency response. The level of signal conditioning achieved was extremely good, operating at the limits of the data acquisition system, i.e. ± 1 DEN (Digital Equivalent Number). Table 5.5 shows details of the signal conditioning circuitry.

Description of Transducer (* = existing machine transducer)	Symbolic Name	Signal Noise	Calibrated Range	Sensitivity \pm unit / DEN
- Nozzle Melt Pressure Transducer	NMP 1	± 1 DEN	0-1200 bar	0.34 bar
- Nozzle Melt Pressure Transducer	NMP 2	± 1 DEN	0-1200 bar	0.34 bar
- Tool Cavity Pressure Transducer	TOOLP 1	± 1 DEN	0-680 bar	0.17 bar
- Tool Cavity Pressure Transducer	TOOLP 2	± 1 DEN	0-680 bar	0.17 bar
- Tool Cavity Pressure Transducer	TOOLP 3	± 1 DEN	0-680 bar	0.17 bar
* Hydraulic Injection Pressure	HYDP	± 1 DEN	0-110 bar	0.030 bar
* Screw Displacement	SDISP 1	± 1 DEN	0.4-53.4 mm	0.025 mm
- Reference Screw Displacement	SDISP 2	± 1 DEN	0.4-53.4 mm	0.025 mm
- Screw Displacement	SDISP 3	± 1 DEN	0.4-53.4 mm	0.016 mm
* Screw Displacement	SDISP 4	± 1 DEN	0.4-11.7 mm	0.003 mm
- Screw Velocity	SVEL 1	± 2 DEN	10-60 mm/s	0.016 mm/s
* Screw Rotational Speed	SRPM	± 2 DEN	0-200 RPM	0.05 RPM

Table 5.5 Signal conditioning of machine and process monitoring transducers

The analogue signals were conditioned for the range 0 to 10.24 Volts. The choice of 10.24 volts assisted in maintaining a low signal/noise ratio. The output of the signal conditioning circuits were voltage followed to prevent, (i) the analogue signal conditioning and digital data acquisition circuitry from being damaged, and (ii) the signal conditioning circuitry from being 'over-loaded' and possible damage.

Description of Transducer	Symbolic Name	Description of Signal Conditioning Circuitry
Nozzle and Tool Melt Pressure Transducers	NMP and TOOLP	Radio Spares strain gauge amplifier
Hydraulic Injection Pressure	HYDP	Operational Amplifier First order low pass passive filter
Screw Displacement	SDISP1	Level Detector ($f_o = 2.4$ KHz) Second order Butterworth active filter
Reference Screw Displacement	SDISP2	First order low pass active filter
Screw Displacement	SDISP3	Operational amplifier
Screw Displacement	SDISP4	Operational amplifier First order low pass active filter
Screw Velocity Filtered	SVEL1	None
Screw Velocity Unfiltered	SVEL2	First order low pass active filter
Screw Rotational Speed	SRPM	Frequency to voltage converter Fourth order Butterworth active filter

Table 5.6 Signal conditioning circuitry of Sandretto injection moulding machine

5.5 Transducer Calibration

The transducers used for data acquisition were calibrated under static conditions. The dynamic response of displacement and temperature transducers were investigated. The measured quantity to DEN (digital equivalent number) relationships, were modelled using a fourth order polynomial curve fit, for transducer calibration.

5.5.1 Pressure Transducers (Static Calibration)

Pressure transducers were calibrated using the improved configuration high temperature pressure transducer test and calibration facility (see chapter 4.5), shown in figures 4.26 and 4.27, based on a Budenburg dead weight tester. The two nozzle and three tool pressure transducers were calibrated for ambient temperature and for typical operating temperatures. Table 5.6 shows details of calibration pressure and temperature values. The nozzle melt pressure transducers were calibrated for the pressure range 0-1200 bar, and tool cavity pressure transducers 0-680 bar. The Budenburg dead weight tester generates a maximum pressure of 1200 bar. The calibration data for each pressure transducer, at different temperatures formed the basis of a pressure transducer calibration 'look-up' table. The pressure to digital equivalent number (DEN) relationships for the pressure transducers were modelled using a fourth order polynomial curve fit, for calibration purposes.

Transducer Location	Pressure Range	Temperature Range
Nozzle Melt Pressure	0-1200-0 bar, 100 bar increments	20C , 150-250C, 10 C increments (215C additional for POM)
Tool Cavity Melt Pressure	0-680-0 bar, 100 bar increments	20-120 C, increments of 10 C

Table 5.7 Pressure transducer calibration information

5.5.2 Displacement Transducers (Static/Dynamic Calibration)

Static Calibration, The displacement transducers were calibrated using a vernier measuring scale (accuracy 0.02 mm), attached to the injection unit. Figure 5.9 shows the linear displacement and velocity transducers located on the machines injection unit.

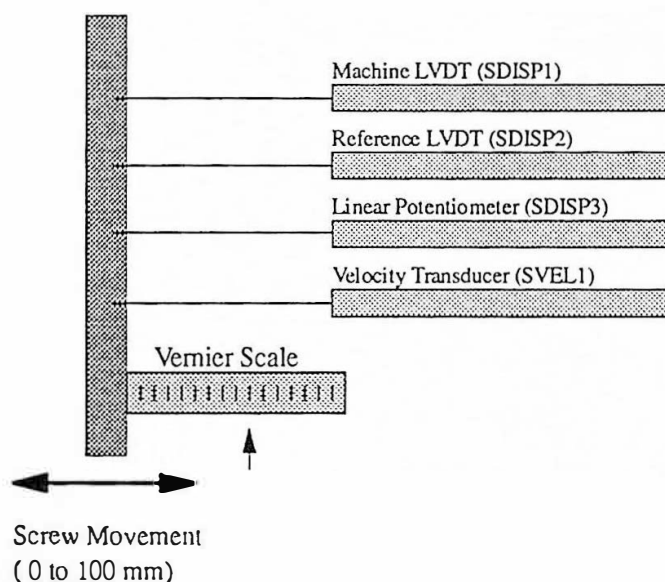


Figure 5.9 Schematic diagram of screw displacement and velocity transducers located on the injection unit

Dynamic Calibration, The dynamic response of the screw displacement measurements was investigated, following work by Sivakumar (1986 p 123), outlining possible problems with the dynamic response of LVDT. The measured screw displacement obtained from the linear potentiometer and CEI LVDT were compared. Figure 5.10 shows the steady state mean screw displacement error for increasing screw injection velocity (10 to 97 mm/s). It is apparent that the LVDT measurement lags the potentiometer measurement, with increasing magnitude for increasing screw injection velocity. Figure 5.11 shows the steady state screw displacement error for an injection velocity of 97 mm/s. The mean steady state error = -1.13 mm, for the time period $t = 0.10$ to 0.34 seconds.

Figure 5.10 Steady state dynamic error lag of LVDT measurements referenced to linear potentiometer measurements

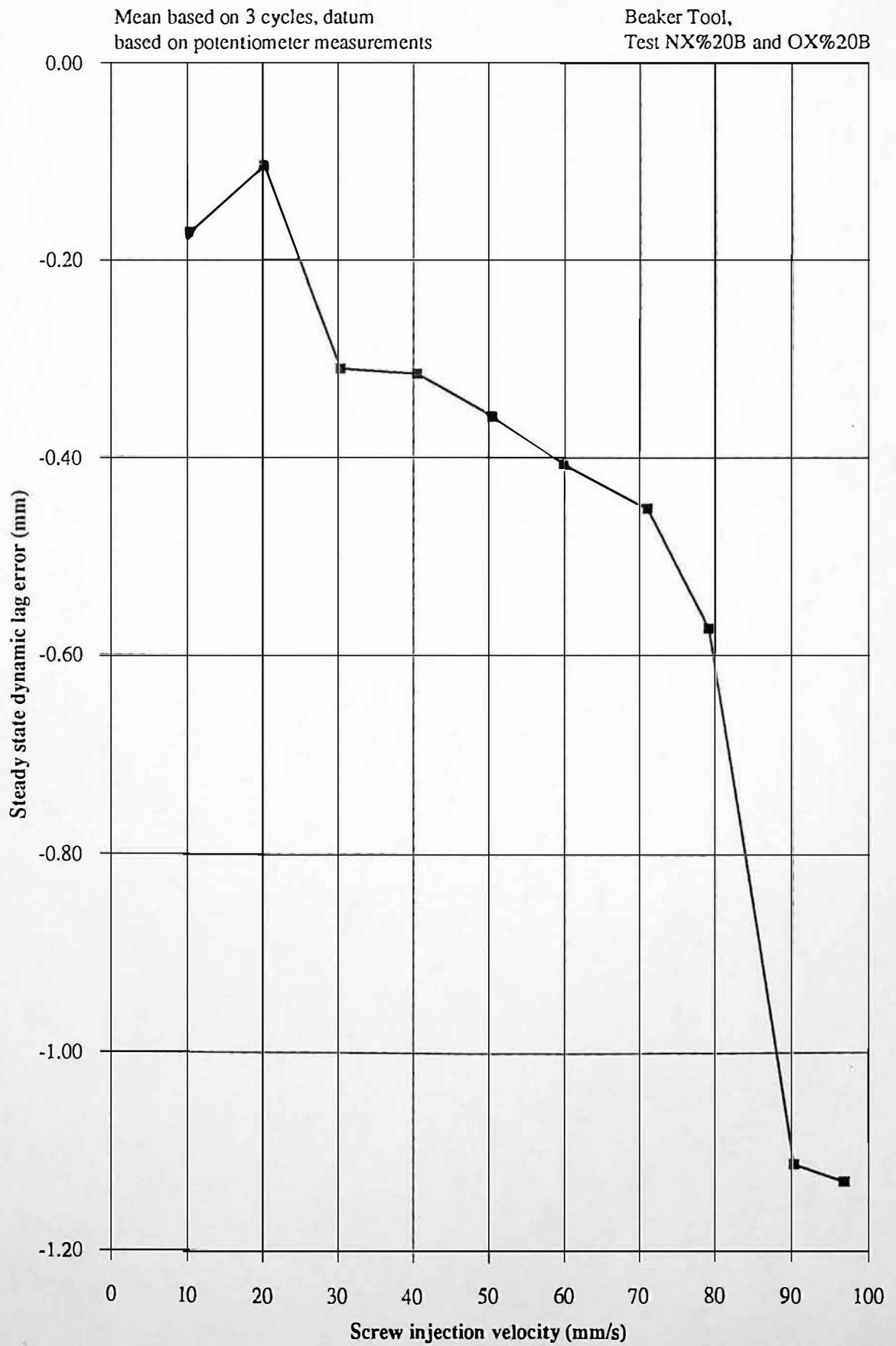
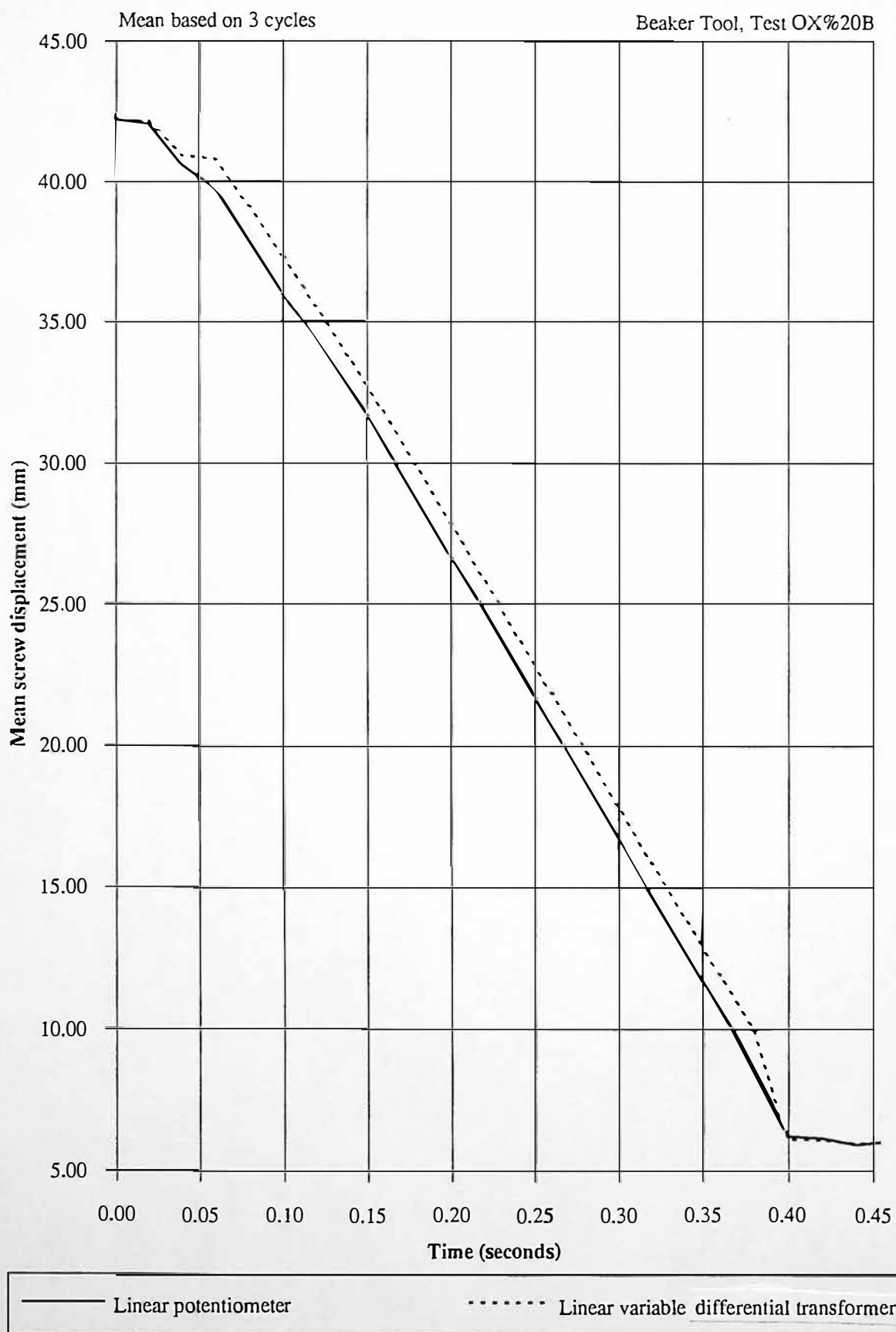


Figure 5.11 Dynamic response of LVDT and linear potentiometer transducers for an injection screw velocity of 97 mm/s



During typical moulding conditions injection velocities of 10 to 70 mm/s are used, the maximum error for this range is -0.41 at 60 mm/s. The steady state error between LVDT and potentiometer increases significantly between 70 and 80 mm/s.

The potentiometer displacement values were used for calibration of the velocity transducer. The potentiometer was shown to have a better dynamic response, as it led the LVDT response. The velocity transducer was calibrated for static conditions, i.e. at constant velocity, the dynamic response of the LVDT would not cause significant errors at constant velocity.

5.5.3 Temperature Transducers (Static/Dynamic Calibration)

Static Calibration, The temperature transducers were calibrated by use of standard linearisation tables. Thermocouples and an infra-red temperature transducer were used, the Infra red transducer having a type 'J' thermocouple output. The thermocouple outputs were calibrated using standard linearisation tables. The tables consist of fourth order polynomial coefficients, curve fitted for different temperature ranges, Biodata (1990). The type 'T' thermocouples were linearised for the temperature range 0 to 400C, with an accuracy of -0.15 to +0.17C. The type 'J' thermocouples were linearised for the temperature range -20 to 500C, with an accuracy of -0.07 to +0.06C.

Dynamic Calibration, Figures 5.12 and 5.13 show the dynamic response of a 1 mm diameter type 'J' thermocouple for a temperature step change, compared to an industrial nozzle thermocouple. The first order time constant of the 1 mm diameter thermocouple = 0.21 seconds compared to 2.30 seconds for the industrial nozzle thermocouple. The 1 mm thermocouple response is faster than the predicted first order response, and possibly indicates a damped higher order system.

Figure 5.12 Dynamic response of 1 mm diameter thermocouple to temperature step change

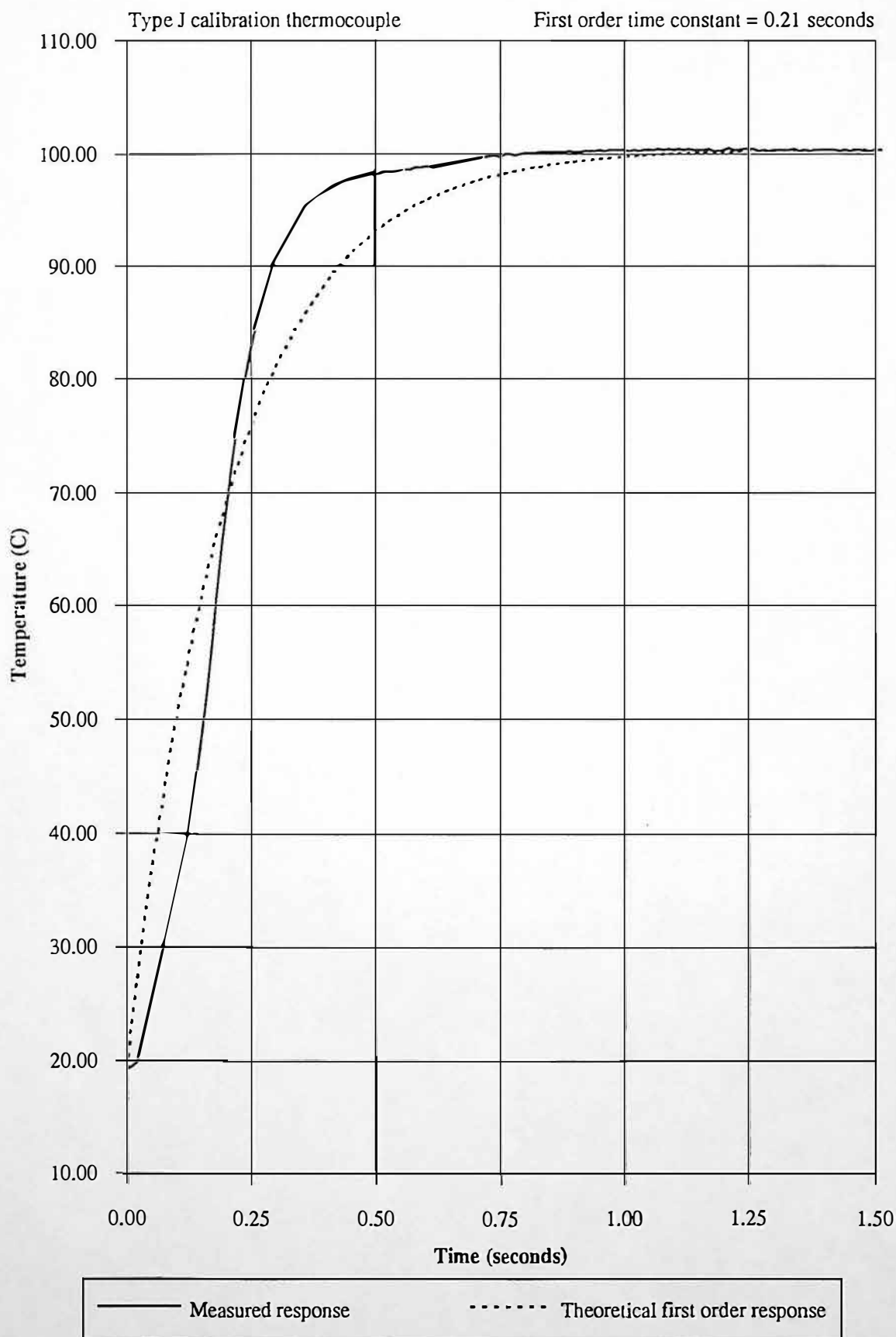
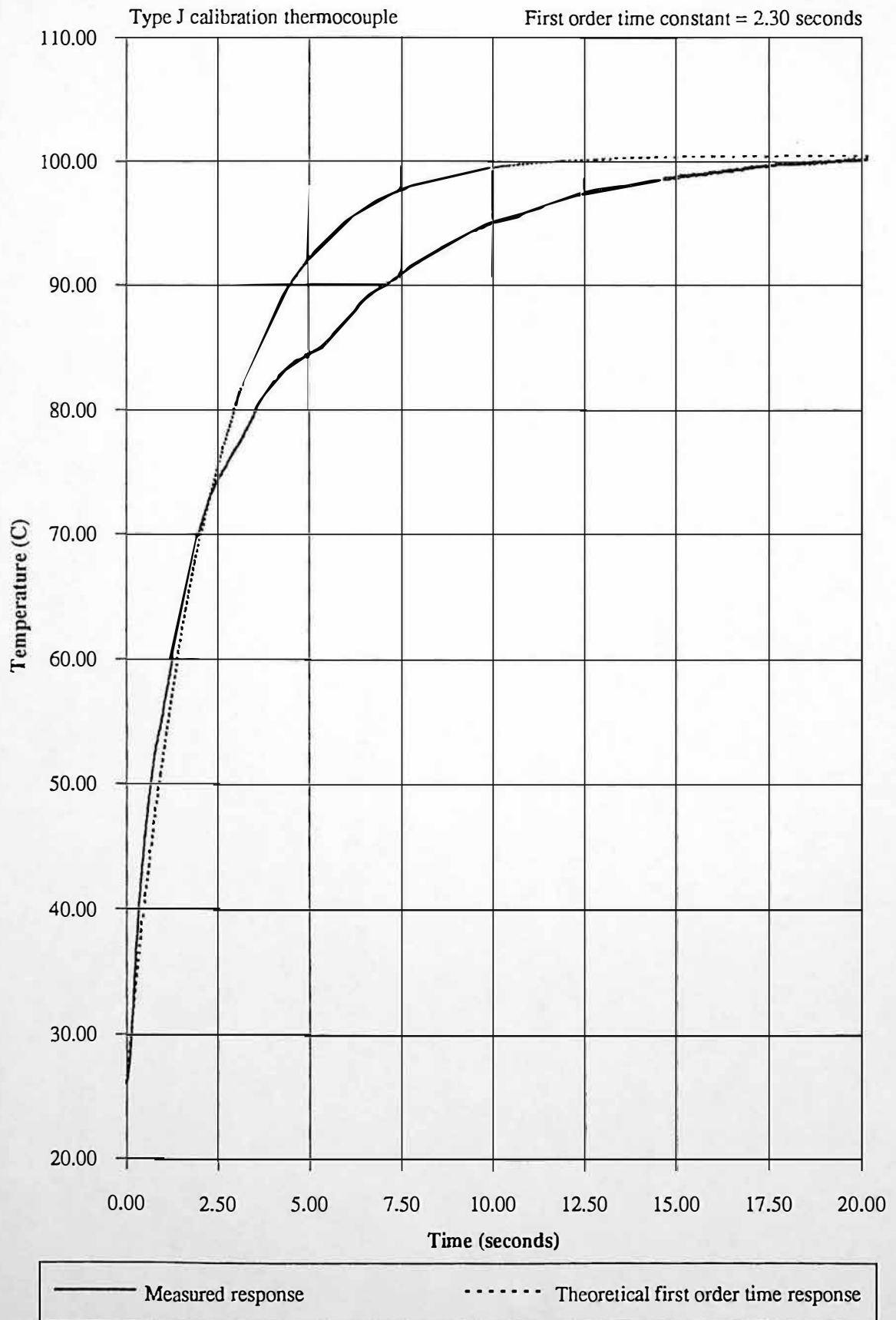


Figure 5.13 Dynamic response of industrial nozzle thermocouple to temperature step change



5.5.4 Velocity Transducer (Static Calibration)

The velocity transducer was calibrated using screw velocity derived from a linear potentiometer. The linear potentiometer formed the basis of velocity transducer calibration, due to its dynamic performance, compared the LVDT. The mean screw velocities were calculated for 2.00, 1.00, 0.60, 0.40 and 0.36 seconds for injection velocities 10.43, 20.15, 30.33, 41.14, 50.53 and 59.99 mm/s, respectively. The mean velocity was calculated for the largest time period possible, to minimise velocity quantification errors, data was monitored at 50 Hz.

5.5.5 Screw Rotational Speed (Static Calibration)

The screw rotational speed is measured by use of a magnetic pick-up counting the number of teeth, of a rotating gear wheel located on the screw motor. The screw rotational speed is calibrated by use of a frequency counting circuit, counting the number of teeth that pass the magnetic pickup per second, as shown in figure 5.4.

CHAPTER 6

Machine and Process Variable Monitoring Technique

6.1 Introduction

Injection moulding is a batch process operation consisting of several phases, injection, plasticisation and cooling. This research has concentrated on the injection and plasticisation phases, for typical injection moulding conditions. The injection phase is extremely important for measurement of polymer melt viscosity and assessment (prediction) of product quality. The plasticisation phase was monitored to ensure that plasticising process conditions were steady. Plasticisation data is important for determining control actions, particularly plasticising melt back pressure.

Measurements of tool process and machine parameters were made during the injection and plasticisation phases. Figure 6.1 shows a schematic diagram of the machine and process variable monitoring system.

Process and machine variable monitoring use two separate data acquisition systems, for the injection and plasticisation phases. Two systems were used to monitor the injection and plasticisation phases at different sample rates. The injection and plasticisation phases were sampled at 50 or 100 Hz and 10 or 20 Hz, respectively. The data sampling rates were chosen to produce an accurate representation of the process dynamics. The difference in sample rate was due to the differing dynamic responses of these phases. The choice of too fast a sampling rate may provide no additional process information, therefore, only using valuable system resources. Sampling the plasticisation phase at 100 Hz may produce no additional dynamic information than sampling at 20 Hz.

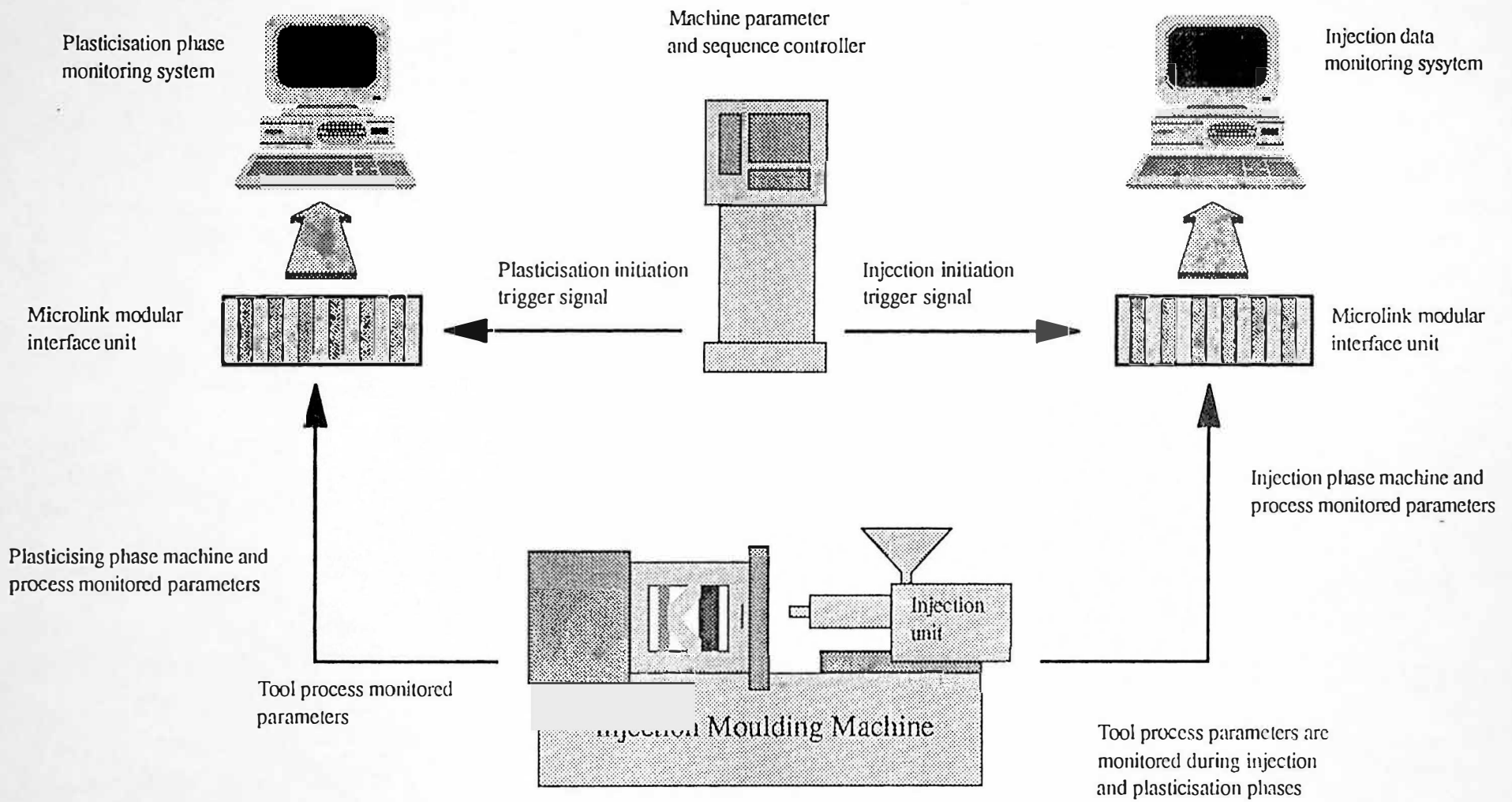


Figure 6.1 Schematic diagram of machine and process variable monitoring system

To ensure that an accurate and precise measurement of polymer melt viscosity is achieved, it is vital to have precise timing of the injection and plasticisation phases. The exact start of the injection and plasticisation phases should be used to initiate data monitoring. The use of precise data monitoring triggers allows data to be compared on a cycle to cycles basis, therefore allowing identification of process variation. Machine and process monitoring hardware consisted of a personal computer (80386 DX, IBM Compatible) and Biodata Microlink 2000, Biodata (1990). Data were analysed using a personal computer with spreadsheet, Microsoft Excel, combining statistical analysis with excellent graphical display facilities.

6.2 Machine and Process Variable Monitoring Initiation Triggers

The machine parameter and sequence controller provides a synoptic cycle indication screen, as shown in figure 6.2. This screen summarises the machine sequencing during the injection moulding process. The start of primary injection and plasticisation phases are clearly shown during a typical machine cycle. This synoptic screen indicates the status of the control relays, for the hydraulic machine functions. The control signals to the relays are direct current voltages, 24 Volts indicates signal low (relay off) and 4 volts indicates signal high (relay on). This 24 to 4 Volt relay signal was conditioned by an electronic circuit, to operate the trigger function (TRIG IN) of the Microlink HSC (High Speed Clock) card. These signals allow precise initiation of data monitoring, therefore the monitored data can be compared using a common timebase. A common timebase is extremely important when post-processing the monitored data, to ensure an accurate impression of process variation. Figure 9.16 shows the benefit of using a precise trigger for the start of injection monitoring. This figure shows mean nozzle melt pressure is shown for five different injection velocities.

The implications of not using precise triggers for the start of injection and plasticisation monitoring, means cycle to cycle data would have to be manually adjusted on the timebase. This procedure may introduce accuracy problems and increases data analysis time. During the injection moulding process a time period window may exist (0.10 seconds), where process variations are low. Therefore manual adjustment of the timebase, may introduce accuracy problems preventing this window from being realised.

		1/1 N
MOULD CLOSING d04 []s	MOULD OPENING d06 []s	AWAITING ANCILLARY
CARRIAGE FORWARD d08 []s	CARRIAGE BACKWARD	ANCILLARY
I INJECTION d02 []s	II-III INJECTION d14 []s	I DECOMPRESSION
PLASTICISING d01 []s	II DECOMPRESSION	ACCUMULATOR RECHARGE
COOLING d05 []s	CYCLE DWELL TIME d11 []s	ROBOT d07 []s
EJECTION d10 []s	EJECTOR RETURN d09 []s	STOP d15 []s
AWAITING SYNCHRONISM	CYCLE TOTAL TIME ACTUAL d12 []s PREVIOUS d03 []s	

BARREL
MOULD CLOSING
MOULD OPENING
EJECTION
INJECTION
PROFILES
PLASTICIS
CARRIAGE

06-05-93
12:29:07

Figure 6.2 Synoptic cycle indication VDU screen display for Selec machine controller

6.3 Machine and Process Variable Monitoring System Hardware

The data acquisition hardware used, comprises of two main components, a computer and a modular interface unit, shown in figure 6.3. The computer performs several functions: (i) control of the modular interface unit, (ii) storage of the monitored process and machine variable data, and (iii) data processing and analysis.

6.3.1 Computer Specification

The two 80386 IBM compatible personal computers, used for data acquisition are described in tables 6.1 a and 6.1 b.

<p>Manufacturer: Olivetti, Model: XP4</p> <p>CPU: 80386 DX and 80387 (Math Coprocessor)</p> <p>Clock Speed: 25 MHz, RAM: 4 MB</p> <p>Harddisc: 135 MB</p> <p>VGA Colour Monitor</p> <p>3.5" and 5.25" floppy drives</p> <p>120 MB Tape Streamer</p>

Table 6.1 a Personal computer specification for injection monitoring

<p>Manufacturer: Everex, Model: 386/33</p> <p>CPU: 80386 DX and 80387 (Math Coprocessor)</p> <p>Clock Speed: 33 MHz, RAM: 6 MB</p> <p>Harddisc: 200 MB</p> <p>VGA Colour Monitor</p> <p>3.5" and 5.25" floppy drives</p>
--

Table 6.1 b Personal computer specification for plasticisation monitoring

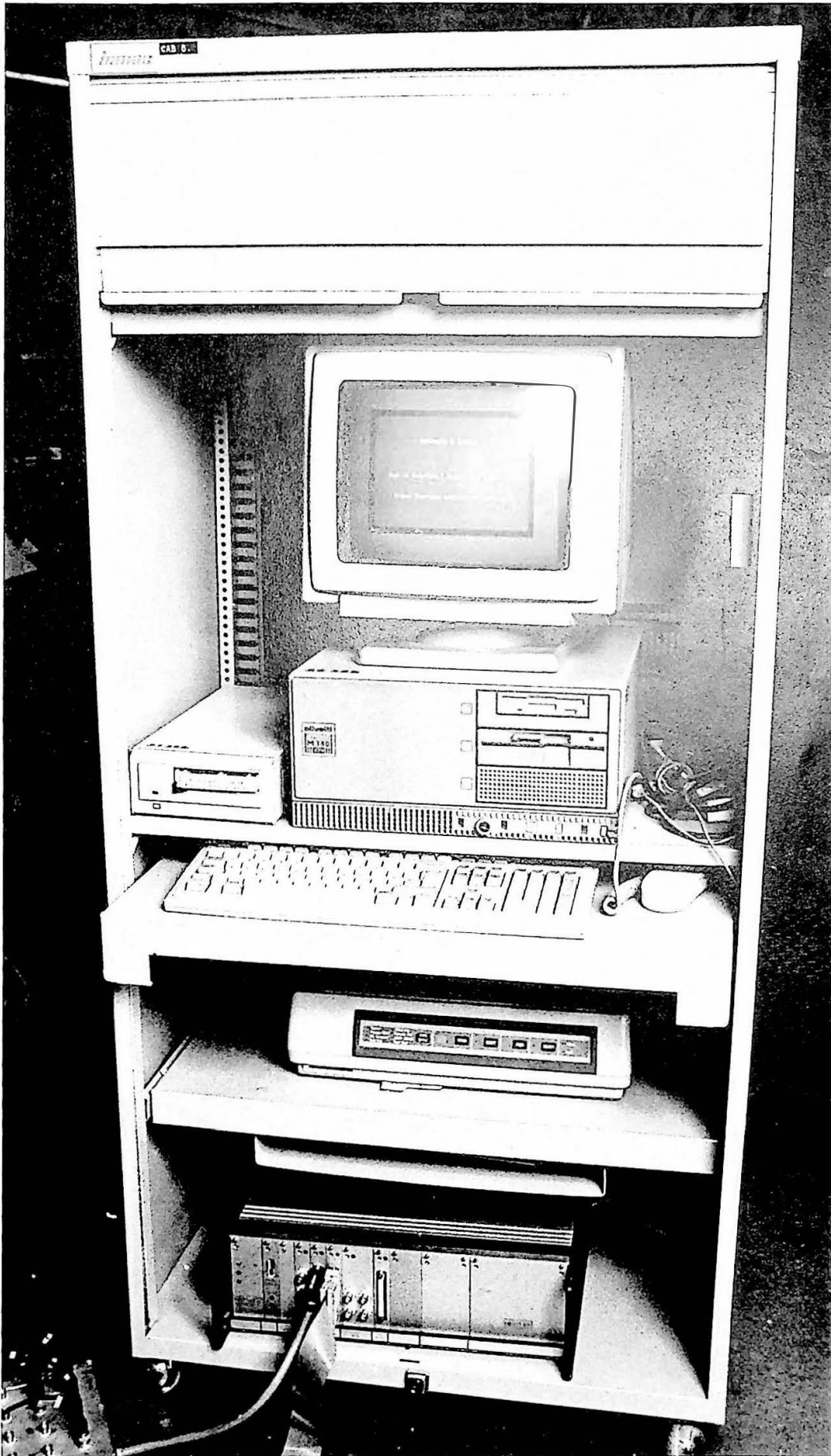


Figure 6.3 Machine and process variable monitoring system hardware

A parallel port tape streamer is available for 'backing-up' data of both personal computers. A parallel port 128 MB optical drive provides easy access to archived data.

6.3.2 Modular Interface Unit

The Biodata Microlink Series 2000 (Original Microlink) modular interface unit was chosen, as a result of an extensive survey, Rose (1990 p 89), shown in figure 6.4. The three major computer and interface systems evaluated were: (i) computer with internal bus interface cards fitted to main data bus, (ii) computer and separate interface communicating by parallel data transfer, and (iii) computer and separate interface communicating by serial data transfer.

The Biodata Microlink modular interface unit has a wide variety of cards available, therefore allowing a custom interface configuration to be designed. The computer and Biodata Microlink modular interface unit communicate via an IEEE 488 Parallel bus. It was therefore necessary to install an IEEE 488 interface card on computers bus, inside the computer. Data transmission between the computer and Biodata Microlink is bi-directional, as eight parallel bits (one byte) at a time. The maximum data transmission rate of the IEEE 488 bus is 16000 samples per second.

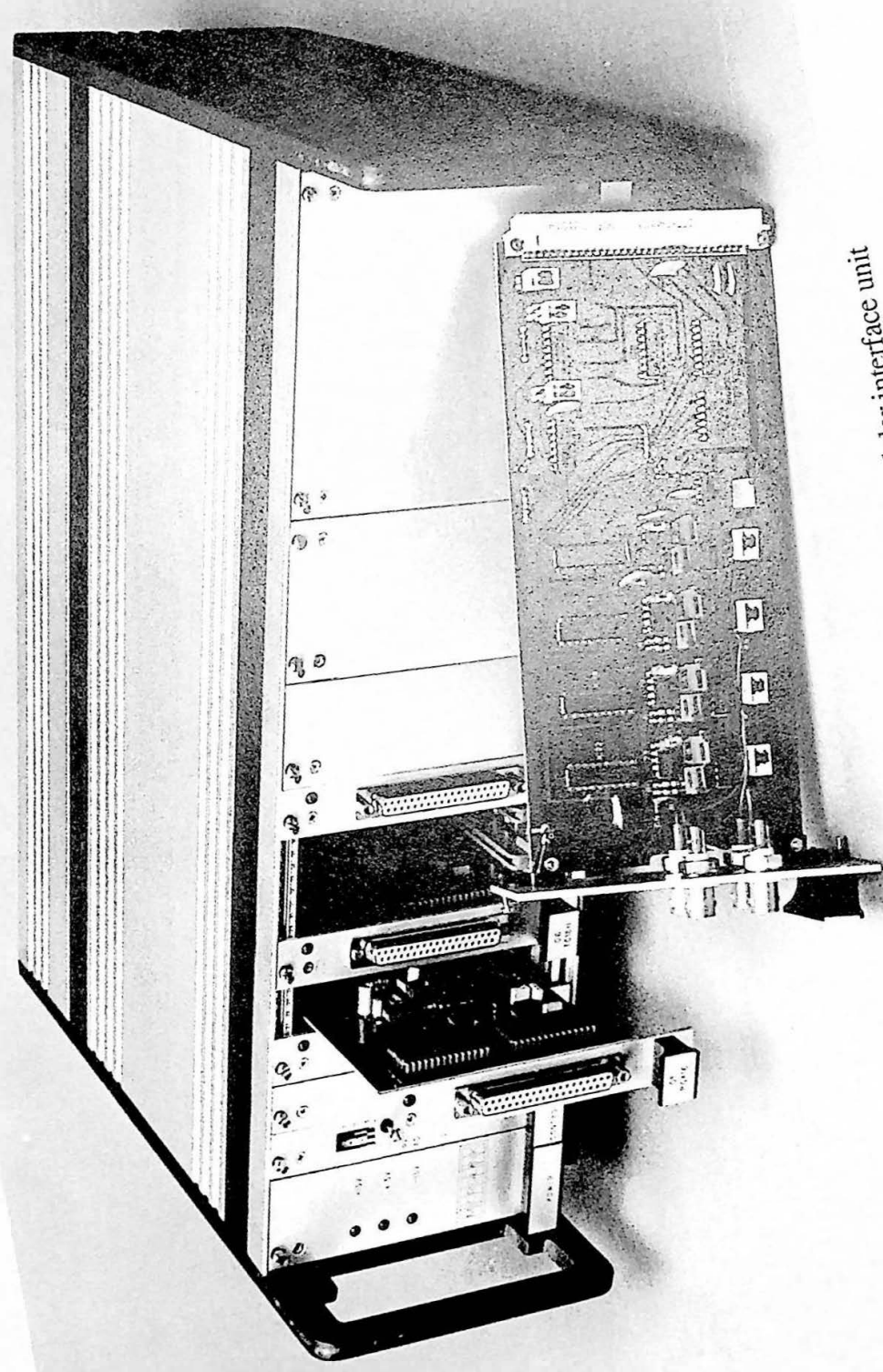


Figure 6.4 Biodata Microlink modular interface unit

6.4 Machine and Process Variable Monitoring System Software

6.4.1 Software for Injection Moulding Process

A sophisticated data acquisition package was used for monitoring the injection and plasticisation phases, written in 'C' by Dr R M Rose, Wolfson Research Fellow, Rose (1991).

The maximum sampling rate was 1000 samples per second for a maximum number of 4000 readings per channel. The number of channels monitored was limited only by the number of analogue input interface cards present.

Calibration was by fourth order polynomial curve fit, except for screw rotational speed and screw velocity which were linear fits. The maximum order of the calibration was easily changed within the program, due to its logical coding structure. Calibration data is written to the calibration file CALIB.DAT, this file is stored as a reference for each separate test.

Process monitoring was initiated by an external trigger. Data was recorded on the computers harddisc. Both uncalibrated RAW and calibrated CSV data were recorded and stored. The calibrated data was stored in a CSV (comma separated variable format). The combination of analogue and thermocouple inputs was easily varied, due to the logical structure of the software.

The software allows a cycle storage interval to be specified, whereby data from every tenth cycle is stored, for a data storage interval of ten. Uncalibrated data (RAW) for a selected channel is displayed on the VDU for every cycle, six cycles of data were overlaid before the screen was updated, this value can easily be changed. The range of the y-axis scale can easily be changed. A typical nozzle melt pressure profile during

the injection phase is shown in figure 6.5, during machine and process variable monitoring. Figure 6.5 shows four nozzle melt pressure profiles during primary injection and packing phase, overlaid and the cycle monitor above the profiles, indicates that four cycles of data has been stored and cycle five is being collected.

6.4.2 Software for Transducer Static Calibration and Performance Assessment

A modular range of software called Windmill was utilised for the transducer static calibration and testing. The Windmill software modules operate under a Microsoft Windows environment, performing tasks such as logging and charting data. The software collects data at a maximum rate of one sample per second and is ideally suited for static calibration and transducer testing. The software is executed using Microsoft DOS, and utilises the personal computers internal clock. This clock is not as precise as the Biodata Microlink High Speed Clock (HSC), Biodata (1990). The displayed values used for the experimental work were in the ranges 0 to 10.24 Volts or 0 to 4095 DEN (Digital Equivalent Number).

6.5 Data Processing and Analysis

Data monitoring of the injection moulding process generates large amounts of data. The injection uncalibrated (raw) data files for test P30%20B were 57,150 bytes compared to the 115,425 bytes for the calibrated data, monitoring 10 analogue channels and 5 thermocouples (including a cold junction reference channel) at 100 Hz for 6.98 seconds. The plasticisation uncalibrated data files of test P30%20B were 8966 bytes compared to the 18524 bytes for the calibrated data, monitoring 4 analogue channels and 3 thermocouples (including a cold junction reference channel) at 20 Hz for 11.95 seconds.

The monitored data was analysed using a spreadsheet (Microsoft Excel), allowing statistical analysis and graphical display of analysed results.

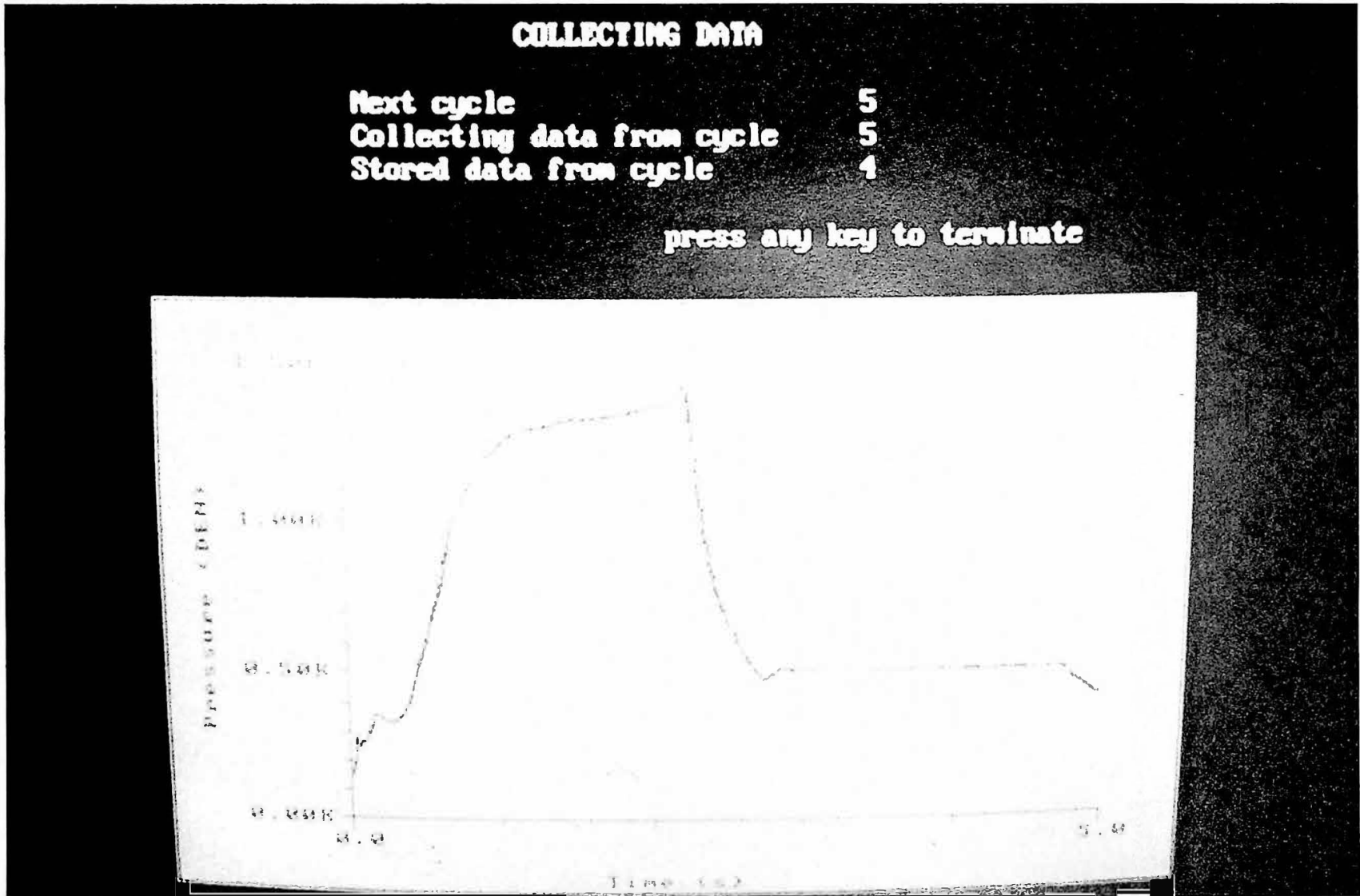


Figure 6.5 Typical nozzle melt pressure profiles during primary injection and packing phase

CHAPTER 7

In-line Capillary Rheometry

7.1 Introduction

Injection moulding machine parameter and sequence control has improved in recent years, to such an extent that polymer melt viscosity variations have become a significant processing problem. Polymer melt viscosity variations result from raw material batch changes, use of 'regrind' and recycled materials, Ross et al (1990). To compensate for polymer melt viscosity variations, true closed loop process control is required. The basis of such control is most likely to be an accurate and precise in-line measurement of polymer melt viscosity, Speight and Coates (1991). Nozzle melt pressure measurement is essential for calculating true viscosity: In-line nozzle rheometry (nozzle injection melt pressure) yields a first hand assessment of polymer melt viscosity, whereas in-line process measurements (hydraulic screw injection pressure) provide a relative assessment. The measurement of melt pressure using an in-line nozzle rheometer, may introduce measurement accuracy errors, due to inherent processing problems: (i) leakage of polymer melt past the screw non-return valve, (ii) flow variations (vortices) induced by the presence of in-line transducers in the nozzle reservoir, (iii) residence time problems, due to the increase of the nozzle reservoir geometry, and (iv) material degradation in adjacent areas to the in-line transducers. Therefore, it is necessary to investigate similarities and differences between in-line and off-line capillary rheometry, to assess the usefulness and accuracy of in-line nozzle rheometry as a scientific technique. Malloy (1988) reports that results obtained from in-line and off-line capillary rheometry were in good agreement for the wall shear rate range 100 to 10000 (sec^{-1}). During the injection moulding process extremely high wall shear rates are encountered, in the region of 100000 (sec^{-1}) depending on geometry, especially at the entrance to the gate, Dobbie (1993b).

7.1.1 Scope of this Chapter

In-line capillary rheometry is undertaken on polymer melts with a true process shear history, whereas a different shear history exists for off-line capillary rheometry. Therefore significantly different results may be obtained from the two techniques for polymer melts with a narrow processing window. The work reported here compares apparent and true wall shear stress versus wall shear rate relationships, for in-line and off-line capillary rheometry, using essentially identical capillary die geometries. The work described compares high wall shear rate in-line capillary rheometry data, with off-line data. High wall shear rates are typical of the injection moulding process, and therefore should be investigated. The analysis of wall shear stress, wall shear rate relationships, reduces the necessity to pressure and temperature correct viscosity data (see chapter 3.3.3), as wall shear stress is the major concern. The use of essentially the same capillary die geometries means that data can be more accurately compared, regarding polymer melt pressure effects. Higher volumetric flow rates are present for in-line capillary rheometry, therefore higher shear rates are developed, compared to off-line capillary rheometry, for the same capillary die radius. The significance of wall shear rate on polymer melt shear heating effects for in-line and off-line capillary rheometry was investigated, (see chapter 7.5.2).

Analysis described in this chapter concerns shear flow, although extensional viscosity can be readily calculated from the pressure drop through a zero length capillary die. Off-line capillary rheometry uses an effective zero length capillary die. Due to the velocity control algorithm of the in-line injection unit (see chapter 7.3), an effective zero length capillary die would produce inaccurate P_0 measurements. Therefore in the case of in-line capillary rheometry, the zero length pressure drop is calculated by linear extrapolation from long and short capillary dies (P_1 and P_s respectively). This calculated extensional viscosity from an extrapolated value of P_0 is likely to include inaccuracies, therefore shear flow are analysed.

7.1.2 In-line Capillary Rheometry

In-line capillary rheometry is used to determine the precise processing properties of polymer melts. Accurate and reliable polymer melt viscosity data obtained under true processing conditions, forms an increasingly important part of Finite Element Analysis (FEA) and Computer Aided Design (CAD) analysis. This research utilises a modular rheological nozzle installed on the injection unit of the Sandretto 60 tonne hydraulic injection moulding machine (see chapter 4.1 and Appendix A). An assessment of polymer melt rheology can therefore be determined, for melts subjected to the same process shear history as that encountered during actual moulding operations. In-line capillary rheometry tests are here referred to as 'airshots', where polymer melt is injected to air, instead of a tool cavity. The presence of two pressure transducers in the nozzle reservoir bore, as shown in figure 7.1 and 7.2, allows the capillary die entrance pressure to be calculated by linear extrapolation, as described in chapter 7.4. The corrected capillary die entrance pressures were used directly for stress analysis as they did not include end effect errors. A Bagley correction was implemented using two capillary dies, the first having length $L = 16.0$ mm, radius $R = 0.5$ mm, aspect ratio $L/R = 32$ and the second $L = 3.0$ mm, $R = 0.5$ mm, $L/R = 6$.

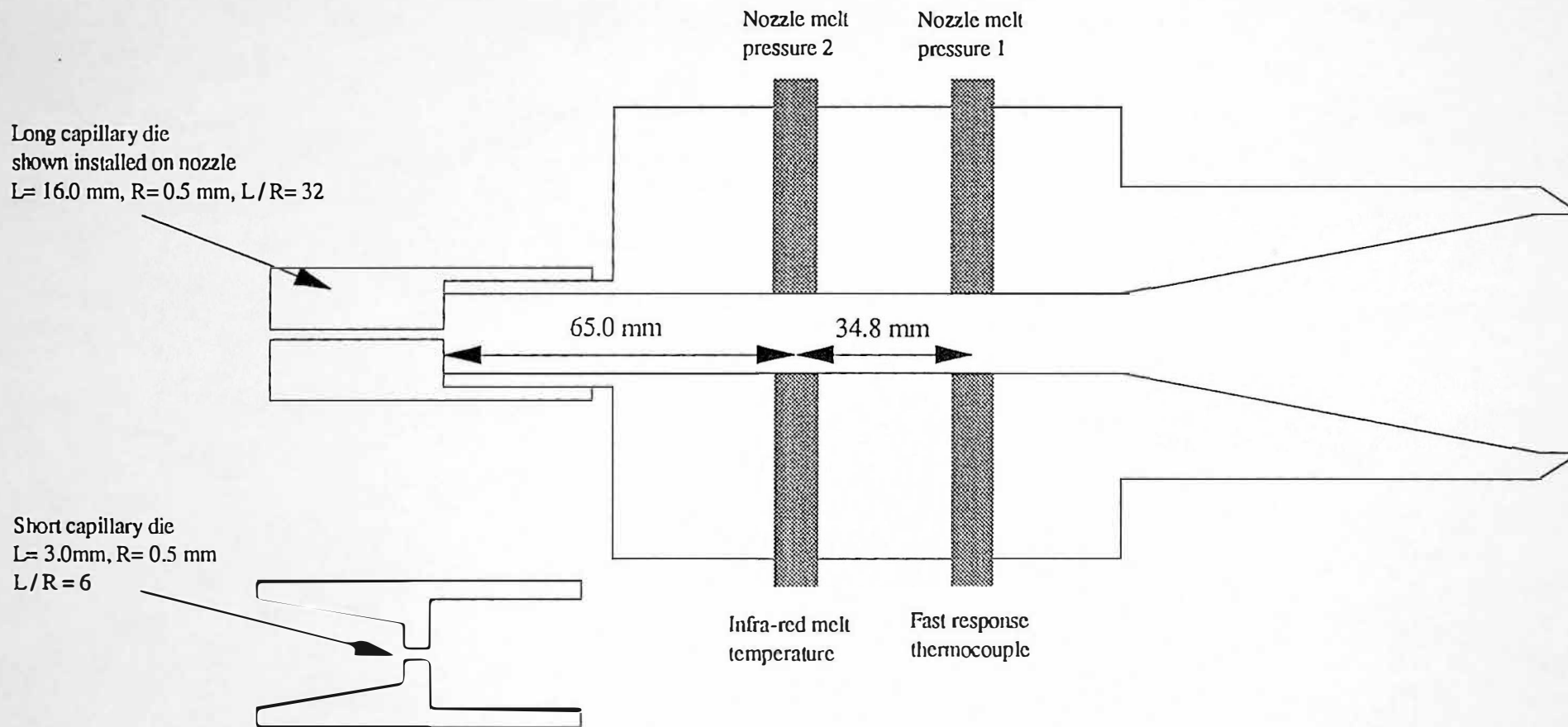


Figure 7.1 Schematic diagram of the modular nozzle configuration for in-line capillary rheometry

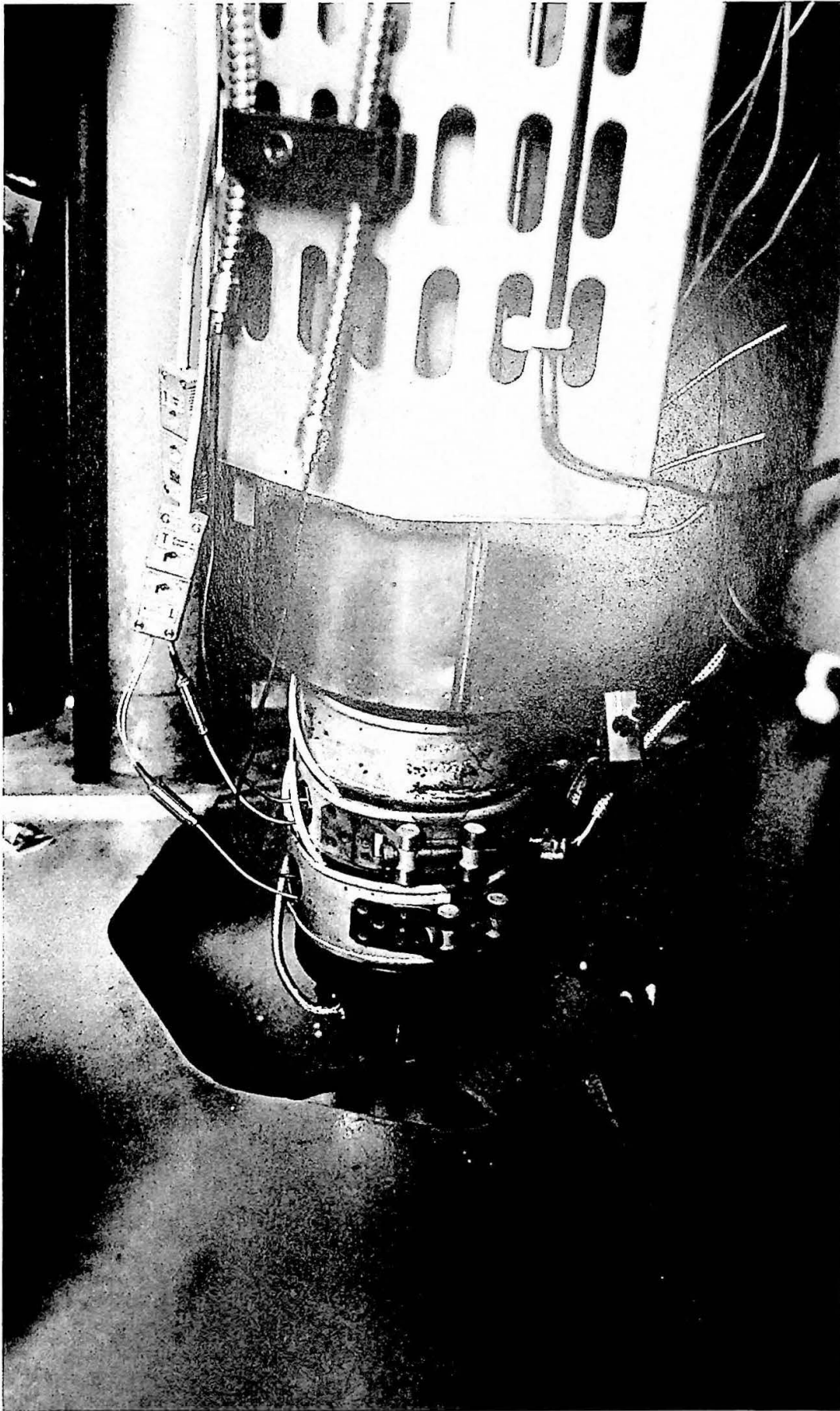


Figure 7.2 Modular nozzle rheometer configured for in-line capillary rheometry

7.1.3 Off-line Capillary Rheometry

However, off-line capillary rheometry is widely used in laboratories, and provides a useful datum for comparison with in-line capillary rheometry. Off-line capillary rheometry, based here on a Rosand RH7-2 twin bore computer controlled capillary rheometer (see section 4.1 and Appendix B), allows accurate and precise measurement of polymer melt rheology, but under non-typical shear and temperature histories. The Rosand twin bore configuration allows the measurements necessary for a Bagley correction to be implemented simultaneously, by use of two capillary dies, the first having length $L = 16.0$ mm, radius $R = 0.5$ mm, aspect ratio $L/R = 32$, the second having $L = 0.25$ mm, $R = 0.5$ mm, $L/R = 0.5$. For calculations, the off-line capillary rheometer software regards the zero length capillary die as 0.0 mm. This assumption is made for short length capillary dies in the range 0.0 to 0.3 mm.

7.2 Materials Investigated

7.2.1 High Density Polyethylene (HDPE)

The melt flow index (MFI) data quoted below complies with ISO 1133-1981 condition 4 (2.16 kg). This test uses a 2.16 kg load for a 10 minute (600 second) duration.

BP Rigidex is a high density polyethylene copolymer with a narrow molecular weight distribution.

BP Rigidex HD5226EA and HD5050EA

Density = 950 kg/m³

Specific Heat = 2300 J/kg/C

Approximate Shrinkage = 4.0 %, Morton-Jones (1989 p 166)

BP Rigidex, HD5226EA

MFI = 26 grams / 600 seconds at 190C, 2.16 kg Load

Number Average Molecular Weight \bar{M}_n = 11100

Weight Average Molecular Weight \bar{M}_w = 46500, Polydispersity Index = 4.2

Batch Number: HD 5226 1 EA 0F 245 Internal Ref. 4.164.179

See Appendix H(i) for BP Technical Information Sheet T211/1

Tests: I40%20B, J40%20B, L40%20B, NX%20B and OX%20B

BP Rigidex, HD5050EA

MFI = 4 grams / 600 seconds at 190C, 2.16 kg Load

Number Average Molecular Weight \bar{M}_n = 15000

Weight Average Molecular Weight \bar{M}_w = 90000, Polydispersity Index = 6.0

Batch Number: HD 5050 EA 1F 020 Internal Ref. 4.B0.012.127

See Appendix H(ii) for BP Technical Information Sheet T206/1

Test: G40%20B

Table 7.1 a Specification of high density polyethylene (HDPE)

7.2.2 Polyoxymethylene (POM)

Du Pont Delrin is a homopolymer with a regular structure and a high degree of crystallinity.

Du Pont Delrin II 900F, 500 and 100

Density = 1042 kg/m³

Specific Heat Average over temperature range -18C to +100C = 0.35

Approximate Shrinkage = 0.0 - 2.2 %, Morton-Jones (1989 p 166)

Du Pont Delrin II 900F

MFI = 22-24 grams / 600 seconds at 190C, 2.16 kg Load

Batch Number: TYPE II 900 F NC-010 LOT 262007K02

Du Pont Delrin II 500

MFI = 12-14 grams / 600 seconds at 190C, 2.16 kg Load

Batch Number: TYPE II 500 NC-010

Bag1 LOT 347008K011 Tests: 3-500D, L-D500B1

Bag2 LOT 25104K008 Test: N-D500B2

Bag3 LOT 276108L003 Test: P30%20B

Du Pont Delrin II 100

MFI = 2 grams / 600 seconds at 190C, 2.16 kg Load

Batch number: TYPE II 100 NC-010 LOT 085010L010

Table 7.1 b Specification of polyoxymethylene (POM)

See Appendix H(iii) for Du Pont Technical Information.

7.3 Experimental Comparison of In-line and Off-line Capillary Rheometry

The Poiseuille flow equations for capillary flow yields an apparent rather than a true measure of wall shear viscosity, see chapter 3.3.1) To determine true shear viscosity a series of corrections are made, Bagley (ends pressure drop), see chapter 3.3.3.1 and Rabinowitsch correction (non-parabolic velocity profile), see chapter 3.3.3.2.

Apparent shear wall viscosity is calculated from wall shear stress and apparent wall shear rate. Wall shear stress is derived from the pressure drop developed by a long capillary die (L/R aspect ratio = 32). Apparent wall shear rate is derived from the polymer melt volumetric flow rate (inferred from linear screw velocity), assuming negligible leakage from the screw non-return valve.

True shear viscosity is calculated from wall shear stress and true wall shear rate. Wall shear stress is derived from the pressure drop associated with the difference between long and short capillary dies (Bagley end pressure drop correction). True wall shear rate is derived from apparent (Newtonian) wall shear rate, by compensating for the fact that the assumed polymer melt parabolic velocity profile is more 'plug-like' because of non-Newtonian behaviour (Rabinowitsch correction).

Results are presented as wall shear stress versus apparent wall shear rate, thus allowing the non-Newtonian behaviour of the polymer melt to be assessed, and modelled using a power law curve fit (see chapter 3.5). The gradient of the wall shear stress versus wall shear rate flow curve reflects the polymer melt shear viscosity. Further analysis investigates the influence of a Bagley correction on the power law curve fit. The influence of a Rabinowitsch correction on apparent wall shear rate is described and the possible causes of error are investigated.

Particular experimental points of note are:

1. Essentially the same capillary die geometries were used for both techniques, see chapter 7.1.2. The reservoir bore diameter of the In-line rheometer is 16.0 mm compared to 15.0 mm for the off-line rheometer, both with 180 degree capillary die entrance angles. In-line and off-line capillary rheometers both use capillary dies of radius 0.5 mm, this allows a direct comparison of wall shear stress versus wall shear rate data, regarding the influence of pressure and temperature effects on viscosity (see chapter 3.3.3). Fenner (1979 p 149) reports that for pressure driven flows the effect on viscosity of a pressure difference ΔP and temperature rise ΔT may balance, eliminating the need for pressure and temperature correction.

The following reasons are given for the choice of a short capillary die of length of 3.0 mm, rather than an effective zero length capillary die:

- (i) The Sandretto injection moulding machine uses a screw velocity control algorithm called Logiflux. Observation has shown this algorithm to oscillate hydraulic pressure (approximate frequency of oscillations = 10 Hz) for low screw velocities (low In-line capillary rheometry shear rate range), where screw load is low. The effectively zero length capillary die would generate a low screw load and low hydraulic injection pressure. Therefore zero length capillary die measurements would be subject to large errors. (It should be noted that for normal moulding conditions the Logiflux control algorithm does not produce hydraulic pressure oscillations).
- (ii) An effectively zero length capillary die ($L= 0.25$ mm) would be highly susceptible to damage during the plasticising phase, when the capillary die is physically sealed.
- (iii) Due to the high wall shear rates developed by the in-line nozzle rheometer (for the same capillary die radius as off-line capillary rheometry), capillary die wear would be a significant problem. Abrasive polymers would enlarge the capillary die orifice, after a short processing period.

2. The in-line capillary rheometer based on the Sandretto injection moulding machine has a higher volumetric flow capacity, than the off-line rheometer, resulting in a higher shear rate range. Table 7.3 shows the apparent shear rate range for in-line and off-line capillary rheometry. The Apparent wall shear rate calculations are based on a capillary die radius of 0.5 mm.

Capillary Rheometry Technique	Minimum Apparent Wall Shear Rate (sec^{-1})	Maximum Apparent Wall Shear Rate (sec^{-1})
In-line	3.84×10^4	1.27×10^6
Off-line	3.00×10^{-1}	1.50×10^4

Table 7.2 Apparent wall shear rate range for in-line and off-line capillary rheometry

3. The twin bore design of the off-line rheometer enables the measurements for an end pressure drop correction to be made simultaneously. Therefore ensuring that both P_L and P_S measurements are made for the same piston velocities (apparent wall shear rates). In-line capillary rheometry requires two separate airshots to measure P_L and P_S , therefore introducing the possibility of shear rate errors, i.e. injection velocity may not be exactly the same for each airshot.

4. The in-line capillary rheometer uses polymer melt with a well defined shear history, for true injection moulding process conditions, unlike off-line devices. The off-line capillary rheometer also requires the operator to pack the polymer into the barrels, and is therefore is subject to variation. The presence of two barrels on the off-line capillary rheometer means that packing errors are more significant.

5. The off-line capillary rheometer has one pressure transducer for each bore, to measure the capillary die pressure drops. The centre of the off-line pressure transducers 8 mm diaphragm are located 10 mm from the capillary die entrance. The

two In-line capillary rheometer pressure transducers Nozzle Melt Pressure 1 (NMP 1) and Nozzle Melt Pressure 2 (NMP 2) are located in the nozzle reservoir bore, 34.8 mm between diaphragm centres. The diaphragm centre of NMP 2 is located 65.0 mm from the capillary die entrance. The In-line melt pressure measurements are utilised to extrapolate a corrected capillary die entrance pressure (CDEP) for the same location, as the off-line capillary pressure measurement (see chapter 7.4). The CDEP allows a more accurate comparison between In-line and off-line capillary rheometry. This work therefore investigates the importance of pressure transducer location in the reservoir bore.

7.3.1 Configuration of In-line Modular Nozzle Rheometer

In-line capillary rheometry requires the removal of the tool from between the injection moulding machines fixed and moving platens. The in-line modular nozzle rheometer is advanced forward, through the fixed platen tool location ring, enabling the nozzle capillary dies to contact with a capillary aluminium die seal, attached to the moving platen. The moving platen was retracted after plasticisation for each 'Airshot'. The airshots were manually sequenced at two minute intervals, with 3 'airshots' at each injection velocity. Extreme care was necessary with the experimental procedures, as delicate nozzle instrumentation could easily be damaged. Figure 7.3 shows a schematic diagram of the experimental installation. Figure 7.4 shows a general view of the Sandretto 60 tonne injection moulding machine configured for in-line capillary rheometry and figure 7.5 shows a short capillary die located on modular nozzle rheometer.

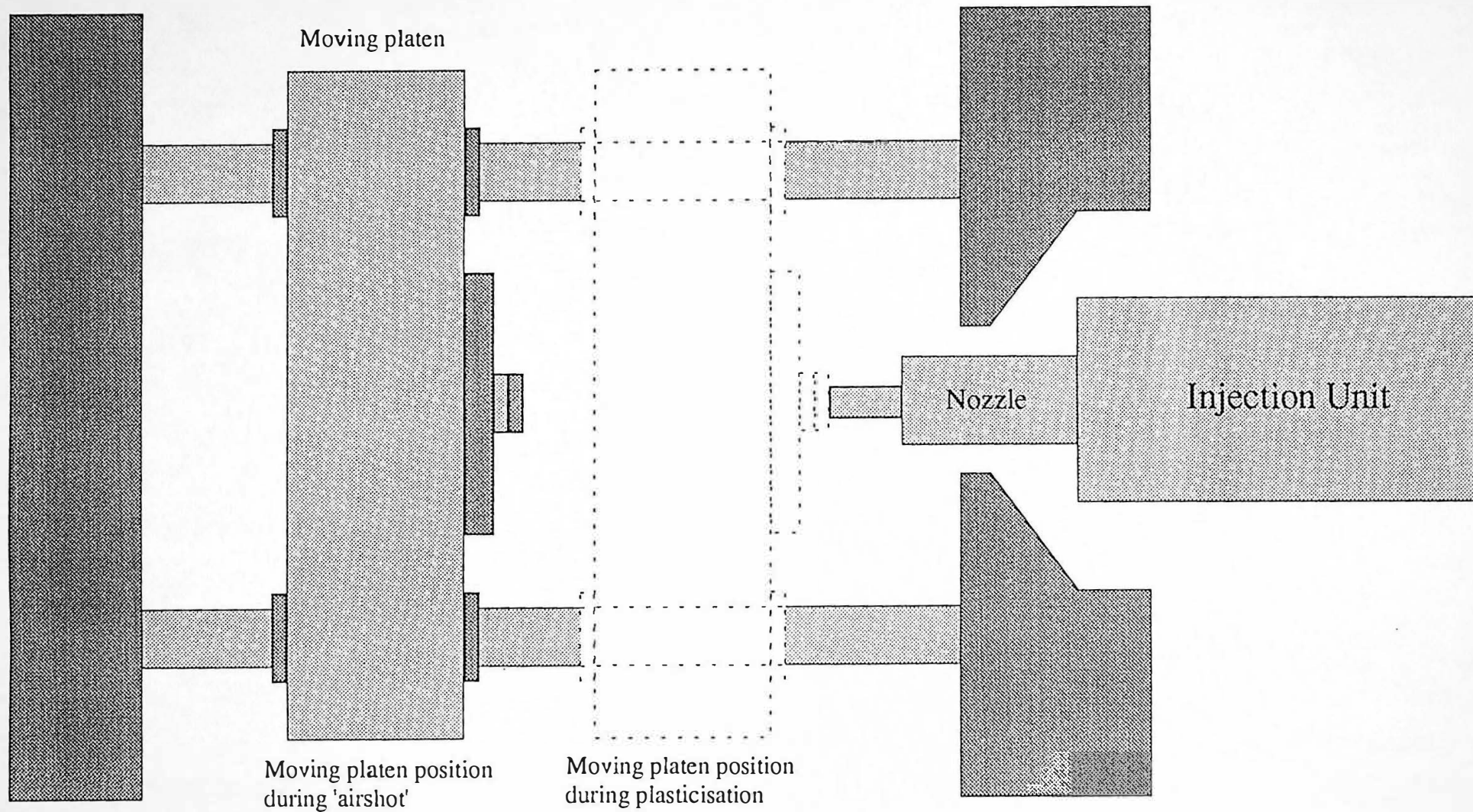


Figure 7.3 Schematic diagram of in-line capillary rheometer installation

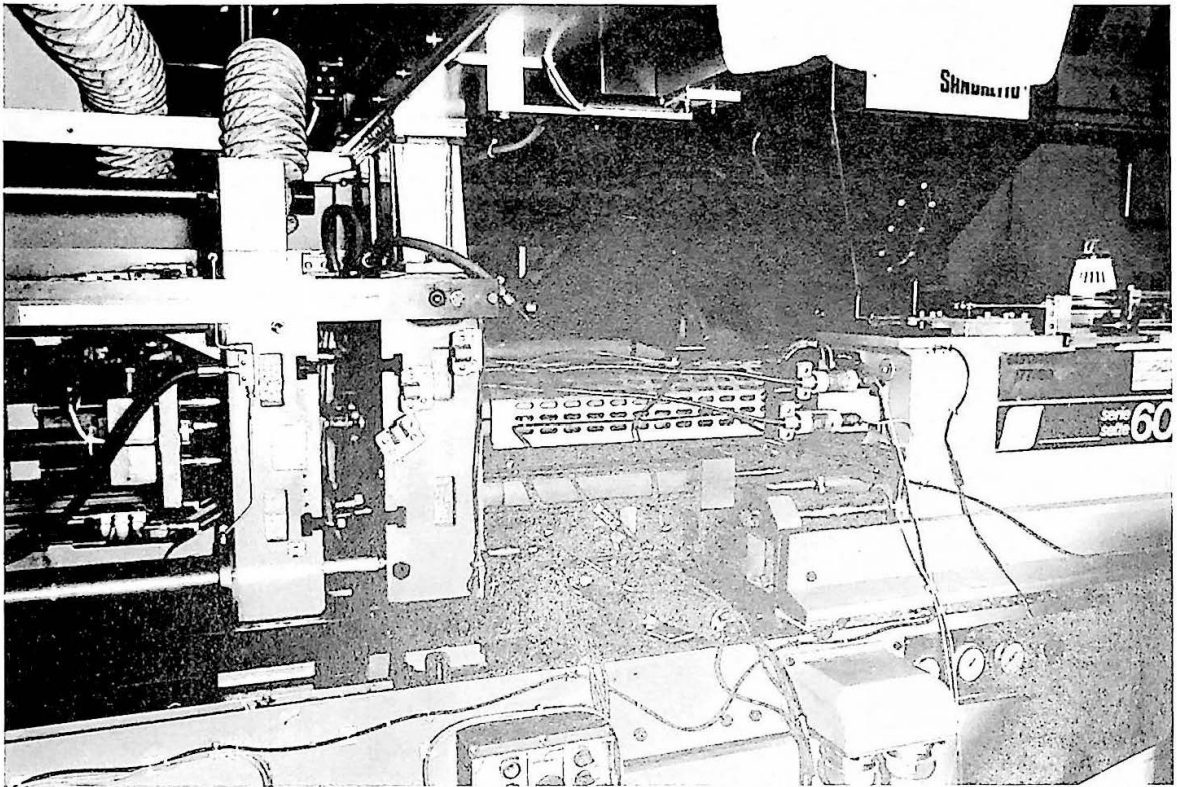


Figure 7.4 General view of Sandretto 60 tonne injection moulding machine configured for in-line capillary rheometry

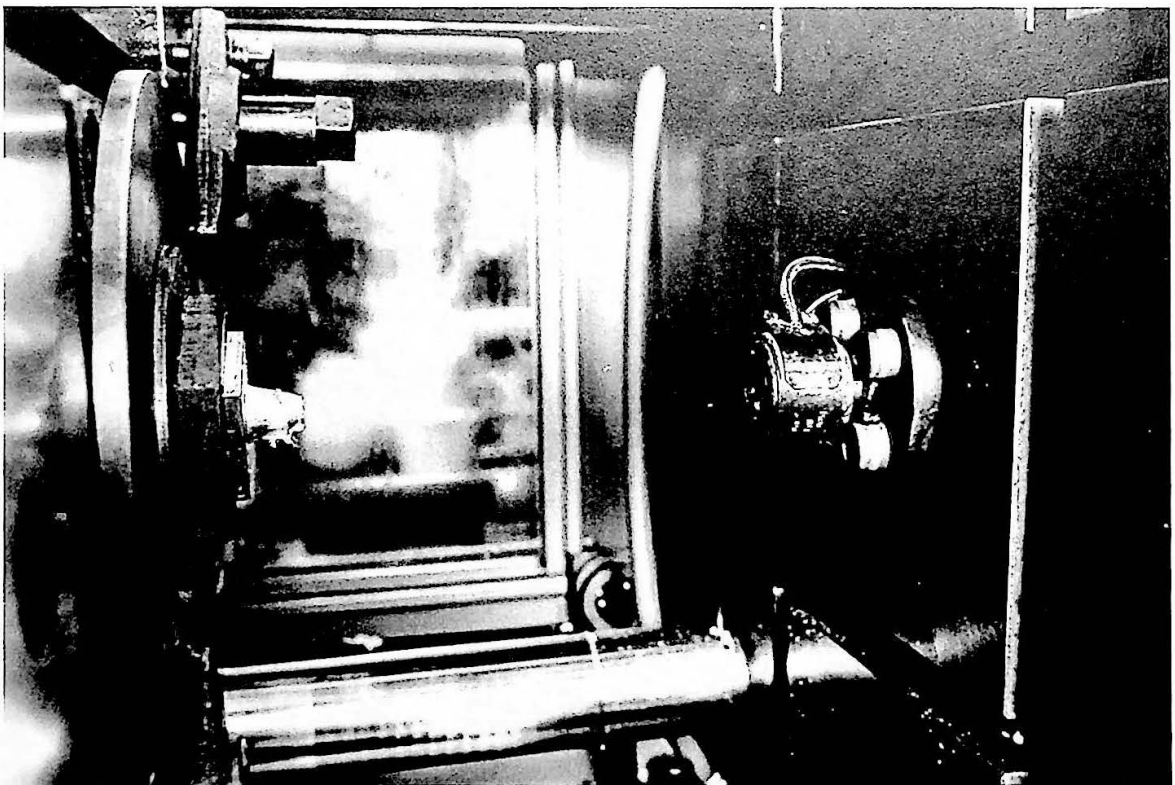


Figure 7.5 Short capillary die located on modular nozzle rheometer

The following injection parameters shown in Table 7.3 a, were monitored for 30.00 seconds at 50 Hz, initiated from the start of the injection phase.

Channel Number	Description of Monitored Parameter	Symbolic Name	Transducer Type
PGA 0	Nozzle Melt Pressure 1	NMP 1	Diaphragm device
PGA 1	Nozzle Melt Pressure 2	NMP 2	Diaphragm device
PGA 2	Hydraulic Injection Pressure	HYDP	Diaphragm device
PGA 5	Injection Screw Displacement	SDISP 1	LVDT
PGA 6	Reference Injection Screw Displacement	SDISP 2	LVDT
PGA 7	Injection Screw Displacement. Packing Phase	SDISP 3	LVDT
PGA 8	Injection Screw Displacement	SDISP 4	Linear potentiometer
PGA 9	Screw Injection Velocity	SVEL	Inductive device
TC 0	Nozzle Melt Temperature	NMT 1	Infra red device
TC 1	Nozzle Melt Temperature	NMT 2	Fast resp. thermocouple
TC 2	Hydraulic Oil Temperature	OILT	Type J thermocouple
TC 3	Air Temperature	AIRT	Type J Thermocouple

Table 7.3 a In-line capillary rheometry injection monitored parameters

The following plasticising parameters shown in Table 7.3 b, were monitored for 30.00 seconds at 10 Hz, initiated from the start of the plasticisation phase.

Channel Number	Description of Monitored Parameter	Symbolic Name	Transducer Type
PGA 0	Plasticising Nozzle Back Pressure	NMP 1	Diaphragm device
PGA 1	Plasticising Nozzle Back Pressure	NMP 2	Diaphragm device
PGA 2	Plasticising Screw Rotational Speed	SRPM	Magnetic pickup
PGA 3	Plasticising Screw Displacement	SDISP 1	LVDT

Table 7.3 b In-line capillary rheometry plasticisation monitored parameters

Table 7.4 shows the machine parameter settings for the in-line capillary rheometer, for both high density polyethylene and polyoxymethylene respectively.

Machine Parameter Settings	High Density Polyethylene (HDPE)	Polyoxymethylene (POM)
Plasticising screw rotation speed (RPM)	80	80
Plasticising back pressure (bar)	5	5
Plasticising end position (%)	50.0	50.0
Primary injection velocity (%)	3, 5, 7, 9, 11	3, 5, 7, 9, 11
Maximum hydraulic injection pressure (bar)	115	115
Die Temperature Control Zone (C)	190	215
Nozzle Temperature Control Zone 1 (C)	190	215
Nozzle Temperature Control Zone 2 (C)	190	215
Barrel Temperature Control Zone A (C)	190	215
Barrel Temperature Control Zone B (C)	185	210
Barrel Temperature Control Zone C (C)	180	205
Feed zone cooling, water flow rate (YES/NO)	YES	YES

Table 7.4 In-line nozzle rheometer machine parameter settings

Figure 7.6 shows the nozzle short capillary die in contact with the capillary die seal on the moving platen, during the plasticisation phase. Figure 7.7 shows an in-line nozzle rheometer 'airshot' of POM, Delrin II 500 at an injection screw velocity of 5 mm/s, nozzle temperature 215C. Figure 7.8 shows the corrected long capillary die entrance pressure profile and screw displacement for the same experimental conditions as shown in figure 7.7. The mean nozzle capillary die entrance pressure was calculated for the time period $t = 8.00$ to 8.50 seconds.



Figure 7.6 Short capillary die sealed by moving platen plate during plasticisation phase

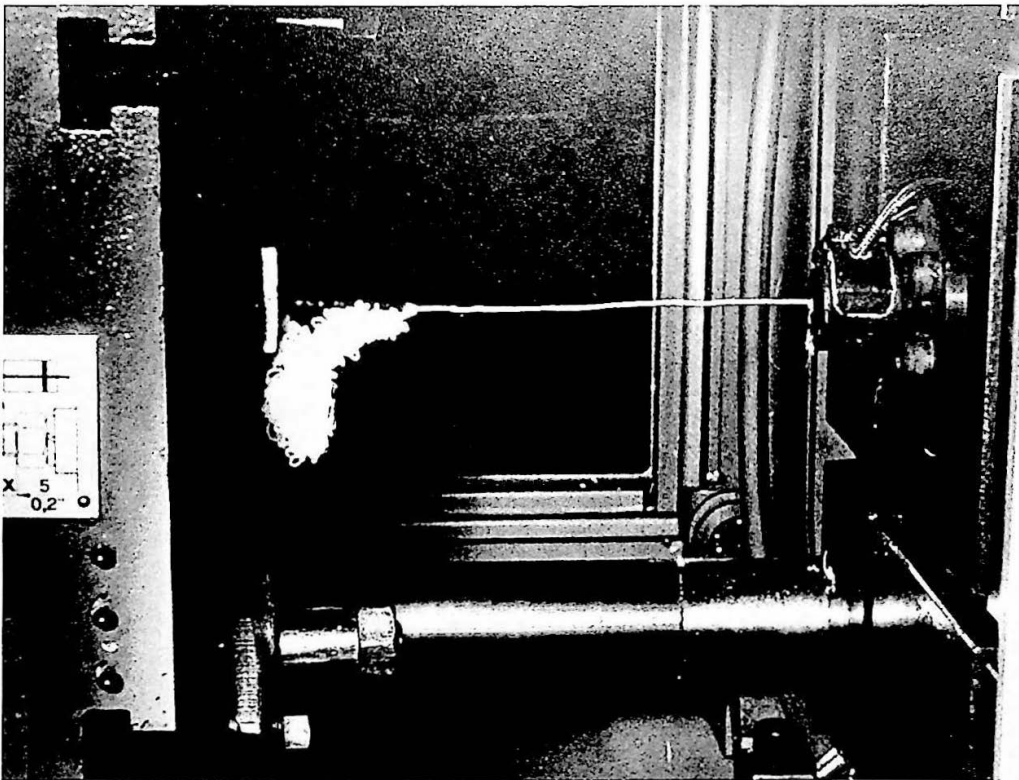
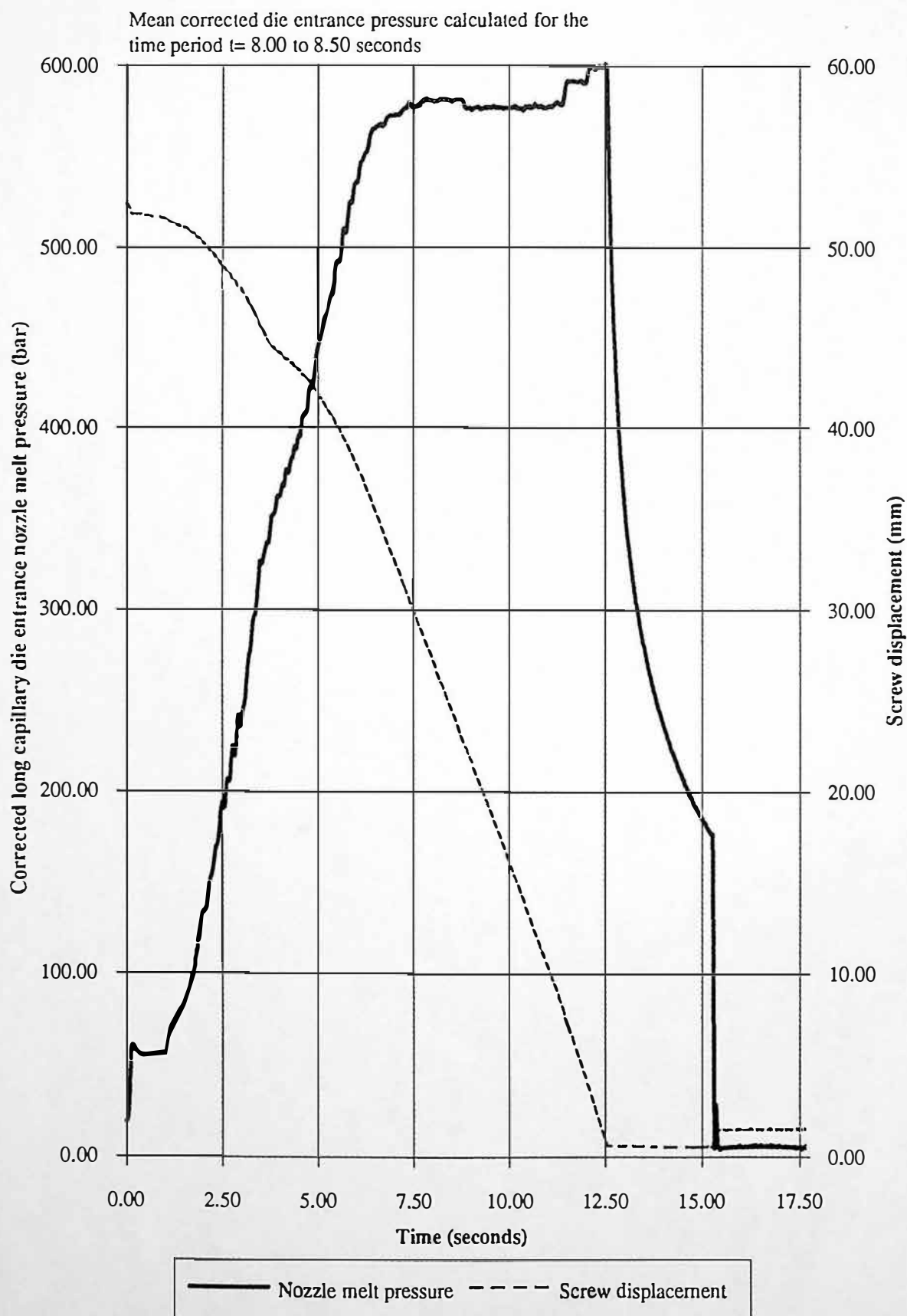


Figure 7.7 In-line capillary rheometry 'airshot', POM Delrin II 500, long capillary die, 5 mm/s screw injection velocity

Figure 7.8 In-line corrected long capillary die entrance pressure and screw displacement for Du Pont Delrin II 500 at 5 mm/s screw injection velocity during a typical 'airshot'



7.3.2 Configuration of Rosand RH7-2 Twin Bore Off-line Capillary Rheometer

Table 7.5 shows the monitored parameters for the off-line capillary rheometer. Figure 7.9 shows a schematic diagram of the Rosand RH7-2 twin bore off-line capillary rheometer. Tables 7.6 a and 7.6 b show the machine parameter settings for the off-line capillary rheometer, for both high density polyethylene and polyoxymethylene, respectively. The transducers are monitored at a sample frequency dependent on the crosshead velocity. Experimental Procedures for the Rosand twin bore off-line capillary rheometer are shown in Appendix C(i).

The Monitored Parameters were:

Parameter Number	Description of Monitored Parameters	Symbolic Name	Transducer Type
1	Entrance Pressure to Long Die	PL	Diaphragm
2	Entrance Pressure to Short Die	Ps	Diaphragm
3	Load on Crosshead (for safety)	LOAD	Strain gauge load cell
4	Crosshead Piston Velocity	VEL	Tacho. and encoder
5	Top Zone Temperature	TOPZONE	Type J thermocouple
6	Middle Zone Temperature	MIDZONE	Type J thermocouple
7	Bottom Zone Temperature	BOTZONE	Type J thermocouple

Table 7.5 Off-line capillary rheometer monitored parameters

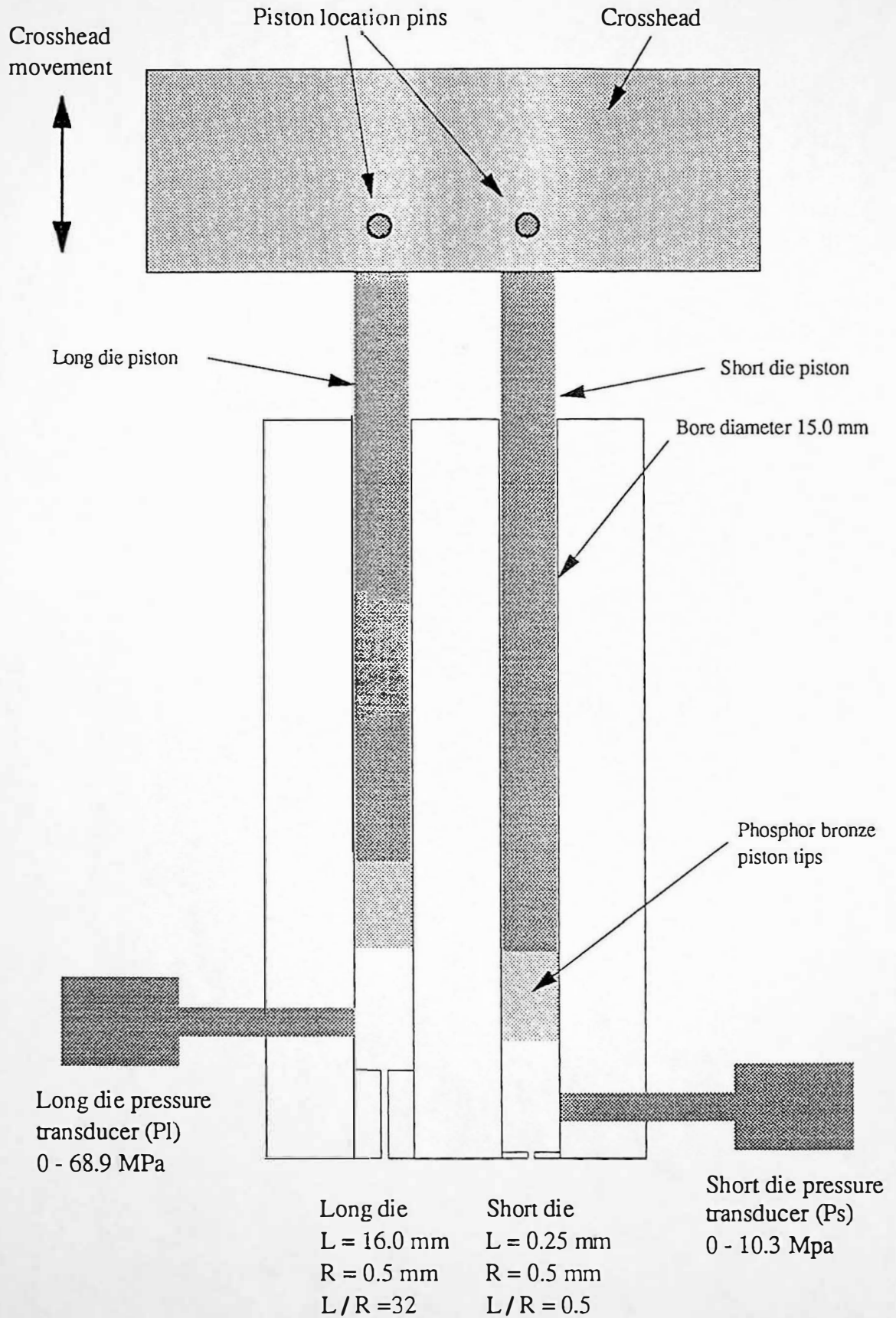


Figure 7.9 Schematic diagram of Rosand RH7-2 twin bore off-line capillary rheometer

Material: High Density Polyethylene Test Information			
Polymer type	High Density Polyethylene		
Trade name	BP Rigidex		
Grade	HD5226EA and HD5050EA		
Lab code number	-	Operator's initials	RGS
Molecular weight Mw	-	Mw/Mn	-
Filler percentage	-	Drying temperatures (C)	-
Filler types	-	Drying atmosphere	-
Sample original	BP Chemicals Ltd	Drying hours	-
Additional Information	-		
Test Temperatures		Test Geometry	
Top zone temp (C)	190.0C	Long die length (mm)	16
Middle zone temp (C)	190.0C	Long die diameter (mm)	1
Bottom zone temp (C)	190.0C	Short die length (mm)	0
		Short die diameter (mm)	1
		Die entry angle (degrees)	180
RUN SCHEDULE - Piston Speeds mm/min 0.50 to 500 depending on shear rate range, 16 stages.			
PRESSURE TRANSDUCERS		PREHEAT SEQUENCE	
Transducer at long die	387216	1st Compression Speed (mm/min)	100
Max. pressure (MPa)	68.97	Initial pressure long die (MPa)	0.2
Information	Nominal value	Initial pressure short die (MPa)	0.2
Transducer at short die	390534	Time before 2nd compression (min)	6
Max. pressure (MPa)	10.34	2nd Compression Speed (mm/min)	200
Information	Nominal value	Final pressure long die (MPa)	0.2
		Final pressure short die (MPa)	0.2
		Preheat Time (min)	3
CONTROL FACTORS			
Variation on standard sample rate	1		
Max no. of samples at any speed	50		
Endpoint filter time constant	2		
Allowable deviation at end point	0.35		
Disc title	HDPE		
File title	*.DAT. *.CAL		

Table 7.6 a Off-line capillary rheometer machine parameter settings

Material: Polyoxymethylene Test Information			
Polymer type	Polyoxymethylene		
Trade name	Du Pont Delrin II		
Grade	100, 500 and 900F		
Lab code number	-	Operator's initials	RGS
Molecular weight Mw	-	Mw/Mn	-
Filler percentage	-	Drying temperatures (C)	-
Filler types	-	Drying atmosphere	-
Sample original	Du Pont (UK) Ltd	Drying hours	-
Additional Information	-		
Test Temperatures		Test Geometry	
Top zone temp (C)	215.0C	Long die length (mm)	16
Middle zone temp (C)	215.0C	Long die diameter (mm)	1
Bottom zone temp (C)	215.0C	Short die length (mm)	0
		Short die diameter (mm)	1
		Die entry angle (degrees)	180
RUN SCHEDULE - Piston Speeds mm/min 0.50 to 500 depending on shear rate range, 16 stages.			
PRESSURE TRANSDUCERS		PREHEAT SEQUENCE	
Transducer at long die	387216	1st Compression Speed (mm/min)	100
Max. pressure (MPa)	68.97	Initial pressure long die (MPa)	0.5
Information	Nominal value	Initial pressure short die (MPa)	0.5
Transducer at short die	390534	Time before 2nd compression (min)	4
Max. pressure (MPa)	10.34	2nd Compression Speed (mm/min)	200
Information	Nominal value	Final pressure long die (MPa)	1
		Final pressure short die (MPa)	1
		Preheat Time (min)	4
CONTROL FACTORS			
Variation on standard sample rate	1		
Max no. of samples at any speed	10 or 25		
Endpoint filter time constant	2		
Allowable deviation at end point	0.35		
Disc title	POM		
File title	*.DAT. *.CAL		

Table 7.6 b Off-line capillary rheometer machine parameter settings

7.4 Correction of In-line Capillary Die Entrance Pressure

In-line and off-line polymer melt pressure drop measurements are fundamental to the calculation of viscosity. The pressure transducers used in the current work are located at different distances with respect to capillary die entrance, for in-line and off-line capillary rheometry, for practical reasons. Malloy (1988), Malloy et al (1989), used linear extrapolation between three pressure transducers for die entrance pressure during in-line capillary rheometry, processing HDPE. Laun (1983 p 176) used polynomial extrapolation between three pressure transducers, for an extrusion slit die entrance and exit pressures, processing LDPE. This chapter describes the procedure used to correct for the different pressure transducer locations. Figures 7.10 a and 7.10 b show the reservoir, capillary configurations for in-line and off-line capillary rheometry, respectively.

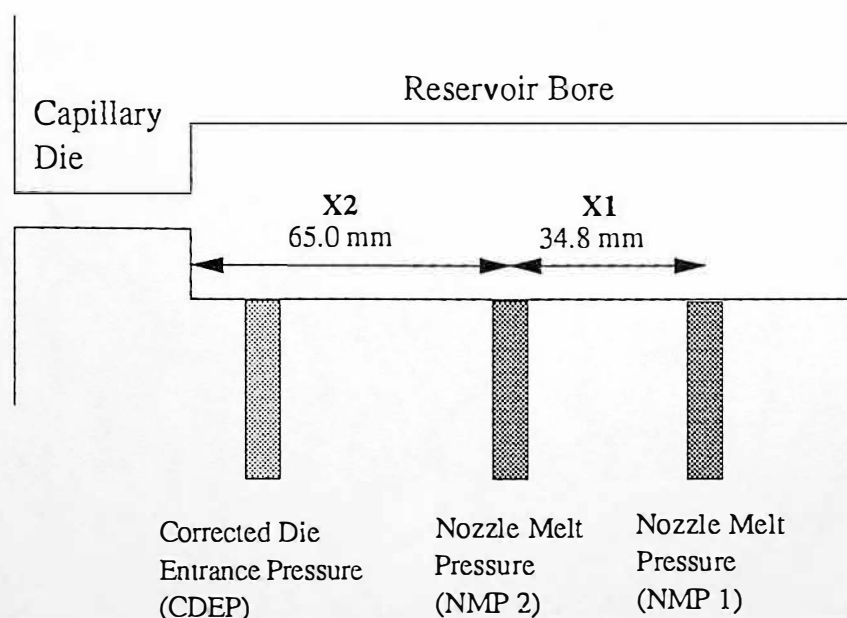


Figure 7.10 a Pressure transducer location for in-line capillary rheometry

Linear extrapolation of the two in-line pressure measurements, leads to an in-line pressure measurement for the same location as the off-line rheometer. The corrected

die entrance pressure allows a more accurate comparison of in-line and off-line capillary rheometry. This analysis therefore investigates the significance of pressure transducer location within a reservoir bore, regarding distance from the capillary die entrance.

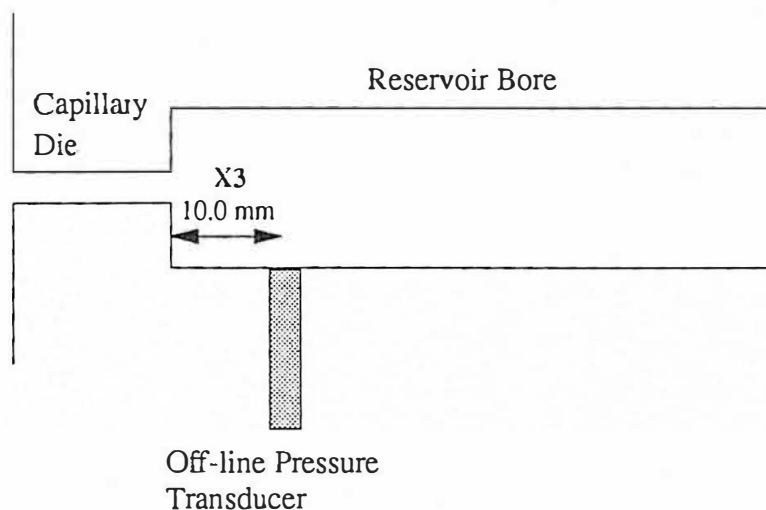


Figure 7.10 b Pressure transducer location for off-line capillary rheometry

7.4.1 Calculation of In-line Die Entrance Pressure

The two in-line pressure transducers were used to extrapolate the in-line capillary die entrance pressures for 10.0 mm from the capillary die entrance.

$$\Delta P = (NMP1 - NMP2) \quad \text{Eq. 7.1}$$

$$\text{Corrected Capillary Die Entrance Pressure} = NMP2 - (((X2 - X3) / X1) \times \Delta P) \quad \text{Eq. 7.2}$$

Where:

NMP 1 = Nozzle Melt Pressure 1

NMP 2 = Nozzle Melt Pressure 2

X1 = distance between in-line melt pressure transducers (NMP 1 and NMP 2) (mm),	34.8 mm
X2 = distance between melt pressure transducer 2 (NMP 2) and die entrance (mm),	65.0 mm
X3 = distance between off-line melt pressure transducer and die entrance (mm),	10.0 mm

Assuming that melt pressure and dimensions are measured at the centre of the pressure transducers diaphragm.

7.4.2 Accuracy of Corrected Capillary Die Entrance Pressure

The use of a corrected die entrance pressure (CDEP) measurement may introduce accuracy errors, compared to the accuracy of an actual nozzle melt pressure measurement. The CDEP measurement is subject to the calculated combined errors of two pressure transducers, with associated extrapolation errors. The accuracy error of each pressure transducer is ± 0.5 bit, therefore the combined error of the CDEP is ± 1.0 bit excluding extrapolation errors and ± 1.6 bits including extrapolation errors. Table 7.7 shows statistical data for two in-line nozzle melt pressure measurements (NMP 1 and NMP 2) and a corrected mean die entrance pressure, during a typical 'airshot' (see figures 7.7 and 7.8). The mean pressure measurements were analysed for the period $t = 8.00$ to 8.50 seconds (sample rate 50 Hz). Polyoxymethylene (Du Pont Delrin II 500) was injected at a screw velocity of 5 mm/s, through a capillary die (long die, L/R aspect ratio = 32) to air.

	Nozzle Melt Pres. (NMP1)	Nozzle Melt Pres. (NMP2)	Corrected Die Entrance Pres. (CDEP)
Mean (bar)	585.23	583.49	580.75
Standard Deviation (bar)	0.52	0.51	0.54
Coefficient of Variation (%)	0.089	0.087	0.092

Table 7.7 Nozzle melt pressure accuracy data for typical 'airshot'

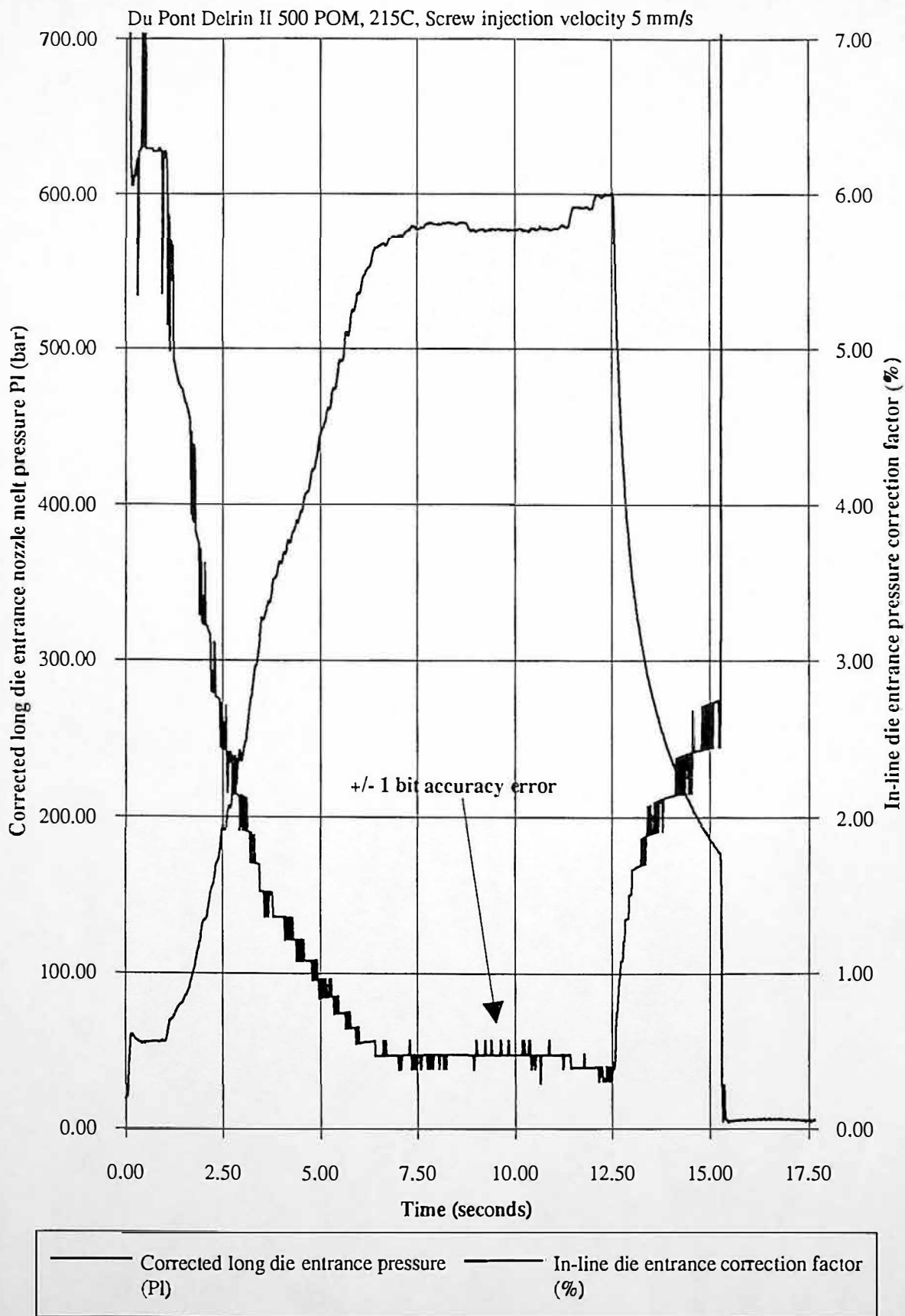
Table 7.7 shows that the mean CDEP has a coefficient of variation of 0.092, compared to 0.089 and 0.087 for NMP 1 and NMP 2. The coefficient of variation for the CDEP is not significantly larger than that of NMP 1 and NMP 2. Therefore the accuracy of the extrapolated capillary die entrance pressure is not adversely effected.

A nozzle melt pressure correction factor (see Eq. 7.3) can be derived from the data contained in Table 7.7. The correction factor is -0.47%, representing an apparent wall shear stress correction of 7.14×10^3 Pa. During current work a maximum correction factor ranges of -1.08 to 1.27% and -3.99 to 2.05% were experienced for P_L and P_S respectively, during periods of steady pressure. The implications of positive nozzle melt pressure correction factors are discussed in chapter 7.7. Figure 7.11 shows the corrected long capillary die entrance pressure compared to the nozzle melt pressure correction factor, for the typical 'airshot' of Table 7.7. It is apparent from figure 7.11 that the correction factor is significant during periods of pressure change. It is also apparent for figure 7.11 that the combined accuracy error of the two pressure transducers is ± 1 bit. Therefore, despite extrapolation errors, a high level of measurement accuracy is maintained. Regarding measurement accuracy, it is important to note that commercially available signal conditioning units, typically have accuracy errors of ± 2 to ± 20 bits.

$$\text{Nozzle Melt Pressure Correction Factor} = \frac{100 \times (\text{CDEP} - \text{NMP2})}{\text{NMP2}} \quad (\%) \quad \text{Eq. 7.3}$$

The calculation of a corrected capillary die entrance pressure (CDEP) has shown that pressure transducer location within the nozzle reservoir, has minimal effect on the calculated wall shear stress.

Figure 7.11 Influence of correction factor on in-line nozzle melt pressure



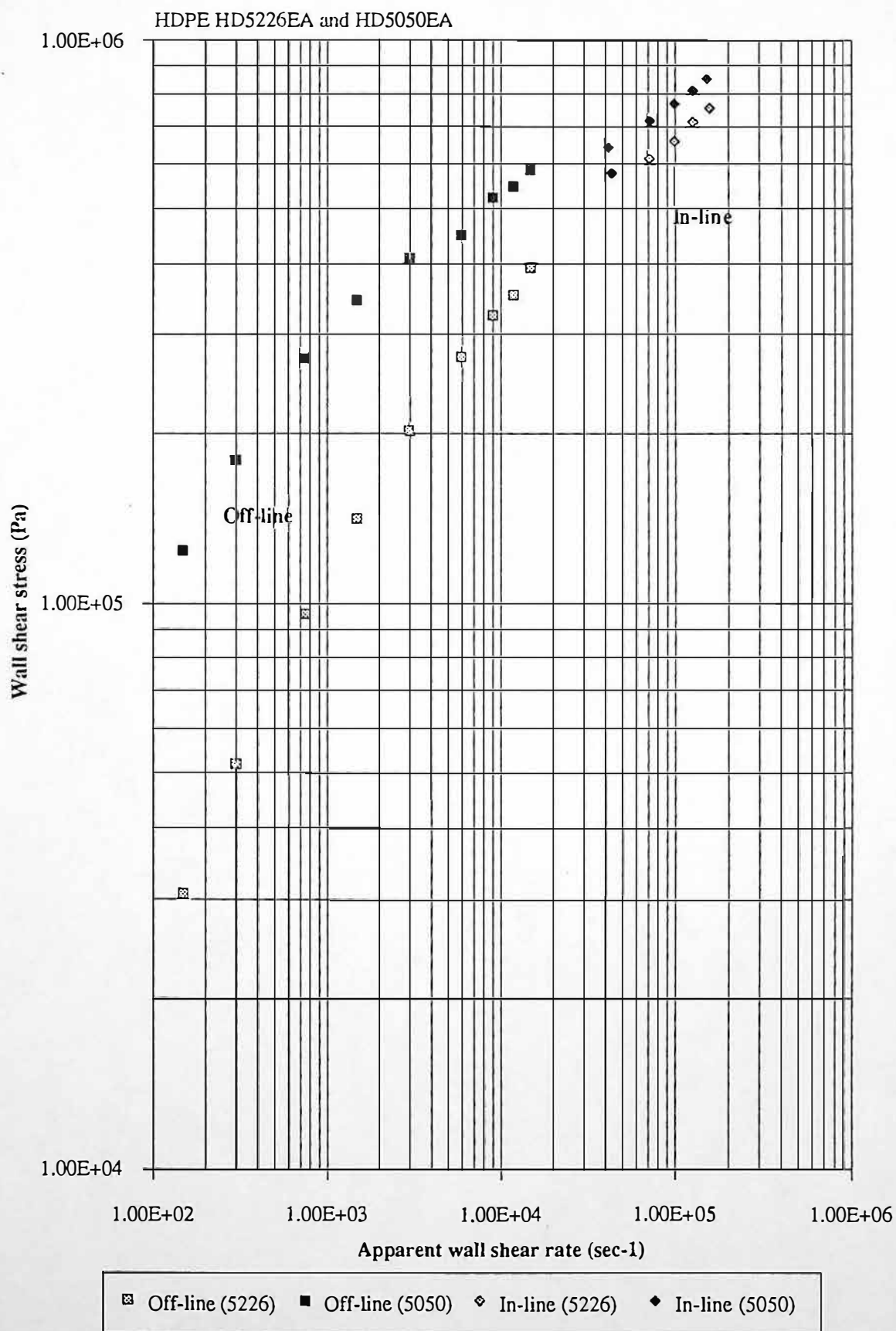
7.5 Comparison of In-line and Off-line Capillary Rheometry Experimental Results for High Density Polyethylene

7.5.1 Comparison of Wall Shear Stress Versus Apparent Wall Shear Rate Data

Figure 7.12 shows apparent wall shear stress versus wall shear rate, for two molecular weight grades of HDPE (BP Rigidex HD5226EA and HD5050EA), see chapter 7.2.1. It can be seen that in-line and off-line capillary rheometry techniques are both clearly capable of distinguishing between two different molecular weight grades of HDPE. Figure 7.12 shows that in-line and off-line capillary rheometry have comparable wall shear stress versus apparent wall shear rate relationships for the two molecular weight grades of HDPE.

Figure 7.12 also shows that the in-line data for HDPE HD5050EA has deviated from the general trend of the off-line data. This deviation can be described by: (i) an increase of apparent wall shear rate by approximately $2 \times 10^4 \text{ sec}^{-1}$, and (ii) a reduction of shear stress by approximately $1 \times 10^5 \text{ Pa}$. The reason for this phenomenon may be explained by: (i) leakage past the screw non-return valve, and (ii) polymer melt slip at the capillary die wall. Comparison of in-line and off-line capillary rheometry data for HD5226EA shows a good agreement, compared to the HDPE HD5050EA data. HDPE grade HD5226EA is a lower molecular weight grade HDPE than HD5050EA, and is therefore more susceptible to leak past the screw non-return valve, due to its inherently lower viscosity. Therefore, for the high molecular weight grade of HDPE (HD5050EA), it is likely that polymer melt slip at the die wall has occurred, Cogswell (1981 p 98), Hatziliriakos and Dealy (1992), Hatziliriakos et al (1992), unless the higher molecular weight HDPE prevented the non-return valve from proper operation.

Figure 7.12 In-line and off-line capillary rheometry
(uncorrected HDPE data)



In-line wall shear stress shows greatest deviation from the general trend at an apparent wall shear rate of $4.38 \times 10^4 \text{ sec}^{-1}$, the reason being experimental error. On inspection, it is apparent from the respective pressure profiles that the polymer had not reached steady flow conditions, this point is therefore only illustrated for experimental completeness and not included in the following analysis.

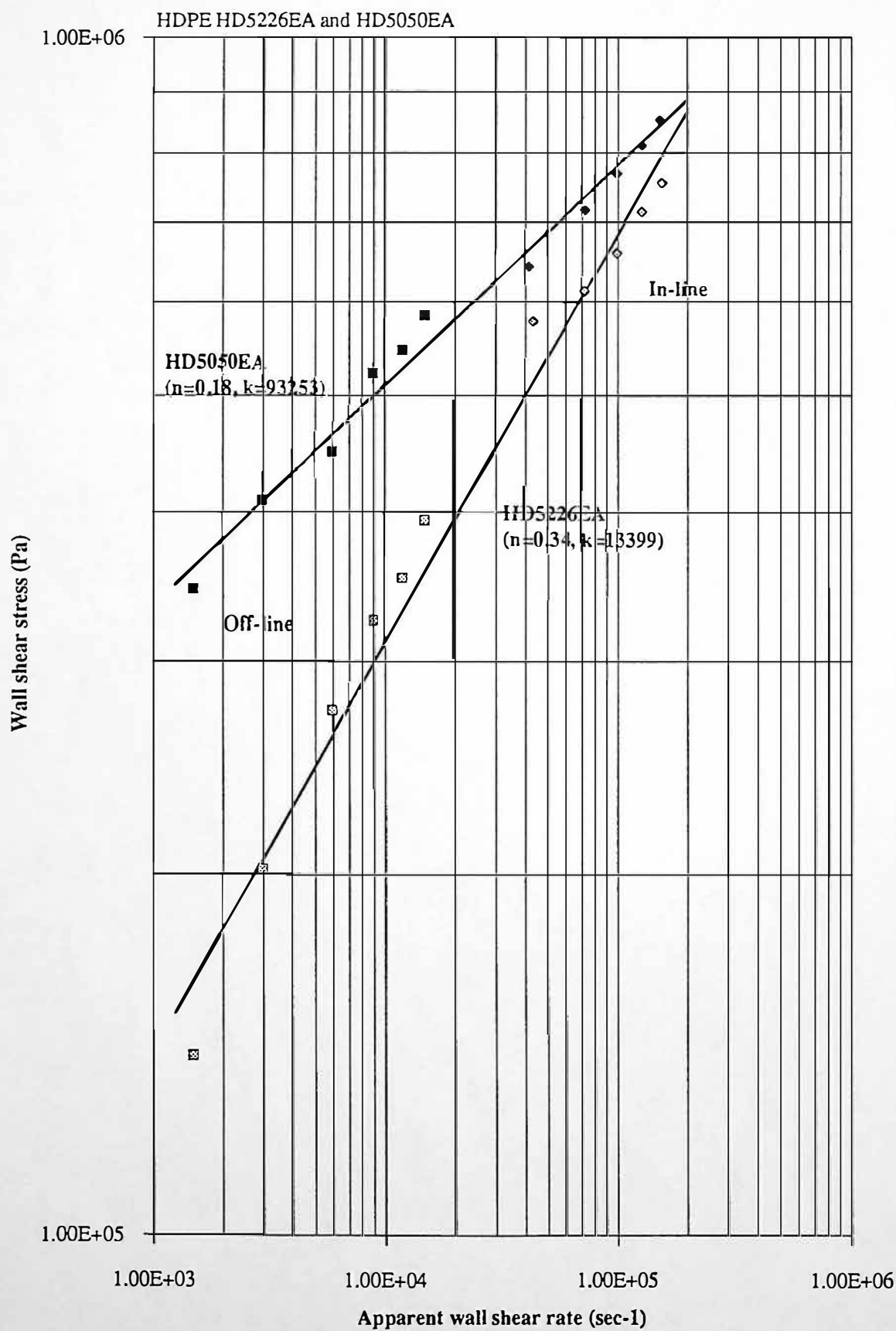
Figure 7.13 shows a comparison of in-line and off-line capillary rheometry data, for HDPE grade HD5226EA and HD5050EA, over the apparent wall shear rate range 1500 to 157082 sec^{-1} .

Tables 7.8 a and 7.8 b show the summarised results of power law analysis for the two molecular weight grades HDPE grades HD5226EA and HD5050EA. Power law curve fits of wall shear stress versus apparent wall shear rate for in-line and off-line rheometry are described. Also described are the combined power law curve fits for in-line and off-line capillary rheometry.

Rheometry Technique	Shear rate Range (sec^{-1})	Power n	Constant k	Coefficient of Correlation	Standard Error
In-line Capillary Rheometry	43763 - 157082	0.27	29382	0.998	0.0028
Off-line Capillary Rheometry	150 - 15000	0.54	2404	0.994	0.0470
Off-line and In-line Capillary Rheometry	1500 - 157082	0.34	13399	0.992	0.0337

Table 7.8 a Summary of power law results for HDPE grade HD5226EA (uncorrected data)

Figure 7.13 Comparison of in-line and off-line capillary rheometry (uncorrected HDPE data)



Rheometry Technique	Shear rate Range (sec ⁻¹)	Power n	Constant k	Coefficient of Correlation	Standard Error
In-line Capillary Rheometry	42010 - 154240	0.22	64643	0.999	0.0027
Off-line Capillary Rheometry	150 - 15000	0.32	27942	0.978	0.0525
Off-line and In-line Capillary Rheometry	1500 - 154240	0.18	93253	0.993	0.0157

Table 7.8 b Summary of power law results for HDPE grade HD5050EA (uncorrected data)

It is apparent from tables 7.8 a and 7.8 b that the n values are lower for in-line capillary rheometry data, than for off-line data. For HDPE grade HD5226EA the n values are 0.27 and 0.54 for in-line and off-line capillary rheometry, respectively. For HDPE grade HD5050EA the n values are 0.22 and 0.32 for in-line and off-line capillary rheometry, respectively. This difference in n value is most likely due to the different shear rate ranges investigated, for in-line and off-line capillary rheometry. Theoretically, wall shear stress versus wall shear rate flow curves, that perfectly obey the power law, can be described by a single n and K value. In practice there are only a few polymeric materials that follow the power ^{law} accurately, over a wide wall shear rate range (4 to 5 decades of wall shear rate). It is common practice to use the power law over a maximum of two decades, or less, fitting a number of curves. It is apparent from the off-line capillary rheometry data shown in Figure 7.12 that the n values are decreasing, for the two molecular weight HDPE grades. The decreasing values of n for increasing apparent wall shear rate are indicative of a pseudoplastic (shear thinning) polymer. The following analysis investigates this shear thinning behaviour.

A more accurate model of the wall shear stress versus apparent wall shear rate flow curve, can be derived by a second order polynomial curve fit, the results of which are shown in Table 7.13 for HD5226EA and HD5050EA.

Rigidex HDPE Grade	Coeff. 1 A	Coeff. 2 B	Constant C	Coefficient of Correlation	Standard Error
HD5226EA	2.26869	1.266818	-0.1130967	0.9999	0.0057
HD5050EA	3.480474	0.9651868	-0.1010375	0.9983	0.0154

Table 7.9 Second order polynomial curve fit data for HDPE grades HD52256EA and HD5050EA

Equation 7.4 is a second order polynomial, relating wall shear stress to apparent wall shear rate. Differentiation of equation 7.4, results in equation 7.5, which relates apparent wall shear rate to a specific n value.

$$\tau = A\dot{\gamma}^2 + B\dot{\gamma} + C \quad \text{Eq. 7.4}$$

$$n = 2A\dot{\gamma} + B \quad \text{Eq. 7.5}$$

Where:

τ = wall shear stress (Pa)

$\dot{\gamma}$ = apparent wall shear rate (sec^{-1})

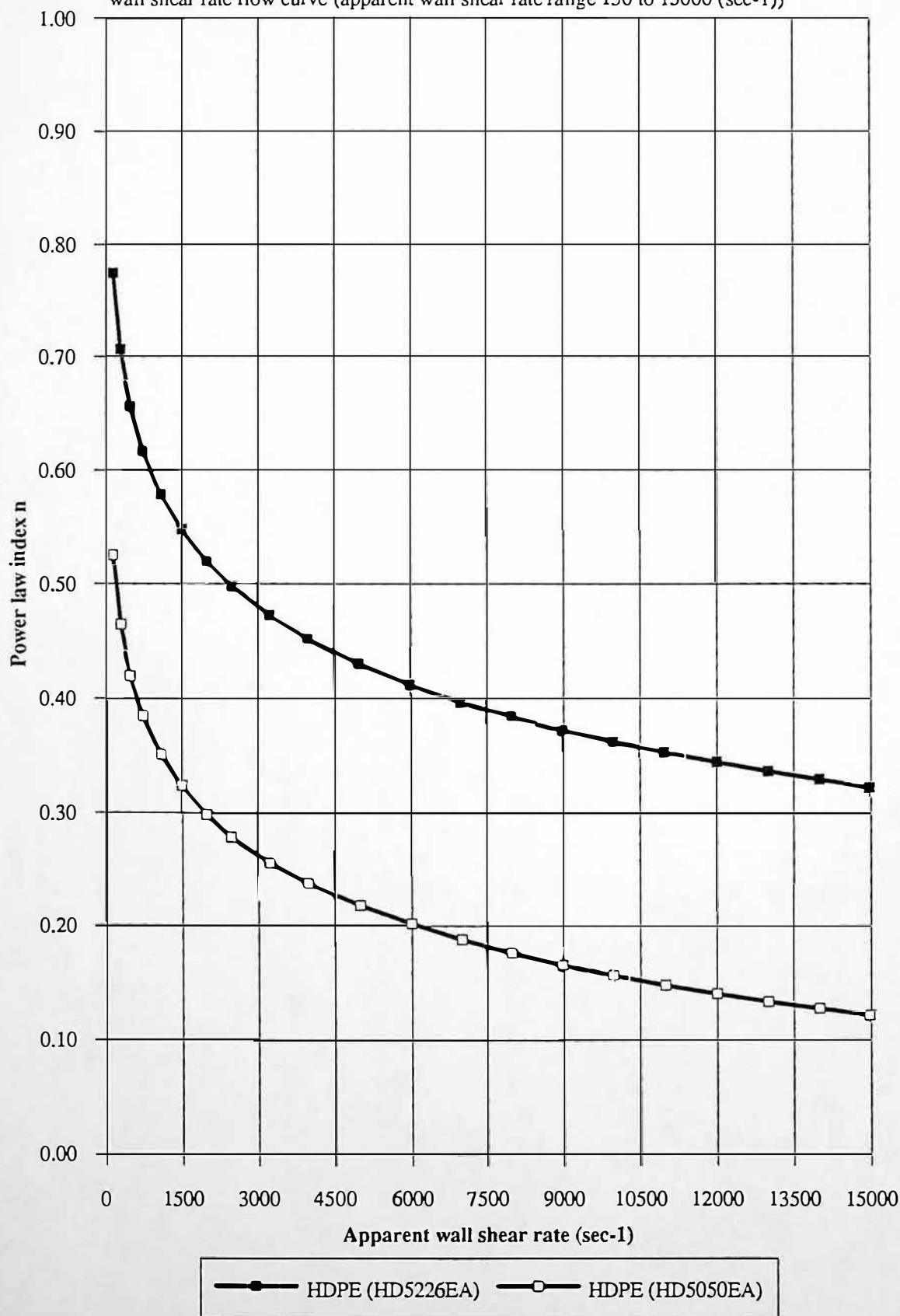
n = Power law Index

A, B and C are the second order polynomial coefficients

Figure 7.14 shows the influence of apparent wall shear rate on the n values for the shear rate range 150 to 15000 sec^{-1} , for HDPE grades HD5226EA and HD5050EA.

Figure 7.14 Influence of apparent wall shear rate on power law index n (uncorrected HDPE data)

Based on second order polynomial curve fit to off-line wall shear stress versus apparent wall shear rate flow curve (apparent wall shear rate range 150 to 15000 (sec⁻¹))



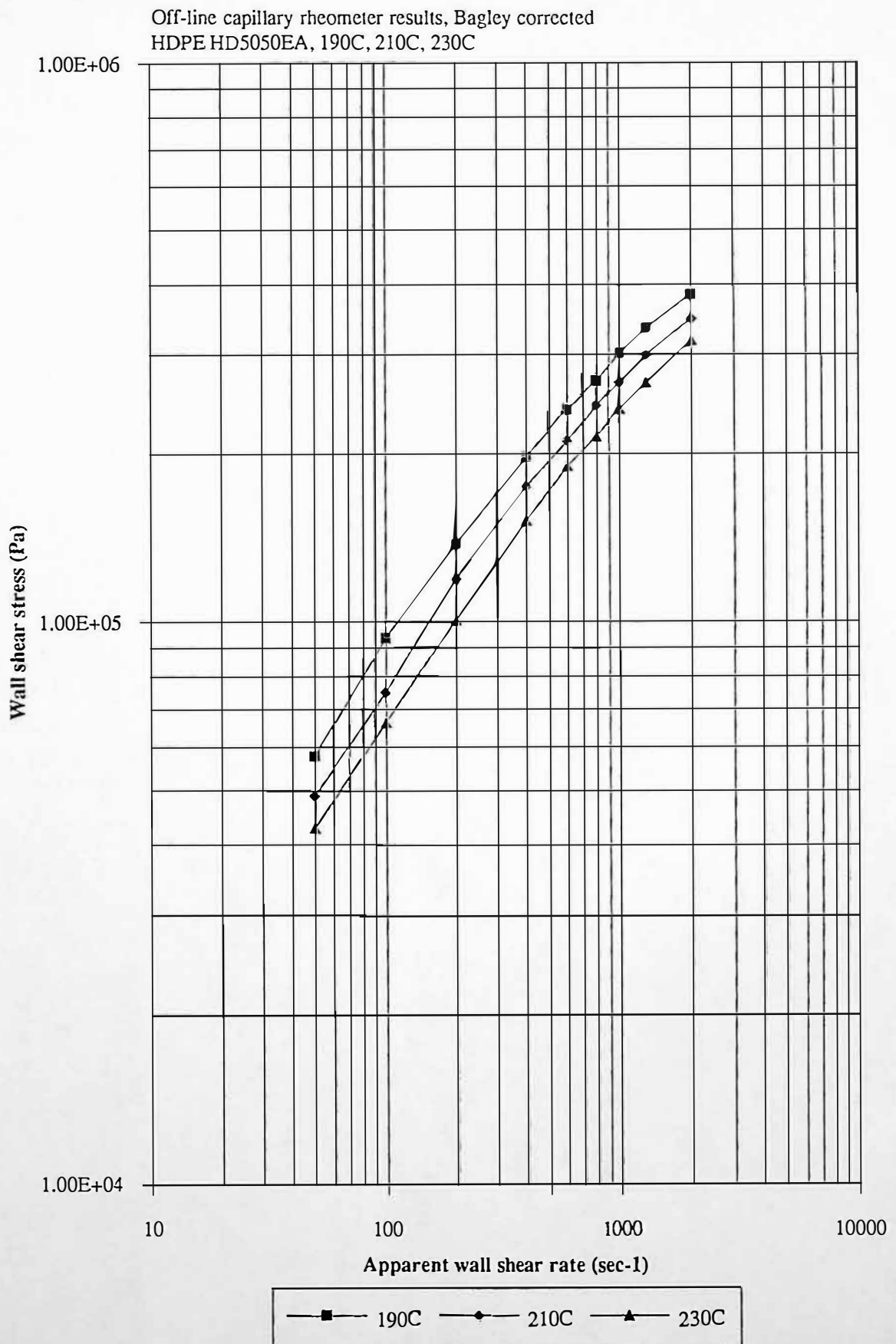
Considering HDPE grade HD5226EA, the off-line capillary rheometry n value for the wall shear rate range 150 to 15000 sec^{-1} is 0.54; the derived value of n for a shear rate of 15000 sec^{-1} is 0.32; therefore the in-line capillary rheometry n value of 0.27 for the shear range 72525 to 157082 sec^{-1} is a realistic n value. The reduction of n from 0.32 to 0.27 is most likely as a result of continued shear thinning, for the apparent wall shear rate range 15000 to 72525 sec^{-1} . An extrapolated n value calculated using equation 7.5 for the shear rate 72525 sec^{-1} = 0.17. Therefore, extrapolated n values for apparent wall shear rates outside the original curve fit range, may be subject to large inaccuracies, as shown.

Considering HDPE grade HD5050EA, the off-line capillary rheometry n value for the shear rate range 150 to 1500 sec^{-1} is 0.32, the derived value of n for a shear rate of 15000 sec^{-1} is 0.12; therefore the in-line capillary rheometry n value of 0.22 is higher than the derived value. The reason for the high n values is most likely due to the leakage past the screw non-return valve or the slip at the wall of the capillary die. An extrapolated n value calculated using equation 7.5 for the apparent wall shear rate 41010 sec^{-1} = 0.03. This very low n value emphasises that polynomial extrapolation outside the original curve fit range may be subject to large inaccuracies.

7.5.2 Influence of Melt Temperature on Wall Shear Stress

Data from tables 7.8 a and 7.8 b have shown in-line and off-line capillary rheometry to have different n values. In-line capillary rheometry having substantially lower n values. Analysis has shown the different n values are most likely a result of the different apparent wall shear rate ranges. The following investigation analyses the influence of melt temperature changes due to shear heating effect through the die. Figure 7.15 shows off-line capillary rheometry data for HDPE grade HD5050EA, for three melt temperatures 190C, 210 and 230 C. Wall shear stress versus apparent wall shear rate is shown.

**Figure 7.15 Influence of temperature on wall shear stress
(uncorrected HDPE data)**



It can be seen from figure 7.15 that wall shear stress decreases as melt temperature increases. The mean shear stress change with temperature ΔT , was calculated to be 1172 Pa/C.

The influence of shear heating effects on polymer melt temperature during 'airshot' tests was investigated. Figure 7.16 shows the result of tests on HDPE grade HD5050EA, for set injection velocities of 3, 5, 7, 9, 11 mm/s.

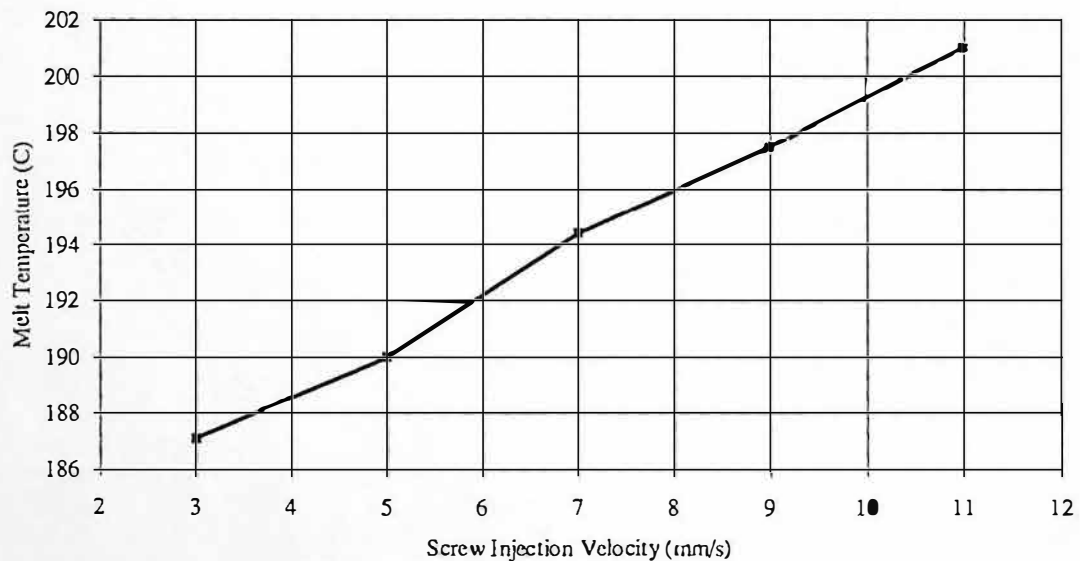


Figure 7.16 Influence of shear heating on polymer melt temperature

The machine parameter settings are shown in Table 7.3. Five 'airshots' were initiated, prior to melt temperature measurement, this ensured that the melt temperature was a true reflection of process conditions. The nozzle temperatures were set at 190C, the measured melt temperature for the screw injection velocity of 3 mm/s = 187C. It is apparent that the measured temperatures are subject to constant error. The loss in heat may be due to: (i) machine parameter variation of the temperature controller, (ii) poor

(uneven) heating of the polymer melt in the barrel, and (iii) cooling of the polymer melt after the 'airshot', before reaching the bulk of the material. The measured temperature rise $\Delta T = 13.9\text{C}$, this compares with the calculated adiabatic temperature rise of $\Delta T = 24.9\text{C}$ based on $\Delta P = 5.45 \times 10^7\text{ Pa}$, specific heat = 2300 J/Kg/C , density = 950 Kg/m^3 . The difference between the measured and calculated temperatures, is most likely due to thermal conduction from the polymer melt to the nozzle and capillary die, during the 'airshot'.

The n values for in-line and off-line rheometry are 0.32 and 0.22 respectively. A corrected n value for the in-line capillary rheometry data can be derived. The n value correction procedure uses the data shown in figure 7.16, combined with the calculated shear stress change with temperature (1172 Pa / C), assuming a linear relationship between melt temperature and apparent wall shear rate. The corrected n value is 0.23, showing that shear heating effects cause a minimal change of the n value, for these specific test conditions.

For shear heating effects to be sufficient to cause the drop of n from 0.32 to 0.22, the shear stress change per degree C would have to at least equal 8400 Pa / C or $\Delta T = 99.6\text{ C}$. The calculated adiabatic temperature rise $\Delta T = 24.9\text{ C}$, showing that an increase of melt temperature by 99.6 C , due to shear heating effects, is most unlikely, for these specific process conditions.

7.5.3 Effect of Bagley Correction

Figure 7.17 shows wall shear stress (Bagley corrected) versus apparent wall shear rate for the two molecular weight HDPE grades. Tables 7.10 a and 7.10 b show the summarised results of power law analysis for the two molecular weight grade HDPE (HD5226EA and HD5050EA). Power law curve fits of wall shear stress (Bagley corrected) versus apparent wall shear rate for in-line and off-line rheometry are described. Also described are the combined power law curve fits for in-line and off-line capillary rheometry.

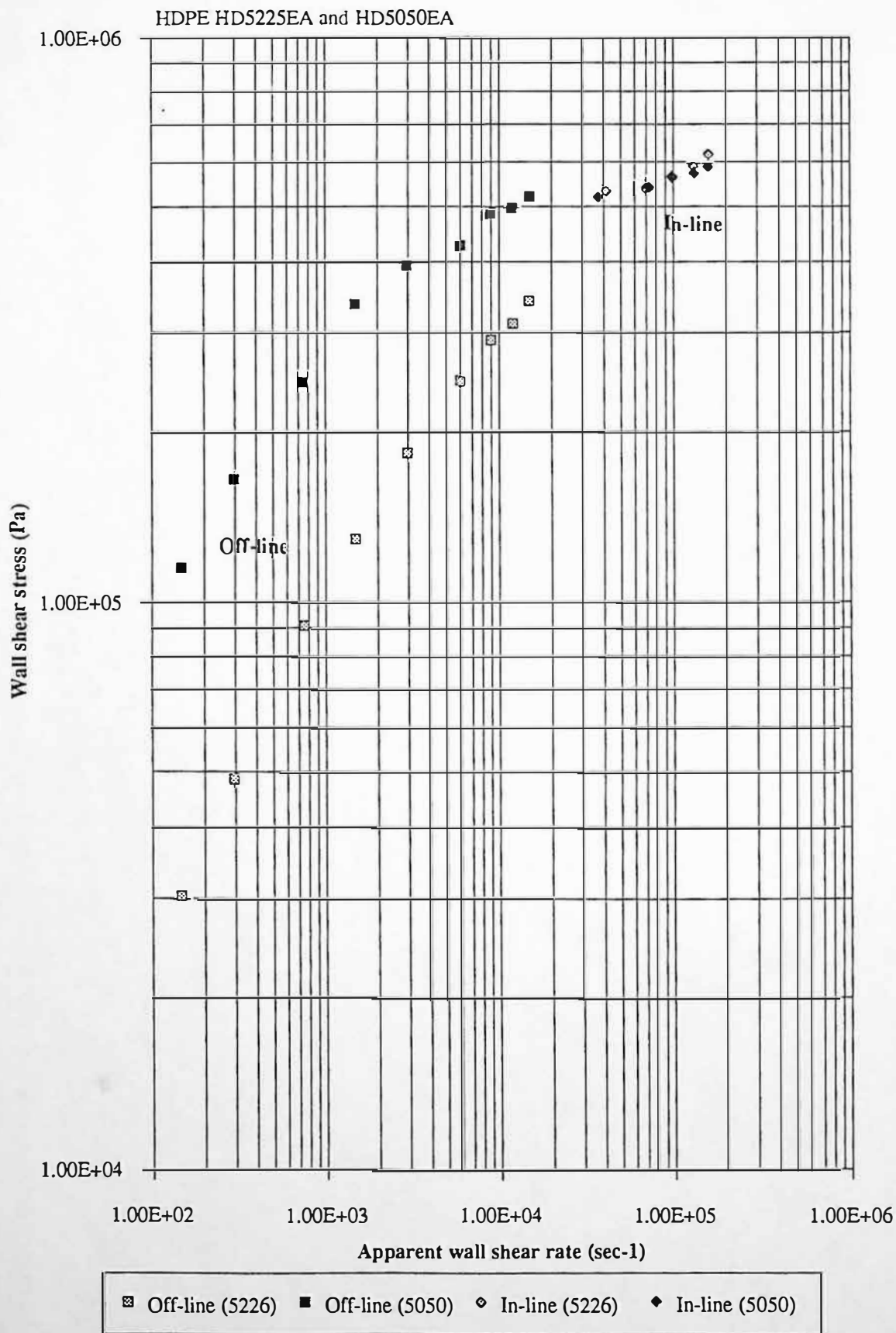
Rheometry Technique	Shear rate Range (sec ⁻¹)	Power n	Constant k	Coefficient of Correlation	Standard Error
In-line Capillary Rheometry	41914 - 158579	0.17	85039	0.994	0.0035
Off-line Capillary Rheometry	150 - 15000	0.52	2635	0.993	0.0464
Off-line and In-line Capillary Rheometry	1500 - 158579	0.32	14319	0.990	0.0357

Table 7.10 a Summary of power law results for HDPE grade HD5226EA (Bagley corrected data)

Rheometry Technique	Shear rate Range (sec ⁻¹)	Power n	Constant k	Coefficient of Correlation	Standard Error
In-line Capillary Rheometry	37591 - 159173	0.09	211394	0.987	0.0039
Off-line Capillary Rheometry	150 - 15000	0.32	29791	0.984	0.0446
Off-line and In-line Capillary Rheometry	1500 - 159173	0.10	176140	0.941	0.0271

Table 7.10 b Summary of power law results for HDPE grade HD5050EA (Bagley corrected data)

Figure 7.17 In-line and off-line capillary rheometry (Bagley corrected HDPE data)



Identification of the two HDPE molecular weight grades for off-line capillary rheometry is clearly possible, the in-line data after being Bagley corrected are not so clearly separated.

Table 7.11 Summarises the n values for uncorrected and Bagley corrected data, for in-line and off-line capillary rheometry.

	In-line Capillary Rheometry		Off-line Capillary Rheometry	
	Uncorrected	Bagley Corr.	Uncorrected	Bagley Corr.
HD5226EA	0.27	0.17	0.54	0.52
HD5050EA	0.22	0.09	0.32	0.32

Table 7.11 Summary of n values for uncorrected and Bagley corrected HDPE data

The Bagley correction does not significantly influence the n values derived from the off-line capillary rheometer. For HDPE grades HD5226EA and HD5050EA the n values only change for HDPE grade HD5226EA from 0.54 to 0.52, representing a 4% change. The HDPE grade HD5050EA n value remained constant at 0.32, representing a 0% change. For the off-line capillary rheometry wall shear rate range 150 to 15000 sec^{-1} the ends pressure drop are low (Bagley correction).

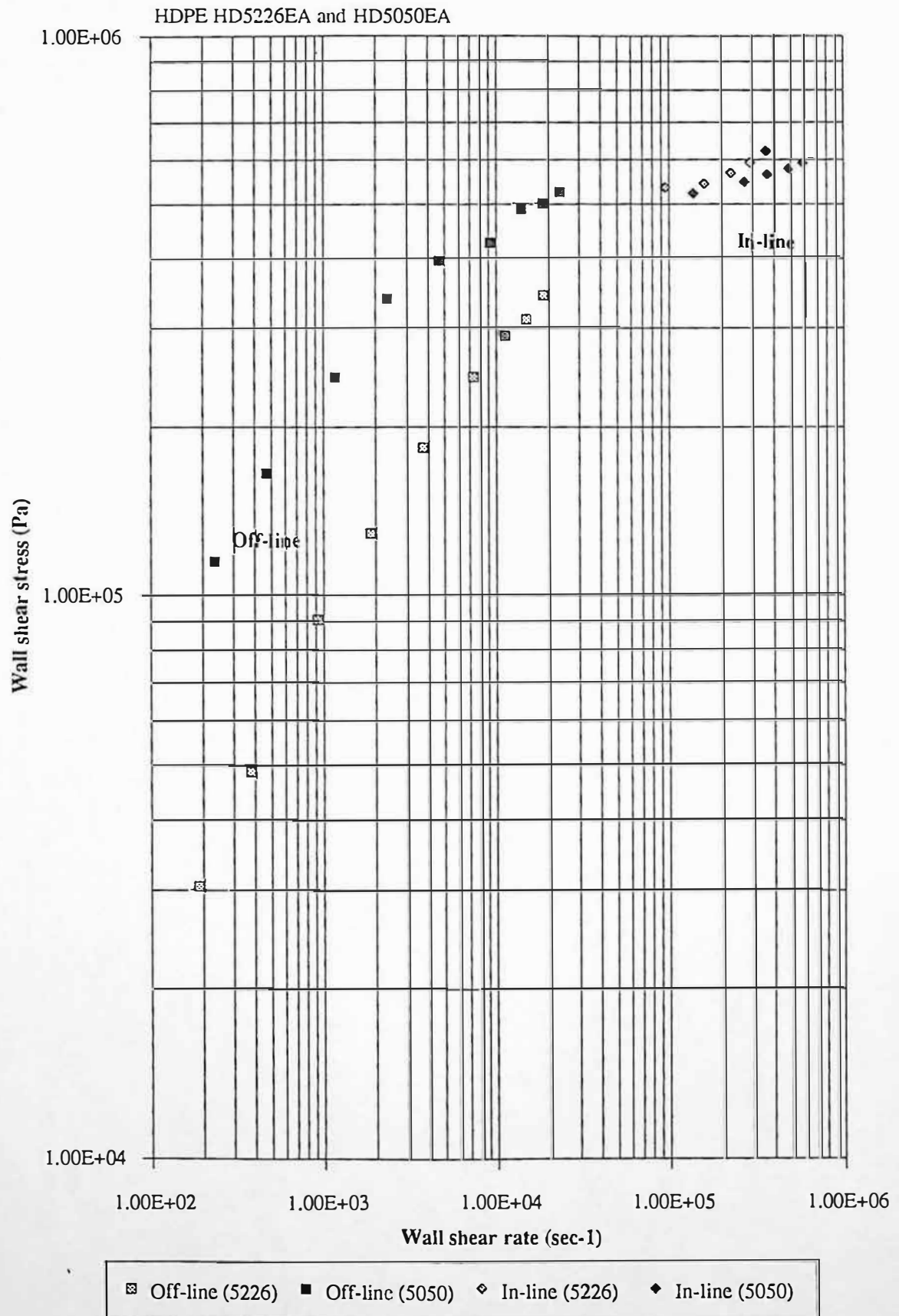
However, the Bagley correction has a strong influence on the n values for in-line capillary rheometry for the wall shear rate ranges 41914 - 158579 sec^{-1} and 37591 - 159173 sec^{-1} . For HDPE grades HD5226EA and HD5050EA the n values are reduced from 0.27 to 0.17 and 0.22 to 0.09, representing percentage changes of 37% and 59% respectively. The in-line n values for HDPE grades HD5226EA and HD5050EA can be seen from figures 7.5.6, as different gradients.

The very low in-line n value for HD5050EA indicates that polymer melt slip at the capillary die wall is most likely occurring. This low n value is evidence for the assumption made in chapter 7.5.1, that polymer melt slip at the capillary die wall is occurring, for the uncorrected wall shear stress versus apparent wall shear rate data. Slip must be suspected in capillary rheometer data if the n value is very low, i.e. less than 0.1, Fenner (1979 p 28). It is apparent from figure 7.12 that the two molecular weight grades of HDPE are clearly separable. Figure 7.17 shows that the Bagley corrected data for the two molecular weight grades HDPE are not so clearly separable. The low n value for the Bagley corrected data indicates that, due to the plug-flow, volumetric flow rate is almost independent of shear stress. Therefore the end pressure drop data are indicative of the two molecular weight grades of HDPE.

7.5.4 Effect of Rabinowitsch Correction

Figure 7.18 shows wall shear stress (Bagley corrected) versus true wall shear rate (Rabinowitsch correction) for the two molecular weight grades of HDPE. It is necessary to ignore the data point for HD5226EA at a shear rate of $9.48 \times 10^4 \text{ sec}^{-1}$, $4.19 \times 10^4 \text{ sec}^{-1}$ (before Rabinowitsch corrected), due to the fore mentioned experimental error (see chapter 7.5.1). The corrected off-line capillary rheometry data clearly determines a difference between the two HDPE grades. The in-line capillary rheometry data show the two different molecular weight grades of HDPE as different slopes of the wall shear stress versus wall shear rate flow curve. The low n values of the Bagley corrected HDPE grade HD5050EA data, influence the Rabinowitsch correction for true wall shear rate, by an additional $3 \times 10^5 \text{ sec}^{-1}$ (approximately), compared to the HDPE HD5226EA data. This level of wall shear rate correction indicates that polymer melt slip at the capillary die wall may have occurred.

Figure 7.18 In-line and off-line capillary rheometry
(Bagley and Rabinowitsch corrected HDPE data)



7.6 Comparison of In-line and Off-line Capillary Rheometry Experimental Results for Polyoxymethylene

7.6.1 Comparison of Wall Shear Stress Versus Apparent Wall Shear Rate Data

Figure 7.19 shows wall shear stress versus apparent wall shear rate for three molecular weight grades of POM (Du Pont Delrin II 900F, 500 and 100), see chapter 7.2.2. It can be seen that in-line and off-line capillary rheometry techniques are both clearly capable of distinguishing between three different molecular weight grades of POM. It can also be seen from figure 7.19, that the POM data can best be described by two linear flow regions, as shown in figure 7.20. The two linear regions are above and below the shear rates of 4500, 3600 and 5000 sec^{-1} , for POM 900F, 500 and 100 respectively. Considering POM Delrin II grade 500, the wall shear stress versus apparent wall shear rate relationship is described by the following expressions:

$$250 \leq \dot{\gamma} \leq 3600 \quad (\text{sec}^{-1}) \quad \text{Wall Shear Stress} = 3913\dot{\gamma}^{0.58}$$

$$3600 \leq \dot{\gamma} \leq 158129 \quad (\text{sec}^{-1}) \quad \text{Wall Shear Stress} = 62700\dot{\gamma}^{0.24}$$

Table 7.17 shows off-line capillary rheometry power law curve fit results, for apparent wall shear rates of 250 to 6000 sec^{-1} , for the lower linear region.

Delrin II POM Grade	Power n	Constant k	Coefficient of Correlation	Standard Error
900F	0.64	1881	0.997	0.035
500	0.58	3913	0.994	0.040
100	0.45	16523	0.990	0.018

Table 7.12 Off-line capillary rheometry power law results for POM

Figure 7.21 shows a comparison between in-line and off-line data for the upper linear region, for the three molecular weight grades of POM.

Figure 7.19 In-line and off-line capillary rheometry
(uncorrected POM data)

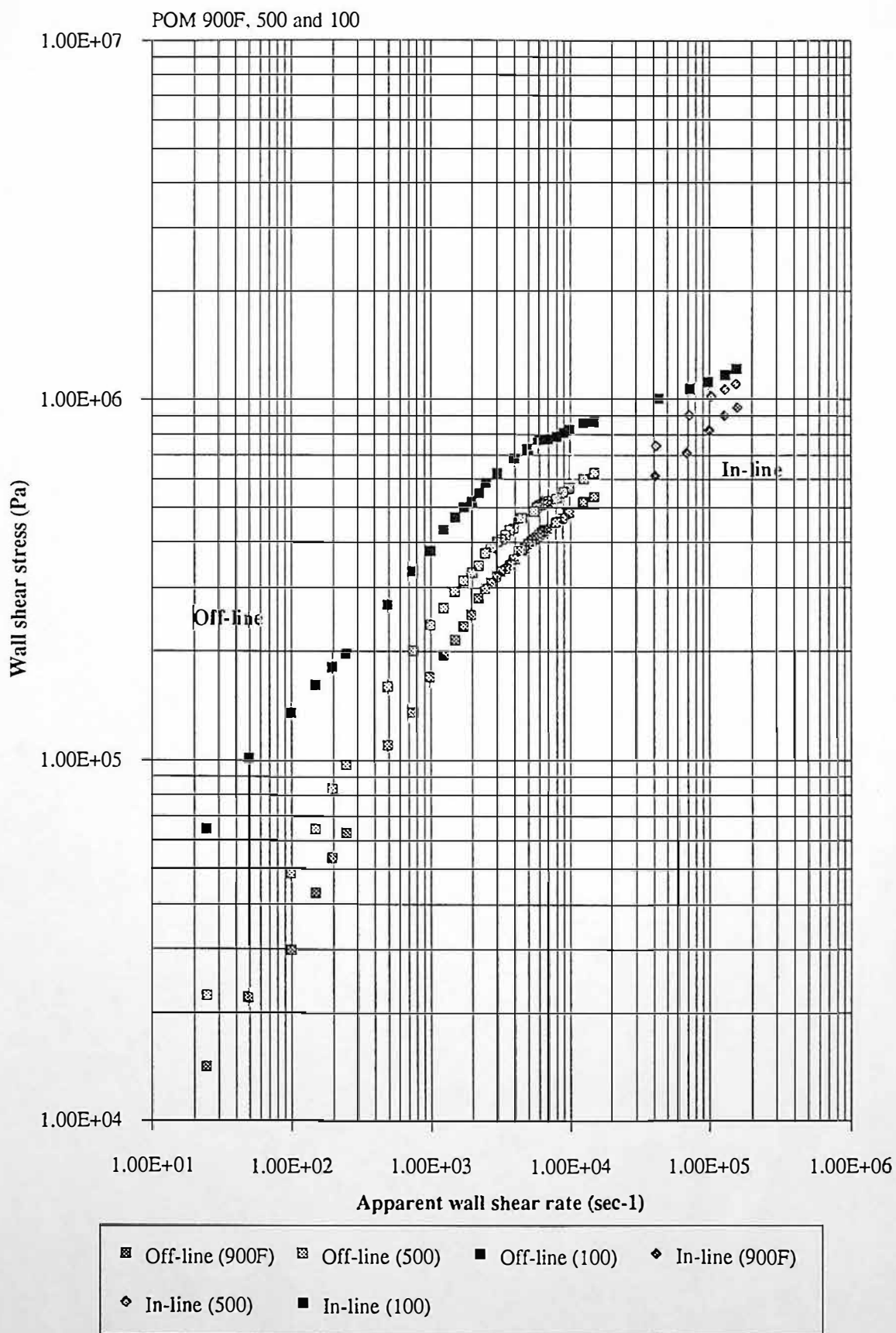


Figure 7.20 Two non-Newtonian linear flow regions for three molecular weight grades of POM (uncorrected data)

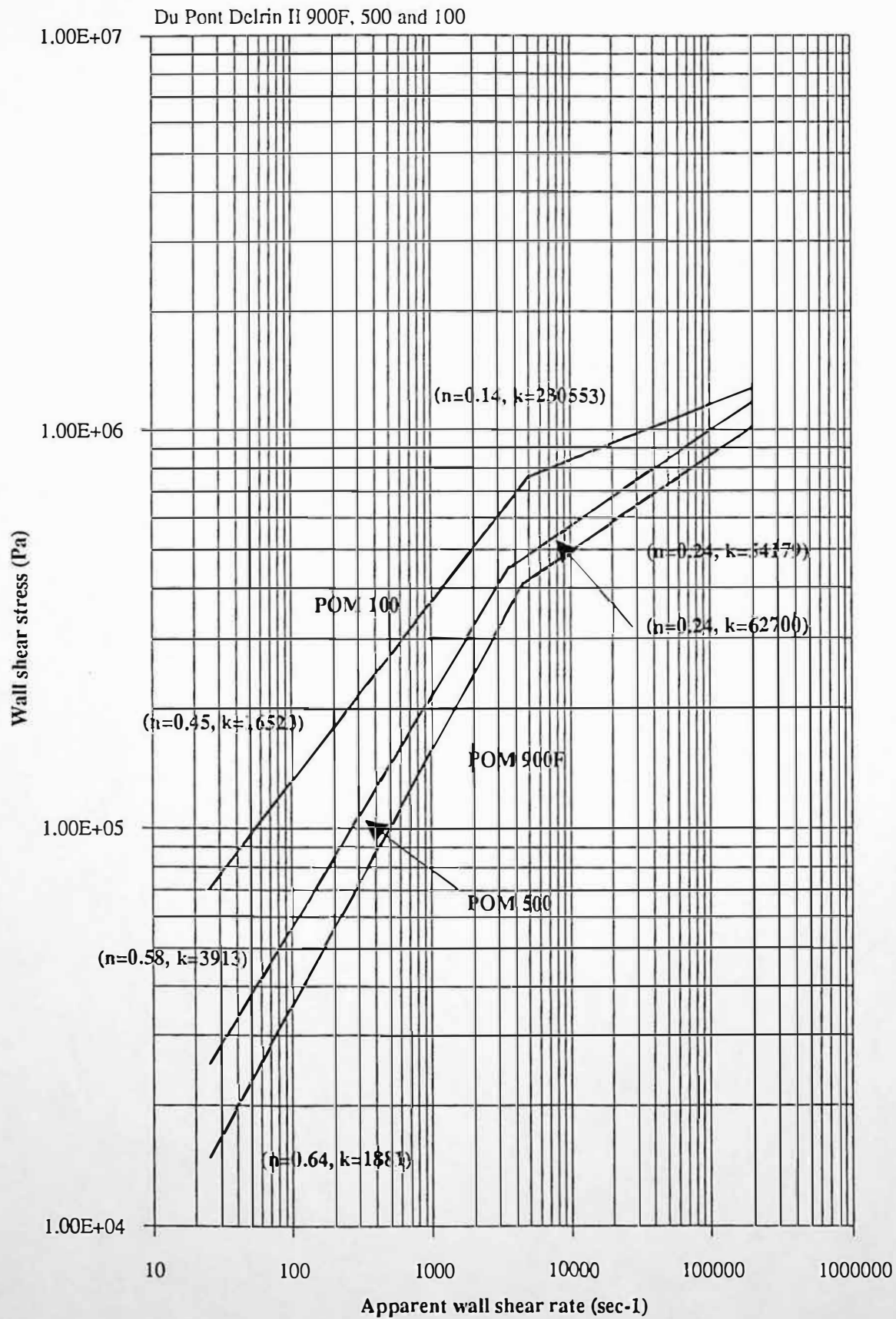
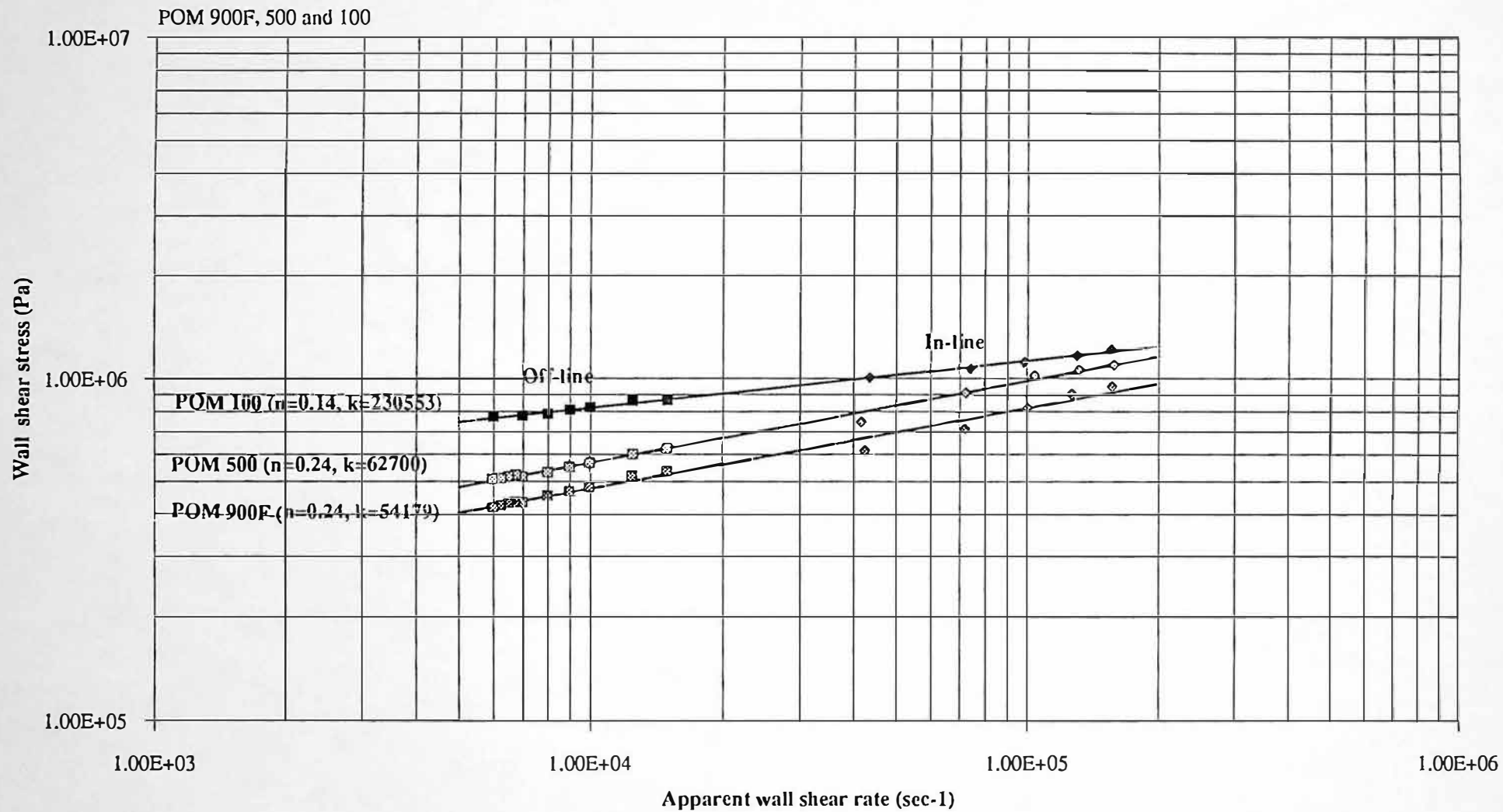


Figure 7.21 Comparison of in-line and off-line capillary rheometry (uncorrected POM data)



Tables 7.13 a, 7.13 b and 7.213 c show the summarised results of power law analysis for the upper linear region, for the three molecular weight grades of POM for in-line, off-line and combined in-line and off-line data.

Rheometry Technique	Shear rate Range (sec-1)	Power n	Constant k	Coefficient of Correlation	Standard Error
In-line Capillary Rheometry	42547 - 156455	0.35	15208	0.996	0.0080
Off-line Capillary Rheometry	6000 - 15000	0.27	39317	0.998	0.0027
Off-line and In-line Capillary Rheometry	6000 - 155455	0.24	54179	0.993	0.0154

Table 7.13 a Summary of power law results for POM grade 900F (uncorrected data)

Rheometry Technique	Shear rate Range (sec-1)	Power n	Constant k	Coefficient of Correlation	Standard Error
In-line Capillary Rheometry	41741 - 158129	0.30	32866	0.990	0.0109
Off-line Capillary Rheometry	6000 - 15000	0.23	66865	0.994	0.0036
Off-line and In-line Capillary Rheometry	6000 - 158129	0.24	62700	0.997	0.0095

Table 7.13 b Summary of power law results for POM grade 500 (uncorrected data)

Rheometry Technique	Shear rate Range (sec-1)	Power n	Constant k	Coefficient of Correlation	Standard Error
In-line Capillary Rheometry	43443 - 156256	0.15	208703	0.994	0.0039
Off-line Capillary Rheometry	6000 - 15000	0.14	226204	0.979	0.0044
Off-line and In-line Capillary Rheometry	6000 - 156256	0.14	230553	0.999	0.0040

Table 7.13 c Summary of power law results for POM grade 100 (uncorrected data)

It is apparent from tables 7.13 a and 7.13 b that n values are higher for the in-line data, compared to the off-line data, for the POM grades 900F and 500. The in-line n values = 0.35 and 0.30 compared to the off-line n values = 0.27 and 0.23 for POM 900F and 500. The *in*-line wall shear stress data for POM 900F and 500 are low for screw injection velocities of 3 and 5 mm/s. This is most likely a result of polymer melt leakage past the screw non-return valve. Above 5 mm/s the polymer melt is likely to tension stiffen due to extensional viscosity effects, therefore leakage past the screw non-return valve may be reduced.

Data for POM 100 shows good agreement between in-line and off-line n values, 0.15 and 0.14 respectively. Figure 7.22 shows the velocity profiles in the capillary dies for the two linear flow regions of the POM 100 data, at a constant wall shear stress of 4.69×10^5 Pa. The low value of n obtained for the POM 100 indicates a predominately 'plug-like' flow, this can be seen in figure 7.22. For $n = 0.14$ the velocity is almost constant over the central region of flow from $r = 0.00$ to 0.30 mm, where shear flow is limited to an outer skin of material in the region $r = 0.30$ to 0.50 mm. It is apparent that decreasing values of n , increase the influence of plug-flow, resulting in increased shear flow in the outer skin.

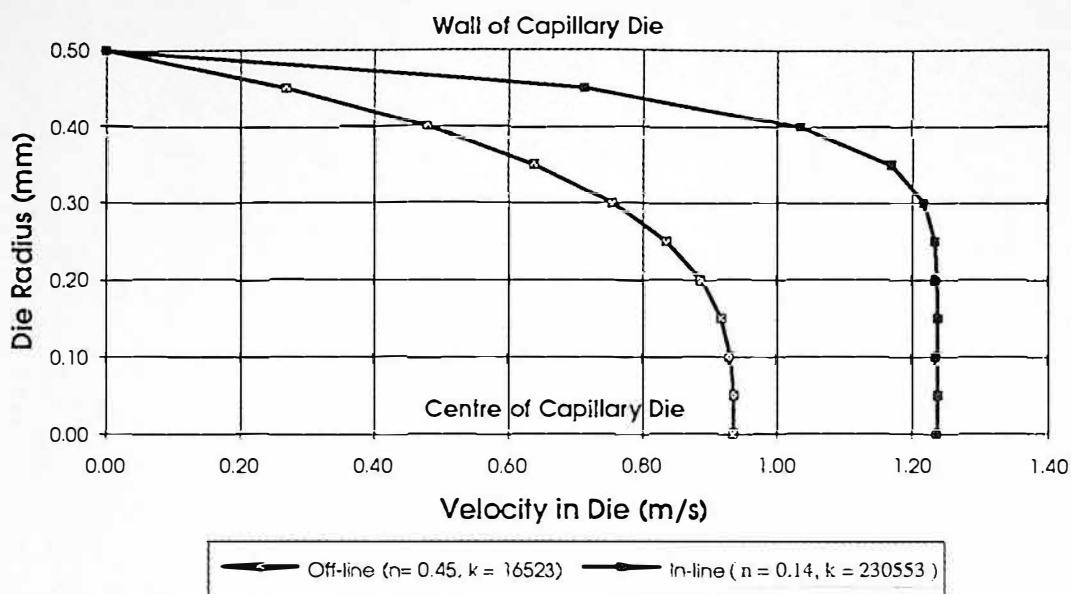
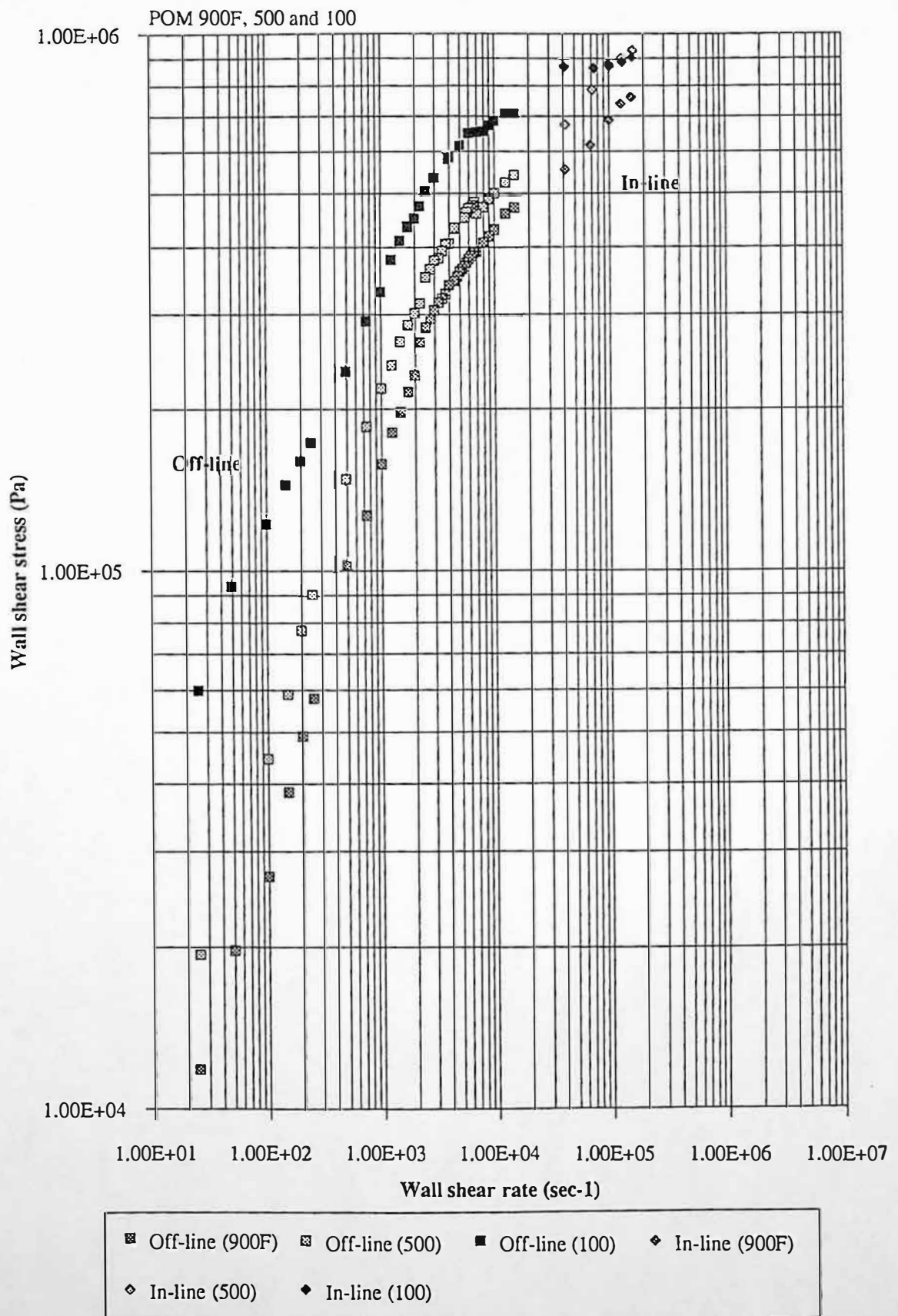


Figure 7.22 Velocity profiles in capillary die

7.6.2 Effect of Bagley Correction

Figure 7.23 shows wall shear stress (Bagley corrected) versus apparent wall shear rate for the three molecular weight grades of POM (900F, 500 and 100) respectively. It is apparent from figure 7.19 that the Bagley corrected data is uncharacteristically high for off-line capillary rheometry for the wall shear rate 2500 to 6750 sec^{-1} . The reason for the high shear stress values is due to low P_s measurements, probably resulting from contamination on the short die pressure transducer diaphragm.

Figure 7.23 In-line and off-line capillary rheometry
(Bagley corrected POM data)



Tables 7.14 a, 7.14 b and 7.14 c show the results of power law analysis for the upper linear region, on the three POM molecular weight grades, for in-line, off-line and combined data.

Rheometry Technique	Shear rate Range (1/s)	Power n	Constant k	Coefficient of Correlation	Standard Error
In-line Capillary Rheometry	41235 - 158351	0.25	40309	0.996	0.0063
Off-line Capillary Rheometry	6000 - 15000	0.24	46445	0.997	0.0026
Off-line and In-line Capillary Rheometry	6000 - 158351	0.22	54339	0.988	0.0191

Table 7.14 a Summary of power law results for POM grade 900F (Bagley corrected data)

Rheometry Technique	Shear rate Range (1/s)	Power n	Constant k	Coefficient of Correlation	Standard Error
In-line Capillary Rheometry	41600 - 162905	0.25	50116	0.987	0.0107
Off-line Capillary Rheometry	7000 - 15000	0.23	62283	0.999	0.0017
Off-line and In-line Capillary Rheometry	7000 - 162905	0.23	59030	0.999	0.0067

Table 7.14 b Summary of power law results for POM grade 500 (Bagley corrected data)

Rheometry Technique	Shear rate Range (1/s)	Power n	Constant k	Coefficient of Correlation	Standard Error
In-line Capillary Rheometry	41082 - 159920	0.03	651231	0.731	0.0066
Off-line Capillary Rheometry	6000 - 15000	0.11	240427	0.965	0.0047
Off-line and In-line Capillary Rheometry	6000 - 159920	0.11	252468	0.977	0.0134

Table 7.14 c Summary of power law results for POM grade 100 (Bagley corrected data)

Table 7.15 Summarises the n values for uncorrected and Bagley corrected data, for in-line and off-line capillary rheometry.

Delrin II POM Grade	In-line Capillary Rheometry		Off-line Capillary Rheometry	
	Uncorrected	Bagley Corr.	Uncorrected	Bagley Corr.
900F	0.35	0.25	0.27	0.24
500	0.30	0.25	0.23	0.23
100	0.15	0.03	0.14	0.11

Table 7.15 Summary of n values for uncorrected and Bagley corrected POM data

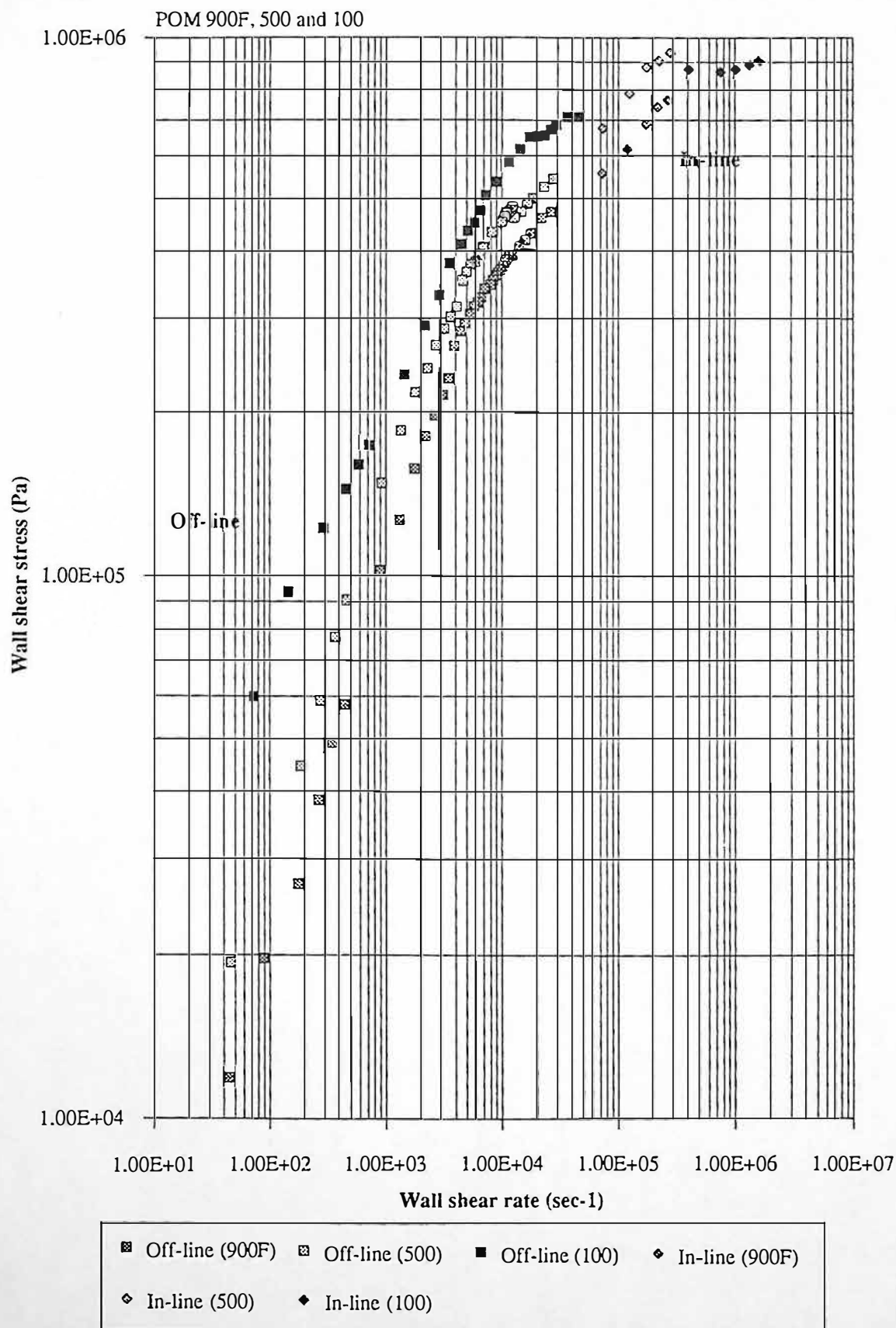
The Bagley correction does not significantly influence the n values from the off-line capillary rheometer. The Bagley correction reduced the n values for POM 900F, 500 and 100 by 11%, 0% and 21% respectively. The uncorrected and Bagley corrected n values for POM 100 are low 0.14 and 0.11 respectively. These low n values indicate that polymer melt slip at the capillary die wall is most likely occurring.

Figure 7.23 shows that in-line capillary rheometry data is clearly separable for the three molecular weight POM grades. It is apparent from tables 7.14 a and 7.14 b that n values have close agreement for in-line and off-line capillary rheometry, for the POM 900F and 500. The in-line n values = 0.25 and 0.25 compared to off-line n values = 0.24 and 0.23 for POM 900F and 500, respectively. The n values for POM 100 are 0.03 and 0.11 for in-line and off-line data respectively. The n value for in-line data is very low at 0.03, polymer melt slip in the capillary die wall is most likely occurring. The very low n value indicates that volumetric flow rate is almost independent of shear stress.

7.6.3 Effect of Rabinowitsch Correction

Figure 7.24 shows wall shear stress (Bagley correction) versus true shear wall shear rate (Rabinowitsch correction) for the three different molecular grades of POM. The low n values of the Bagley corrected POM 100 data, influence the Rabinowitsch correction for true wall shear rate, by an additional $1 \times 10^6 \text{ sec}^{-1}$ (approximately), compared to the POM 900F and POM 500 data. This level of wall shear rate correction indicates that polymer melt slip at the capillary die wall may have occurred.

Figure 7.24 In-line and off-line capillary rheometry
(Bagley and Rabinowitsch corrected POM data)



7.7 Discussion of Results

In-line and off-line capillary rheometry tests are discussed, regarding measurement of material variation by consideration of wall shear stress versus wall shear rate flow curves. Data are analysed in an uncorrected form, Bagley corrected and Rabinowitsch corrected forms.

In-line capillary rheometer tests were manually sequenced, demanding high operator concentration, as experimental errors may dictate that tests are repeated. Automatic operation during actual moulding conditions should improve machine sequencing accuracy, Speight and Coates (1991), therefore improving the repeatability of results. An example of experimental error is described in chapter 7.5.1, whereby the polymer melt had not reached a steady flow condition, airshot to airshot.

7.7.1 High Density Polyethylene (HDPE) Data

It can be seen from Figure 7.12 that in-line and off-line capillary rheometry techniques are both clearly capable of distinguishing between two different molecular weight grades of HDPE. Figure 7.12 also shows that the in-line data for HDPE HD5050EA has deviated from the general trend of the off-line data. The reason for this phenomenon may be explained by: (i) leakage past the screw non-return valve, (ii) polymer melt slip at the capillary die wall. HDPE grade HD5226EA is a lower molecular weight grade HDPE than HD5050EA, and is therefore more susceptible to leak past the screw non-return valve, due to its inherently lower viscosity. Analysis of the low molecular weight grade HDPE (HD5226EA), shows good agreement between in-line and off-line data. Therefore, as HDPE grade HD5050EA is a higher molecular weight than grade HD5226EA, it is most likely that polymer melt slip at the capillary die wall has occurred.

Capillary Rheometry Technique / Material Grade	In-line (A)	Off-line (B)	Deviation (A - B)	In-line and Off-line
HDPE HD5226EA	0.27	0.54	- 0.27	0.34
HDPE HD5050EA	0.22	0.32	- 0.10	0.18

Table 7.16 Summary of HDPE power law index n values (uncorrected data)

It is apparent from table 7.16 that the n values are lower for in-line capillary rheometry data, than off-line data. For HDPE HD5226EA the n values are 0.27 and 0.54 for in-line and off-line capillary rheometry, respectively. For HDPE HD5050EA the n values are 0.22 and 0.32 for in-line and off-line capillary rheometry, respectively. This difference in n value is most likely due to the different wall shear rate ranges investigated, for in-line and off-line capillary rheometry. It is apparent from the off-line capillary rheometry data shown in Figure 7.12 that the n values are decreasing, for the two molecular weight HDPE grades. The decreasing values of n for increasing apparent wall shear rates are indicative of pseudoplastic (shear thinning) polymer melts. Figure 7.14 shows the relationship between the power law index n and shear rate for off-line capillary rheometry, the relationship is modelled using a second order polynomial. Due to higher shear rates for in-line capillary rheometry, the influence of shear heating effects (melt temperature) were investigated. Results show that shear heating effects of the polymer melt were not significant in influencing n values.

Capillary Rheometry Technique / Material Grade	In-line (A)	Off-line (B)	Deviation (A - B)	In-line and Off-line
HDPE HD5226EA	0.17	0.52	- 0.35	0.32
HDPE HD5050EA	0.09	0.32	- 0.21	0.10

Table 7.17 Summary of HDPE power law index n values (Bagley corrected data)

It can be seen from tables 7.16 and 7.17 that the n values for off-line capillary rheometry, are not significantly changed by the Bagley correction. Therefore, at the lower wall shear rates

the end pressure drop errors are low. The in-line capillary rheometry n values are reduced by 37% and 59% for HDPE HD5226EA and HD5050EA respectively. The very low n value for HD5050EA indicates that slip at the capillary die wall is most likely occurring. The in-line capillary rheometry data show the two different molecular weight grades of HDPE as different slopes of the wall shear stress versus wall shear rate flow curve. The low n values of the Bagley corrected HDPE grade HD5050EA data, influence the Rabinowitsch correction for true wall shear rate, by an additional $3 \times 10^5 \text{ sec}^{-1}$ (approximately), compared to the HDPE HD5226EA data. This level of wall shear rate correction indicates that polymer melt slip at the capillary die wall may have occurred. It is apparent that the use of a Bagley correction may eliminate the nozzle melt pressure information that is of potential use for closed loop process control.

Bagley corrected off-line capillary rheometry data for HDPE grades HD5226EA and HD5050EA are reported by Bonner (1991). The wall shear rates investigated were 70 to 7000 sec^{-1} and 300 to 7000 sec^{-1} , respectively for grades HD5226EA and HD5050EA. The off-line capillary rheometer wall shear stress versus apparent wall shear rate flow curves reported by Bonner (1991), compare to a high degree with those shown in figure 7.17.

7.7.2 Polyoxymethylene (POM) Data

It can also be seen from figure 7.19, that the POM data can best be described by two linear flow regions, as shown in figure 7.20. The two linear regions are above and below the shear rates of 4500, 3600 and 5000 sec^{-1} , for POM 900F, 500 and 100 respectively. A change of slope on the wall shear stress versus wall shear rate flow curve, is a common occurrence for most linear polymers that have been studied, Hatzikiriakos and Dealy (1992b). There is strong evidence to show that this change of slope is caused by melt slip at the capillary die

wall, resulting from an oscillatory flow regime, Lupton and Register (1965), Ramurthy (1986), Kalika and Denn (1987) and Hatzikiriakos and Dealy (1992a).

It can be seen from figure 7.19 that in-line and off-line capillary rheometry techniques are both clearly capable of distinguishing between three different molecular weight grades of POM.

Capillary Rheometry Technique / Material Grade	In-line (A)	Off-line (B)	Deviation (A - B)	In-line and Off-line
POM 900 F	0.35	0.27	+ 0.08	0.24
POM 500	0.30	0.23	+ 0.07	0.24
POM 100	0.15	0.14	+ 0.01	0.14

Table 7.18 Summary of POM power law index n values (uncorrected data)

It is apparent from tables 7.18 that n values are higher for the in-line data, compared to the off-line data, for the three molecular weight grades of POM. The in-line n values = 0.35 and 0.30 compared to the off-line n values = 0.27 and 0.23 for POM 900F and 500. This is most likely a result of polymer melt leakage past the screw non-return valve for the lower screw velocities. Table 7.19 shows that the uncorrected data for POM 100 is similar for in-line and off-line capillary rheometry, 0.15 and 0.14, respectively.

Capillary Rheometry Technique / Material Grade	In-line (A)	Off-line (B)	Deviation (A - B)	In-line and Off-line
POM 900 F	0.25	0.24	+ 0.01	0.21
POM 500	0.25	0.23	+ 0.02	0.23
POM 100	0.03	0.11	- 0.08	0.11

Table 7.19 Summary of POM power law index n values (Bagley corrected data)

It can be seen from tables 7.18 and 7.19 that the n values for off-line capillary rheometry, are not significantly changed by the Bagley correction. It is apparent from table 7.19 that n

values have close agreement for in-line and off-line capillary rheometry, for the POM 900f and 500. The in-line n values = 0.25 and 0.25 compared to off-line n values = 0.24 and 0.23 for POM 900F and 500, respectively. The very low n value for POM 100 indicates that melt slip at the capillary die wall is most likely occurring. It can be seen from figure 7.23 and 7.24 that in-line and off-line capillary rheometry data are both clearly capable of identifying, between the three different molecular weight grades of POM. The low n values of the Bagley corrected POM 100 data, influence the Rabinowitsch correction for true wall shear rate, by an additional $1 \times 10^6 \text{ sec}^{-1}$ (approximately), compared to the POM 900F and POM 500 data. This level of wall shear rate correction indicates that polymer melt slip at the capillary die wall may have occurred.

7.7.3 Corrected In-line Capillary Die Entrance Pressure (CDEP)

Table 7.20 shows the nozzle melt pressure correction factors for different molecular weight grades of HDPE and POM. It is apparent from table 7.20 that positive values (shaded regions) of melt pressure correction factor, indicate a positive pressure gradient in the nozzle reservoir bore. For a laminar flow regime a negative pressure gradient would normally be expected, therefore the positive gradient may indicate a turbulent flow regime.

Set Velocity (mm/s)	HDPE 5226		HDPE 5050		POM 900F		POM 500		POM 100	
	PL	Ps	PL	Ps	PL	Ps	PL	Ps	PL	Ps
3	-0.80	-3.99	-0.37	-1.42	-1.08	-3.79	-0.81	-3.05	+0.04	-0.92
5	-0.75	-3.10	-0.11	-0.23	-0.79	-2.88	-0.47	-2.05	+0.40	+0.38
7	-0.67	-2.55	+0.30	+0.45	-0.56	-2.18	-0.26	-1.57	+0.71	+1.08
9	-0.51	-1.96	+0.62	+0.93	-0.43	-1.88	-0.19	-1.24	+1.00	+1.63
11	-0.43	-1.77	+0.88	+1.34	-0.35	-1.57	-0.05	-1.16	+1.27	+2.05

Table 7.20 Nozzle melt pressure correction factors

These positive gradients apparently correspond with low power law index n values, shown in table 7.21, indicating that polymer melt slip in the capillary die may have occurred.

	HD5226EA	HD5050EA	POM900F	POM500	POM100
Uncorrected Data	0.27	0.22	0.35	0.30	0.15
Bagley Corrected Data	0.17	0.09	0.25	0.25	0.03

Table 7.21 Power law index n values for Bagley corrected in-line capillary rheometry data

The positive pressure gradients may be explained by pressure transducer calibration errors, but on consideration of the pressure data this is clearly not the case, as shown in table 7.22.

Positive pressure gradients occur for the short capillary die data, where pressure values are lower than those for the long capillary die. The positive pressure gradients occur over a large pressure range, indicating that pressure transducer calibration is not main influence.

Set Velocity (mm/s)	HDPE 5226		HDPE 5050		POM 900F		POM 500		POM 100	
	PL	Ps	PL	Ps	PL	Ps	PL	Ps	PL	Ps
3	369.37	90.97	411.13	139.48	393.66	104.09	477.18	126.15	642.41	188.79
5	392.35	111.50	458.26	175.53	456.41	135.40	580.75	172.07	684.17	235.46
7	422.36	128.48	491.76	199.72	526.91	168.99	653.57	195.09	715.40	261.94
9	457.01	148.72	519.20	219.70	577.33	191.11	679.96	209.43	746.79	284.00
11	482.92	161.08	545.13	237.23	607.57	210.05	703.01	216.27	776.52	305.63

Table 7.22 Nozzle melt pressure values

The reason of the positive pressure gradients may be an oscillatory flow regime, resulting in melt slip at the capillary die wall. The following explanations for the positive pressure gradients were given by Groves (1993): (i) stagnant flow due to polymer melt recirculation zones or 'dead space' (oscillatory flow regime), (ii) back flow within the nozzle rheometer, (iii) local degradation due to recirculation zones, and (iv) localised temperature gradient within the nozzle rheometer.

Figure 7.25 shows samples of extruded HDPE grade HD5050EA, from in-line and off-line capillary rheometry, for the respective short length dies. Figures 7.25 a to 7.25 c show the extrudate from in-line capillary rheometry tests, for wall shear rates of 38400, 89600 and 140800 sec^{-1} . The surface appearance of the extrudate samples is random (chaotic), sometimes described as 'wavy', indicating that melt fracture may have occurred, Tordella (1956). The extrudate samples show that the positive pressure gradients are most likely a result of an oscillatory flow regime (non-laminar flow) in the nozzle reservoir bore. The 'wavy' extrudate surface appearance is a result of melt rupture at the die entry, resulting from tension stiffening melts, Cogswell (1981 p 100). In-line capillary rheometry tests were for relatively high wall shear rates, resulting from the die radius (0.5 mm), low wall shear rate tests were not investigated, therefore the 'wavy' extrudate surface appearance may be a result of a poor surface finish on the internal bore of the capillary dies.

Figures 7.25 d to 7.25 f show extrudate from off-line capillary rheometry tests for wall shear rates of 300, 3000 and 15000 sec^{-1} , respectively. The extrudate is smooth and uniform at a wall shear rates of 300 sec^{-1} . At wall shear rates of 3000 sec^{-1} a slight regular surface defect is apparent. The regular surface defect becomes pronounced for wall shear rates of 15000 sec^{-1} . This regular surface defect can be described as a 'screw thread', and like sharkskin arises from the tearing of melt at the exit of the capillary die, Hatzikiriakos and Dealy (1992b) and Hatzikiriakos et al (1993). A regular 'zig-zag' extrudate occurs for tension thinning melts, where the surface defect is triggered in the die.



Figure 7.25 a In-line capillary rheometry extrudate - 38400 sec^{-1}

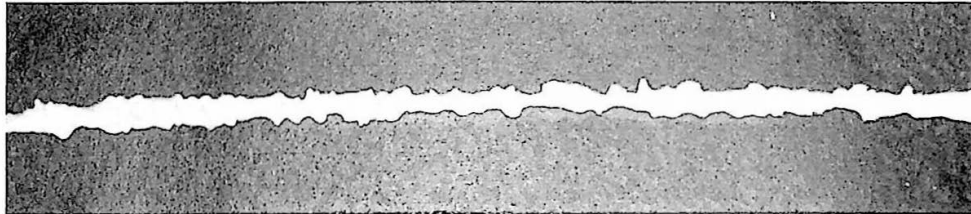


Figure 7.25 b In-line capillary rheometry extrudate - 89600 sec^{-1}

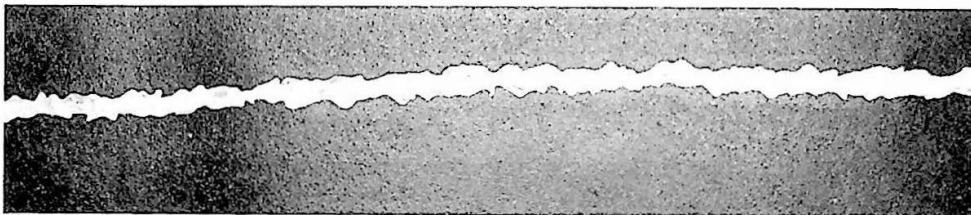


Figure 7.25 c In-line capillary rheometry extrudate 140800 sec^{-1}



Figure 7.25 d Off-line capillary rheometry extrudate - 300 sec^{-1}

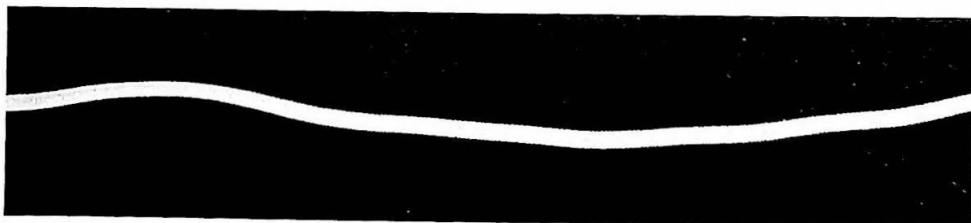


Figure 7.25 e Off-line capillary rheometry extrudate - 3000 sec^{-1}



Figure 7.25 f Off-line capillary rheometry extrudate - 15000 sec^{-1}

Figure 7.25 In-line and off-line capillary rheometry extrudate surface appearance

7.8 Concluding Comments

- In-line and off-line capillary rheometry techniques are both clearly capable of distinguishing between different molecular weight grades of high density polyethylene (HDPE) and polyoxymethylene (POM).
- Significantly different results may be obtained from in-line capillary rheometry, compared to off-line capillary rheometry, for polymer melts, due to different shear rate ranges investigated.
- The different molecular weight grades were more distinguishable before Bagley or Rabinowitsch corrections. The Bagley correction removed the capillary die ends pressure drop, showing that polymer melt slip at the die wall was most likely occurring. The ends pressure drop therefore clearly distinguished between the different molecular weight grades of HDPE and POM.
- The Rabinowitsch correction may over correct wall shear rate data for low power law index 'n' values.
- Polymer melt leakage past the screw non-return valve may occur for low molecular weight grade polymers, with associated low melt viscosity.
- The nozzle melt pressure correction factor was shown to be largest, at lower nozzle melt pressures. Positive nozzle melt pressure corrections may indicate if polymer melt slip at the wall of the capillary die has occurred.

- Analysis has shown that high molecular weight grades of HDPE (HD5050EA) and POM (100) are most likely subject to slip at the capillary die wall. Volumetric flow rate is almost independent of wall shear stress, when a Bagley correction is implemented.

CHAPTER 8

In-line Nozzle Rheometry and Process Measurements for Injection Moulding

8.1 Introduction

Modern day injection moulding machines use sophisticated machine parameter and sequence control. Microprocessors form the basis of this machine control, therefore technological advances are continually being incorporated into machine design. Machine control has improved in recent years, to such an extent that melt viscosity variations have become an apparent processing problem. The significance of melt viscosity variations, depends on the sophistication of the machine control employed and quality of raw materials supplied. To compensate for the melt viscosity variations, closed loop process control is required. The basis of such a control strategy is most likely an accurate and precise measurement of melt viscosity.

The strategy for melt viscosity assessment adopted by machine manufacturers has been to integrate a previously specified region of the primary injection hydraulic pressure profile, for example the Sandretto viscosity index calculation. Some machine manufacturers simply ignore sections of the injection hydraulic pressure profiles, for example the Sandretto viscosity index. This index effectively clips the start and finish of the hydraulic injection pressure profile, during primary injection, in an attempt to increase measurement precision, as described in appendix A(iii). An important factor to note is the performance of machine instrumentation, this factor strongly influences measurement accuracy and precision. The melt viscosity measurement accuracy and precision may be influenced by the screw velocity control relative performance of the machine. Signal conditioning circuitry for hydraulic injection pressure transducers often only have adequate performance. The Cincinnati Milacron in-line nozzle

rheometer system is based on nozzle rheometer technology developed at Lowell University, Massachusetts, USA, Malloy (1988), Malloy et al (1989), Ross et al (1990) and Wu and Chen (1990). This work describes a trace of apparent viscosity, injection pressure and screw injection velocity versus screw position. A percentage viscosity deviation is reported for the material being processed compared to the database. This percentage viscosity deviation may include machine parameter variation, as a result of the screw acceleration period up to the set screw injection velocity. For a precise assessment of melt viscosity variation it is necessary to deconvolve machine and process parameters.

Typical off-line capillary rheometry assessments of melt viscosity are measured at constant wall shear rates. Constant wall shear rates are achieved by accurate and precise velocity control of a rheometer's injection unit (pistons). Regarding the injection moulding process, the primary injection phase is velocity controlled, and therefore is the logical phase to concentrate upon, to initiate assessment of melt viscosity.

Chapter 7 shows that in-line capillary rheometry is an accurate and precise technique for determining melt viscosity, during actual process conditions. Mean nozzle melt pressure is determined by manual inspection of the melt pressure profiles. Figure 7.8 shows the screw displacement and nozzle melt pressure for a typical 'airshot'. The mean nozzle melt pressure is calculated for the time period $t = 8.00$ to 8.50 seconds, where nozzle melt pressure is steady. Nozzle melt pressure profiles for actual moulding conditions are likely to be more complex than that shown in figure 7.8. The use of complex tool geometries, different injection moulding machines, machine parameter settings and materials, all influence the nozzle melt pressure and hydraulic injection profiles. Therefore, it is necessary to investigate on a cycle to cycle basis melt pressure profiles for typical process conditions. These investigations should determine where optimum accuracy and precision of nozzle melt pressure and hydraulic

injection pressure measurements can be achieved. Nozzle melt pressure profiles are influenced by a diverse range of machine and process parameters. Therefore, investigations were necessary to determine the main influence on nozzle melt pressure and hydraulic injection pressure accuracy and precision.

8.1.1 Scope of this Chapter

The aim of this chapter is to determine the accuracy and precision of in-line polymer melt viscosity measurements, during typical moulding conditions. This chapter describes the procedures for determining the optimum accuracy and precision of in-line nozzle rheometry (nozzle melt pressure measurements) and process measurements (hydraulic injection pressure measurements) during the velocity controlled primary injection phase. The main influences on the accuracy and precision of nozzle melt pressure were investigated.

8.1.2 Experimental Moulding Tests Analysed

This chapter concentrates analysis on nine experimental moulding tests:

Polyoxymethylene (see chapter 7.2.2) injection moulding process data was collected from 50 experimental tests producing injection and plasticising data for 887 individual moulding cycles. The 70 cycles analysed in this chapter are from test P30%20B (25 cycles, Du Pont Delrin II 500, Bag 3, (beaker tool), test 3-500D (25 cycles, Du Pont Delrin II 500, Bag 1, container tool), test L-D500B1 (10 cycles, Du Pont Delrin II 500, Bag 1, Container tool) and test N-D500B2 (10 cycles, Du Pont Delrin II 500, Bag 2, container tool). These tests were analysed to show the methodology, for determining an optimum accuracy and precision for in-line nozzle rheometry and process measurements.

High density polyethylene (see chapter 7.2.1) injection moulding process data was collected from a total of 29 experimental tests producing injection and plasticising data for 644 individual moulding cycles. The 50 cycles analysed in this chapter are from test NX%20B (15 cycles, BP Rigidex HD5226EA), test OX%20B (15 cycles, BP Rigidex HD5226EA), test I40%20B (10 cycles, BP Rigidex HD5226EA) and test L40%20B (10 cycles, BP Rigidex HD5226EA). Test NX%20B includes monitored data from 15 moulding cycles for 5 injection velocities 10, 20, 30, 40 and 50 mm/s, 3 cycles were monitored at each selected velocity. Test OX%20B includes monitored data from 15 moulding cycles for 5 injection velocities 60, 70, 80, 90 and 99 mm/s. Tests NX%20B and OX%20B are analysed to show the comparison between in-line nozzle melt pressure measurements and hydraulic injection pressure measurements. Tests L40%20B and I40%20B, used different levels of velocity control performance, achieved by changing the accuracy of screw displacement (LVDT) signal conditioning circuitry (Levels A and B screw displacement accuracies), to investigate the effect on nozzle melt pressure measurements. Details of the high density polyethylene (HDPE) and Polyoxymethylene (POM) are described in chapter 7.2.1 and 7.2.2 respectively.

Industrial data were analysed, from a production environment at Birkbys Plastics Ltd. The product moulded was a complex automotive component (instrument cluster housing) for the Ford Motor Company (UK) Ltd. The presentation of industrial data, consolidates the analysis described, as a different injection moulding machine, tool, material and machine parameter settings were used.

Details of all experimental moulding tests are outlined in Appendix I(i), (ii) and (iii) for Sandretto, Stork and Cincinnati Milacron, respectively.

8.2 Experimental Configuration

8.2.1 In-line Modular Nozzle Rheometer Configuration

The same modular nozzle configuration was used for all experimental moulding tests, see Appendix I(i). The modular nozzle was configured to give minimal disturbance to polymer melt rheology, i.e. only one instrumentation module was used. The additional volume of the nozzle rheometer bore compared to the original machine nozzle bore was approximately $6 \times 10^{-6} \text{ m}^3$, an approximate increase in volume of 5 % with the screw fully retracted. Figures 8.1 and 8.2 show a schematic diagram and general view of the modular nozzle rheometer configured for experimental moulding trials, respectively. The location of the Dynisco melt pressure transducer PT435A and Dynisco infra-red melt temperature transducer MTT935A can be seen. Figure 8.1 also shows the location of the type T calibration thermocouples and heater bands (elements).

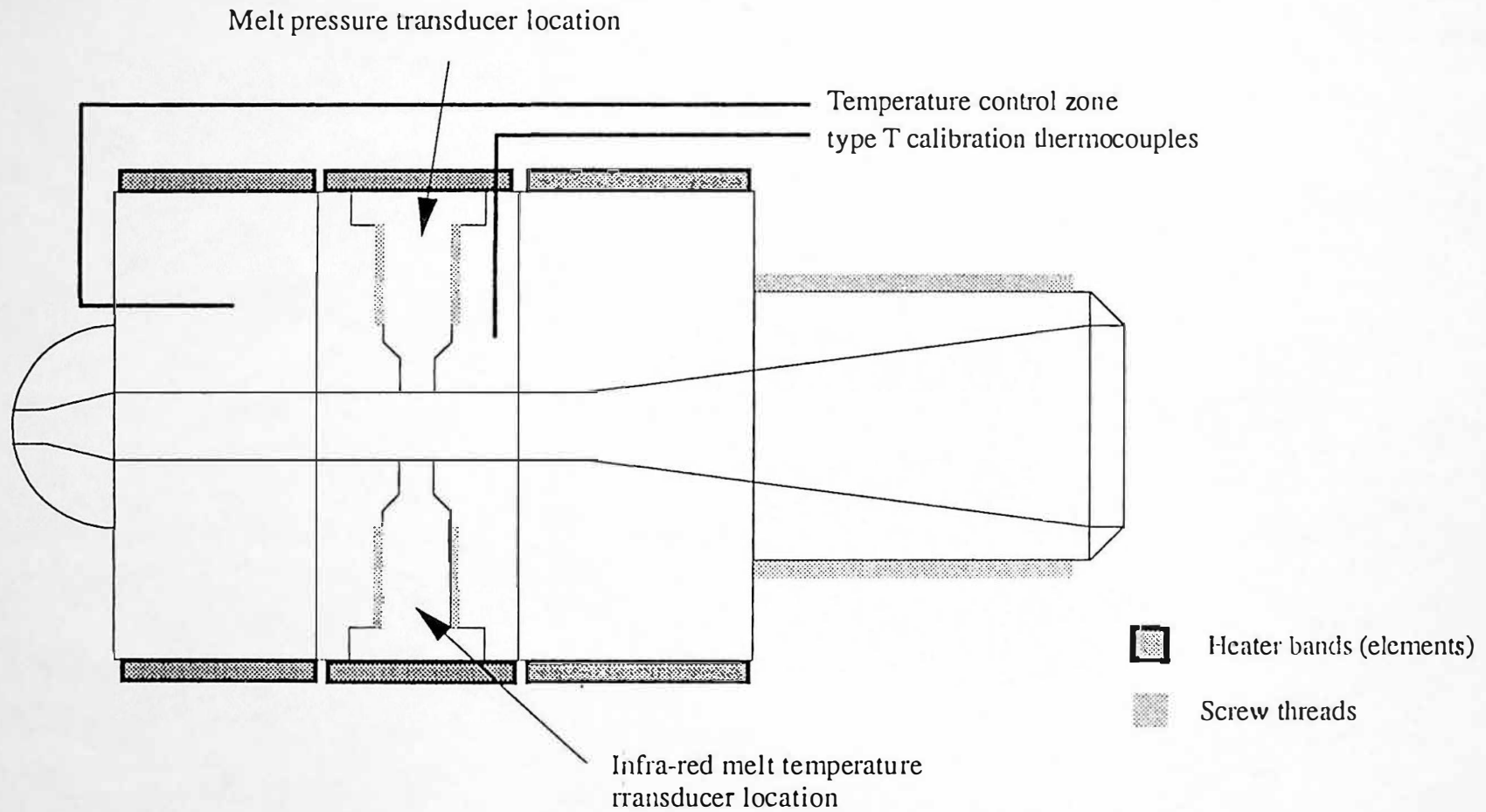


Figure 8.1 Schematic diagram of in-line modular nozzle rheometer configured for injection moulding experimental tests

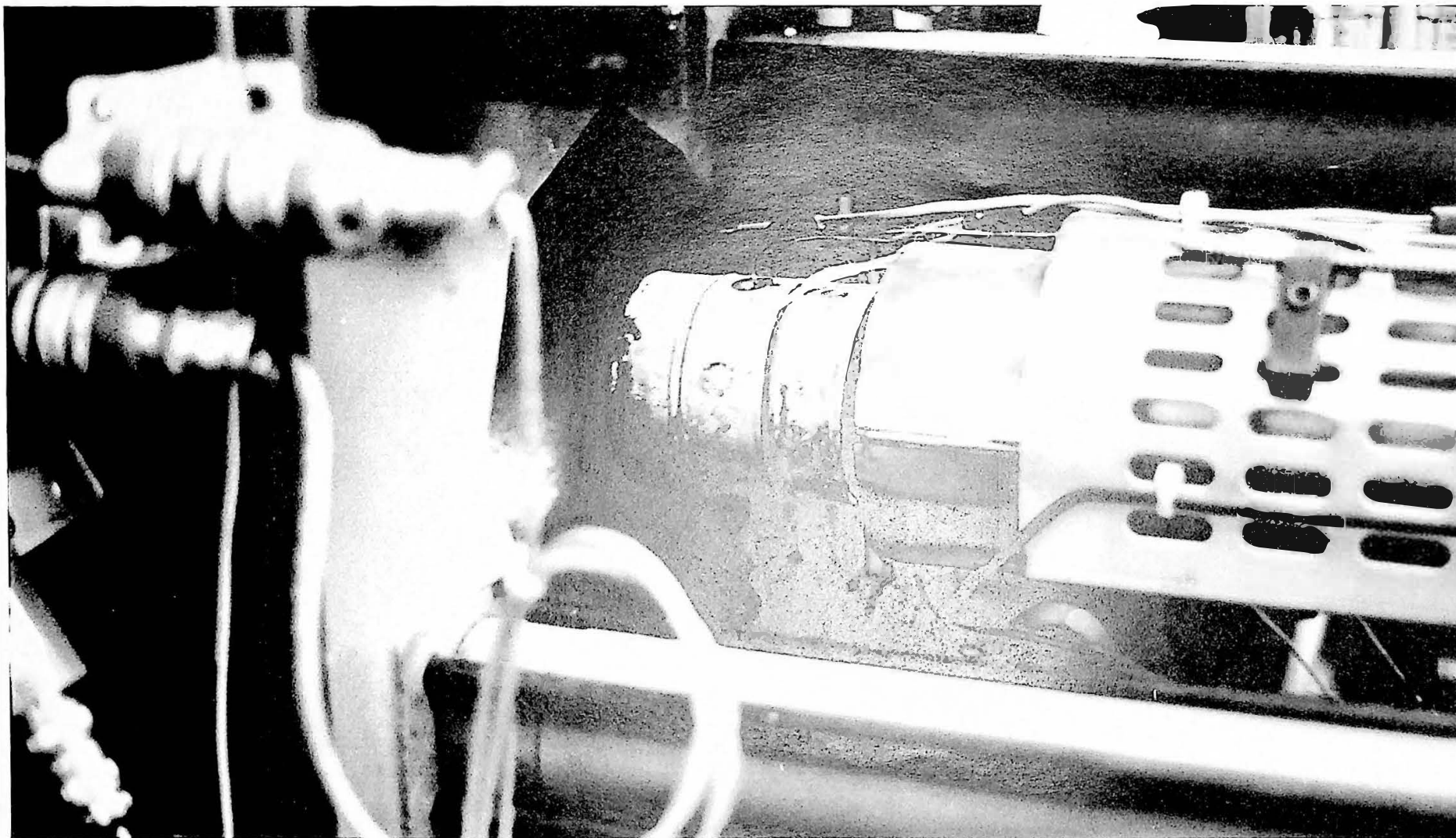


Figure 8.2 In-line modular nozzle configured for injection moulding experimental tests

8.2.2 Monitored Parameters

Beaker Tool: each of the following injection parameters were monitored at 50 Hz for 6.96 seconds, from the start of the injection phase.

Channel Number	Description of Monitored Parameter	Symbolic Name	Transducer Type
PGA 0	Nozzle Melt Pressure 1	NMP 1	Diaphragm device
PGA 1	Hydraulic Injection Pressure	HYDP	Diaphragm device
PGA 2	Tool Pressure 1	TOOLP 1	Diaphragm device
PGA 3	Tool Pressure 2	TOOLP 2	Diaphragm device
PGA 4	Tool Pressure 3	TOOLP 3	Diaphragm device
PGA 5	Injection Screw Displacement	SDISP 1	LVDT
PGA 6	Reference Injection Screw Displacement	SDISP 2	LVDT
PGA 7	Injection Screw Displacement. Packing Phase	SDISP 3	LVDT
PGA 8	Injection Screw Displacement	SDISP 4	Linear potentiometer
PGA 9	Injection Screw Velocity	SVEL 1	Inductive device
TC 1	Injection Melt Temperature	NMT 1	Infra red device
TC 2	Tool Temperature 1	TOOLT 1	Type J Thermocouple
TC 3	Tool Temperature 2	TOOLT 2	Type J Thermocouple
TC 4	Tool Temperature 3	TOOLT 3	Type J Thermocouple

Table 8.1 a Beaker tool injection monitored parameters

Each of the following plasticising parameters were monitored at 20 Hz for 19.95 seconds from the start of the plasticisation phase.

Channel Number	Description of Monitored Parameter	Symbolic Name	Transducer Type
PGA 0	Plasticising Back Pressure	NMP 1	Diaphragm device
PGA 2	Plasticising Screw Rotational Speed	SRPM	Magnetic pickup
PGA 1	Plasticising Screw Displacement	SDISP 1	LVDT
PGA 3	Tool Melt Pressure 1	TOOLP 1	Diaphragm device
TC 1	Hydraulic Oil Temperature	OILT	Type J thermocouple
TC 2	Air Temperature	AIRT	Type J thermocouple

Table 8.1 b Beaker tool plasticisation monitored parameters

Container Tool (Test 3-D500), each of the following injection parameters were monitored at 50 Hz for 7.96 seconds, from the start of the injection phase.

Channel Number	Description of Monitored Parameter	Symbolic Name	Transducer Type
PGA 0	Nozzle Melt Pressure 1	NMP 1	Diaphragm device
PGA 1	Injection Screw Displacement	SDISP 1	LVDT
PGA 2	Reference Injection Screw Displacement	SDISP 2	LVDT
PGA 3	Hydraulic Injection Pressure	HYDP	Diaphragm device
PGA 4	Filtered Screw Injection Velocity	SVEL 1	Inductive device
PGA5	Unfiltered Screw Injection Velocity	SVEL 2	Inductive device
TC 1	Nozzle Melt Temperature	NMT 1	Type J Thermocouple

Table 8.2 Container tool injection monitored parameters (Test 3-D500)

Each of the six tool temperature thermocouples (Type T calibration, TC-1 to TC-6, see chapter 4) and air temperature thermocouple (Type J calibration) were continually monitored at 1 Hz, using the Biodata Windmill software, (see chapter 6.4.2) for the test duration.

Container Tool: each of the following injection parameters were monitored at 50 Hz for 4.96 seconds, from the start of the injection phase.

Channel Number	Description of Monitored Parameter	Symbolic Name	Transducer Type
PGA 0	Nozzle Melt Pressure 1	NMP 1	Diaphragm device
PGA 1	Injection Screw Displacement	SDISP 1	LVDT
PGA 2	Screw Injection Velocity	SVEL 1	Inductive device
TC 1	Nozzle Melt Temperature	NMT 1	Infra red device

Table 8.3 a Container tool injection monitored parameters

Each of the following plasticising parameters were monitored at 10 Hz for 11.90 seconds from the start of the plasticisation phase.

Channel Number	Description of Monitored Parameter	Symbolic Name	Transducer Type
PGA 0	Plasticising Nozzle Back Pressure	NMP 1	Diaphragm device
PGA 1	Injection Screw Displacement	SDISP	LVDT
PGA 2	Plasticising Screw Rotational Speed	SRPM	Magnetic pickup
TC 1	Fixed Platen Temperature	FPTEMP	Type T thermocouple
TC 2	Moving Platen Temperature	MPTEMP	Type T thermocouple

Table 8.3 b Container tool plasticisation monitored parameters

8.2.3 Machine Parameters

Machine Parameter Settings	Beaker Tool	Contained Tool
Plasticising Screw Rotation Speed (RPM)	80	80
Plasticising Back Pressure (bar)	3	1
Plasticising End Position (%)	39.0	50.0
Decompression Stroke at Plasticisation end (%)	3	6
Total Injection Time. Primary and Packing (seconds)	5.20	6.00
Primary Injection Velocity (%)	30	30
Maximum Hydraulic Injection Pressure (bar)	115	115
Switch Over Position to Packing Phase (%)	7.00	7.00
Secondary Packing Hydraulic Injection (bar)	20	40
Secondary Packing Time (seconds)	3.00	3.00
Decompression Stroke at Injection End (%)	0	1
Cooling Time (seconds)	35	30
Nozzle Temperature Control Zone 1 (C)	215	215
Nozzle Temperature Control Zone 2 (C)	215	215
Barrel Temperature Control Zone A (C)	215	210
Barrel Temperature Control Zone B (C)	210	205
Barrel Temperature Control Zone C (C)	205	200
'Hot Tip' Temperature (C)	215	N/A
Feed Zone Cooling. (YES/NO)	YES	YES
Tool Temperature. Polymer Melt Feed Zone (C)	70	N/A
Tool Temperature. Fixed Platen (C)	70	70
Tool Temperature. Moving Platen (C)	60	60

Table 8.4 Machine parameter settings for polyoxymethylene (POM)

Machine Parameter Settings	Beaker Tool
Plasticising Screw Rotation Speed (RPM)	80
Plasticising Back Pressure (bar)	5
Plasticising End Position (%)	38
Decompression Stroke at Injection End (%)	3
Total Injection Time, Primary and Packing (seconds)	4.40
Primary Injection Velocity (%)	
Maximum Hydraulic Injection Pressure (bar)	115
Switch Over Position to Packing Phase (%)	7
Secondary Packing Hydraulic Injection (bar)	20
Secondary Packing Time (seconds)	3
Decompression Stroke at Injection End (%)	0
Cooling Time (seconds)	35
Nozzle Temperature Control Zone 1 (C)	190
Nozzle Temperature Control Zone 2 (C)	190
Barrel Temperature Control Zone A (C)	190
Barrel Temperature Control Zone B (C)	185
Barrel Temperature Control Zone C (C)	180
'Hot Tip' Temperature (C)	190
Feed Zone Cooling (YES/NO)	YES
Tool Temperature, Polymer Melt Feed Zone (C)	40
Tool Temperature, Fixed Platen (C)	40
Tool Temperature, Moving Platen (C)	40

Table 8.5 Machine parameter settings for high density polyethylene (HDPE)

8.3 Beaker Tool Experimental Results

8.3.1 Introduction

Experimental results from test P30%20B are analysed in this chapter. The injection phase for 25 injection moulding cycles were accurately monitored, processing polyoxymethylene (POM) Du Pont Delrin II 500 (see chapter 7.2.2), using the instrumented beaker tool (single impression).

8.3.2 Initial Experimental Observations

Figure 8.3 shows mean nozzle melt pressure, mean hydraulic injection pressure and mean screw displacement for the 25 moulding cycles. The scope of this analysis concentrates on the primary injection phase, for $t = 0.00$ to 1.75 seconds.

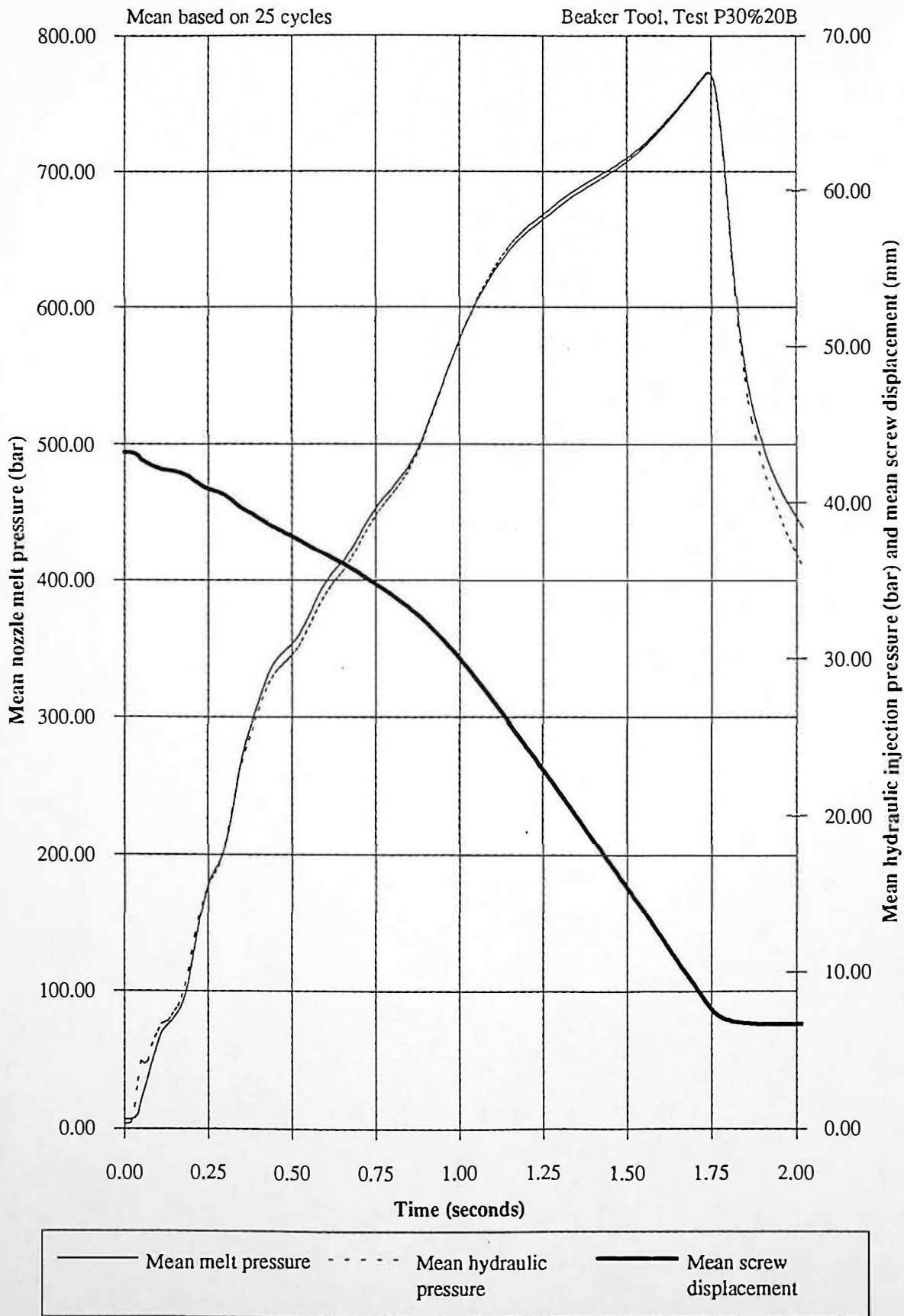
It is apparent from figure 8.3 that mean nozzle melt pressure compares to mean hydraulic injection pressure, with a high degree of correlation, coefficient of correlation = 1.00, for $t = 0.00$ to 1.75 seconds. This relationship is investigated in chapter 8.3.6 and further investigations are made in chapter 8.7, where polymer melt compressibility is investigated, for a range of injection velocities.

8.3.3 Integration of Full Pressure Profiles During Primary Injection

The following statistical analysis assumes knowledge of mean, variance, standard deviation and coefficient of variation, these parameters are described in Appendix J.

The first stage of analysis integrates the nozzle melt pressure and hydraulic injection pressure measurements for the full period of primary injection ($t = 0.00$ to 1.75 seconds) for the 25 moulding cycles.

Figure 8.3 Mean nozzle melt pressure, mean hydraulic injection pressure and mean screw displacement during primary injection



The mean nozzle melt pressure integral for the full period of primary injection = 832.50 bar.sec, with coefficient of variation = 0.73%. The mean hydraulic injection pressure integral for the full period of primary injection = 72.87 bar.sec, with coefficient of variation = 0.72%.

8.3.4 Integration of Specific Area of the Pressure Profiles

Figure 8.4 shows mean nozzle melt pressure and coefficient of variation for the 25 moulding cycles. Figure 8.5 shows mean hydraulic injection pressure and coefficient of variation for the 25 moulding cycles. It is apparent that coefficient of variation may indicate the time period during the primary injection phase, where injection velocity control has minimal variation, (see chapter 8.6). The coefficient of variation of mean nozzle melt pressure and hydraulic injection pressure, for the 25 moulding cycles, stabilises to a minimum for the time period $t = 1.20$ to 1.70 seconds.

The second stage of analysis integrates the pressure profiles for the time period $t = 1.20$ to 1.70 seconds. The mean nozzle melt pressure integral ($t = 1.20$ to 1.70 seconds) = 357.96 bar.sec, with a coefficient of variation = 0.54%. The mean hydraulic injection pressure integral ($t = 1.20$ to 1.70 seconds) = 31.45 bar.sec, with a coefficient of variation = 0.51%.

Therefore, analysis of mean nozzle melt pressure and mean hydraulic injection pressure profiles, during primary injection, has resulted in a pressure integral for $t = 1.20$ to 1.70 seconds. The following comparisons are made with respect to the integrals for full primary injection ($t = 0.00$ to 1.75 seconds). The nozzle melt pressure integral ($t = 1.50$ to 2.00 seconds) represents an increase in measurement precision by a factor of $0.73/0.54 = 1.35$. The hydraulic pressure integral ($t = 1.20$ to 1.70 seconds) represents an increase in measurement precision by a factor of $0.72/0.51 = 1.41$.

Figure 8.4 Mean nozzle melt pressure and coefficient of variation during primary injection

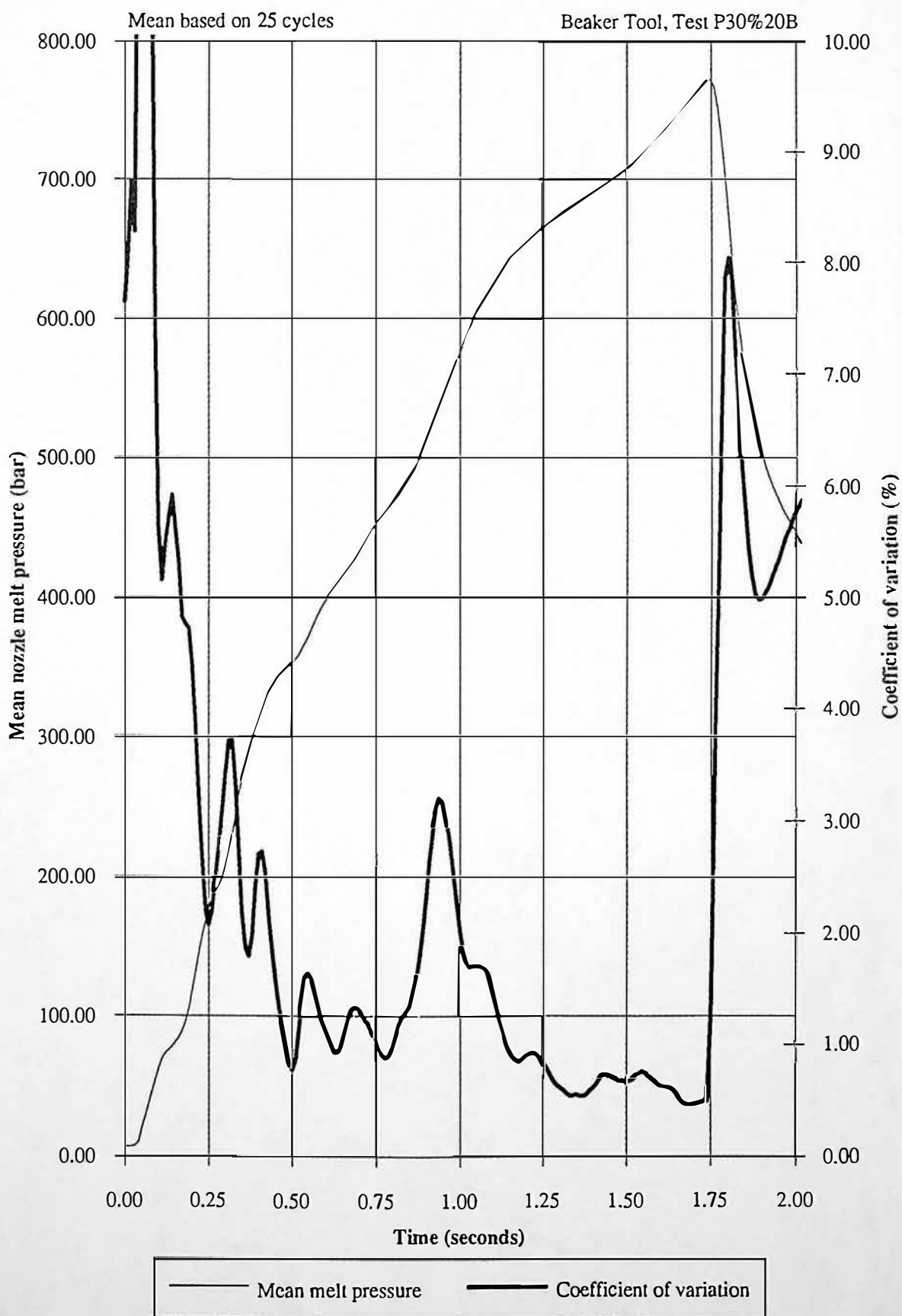
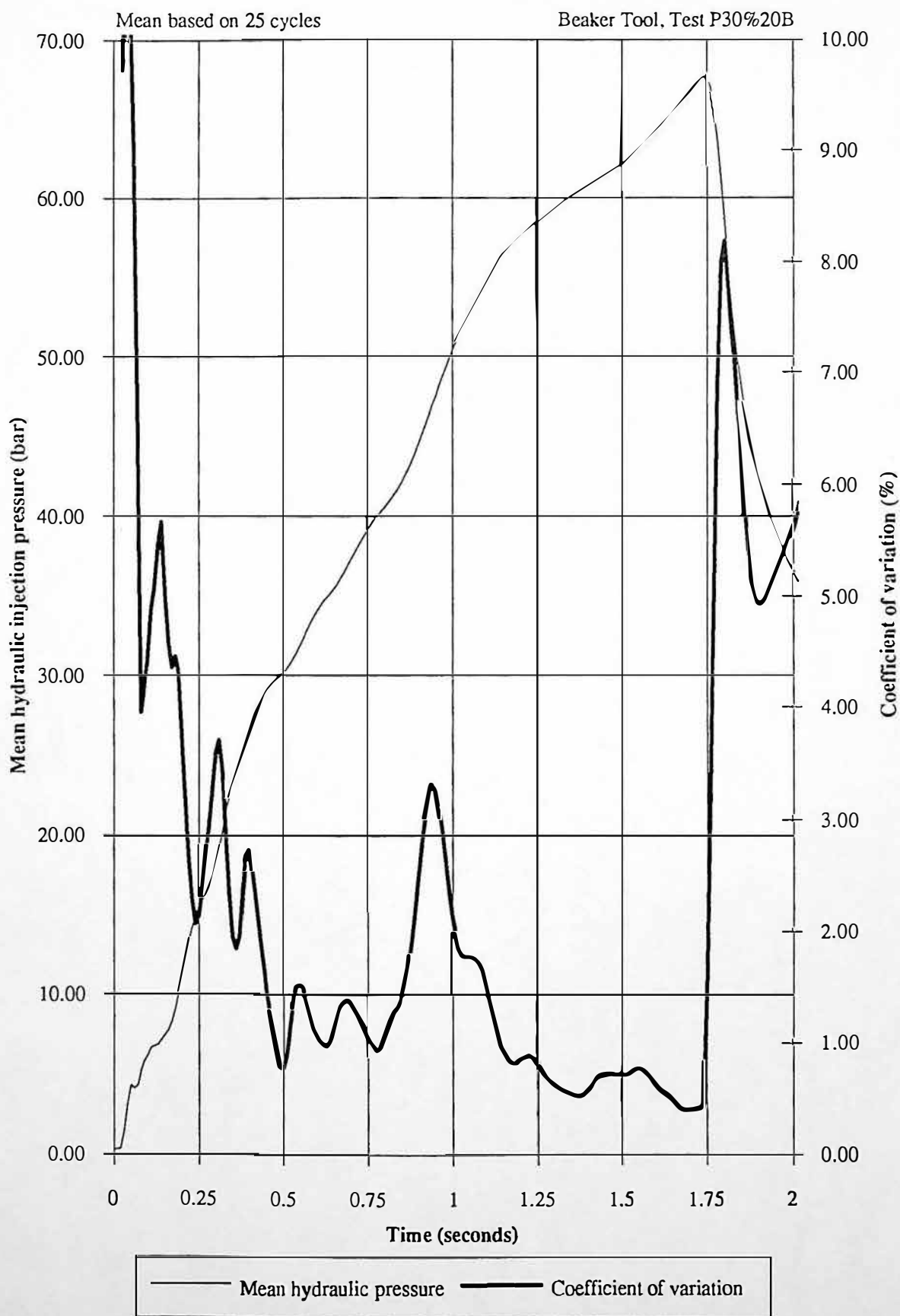


Figure 8.5 Mean hydraulic injection pressure and coefficient of variation during primary injection



8.3.5 Summary of Results

Table 8.6 summarises the results, allowing comparison of the coefficients of variation of nozzle melt pressure and hydraulic injection pressure.

	Full Pressure Integral (t= 0.00 to 1.75 seconds)	Specific Pressure Integral (t= 1.20 to 1.70 seconds)
In-line Nozzle Rheometry (Nozzle Melt Pressure)	0.73%	0.55%
Process Measurements (Hydraulic Injection Pressure)	0.72%	0.51%

Table 8.6 Summary of coefficient of variation results for test P30%20B

The advantage of calculating a specific pressure integral, can be seen in table 8.6, as the coefficients of variation are reduced by factors of 1.37 and 1.41, for nozzle melt pressure and hydraulic injection pressure measurements, respectively.

The coefficient of variation can be used to calculate the measurement accuracy. Measurement accuracy was based on a 99.7% spread of data i.e. ± 3 standard deviations about the mean value, assuming a normal distribution. The calculated measurement accuracy for each coefficient of variation are shown in Table 8.7.

	Full Pressure Integral (t= 0.00 to 1.75 seconds)	Specific Pressure Integral (t= 1.20 to 1.70 seconds)
In-line Nozzle Rheometry (Nozzle Melt Pressure)	$\pm 2.19\%$	$\pm 1.62\%$
Process Measurements (Hydraulic Injection Pressure)	$\pm 2.16\%$	$\pm 1.53\%$

Table 8.7 Summary of measurement accuracy results for test P30%20B

The results of tables 8.6 and 8.7 show that nozzle melt pressure and hydraulic injection pressure integrals have a similar precision.

8.3.6 Comparison of Nozzle Melt Pressure and Hydraulic Injection Pressure Integrals During Primary Injection

The following work investigates the relationship between nozzle melt pressure and hydraulic injection pressure integrals. It can be seen from figures 8.6 and 8.7, that both pressure integrals have a high degree of correlation, and therefore both reflect the same polymer melt viscosity variations. The coefficient of correlation between mean nozzle melt pressure integral and mean hydraulic injection pressure integral for the full period of primary injection ($t=0.00$ to 1.75 seconds) = 0.99 and for the specific integral ($t=1.20$ to 1.70 seconds) = 0.97.

Figure 8.6 Relationship between nozzle melt pressure and hydraulic injection pressure integrals for the full period of primary injection

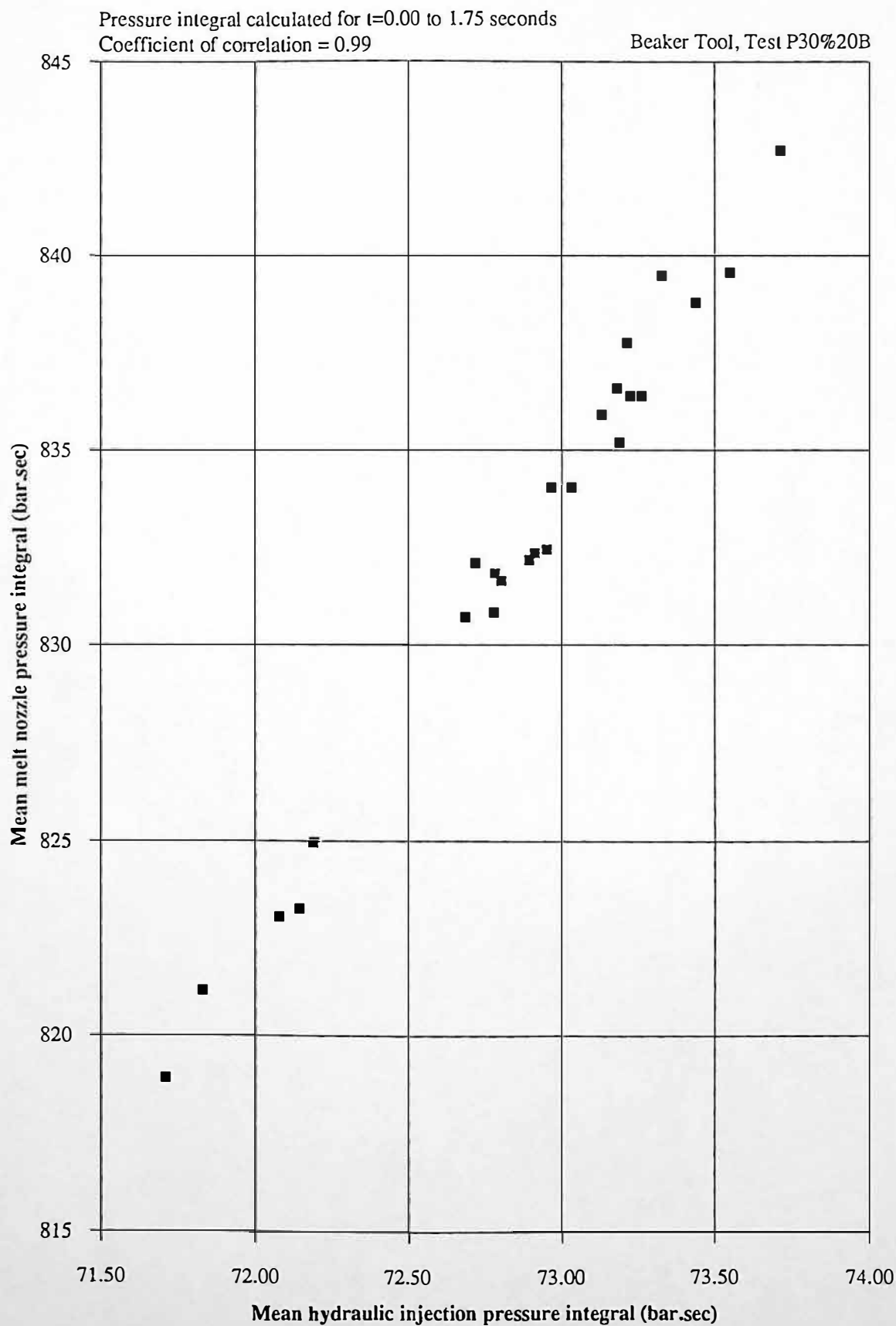
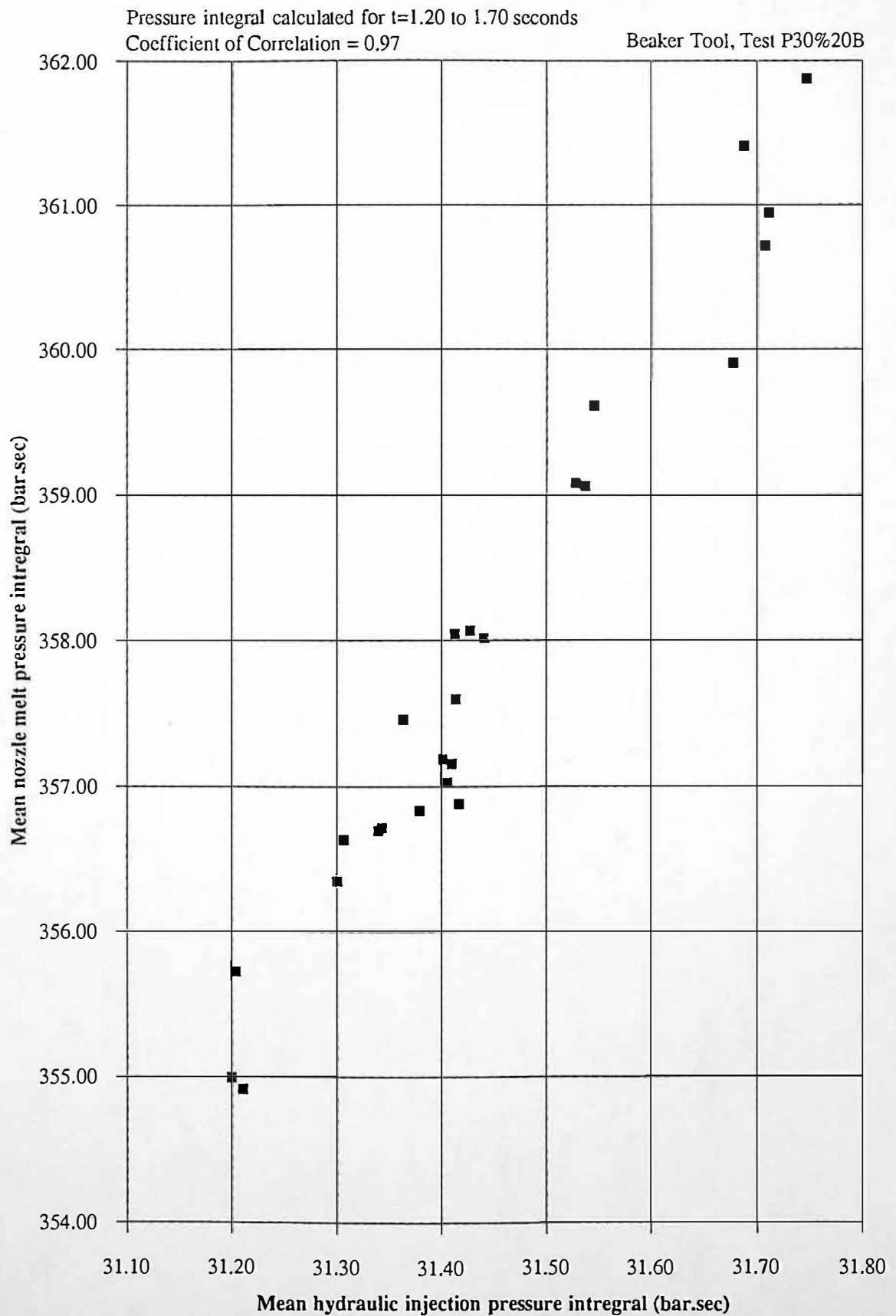


Figure 8.7 Relationship between nozzle melt pressure and hydraulic injection pressure integrals for a specific period of primary injection



8.4 Container Tool Experimental Results

8.4.1 Introduction

Experimental results from test 3-500D are analysed in this chapter. The injection phase for 25 injection moulding cycles were accurately monitored, processing polyoxymethylene (POM) Du Pont Delrin II 500 (see chapter 7.2.2), using the instrumented (two impression 'family' tool) container tool.

8.4.2 Initial Experimental Observations

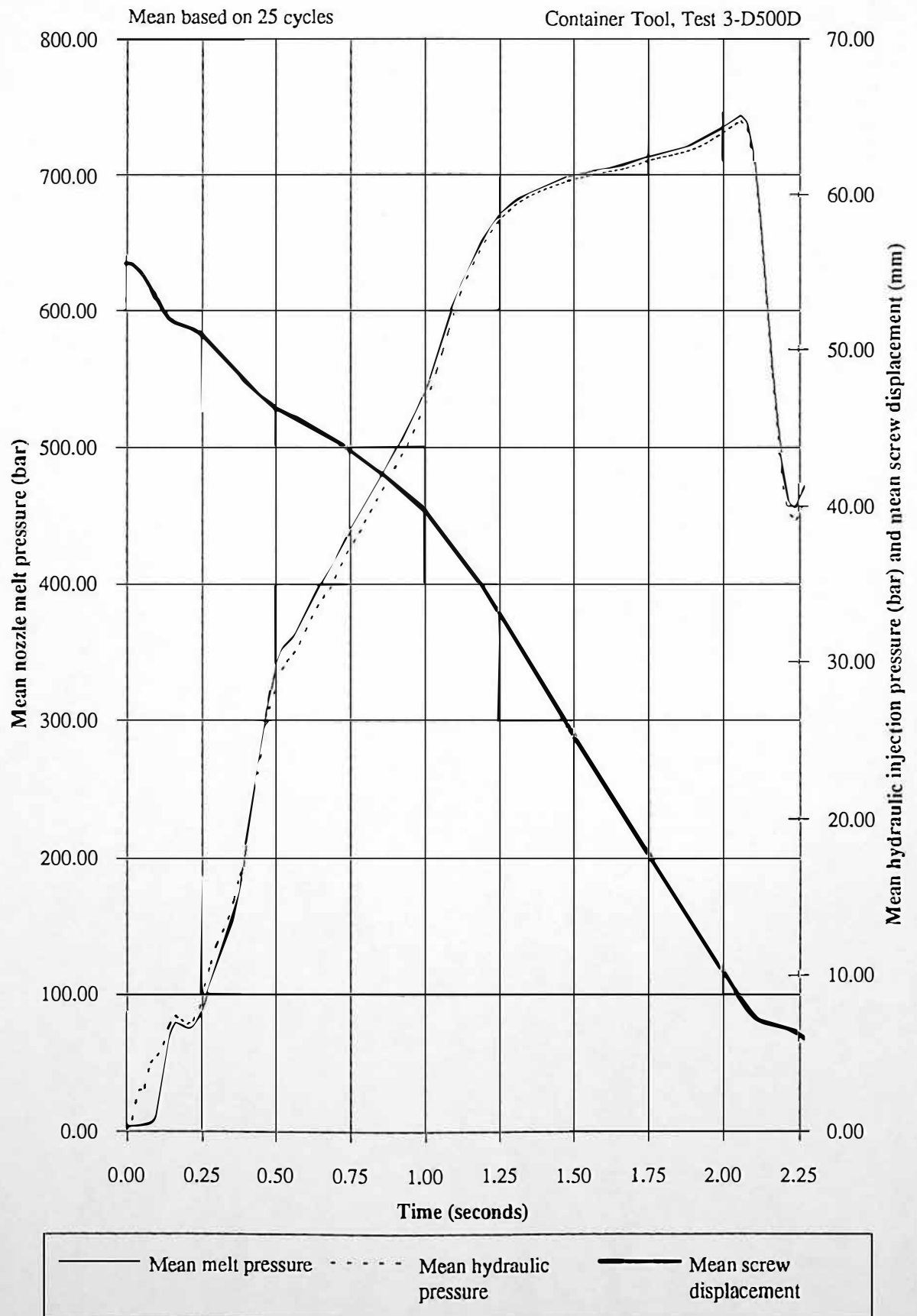
Figure 8.8 shows mean nozzle melt pressure, mean hydraulic injection pressure and mean screw displacement for the 25 moulding cycles. This analysis concentrates on the primary injection phase, for $t = 0.00$ to 2.06 seconds.

It is apparent from figure 8.8 that mean nozzle melt pressure compares to mean hydraulic injection pressure, with a high degree of correlation, coefficient of correlation = 1.00, for $t = 0.00$ to 2.06 seconds. This relationship is investigated in chapter 8.4.6 and further investigations are made in chapter 8.7, where polymer melt compressibility effects are investigated, for a range of injection velocities.

8.4.3 Integration of Full Pressure Profiles During Primary Injection

This first stage of analysis integrates nozzle melt pressure and hydraulic injection pressure measurements for the full period of primary injection ($t = 0.00$ to $t = 2.06$ seconds) for the 25 moulding cycles. The mean nozzle melt pressure integral for the full period of primary injection = 1013.53 bar.sec, with coefficient of variation = 0.84%. The mean hydraulic injection pressure integral for the full period of primary injection = 88.16 bar.sec, with coefficient of variation = 0.83%.

Figure 8.8 Mean nozzle melt pressure, mean hydraulic injection pressure and mean screw displacement during primary injection



8.4.4 Integration of Specific Area of Pressure Profiles

Figure 8.10 shows mean nozzle melt pressure and coefficient of variation for the 25 moulding cycles. Figure 8.9 shows mean hydraulic injection pressure and coefficient of variation for the 25 moulding cycles. It is apparent that coefficient of variation may indicate the time period during the primary injection phase, where injection velocity control has minimal variation, (see chapter 8.6). The coefficient of variation of mean nozzle melt pressure and mean hydraulic injection pressure for the 25 moulding cycles, stabilises to a minimum for $t = 1.50$ to $t = 2.00$ seconds.

The second stage of analysis integrates the pressure profiles for the time period $t = 1.50$ to 2.00 seconds. The mean nozzle melt pressure integral ($t = 1.50$ to 2.00 seconds) = 371.27 bar.sec, with a coefficient of variation = 0.21%. The mean hydraulic injection pressure integral ($t = 1.50$ to 2.00 seconds) = 32.34 bar.sec, with a coefficient of variation = 0.17%.

Therefore, analysis of mean nozzle melt pressure and hydraulic injection pressure profiles during primary injection, has resulted in a pressure integral for $t = 1.50$ to 2.00 seconds. The following comparisons are made with respect to the integrals for full primary injection ($t = 0.00$ to 1.75 seconds). The nozzle melt pressure integral ($t = 1.50$ to 2.00 seconds) represents an increase in measurement precision by a factor of $0.84/0.21 = 4.00$. The hydraulic injection pressure integral ($t = 1.50$ to 2.00 seconds) represents an increase in measurement precision by a factor of $0.83/0.17 = 4.88$.

Figure 8.9 Mean nozzle melt pressure and coefficient of variation during primary injection

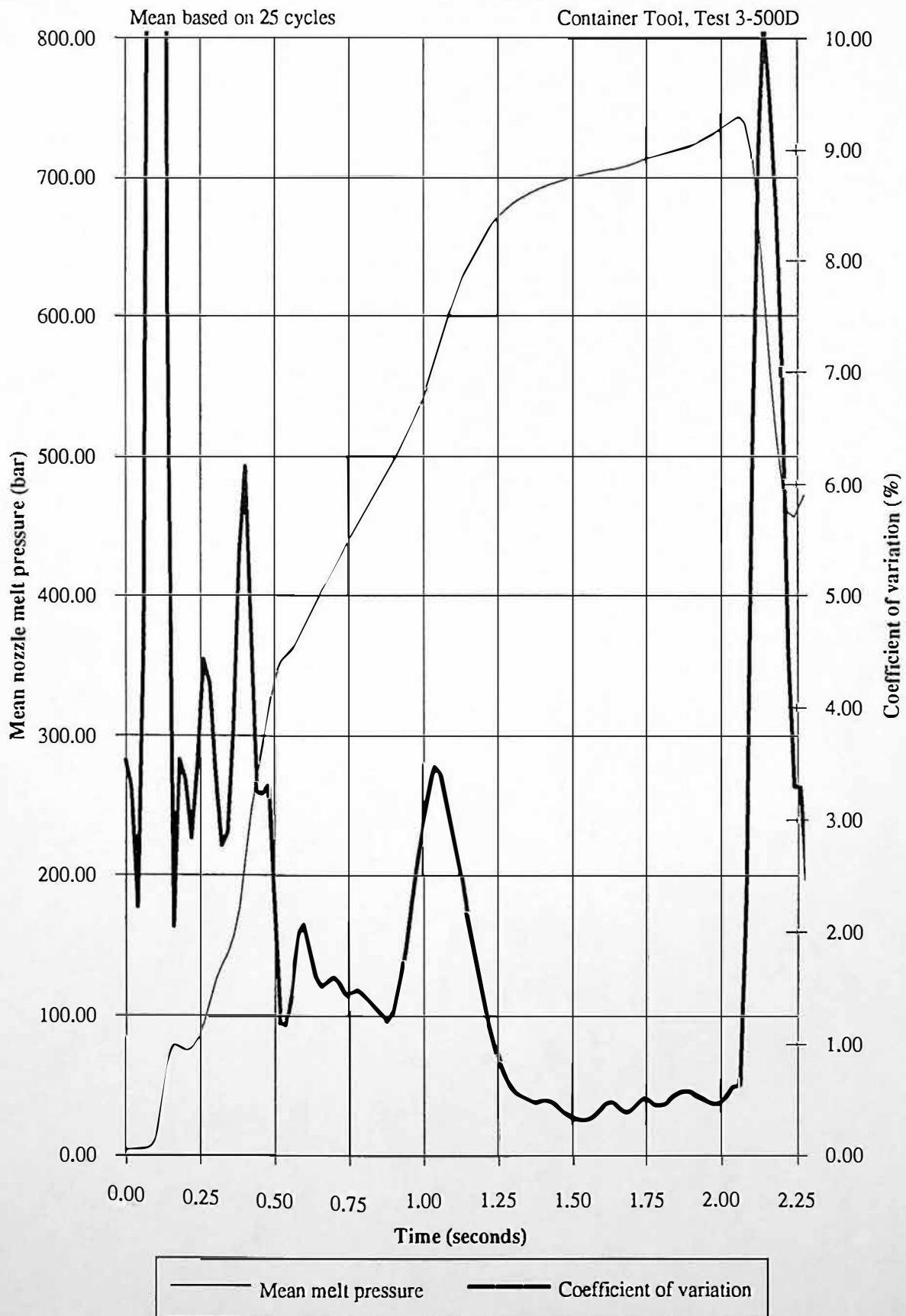
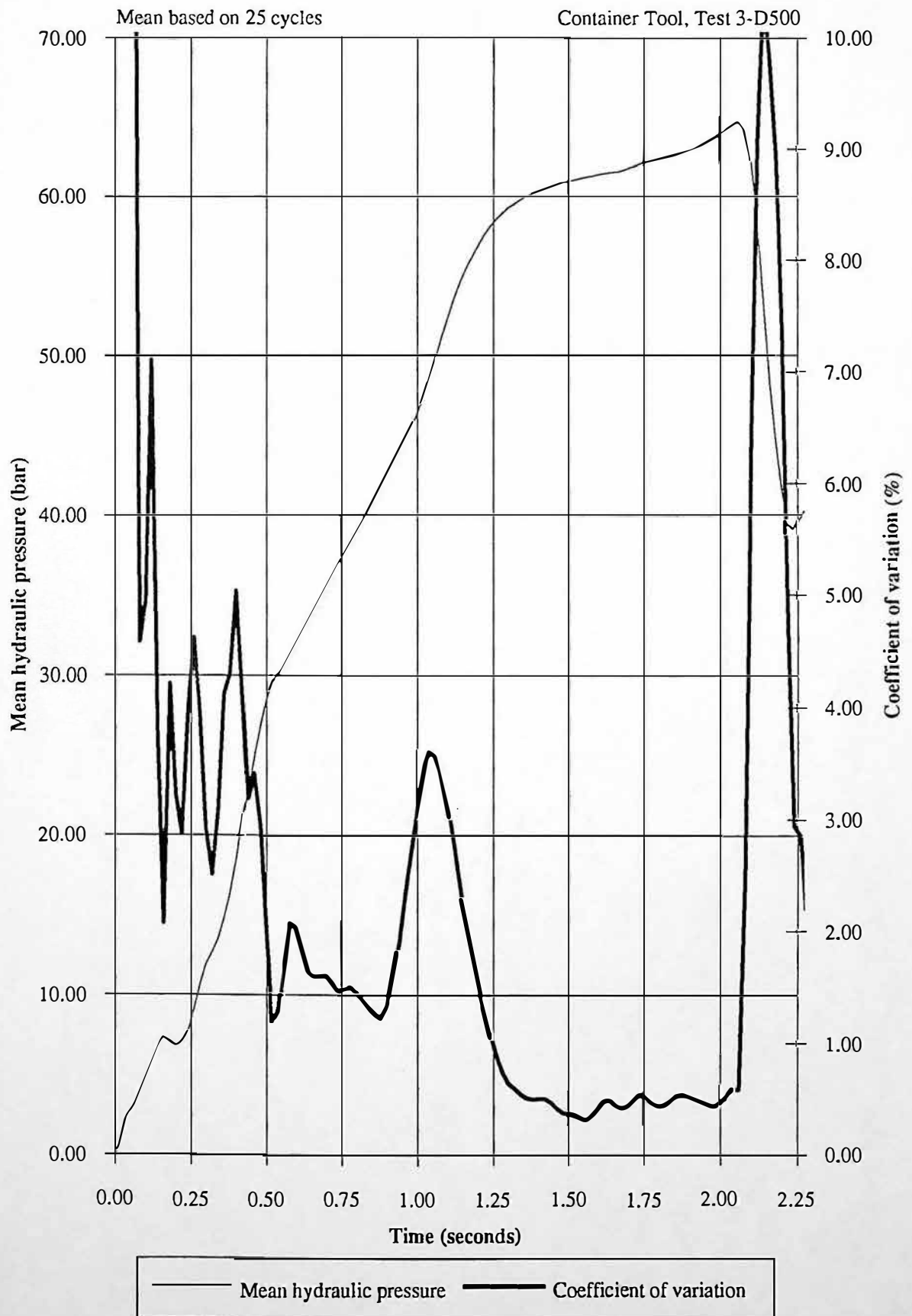


Figure 8.10 Mean hydraulic injection pressure and coefficient of variation during primary injection



8.4.5 Summary of Results

Table 8.8 summarises the results, allowing comparison of the coefficients of variation of nozzle melt pressure and hydraulic injection pressure.

	Full Pressure Integral (t= 0.00 to 2.06 seconds)	Specific Pressure Integral (t= 1.50 to 2.00 seconds)
In-line Nozzle Rheometry (Nozzle Melt Pressure)	0.84%	0.21%
Process Measurements (Hydraulic Injection Pressure)	0.83%	0.17%

Table 8.8 Summary of coefficient of variation results for test 3-D500

The advantage of calculating a specific pressure integral, can be seen in table 8.8, as the coefficients of variation are reduced by a factors of 4.88 and 4.00, for nozzle melt pressure and hydraulic injection pressure measurements, respectively.

The coefficient of variation can be used to calculate the measurement accuracy. Measurement accuracy was based on a 99.7% spread of data i.e. ± 3 standard deviations about the mean value, assuming normal distribution. The calculated measurement accuracy for each coefficient of variation are shown in table 8.9.

	Full Pressure Integral (t= 0.00 to 2.06 seconds)	Specific Pressure Integral (t= 1.50 to 2.00 seconds)
In-line Nozzle Rheometry (Nozzle Melt Pressure)	$\pm 2.52\%$	$\pm 0.63\%$
Process Measurements (Hydraulic Injection Pressure)	$\pm 2.49\%$	$\pm 0.51\%$

Table 8.9 Summary of measurement accuracy results for test 3-D500

The results of tables 8.8 and 8.9 show that nozzle melt pressure and hydraulic injection pressure integrals have a similar precision.

8.4.6 Comparison of Nozzle Melt Pressure and Hydraulic Injection Pressure Integrals During Primary Injection

The following work investigates the relationship between nozzle melt pressure and hydraulic injection pressure integrals. It can be seen from figures 8.11 and 8.12, that both pressure integrals have a high degree of correlation, and therefore both reflect the same polymer melt viscosity variations. The coefficient of correlation between mean nozzle melt pressure integral and mean hydraulic injection pressure integral for the full period of primary injection ($t=0.00$ to 2.06 seconds) = 0.99 and for the specific integral ($t=1.50$ to 2.00 seconds) = 0.90 .

Figure 8.11 Relationship between nozzle melt pressure and hydraulic injection pressure integrals for the full period of primary injection

Pressure integrals calculated for $t=0.00$ to 2.06 seconds

Coefficient of correlation = 0.99

Container Tool, Test 3-D500

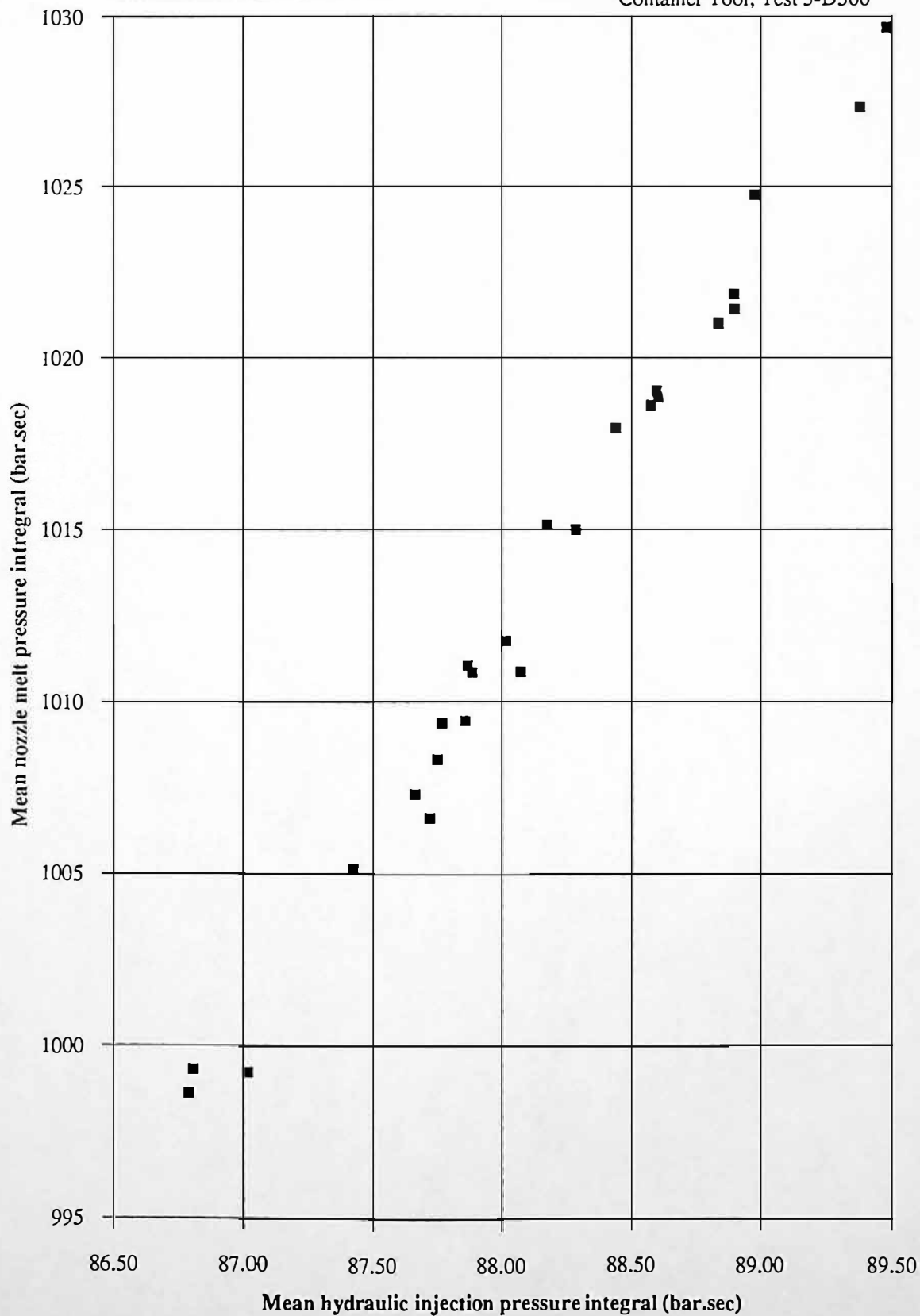
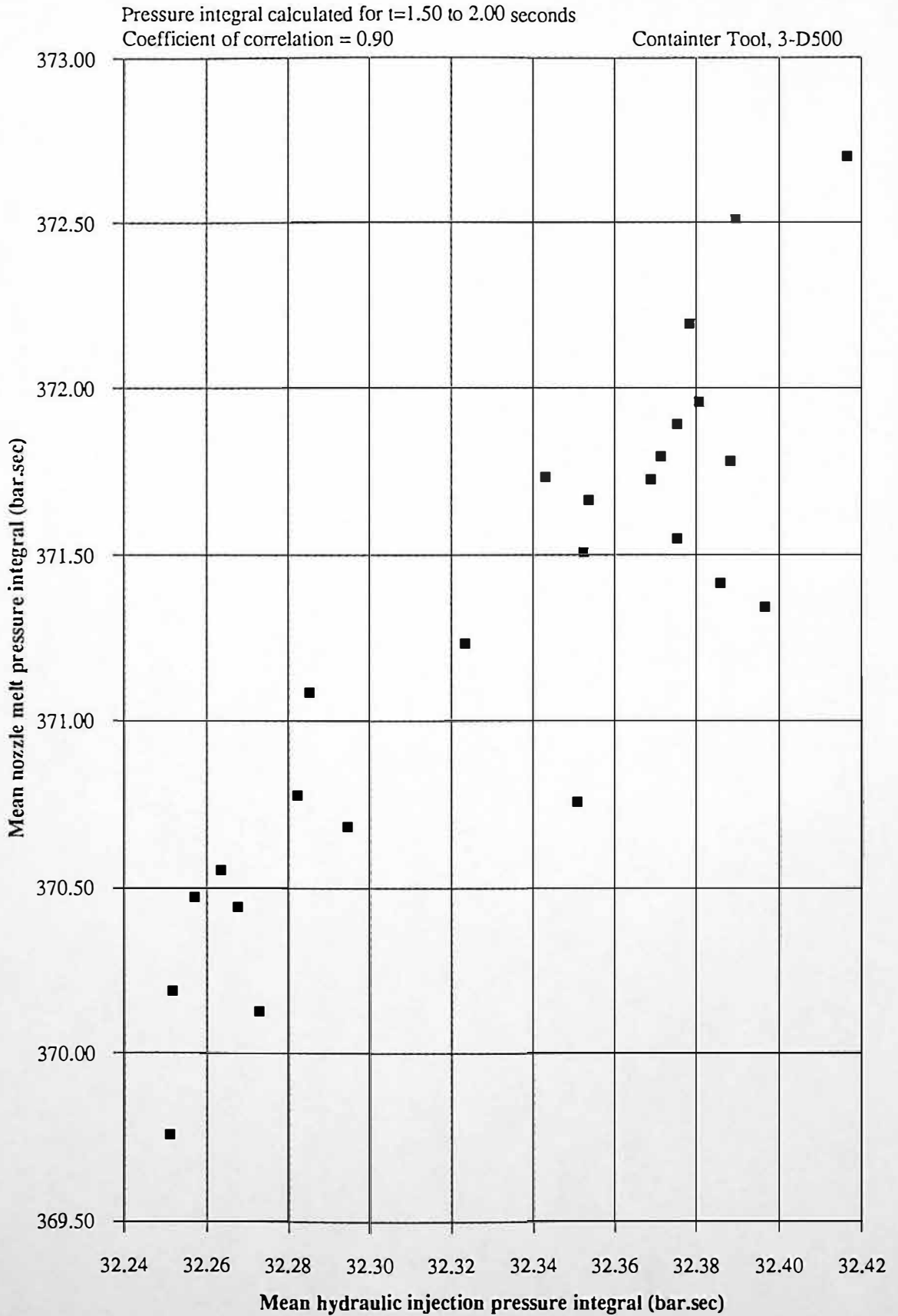


Figure 8.12 Relationship between nozzle melt pressure and hydraulic injection pressure integrals for a specific period of primary injection



8.5 Measurement of Specific Nozzle Melt Pressure Integrals for Material Batch to Batch Variation Identification

Experimental results from tests L-D500B1 and N-D500B2 are analysed, using two different batches of the same grade material, see table 8.10. The injection phase for 10 injection moulding cycles were accurately monitored, processing polyoxymethylene (POM), Du Pont Delrin II 500, using the instrumented (two impression 'family') container tool.

	Test	Material Batch Number
Batch 1	L-D500B1	LOT 347008K011
Batch 2	N-D500B2	LOT 258104K008

Table 8.10 Material batch information

Chapters 8.3 and 8.4 have described procedures for determining an optimum assessment of polymer melt viscosity for a specific nozzle geometry, using two different tools. To show the benefits that result from determining a specific nozzle melt pressure integral two batches of the same grade polymer were processed.

Figure 8.13 and 8.14 show the mean nozzle melt pressure and mean screw displacement for 10 moulding cycles, for tests L-D500B1 and N-D500B2, respectively. Figure 8.15 shows the result of calculating a nozzle melt pressure integral for the full period of primary injection $t = 0.00$ to 1.70 seconds. The mean difference between the mean nozzle melt pressure integrals is 13.9 bar.sec.

Figure 8.16 shows the result of calculating a nozzle melt pressure integral based on the Sandretto viscosity index, i.e. an industrial practice as described in appendix A(iii).

The difference between the mean nozzle melt viscosity index is 7.8 bar.sec. The nozzle melt pressure integral was calculated for $t= 0.34$ to 1.34 seconds.

Figures 8.17 and 8.18 show the mean nozzle melt pressure and coefficient of variation for both material batches. It can be seen that between $t= 1.40$ and 1.48 seconds that the coefficient of variation is a minimum for both material batches. Figure 8.19 show the nozzle melt pressure integral calculated for $t= 1.40$ to 1.48 seconds. The results show a clear difference between the material batches, using a ± 3 standard deviation spread of about the mean.

	Du Pont Delrin II (POM) 500	
	Batch 1	Batch 2
Full Pressure Integral ($t=0.00$ to 1.70 seconds)	0.73%	0.85%
Melt Viscosity Index Pressure Integral ($t=0.34$ to 1.34 seconds)	0.99%	1.12%
Specific Pressure Integral ($t=1.40$ to 1.48 seconds)	0.08%	0.12%

Table 8.11 Coefficients of variation results for material batch 1 and batch 2

Table 8.11 shows the coefficient of variations for tests L-D500B1 and N-D500B2. The calculation of a specific pressure integral are reduces the coefficient of variation by factors 9.33 and 6.94, for tests L-D500B1 and N-D500B2 respectively, when compared to the full pressure integral.

The calculation of a specific pressure integral based on the Sandretto viscosity index function, see Appendix A(iii), increases the coefficient of variation by factors of 1.36 and 1.32 for tests L-D500B1 and N-D500B2 respectively.

Figure 8.13 Mean nozzle melt pressure and mean screw displacement during primary injection for batch 1

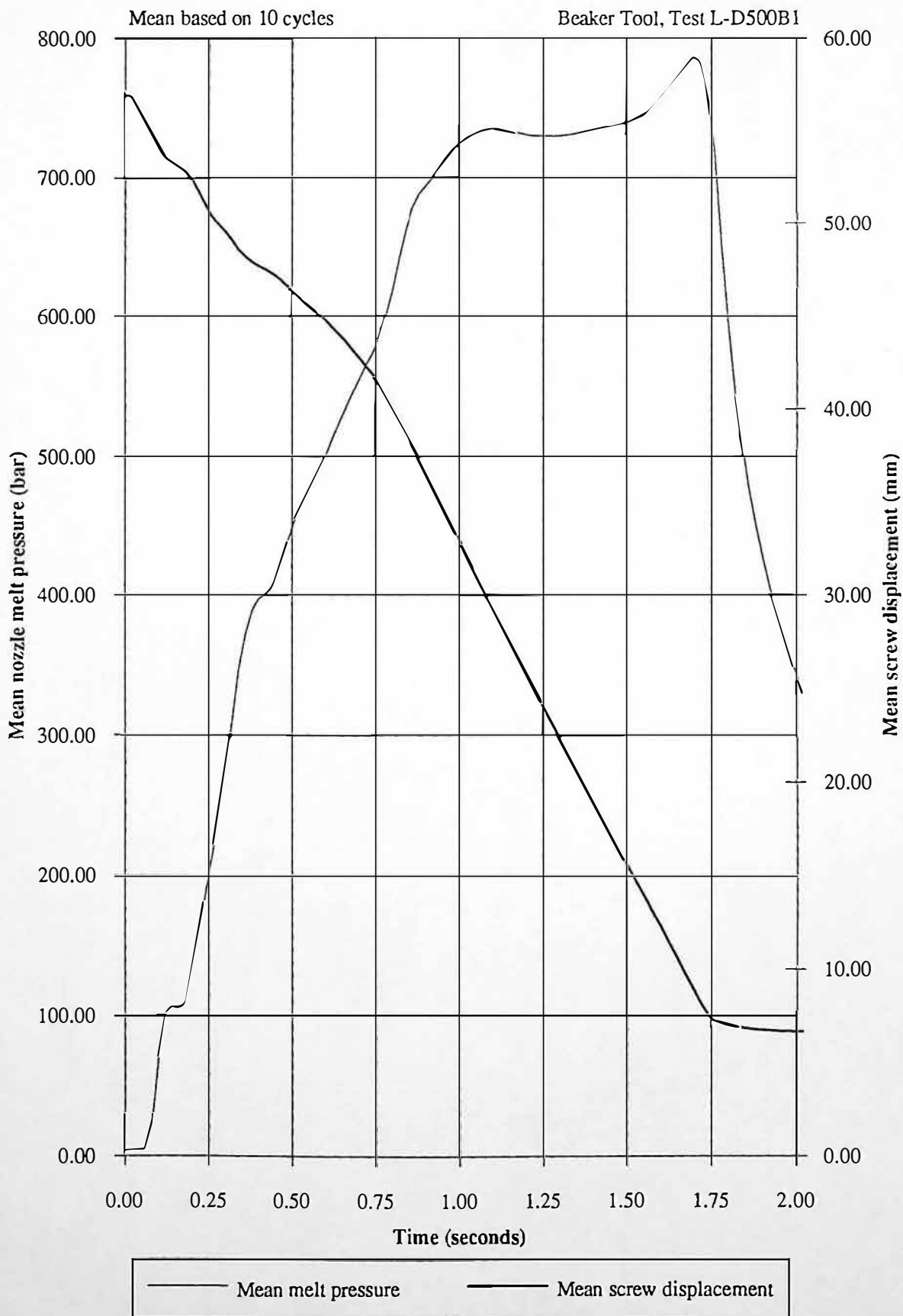


Figure 8.14 Mean nozzle melt pressure and mean screw displacement during primary injection for batch 2

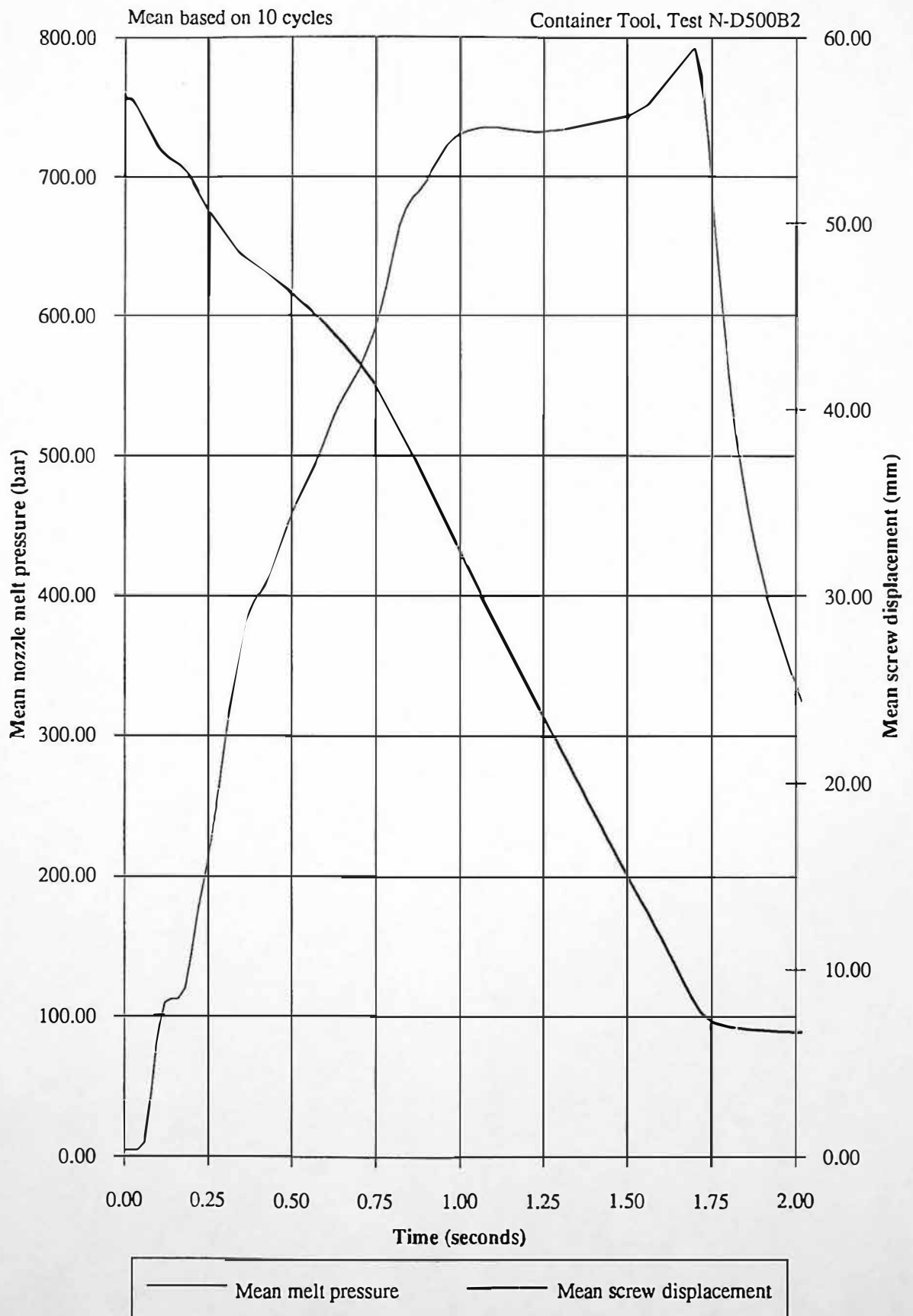


Figure 8.15 Nozzle melt pressure integrals for the full period of primary injection

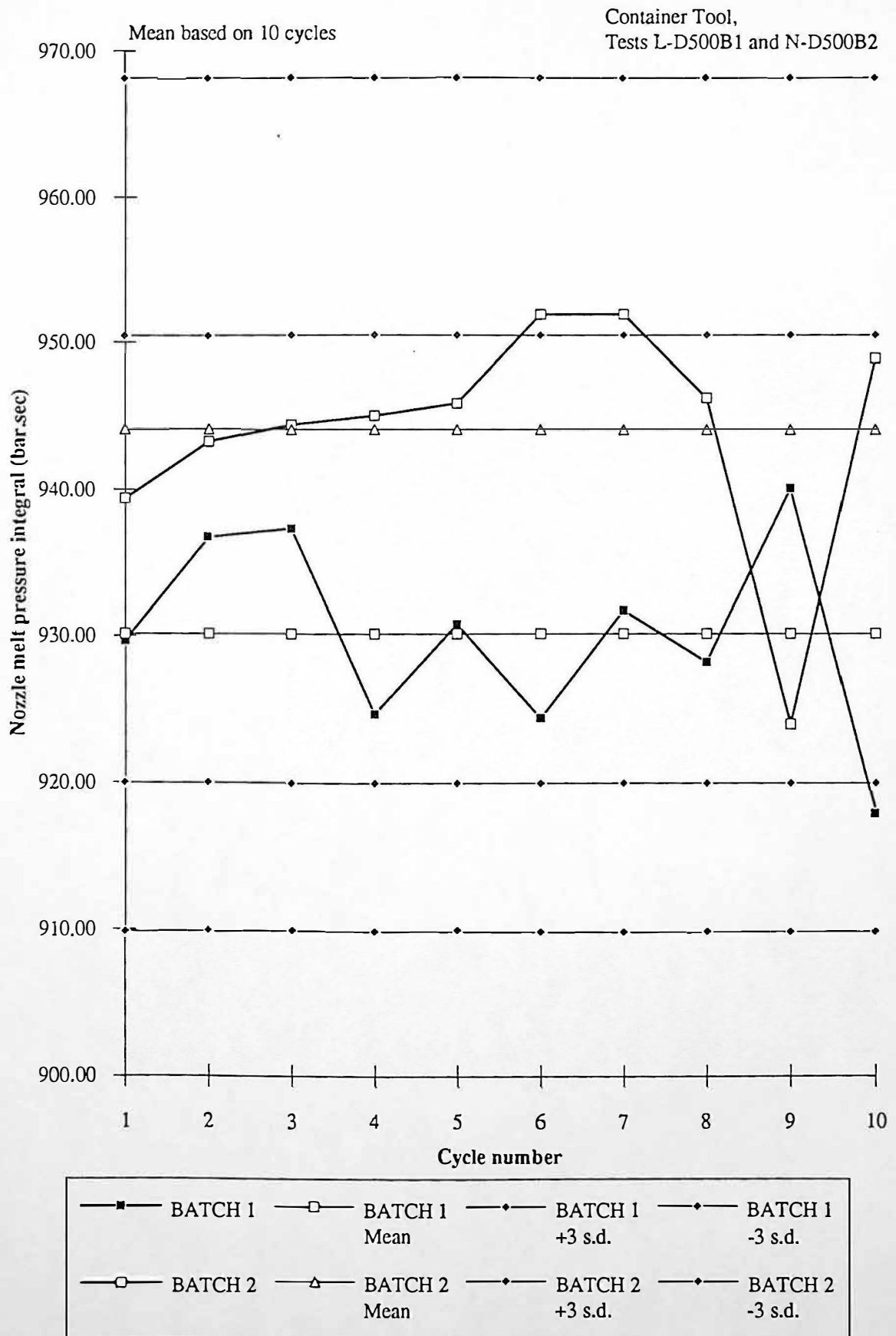


Figure 8.16 Nozzle melt pressure integrals based on the Sandretto viscosity index calculation

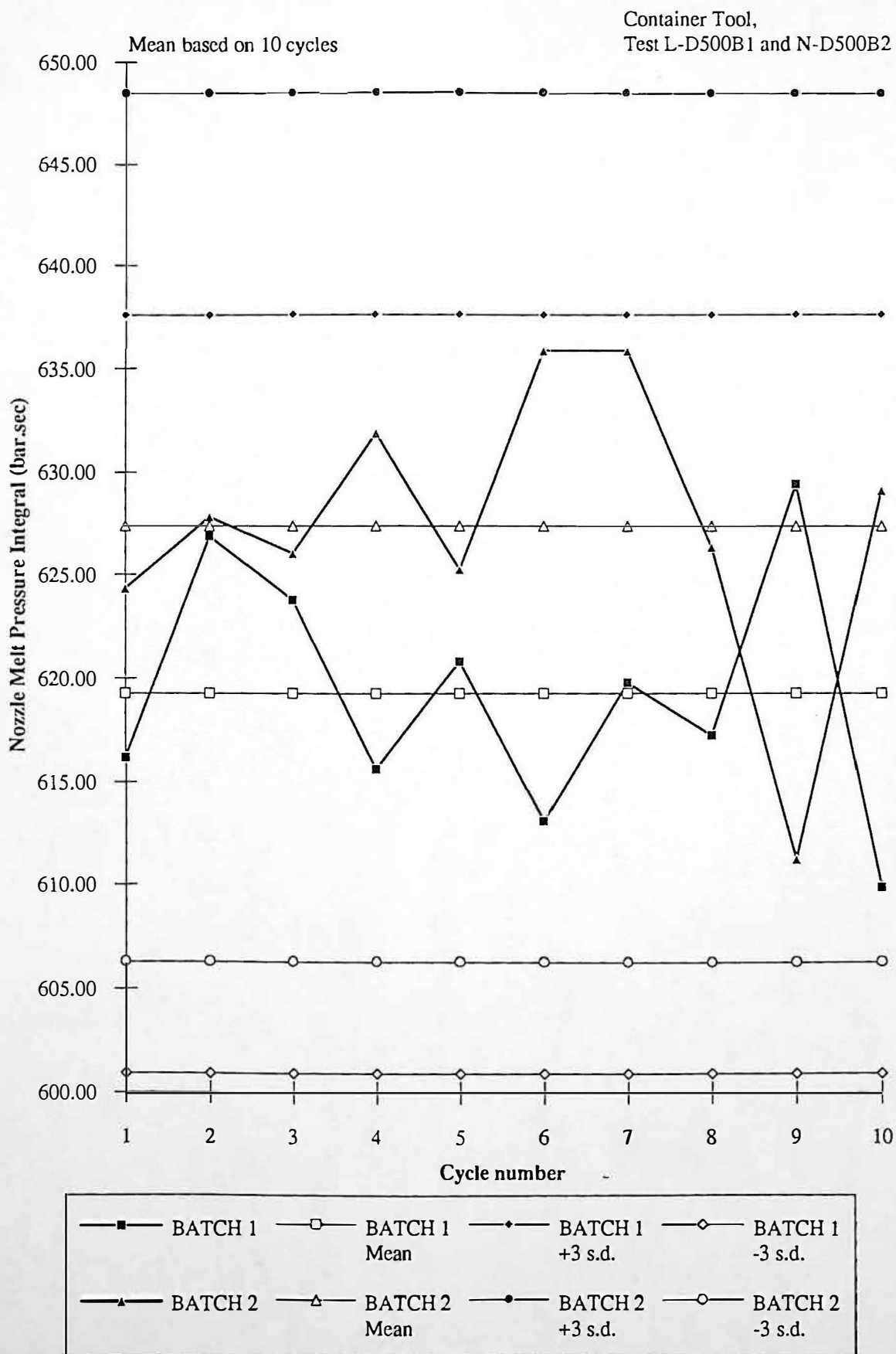


Figure 8.17 Mean nozzle melt pressure and coefficient of variation during primary injection for batch 1

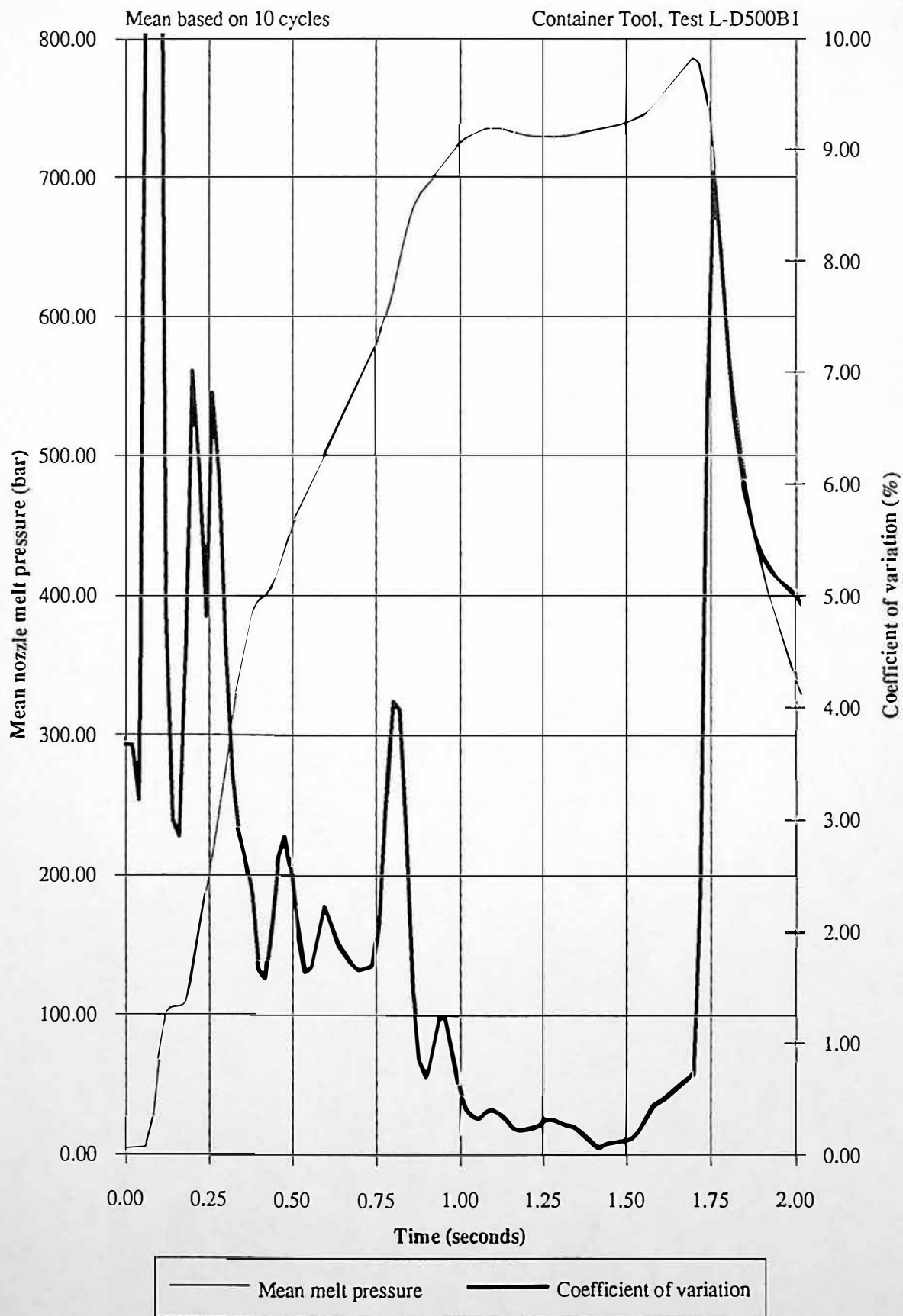


Figure 8.18 Mean nozzle melt pressure and coefficient of variation during primary injection for batch 2

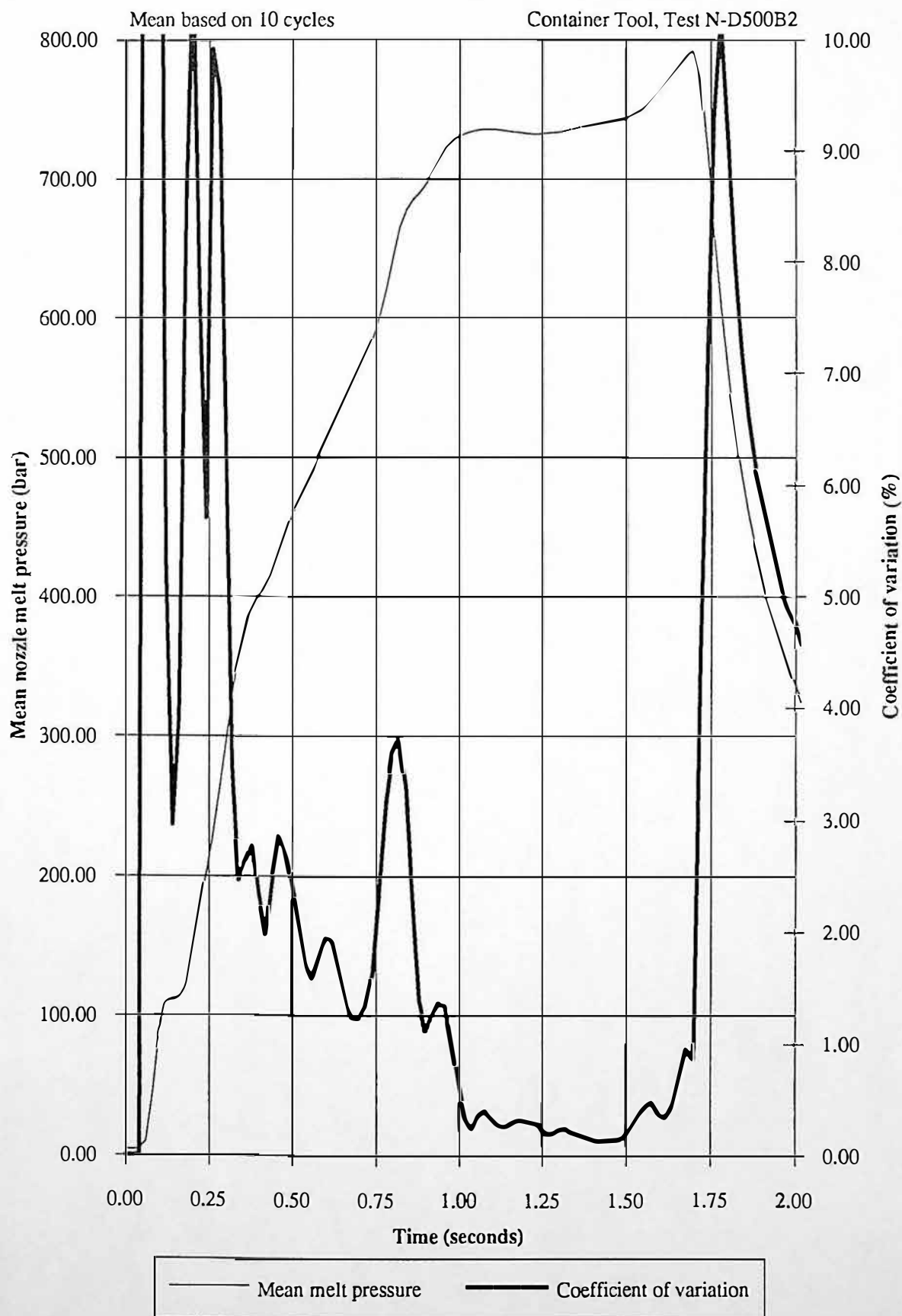
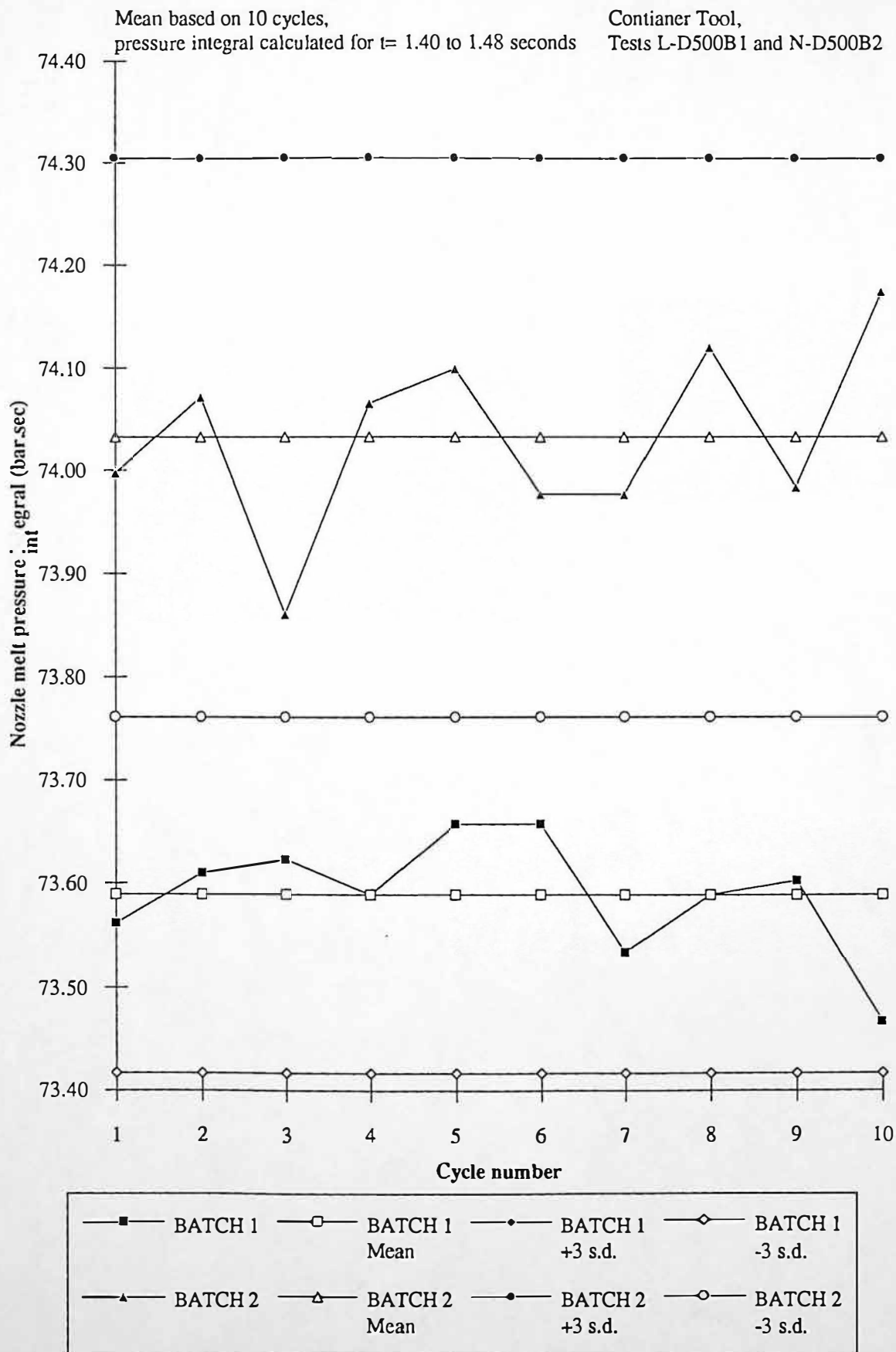


Figure 8.19 Nozzle melt pressure integrals for a specific period of primary injection



8.6 Influence of Screw Injection Velocity Control Performance on In-line Rheological and Process Measurements

8.6.1 Introduction

Chapters 8.3 and 8.4 have shown that during primary injection, specific nozzle melt pressure and hydraulic injection pressure integrals, can be determined, that optimise the measurement precision of in-line nozzle melt pressure and hydraulic injection pressure measurements. This chapter shows that quality of velocity control achieved during primary injection has a major influence in determining the location of specific pressure integrals.

8.6.2 Theoretical Considerations of In-line Nozzle Rheometry

Polymer melt rheology in the injection moulding machine nozzle convergence section is predominantly shear flow, with minimal deformation from extensional flow, due to the low angle of convergence within the nozzle (10 degrees convergence half angle). This idealised model may be subject to an extensional viscosity pressure component depending on gate geometry. In-line rheological measurements of apparent shear viscosity during primary injection are derived from the Poiseuille law for capillary flow i.e. from fundamental knowledge of volumetric flow rate (Q) and melt pressure (P) for a well defined geometry.

$$\text{Apparent Shear Viscosity } \eta = \frac{\tau_s}{\dot{\gamma}} \text{ (Pa.s)} \quad \text{Eq. 8.1}$$

$$\text{Apparent wall shear stress } \tau_s = \frac{PR}{2L} \text{ (Pa)} \quad \text{Eq. 8.2}$$

$$\text{Apparent wall shear rate } \dot{\gamma} = \frac{4Q}{\pi R^3} \text{ (s}^{-1}\text{)} \quad \text{Eq. 8.3}$$

where: P = Nozzle melt pressure (Pa)
 R = Capillary Radius (m)
 L = Capillary Length (m)

Volumetric flow rate Q (m^3/s) is calculated from the continuity equation:

$$Q = (v \cdot A) - Q_{\text{leak}} \quad \text{Eq. 8.4}$$

where:

v = Linear injection velocity (m/s)
 A = Cross sectional area of the screw (m^2)
 Q_{leak} = Leakage flow due to back flow past check ring (m^3/s)

From the continuity equation it can be seen that volumetric flow rate (Q) is directly related to screw velocity, assuming that leakage flow (Q_{leak}) is negligible. Therefore, if screw velocity is constant, variations in apparent shear viscosity are reflected in the measured nozzle melt pressure, assuming the maximum hydraulic line pressure limit is not reached. As primary injection operates with closed loop velocity control, the performance of the control algorithm determines the accuracy of screw velocity, which influences the accuracy of the nozzle melt pressure measurements.

8.6.3 Experimental Results

Figure 8.20 shows mean screw injection velocity and coefficient of variation for 25 cycles of test P30%20B. Measuring screw velocity directly allows the variations in velocity control to be assessed. Screw velocity can be derived from screw displacement, but quantification errors may be large, for high data sample rates, Sivakumar (1986 p 123). It can be seen from figure 8.20 that there is a region of low coefficient of variation between $t=1.20$ and $t=1.70$ seconds. This region corresponds to the specified pressure integral region as shown in figures 8.4 and 8.5. Therefore, the quality of the screw velocity control apparently has a strong influence on the quality of in-line nozzle melt pressure measurements and hydraulic injection pressure measurements. Figure 8.21 shows mean screw injection velocity and mean screw acceleration. It can be seen that between $t=1.20$ and $t=1.70$ seconds where screw acceleration is low, this period corresponds to the period of good velocity control $t=1.20$ and $t=1.70$ seconds.

It can be seen from figure 8.22 that there is a region of low coefficient of variation between $t=1.50$ and $t=2.00$ seconds. This region corresponds to the specified pressure integral region as shown in figures 8.9 and 8.10. Figure 8.23 shows mean screw injection velocity and mean screw acceleration. It can be seen that between $t=1.50$ and $t=2.00$ seconds where screw acceleration is low, this period corresponds to the period of good velocity control $t=1.50$ and $t=2.00$ seconds.

The analysis of screw velocity for tests P30%20B and 3-500D has shown that the quality of screw velocity control influences the quality of in-line rheometry and process measurements. It can be seen that regions of low acceleration show where velocity control is good and therefore where to integrate the nozzle melt pressure and hydraulic injection profiles.

Figure 8.20 Mean screw injection velocity and coefficient of variation during primary injection

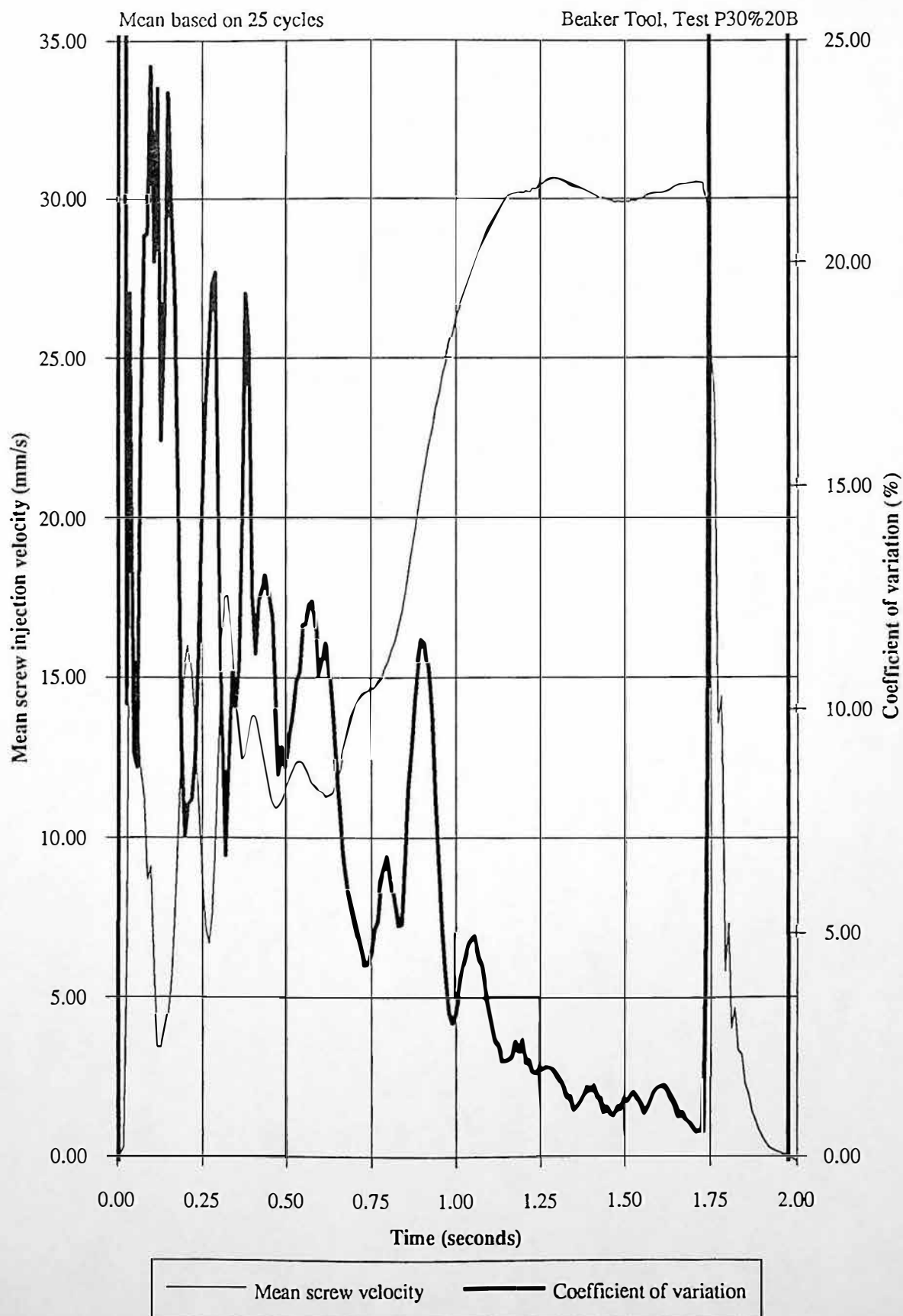


Figure 8.21 Mean screw injection velocity and mean screw acceleration during primary injection

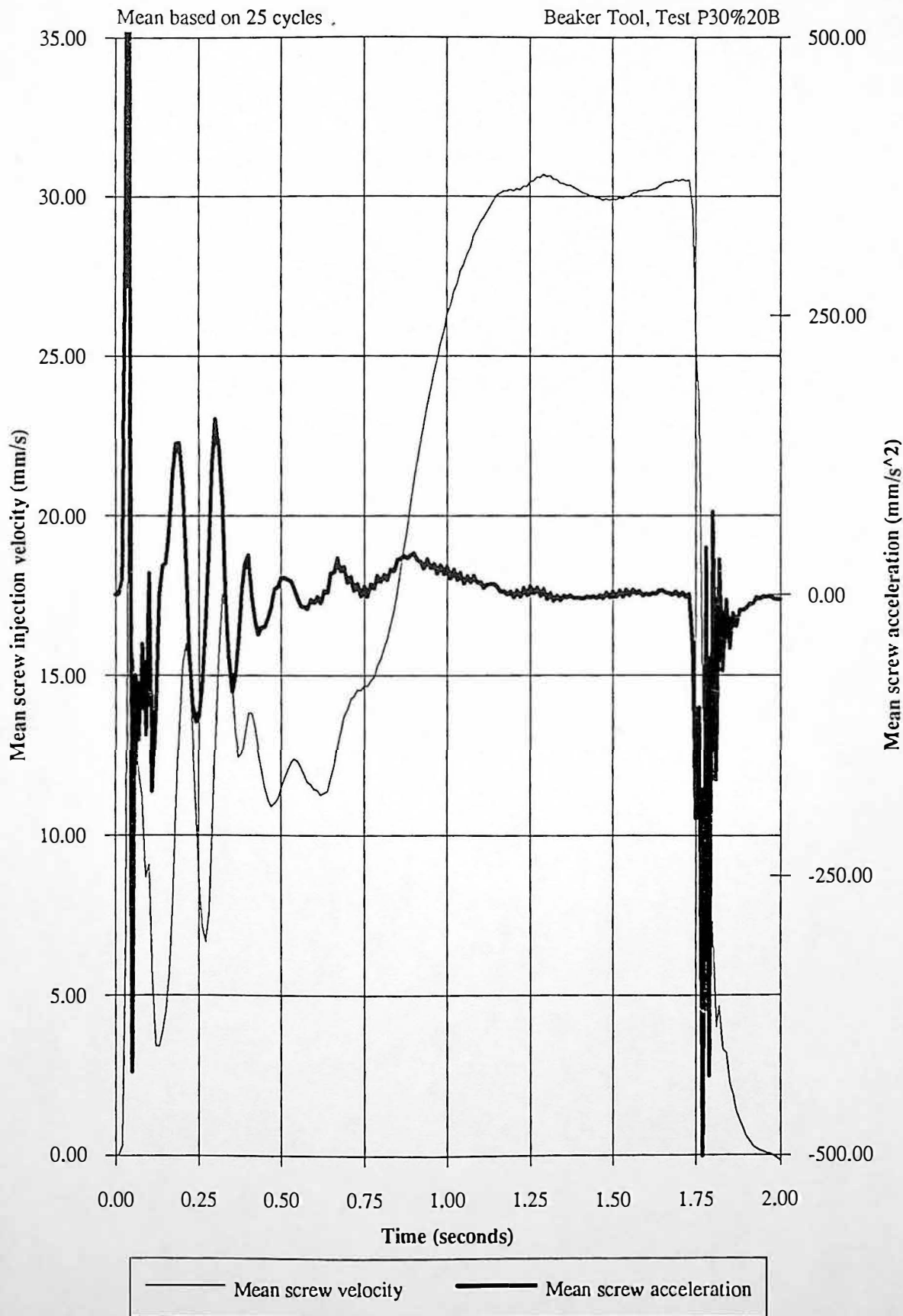


Figure 8.22 Mean screw injection velocity and coefficient of variation for primary injection

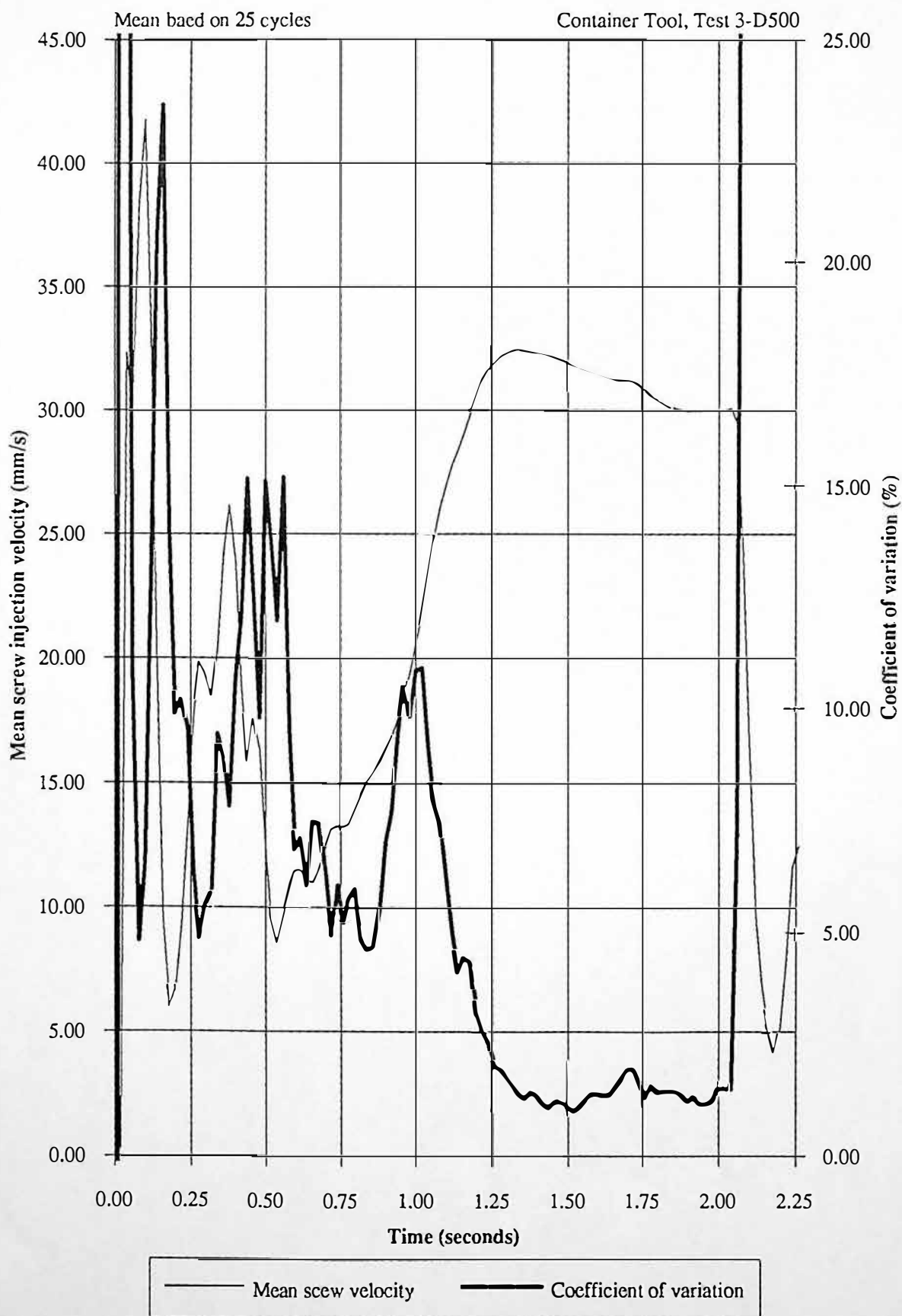
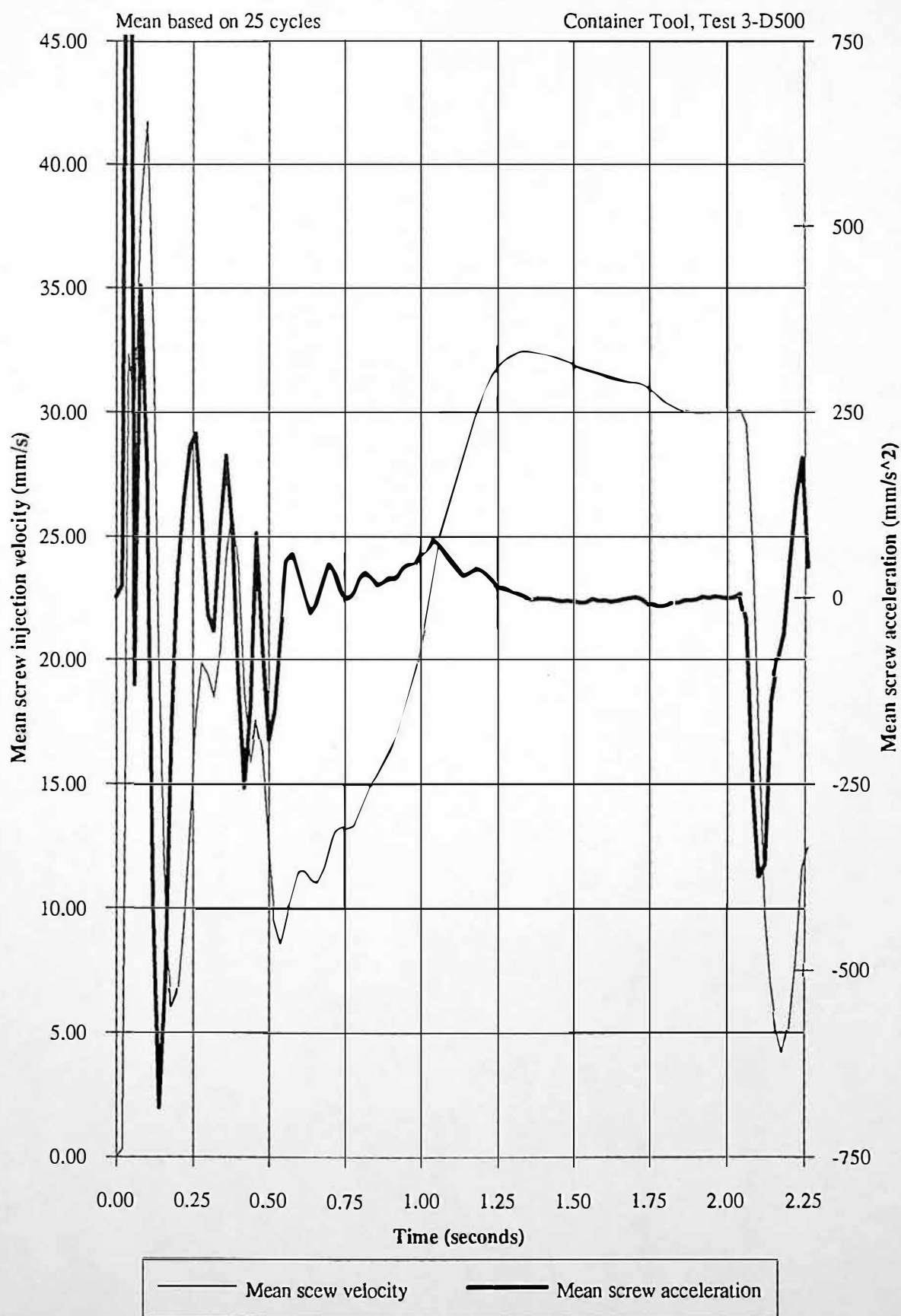


Figure 8.23 Mean screw injection velocity and mean screw acceleration during primary injection



8.6.4 Changing the Performance of the Screw Injection Velocity Control

For this work the screw displacement accuracy has been improved from ± 0.22 mm (level A screw displacement accuracy) to ± 0.06 mm (level B screw displacement accuracy), see chapter 4.6.

The screw position signal is converted into a digital value by the machine controlled, for quantitative differentiation to determine screw velocity. Therefore, the accuracy of the screw displacement signal directly influences the performance of the screw velocity controller. The differences in the velocity control performance should directly affect the precision of a polymer melt viscosity assessment, if the hypothesis of chapter 8.6 is correct.

Data is investigated from tests L40%20B and I40%20B, 10 cycles were monitored from each test. Figures 8.24 and 8.25 show mean screw injection velocity and mean nozzle melt pressure, respectively for test L40%20B, both figures showing the respective coefficient of variation. Figures 8.26 and 8.27 show mean screw injection velocity and mean nozzle melt pressure, respectively for test I40%20B, both figures showing the respective coefficient of variation.

Table 8.12 shows the mean coefficient of variation results for mean screw injection velocity, mean nozzle melt pressure and product weight for tests L40%20B and I40%20B respectively. The different levels of velocity control performance also reflects in the product quality, i.e. product weight distribution, as shown in figure 8.28.

	Test L40%20B: Level A Screw Displacement Accuracy		Test I40%20B: Level B Screw Displacement Accuracy	
	Mean	Coefficient of variation	Mean	Coefficient of variation
Mean Screw Injection Velocity	42.54 mm/s	1.99 %	40.62 mm/s	1.34 %
Mean Nozzle Melt Pressure	443.86 bar	2.05 %	443.30 bar	0.63 %
Mean Product Weight	32.77 grams	0.08 %	32.76 grams	0.02 %

Table 8.12 Coefficient of variation results for level A and B screw displacement accuracy

Figure 8.24 Mean screw injection velocity and coefficient of variation during primary injection for level A screw displacement accuracy

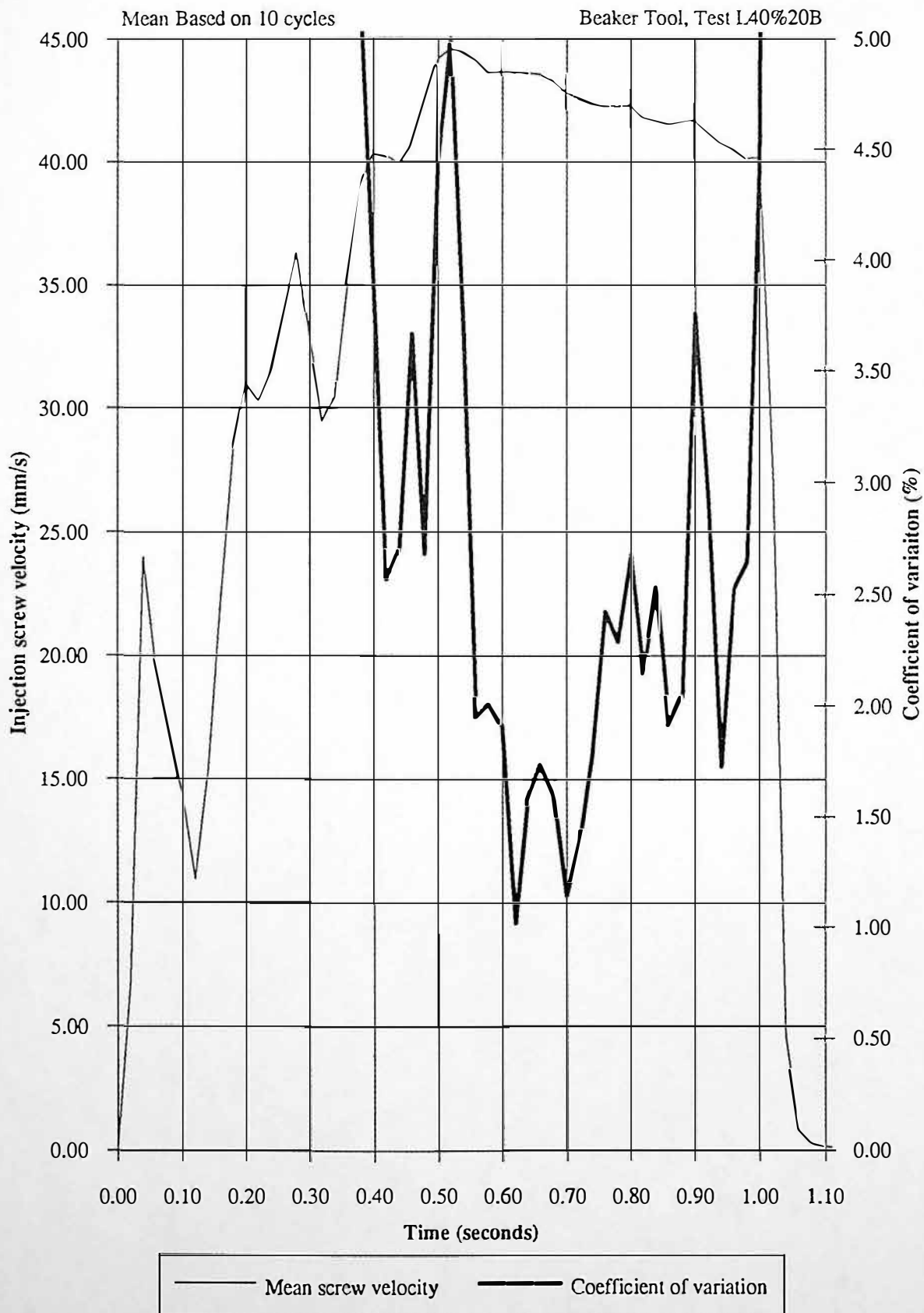


Figure 8.25 Mean nozzle melt pressure and coefficient of variation during primary injection for level A screw displacement accuracy

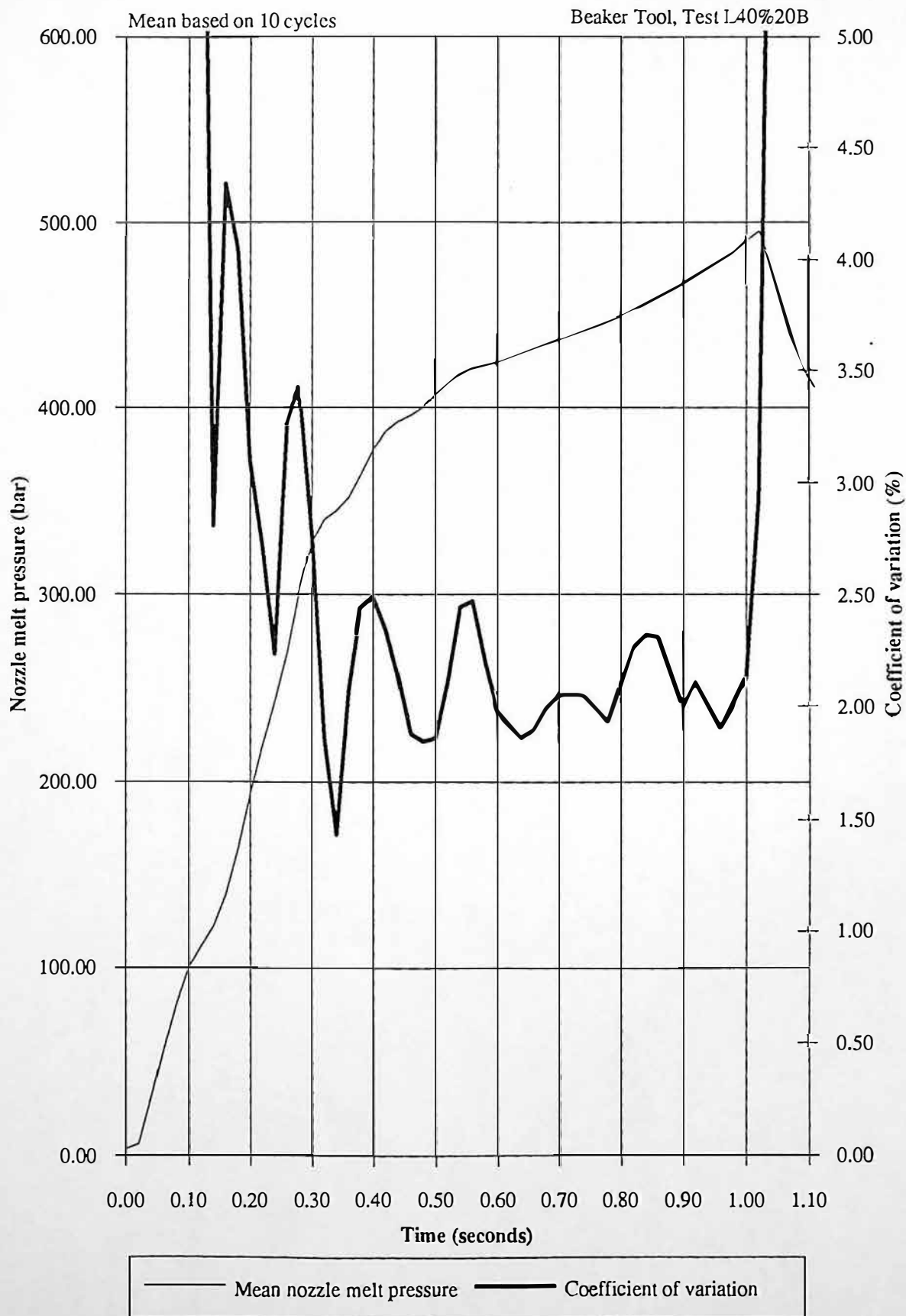


Figure 8.26 Mean screw injection velocity and coefficient of variation during primary injection for level B screw displacement accuracy

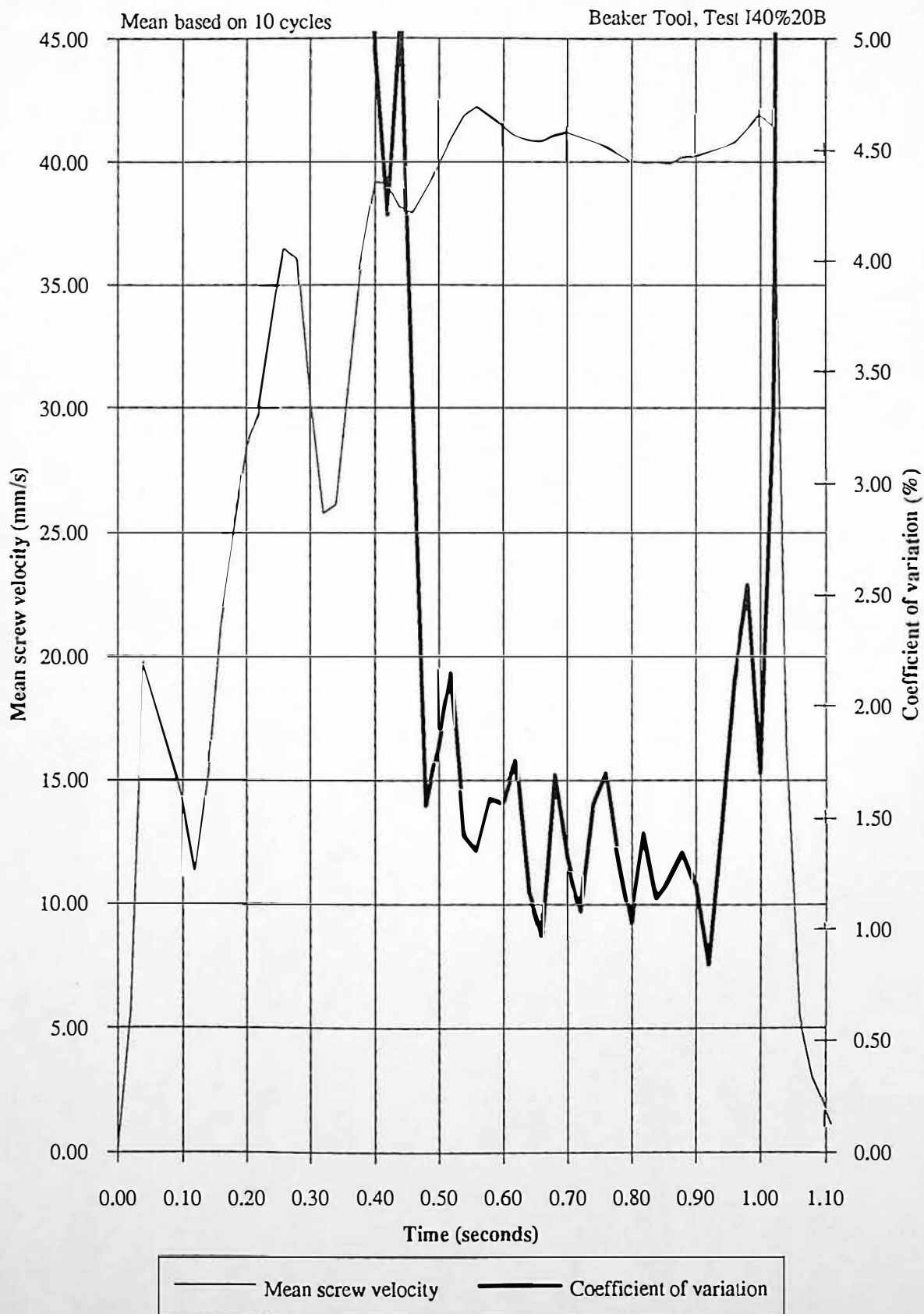


Figure 8.27 Mean nozzle melt pressure and coefficient of variation during primary injection for level B screw displacement accuracy

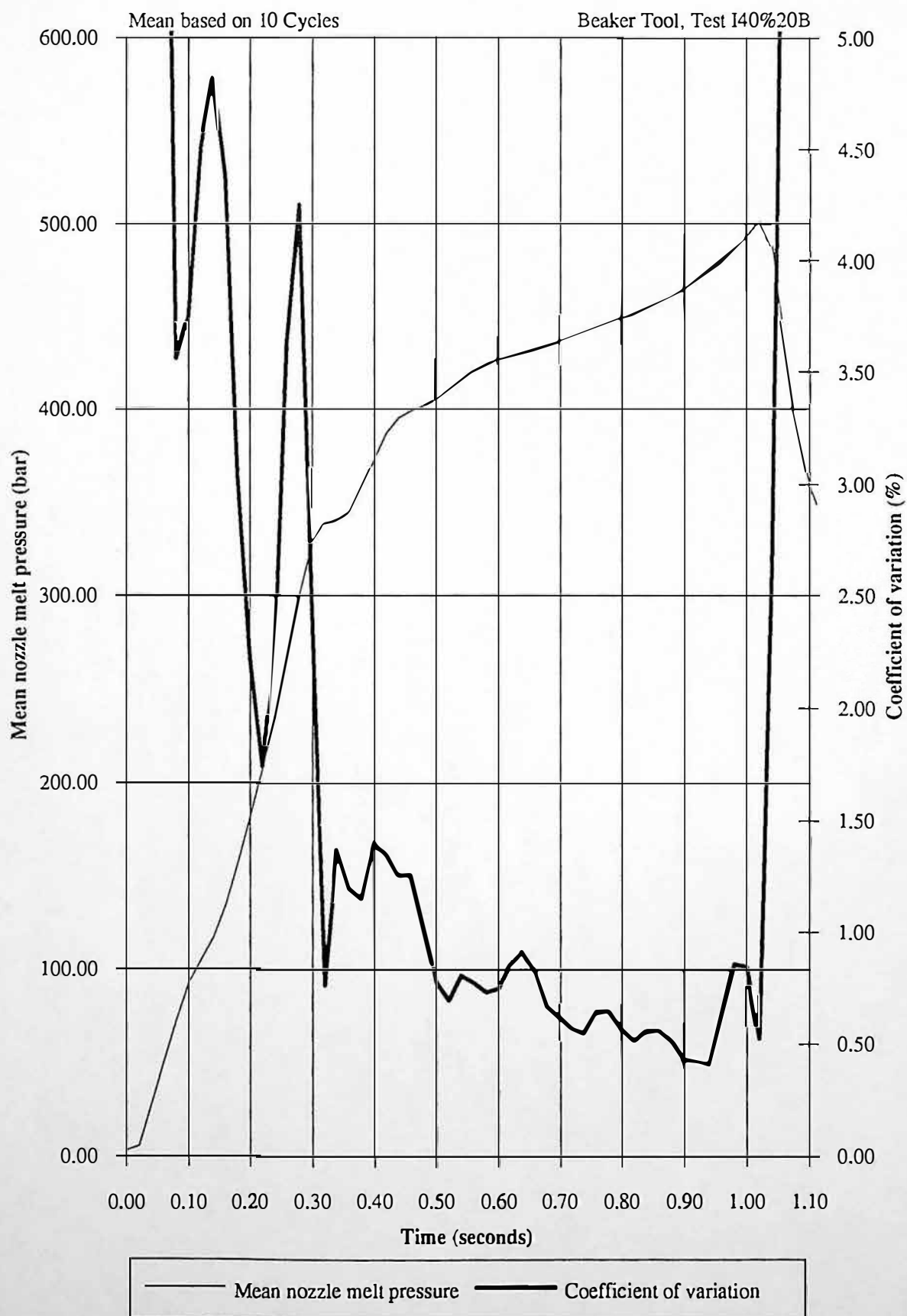
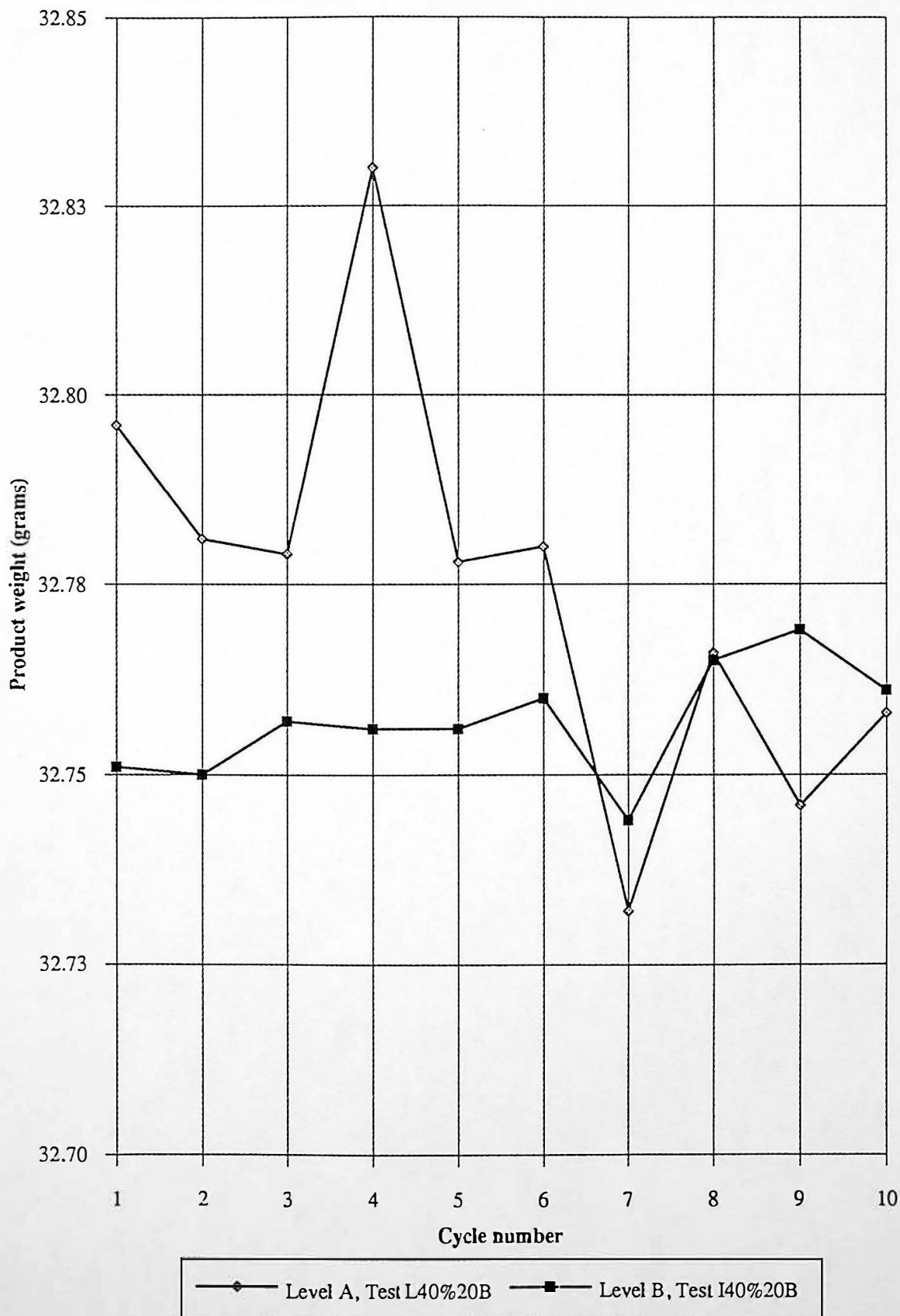


Figure 8.28 Product weight distribution for level A and B screw displacement accuracy

Level A, Test L40%20B, mean = 32.77 grams, standard deviation = 0.03 grams

Level B, Test I40%20B, mean = 32.76 grams, standard deviation = 0.01 grams



8.7 Relationship Between In-line Nozzle Melt Pressure and Hydraulic Injection Pressure Measurements During Primary Injection

8.7.1 Introduction

It has been shown in chapters 8.3 and 8.4 that in-line nozzle melt pressure and hydraulic injection pressure measurements have comparable precision. The aforementioned measurements also have a comparable accuracy, but only for specific process conditions. This chapter investigates the relationship between hydraulic injection pressure and nozzle melt pressure. Chapter 8.6 described a procedure for determining where to integrate nozzle melt pressure and hydraulic injection pressure, an alternative method is described.

8.7.2 Comparison of Nozzle Melt Pressure and Hydraulic Injection Pressure Measurements During Primary Injection

- (i) An accurate and precise measurement of nozzle melt pressure allows an absolute rheological assessment of melt viscosity. For process control an absolute measurement of polymer melt viscosity during primary injection is desirable, but a relative assessment of melt viscosity may be adequate.
- (ii) An accurate measurement of polymer melt temperature is possible, using an in-line nozzle rheometer.
- (iii) In an industrial environment a nozzle rheometer may be susceptible to damage. Implementation of process control based on hydraulic injection pressure would be more favourable for some industrial environments, where measurements are made away from machine nozzle, therefore making maintenance easier. Improvements to

the signal conditioning circuits of the hydraulic injection pressure transducer may be necessary, to obtain the required accuracy and precision.

8.7.3 Theoretical Considerations for The Relationship Between Nozzle Melt and Hydraulic Injection Pressure Measurements

The relationship between nozzle melt pressure and hydraulic injection pressure would be constant for an ideal injection unit, assuming no mechanical losses from the injection unit and no compressibility of the polymer melt.

$$\text{Nozzle Melt Pressure} = \frac{A_{\text{Piston}}}{A_{\text{Screw}}} \times \text{Hydraulic Injection Pressure} \quad \text{Eq. 8.5}$$

Where:

$$A_{\text{Piston}} = \text{Area of Hydraulic Piston (m}^2\text{)}$$

$$A_{\text{Screw}} = \text{Area of Screw (m}^2\text{)}$$

The ratio of Nozzle melt pressure to hydraulic injection pressure can be calculated for the injection unit of the Sandretto 60 injection moulding machine, see Appendices A(i) and A (ii), where hydraulic piston diameter = 140 mm and screw diameter = 40 mm.

$$A_{\text{Piston}} = \frac{\pi d^2}{4} = \frac{\pi \cdot (0.140)^2}{4} = 1.539 \times 10^{-2} \text{ m}^2$$

$$A_{\text{Screw}} = \frac{\pi d^2}{4} = \frac{\pi \cdot (0.040)^2}{4} = 1.257 \times 10^{-3} \text{ m}^2$$

$$\text{Therefore, } \frac{A_{\text{Piston}}}{A_{\text{Screw}}} = \frac{1.539 \times 10^{-2}}{1.257 \times 10^{-3}} = 12.25$$

8.7.4 Experimental Results

It can be seen from figure 8.29 that the ratio between maximum nozzle melt pressure and hydraulic injection pressure during primary injection, depends on the screw injection velocity.

At an injection velocity of 10 mm/s the ratio is 11.75, this ratio reduces to 10.60 at 97 mm/s. There is a linear relationship between injection velocity and ratio of maximum nozzle melt pressure and maximum hydraulic injection pressure. This relationship has a coefficient of correlation of 0.99. Figure 8.30 shows the mean hydraulic oil temperature during tests NX%20B and OX%20B. It is apparent that the variation of the ratio was not a direct result of hydraulic oil temperature changes.

To derive absolute nozzle melt pressure from hydraulic injection pressure, it is apparent that material compressibility and hydraulic efficiency may need to be modelled.

Analysis of the ratio between nozzle melt pressure and hydraulic injection pressure during primary injection can be used to determine where to integrate the nozzle melt pressure and hydraulic injection pressure profiles.

Figure 8.31 shows the ratio of hydraulic/melt pressure compared to injection screw velocity for test P30%20B. During the screw acceleration period the ratio reduces as expected. Once the desired injection velocity is achieved the ratio stabilises. Therefore, if the ratio is differentiated as shown in figures 8.32 and 8.33, the lowest value of the differential indicates where screw velocity control is good. From the previous section this period indicates where to integrate the pressure profiles.

Figure 8.34 shows the ratio of hydraulic/melt pressure compared to injection screw velocity for test 3-500D. During the screw acceleration period the ratio reduces as expected. Once the desired injection velocity is achieved the ratio stabilises.

Therefore, if the ratio is differentiated as shown in figure 8.35 and figure 8.36, the lowest value of the differential indicates where screw velocity control is good. From the previous section this period indicates where to integrate the pressure profiles.

Figure 8.29 Relationship between maximum nozzle melt pressure and hydraulic injection pressure, during primary injection

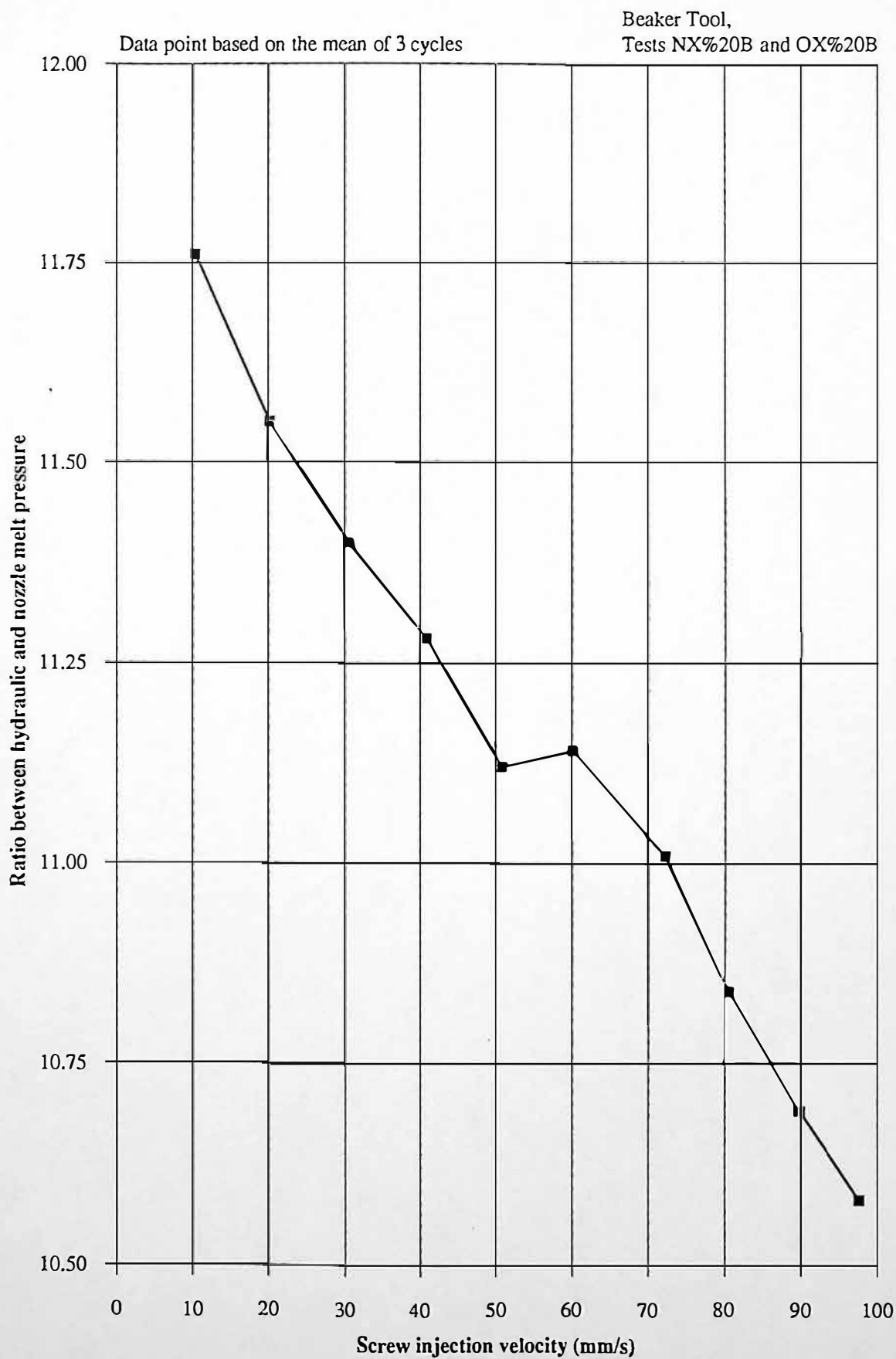


Figure 8.30 Hydraulic oil temperature distribution for increasing screw injection velocity

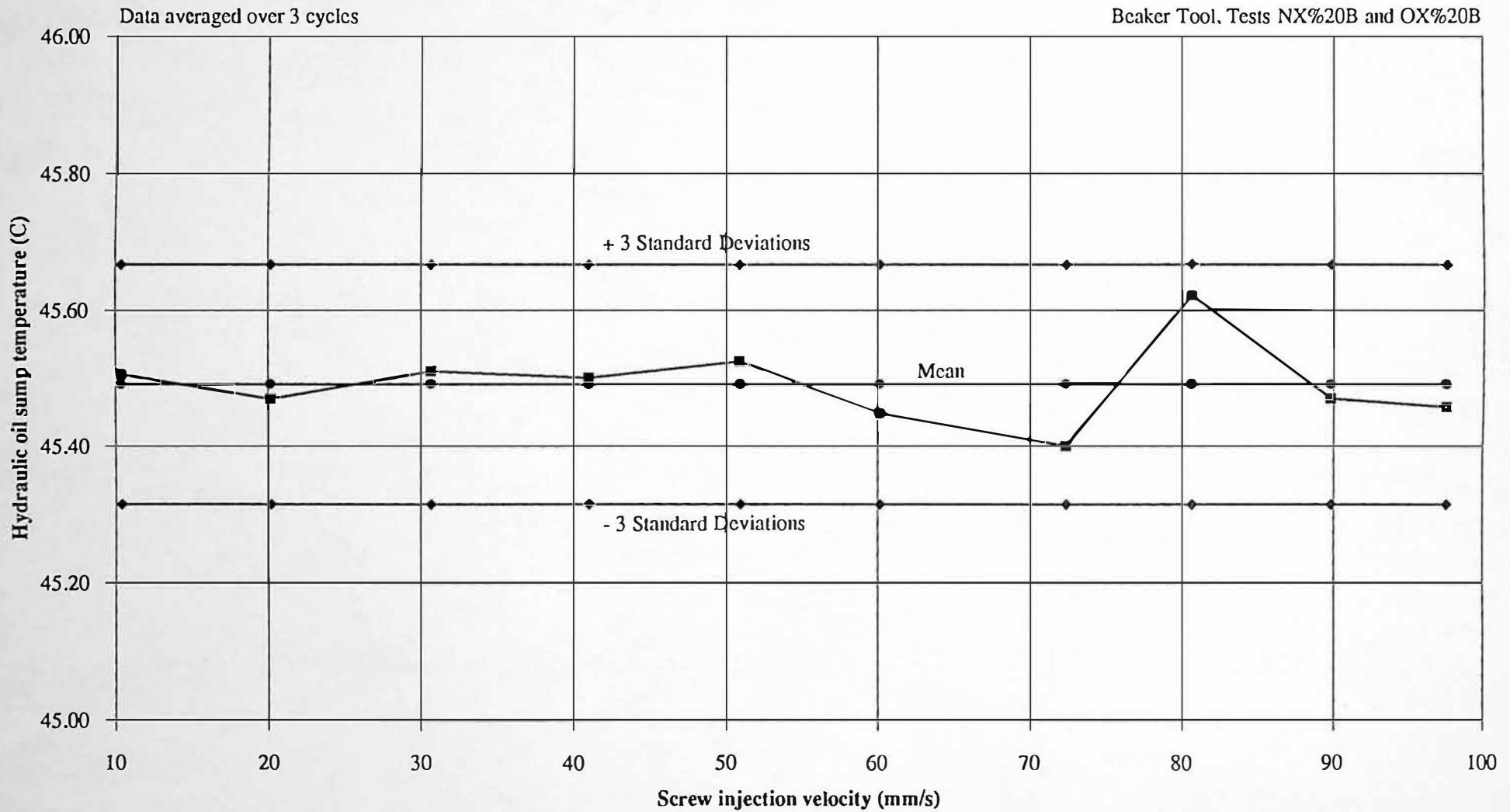


Figure 8.31 Mean screw injection velocity and mean ratio of nozzle melt pressure to hydraulic injection pressure during primary injection

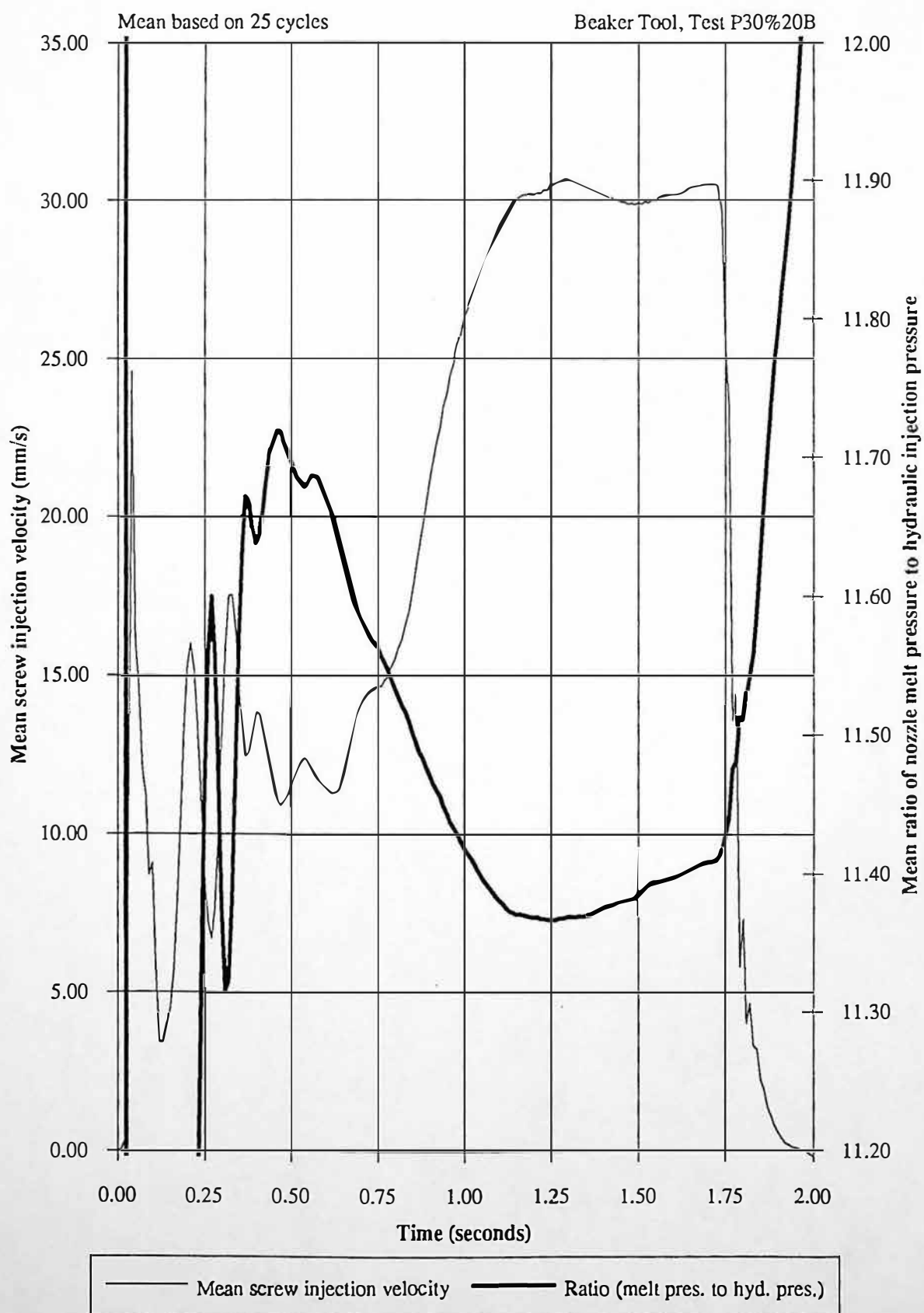


Figure 8.32 Differential of mean ratio of nozzle melt pressure to hydraulic injection pressure and coefficient of variation of nozzle melt pressure during primary injection

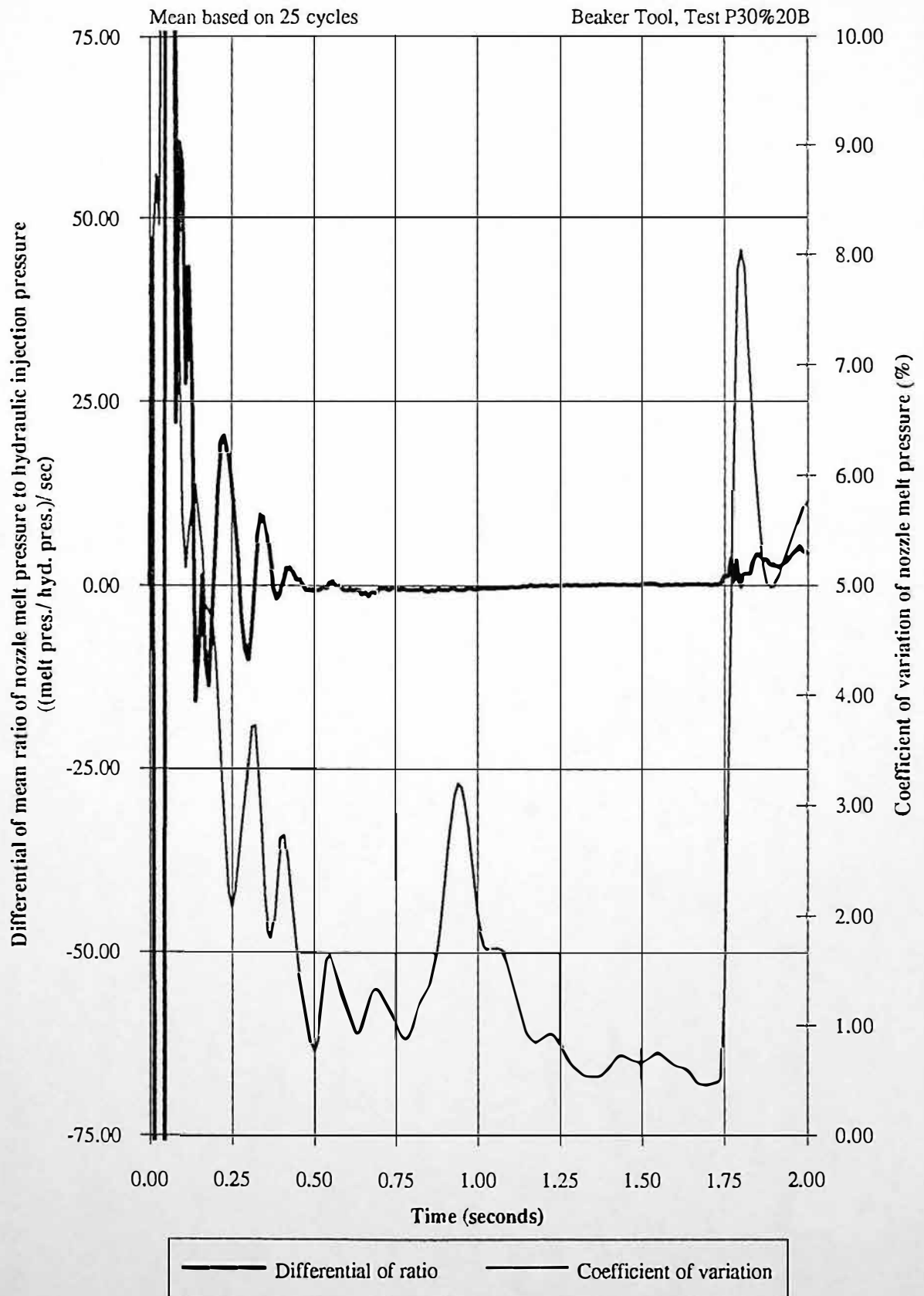


Figure 8.33 Differential of mean ratio of nozzle melt pressure to hydraulic injection pressure and coefficient of variation of nozzle melt pressure during primary injection

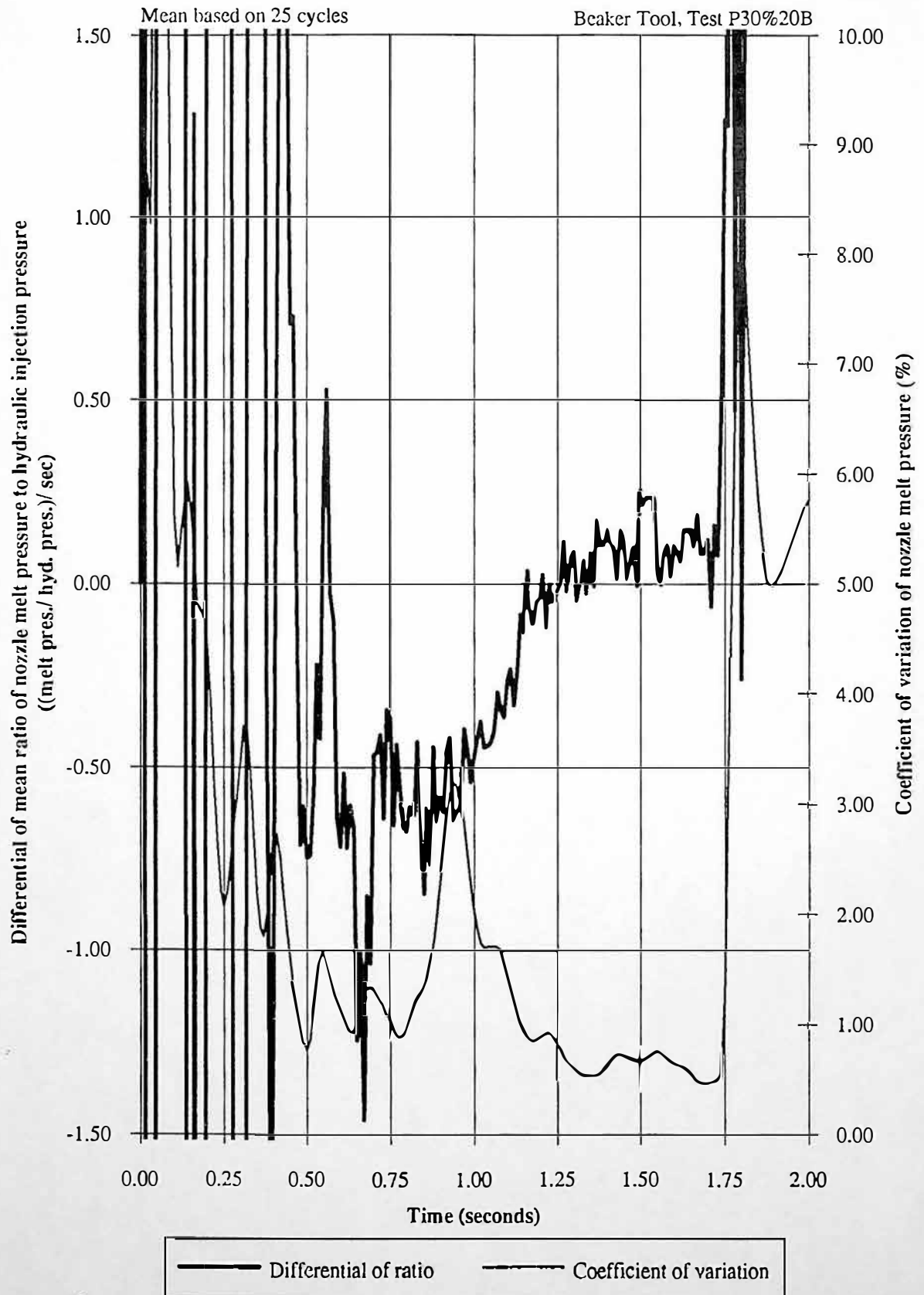


Figure 8.34 Mean screw injection velocity and mean ratio of nozzle melt pressure to hydraulic injection pressure during primary injection

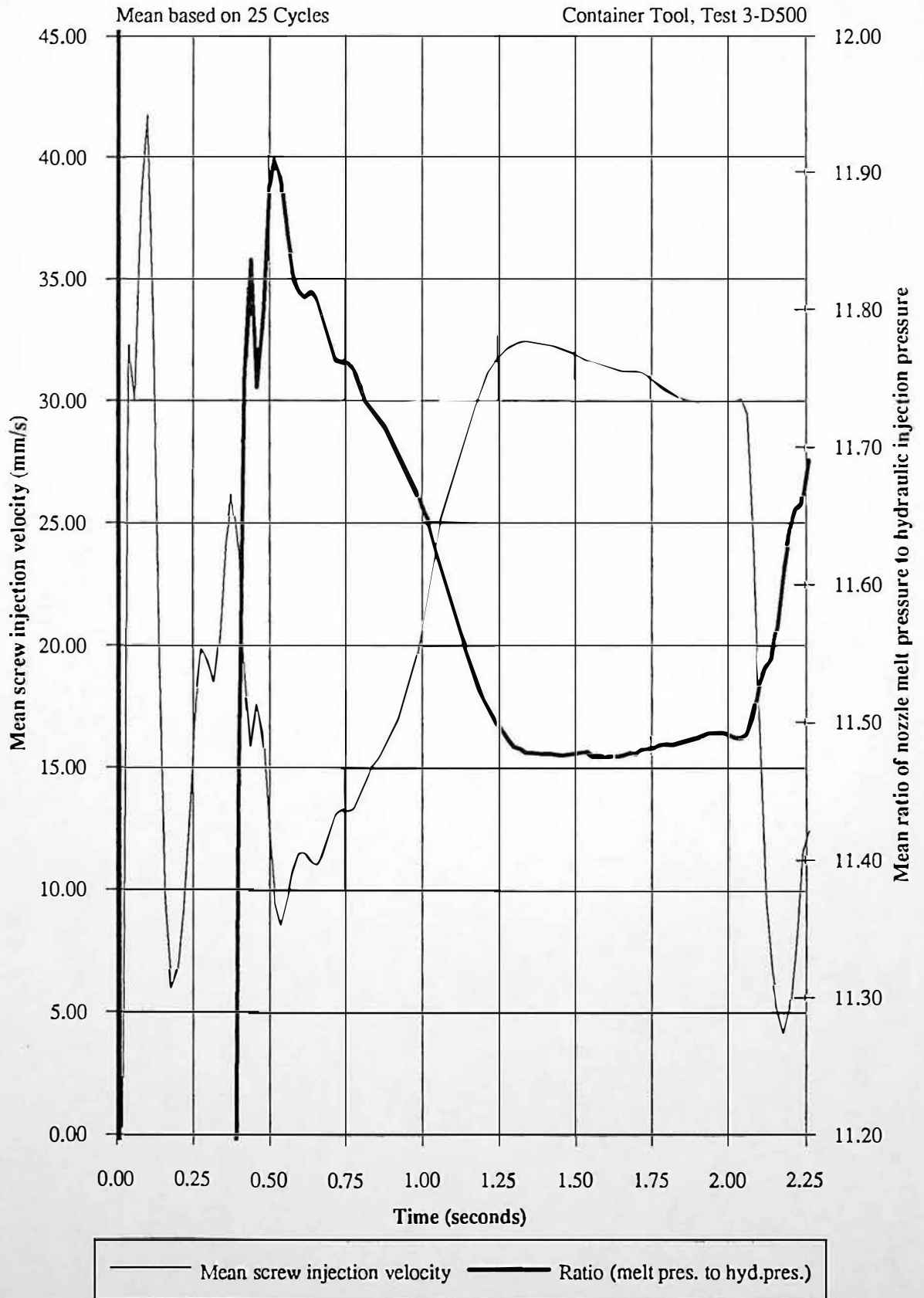


Figure 8.35 Differential of mean ratio of nozzle melt pressure to hydraulic injection pressure and coefficient of variation of nozzle melt pressure during primary injection

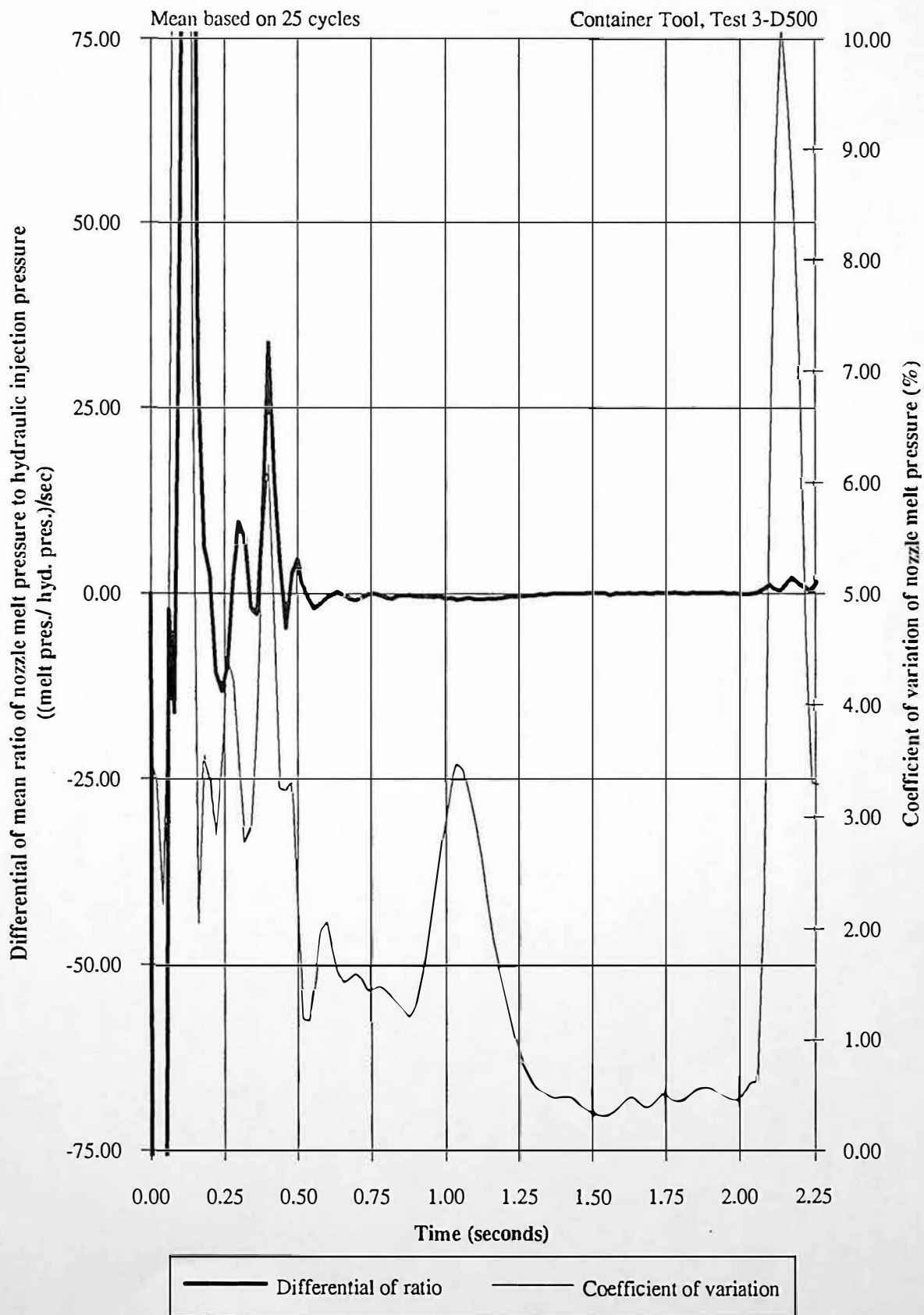
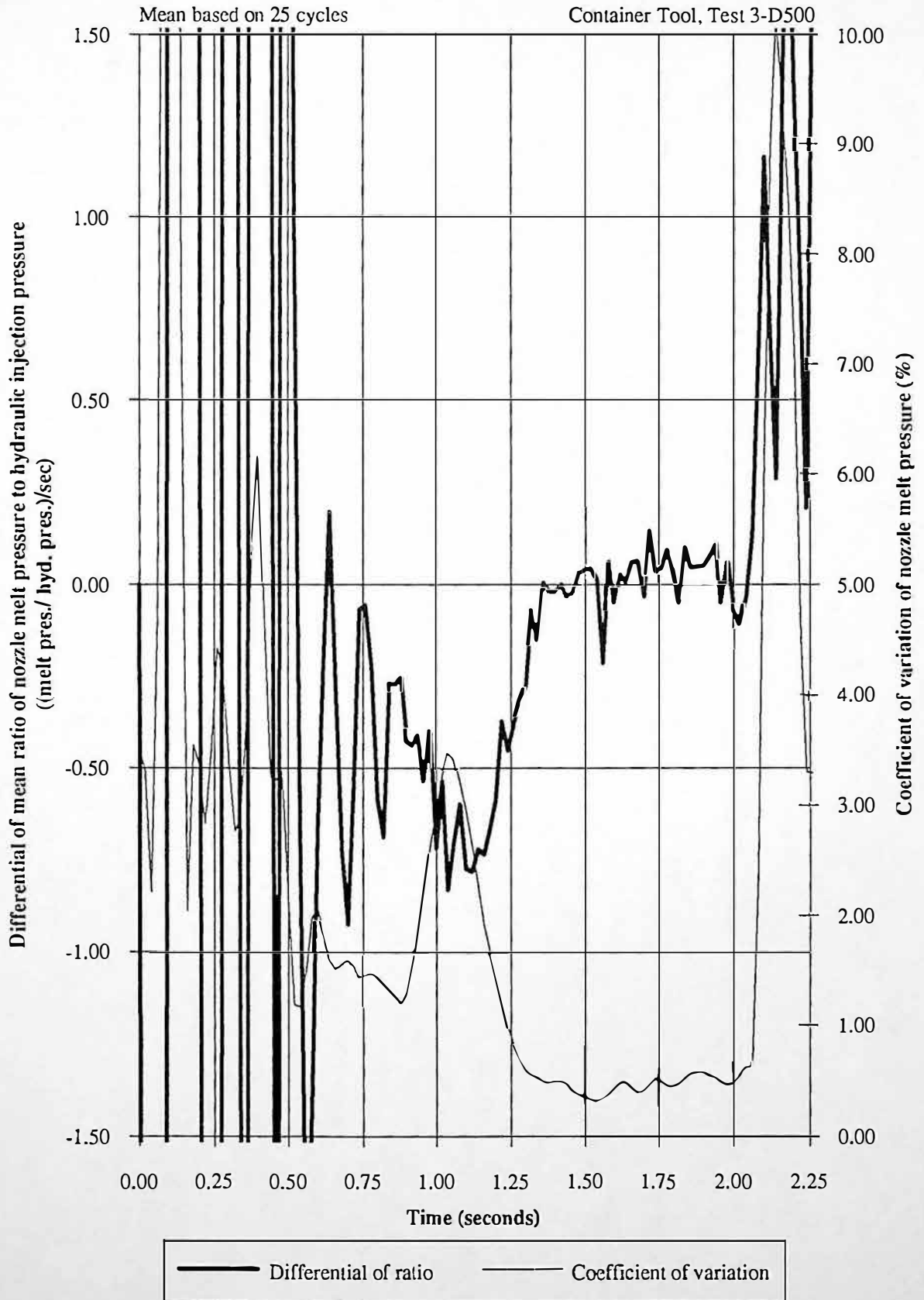


Figure 8.36 Differential of mean ratio of nozzle melt pressure to hydraulic injection pressure and coefficient of variation of nozzle melt pressure during primary injection



8.8 Industrial Process Monitoring

8.8.1 Introduction

Process data was monitored at Birkbys Plastics Ltd. The data presented in this chapter consolidates the procedures for assessment of polymer viscosity measurements, as described in chapters 8.3 and 8.4. It is important to note that a different machine, tool, material and machine parameters were used for industrial process monitoring.

Experimental results from test A11-2511 are analysed in this chapter. Appendix I(iii) has a list of all the experimental tests carried out at Birkbys Plastics Ltd. The injection phase for 25 injection moulding cycles were accurately monitored, processing BASF Turluran ABS (amorphous material) at 260C.

8.8.2 Experimental Configuration

Injection Moulding Machine and Tool: a Stork 440 Tonne injection moulding machine was utilised for these experimental moulding tests. Figure 8.37 shows the 440 Tonne Stork injection moulding machine, complete with robot at Birkbys Plastic Ltd. The machine was producing instrument cluster housings from a two impression tool for the Ford Motor Company Ltd. Figure 8.38 shows the moulded product (one impression), sprue and runner system.

In-line Nozzle Rheometer: Design for the rheological nozzle was based on the machines original nozzle. Figure 8.39 shows a detail drawing of the rheological nozzle, it is apparent that the nozzle reservoir bore has been enlarged from 12.0 mm to 16.0 mm to accommodate the instrumentation. Figure 8.40 shows the configured rheological nozzle during experimental tests. A guard was located on the nozzle to protect the instrumentation from becoming damaged by a polymer melt 'blow-back'.

Data Monitoring Equipment: a Biodata Microlink 2000 system was used for data acquisition. The Microlink was configured with the following modules PGA16, HSC and TC16H, Biodata (1990). A 80486 IBM compatible personal computer provided the necessary control. Data collection was initiated using the same software as described in chapter 6.4, Rose (1991).

Monitored Parameters: The injection and plasticisation phases were monitored together, with data monitoring being initiated by an electronic trigger for the start of the injection phase. Table 8.13 lists the injection and plasticisation machine and process monitored parameters. Figure 8.41 shows the mean nozzle melt pressure and screw displacement for a typical industrial monitored injection moulding cycle. Each of the following parameters were monitored at 50 Hz for $t = 0.00$ to 35.96 seconds. Linear calibrations were used for the pressure and displacement transducers.

Channel Number	Description of Monitored Parameter	Symbolic Name	Transducer Type
PGA 0	Nozzle Melt Pressure	NMP 1	Diaphragm device
PGA 1	Hydraulic Pressure	HYDP	Diaphragm device
PGA 2	Injection Screw Displacement	SDISP 1	(LVDT)
TC 1	Nozzle Melt Temperature	NMT 1	Infra-red device
TC 2	Hydraulic Oil Temperature	OILT	Type J thermocouple
TC 3	Fixed Platen Tool Temperature	FPTEMP	Type J thermocouple
TC 4	Moving Platen Tool Temperature	MPTEMP	Type J thermocouple

Table 8.13 Injection and plasticisation machine and process monitored parameters

Material Processed: BASF Terluran 968SM Black
 Acrylonitrile Butadiene Styrene (ABS)
 Density = 1.06 g/ml

Melt Volume Index MVI (1.value)	= 7 ml/10 min
at test temperature	= 200 C
at test load	= 21.6 kg
Melt Volume Index MVI (2.value)	= 5 ml/10 min
at test temperature	= 220 C
at test load	= 10 kg

Table 8.14 Processing properties of Terluran 968SM Black (BASF Campus Database)

Table 8.14 describes the melt flow index values for BASF Terluran 968SM. During normal operating conditions the sprue/runner system were continuously reground, mixed with the virgin material and fed to the hopper. The material was processed with a ratio of 90% virgin material to 10% regrind material.

Machine Parameters, details of machine settings are described in Table 8.15.

Machine Parameter Settings	
Plasticising screw rotation speed (RPM)	121
Plasticising back pressure (bar)	28
Plasticising end position (%)	121.0
Decompression stroke at injection end (%)	0.0
Cooling Time (seconds)	9.0
Full primary injection time (seconds)	4.5
Primary injection velocity (%)	32
Maximum hydraulic injection pressure (bar)	140
Switch over position to packing phase (%)	17.0
Secondary packing hydraulic injection (bar)	75
Secondary packing time (seconds)	19.0
Decompression stroke at injection end (%)	0.0
Nozzle Temperature Control (C)	260
Barrel Temperature Control Zone 5 (C)	245
Barrel Temperature Control Zone 4 (C)	240
Barrel Temperature Control Zone 3 (C)	240
Barrel Temperature Control Zone 2 (C)	230
Barrel Temperature Control Zone 1 (C)	230
Hot tip Temperature (C)	N/A
Feed zone cooling, water flow rate (YES/NO)	YES
Tool temperature, (C)	40

Table 8.15 Machine parameter settings for Stork machine

8.8.3 Experimental Results

Initial Experimental Observations, figure 8.42 shows mean nozzle melt pressure, mean hydraulic injection pressure and mean screw displacement for the 25 moulding cycles.

The scope of this analysis concentrates on the primary injection phase, for $t=0.00$ to 4.10 seconds. It can be seen from figure 8.42 that mean nozzle melt pressure compares to hydraulic injection pressure, with a high degree of correlation, coefficient of correlation =

1.00, for the period $t=0.00$ to 4.10 seconds. This relationship is investigated in chapter 8.8.5 and further investigations were made in chapter 8.7, where polymer melt compressibility was investigated, for a range of injection velocities.

Integration of Full Primary Injection Pressure Profiles: The first stage of analysis integrates the nozzle melt pressure and hydraulic injection pressure profiles for the full period of primary injection ($t= 0.00$ to 4.10 seconds) for the 25 moulding cycles. The mean nozzle melt pressure integral for the full period of primary injection = 3362.35 bar.sec, with coefficient of variation = 0.20%. The mean hydraulic injection pressure integral for the full period of primary injection = 405.77 bar.sec, with coefficient of variation = 0.18%.

Integration of Specific Area of Primary Injection Pressure Profiles: Figure 8.43 shows mean nozzle melt pressure and coefficient of variation for the 25 moulding cycles. Figure 8.44 shows mean hydraulic injection pressure and coefficient of variation for the 25 moulding cycles. It is apparent that periods of low coefficient of variation of nozzle melt pressure and hydraulic injection pressure indicate the time period during primary injection, where injection velocity control has minimal variation, as investigated in chapter 8.6. The coefficient of variation of mean hydraulic injection and nozzle melt pressures for the 25 moulding cycles, stabilises to a minimum for $t=2.20$ to 2.70 seconds. It is important to observe that between 2.70 and 4.10 seconds that the coefficient of variation for nozzle melt pressure and hydraulic injection pressure does not stabilise and increases to a maximum at 3.28 seconds, 0.65% for nozzle melt pressure and 0.58% for hydraulic injection pressure. This phenomenon shows that the periods of low coefficient of variation are not a direct result of high nozzle melt pressure and hydraulic injection pressures.

The second stage of analysis was to integrate the pressure profiles for the time period $t=2.20$ to 2.70 seconds. The mean nozzle melt pressure integral ($t=2.20$ to 2.70 seconds)

= 517.27 bar.sec, with a coefficient of variation = 0.12%. The mean hydraulic injection pressure integral (t=2.20 and 2.70 seconds) = 61.62 bar.sec, with a coefficient of variation = 0.12%. Therefore, analysis of mean pressure profiles during primary injection, has resulted in a pressure integral (t=2.20 to 2.70 seconds). The nozzle melt pressure integral (t=2.20 to 2.70 seconds) represents an increase in measurement precision by a factor of $0.20/0.12 = 1.67$. The hydraulic pressure integral (t=2.20 to 2.70 seconds) represents an increase in measurement precision by a factor of $0.18/0.12 = 1.50$. The preceding comparisons are made with respect to the integrals for full primary injection (t= 0.00 to 4.10 seconds).

8.8.4 Summary of Experimental Results

	Full Pressure Integral (t= 0.00 to 4.10 seconds)	Specific Pressure Integral (t= 2.20 to 2.70 seconds)
In-line Nozzle Rheometry (Nozzle Melt Pressure)	0.20%	0.12%
Process Measurements (Hydraulic Injection Pressure)	0.18%	0.12%

Table 8.16 Summary of coefficient of variation results for industrial process monitored data

Table 8.16 allows the coefficients of variation for process measurements and in-line nozzle rheometry to be compared. The advantage of calculating a specific pressure integral, can be seen in table 8.16, as the coefficients of variation are reduced by a factor of 1.5 and 1.67 respectively, for in-line nozzle melt pressure and hydraulic injection pressure measurements. The coefficient of variation can be used to calculate the measurement accuracy. Measurement accuracy was based on a 99.7% spread of data, i.e. ± 3 standard deviations about the mean value, assuming a normal distribution. The calculated measurement accuracy for each coefficient of variation are shown in Table 8.17. This

chapter has shown that in-line nozzle melt pressure and hydraulic injection pressure integrals have a similar precision.

	Full Pressure Integral (t= 0.00 to 4.10 seconds)	Specific Pressure Integral (t= 2.20 to 2.70 seconds)
In-line Nozzle Rheometry (Nozzle Melt Pressure)	±0.60%	±0.36%
Process Measurements (Hydraulic Injection Pressure)	±0.54%	±0.36%

Table 8.17 Summary of measurement accuracy results for industrial process monitored data

8.8.5 Comparison Nozzle Melt Pressure and Hydraulic Injection Pressure During Primary Injection

The following work investigates the relationship between nozzle melt pressure and hydraulic injection pressure integrals. It can be seen from figures 8.45 and 8.46, that both pressure integrals have a high degree of correlation, and therefore both reflect the same polymer melt viscosity variations. The coefficient of correlation between mean nozzle melt pressure integral and mean hydraulic injection pressure integral for the full period of primary injection (t=0.00 to 4.10 seconds) = 0.97 and for the specific integral (t=2.20 to 2.70 seconds) = 0.93.

8.8.6 Identification of Specific Pressure Integral Time Periods

Figure 8.47 shows the mean ratio of nozzle melt pressure to hydraulic injection pressure and differential of the ratio. Figures 8.48 and 8.49 show the differential of the mean ratio of nozzle melt pressure to hydraulic injection pressure and coefficient of variation of nozzle melt pressure. Figure 8.49 shows an enlarged scale for the differential of the mean ratio of nozzle melt pressure to hydraulic injection pressure. The ratio is lowest at t=2.20 to 2.70 seconds, which corresponds to the specified pressure integral time period.

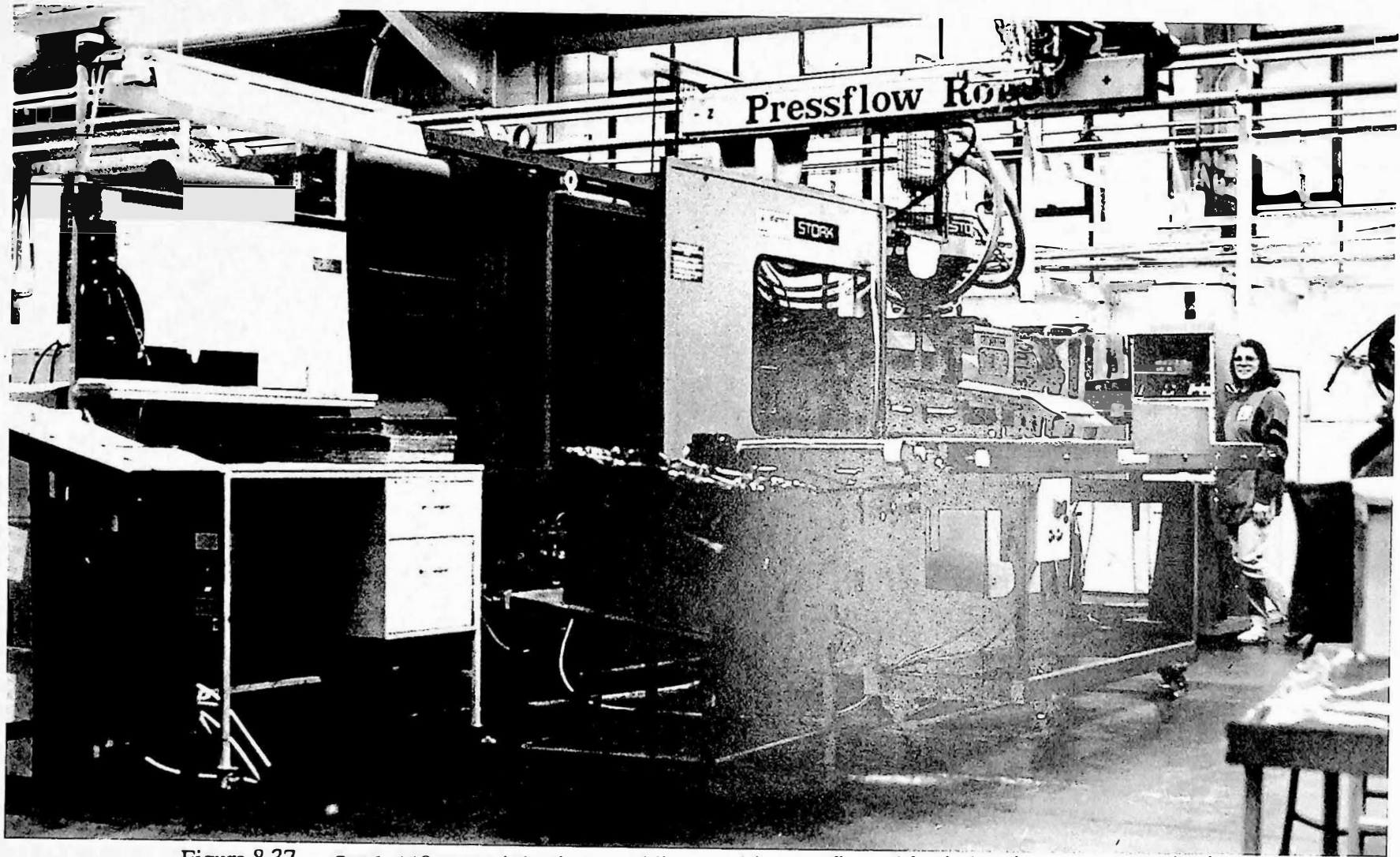


Figure 8.37 Stork 440 tonne injection moulding machine configured for industrial process monitoring

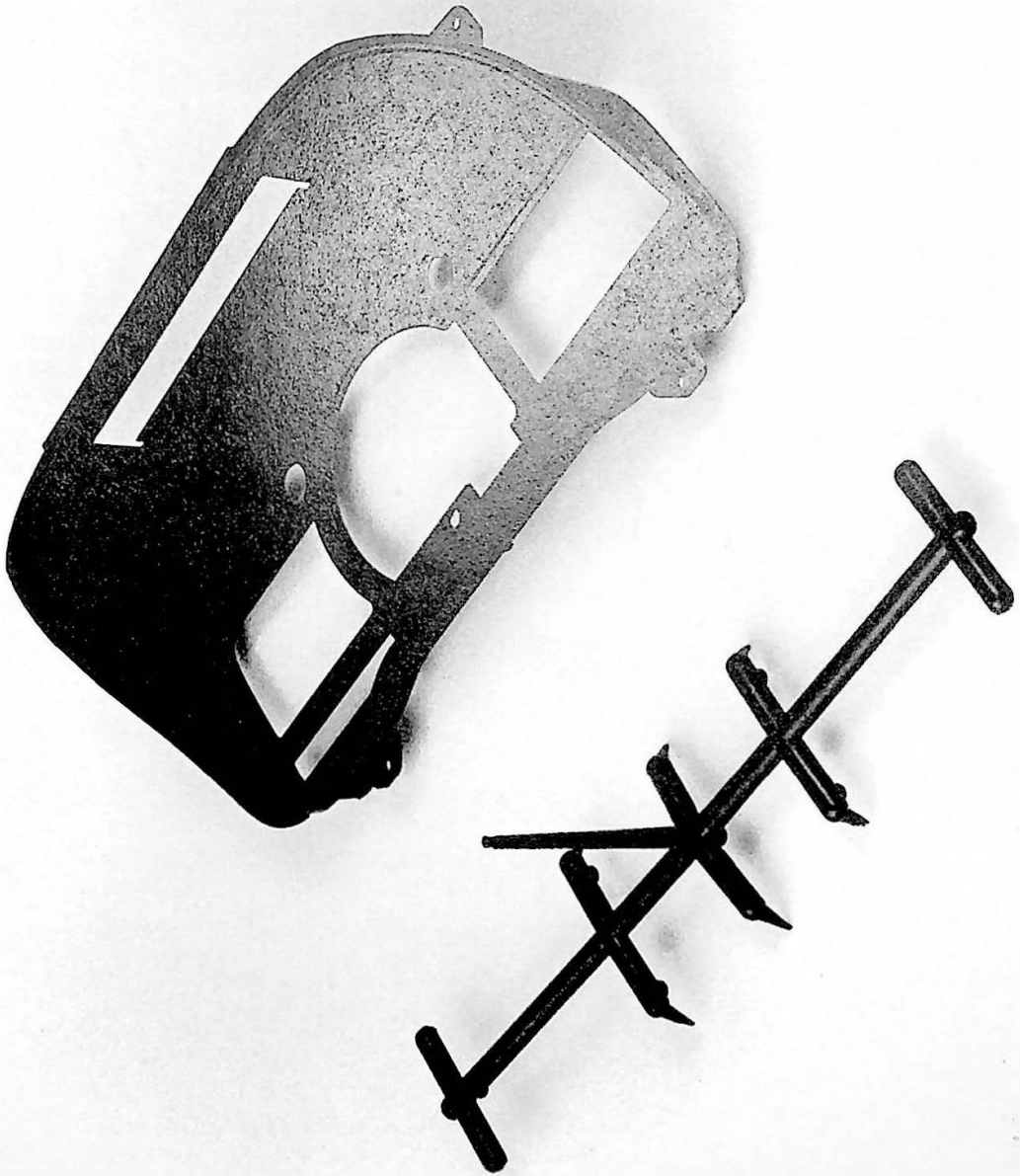


Figure 8.38 Moulded product, sprue and runner system

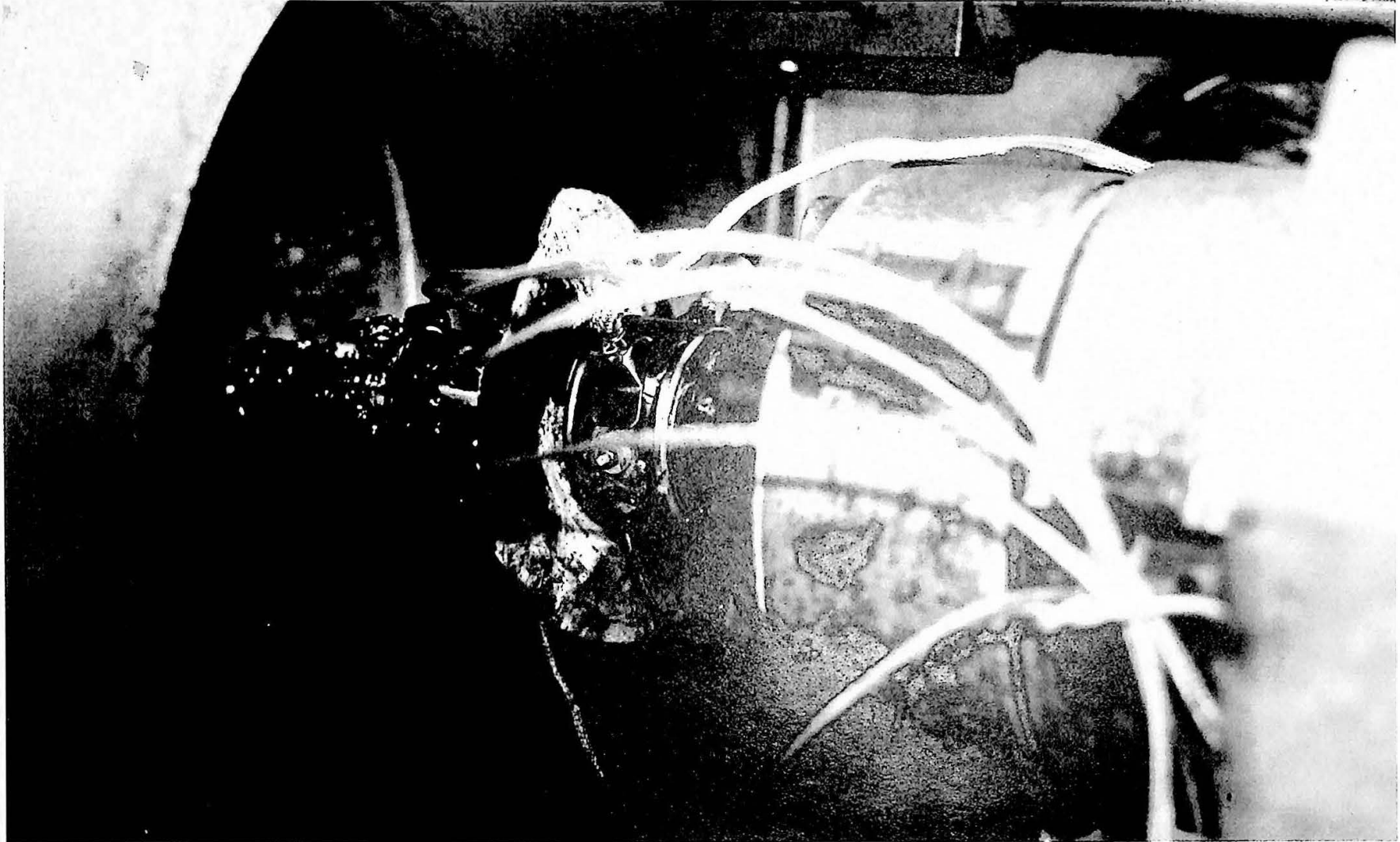


Figure 8.40 In-line nozzle rheometer during industrial process monitoring

Figure 8.41 Mean nozzle melt pressure and mean screw displacement during a typical industrial monitored injection moulding cycle

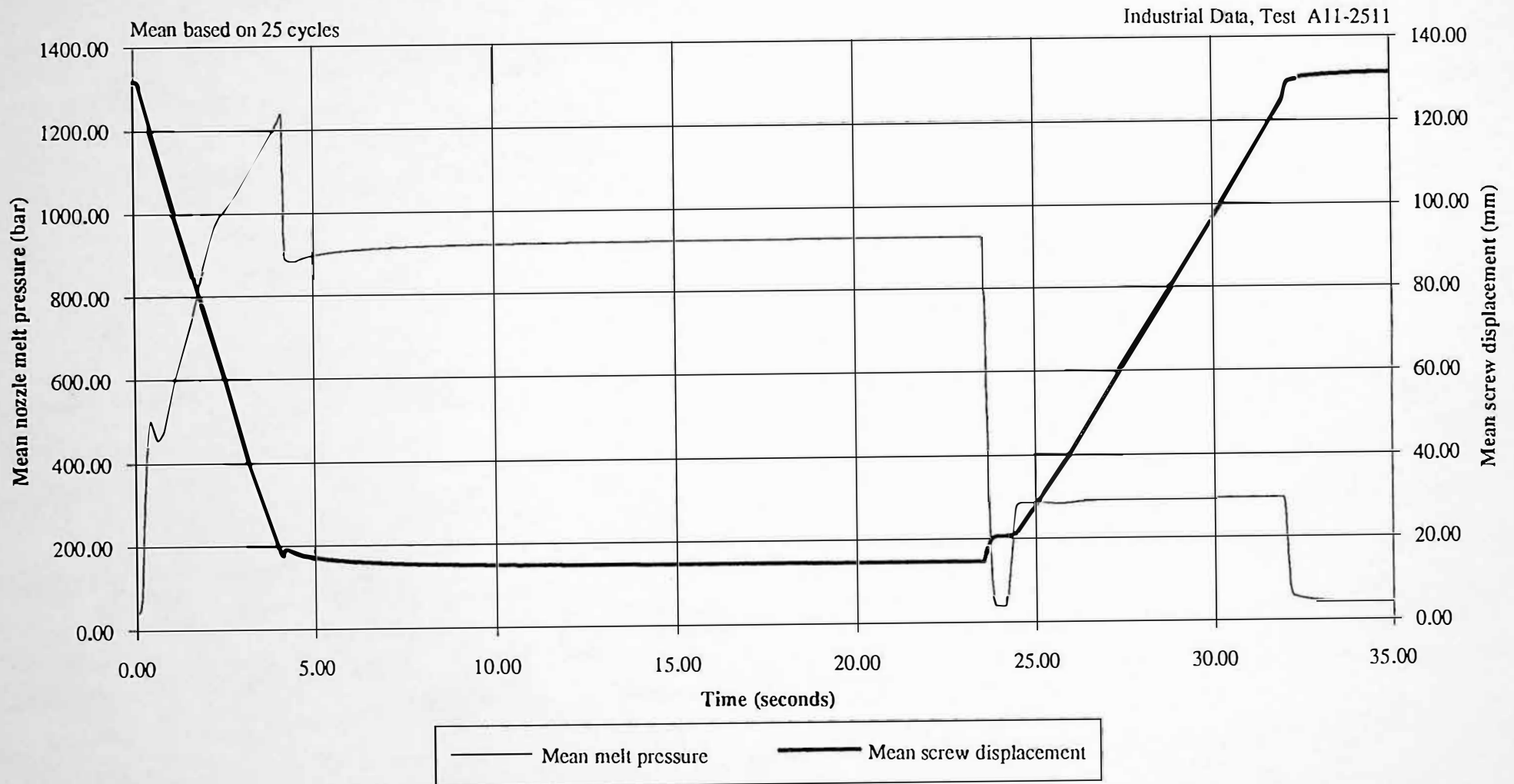


Figure 8.42 Mean nozzle melt pressure, mean hydraulic injection pressure and mean screw displacement during primary injection

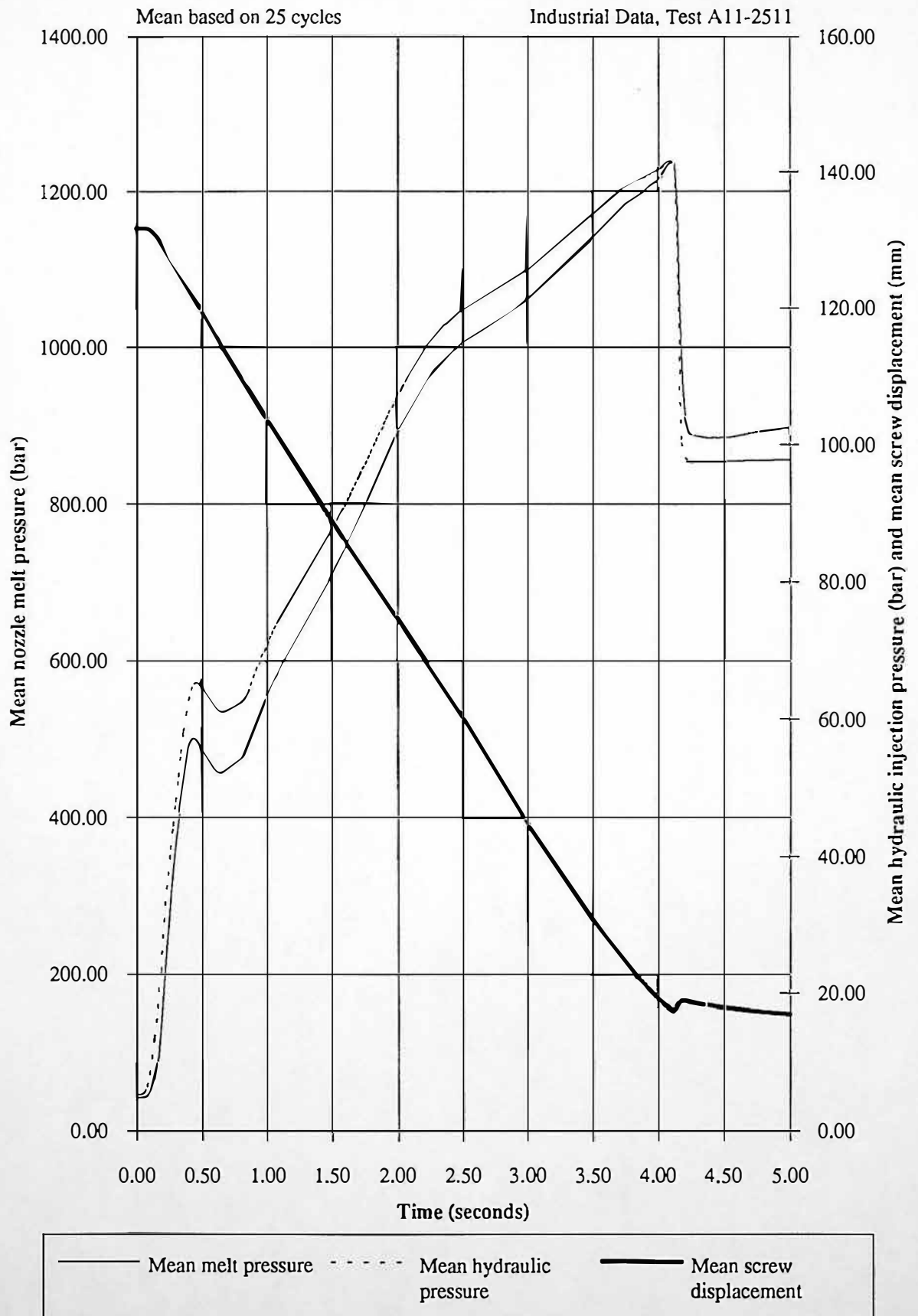


Figure 8.43 Mean nozzle melt pressure and coefficient of variation during primary injection

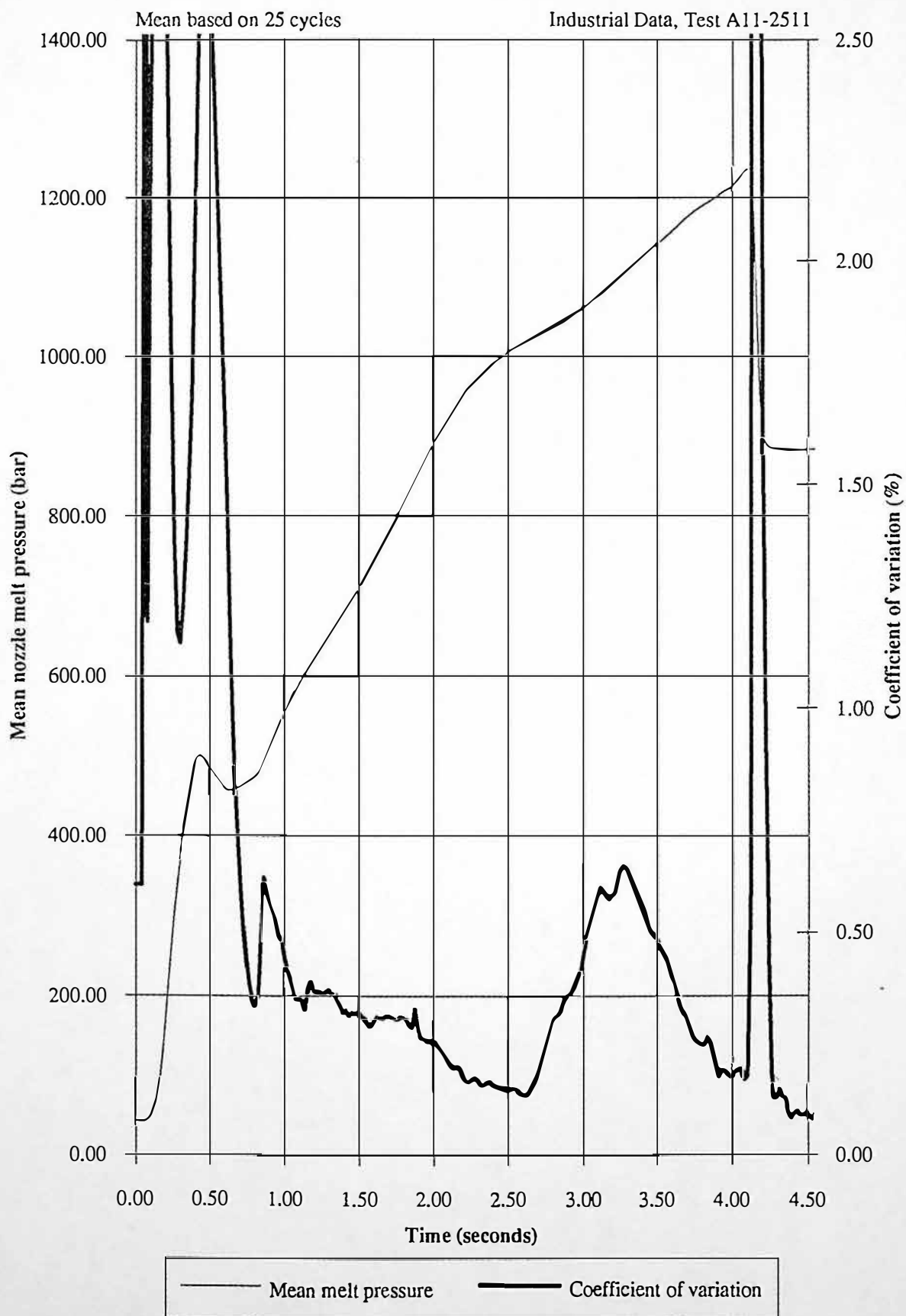


Figure 8.44 Mean hydraulic injection pressure and coefficient of variation during primary injection

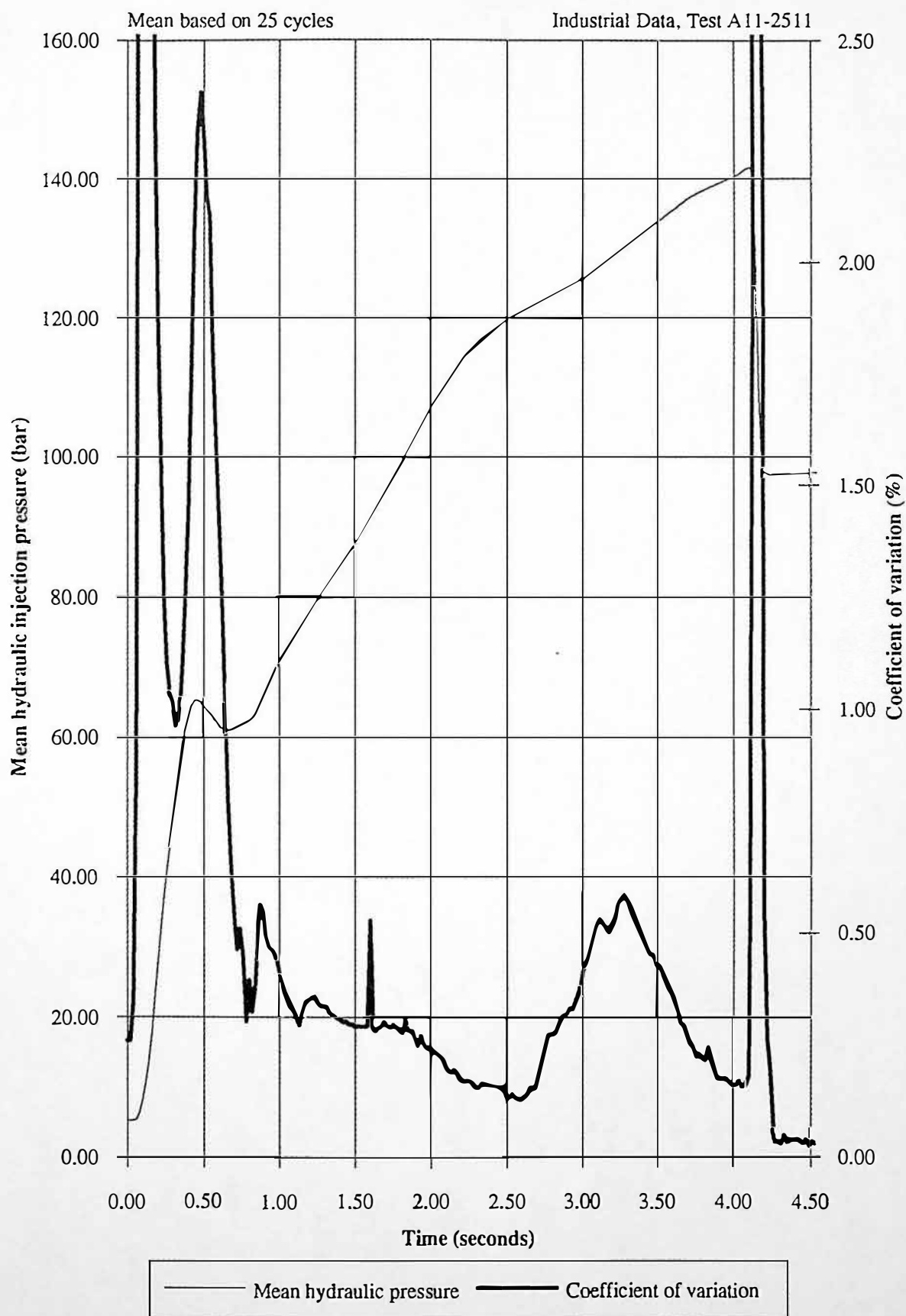


Figure 8.45 Relationship between nozzle melt pressure and hydraulic injection pressure integrals for the full period of primary injection

Pressure integral calculated for t= 0.00 to 4.10 seconds
Coefficient of correlation = 0.97
Industrial Data, Test A11-251 I

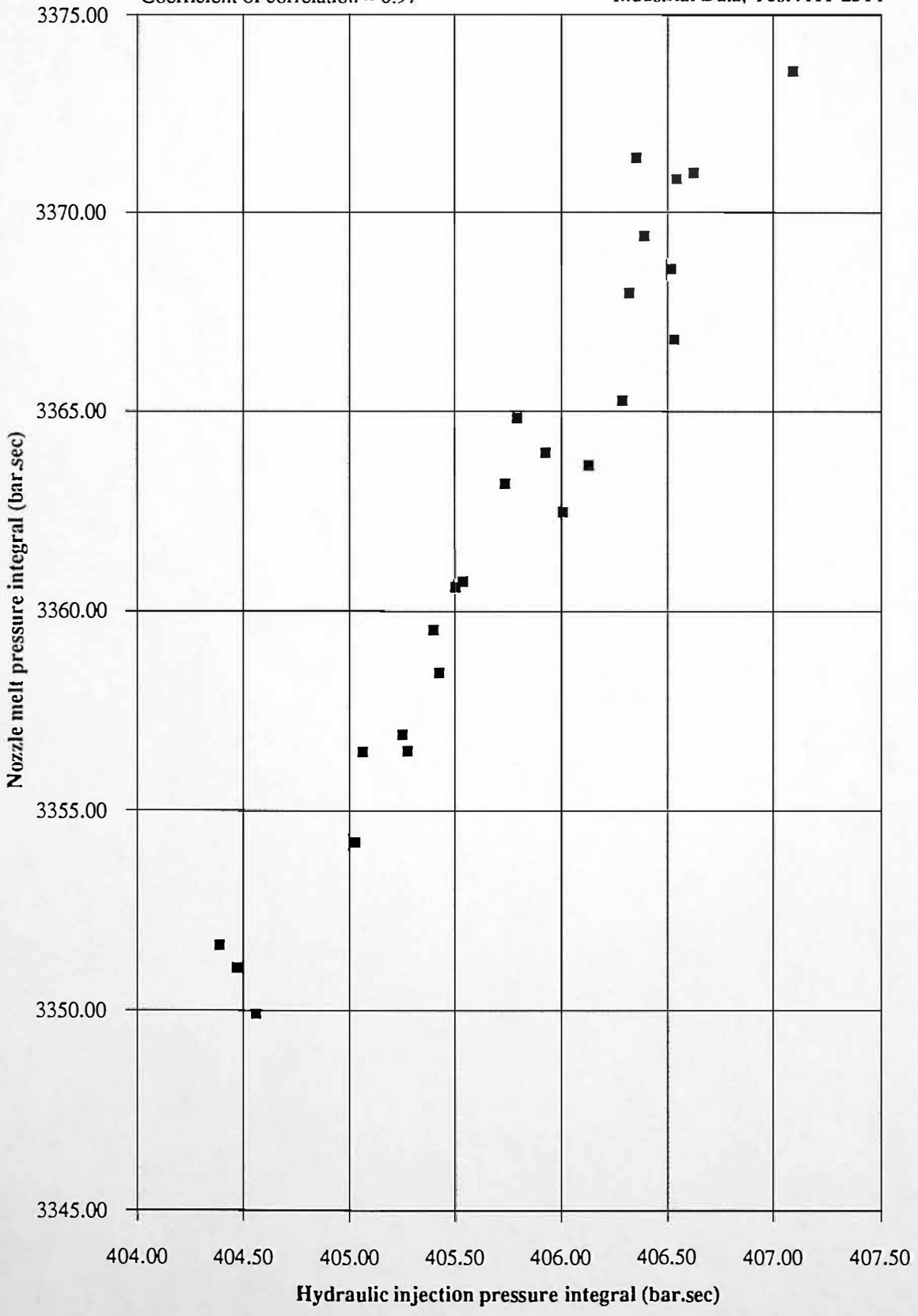


Figure 8.46 Relationship between nozzle melt pressure and hydraulic injection pressure integrals for a specific period of primary injection

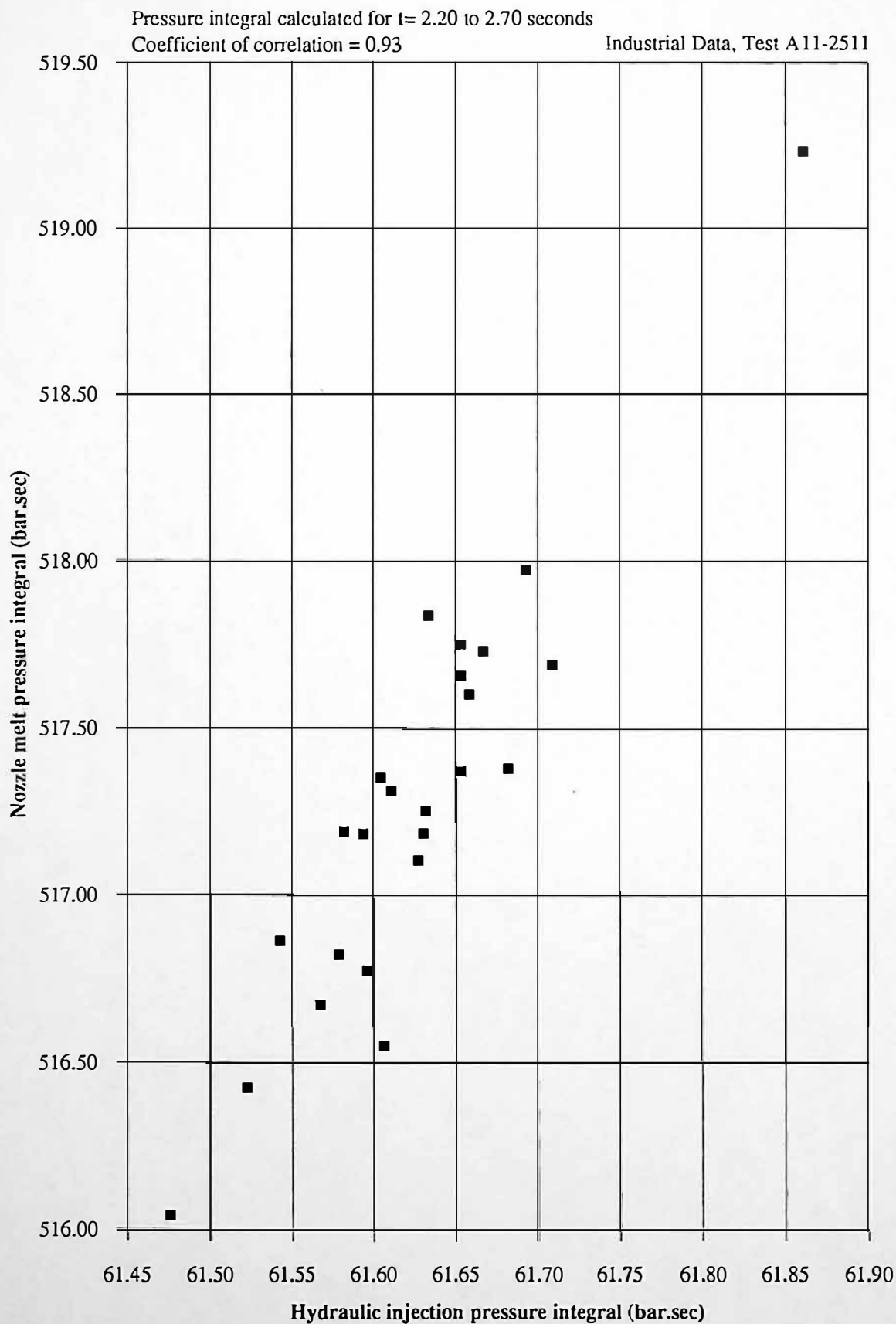


Figure 8.47 Mean ratio of nozzle melt pressure to hydraulic injection pressure and differential of ratio during primary injection

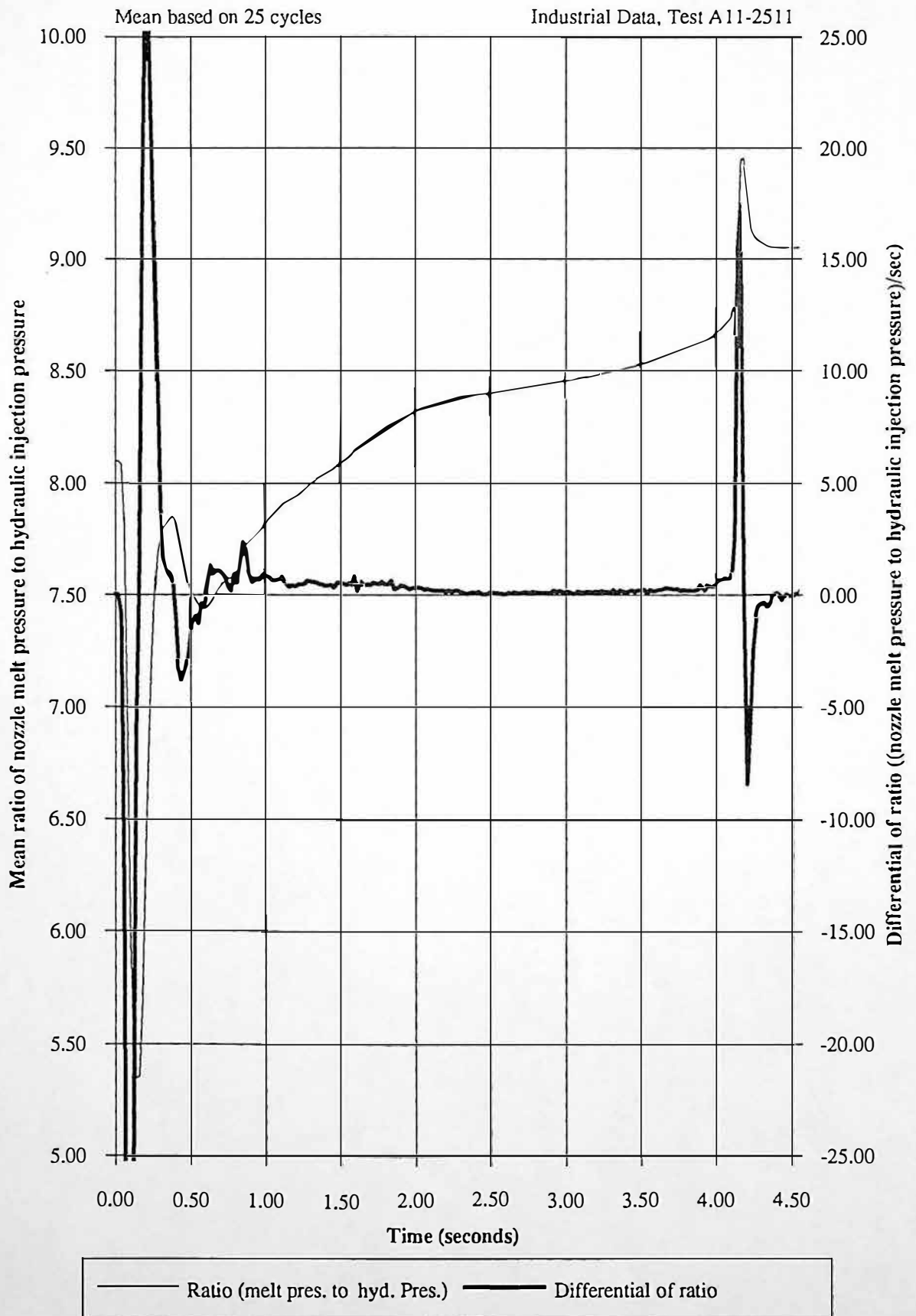


Figure 8.48 Differential of mean ratio of nozzle melt pressure to hydraulic injection pressure and coefficient of variation of nozzle melt pressure during primary injection

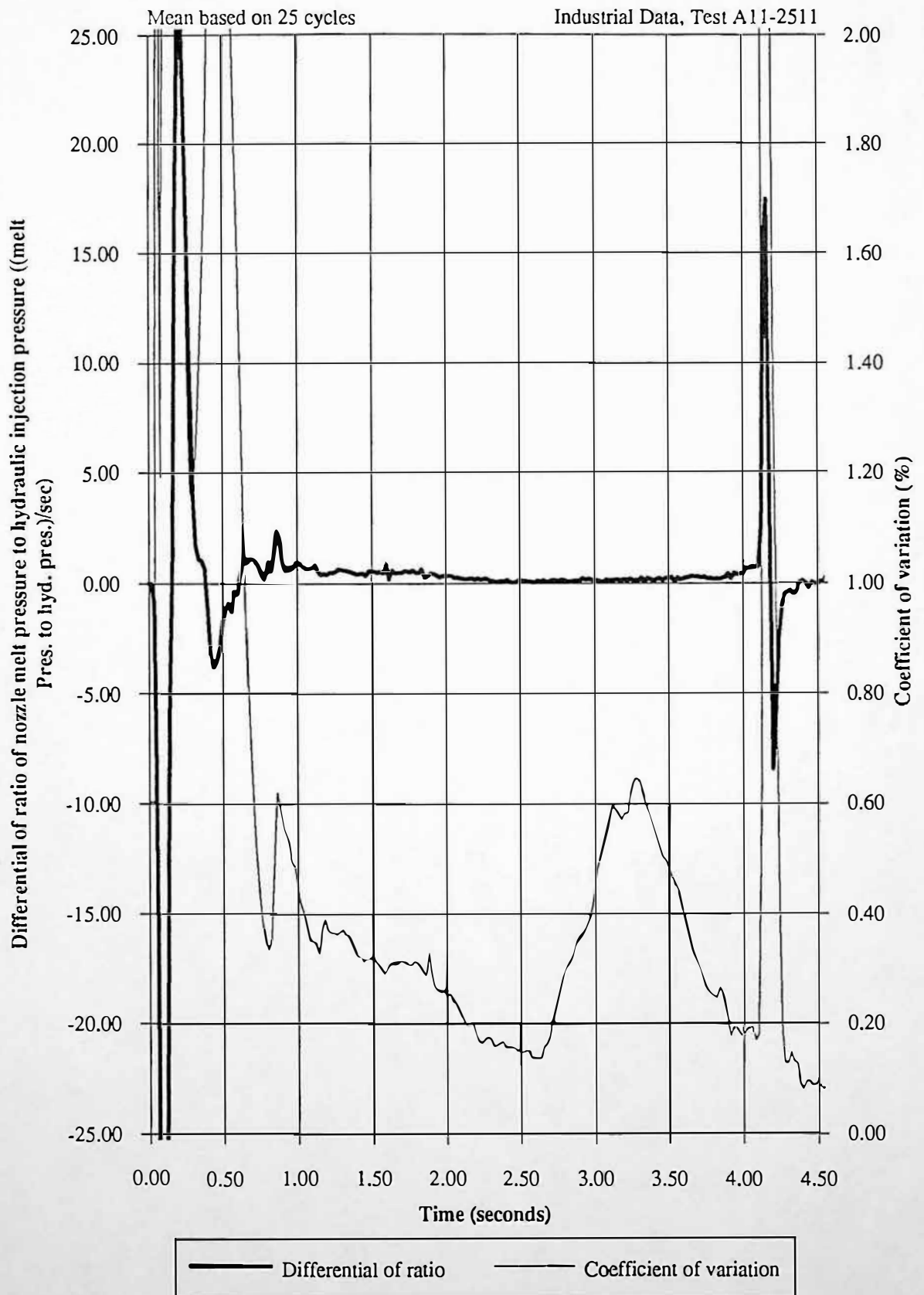
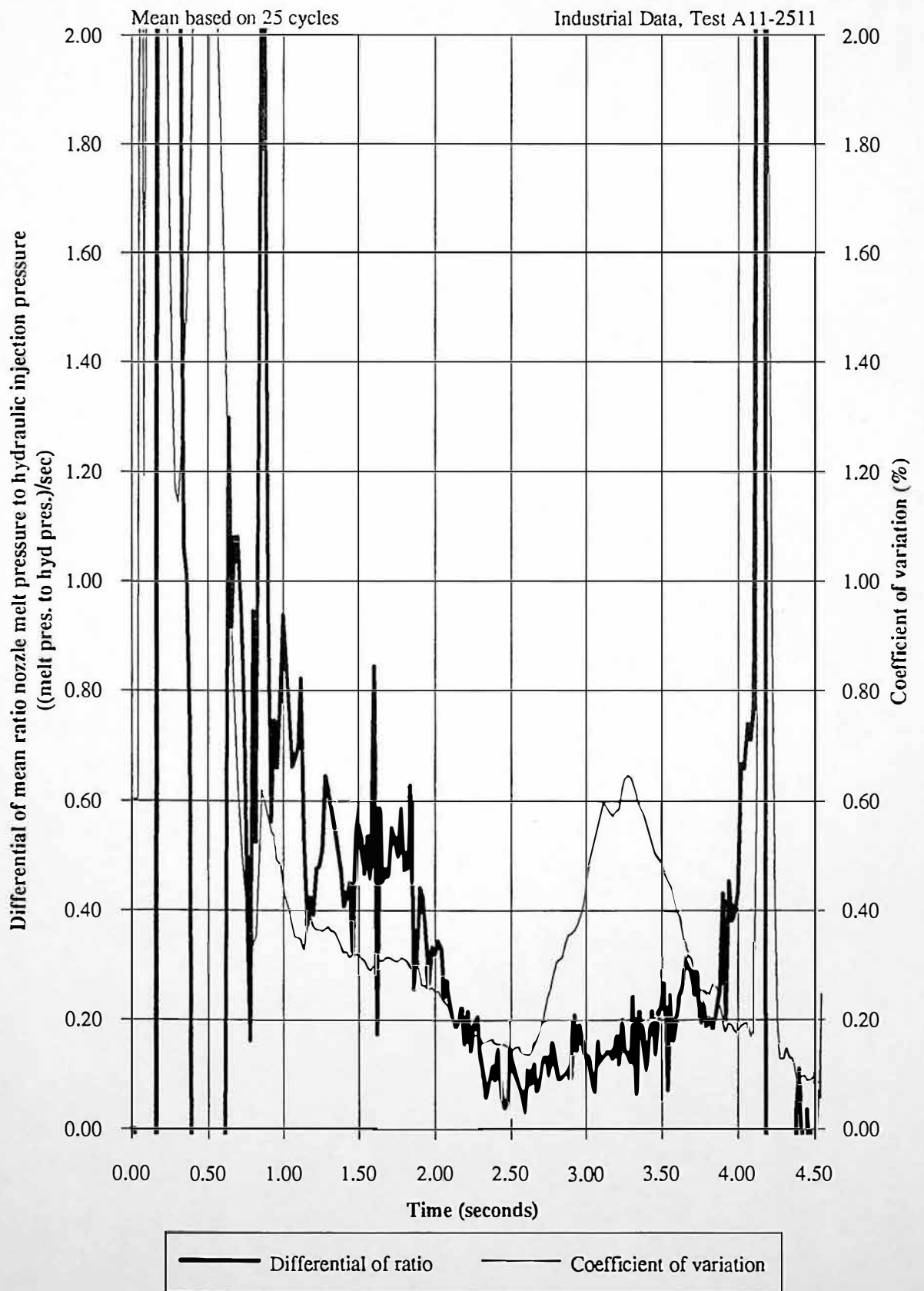


Figure 8.49 Differential of mean ratio of nozzle melt pressure to hydraulic injection pressure and coefficient of variation of nozzle melt pressure during primary injection



8.9 Discussion of Results

The work of this chapter investigates nozzle melt pressure and hydraulic injection pressure profiles, during the primary injection phase, on a cycle to cycle basis. The main influences to nozzle melt pressure and hydraulic injection pressure measurements are investigated, relating to process variation.

8.9.1 Determination of an Optimum Assessment of Polymer Melt Viscosity During Primary Injection

Polymer melt viscosity is derived from nozzle melt pressure, reflecting interactions of shear and extensional stress, for constant wall shear rates. Nozzle melt pressure and hydraulic injection pressure data from typical injection moulding cycles, has shown that it is possible to determine an area of the pressure profile, that is subject to low variation. During this period of low pressure variation, an integral can be derived, that reflects polymer melt viscosity, subject to a minimal disturbance from machine parameter variation.

Chapters 8.3. and 8.4 determine pressure integral measurement accuracies for typical moulding conditions, for two different tools, the results are shown in tables 8.18 and 8.19.

Chapter 8.8 shows industrially monitored data for a different machine, material, tool and machine parameter settings, the results are shown in table 8.20.

	Full Pressure Integral (t=0.00 to 1.75 seconds)	Specific Pressure Integral (t=1.20 to 1.70 seconds)
In-line Nozzle Rheometry (Nozzle Melt Pressure)	0.73%	0.54%
Process Measurements (Hydraulic Injection Pressure)	0.72%	0.51%

Table 8.18 Summary of coefficient of variation results for test P30%20B

	Total Pressure Integral (t= 0.00 to 2.06 seconds)	Specific Pressure Integral (t= 1.50 to 2.00 seconds)
In-line Nozzle Rheometry (Nozzle Melt Pressure)	0.84%	0.21%
Process Measurements (Hydraulic Injection Pressure)	0.83%	0.17%

Table 8.19 Summary of coefficient of variation results for test 3-D500

	Full Pressure Integral (t= 0.00 to 4.10 seconds)	Specific Pressure Integral (t= 2.20 to 2.70 seconds)
In-line Nozzle Rheometry (Nozzle Melt Pressure)	0.20%	0.12%
Process Measurements (Hydraulic Injection Pressure)	0.18%	0.12%

Table 8.20 Summary coefficient of variation results for industrial process monitored data

It is apparent that total nozzle melt pressure integrals are reduced by factors of 1.35, 4.00 and 1.67, for the work of chapters 8.3, 8.4 and 8.8, respectively, by the calculation of specific pressure integrals. The full hydraulic injection pressure integrals are reduced by factors of 1.41, 4.88 and 1.5, for the work of chapters 8.3, 8.4 and 8.8, respectively. These results show that hydraulic injection pressure provides the same accuracy measurements as nozzle melt pressure measurements. In the case of the industrially monitored data, the coefficient of variation is 0.20% for the nozzle melt pressure, compared to 0.18% for the hydraulic injection pressure. This may reflect the fact that the 440 tonne Stork machine uses a Moog valve to control injection velocity, as opposed to the Sandretto Logiflux screw velocity control algorithm. Hydraulic injection pressure measurements determine a relative assessment of polymer melt viscosity, by means of a hydraulic injection pressure integral. For closed loop process control a relative assessment of polymer melt viscosity is adequate, but for scientific polymer melt rheology an absolute nozzle melt pressure measurement is necessary.

Results from an all electric injection moulding machine Cincinnati Milacron ACT30, are shown in figure 8.50. The nozzle melt pressure integral for the period $t = 0.90$ to 1.10 seconds = 120.40 bar.sec, with a coefficient of variation of 0.12% .

Results from chapter 8.5 show that nozzle melt pressure measurements, with a typical coefficient of variation of 0.10% , are able to distinguish between different batches of the same molecular weight grade polyoxymethylene. This fact shows the usefulness of such measurement techniques for closed loop process control for the injection moulding.

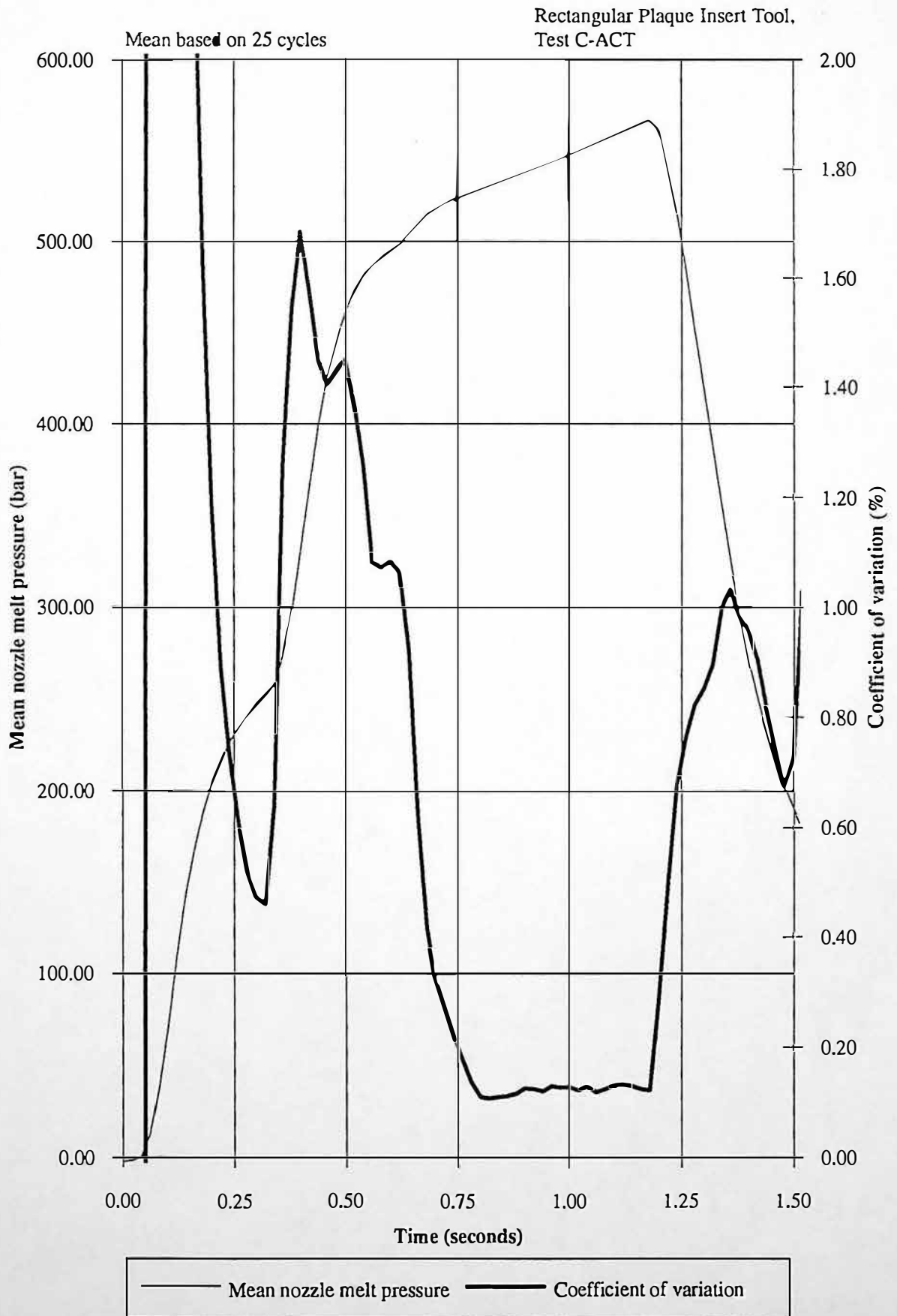
Periods of low pressure variation can be determined by analysing the screw dynamics during the primary injection phase. Screw acceleration is derived from measured screw velocity and therefore may be subject to significant quantification errors at low screw accelerations.

A second method for determining the location of the periods of steady pressure, with an improved precision is described in chapter 8.7, whereby, the ratio between nozzle melt pressure and hydraulic injection pressure is differentiated. The resultant differential indicates the period of low pressure variation, with an increased precision, compared to the screw acceleration techniques.

Both methods for determining the period of low pressure variation, have their benefits:

Screw Acceleration: (i) this is best measured using a velocity transducer and differentiating. These transducers are not standard machine and would therefore need installation, as double differentiation of screw displacement would be subject to large quantification errors, (ii) numerical differentiation of screw velocity is subject to quantification errors when acceleration is low, and (iii) may not reflect polymer melt compression for complex tools.

Figure 8.50 Mean nozzle melt pressure and coefficient of variation during primary injection - Cincinnati Milacron ACT30



Differential of Ratio of Nozzle Melt Pressure to Hydraulic Injection Pressure: (i) has a greater precision than derived screw acceleration, (ii) requires both nozzle melt and hydraulic injection pressure transducers, (iii) reflects polymer melt compression for complex tools.

8.9.2 Importance of Screw Injection Velocity Control

The influence of screw velocity control on the accuracy of nozzle melt pressure and hydraulic injection pressure measurements is investigated in chapter 8.6. Results from chapter 8.6 show that periods of low pressure variation are due to periods of steady velocity control. The quality of screw velocity control directly influences the period of pressure variation, during primary injection, as shown in figure 8.51.

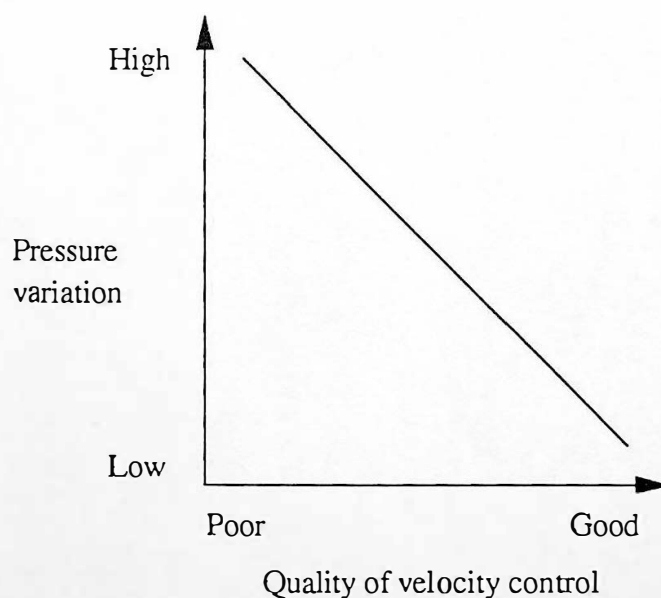


Figure 8.51 Relationship between screw velocity control and pressure variation

8.10 Concluding Comments

- The use of high accuracy instrumentation combined with a precisely timed machine and process variable monitoring system, allows an accurate and precise assessment of polymer melt viscosity, for typical injection moulding conditions. The assessment of polymer viscosity is achieved by integration of nozzle melt pressure and hydraulic injection pressure profiles, for specific time periods.
- Two procedures are presented that allow an optimum nozzle melt pressure integral to be identified: (i) identification of periods of steady screw velocity during primary injection phase, i.e. periods of low screw acceleration, and (ii) differentiation of the ratio between nozzle melt pressure and hydraulic injection pressure during primary injection phase. These procedures would form the basis of an algorithm to determine where to integrate nozzle melt pressure and hydraulic injection profiles.
- Nozzle melt pressure integrals were able to distinguish between two different batches of the same molecular weight grade polyoxymethylene. A measurement accuracy of $\pm 0.3\%$ was achieved, based on a ± 3 standard deviation distribution about the mean.
- Techniques for optimising polymer melt viscosity assessment have been tested on three different technology injection moulding machines, Sandretto 60 tonne, Stork 440 tonne and a Cincinnati Milacron ACT30 30 tonne machines.

CHAPTER 9

Influence of Process Variation on Product Quality

9.1 Introduction

Injection moulding is a complex process, with many interacting machine and process parameters influencing product quality. Modern day injection moulding machines utilise the latest microprocessor technology to control machine parameters. Associated with the continual improvement of machine parameter performance, is the fact that polymer melt viscosity variations are becoming a more significant processing problem.

The experimental work of chapters 7 and 8 show that an accurate and precise in-line assessment of polymer melt viscosity can be determined. The experimental research of chapter 7 has shown that in-line capillary rheometry provides an accurate assessment of polymer melt viscosity, for polymer melts with a true process history. The experimental work of chapter 8 describes a methodology for determining an optimum accuracy and precision, of polymer melt viscosity measurement. The assessment was made for in-line nozzle rheometry (nozzle melt pressure) and process measurements (hydraulic Injection pressure), during the velocity controlled primary injection phase. The results described are for the previously described (see chapter 5) highly accurate instrumentation (see chapter 5) and typical injection moulding process conditions.

9.1.1 Scope of this Chapter

The experimental research described in this chapter investigates the influence of polymer melt viscosity variation on product quality (product weight and dimension), for semi-crystalline materials, during primary injection.

The specific aims of this chapter are:

- (i) Show the influence of the heat transfer rate from polymer melt in the cavity to adjacent tool, on product quality.
- (ii) Show that tool and polymer melt temperature are primary influences on the heat transfer rate from polymer melt in the cavity to adjacent tool.
- (ii) Establish the interrelationship between polymer melt viscosity and nozzle melt pressure and temperature.

The establishment of such a relationship provides information necessary for closed loop process control. Figure 9.1 shows a schematic flow diagram of closed loop process control of injection moulding. The work of this chapter forms an important part of a process control algorithm, whereby intelligent interpretation of polymer melt viscosity is related to product quality.

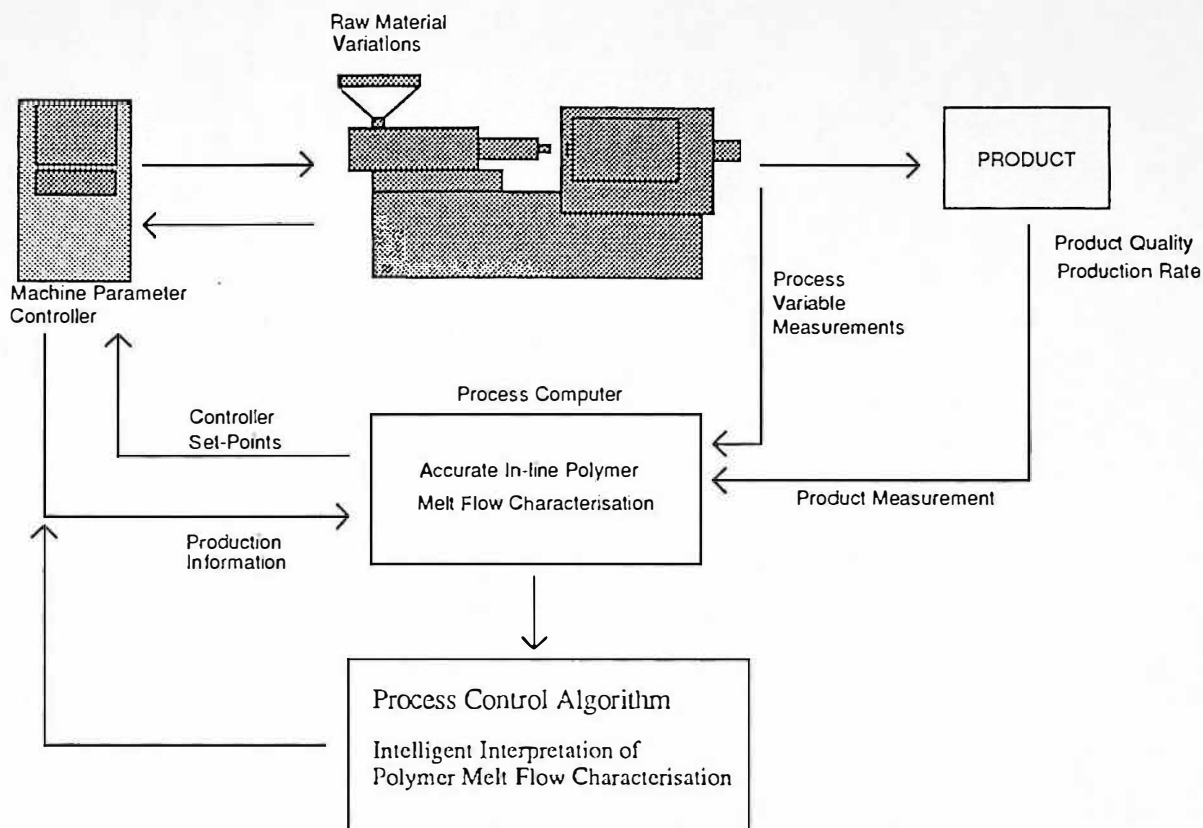


Figure 9.1 Closed loop process control for injection moulding

The experimental work described uses two different molecular weight grades of high density polyethylene (HDPE), BP Rigidex grades HD5226EA and HD5050EA (see chapter 7.2.1). This material is semi-crystalline with an approximate shrinkage of 4% Morton-Jones (1989 p 166). Amorphous polymers, Acrylonitrile Butadiene Styrene (ABS) and Poly(methyl-methacrylate), Acrylic, are currently being investigated, with regard the influence of polymer melt viscosity on product quality. Amorphous polymers typically have low shrinkage rates, the approximate shrinkage for ABS = 0.3 to 0.8%, Morton-Jones (1989 p 166).

9.1.2 Experimental Moulding Tests

The results from four experimental tests are described in this chapter, tests J40%20B, I40%20B, G40%20B and NX%20B producing 60 moulded products, utilising the instrumented beaker tool. Chapter 8.2 describes the experimental configuration, necessary for these experimental tests.

Tool temperature was purposefully varied (over 25 injection moulding cycles), test J40%20B processing HDPE (HD5226EA). The tool temperature variation influenced the rate of heat transfer from the polymer melt in the cavity to the adjacent tool, which in turn influences polymer melt shrinkage rate. The analysis shows that polymer melt shrinkage is a primary factor influencing product quality for semi-crystalline materials (HDPE). Work described by Woodhead (1990), Speight and Coates (1993a) and Wu and Chen (1990) investigates the influence of intentionally changing tool temperature on product weight.

The influence of polymer melt viscosity on nozzle melt pressure and temperature was investigated. Two different molecular weight grades of HDPE were processed and analysed, tests I40%20B (HD5226EA) and G40%20B (HD5050EA).

The influence of injection velocity on nozzle melt pressure and temperature was investigated. HDPE (HD5226EA) was processed for five single stage injection velocities (3 cycles per velocity). The influence of melt pressure and temperature on product quality was analysed, test NX%20B.

The experimental results shown in this chapter include data sampling points, this is to ease quantification of the data.

9.2 Influence of Tool and Melt Temperature on Heat Transfer Rate from Polymer Melt in the Cavity to Adjacent Tool

Melt temperature and tool temperature are extremely important process parameters that influence product quality. Melt temperature is influenced by polymer type, melt viscosity, screw injection velocity, screw rotational speed and plasticising back pressure. Tool temperature is influenced by melt temperature, injection time and cooling time. Tool and melt temperature both influence the rate of heat transfer from polymer melt in the cavity to adjacent tool. Research by Isayev and Hariharan (1984) investigates density distribution of moulded components, Sepe (1991) investigates the use of shrinkage time plots to improve productivity in fine tolerance moulding and Pierick and Noller (1991) investigates the effect of processing conditions on shrinkage. Polymer melt subject to high shrinkage, produces moulded products with a higher relative density, than products moulded with low rates of polymer melt shrinkage. A higher relative density produces moulded products with higher weight and greater specific dimensions.

9.2.1 Influence of Tool Temperature on Heat Transfer Rate

The experimental work described, shows the influence of the heat transfer rate from polymer melt in the cavity to adjacent tool, on product quality. Heat transfer from polymer melt in the cavity to adjacent tool, is a important factor affecting product quality. The rate of heat transfer is influenced by tool and melt temperatures. Experimental results from test J40%20B are analysed in this section. The injection and plasticising phases were accurately monitored for 25 injection moulding cycles. Tool temperature control settings were purposefully varied to influence the heat transfer rate from the tool, which in turn influences polymer melt shrinkage rate within the cavity. The initial 5 cycles were processed with the tool temperatures set at 60C, the next 10 cycles at 70C and the final 10 cycles at 50C.

9.2.2 Transient Response of Tool Temperature Controller

Figure 9.2 shows the set tool temperature compared to measured tool temperature. The mean tool temperature is calculated for the time period that the injection phase is monitored ($t=0.00$ to 6.96 seconds). Set tool temperature refers to the set temperatures on all three tool temperature controllers. After cycle 5 the set tool temperatures were changed from 60°C to 70°C , the data from this step change is sufficient to derive an approximate first order time constant of 3 cycles. This time constant is a function of many variables, of which; tool temperature control zone location, tool temperature controller parameters, temperature transducer location and machine parameter set up are important. These experimental results show the influence of tool temperature on product quality, for typical tool temperature control.

9.2.3 Influence of Tool Temperature on Product Quality

Figures 9.3 and 9.4 show the influence of tool temperature variations on product quality (weight and dimension), respectively. It is apparent that product weight and dimensions are inversely proportional to tool temperature. Polymer melt shrinkage is shown to be inversely proportional to temperature. Figure 9.5 shows the correlation between product weight and product dimension (height).

	Coefficient of Correlation
Product Weight to Product Height	0.93
Tool Temp. to Product Weight	-0.75
Tool Temp. to Product Height	-0.68

Table 9.1 Comparison of coefficients of correlation for tool temperature and product quality (weight and height dimension)

Table 9.1 shows the coefficients of correlation for mean tool temperature, product weight and product height.

Figure 9.2 Set tool temperature and mean measured tool temperature

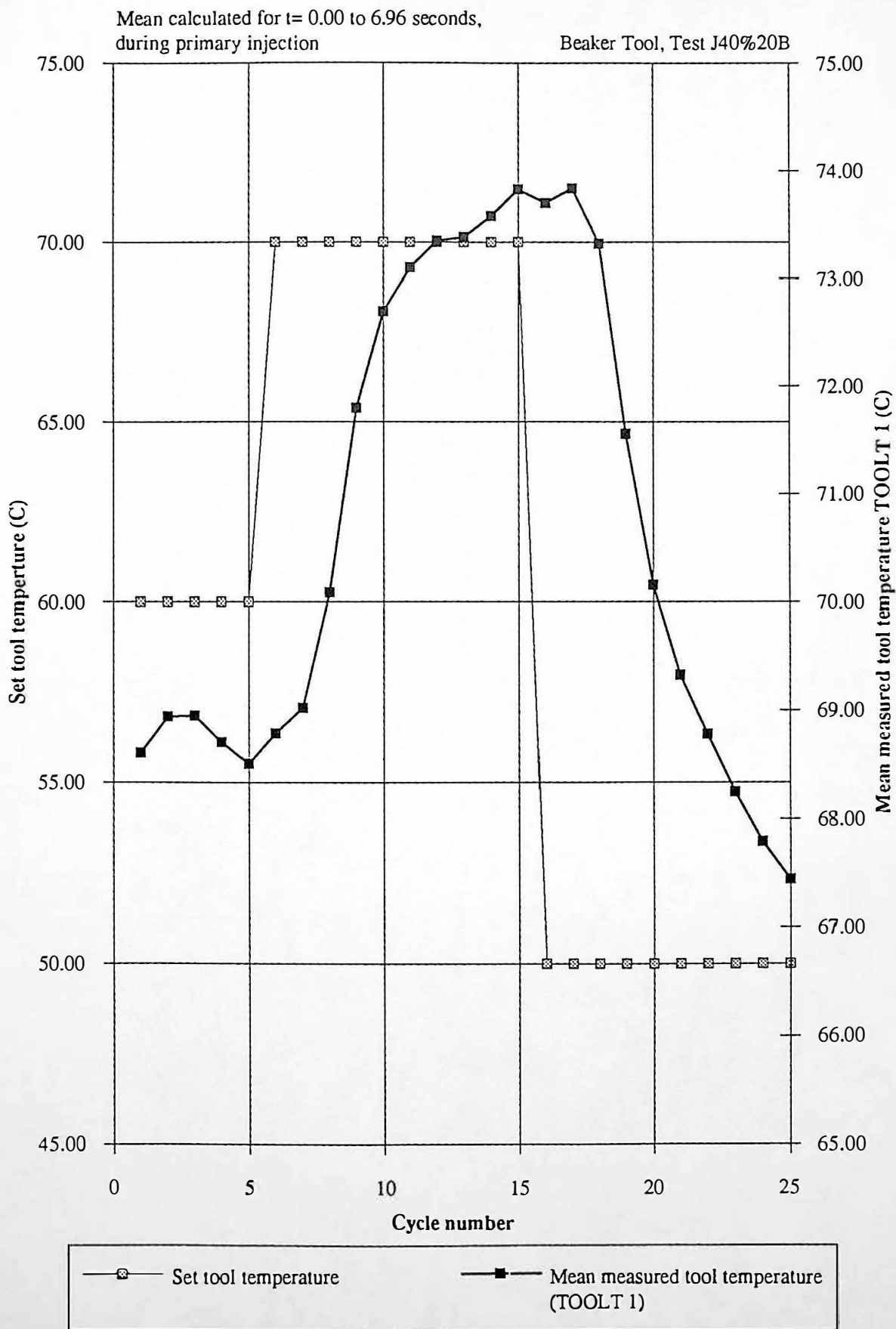


Figure 9.3 Mean measured tool temperature and product weight

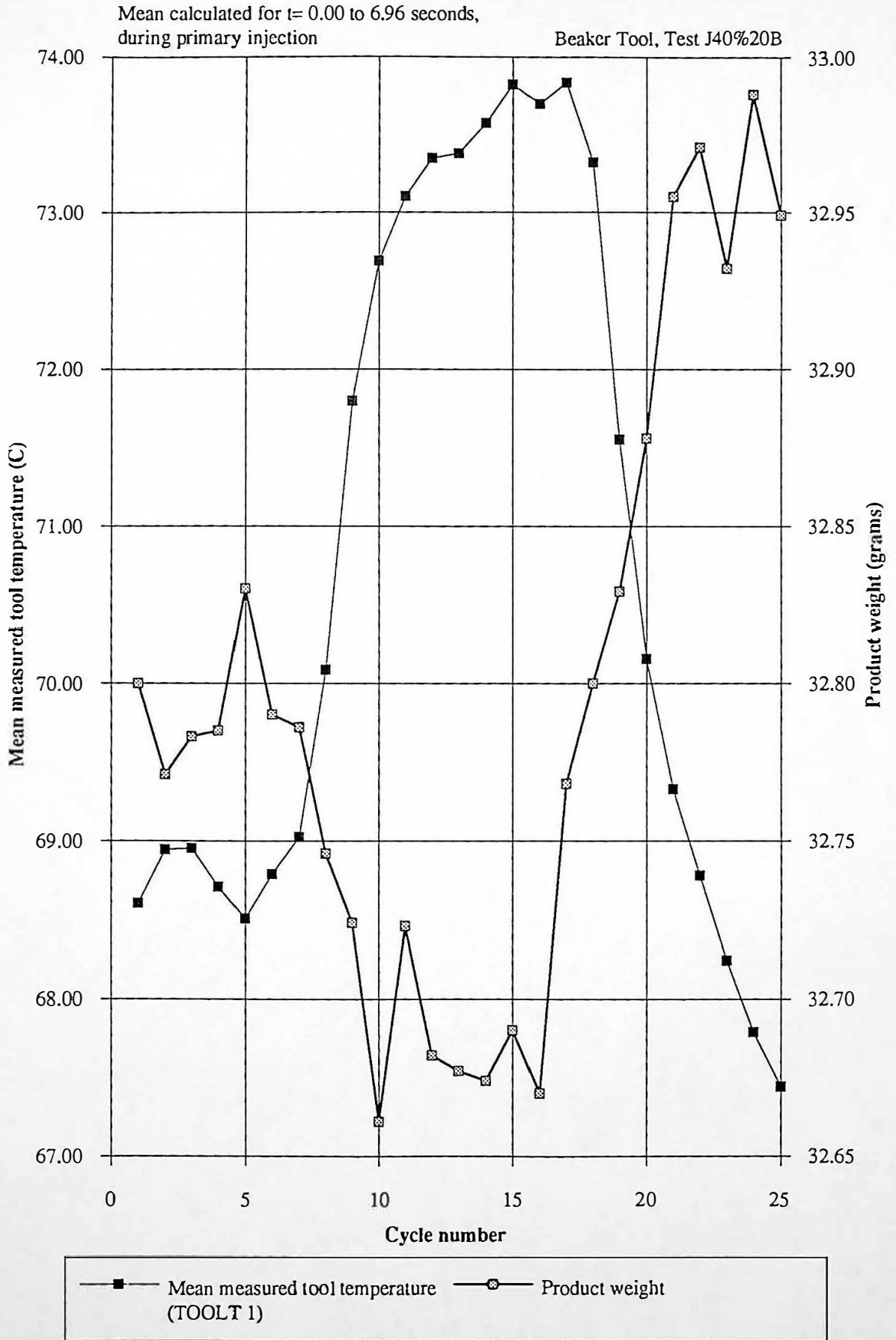


Figure 9.4 Mean measured tool temperature and product height dimension

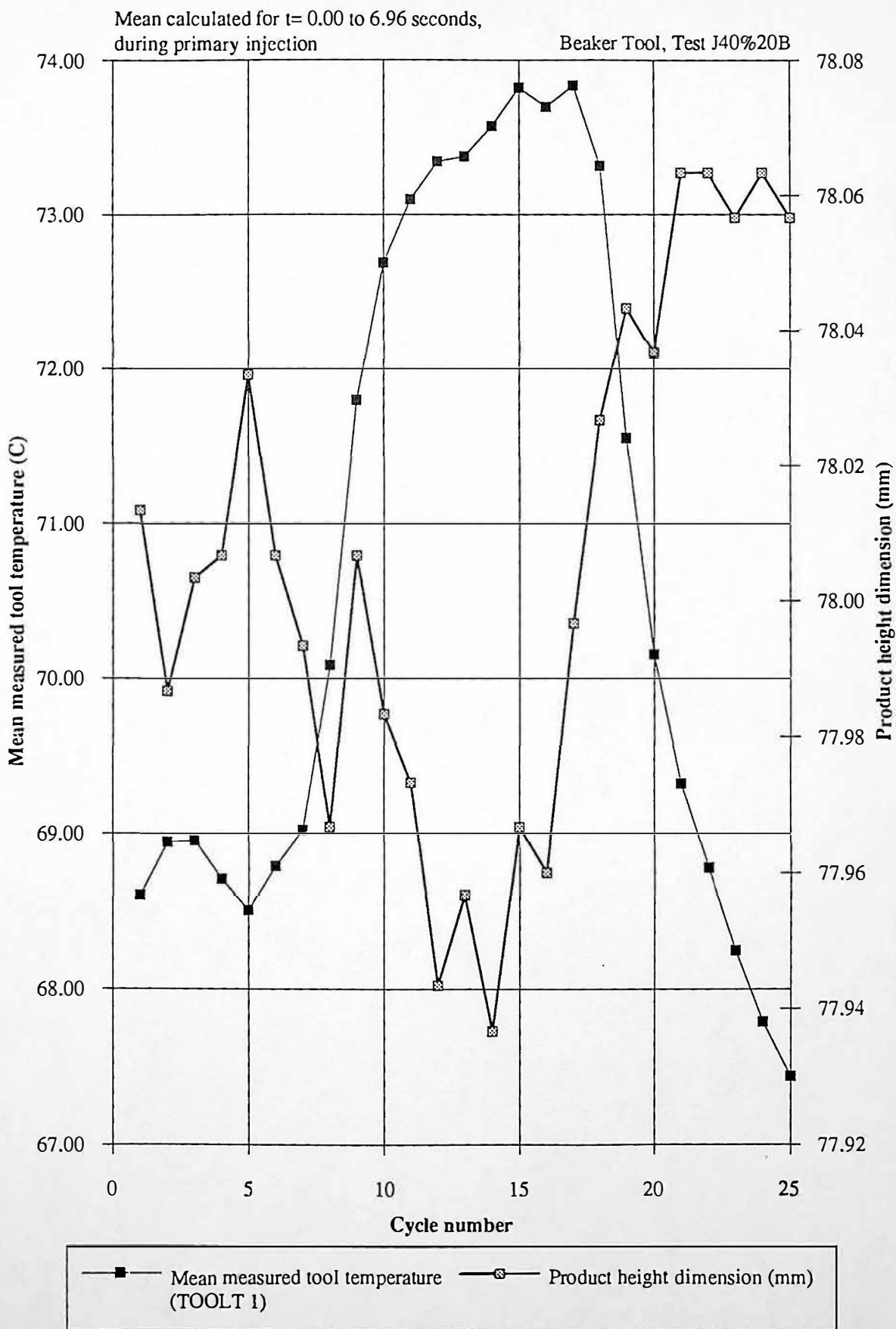
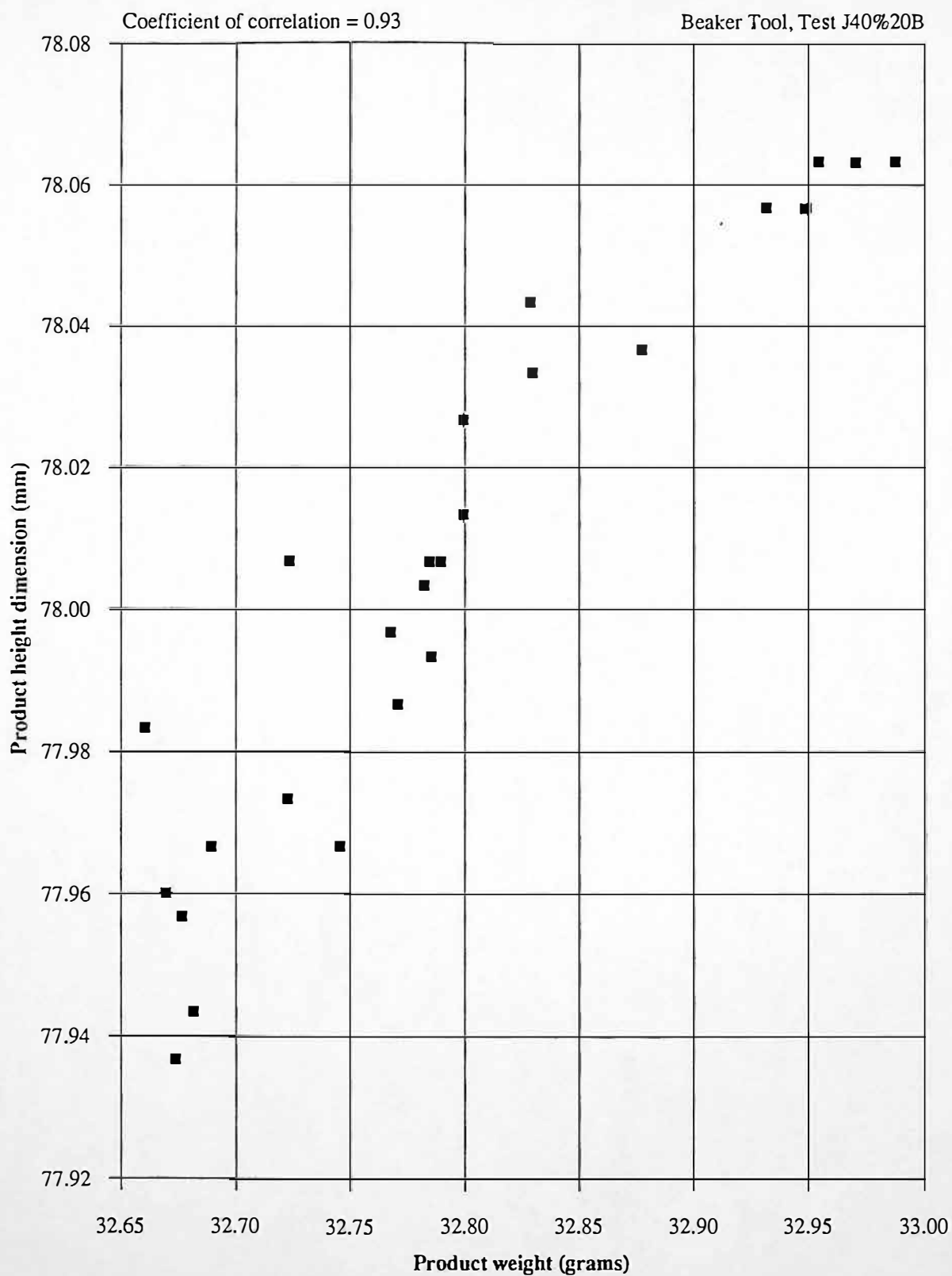


Figure 9.5 Relationship between product weight and product height dimension



It is apparent that product weight and height correlate to a high degree, coefficient of correlation = 0.93. The correlations between tool temperature and product weight and height are lower at -0.75 and -0.68, respectively. The explanation for this may be due to the dynamic response of the tool, to temperature changes. The mean tool temperature = 70.70 C, with coefficient of variation 3.25%, the mean product weight = 32.79 g, with coefficient of variation 0.31%, the mean product height dimension = 78.01 mm, with coefficient of variation 0.05%.

9.2.4 Product Density Distribution

Product density influences product weight and dimension, it should be noted that product density distribution may not be uniform, Isayev and Hariharan (1984) and Wimberger-Froedl and Bruin (1993). Therefore, product weight reflects the average product density change, but dimension changes may be restricted to specific product features. The measurement of the beaker height was made at 90 degrees to the transducer location flats, as shown in figure 9.6. The measurement of beaker height made at the pressure transducer flat does not correlate to the product weight, coefficient of correlation = 0.05. The product height measurement made at the pressure transducer flat = 78.23 mm, coefficient of variation = 0.07%.

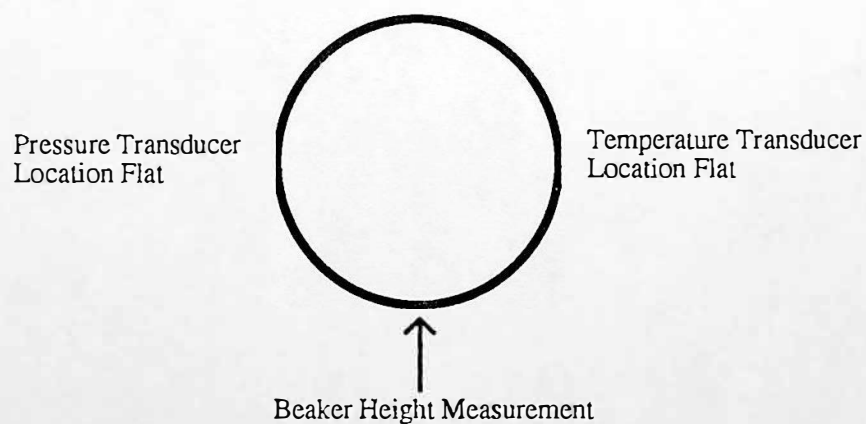


Figure 9.6 Measurement of beaker height dimension

9.3 Influence of Molecular Weight on Polymer Melt Viscosity

The experimental work described in this section investigates the influence of two different molecular weight grades of HDPE (HD5226EA and HD5050EA), on nozzle melt temperature, for the same primary injection velocity (40 mm/s).

Experimental Point to Note:

Due to the higher nozzle melt pressure of test G40%20B, associated with the higher molecular weights, compared to test I40%20B, the packing time was increased from 3.0 to 7.0 seconds. The change of packing time was necessary to ensure that moulding conditions remained typical, for the different molecular weight HDPE grades. Although packing times were different the primary injection phases were set the same, allowing direct comparison of primary injection results. Product quality assessments are not described in this section, due the difference in packing times, which influence product weight.

9.3.1 Initial Experimental Observations

Figures 9.7 and 9.8 show the mean nozzle melt pressure and screw displacement for tests I40%20B and G40%20B, during primary and packing phases, processing two different molecular weight grades of HDPE respectively. It can be seen that primary injection for test I40%20B = 1.02 seconds and for test G40%20B = 1.44 seconds. The peak nozzle melt pressure = 501.1 bar at $t = 1.02$ seconds for test I40%20B and 1003.5 bar at $t = 1.44$ seconds for test G40%20B, reflecting the two grades of HDPE processed.

Figure 9.7 Mean nozzle melt pressure and mean screw displacement during primary injection for HDPE grade HD5226EA

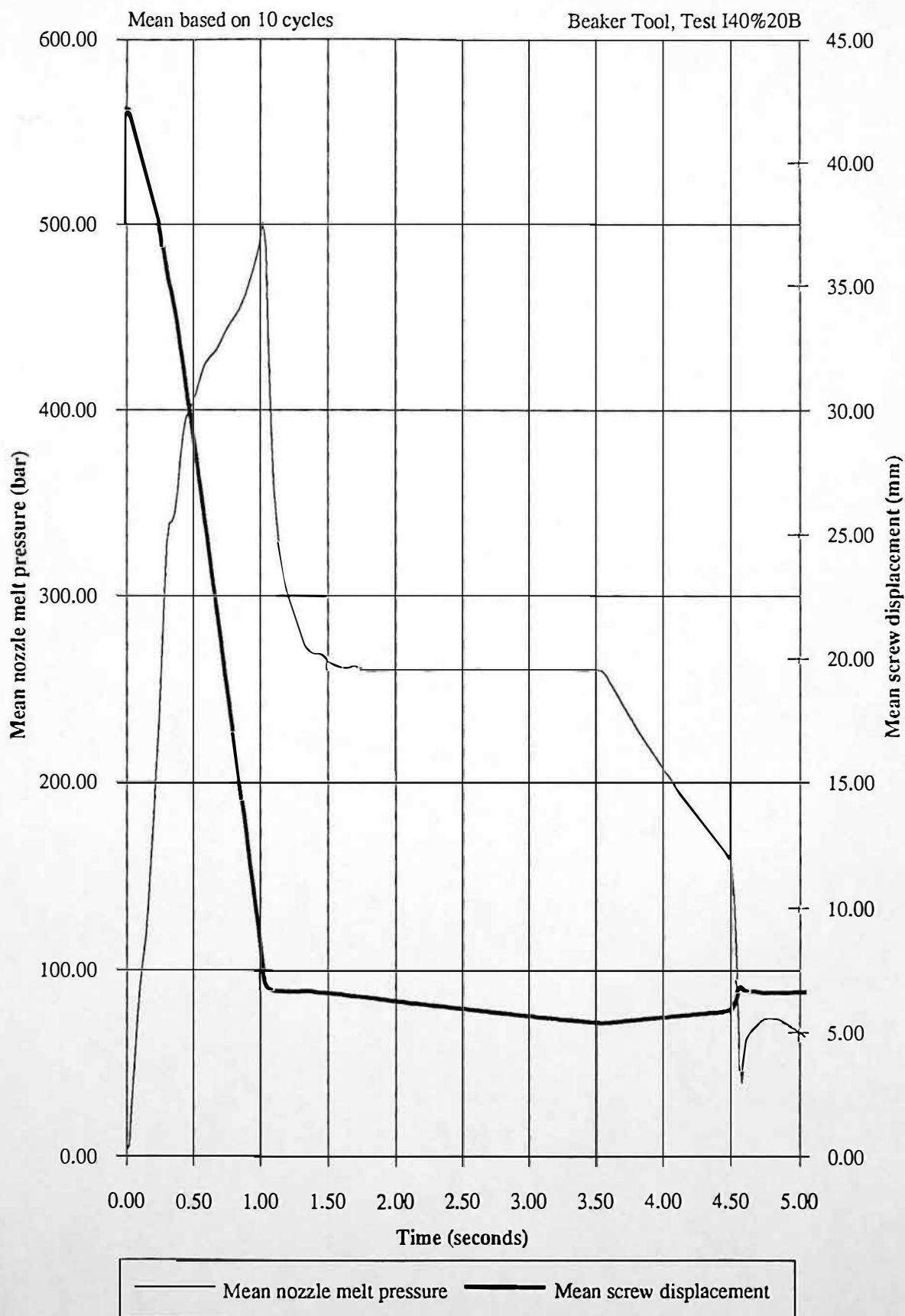
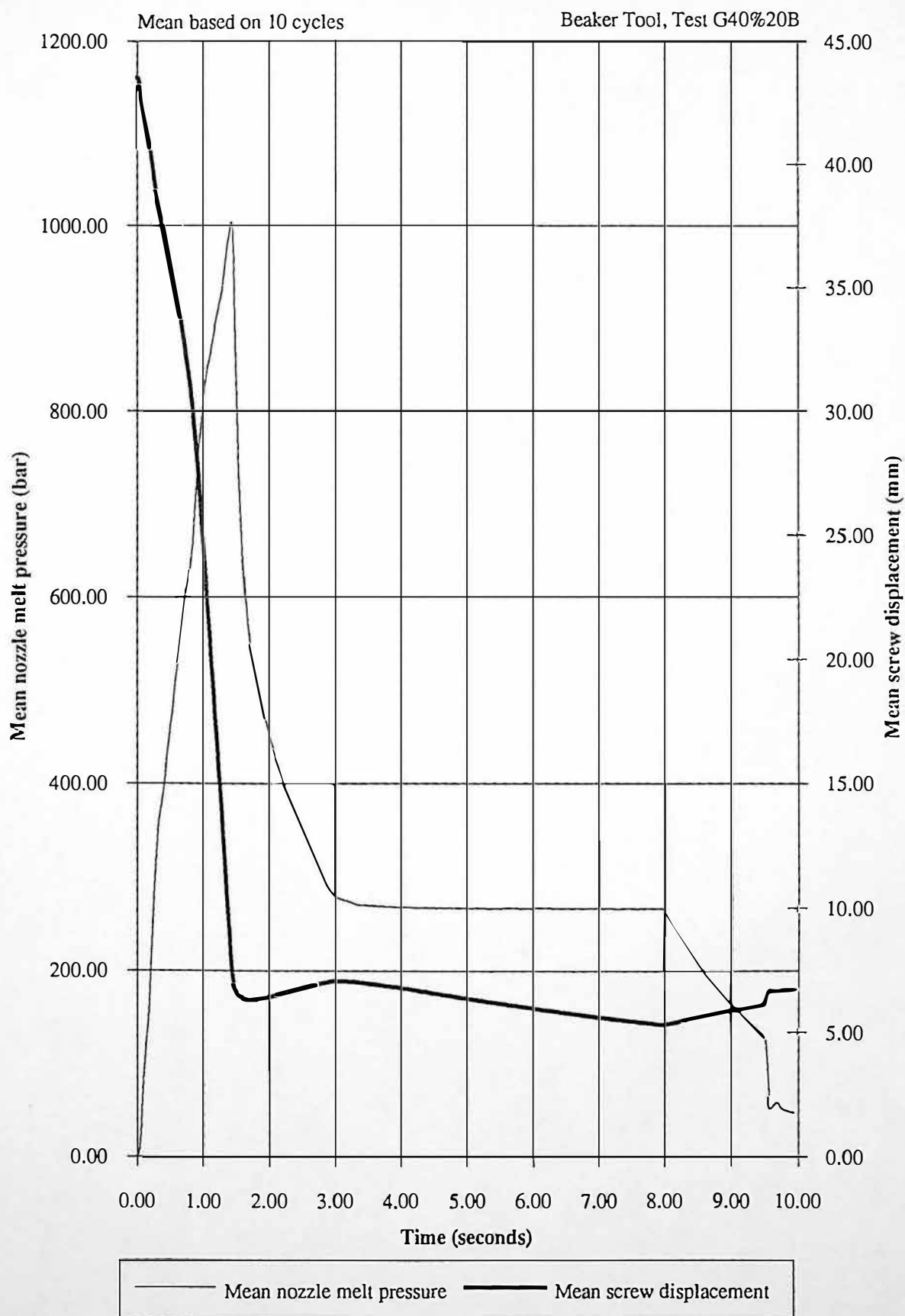


Figure 9.8 Mean nozzle melt pressure and mean screw displacement during primary injection for HDPE grade HD5050EA



9.3.2 Primary Injection Screw Velocity Profile

Figure 9.9 shows the measured velocity for both tests, test I40%20B reached set velocity in 0.46 seconds, test G40%20B reached set velocity in 1.02 seconds. The acceleration period for test G40%20B was prolonged, due to the increased inertia generated by the use of the higher molecular weight (higher viscosity) materials.

9.3.3 Relationship Between Nozzle Melt Pressure and Nozzle Melt Temperature During Primary Injection

Figure 9.10 shows the nozzle melt pressure compared to nozzle melt temperature for test I40%20B. Figure 9.11 shows mean calculated screw acceleration compared to nozzle melt temperature during primary injection for test I40%20B. Comparison of figures 9.10 and 9.11 show that nozzle melt pressure influences nozzle melt temperature for periods of screw acceleration. For the period $t=0.00$ to 0.46 seconds, where nozzle melt temperature and pressure correlate, with a coefficient of correlation of 1.00. For the period 0.46 to 1.02 seconds nozzle melt temperature and pressure correlate with a coefficient of correlation of 0.63. Figure 9.13 shows the nozzle melt pressure compared to nozzle melt temperature for test I40%20B. Figure 9.14 shows mean calculated screw acceleration compared to nozzle melt temperature during primary injection for test G40%20B. Comparison of figures 9.13 and 9.14 show that nozzle melt pressure influences nozzle melt temperature for periods of screw acceleration. For the period $t=0.00$ to 0.94 seconds, where the nozzle melt temperature and pressure correlate, with a coefficient of correlation of 0.99. For the period 0.94 to 1.44 seconds nozzle melt temperature and pressure correlate with a coefficient of correlation of 0.88. Comparison of figure 9.11 to 9.12 and 9.14 to 9.15 shows that nozzle melt pressure influences nozzle melt temperature for low differential values of nozzle melt pressure to hydraulic injection pressure (polymer melt compressibility).

Figure 9.9 Mean screw injection velocity during primary injection for two different molecular weight grades of HDPE (HD5226EA and HD5050EA)

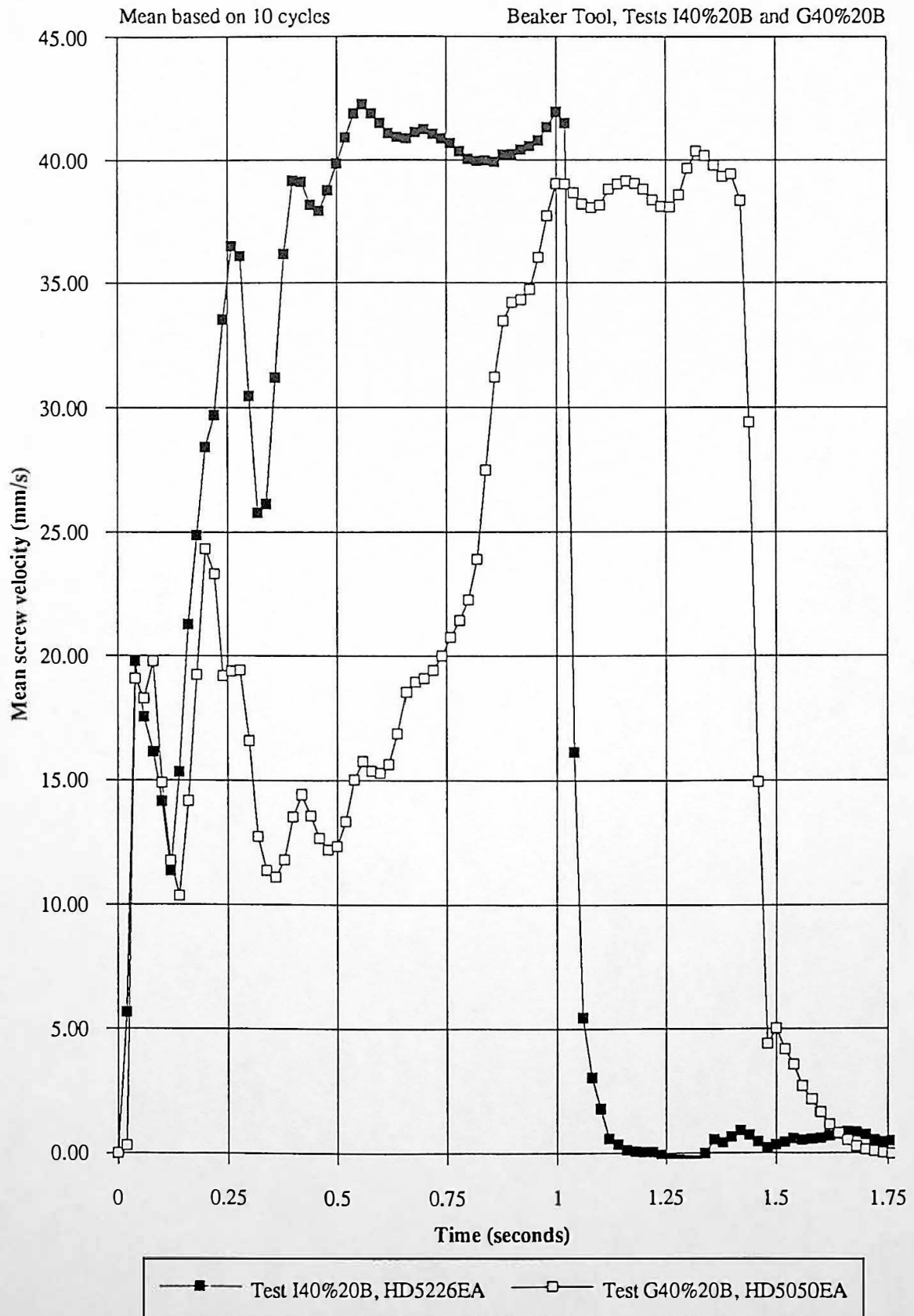


Figure 9.10 Mean nozzle melt pressure and mean nozzle melt temperature during primary injection for HDPE grade HD5226EA

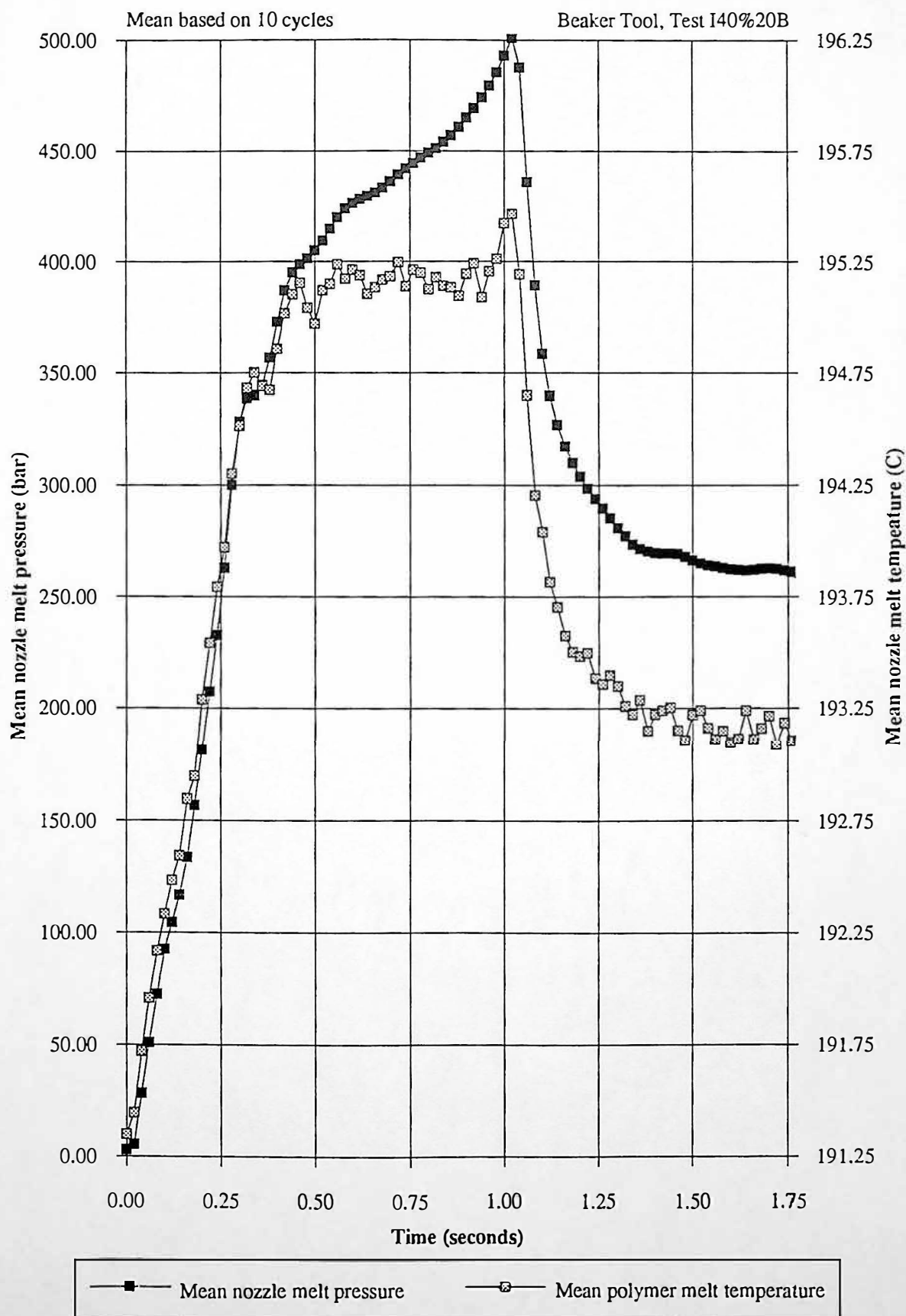


Figure 9.11 Mean screw acceleration and mean nozzle melt temperature during primary injection

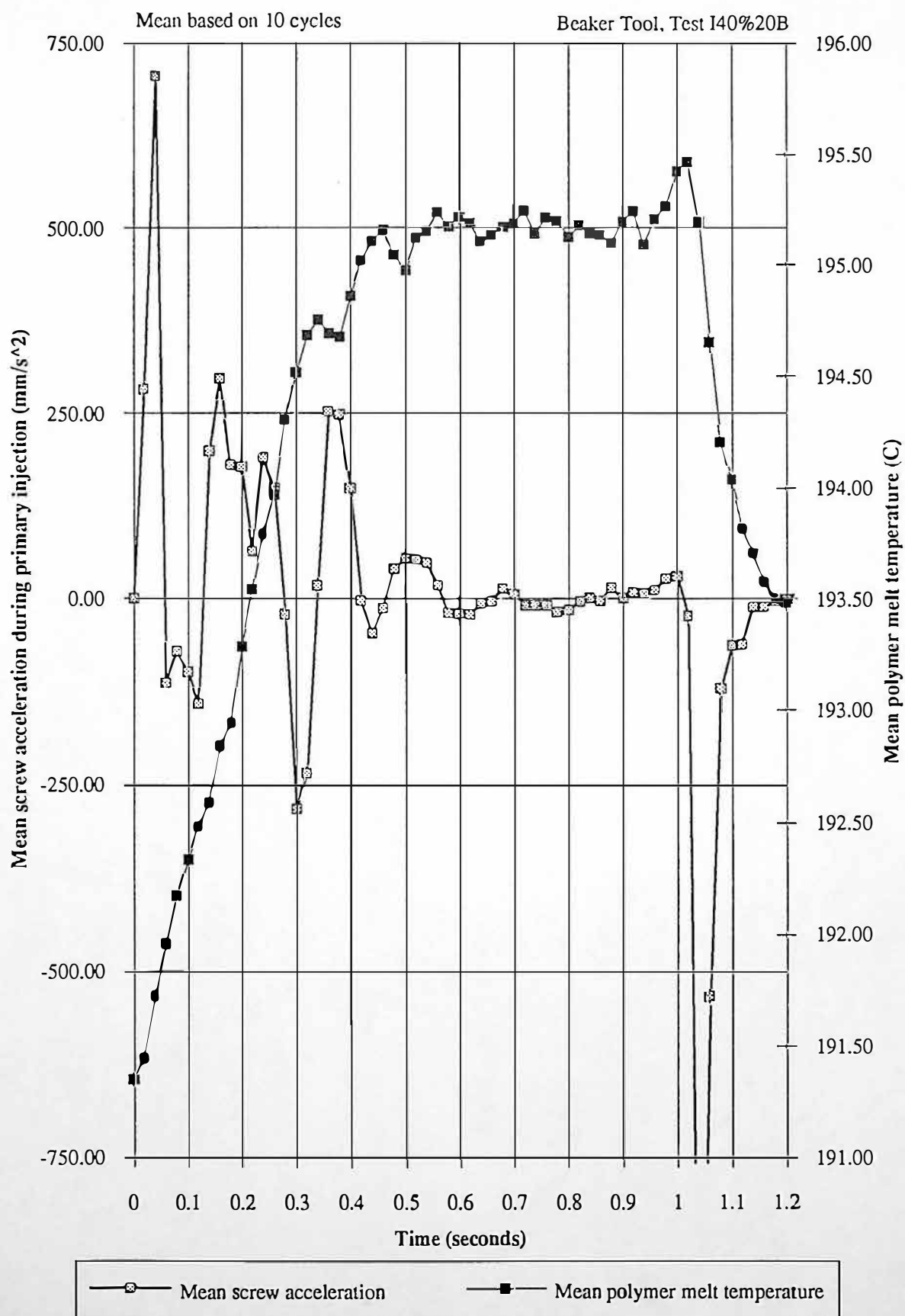


Figure 9.12 Differential of mean ratio of nozzle melt pressure to hydraulic injection pressure and mean nozzle melt temperature during primary injection

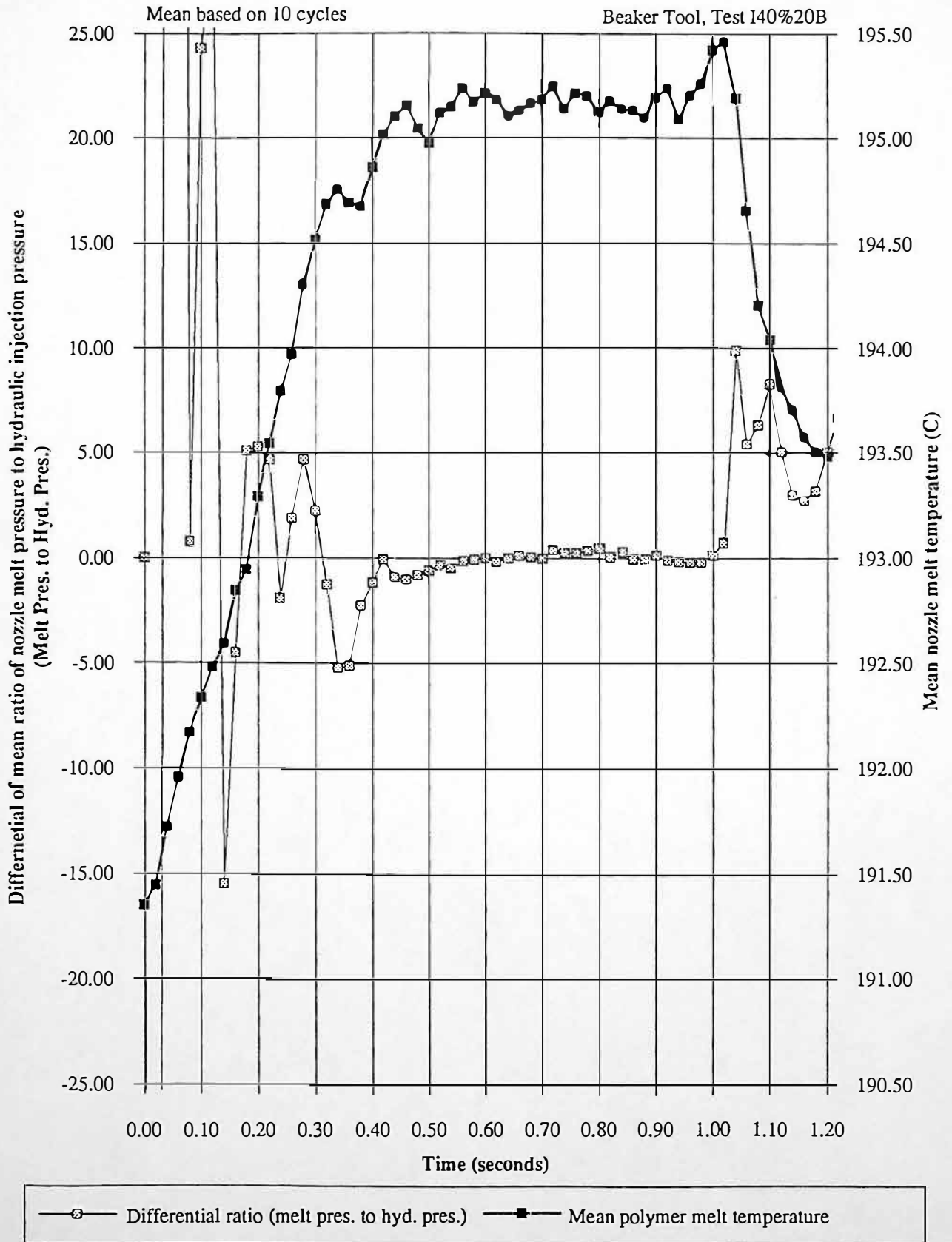


Figure 9.13 Mean nozzle melt pressure and mean nozzle melt temperature during primary injection for HDPE grade HD5050EA

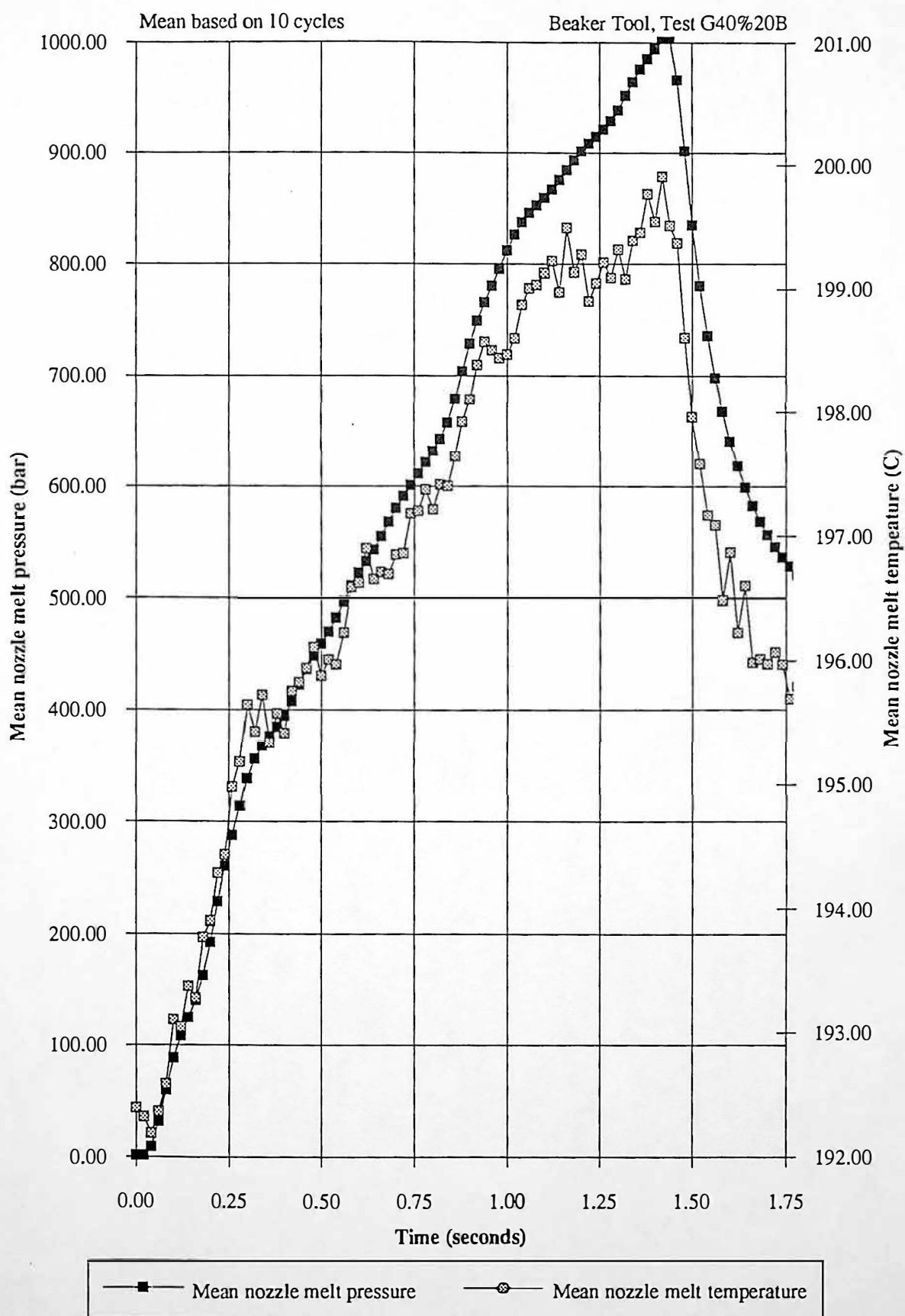


Figure 9.14 Mean screw acceleration and mean nozzle melt temperature during primary injection

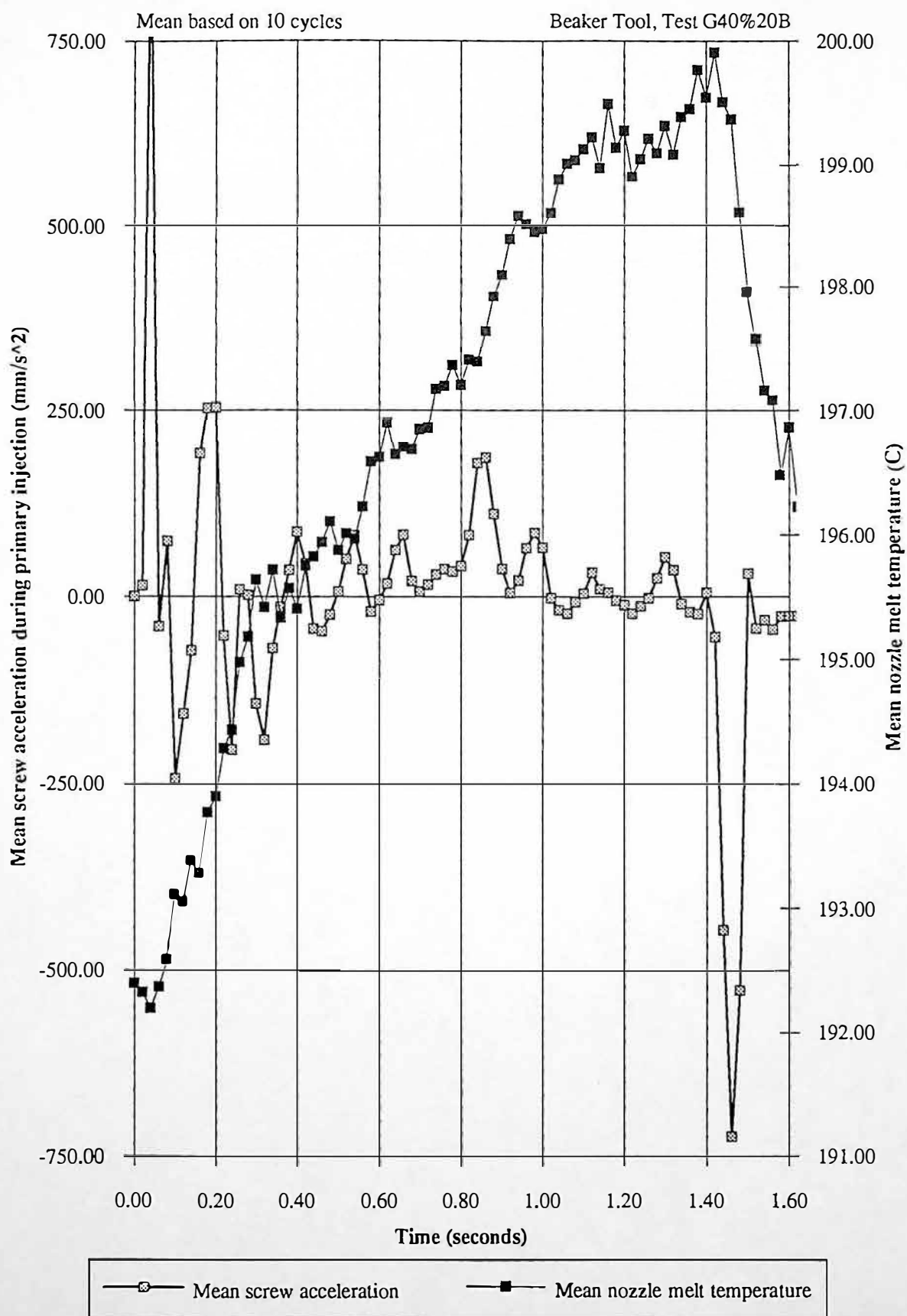
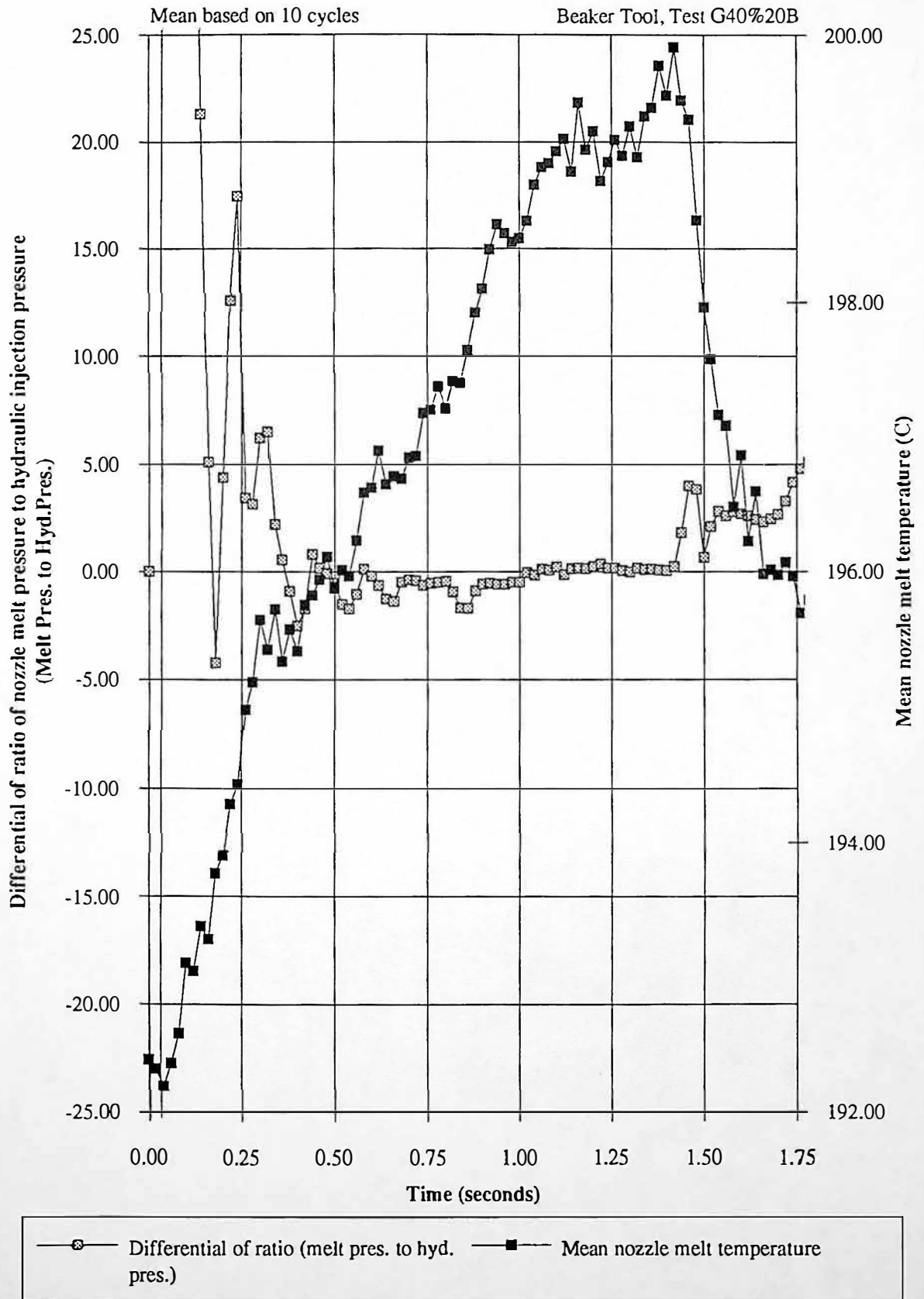


Figure 9.15 Differential of mean ratio of nozzle melt pressure to hydraulic injection pressure and mean nozzle melt temperature during primary injection



9.3.4 Comparison of Theoretical and Practical Nozzle Melt Temperature Differentials

The equation for the first law of thermodynamics allows an adiabatic temperature rise to be calculated, based on nozzle melt pressure, for the screw acceleration period.

$$\Delta T = \frac{\Delta P}{C_p \times \rho} \quad \text{Eq. 9.1}$$

rearranging equation 9.1 gives:

$$C_p = \frac{\Delta P}{\Delta T \times \rho}$$

where:

ΔP = Pressure Change (Pa)

ΔT = Temperature Change (C)

ρ = Density (kg/m^3), assume the polymer melt density = 750 kg/m^3

For test I40%20B at the final stage of screw acceleration $t=0.46$ seconds, nozzle melt pressure = 398.7 bar and nozzle melt temperature $T = 195.2\text{C}$. For test G40%20B at the final stage of screw acceleration $t=0.94$ seconds, nozzle melt pressure = 766.3 bar and nozzle melt temperature $T = 198.6 \text{ C}$.

Therefore:

$$C_p = \frac{(766.3 \times 10^5 - 398.7 \times 10^5)}{(198.6 - 195.2) \times 750} = 14416 \text{ J/kg/C}$$

The quoted value of specific heat = 2300 J/kg/C (Appendix H(i) and H(ii) for BP Chemicals technical information sheets T206/1 and T211/1, respectively), therefore for

idealised conditions, the same pressure change would produce a temperature change of $\Delta T = 21.3 \text{ C}$.

$$\Delta T = \frac{\Delta P}{C_p \times \rho} \Rightarrow \frac{(766.3 \times 10^5 - 398.7 \times 10^5)}{2300 \times 750} = 21.3 \text{ C}$$

The infra-red temperature transducer measured an increase in temperature of $\Delta T = 3.4 \text{ C}$ compared to a calculated temperature increase of $\Delta T = 21.3 \text{ C}$. The difference is a factor of 4.9. Chapter 5 compared the response of a 1 mm diameter thermocouple and a standard industrial thermocouple. The temperature rise would have most likely been $\Delta T = 0.7 \text{ C}$ for a typical industry thermocouple with a time constant of 2.30 seconds, (based on simple ratios).

9.3.5 Process Sensitivity

From a sensitivity point of view:

$$\text{Sensitivity} = \frac{\Delta T}{\Delta P} \Rightarrow \frac{(198.6 - 195.2)}{(766.3 - 398.7)} = \frac{3.4}{367.6} = 9.25 \times 10^{-3} \text{ (C / bar)}$$

It is apparent from these results that nozzle melt pressure is proportional to nozzle melt temperature, for periods of polymer melt compressibility during the primary injection phase.

9.4 Influence of Screw Injection Velocity on Melt Viscosity

Chapter 9.3.1 describes experimental results obtained by processing two different molecular weight grades of HDPE for the same primary injection velocity. Nozzle melt pressure is shown to influence nozzle melt temperature for periods of screw acceleration. Nozzle melt pressure is influenced by the combined effect of polymer melt viscosity and screw injection velocity. The experimental investigation of this section, analyses the influence of nozzle melt pressure on nozzle melt temperature, for five different screw injection velocities. Product quality assessments are made, as the packing phase have the same packing pressure and time period (20 bar hydraulic pressure for 3 seconds). During typical injection moulding operations injection screw velocity varies depending on the quality of machine parameter control.

Figure 9.16 shows the influence of injection velocity on product weight and height dimension. It is apparent that as injection velocity increases, product weight and height dimension decrease. This relationship occurs for typical injection moulding process conditions, using semi-crystalline materials. Figure 9.16 shows the influence of screw injection velocity on product quality (weight and height dimension). The relationship between screw injection velocity and product quality is extremely important. Therefore the work described in this chapter investigates this relationship. The influence of screw injection velocity on product quality reduces for high screw injection velocities, where polymer melt shear heating effects reach a maximum value.

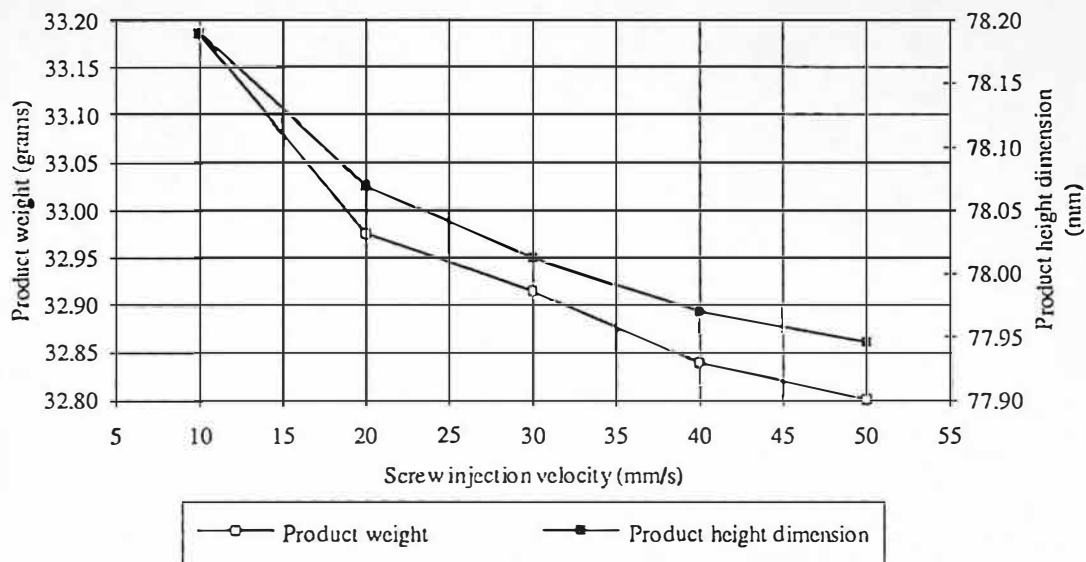


Figure 9.16 Influence of injection velocity on product quality (weight and height dimension)

9.4.1 Initial Experimental Observations

Figures 9.17 and 9.18 show the mean nozzle melt pressure and screw displacement profiles for test NX%20B, each profile is the mean of 3 cycles for 5 injection velocities. The times for primary injection phase for velocities 10, 20, 30, 40 and 50 mm/s are 3.38, 1.96, 1.36, 1.02, and 0.82 seconds respectively. The slower the injection time, the more time is available for the polymer melt to shrink. Figure 9.19 shows the velocity profiles for the 5 injection velocities. The screw acceleration periods are apparent, the screw accelerating greatest for the greater set velocity. Figure 9.20 shows the nozzle melt temperature profiles for the 5 injection velocities.

Figure 9.17 Mean nozzle melt pressure for screw injection velocity range

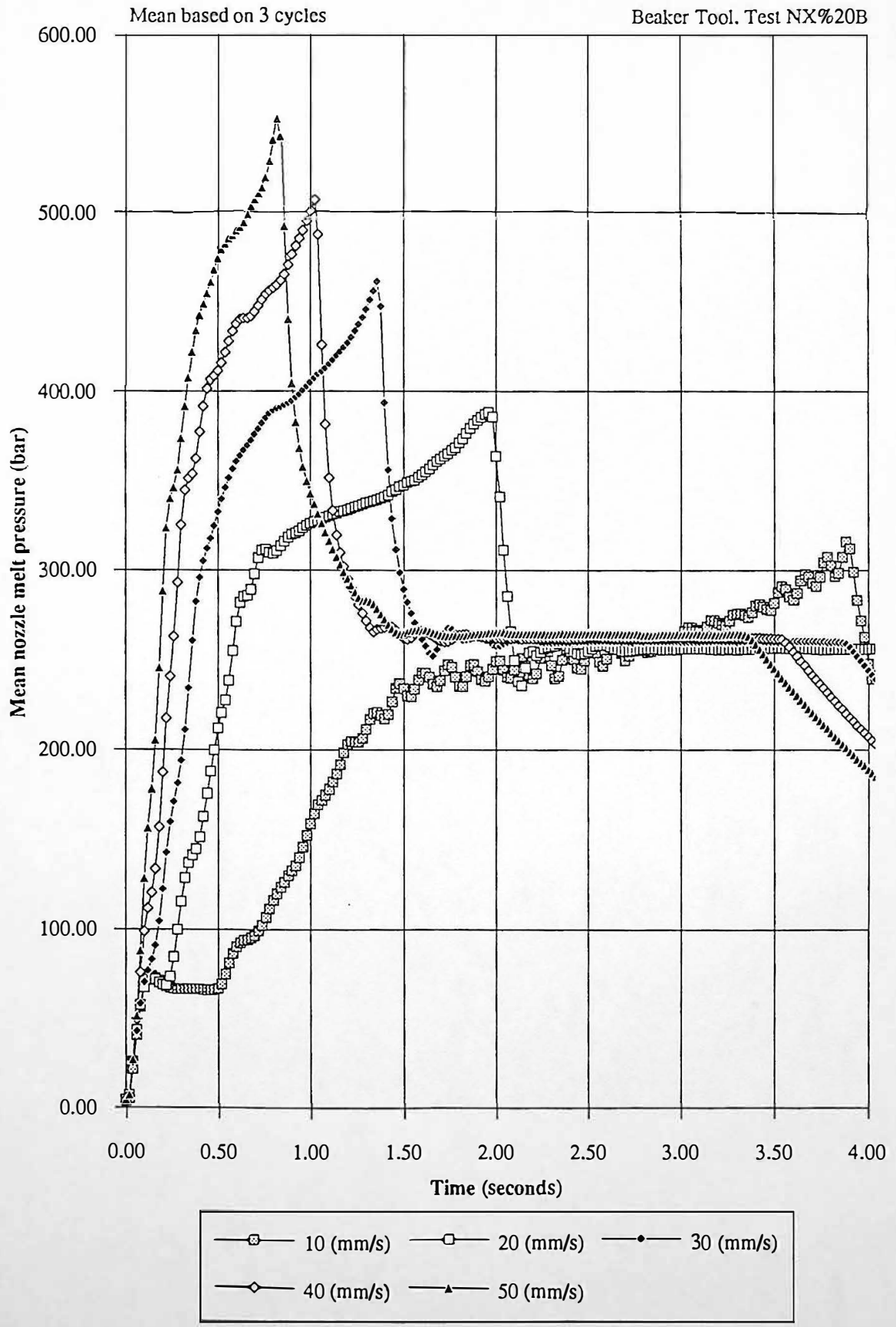


Figure 9.18 Mean screw displacement for screw injection velocity range

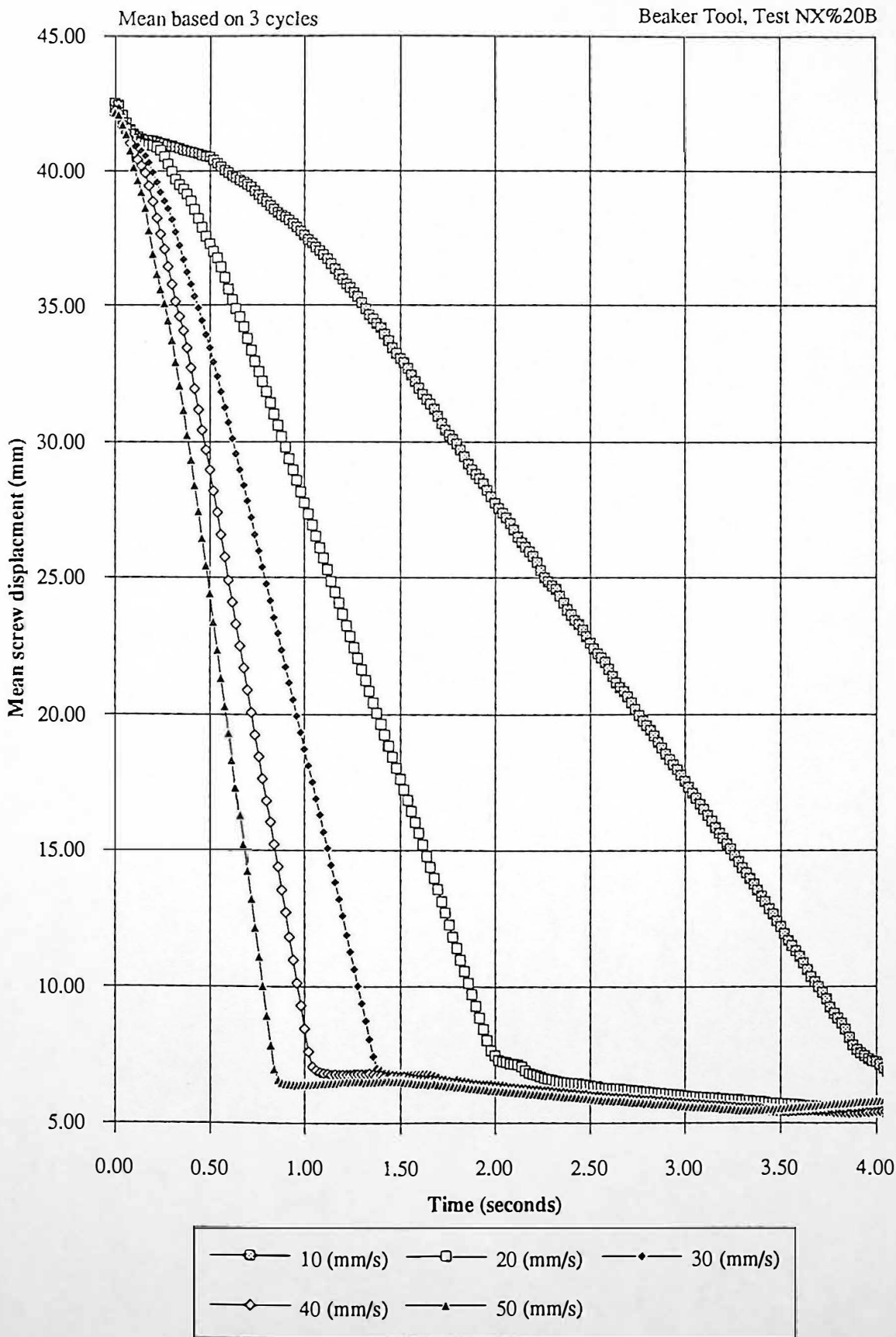


Figure 9.19 Mean screw injection velocity range

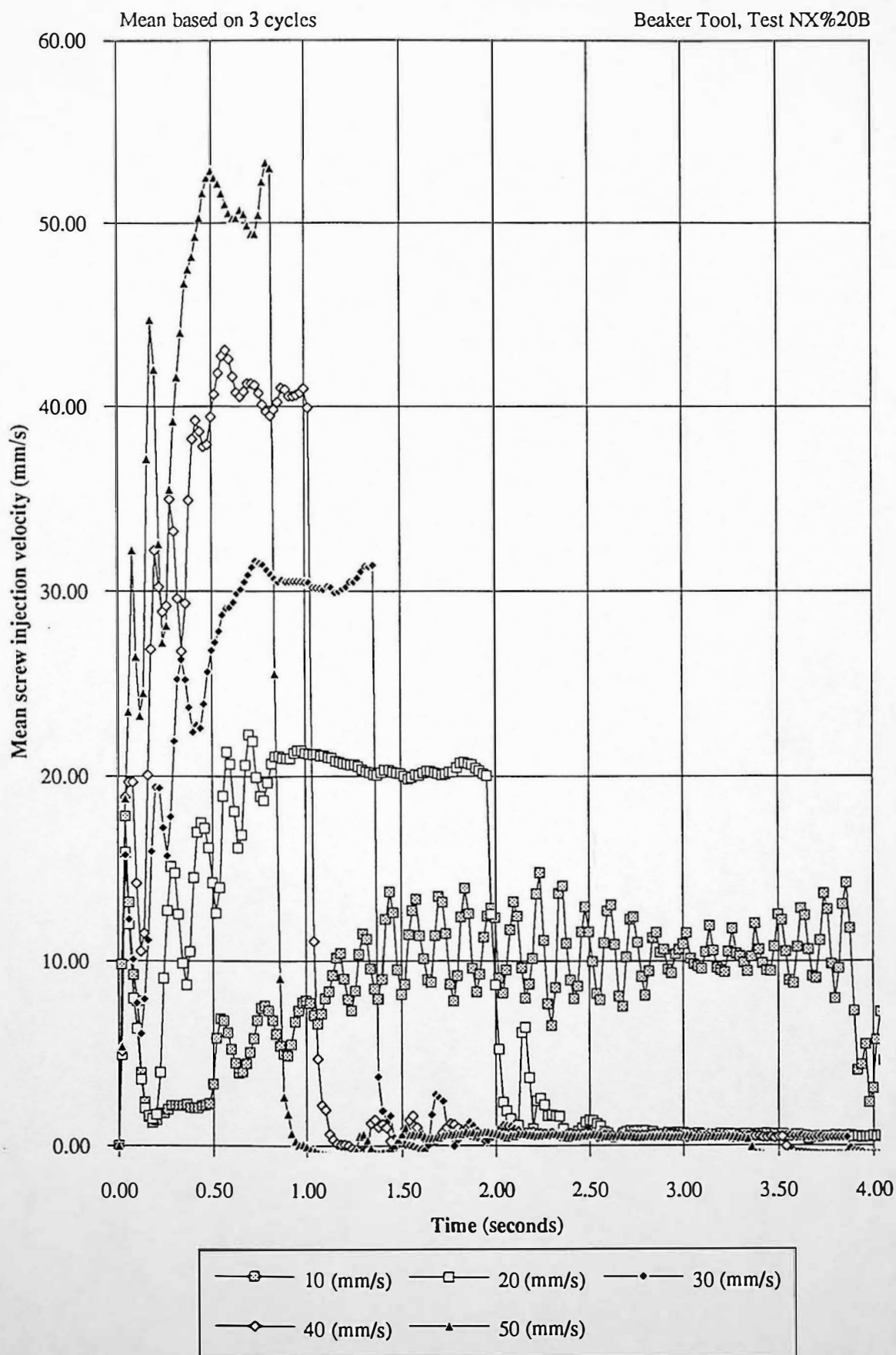
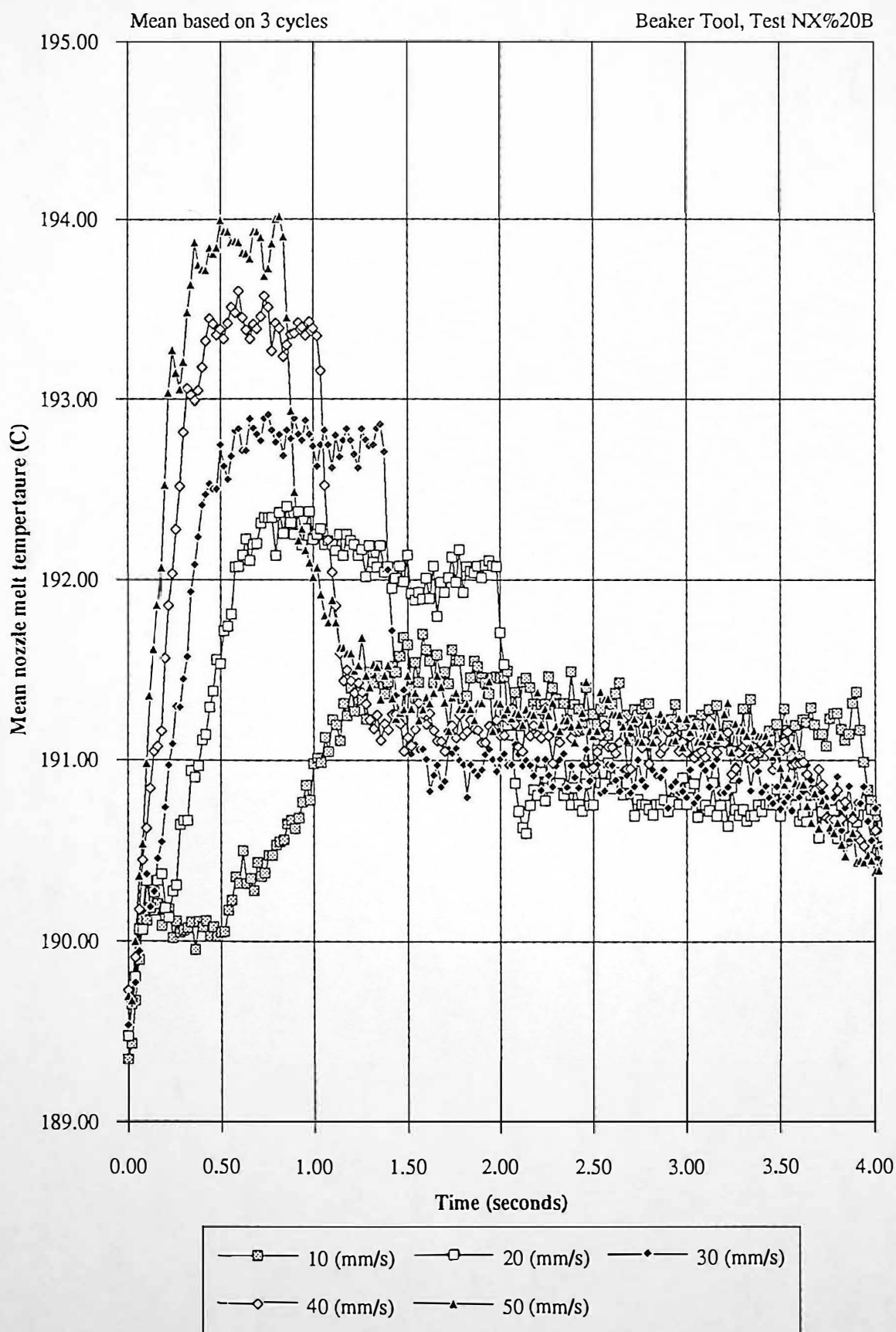


Figure 9.20 Mean nozzle melt temperature for screw injection velocity range



9.4.2 Relationship Between Nozzle Melt Pressure and Nozzle Melt Temperature During Primary Injection

Figure 9.21 shows nozzle melt pressure compared to nozzle melt temperature for an injection velocity of 20 mm/s. Comparison of figures 9.22 and 9.23 shows that nozzle melt pressure influences nozzle melt temperature for periods of screw acceleration and polymer melt compression, respectively.

Figure 9.24 shows nozzle melt pressure compare to nozzle melt temperature for an injection velocity of 50 mm/s. Comparison of figures 9.25 and 9.26 also shows that nozzle melt pressure influences nozzle melt temperature for periods of screw acceleration and polymer melt compression, respectively. Table 9.2 shows the screw acceleration periods for the set screw injection velocities 10 mm/s to 50 mm/s, for test NX%20B.

Set Injection Velocity (mm/s)	Screw Acceleration Period (seconds)	Coefficient of Correlation Between nozzle melt pressure and temperature
10	0.00 to 1.16	0.99
20	0.00 to 0.82	0.99
30	0.00 to 0.64	1.00
40	0.00 to 0.52	1.00
50	0.00 to 0.44	0.99

Table 9.2 Summary of results for periods of screw acceleration

Figure 9.27 shows the relationship between nozzle melt pressure and nozzle melt temperature, for the screw acceleration periods (pressure and temperature measurements were the end of screw acceleration values). The pressure and temperature measurements correlate with a coefficient of correlation of 0.99.

Figure 9.21 Mean nozzle melt pressure and mean nozzle melt temperature during primary injection for set screw injection velocity of 20 mm/s

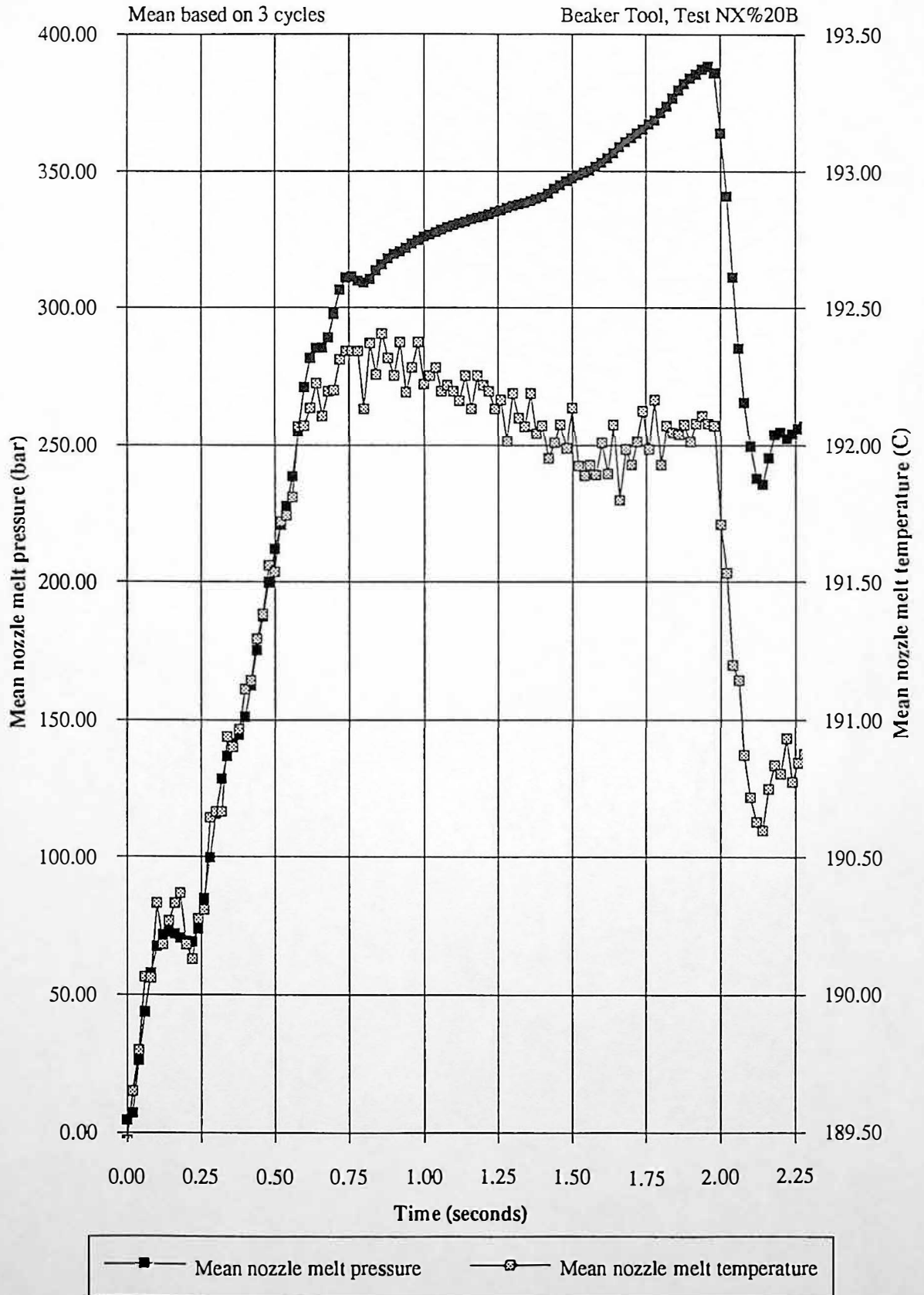


Figure 9.22 Mean screw acceleration and mean nozzle melt temperature during primary injection for a set screw velocity of 20 mm/s

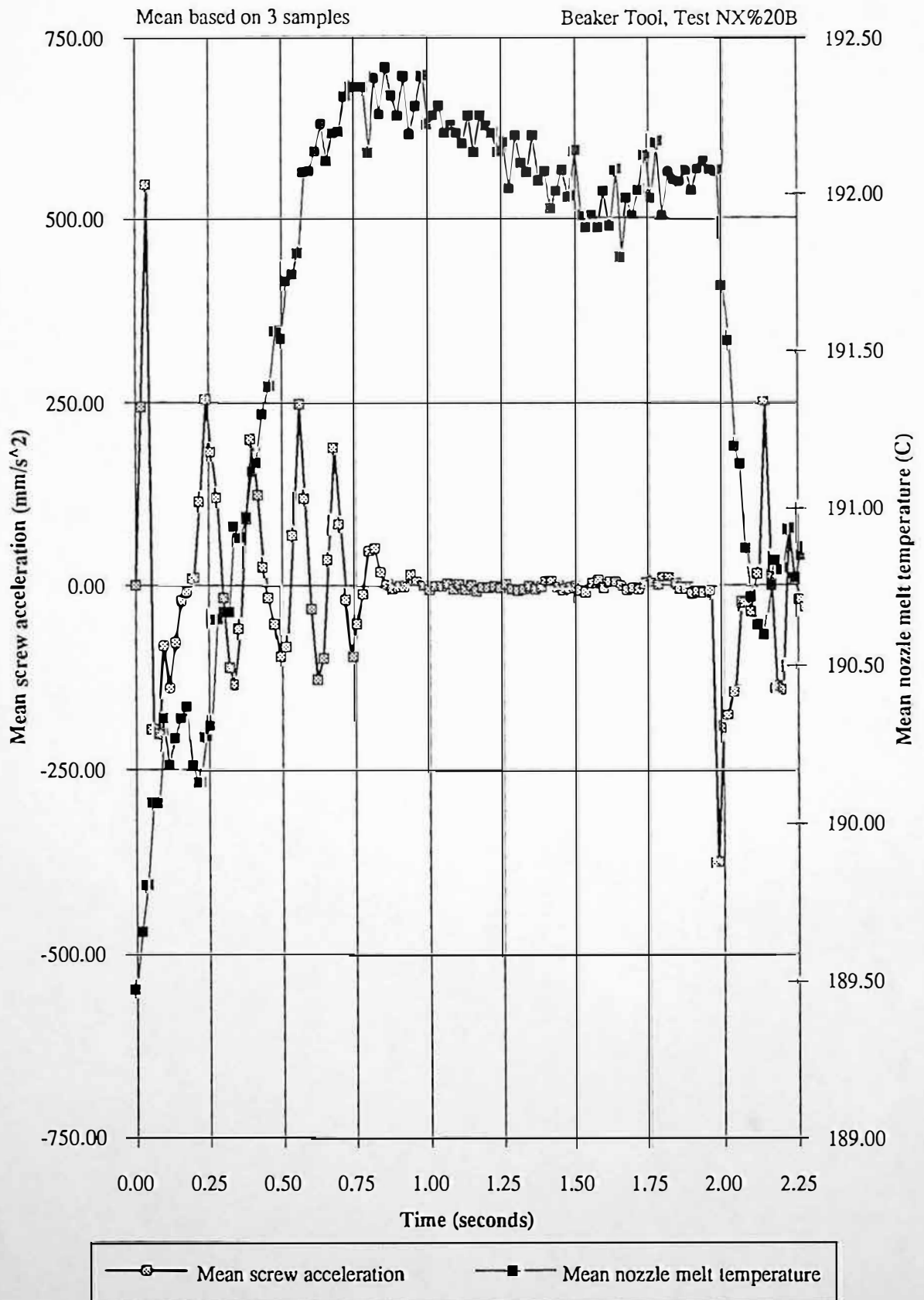


Figure 9.23 Differential of mean ratio of nozzle melt pressure to hydraulic injection pressure and mean nozzle melt temperature during primary injection for set screw injection velocity of 20 mm/s

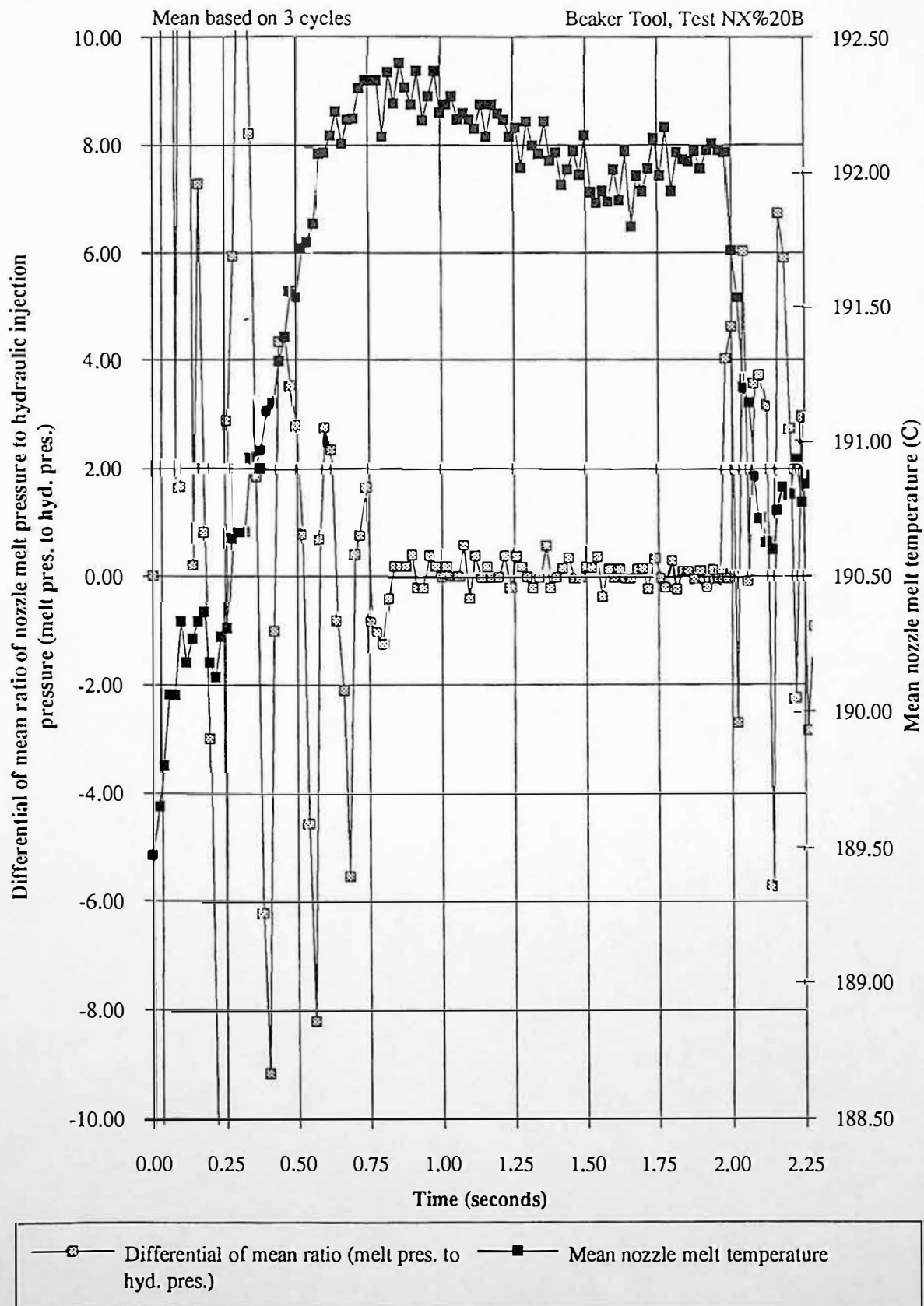


Figure 9.24 Mean nozzle melt pressure and mean nozzle melt temperature during primary injection for set screw velocity of 50mm/s

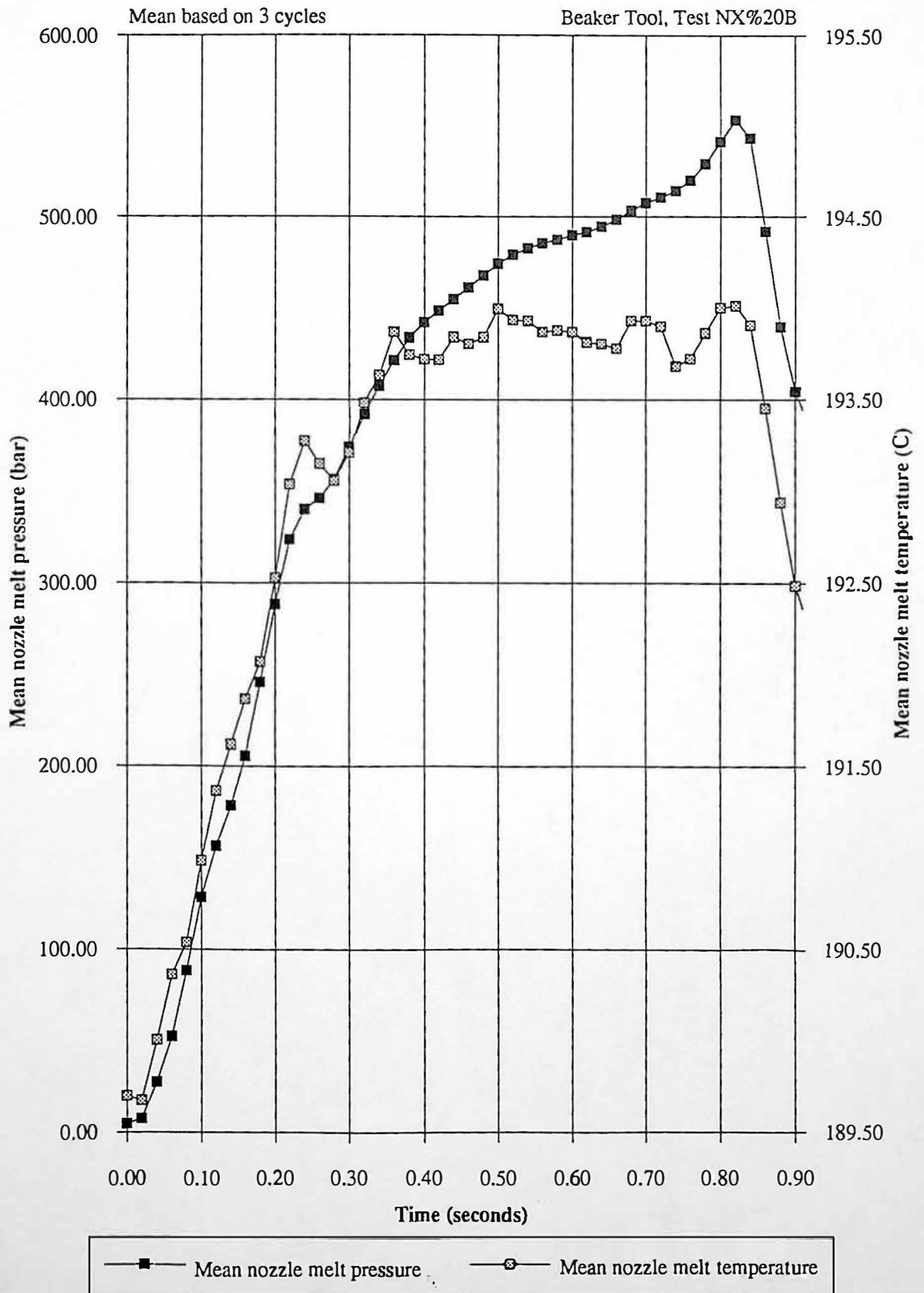


Figure 9.25 Mean screw acceleration and mean nozzle melt temperature during primary injection for a set screw velocity of 50 mm/s

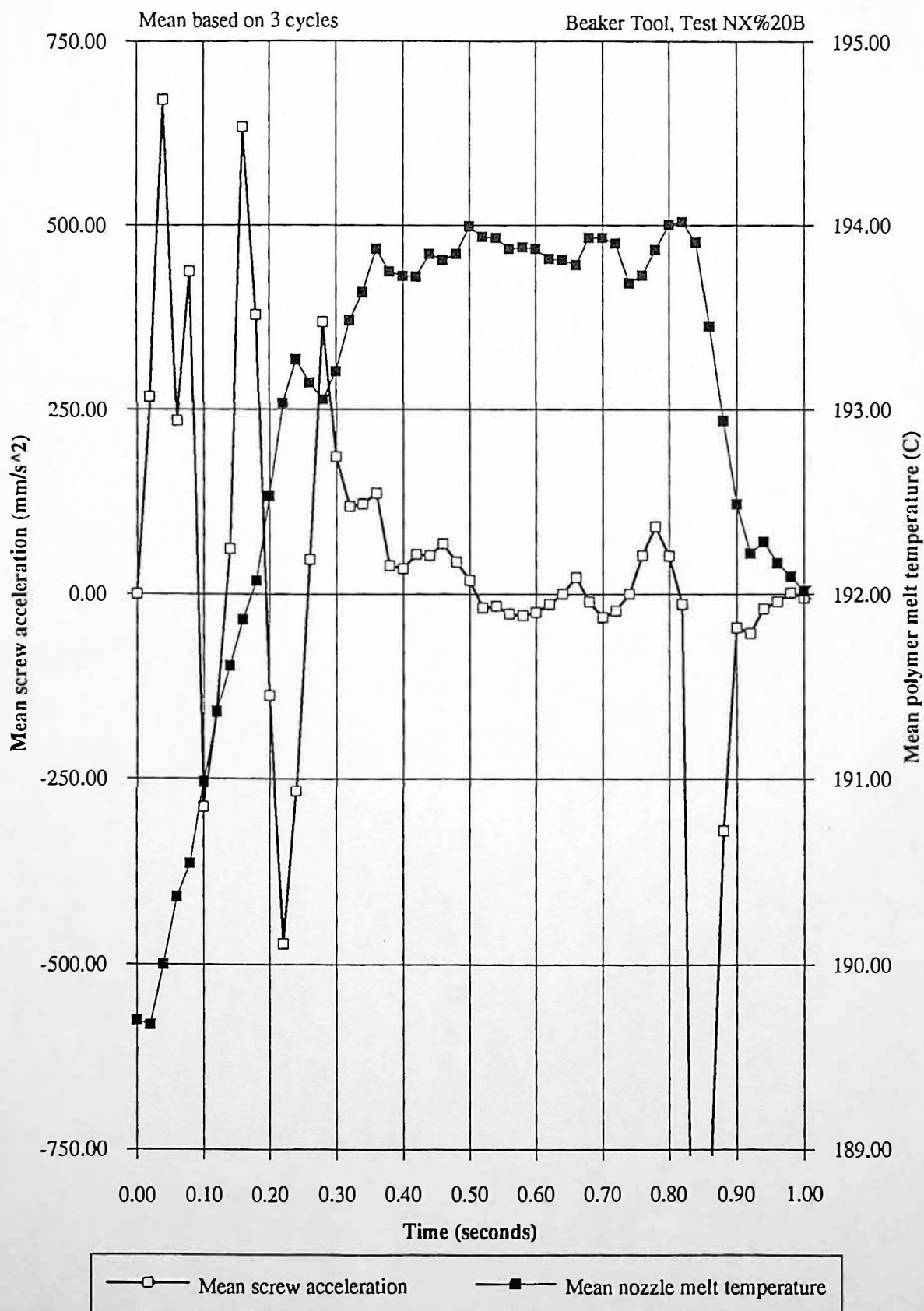


Figure 9.26 Differential of mean ratio of nozzle melt pressure to hydraulic injection pressure and mean nozzle melt temperature during primary injection for set screw injection velocity of 50 mm/s

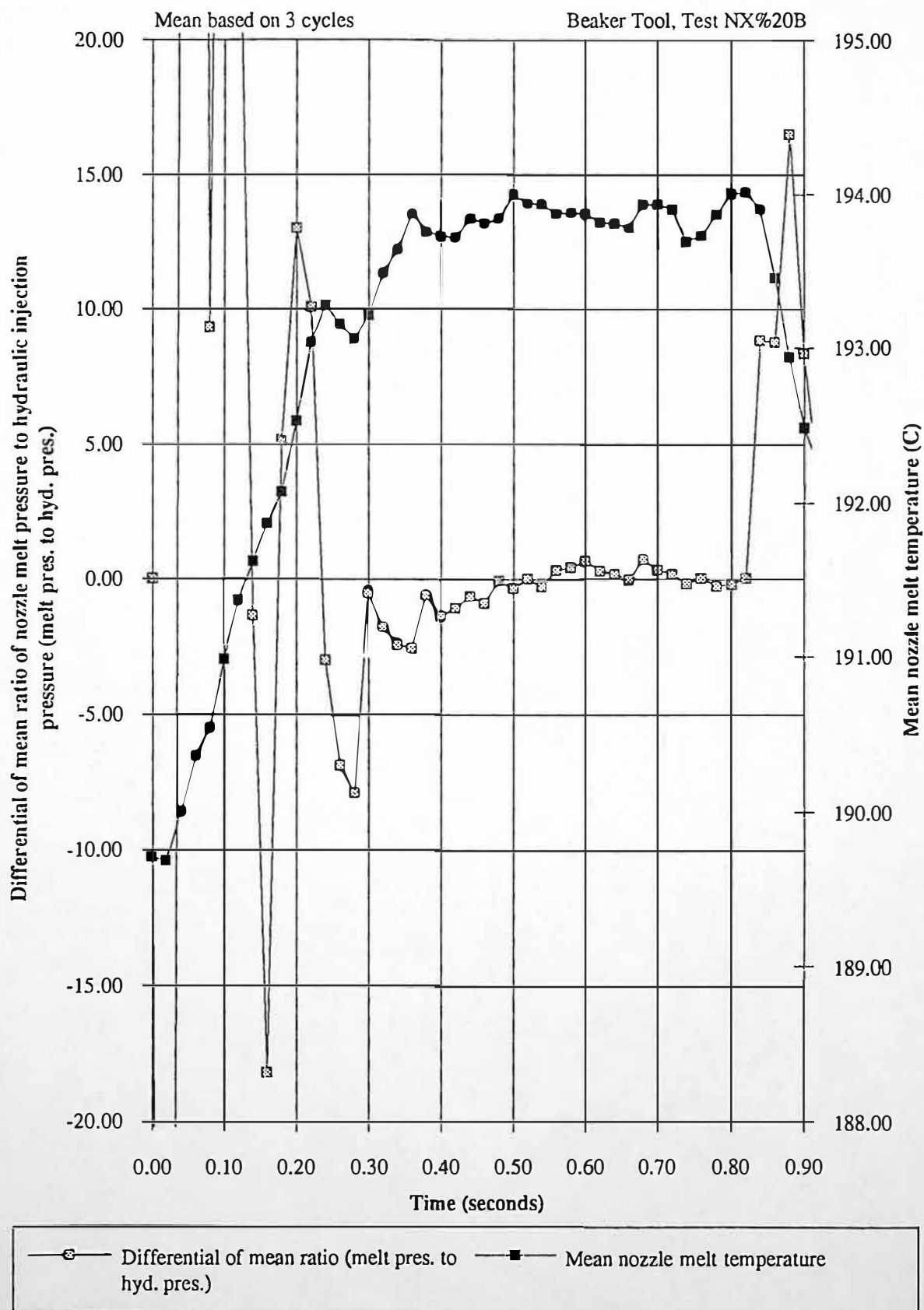
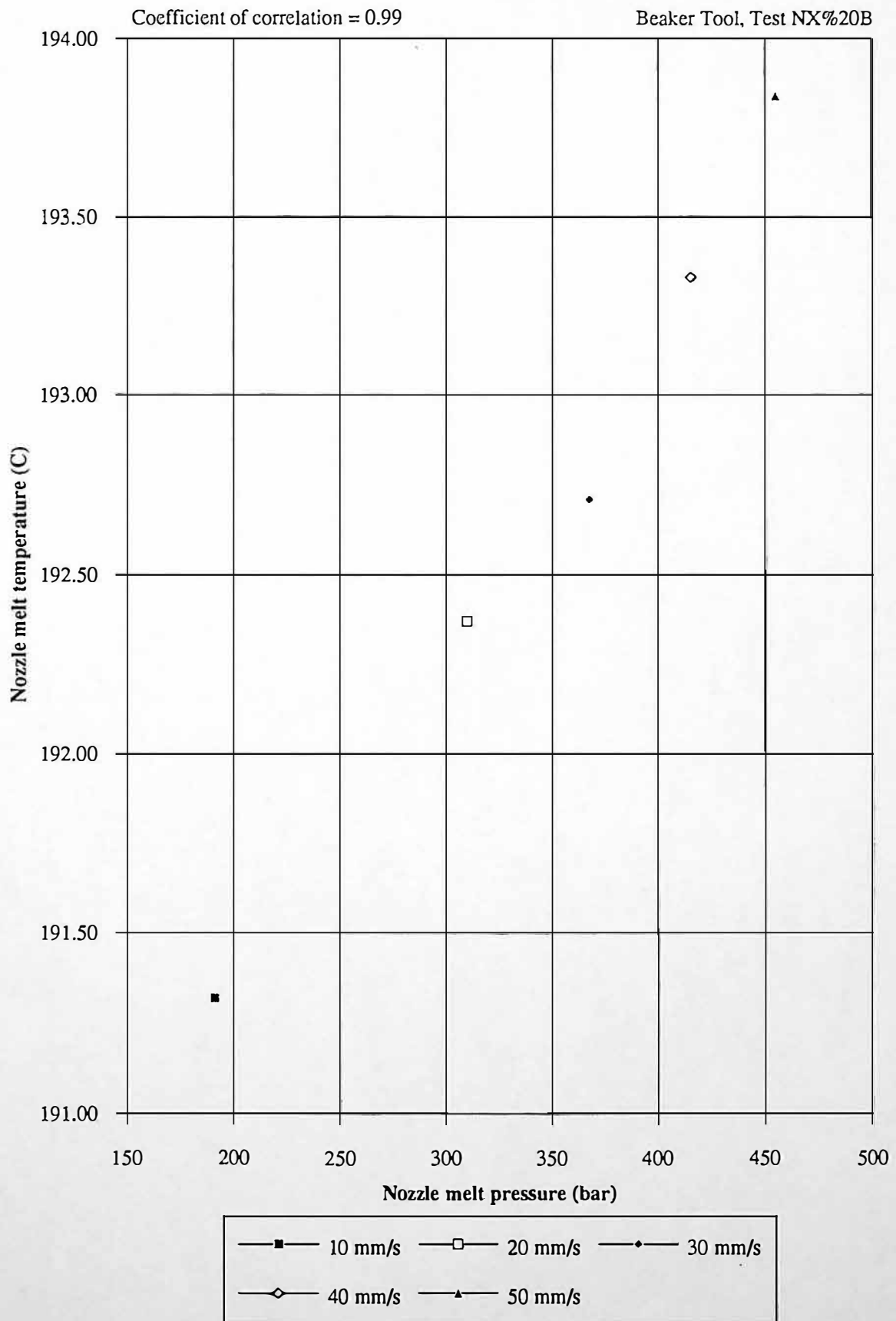


Figure 9.27 Relationship between nozzle melt pressure and nozzle melt temperature for final screw acceleration point



9.4.3 Relationship Between Nozzle Melt Temperature and Product Quality

Figure 9.28 shows the correlation between product weight (grams) and product height dimension (mm), and table 9.3 summaries the product quality assessments. Figure 9.29 shows the influence of nozzle melt temperature on product quality for periods polymer melt compression. Beaker weight and beaker height both correlate to nozzle melt temperature for periods of polymer melt compression.

	Mean	Standard Deviation	Coefficient of Variation (%)
Product Weight	32.94 grams	0.14 grams	0.43
Product Height	78.04 mm	0.09 mm	0.12

Table 9.3 Product quality assessment, weight and dimension

Figures 9.30 to 9.33 show the correlation of product weight to nozzle melt pressure, screw displacement, screw velocity and nozzle melt temperature. A high degree of correlation between product weight and product height has been described by figure 9.27 (coefficient of correlation = 0.99), therefore figures 9.29 to 9.32 also relate to product dimension (height).

Figure 9.28 Relationship between product weight and product height dimension

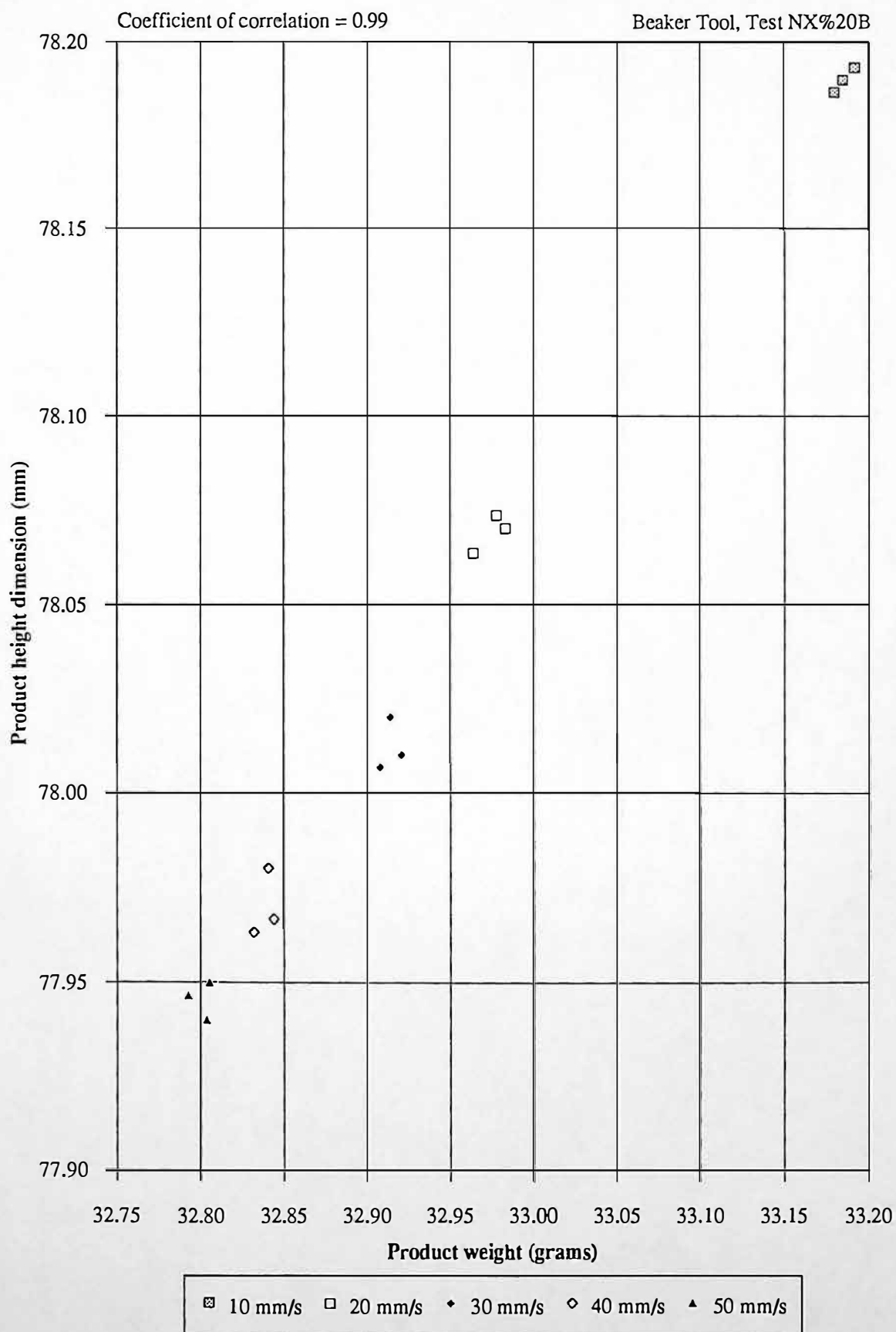


Figure 9.29 Influence of nozzle melt temperature on product quality (weight and height dimension)

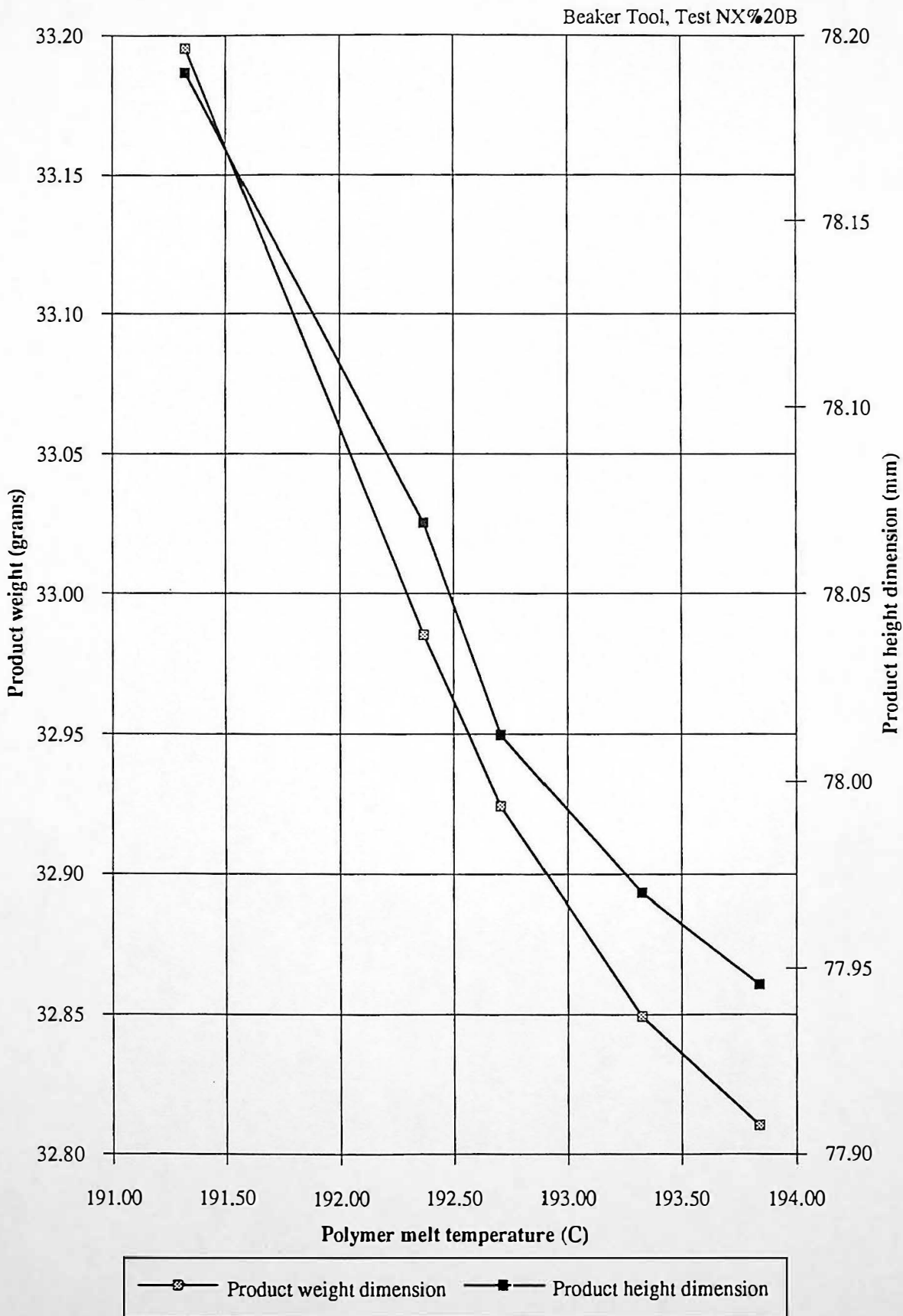


Figure 9.30 Mean nozzle melt pressure and coefficient of correlation between nozzle melt pressure and product weight during primary injection

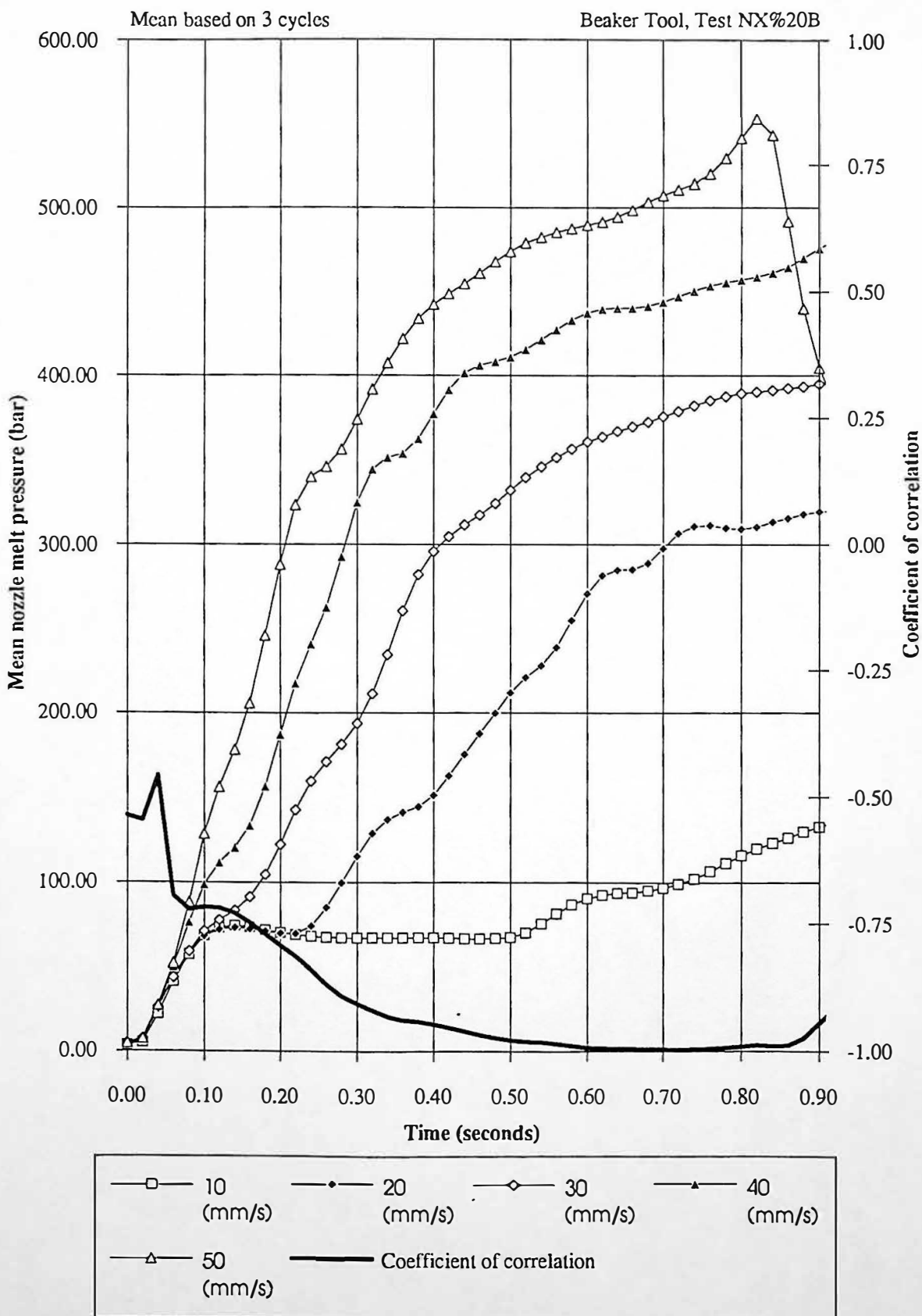


Figure 9.31 Mean screw displacement and coefficient of correlation between screw displacement and product weight during primary injection

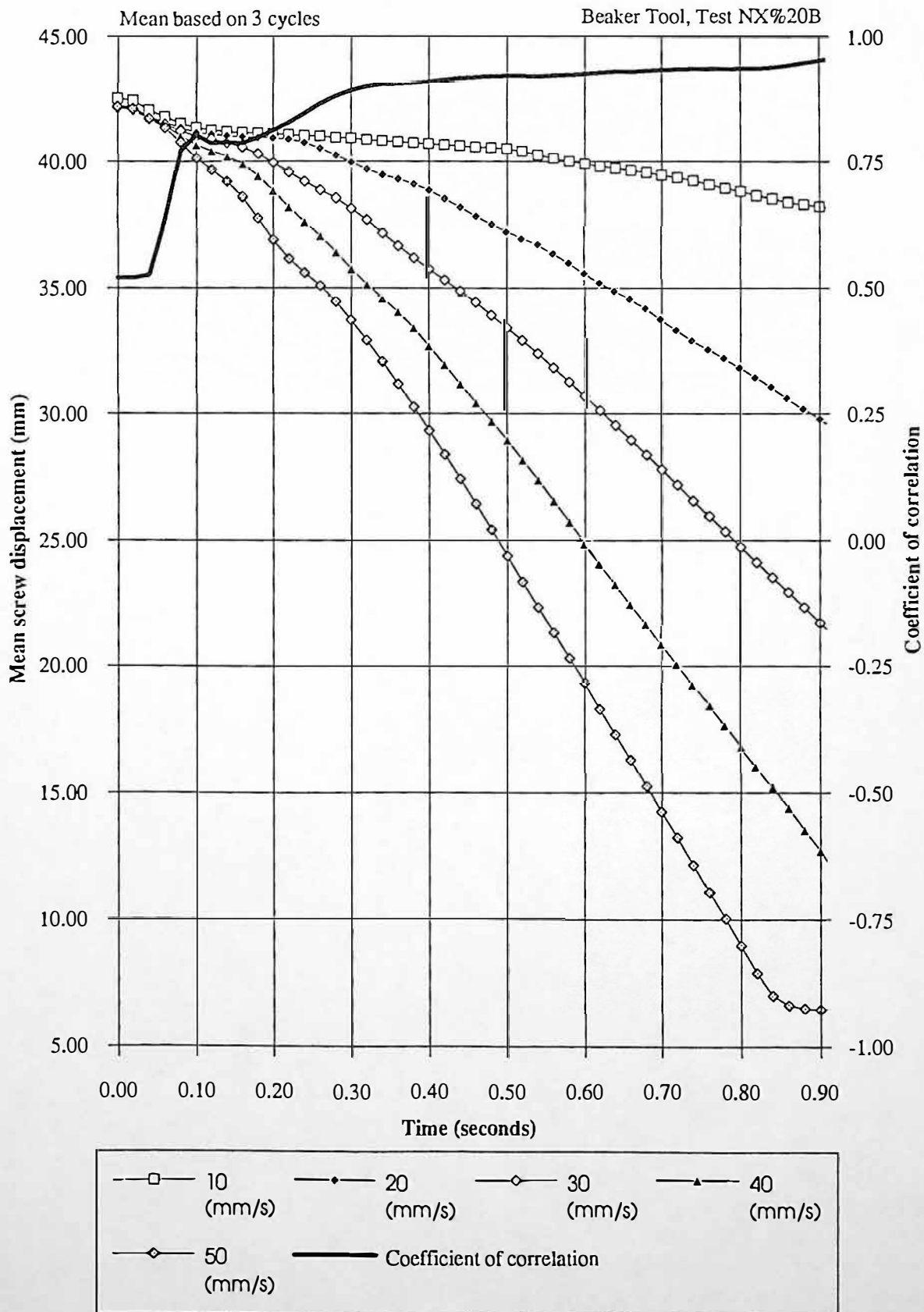


Figure 9.32 Mean screw injection velocity and coefficient of correlation between screw injection velocity and product weight during primary injection

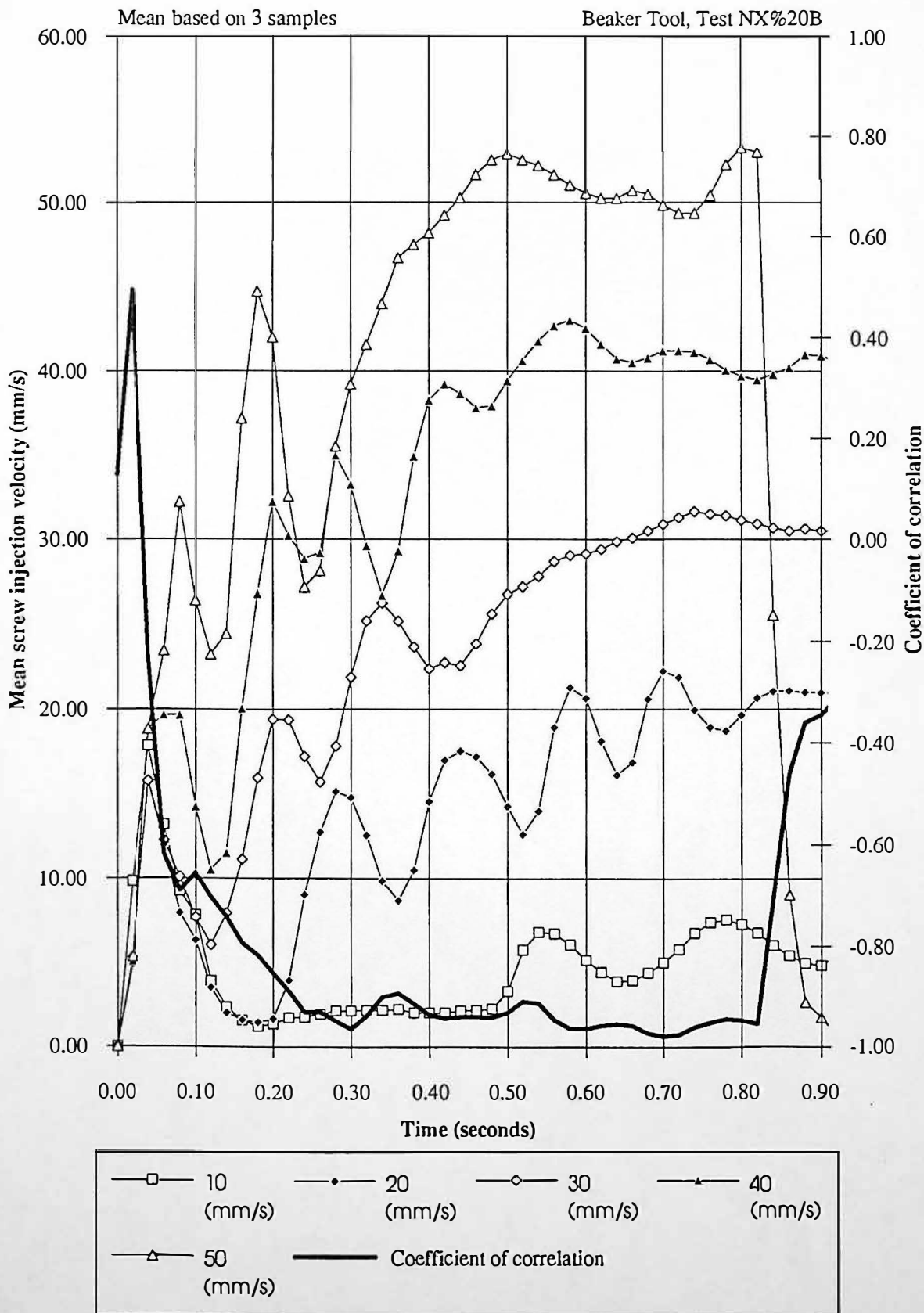
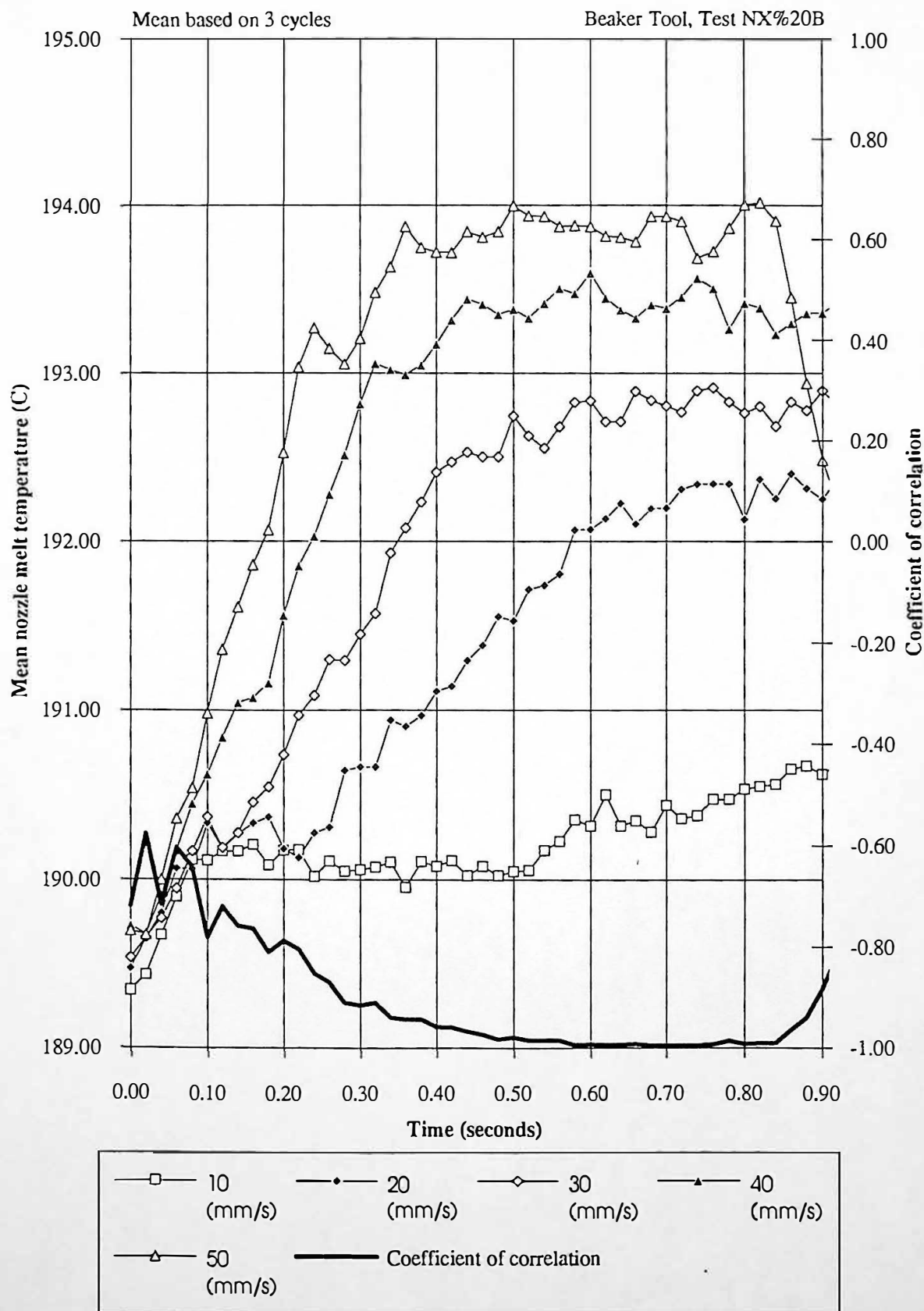


Figure 9.33 Mean nozzle melt temperature and coefficient of correlation between nozzle melt temperature and product weight during primary injection



9.4.4 Comparison of Theoretical and Practical Nozzle Melt Temperature Differentials

An analysis of the pressure and temperature changes yields an assessment of specific heat.

$$C_p = \frac{\Delta P}{\Delta T \times \rho} \Rightarrow \frac{(455.0 \times 10^5 - 191.6 \times 10^5)}{(193.8 - 191.6) \times 750} = 15964 \text{ J/kg/C}$$

The specific heat calculated in section 9.3.4 was 14416 J/kg/C compared to 15964 J/kg/C. The difference is due to test I40%20B and G40%20B utilising high density polyethylene grades HD5226EA and HD5050EA, respectively.

9.4.5 Process Sensitivity

The sensitivity of the influence of nozzle melt pressure variation on nozzle melt temperature follows:

$$\text{Sensitivity} = \frac{(193.8 - 191.3)}{(455.0 - 191.6)} = \frac{2.5}{263.4} = 9.49 \times 10^{-3} \text{ (C/bar)}$$

The sensitivity of the influence of nozzle melt temperature on product weight follows:

$$\text{Sensitivity} = \frac{(33.19 - 32.80)}{(193.8 - 191.3)} = \frac{0.39}{2.5} = 0.156 \text{ (grams / C)}$$

The sensitivity of the influence of nozzle melt temperature on product dimension (height) follows:

$$\text{Sensitivity} = \frac{(78.20 - 77.94)}{(193.8 - 191.3)} = \frac{0.26}{2.5} = 0.104 \text{ (mm / C)}$$

Therefore, the sensitivity of nozzle melt pressure on product weight follows:

$$\text{Sensitivity} = \frac{(33.19 - 32.80)}{(455.0 - 191.6)} = \frac{0.39}{263.4} = 1.48 \times 10^{-3} \text{ (grams / bar)}$$

The sensitivity of nozzle melt pressure on product dimension (height) follows:

$$\text{Sensitivity} = \frac{(78.20 - 77.94)}{(455.0 - 191.6)} = \frac{0.26}{263.4} = 9.87 \times 10^{-4} \text{ (mm / bar)}$$

The results described have strengthened the hypothesis of chapter 9.3, that nozzle melt pressure is proportional to nozzle melt temperature, for periods of polymer melt compressibility during the primary injection phase.

9.5 Discussion of Results

The experimental work reported in this chapter shows the importance of melt temperature on product quality, for typical moulding conditions. The heat transfer rate from polymer melt in the cavity to the adjacent tool is critical to product quality. Figure 9.34 shows the influence of heat transfer rate on product quality.

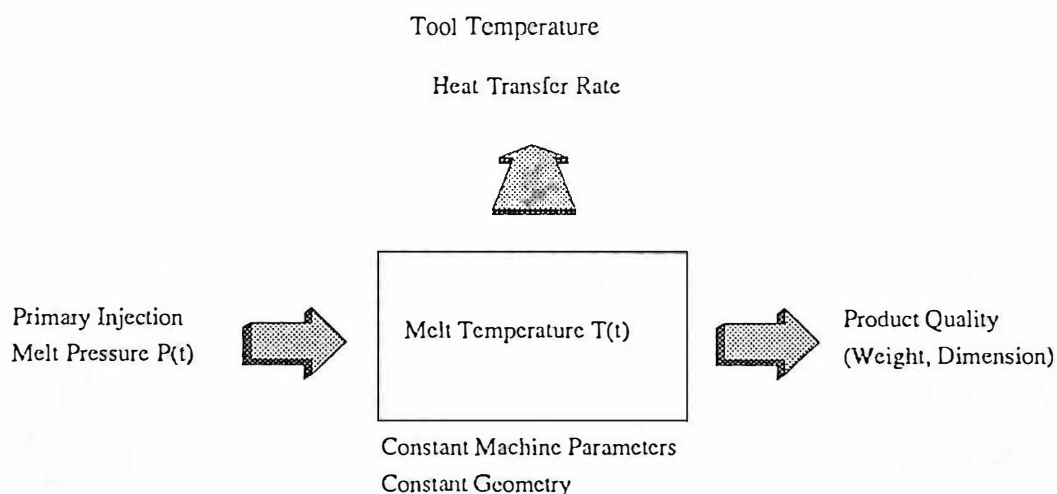


Figure 9.34 Influence of melt temperature on product quality

9.5.1 Influence of Tool Temperature on Product Quality

The experimental work of chapter 9.2 investigates the influence of tool temperature variation on product quality. During typical injection moulding operations, the set tool temperatures were purposefully varied. The changing tool temperature, influenced the heat transfer rate from the polymer melt present in the tool cavity, to the adjacent tool. Therefore, the polymer melt present in the tool cavity, was cooled at different rates, with the varying tool temperature.

The different cooling rates, influences the polymer melt shrinkage rate, for the semi-crystalline HDPE, which influences product density. Product weight and dimensions are determined by polymer melt density, but product density distribution may not be uniform. Product weight reflects the average product density, unlike product dimensions, which may be restricted to specific product features.

9.5.2 Influence of Polymer Melt Viscosity on Product Quality

The experimental work of chapter 9.3 shows that nozzle melt pressure during primary injection, is influenced by material molecular weight (melt shear viscosity) and screw injection velocity (wall shear rate). Nozzle melt pressure is shown to influence nozzle melt temperature for periods of polymer melt compression, i.e. a linear relationship exists between nozzle melt pressure and nozzle melt temperature for periods of polymer melt compression, typical coefficient of correlation = 0.995. Polymer melt compression apparently occurs for periods of screw acceleration for the instrumented container and beaker tools. This relationship can be seen on comparison of screw acceleration and the differential of the ratio of nozzle melt pressure to hydraulic injection pressure. The use of complex tool designs may show that polymer melt compression occurs for time periods longer than the screw acceleration period.

The relationship between nozzle melt pressure and nozzle melt temperature for periods of screw acceleration was established by use of an infra-red melt temperature transducer. The infra-red melt temperature transducer has a time constant of 10 ms, that allows a true reflection of melt temperature process dynamics during primary injection. The mean calculated screw injection velocity for the industrial monitored data described in chapter 8.8, shows screw acceleration during the time period $t = 0.00$ to 0.60 seconds. Figure 8.49 shows the differential of the ratio of nozzle melt pressure to hydraulic injection pressure, indicating that polymer melt compression occurs during the time period $t = 0.00$ to 2.48 seconds.

Figure 9.35 shows a comparison of nozzle melt pressure and nozzle melt temperature, it can be seen that nozzle melt pressure influences nozzle melt temperature for the time period $t=0.00$ to 2.48 seconds. The coefficient of correlation for nozzle melt pressure and nozzle melt temperature for $t=0.00$ to 2.48 seconds = 0.99. The coefficient of correlation for nozzle melt pressure and nozzle melt temperature = 0.80, during the time period $t=2.48$ to 4.10 seconds. It is apparent that screw injection velocity may influence nozzle melt temperature, during the time period $t = 2.48$ to 4.10 seconds.

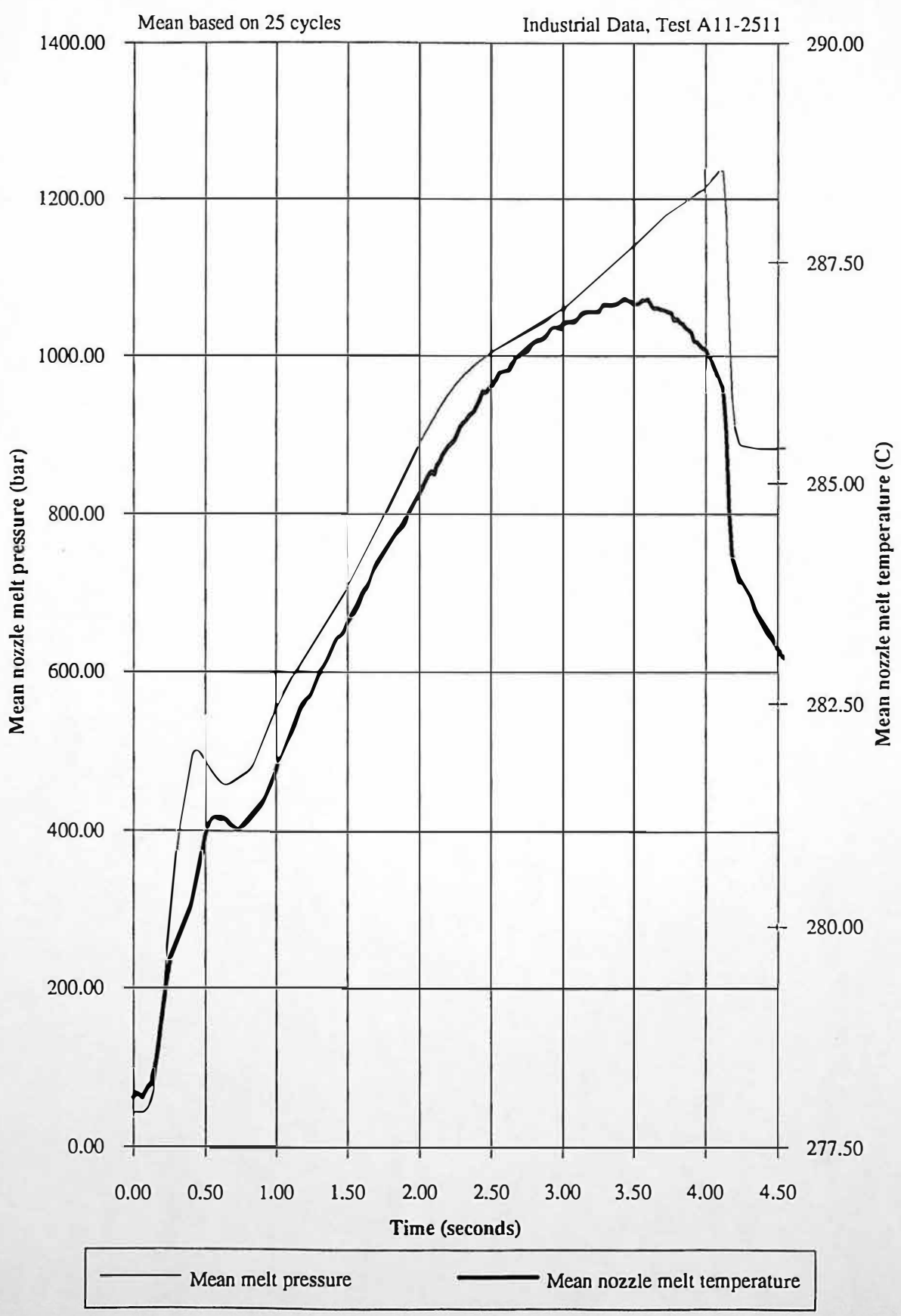
Nozzle melt temperature is an extremely important parameter relating to product quality, influencing the polymer shrinkage rate during primary and packing phases, and influencing the actual operating tool temperature. The rate of polymer melt shrinkage determines the density of the moulded product, a high shrinkage rate results in a high product density, resulting in a high product weight and product dimension (height).

Nozzle melt temperature correlates to nozzle melt temperature, during periods of screw acceleration, typical coefficient of correlation = 0.995. This allows an indirect assessment of nozzle melt temperature to be achieved from nozzle melt pressure and screw acceleration. The resultant process parameter would have a greater degree of accuracy than the melt temperature measurement, due to the greater accuracy of the pressure transducer, as shown in table 9.4.

	Measurement Range	Instrumentation Resolution	Measurement Accuracy
Melt Temperature (Infra-red device)	3.4C	$\pm 0.2C$	$\pm 5.9\%$
Melt Pressure (Diaphragm device)	427 bar	± 0.3 bar	$\pm 0.07\%$

Table 9.4 Melt temperature and pressure measurement accuracy

9.35 Mean nozzle melt pressure and mean nozzle melt temperature during primary injection



The work reported in this chapter has investigated nozzle melt pressure and nozzle melt temperature relationships, for the periods of screw acceleration and polymer melt compression, for the instrumented beaker tool. An assessment of nozzle melt temperature at the end of the polymer melt compression, is used for correlation to product quality, typical coefficient of correlation = - 0.98. The analysis of data from more complex tools, for typical or problematic process conditions may indicate several polymer melt compression zones. The product quality assessment from the infra-red temperature transducer may be determined by summation of the temperature changes, associated with the separate polymer melt compression zones, as shown in equation 9.2.

$$\Delta T = \sum_1^n (\Delta T_1 + \Delta T_2 + \dots + \Delta T_n) \quad \text{Eq. 9.2}$$

9.5.3 Process Sensitivity

It is apparent for periods of screw acceleration and polymer melt compression that nozzle melt pressure influences nozzle melt temperature. Chapters 9.3 and 9.4 have investigated the influence of molecular weight and screw injection velocity on the nozzle melt pressure and nozzle melt temperature relationship. The calculated process sensitivities for molecular weight and screw injection velocity variation are 9.26×10^{-3} (C/bar) and 9.49×10^{-3} (C/bar), which are comparable. Chapter 9.4 investigates process sensitivities relating to product weight and height dimension. The influence of nozzle melt temperature on product weight and height dimension are 0.156 (grams/C) and 0.104 (mm/C), respectively. The influence of nozzle melt pressure sensitivities relating to product height dimension are 1.48×10^{-3} (grams/bar) and 9.86×10^{-4} (mm/bar), respectively.

9.6 Concluding Comments

- Tool temperature and polymer melt temperature for steady moulding conditions influence the heat transfer rate from polymer melt in the cavity to adjacent tool.
- The heat transfer rate from polymer melt in the tool cavity to adjacent tool, determines the polymer melt shrinkage rate, for semi-crystalline materials.
- Nozzle melt pressure influences nozzle melt temperature for periods polymer melt compression, during primary injection.
- Periods of polymer melt compression during primary injection are identified by two analytical methods: (i) analysis of screw acceleration dynamics, and (ii) differentiation of ratio of nozzle melt pressure to hydraulic injection pressure. The second technique is the most precise and reliable.
- Product quality for semi-crystalline materials is primarily determined by the heat transfer rate from polymer melt in the tool cavity to adjacent tool.

CHAPTER 10

Global Discussion of Results

Detailed discussion of results are included in previous chapters 7, 8 and 9

10.1 Introduction

The accuracy and precision of polymer melt viscosity measurements for true process shear and temperature histories was investigated, using in-line and off-line capillary rheometers. A methodology was described for determining an optimum assessment of polymer melt viscosity during typical moulding conditions, in terms of accuracy and precision was investigated. The influence of polymer melt viscosity changes on product quality, during primary injection were investigated. This chapter also describes the influence of the packing phase on product quality, where extensive investigations have been concentrated, but are outside the main body of this work. The work of chapters 7, 8 and 9 describe the concerns necessary for closed loop process control.

10.2 In-line Capillary Rheometry

High density polyethylene (HDPE) and polyoxymethylene (POM) were processed by in-line and off-line capillary rheometry. Two different molecular weight grades of HDPE were processed and three molecular weight grades of POM. In-line and off-line capillary rheometry are both clearly capable of distinguishing between the different molecular weight grades. In-line capillary rheometry is used to process polymer melts with a true process shear and temperature histories.

The power law index 'n' values for both HDPE and POM data are dependant on wall shear rate. Therefore in-line and off-line capillary rheometry techniques may give different 'n' and 'k' values, for different shear rate ranges.

The lower 'n' values for in-line capillary rheometry for HDPE, compared to off-line capillary rheometry, are most likely a result of the pseudoplastic nature of polymer melt for different shear rates. Figure 7.14 shows the relationship between the power law index 'n' and shear rate for off-line capillary rheometry, the relationship is modelled using a second order polynomial.

The POM In-line and off-line capillary rheometry data is comparable for grades 900F and 500, the 100 grade shows that slip at the capillary die wall is most likely occurring.

10.3 Optimum Accuracy and Precision of Polymer Melt Viscosity Measurements

Machine control has improved in recent years, to such an extent that polymer melt viscosity variations have become an apparent processing problem. The significance of polymer melt viscosity variations, depends on the sophistication of the machine control employed and quality of raw materials supplied. To compensate for the material viscosity variations, true closed loop process control is required. The basis of such a control strategy is most likely an accurate and precise measurement of polymer melt viscosity.

10.3.1 Determination of an Optimum Assessment of Polymer Melt Viscosity

Chapter 8 describes the methodology for determining an optimum accuracy and precision of polymer melt rheology, for true process conditions. The methodology has been tested on three injection moulding machine technologies; (i) hydraulic

Sandretto 60 tonne machine, using Logiflux screw velocity control (ii) hydraulic Stork 440 tonne machine, using a Moog valve, and (iii) all electric Cincinnati Milacron ACT30 30 tonne machine, using AC servo motor control. The use of accurate instrumentation results in comparable precision for nozzle melt and hydraulic injection pressure measurements, typically $\pm 0.3\%$ (based on a ± 3 standard deviation from the mean).

10.3.2 Importance of Screw Velocity Control

Results from chapter 8.6 show that periods of low pressure variation are due to periods of steady velocity control. The quality of screw velocity control directly influences the period of pressure variation, during primary injection, as shown in figure 8.51.

10.4 Influence of Polymer Melt Viscosity on Product Quality

The experimental work reported in chapter 9 shows the importance of polymer melt temperature on product quality, for typical moulding conditions. The heat transfer rate from polymer melt in the cavity to the adjacent tool is critical to product quality. Figure 9.33 shows the influence of heat transfer rate on product quality.

Experimental work shows that changing tool temperature, influenced the heat transfer rate from the polymer melt present in the tool cavity, to the adjacent tool. Therefore, the polymer melt present in the tool cavity, was cooled at different rates, with the varying tool temperature.

The different cooling rates, influences the polymer melt shrinkage rate, for the semi-crystalline HDPE, which influences product density. Product weight and dimensions are determined by polymer melt density, but product density distribution may not be

uniform. Product weight reflects the average product density, unlike product dimensions, which may be restricted to specific product features.

The experimental work of chapter 9.3 shows that nozzle melt pressure during primary injection, is influenced by polymer melt viscosity and screw injection velocity, due to the polymer melt viscosity variation. Nozzle melt pressure is shown to influence nozzle melt temperature for periods of polymer melt compression, i.e. a linear relationship exists between nozzle melt pressure and nozzle melt temperature for periods of polymer melt compression, typical coefficient of correlation = 0.995

The work reported in this chapter has investigated nozzle melt pressure and nozzle melt temperature relationships, for the periods of screw acceleration, for the instrumented container and beaker tools (see chapter 4.3 and 4.5). An assessment of nozzle melt temperature at the end of the polymer melt compression, is used for correlation to product quality, typical coefficient of correlation = -0.98. The analysis of data from more complex tools, for typical or problematic process conditions may indicate several polymer melt compression zones. The product quality assessment from the infra red temperature transducers may be determined by the summation of the temperature changes, associated with the polymer melt compression zones, as shown in equation 9.1.

10.5 Influence of Packing Phase on Product Quality

The packing phase of the injection moulding process has a strong influence on product quality. Specific packing phase process parameters are excellent indicators of the performance of the primary injection filling phase. Screw relaxation periods during the packing phase have a strong influence on product quality. Experimental moulding tests using semi-crystalline materials have been carefully analysed, with current investigations using amorphous polymers, Acrylonite Butadiene Styrene (ABS) and

Poly(methyl-methacrylate). Experimental results from test G-5050B2 are presented whereby HDPE Rigidex grade HD5050EA was processed for 25 injection moulding cycles. Figures 10.1 and 10.2 show the correlation between screw displacement and product weight and nozzle melt pressure and product weight, respectively. It is apparent from figures 10.1 and 10.2 that periods of screw relaxation correlate with a high degree to product weight, coefficient of correlation = -0.97. Figure 10.3 shows the correlation between screw packing displacement and product weight. A high correlation between packing displacement and product weight depends on a slight over-packing of the tool cavity. The slight over-packing of the tool cavity may introduce residual stresses in the moulded components, but is necessary to produce a screw relaxation period after switch-over.

10.6 Injection Moulding Closed Loop Process Control

The experimental work described in chapters 7, 8, and 9 provides the necessary information for development of closed loop process control strategies. It is envisaged that controllers of varying complexity be developed. The basis of such control strategies is most likely an accurate and precise measurement of polymer melt viscosity. The work of chapters 8 has described methods for optimising polymer melt viscosity measurements. Chapter 9 describes the influence of polymer melt pressure on melt temperature during primary injection, and the resultant influence on product quality. Three levels of polymer melt viscosity assessment are proposed based on the work of chapters 7, 8 and 9, as shown in figure 10.4.

This first level of melt viscosity assessment (mode 1) is shown in figure 10.4 a. Hydraulic injection pressure is measured to form a relative assessment of melt viscosity. Screw displacement is measured using a LVDT, it is proposed to derive screw velocity and acceleration by analogue differentiation of the screw displacement measurement. The control strategy would use a hydraulic injection pressure integral.

The integration period would be derived by trend analysis, cycle to cycle, combined with knowledge screw injection dynamics, indicating polymer melt compression. Hydraulic injection pressure at the instant set injection velocity is reached is used as a product quality indicator.

An intermediate level of polymer melt viscosity assessment (mode 2) is shown in figure 10.4 b. This level of polymer melt viscosity assessment offers the following benefits, in addition to those of mode 1 operation: (i) an absolute assessment of polymer melt viscosity, based on nozzle melt pressure, (ii) the differentiated ratio of nozzle melt pressure to hydraulic injection pressure is a more reliable assessment of polymer melt compression, for complex tools, than screw injection dynamics, and (iii) nozzle melt pressure at the instant set injection velocity is reached is used as a product quality indicator.

The more sophisticated technique for polymer melt viscosity assessment (mode 3) is shown in figure 10.4 c. This level for polymer melt viscosity assessment offers the benefit of an infra-red melt temperature transducer, in addition to those of modes 1 and 2 operation. An infra red melt temperature transducer is used to measure melt temperature during primary injection. Nozzle melt temperature at the instant set injection velocity is reached is used as a product quality indicator. The variations of melt temperature during and after polymer melt compression are used as a performance indicator for the injection unit, which ultimately influences product quality.

Figure 10.1 Mean screw displacement and coefficient of correlation between screw displacement and product weight for periods of screw relaxation

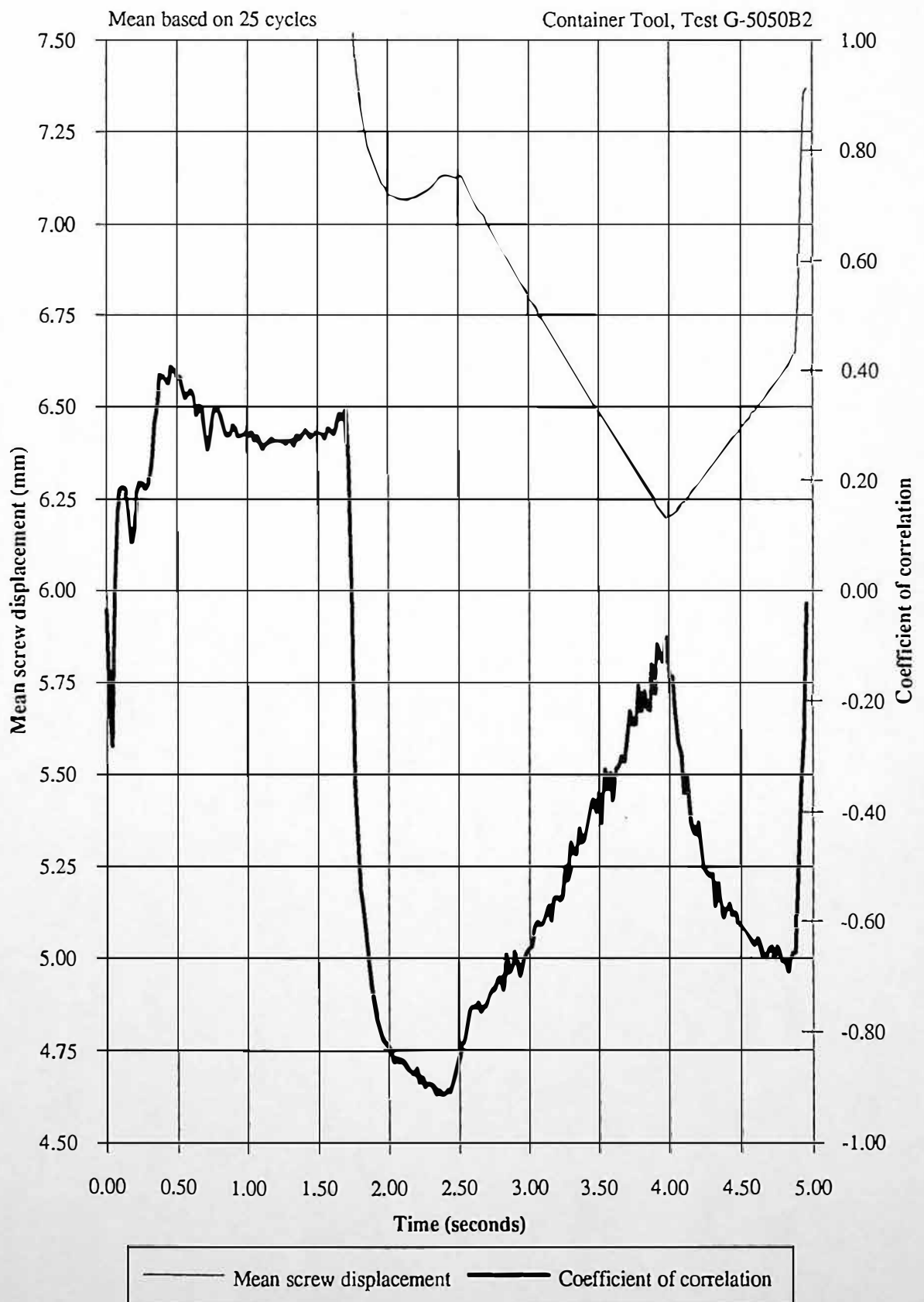


Figure 10.2 Mean nozzle melt pressure and coefficient of correlation between nozzle melt pressure and product weight for periods of screw relaxation.

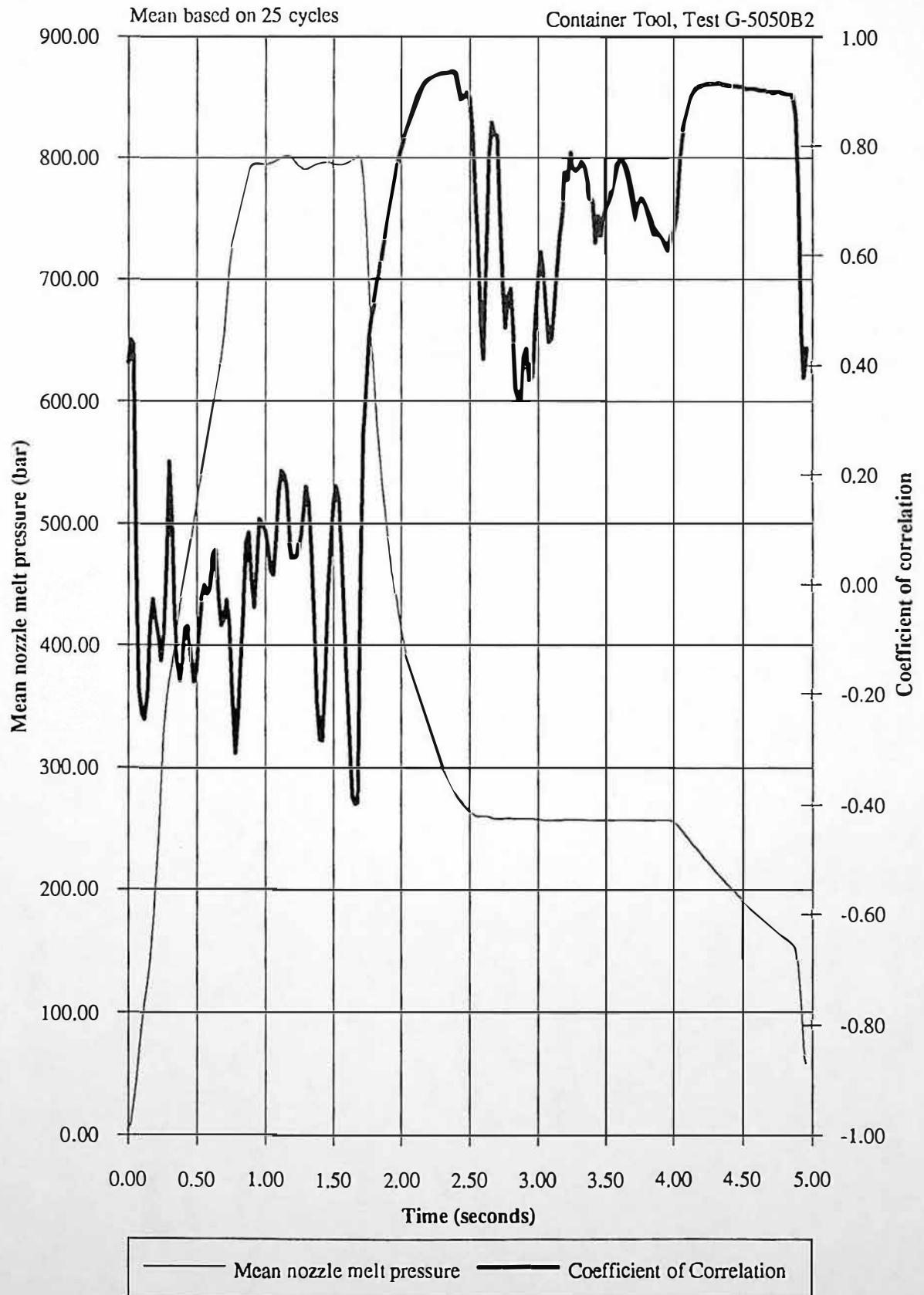
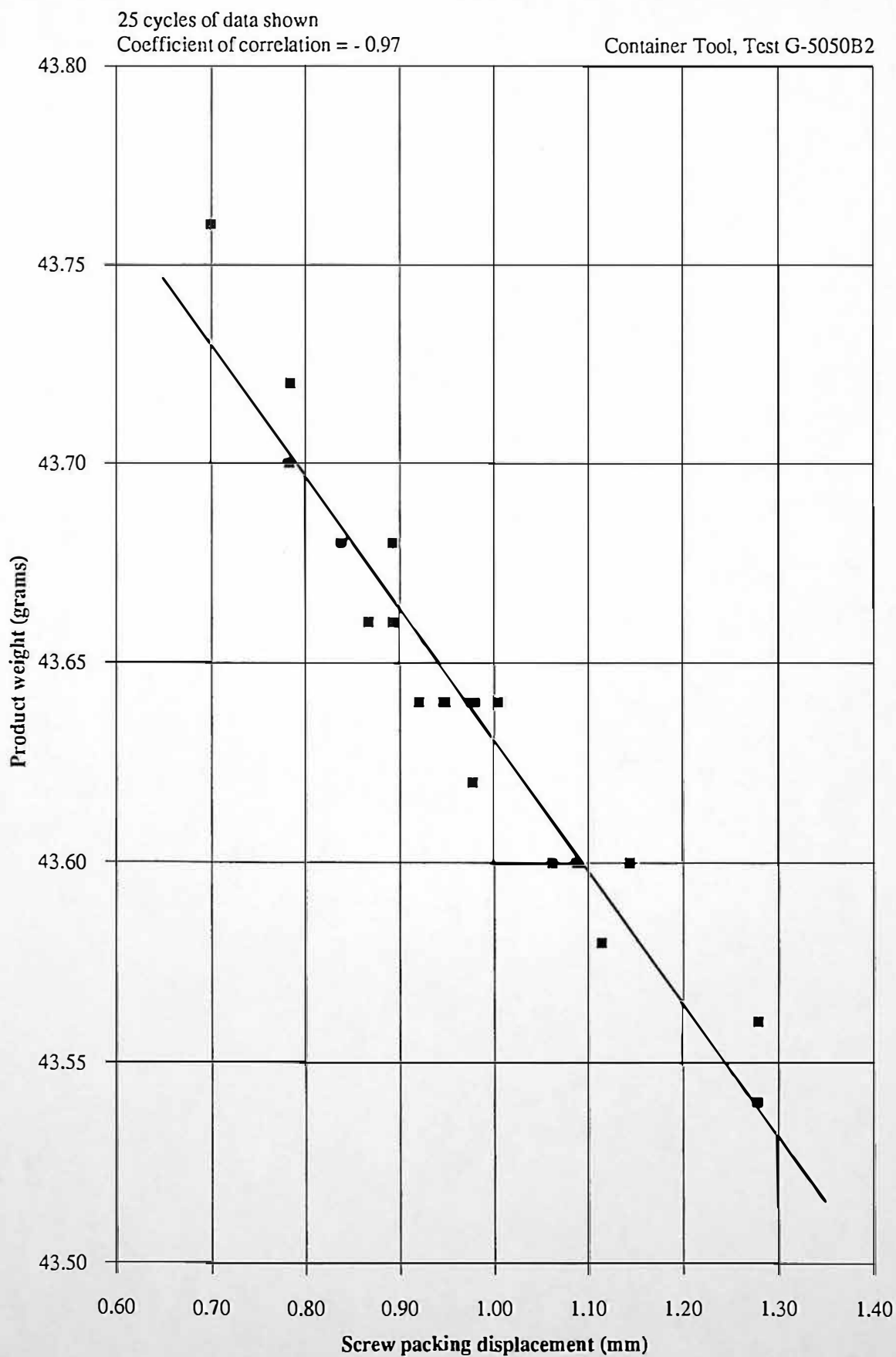


Figure 10.3 Correlation between screw packing displacement and product weight



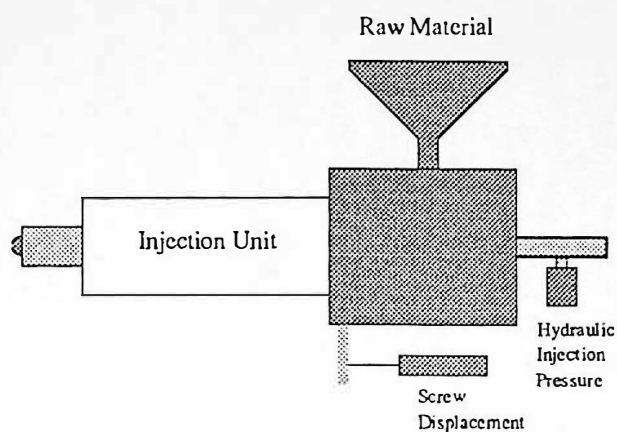


Figure 10.4 a Process control based on hydraulic injection pressure and screw displacement (mode 1)

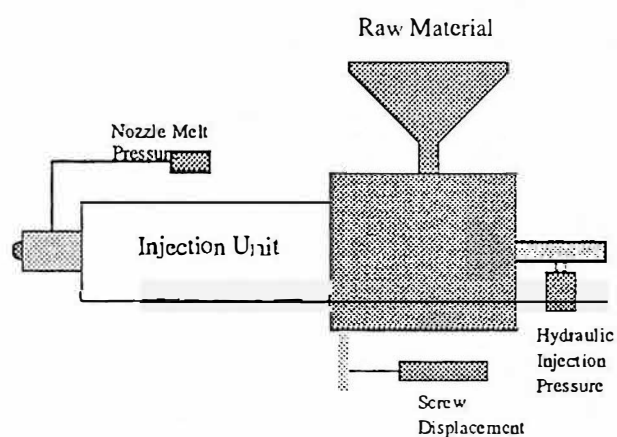


Figure 10.4 b Process control based on nozzle melt pressure, hydraulic injection pressure and screw displacement (mode 2)

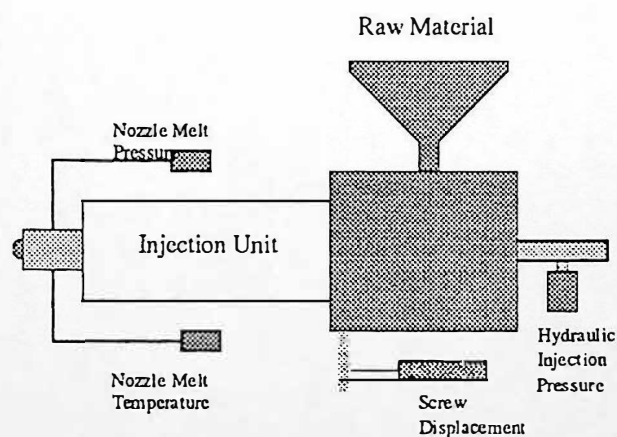


Figure 10.4 c Process control based on nozzle melt pressure, nozzle melt temperature and hydraulic injection pressure and screw displacement (mode 3)

Figure 10.4 Polymer melt viscosity assessment techniques for injection moulding closed loop process control

CHAPTER 11

Conclusions and Recommendations for Future Work

Concluding comments are included in previous chapter 7, 8 and 9

11.1 Conclusions

- An in-line modular nozzle rheometer and instrumented single impression beaker tool have been successfully, designed, constructed and tested. The in-line modular nozzle rheometer provides accurate and precise rheological and process information for polymer melts.

11.1.1 In-line Capillary Rheometry

- In-line and off-line capillary rheometry techniques are both clearly capable of distinguishing between different molecular weight grades of high density polyethylene (HDPE) and polyoxymethylene (POM).
- Significantly different results may be obtained from in-line capillary rheometry, compared to off-line capillary rheometry, for polymer melts, due to different shear rate ranges investigated.
- In-line capillary rheometry shows that distinguishing between different molecular weight grades of semi-crystalline materials was more effective before correction of pressure data (Bagley and Rabinowitsch corrections). Therefore, single nozzle melt pressure transducer provides an assessment of polymer melt viscosity necessary for closed loop process control.

11.1.2 In-line Nozzle Rheometry and Process Measurements in Injection Moulding

- The use of high accuracy instrumentation combined with a precisely timed machine and process variable monitoring system, allows an accurate and precise assessment of polymer melt viscosity, for typical injection moulding conditions. The assessment of polymer viscosity is achieved by integration of nozzle melt pressure and hydraulic injection pressure profiles, for a specific time period.
- Two procedures are presented that allow an optimum nozzle melt pressure integral to be identified: (i) identification of periods of steady screw velocity during primary injection phase, i.e. periods of low screw acceleration, and (ii) differentiation of the ratio between nozzle melt pressure and hydraulic injection pressure during primary injection phase. These procedures would form the basis of an algorithm to determine where to integrate nozzle melt pressure and hydraulic injection profiles.
- Nozzle melt pressure integrals were able to distinguish between two different batches of the same molecular weight grade polyoxymethylene. A measurement accuracy of $\pm 0.3\%$ was achieved, based on a ± 3 standard deviation distribution about the mean.
- Techniques for optimising polymer melt viscosity assessment have been tested on three different technology injection moulding machines, Sandretto 60 tonne, Stork 440 tonne and a Cincinnati Milacron ACT30 30 tonne machine.

11.1.3 Influence of Process Parameter Variations on Product Quality

- Tool temperature and polymer melt temperature for steady moulding conditions influence the heat transfer rate from polymer melt in the cavity to adjacent tool.
- The heat transfer rate from polymer melt in the tool cavity to adjacent tool, determines the polymer melt shrinkage rate, for semi-crystalline materials.
- Nozzle melt pressure influences nozzle melt temperature for periods polymer melt compression, during primary injection.
- Periods of polymer melt compression during primary injection are identified by two analytical methods: (i) analysis of screw acceleration dynamics, and (ii) differentiation of ratio of nozzle melt pressure to hydraulic injection pressure. The second technique is the most precise and reliable.
- Product quality for semi-crystalline materials is primarily determined by the heat transfer rate from polymer melt in the tool cavity to adjacent tool.

11.2 Recommendations for Future Work

11.2.1 Implementation of Closed Loop Process Control

The development of a closed loop process control strategy for semi-crystalline High density polyethylene (HDPE) is proposed. Experimental work of chapters 7, 8 and 9 will form the basis for the control algorithm. The control system will need to be capable of compensating for molecular weight variation of HDPE, by maintaining a specified tolerance on product quality (weight and specific dimensions).

The Injection and plasticisation phases need to be monitored throughout the experimental tests of any control algorithms. Therefore it is proposed to use a third personal computer and modular interface unit, Microlink 3000 intelligent data acquisition and control system, Biodata (1991) for implementation of the control strategy.

Various control strategies will be implemented based on:

- (1) Measurement of polymer melt temperature using an infra red device and tool temperature near the cavity.
- (2) Measurement of polymer melt pressure and screw acceleration (derived by differentiating screw velocity).
- (3) Measurement of hydraulic injection pressure and screw acceleration (derived by differentiating screw velocity).
- (4) Measurement of polymer melt pressure and the differential of the ratio of nozzle melt pressure to hydraulic injection pressure.

The work of chapter 8 will be used to determine an optimum assessment of polymer melt viscosity. This assessment in the form of a specific pressure integral will form the feedback to the control algorithm, indicating any relative melt viscosity variation.

The work of chapter 9 shows the influence of melt temperature and tool temperature on product quality. The conclusions state that polymer melt pressure influences polymer melt pressure for periods of screw acceleration where polymer melt is being compressed.

The control actions will manipulate the polymer melt temperature or heat transfer rate from product to the tool, depending on the magnitude of polymer melt viscosity variation. It is envisaged that plasticising back pressure, injection velocity and tool temperature will form the control action parameters. These parameters are readily controlled and quantifiable. Control of the barrel temperature zones is not desirable unless barrel zones are heated and cooled.

11.2.2 Modular Nozzle Rheometer Design

The presence of instrumentation located directly in the polymer melt may induce disturbances, i.e. vortices. Polymer melt transducers are present for both in-line and off-line capillary rheometry, so disturbances will be present in both. In-line nozzle rheometry utilised four transducers in the reservoir bore, compared to one for off-line rheometry, so in-line nozzle rheometry may cause a larger disturbance. Problems of disturbance to polymer melt in the reservoir bore caused by transducers can be eliminated: (i) the in-line nozzle rheometer can be designed to incorporate a flat section to accommodate the transducers, and (ii) the in-line transducers can be profiled to complement the reservoir bore. The latter option provides a solution that minimises disturbance to the nozzle geometry. Infra-red melt temperature transducers can be

profiled to the reservoir bore. The recent development of an optical pressure transducer, may allow a profiled diaphragm device to be designed. Figure 11.1 shows a schematic diagram of a cross section through such a proposed reservoir bore.

Problems are likely to be encountered with the isometric design, either screw threads need to be precise, copper shims need to be used or a locking device implemented.

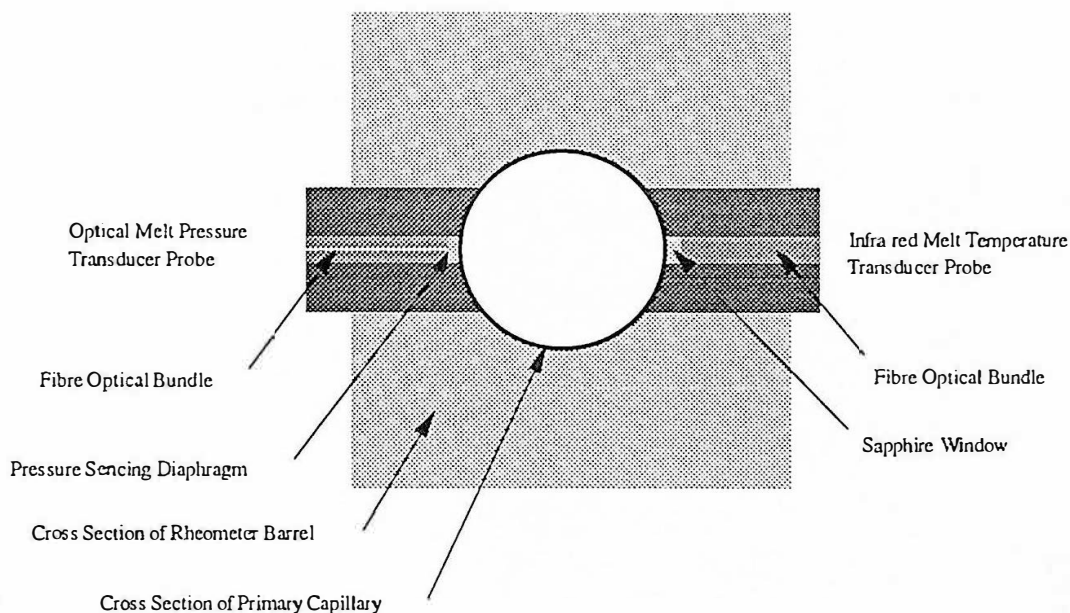


Figure 11.1 Proposed cross section of reservoir bore using optical melt pressure and temperature transducers

Melt temperature is a critical process parameter for influencing product quality (weight and dimensions). Infra-red temperature transducers provide a dynamic measurement of melt shear heating effects, during typical moulding conditions. The present level of technology provides a type J calibration thermocouple output, 0 to 10 Volt, 4 to 20 mA and 0 to 300 mV (corresponding to 0 to 300C) outputs. The accuracy provided by the type J calibration thermocouple output was $\pm 0.2C$, for the experimental work reported. Current developments are investigating the calibration of the 0 to 300 mV output using an offset, for a given ΔT range.

11.2.3 In-Line Capillary Rheometry

The work of chapter 7 has utilised essentially the same die geometries for in-line and off-line capillary rheometry, the only difference being the short die capillary length (see chapter 7.3). The apparent wall shear rate range of the in-line rheometer is determined by the radius of the capillary dies used. Figure 11.2 shows the effective apparent wall shear rate range for different capillary die radii. A capillary die with radius 2.25 mm gives an effective apparent wall shear rate range of 421 to 13906 sec^{-1} , this being nearest to that of the Rosand off-line rheometer with capillary radius of 0.5 mm.

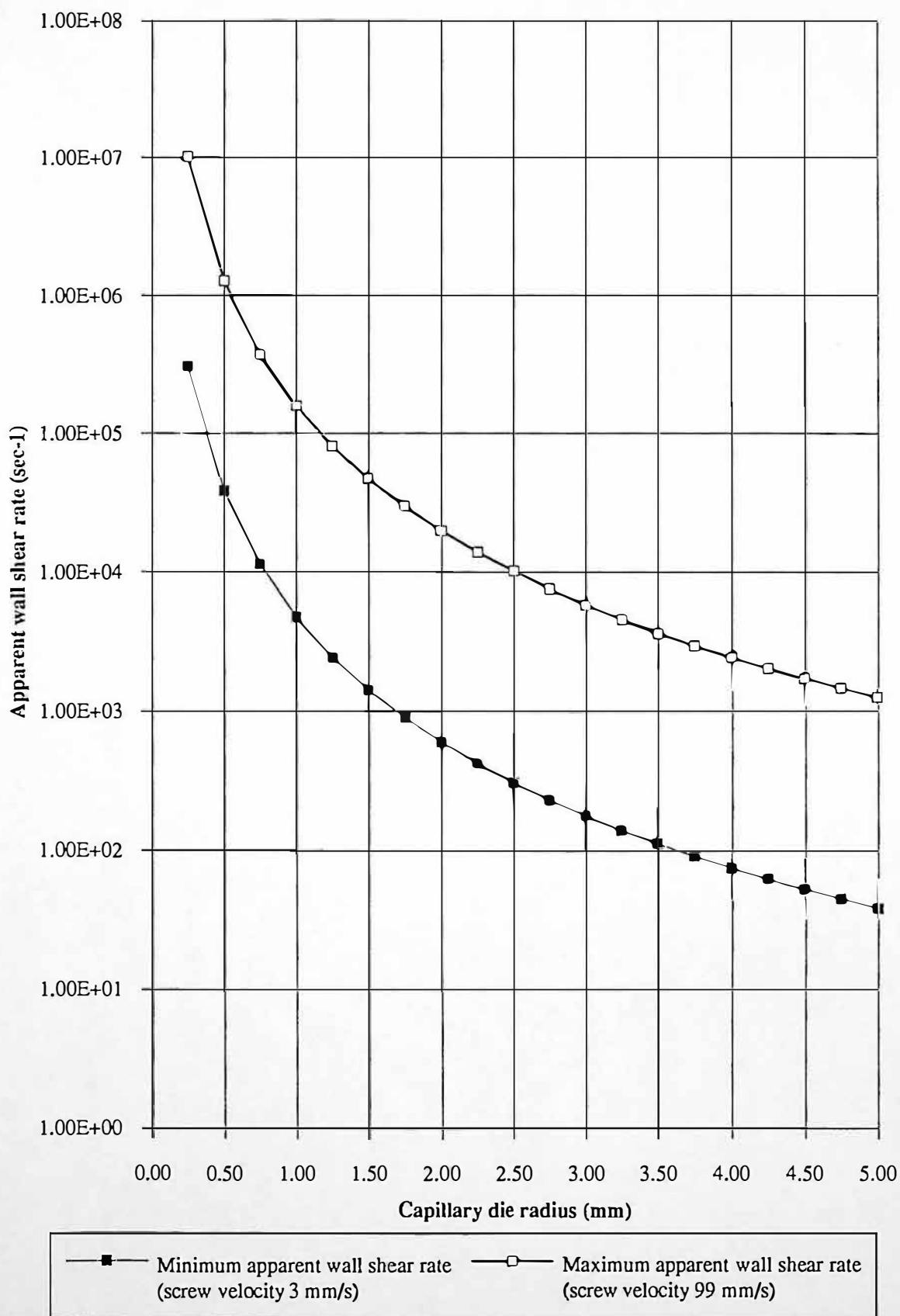
11.2.4 Utilisation of Instrumented Beaker Tool

It is proposed to investigate switch-over from velocity controlled primary injection to pressure controlled packing and holding phases. The use of pressure switch over will be assessed, regarding polymer melt viscosity variation. It is also proposed to utilise the beaker tool for modelling of the polymer melt rheology, as the beaker is essentially a centre gated disc.

11.2.5 Design of a Flexible Cartridge Insert Tool

It is proposed to design and construct a cartridge insert tool that will allow easy change of cavity geometries. This tool will allow the developed closed loop process control strategies to be tested for a range of cavity geometries. The cavity inserts and tool halves will be temperature controlled. An example of an cartridge insert would be for a range of dumbbell mouldings, of variable thickness. This would provide test specimens for tensile testing, to investigate the mechanical properties of mouldings, Coates et al (1993) describe the use of image analysis techniques.

Figure 11.2 Dependence of apparent wall shear rate on capillary die radius



11.2.6 Influence of Process Variation on Product Quality for Amorphous Materials

The work of chapter 9 describes the influence of process variation on product quality for semi-crystalline materials. Semi-crystalline materials generally have a higher shrinkage than amorphous materials, Morton-Jones (1989 p 166), therefore the influence of tool temperature and melt temperature variation for amorphous materials on product quality needs further investigation. Chapter 9 reports that tool temperature and melt temperature influence the heat transfer rate from polymer melt in the cavity to the adjacent tool, whereby the rate of heat transfer directly influences product quality. The experimental work of chapters 9.2 and 9.4, repeated for amorphous materials, or a range of well defined shrinkage polymers, would provide invaluable processing knowledge. Investigations may show for materials of low shrinkage, the importance of other process parameters.

REFERENCES

- Allen P S, Bevis M (1989), New opportunities for the injection moulding process, Proc. 3rd Int. Conf. Polymer Processing Machinery, University of Bradford, UK, 15/1-5, PRI London
- Ali A (1979), Design and manufacture of heat pipes and their application to plastics extruders, PhD thesis, Department in Mechanical and Manufacturing Engineering, University of Bradford
- Ames K (1984), Hydraulic Circuit Design for Micro-Processors Controls on Injection Moulding Machines, SPE ANTEC Tech. Papers, 42, p 792
- Austin C (1987), Flow Algorithms, SPE ANTEC Tech. Papers, 49, p 255
- Bader C, Diez M, Kaiser W (1991), Rheological measurements on the injection moulding machine (aspects of the development of a process monitoring system), Kunststoffe German Plastics 81 3/24-26
- Baker F S, Carter R E, Shales R W (1990), A new environmentally friendly high accuracy melt pressure transducer, Carter Baker Enterprises Ltd, and Francis Shaw and Company Ltd
- Baker W E, Rudin A, Schreiber H P and El-kind M (1993), The effect of processing on rheological and molecular characteristics of a low density polyethylene, Polymer Engineering and Science, Mid-April, Vol. 33, No. 7
- Bakir M A, Marshall D E (1980), Injection Moulding, 16/1-10, Loughborough University of Technology, UK, PRI London
- Barron W R (1990), Fibre-Optic Infrared Thermometry, creating the optimum fibre-optic infra-red temperature sensing system. Sensors, The Journal of Machine Perception, Volume 7, Number 10, September
- BASF Materials data sheet (1982), Review of mathematical design models for thermoplastic machine parts, 82607 July
- Battenfeld (1991), Unilog TC 40, information brochure
- Bernardo C A, Cunha A M and Oliveira M J (1993), The Effect of Fibre Degradation on the Properties of Recycled Polycarbonate, Polymer Processing Society IX Annual Conference, Manchester, 7th April
- Bernhardt E C and Bertacchi G (1984), Applying Computer Aided Engineering (CAE) to Analyse the Interaction of Material Selection, Part Performance, and Part Cost, SPE ANTEC Tech. Papers, 49, p 803
- Bernhardt E C and Bertacchi G (1987), Computer Integrated Injection Moulding (CIIM) Linking Process Simulation with Machine Settings, SPE ANTEC Tech. Papers, 45, p 273
- Bernhardt E C and Bertacchi G (1991), Expert System for Moulding Trouble-Shooting, SPE ANTEC Tech. Papers, 49, p 436
- Binding D M (1988), An Approximate Analysis for Contraction and Converging Flows, Journal of Non-Newtonian Fluid Mechanics, 27, p 173
- Biodata (1990), Microlink Hardware User Manual, Manual Code : MH-M2.03, Copyright Biodata Ltd, January
- Biodata (1991), Microlink Hardware User Manual, Manual Code : M3000-M2.03, Copyright Biodata Ltd, Issue date : May 91

Bonner J G (1991), A study of geometry effect on the flow of melt through extrusion dies, University of Bradford, Department of Mechanical and Manufacturing Engineering, IRC in Polymer Science and Technology, BP Chemicals

British Technology Group (1984), Shear Controlled Orientation Injection Moulding (SCORIM), Patents

Brito A M, Cunha A M, Pouzada A S, Crawford R J (1991), Predicting the skin-core boundary location in injection mouldings, Intern. Polymer Processing VI 4, p 370

Brydson J A (1981), Flow Properties of Polymer Melts, Second Edition, Godwin

Bullen J T (1983), Degree Final Year: Major Project Dissertation, An Analysis of the pressure drop which can be attributed to the gate area in an injection moulding process. Department in Mechanical and Manufacturing Engineering, University of Bradford

Byam J D, Colbert G P (1980), An integrated approach to efficient polymer processing, Proc. Int. Conf. Practical Rheology In Polymer Processing, 1/1-12, Loughborough University of Technology, UK, PRI London

Canovi N (1989), Injection unit: experiences and developments. Sandretto Monographic seminars, Messe Congress Centre, Dusseldorf, November 6th

Carr J J (1991), Microprocessor Interfacing. A Practical Guide for Technicians, Engineers, and Scientists. Prentice-Hall International, Inc.

Chen B S, Liu W H (1989), Numerical simulation and experimental investigation of injection mould filling with melt solidification, Polymer Engineering and Science, mid-August, Vol. 29, No.15, p 1039

Cheng-Ping Chiu, Jong-Hwei Wei, Ming-Chang Shih (1991a), Adaptive model following control of the mould filling process in an injection moulding machine, Polymer Engineering and Science, Mid-August, Vol. 31, No.15, p 1123

Cheng-Ping Chiu, Ming-Chang Shih, Jong-Hwei Wei (1991b), Dynamic modelling of the mould filling process in an injection moulding machine, Polymer Engineering and Science, Mid-October, Vol. 31, No. 19, p 1417

Churchill (1978), Junior SW/140 Water Circulating Temperature Controller, Catalogue Number: 775/4/78

Coates P D (1989a), In-line rheological measurement for control of polymer processing - towards the intelligent processing machine, Proc. 3rd Int. Conf. Polymer Processing Machinery, University of Bradford, UK, 6/1-8, PRI London

Coates P D, Day A J, Bartlett H, Speight R G, Parminter C (1989b), In-line rheometry for injection moulding control, IRC in Polymer Science and Technology, Mechanical and Manufacturing Engineering, University of Bradford, UK

Coates P D (1991), Analysis and Control of Polymer Processing, IRC in Polymer Science and Technology, Mechanical and Manufacturing Engineering, University of Bradford

Coates P D, Chohan R K, Groves D, Speight R G, Rose R M and Woodhead M (1993), In-line and On-line rheometry in extrusion and injection moulding processing, Polymer Processing Society IX Annual Conference, Manchester, 6th April

Coates P D, Haynes A R and Speight R G (1993), In-line Characterisation of Polymer Deformation in Melt and Solid Phase Processing, I M Ward 65th Birthday Conference, Leeds University, April, submitted to Polymer

Cogswell F N (1981), Polymer Melt Rheology, A Guide for Industrial Practice, First published in Great Britain (1981) by George Godwin Limited in association with The Plastics and Rubber Institute, Copyright F N Cogswell

Collyer A A and Clegg D W (1988), Rheological Measurement, Copyright 1988 Elsevier Applied Science Publishers Ltd.

Cooper B E (1969), Statistic of Experimentalists, Pergamon Press Ltd, Oxford.

Crawford R J (1980), The Influence of Injection Moulding Conditions on the Strength of Flow Weld in Thermoplastic, 15/1-9, Loughborough University of Technology, UK, PRI London

Crawford R J (1985a), Plastics Engineering, Copyright R J Crawford, First edition 1981, Published by Pergamon Press Ltd

Crawford R J (1985b), Plastics and Rubber, engineering design and applications, Mechanical Engineering Publications Ltd, London, Copyright R J Crawford

Davies W (1993), Temperature measurement in injection moulding using infrared technology, Dynisco (UK) Ltd

Dobbie T (1993a), Private Communication, University of Bradford, Department of Mechanical and Manufacturing Engineering, IRC in Polymer Science and Technology, June

Dobbie T (1993b), Private Communication, University of Bradford, Department of Mechanical and Manufacturing Engineering, IRC in Polymer Science and Technology, July

Dontula N, Sukanek P C, Devanathan H, Campbell G A (1991), An experimental and theoretical investigation of transient melt temperature during injection moulding, Polymer Engineering and Science, Mid-December, Vol. 31, No. 23, p 1674

Dynisco (1988), MTT900 Series Infra-red Melt Temperature Transducer, information brochure, Dynisco Inc

Dynisco (1989a), Dynisco MTT900 Series Infra-red Melt Temperature Transducer, Installation and Operation Manual, Dynisco Inc

Dynisco (1989b), Injection Moulding Instrumentation, A guide to process improvement, information brochure, Dynisco Inc

Dynisco (1989c), MTC Melt Pressure Transducer Calibrator, information brochure, Dynisco Inc

Dynisco (1990a), Melt pressure instrumentation for the plastics extrusion process, Dynisco Inc

Dynisco (1990b), Instructions for Dynisco PT 411, PT420 Series, PT435A, PT450A, PT460 Series and PT460XL Melt Pressure Transducers, Dynisco Inc

Dynisco (1992), OPT 700 Series Fibre Optic Melt Pressure Transducer Instruction Manual, Dynisco Inc

Dynisco (1993), Optical melt pressure transducer, Design Products and Applications, Dynisco (UK) Ltd, March, Dynisco Inc

Endveco (1992), Dynamic Instrumentation Catalogue, Endveco Corporation

- European Plastics News (1978), Using Recycled Thermoset Scrap as a Filler in Mouldings, February, p48
- European Plastics News (1979), Developments in Closed Process Control, Bodini G, June, p 49
- European Plastics News (1979), Recycling Moulded XPS, August, p 3
- European Plastics News (1989), Market Report, European Sales Leap by 10% in Record Year, January, p 10
- European Plastics News (1993a), Markets. Recycling Industry Takes a Beating, January, p 10
- European Plastics News (1993b), Control, Melt Temperature Profile Defines Quality Limits, April, p 33
- European Plastics News (1993c), Injection Moulding, Controlled Shear Moulding, May, p 25
- Eurotherm (1975), Temperature Controllers Type 070, 071, Instruction Manual, June
- Fellahi S, Boukobbal S and M'Hala M (1991), Additives as Property Improvers for Recycled Mixed Plastics, SPE ANTEC Tech. Papers, 49, p 2170
- Fenner R T (1979), Principles of Polymer Processing, first published in 1979 by The Macmillan Press Ltd, Copyright Roger T Fenner 1979
- Flaman A A M (1993a), Build-up and relaxation of molecular orientation in injection moulding moulding, Part 1: Formulation, Polymer Engineering and Science, February, Vol. 33, No. 4
- Flaman A A M (1993b), Build-up and Relaxation of molecular orientation in injection moulding. Part 2: Experimental Verification, Polymer Engineering and Science, February, Vol. 33, No. 4
- Fornfeld A and Suchanek H-J (1984), Optical Quality Control in Semi-Finished and Finished Plastic Parts, SPE ANTEC Tech. Papers, 42, p 813
- Friel P (1985), Mould temperature control, Kunststoffe 75 12, p 882
- Friel P (1986), Influence of mould surface temperature control on processing and on the quality of injection mouldings, Kunststoffe 76 1, p 23
- Fritch L W (1987), Velocity-Pressure Transfer and Packing: Use them to Optimise Part Properties, SPE ANTEC Tech. Papers, 45, p 218
- Fujiyama M and Wakino T (1988), Journal of Applied Polymer Science, p 29
- Fujiyama M and Wakino T (1992), Molecular Orientation in injection moulding polypropylene copolymers with ethylene, Molecular orientation and properties, Intern. Polymer Processing VII 1
- Fulcher J (1991), University of Wollongong, Australia, An Introduction to Microcomputer Systems, Architecture and Interfacing, First Published in 1989, Addison-Wesley Publishing Company
- Galskoy A and Wang K K (1978), Measuring Melt Temperatures: Thermocouples or Pyrometers, Plastics Engineering, November
- Gaston A (1932), Heating cylinder design of the injection moulding machine, patent issue.
- Genillard A (1993), Financial Times, Technology, Falling Victim to its own success, Wednesday 27th January, p 16

- Gibson A G (1988), *Converging Dies, Contribution, Rheological Measurements*, Collyer A A and Clegg D W, p 49
- Goff J (1993), *Private Communication*, May
- Groves D, Chohan R K, Coates P D (1993), *Converging Flow Measurements for Injection Moulding*, Polymer Processing Society IX Annual Conference, Manchester, 6th April
- Groves D (1993), *Private Communication*, University of Bradford, Department of Mechanical and Manufacturing Engineering, IRC in Polymer Science and Technology, April
- Han C D (1976), *Polytechnic Institute of New York, Rheology in Polymer Processing*, Academic Press, Inc
- Hansberry J and Vanzetti R (1981), *Fibre Optics, A New Approach to Monitor and Control Process Temperature*, Industrial Heating, May
- Haworth B, Sandilands J, White J R (1980), *Characterisation of injection moulding*, Proc. Int. Conf. Practical Rheology in Polymer Processing, Loughborough University of Technology, UK, 12/1-10, PRI London
- Harland W G, Kantas P, Habipis T (1980), *Orientation in injection moulding*, Proc. Int. Conf. Practical Rheology in Polymer Processing, Loughborough University of Technology, UK, 13/1-7, PRI London
- Harrison G (1977), *Degree Final Year: Major Project Dissertation, Design and Construction of a Two Impression Injection Moulding Tool*, Department in Mechanical and Manufacturing Engineering, Department in Mechanical and Manufacturing Engineering, University of Bradford
- Harry D H (1991), *Injection Moulding Machine Control Algorithms*, SPE ANTEC Tech. Papers, 49, p383
- Hastenburg C H V, Widervanck P C, Leenham A J H and Schennink G G J (1992), *The measurement of thermal stress distributions along the flow path in injection-moulded flat plates*, Polymer Engineering and Science, Mid - April (1992), Vol. 32, No. 7
- Hatzikiriakos S G and Dealy J M (1992a), *Wall Slip of Molten High Density Polyethylenes.II. Capillary Rheometer Studies*, Journal of Rheology 36, p 703
- Hatzikiriakos S G and Dealy J M (1992b), *Role of slip and fracture in the oscillating flow of HDPE in a capillary*, Journal of Rheology 36(5) July p 845
- Hauck C (1988), *Computer aided engineering (CAE) for the design of plastic parts and the optimisation of their processing*, Kunststoffzeitschrift, Plastverarbeiter 39, p 20
- Hayashi H (1984), *Measurement of molten resin temperature by MBC 700 system*, Nireco Corporation
- Heason J (1989), *Developments in Gas Injection Moulding*, Proc. 3rd Int. Conf. Polymer Processing Machinery, University of Bradford, UK, 19/1, PRI London
- Hieber C A, Socha L S, Shen S F, Wang K K and Isayev A I (1981), *Experimental and Simulation for Filling Thin Cavities of Variable Gap Thickness*, SPE ANTEC Tech. Papers, 39, p 759
- Hoven-Nievelstein W B (1985), *The use of computational aids in the design of injection moulds*, Kunststoffzeitschrift 75 12, p 866

- Hsiung C M and Cakmak M (1991), Computer simulations of crystallinity gradients developed in injection moulding of slowly crystallising polymers, *Polymer Engineering and Science*, Mid - October, Vol. 31, No. 19
- Hyatt (1872), U.S. Patent for the first injection moulding machine, U.S. Patent 133, 229
- Hull J B, Langton C M (1992), Identification and Characterisation of Materials using Ultrasound, Patent Application Number PCT/GB3/00017, pending publication
- Hull J B, Langton C M and Jones A R (1992), An Ultrasonic Method for Identifying Polymeric Materials/Components for Reclamation and Recycling, *Proc. IMF (Irish Materials Forum) 8*, Dublin, September
- Hull J B, Langton C M, Barker S and Jones A R (1993), Identification and Characterisation of Materials by Broadband Ultrasonic Attenuation Analysis
- Hunkar D B (1987), On-line Statistical Process Control in Injection Moulding, *SPE ANTEC Tech. Papers*, 45, p 275
- Isayev A I (1983), Orientation development in the injection moulding of amorphous polymers, *Polymer Engineering and Science*, mid-April, Vol.23, No. 5, p 271
- Jan T C and O'Brien K T (1991), Architecture of an Expert System for Injection Moulding Problems, *SPE ANTEC Tech. Papers*, 49, p 439
- Johannaber F (1985), *Injection Mould Machines, A Users Guide*, Second Edition, First Printed 1983, Hanser Publishers, Oxford University Press, New York
- Kalika D S, Denn M M (1987), Wall Slip and Extrudate Distortion in Linear Low-Density Polyethylenes, *Journal of Rheology*, 31, p 815
- Kistler (1990), Measurement instruments for plastics processing, information brochure
- Kona (1990), Kona Bushing for Sprueless Moulding, Kona Corporation
- LaBlanc (1980), Studies of Rubber Processability Using a New Automated Capillary Rheometer, Loughborough University of Technology, UK, 18/1-9, PRI London
- Laun M (1983), Polymer melt rheology in a slit die, *Rheol. Acta* 22, p 171
- Lenk R S (1968), *Plastics Rheology*, Published by MacLaren and Sons
- Litherland C (1989), Developments in automated materials handling, *Proc. 3rd Int. Conf. Polymer Processing Machinery*, 21/1-7, PRI London
- Lupton J M and Regester (1965), Melt Flow of Polyethylene at High Rates, *Polymer Engineering Science*, 5, p 235
- Maher R T and Plant H T (1974), Detection of Transient Melt Temperatures in Injection Moulding, A Technical Feature, Kline G M, Technical Editor, *Modern Plastics*, May
- Malloy R A, Chen S J and Orroth S A (1987), A Study of Injection to Holding Pressure Switch-Over Techniques Based in Time, Position or Pressures, *SPE ANTEC Tech. Papers*, 45, p 225
- Malloy R A (1988), Methods for Determining the Shear Viscosity of Polymer Melts Using the Velocity Controlled Reciprocating Screw Injection Moulding Process, Dissertation, University of Lowell, Massachusetts, USA

- Malloy R A, Chen S J, Orroth S A and Farren P J (1989), Melt Viscosity Measurements using an instrumented injection moulding nozzle, Proc. 3rd Int. Conf. Polymer Processing Machinery, 9/1-12, London PRI
- Manziona L T, Cycle Time in Injection Moulding, SPE ANTEC Tech. Papers, 42, p 805
- Mavridis H and Shroff R N (1992), Temperature dependence of polyolefin melt rheology, Polymer Engineering and Science, Mid-December, Vol. 32, No. 23
- McCrum N G, Buckley C P, Bucknall (1988), Principles of Polymer Engineering, Oxford University Press
- Menges G, Fischer R, Lackner (1992), New and Unconventional methods for recycling mixed plastic scrap, Polymer Processing VII December, p 291
- Morton-Jones D M (1989), Polymer Processing, first published in 1989 by Chapman and Hall Ltd, Copyright 1989 D H Morton Jones
- Mullard Ltd (1971), Applications of Infrared Detectors, Copyright Mullard Ltd
- Nanmac Corporation (1992), Temperature Measurement Handbook, Vol. VII, Thermocouples, RTDs and Accessories
- Nanigian J (1993), Private Communication, March
- Nielsen L E, Polymer Rheology (1977), Copyright by Marcel Dekker, Inc
- Neville A M and Kennedy J B (1964), Basic Statistical Methods, for Engineers and Scientists, First published by International Textbook Company in 1964
- Nguyen K T and Kamal M R (1991), Two-Dimensional Packing Analysis of a Viscoelastic Melt, SPE ANTEC Tech. Papers, 49, p 47
- Nolley E, Barlow J W and Paul R (1980), Mechanical properties of polypropylene - low density polyethylene blends, Polymer Engineering and Science, March, Vol. 20, No. 5
- Opolski S W and Kwon T W (1987), Injection Moulding Cooling System Design, SPE ANTEC Tech. Papers, 45, p 264
- Pandelidis I O and Agrawal A R (1987), Self-Tuning Control of Ram Velocity in Injection Moulding, SPE ANTEC Tech. Papers, 45, p 235
- Patel A C (1980), Capillary Rheometry: A Practical Tool to Characterise Carbon Blacks, 9/1-13, Loughborough University of Technology, UK, PRI London
- Plank H (1991), Cincinnati Milacron, Energy saving concepts in injection moulding, Proc. 4th Int. Conf. Polymer Processing Machinery, 14/1-12, PRI London
- Pye R G W (1983), Injection Mould Design, A Design Manual for the Thermoplastic Industry, Third Edition, First Published 1968, Longman Group Ltd.
- Rees D G (1989), Essential Statistics, second edition, First published by Chapman and Hall in 1989
- Richardson S M, Pearson H J, Pearson J R A (1980), Simulation of injection moulding, Proc. Int. Conf. Practical Rheology In Polymer Processing, Loughborough University of Technology, UK, 2/1-13, PRI London
- Ricketson R C and Wang K K (1987), Injection Moulding Process Control Based on Empirical Models, SPE ANTEC Tech. Papers, 45, p 231

- Rietveld J X and Lai G Y (1993), Measured and Predicted Polymer Melt Temperatures for an IR Pyrometer Viewing a Linear Temperature Gradient, Polymer Processing Society IX Annual Conference, Manchester, 7th April
- Rose R M (1990), Computer control of gelation in uPVC compounding, PhD thesis, Department in Mechanical and Manufacturing Engineering, University of Bradford
- Rose R M (1991), Real time batch monitoring software, Wolfson Research Fellow, Department in Mechanical and Manufacturing Engineering, University of Bradford
- Ross C, Malloy R and Chen S J (1990), Melt Viscosity Monitoring as a Measure of Melt Quality in Injection Moulding, SPE ANTEC Tech. Papers, 48, p 243
- Saiu M, Brucato V, Piccarolo S and Titomanlio G (1992), Injection Moulding of iPP, Intern. Polymer Processing VII 3
- Sandretto (1988), Software Development is the Way Forward to Improve Machine Performance, Br. Plast. Rubber 15, 17-18, 20, 23, October
- Schultz J M (1984), Microstructural aspects of failure in semi-crystalline polymers, Polymer Engineering and Science, July, Vol. 24, No. 10
- Science Research Council (1979), Polymer Engineering Directorate, Injection Moulding and the Applications of Microprocessors, A review of recent developments at Kunststoffe 1979
- Sercer M (1989), Trend regulation of the injection moulding process, Proc 3rd Int. Conf. Polymer Processing Machinery, 14/1-10, PRI London
- Sharp D A (1986), Computer monitoring and analysis of thermoset injection moulding, PhD thesis, Department in Mechanical and Manufacturing Engineering, University of Bradford
- Shah S and Hlavaty D (1991), Gas Injection Moulding: Structural Application, SPE ANTEC Tech. Papers, 49, p 1479
- Shen X, Malloy R, Pacini J (1992), An Experimental Evaluation of Melt Temperature Sensors for Thermoplastic Extrusion, ANTEC Tech. Papers, 50, p 918
- Singh K J (1984), Complete Mould Filling Analysis of Thermoplastics with a Single Computer Run, SPE ANTEC Tech. Papers, 42, p 783
- Sivakumar A I (1984), Design, computer monitoring and control of a RRIM machine, Department in Mechanical and Manufacturing Engineering, University of Bradford
- Smud S M, Harper D O, Deshpande P B (1991), Advanced process control for injection moulding, Polymer Engineering and Science, Mid-August, Vol. 31, No. 15, p 1081
- Speight R G, Coates P D (1991), Modular nozzle rheometry for injection moulding control, Proc. 4th Int. Conf. Polymer Processing Machinery, 15/1-12, PRI London, 4th July
- Speight R G and Coates (1990), In-line Rheometry for Injection Moulding Control, SERC Grant GR/F/30222, Third Review Meeting Report, IRC in Polymer Science and Technology, Mechanical and Manufacturing Engineering, University of Bradford, UK, 1st October
- Speight R G and Coates P D (1991), In-line Rheometry for Injection Moulding Control, SERC Grant GR/F/30222, Fifth Review Meeting Report, Executive Progress Report, IRC in Polymer Science and Technology, Mechanical and Manufacturing Engineering, University of Bradford, UK, 25th September

Speight R G and Coates P D (1993a), In-line Rheometry for Injection Moulding Control, SERC Grant GR/H 49351, First Review Meeting Report, IRC in Polymer Science and Technology, Mechanical and Manufacturing Engineering, University of Bradford, UK, 21st January

Speight R G and Coates P D (1993b), Temperature transducer dynamic response assessments, IRC in Polymer Science and Technology, Mechanical and Manufacturing Engineering, University of Bradford, UK, March

Speight R G, Coates P D, Day A J and Hull J B (1993), The Use of Process Measurements for Real Time Injection Moulding Control, Polymer Processing Society IX Annual Conference, Manchester, 7th April

Stoll K E, Ralston P A S, Wright A L and Harper D O (1991), Modelling and control of batch to batch polymer processes, *Polymer Engineering and Science*, Mid-December, Vol. 31, No. 23

Sukanek P C and Campbell G A (1990), Transient melt temperatures in screw injection moulding, *SPE ANTEC Tech. Papers*, 48, p 218

Terwin (1986), Series 1000 pressure transducer data sheet, Terwin Instruments Ltd

Tordella J P (1956), Fracture in the extrusion of amorphous polymers through capillaries, *Journal of Applied Physics*, 27, p 454

Vanzetti R (1972), *Practical Applications of Infrared Techniques, A New Tool in a Dimension for Problem Solving*, A Wiley-Interscience Publication. John Wiley and Sons

Vanzetti Systems Inc (1984), *Fibre Optic Monitoring and Control Systems, Model LTD, Linearised Temperature Detector*

Vanzetti Systems Inc (1989), *Instruction Manual, 5122, Linearised Infra-red Temperature Transducer 4121*

Wagner A H and Kalyon D M (1991), Development of cracks in injection mouldings of Poly (2,6-Dimethyl-1,4 Phenylene Ether), *Polymer Engineering and Science*, Mid-October, Vol. 21, No. 19

Wang L, Chuah S P, Allan P S, Bevis M J (1993), Shear Controlled Orientation in Injection Moulding (SCORIM) for the Control of Microstructure in Moulded Thermoplastic Liquid Crystal Polymers, *Polymer Processing Society IX Annual Conference, Manchester, 7th April*

Whelan A, Craft J L (1978), *Developments In Injection Moulding -1*, Edited by A Whelan and J L Craft, Copyright Applied Science Publishers Ltd

Whelan A, Craft J L (1981), *Developments in Injection Moulding-2*, Edited by A Whelan and J L Craft, Copyright Applied Science Publishers Ltd

Whelan A, Goff J (1991), *The Dynisco Injection Moulders Handbook, 1st Edition 1991*, Sponsored by Dynisco Inc., Copyright Tony Whelan and John Goff

White J L and Spruiell J E (1983), The specification of orientation and its development in polymer processing, *Polymer Engineering and Science*, Mid-April, Vol. 23, No. 5

Whorlow R W (1979), *Rheological Techniques*, Ellis Horwood (distributed by Wiley)

Wilkinson R (1991), Du Pont (UK) Ltd, How good is your injection unit? *Proc 4th Int. Conf. Polymer Processing Machinery, 16/1-8, PRI London*

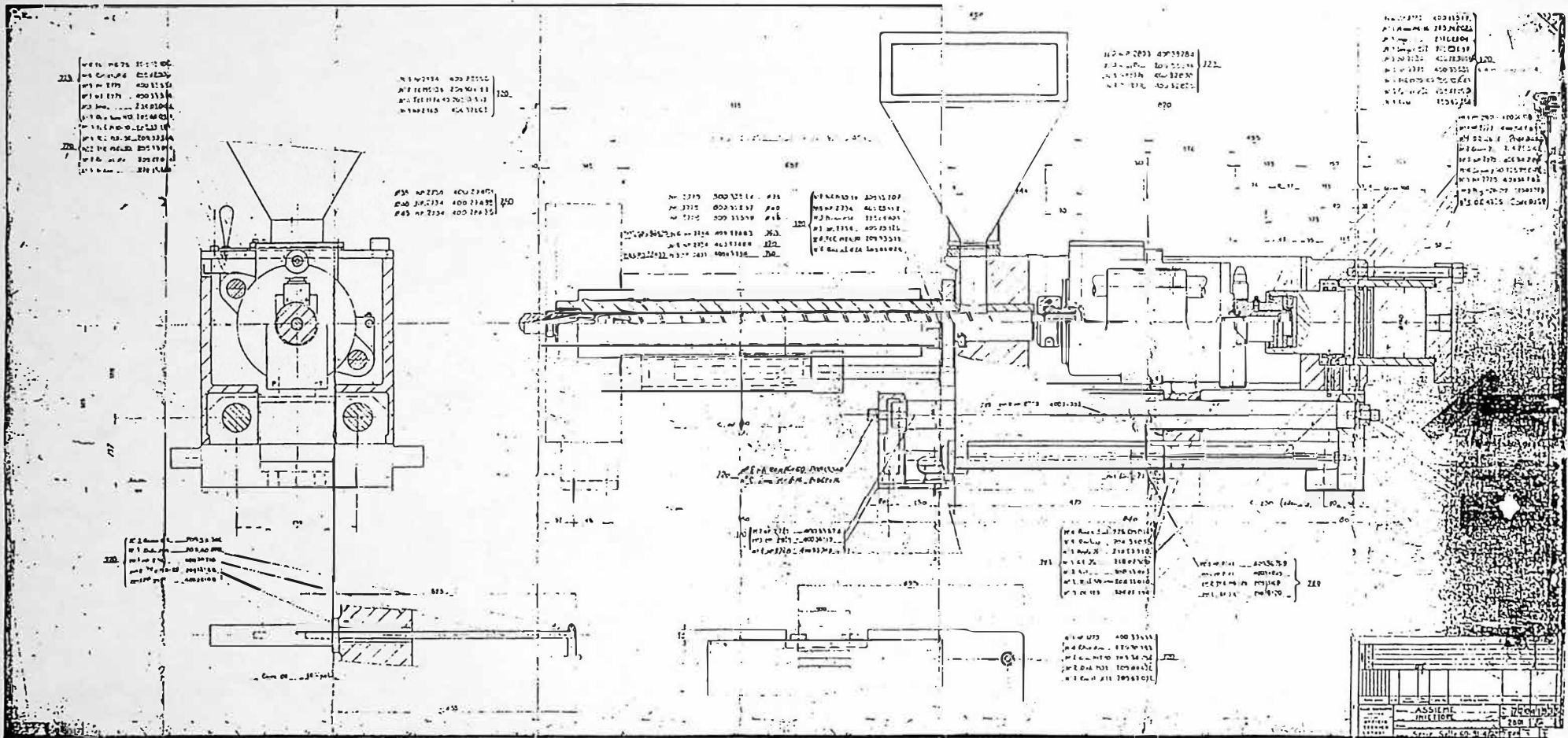
- Wimberger-Friedl R and De Bruin J G (1993), Gapwise Density Distributions in Injection-Moulded Poly(methyl-methacrylate), *Polymer Engineering and Science*, Mid-April, Vol. 33. No. 7, P383
- Windsor Shaw T (1989), Practical experience of SPC for injection moulding, Proc. 3rd Int. Conf. Polymer Processing Machinery, 10/1-10, PRI London
- Winninger H, Effmann J (1989), ACT: Servo technology in injection moulding machines, Proc. 3rd Int. Conf. Polymer Processing Machinery, 17/1-2, PRI London
- Wolf U (1989), Typical injection moulding problems and how to avoid them, BASF technical training, September
- Woodhead M (1990), Degree Final Year: Major Project Dissertation, Statistical Investigations in Injection Moulding, Department in Mechanical and Manufacturing Engineering, University of Bradford
- Wright H C (1973), *Infrared Techniques*, Monographs in Electrical and Electronic Engineering, Oxford University Press
- Wu J L and Chen S J (1990), Pattern Analysis of Injection Moulding Process: Statistical Correlation Study, *SPE ANTEC Tech. Papers*, 48, p 233
- Wu J L, Chen S J and Malloy R (1991), Development of an In-line Cavity Pressure Based Expert System for Injection Moulding Process, *SPE ANTEC Tech. Papers*, 49, p 444
- Wu J P and White J L (1992), Crystalline orientation in injection moulded polyethylene parts, *Intern. Polymer Processing VII* 4
- Yu C J and Sunderland J E (1992), Determination of ejection temperature and cooling time in injection moulding, *Polymer Engineering and Science*, Mid-February, Vol. 32, No. 3

**Appendix A Sandretto Series Seven 60 Tonne Injection
Moulding Machine**

(i) Technical Specification

Clamping force:	60 Tonne (590 kN)
Hydraulic piston diameter	140 mm
Screw diameter:	40 mm
Screw stroke:	99.9 mm
Injection velocity:	0 to 99 mm/s
Type of screw:	General Purpose
Screw aspect ratio:	19 L/ D
Maximum hydraulic pressure:	115 bar
Maximum nozzle melt pressure:	1409 bar *
Tool height:	300 mm
Ejection plate stroke:	90 mm
Screw rotational speed:	0 to 300 RPM
Temperature control zones:	4 (3 Barrel, 1 Nozzle, Type J Thermocouples)
Machine control:	Selec 90, Two 16 bit 8088 Microprocessor
Instrumentation sample speed:	20 ms

* Based on 115 bar hydraulic pressure, area of piston to screw = 12.25, assuming no losses.



Details of Sandretto series seven 60 tonne injection unit (drawing number: 720/41935/2801)

(iii) Sandretto viscosity index calculation

A viscosity Index is calculated in the following way:

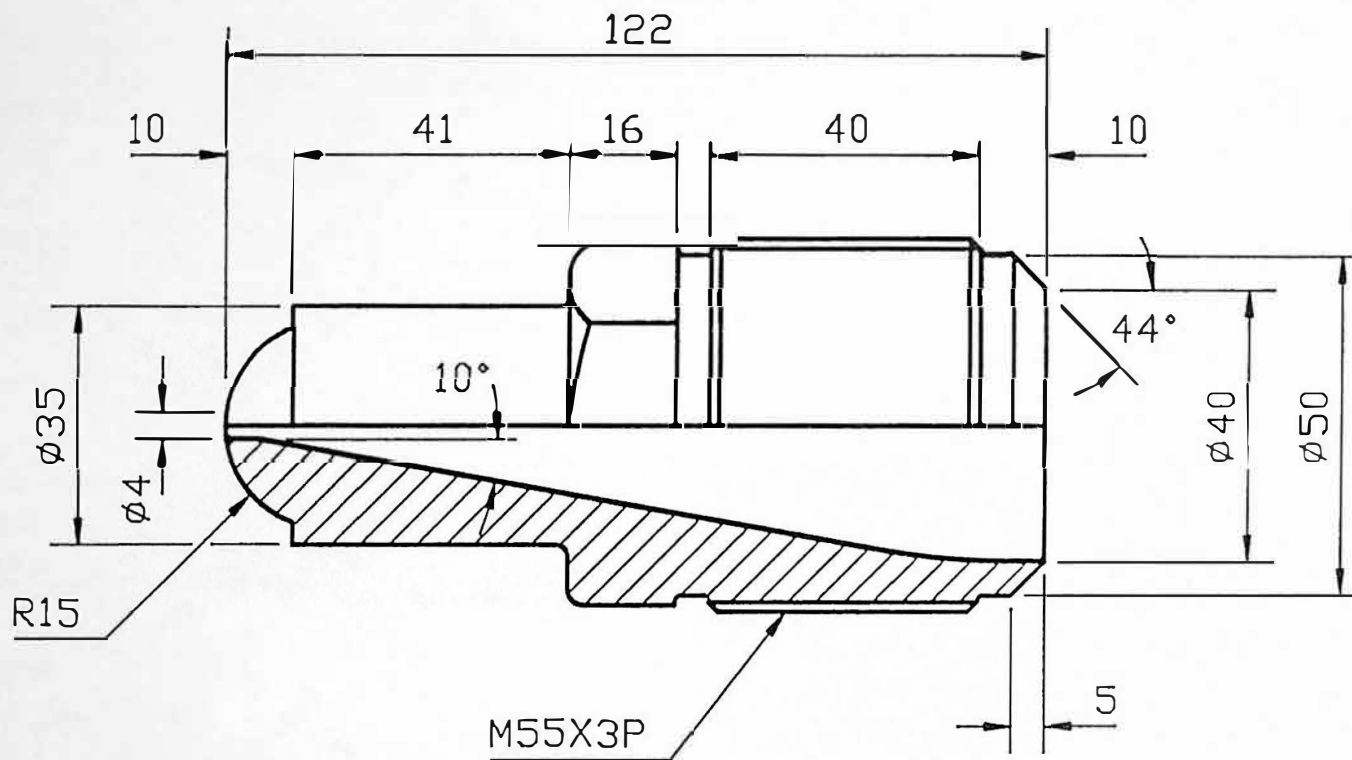
- (1) Injection stroke is split into ten equal lengths i.e. dose to changeover point.
- (2) Steps 1, 2, 9 and 10 are ignored.

Note: 1 and 2 take out initial inaccuracies etc. 9 and 10 to allow computation in real time and to avoid peak pressure at fill.

- (3) A constant time base is used to take readings of pressure at time, then for each stage these pressure readings are added together and divided by a number of readings.
- (4) The six average readings (3-8) are then added together and the average taken.

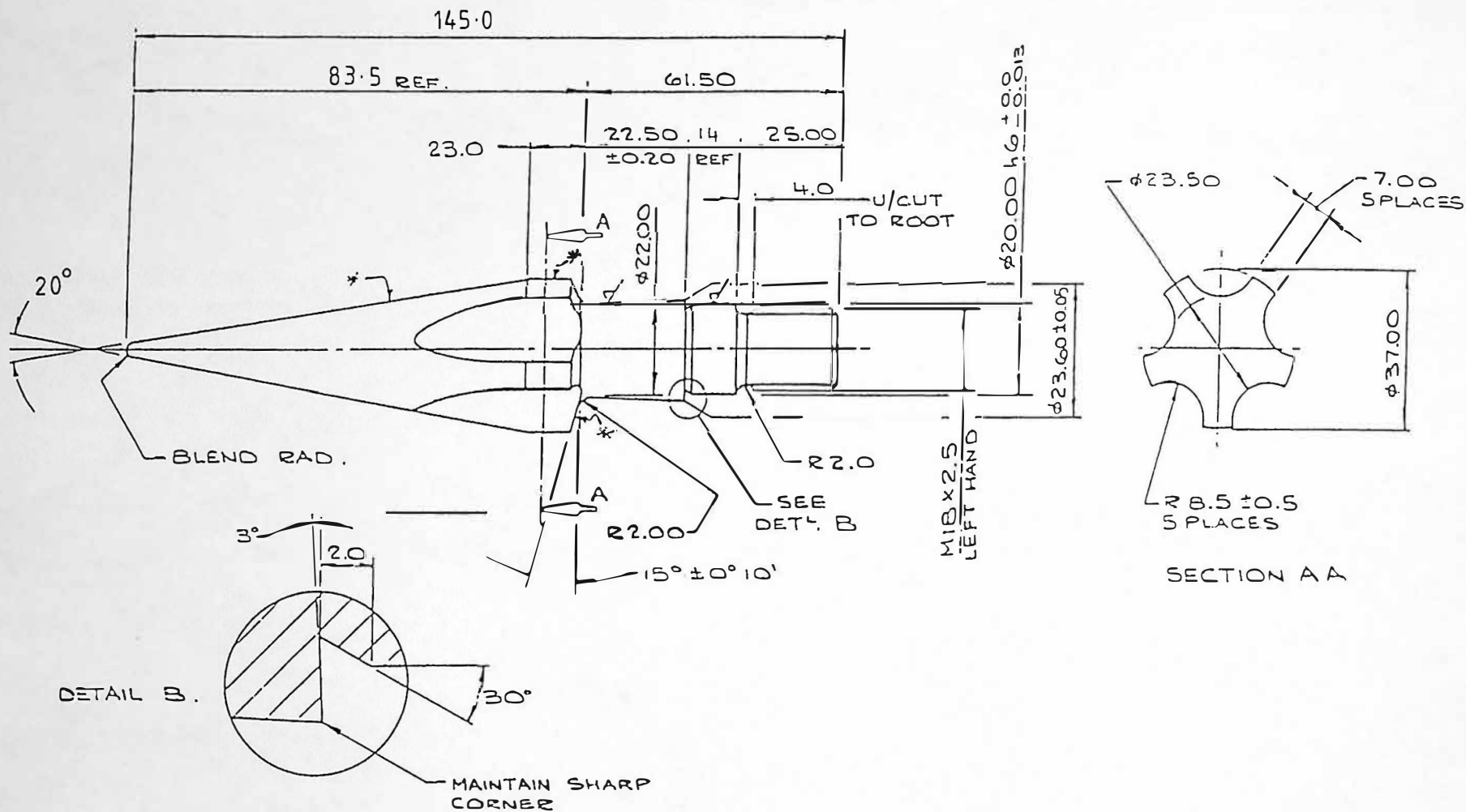
Note:

There is no adjustment for pressure losses, as the system is designed to compare hydraulic injection pressure on a cycle to cycle basis only. Therefore, assume the percentage of the viscosity index number due to losses is constant.



SCALE	1:1	TITLE NOZZLE FOR SANDRETTO 60 TONNE INJECTION MOULDING MACHINE, 40mm SCREW DIAMETER.	DRG. No.	A4
DRN.	MW		400/27489	
APP'D.	RGS		/2734	
DATE	4/6/93		UNIVERSITY OF BRADFORD	

DO NOT SCALE



* = SURFACE TO BE POLISHED AFTER MACHINING
✓ SURFACE FINISH 0.8 MICROMETRES WHERE INDICATED.
UNSPECIFIED RADII 0.75 MAX.

$\phi 40$ SCREW TIP

(vi) **Serial communication, connections and protocol****RS232 Serial Interface Connections**

Function	Selec Controller Pin	to	Personal Computer Pin
Transmitted Data	2	-	3
Received Data	3	-	2
Data Set Ready	6	-	20
Data Terminal Ready	20	-	6

To prevent the occurrence of earth loop problems, ground and signal earth were not connected, as a ground connection already existed between the Selec controller and personal computer. The communication lead operates both ways, due to symmetry.

RS232 Serial Interface Communication Protocol

Baud Rate: 2400 bits/second

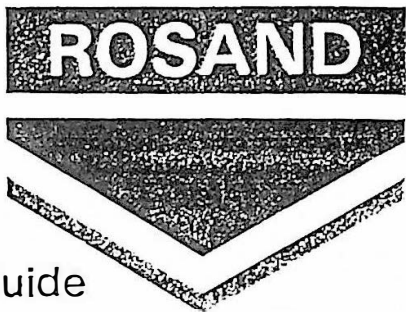
Data Bits: 8

Stop Bits: 1

Parity: None

Flow Control: Xon/Xoff

RH-01

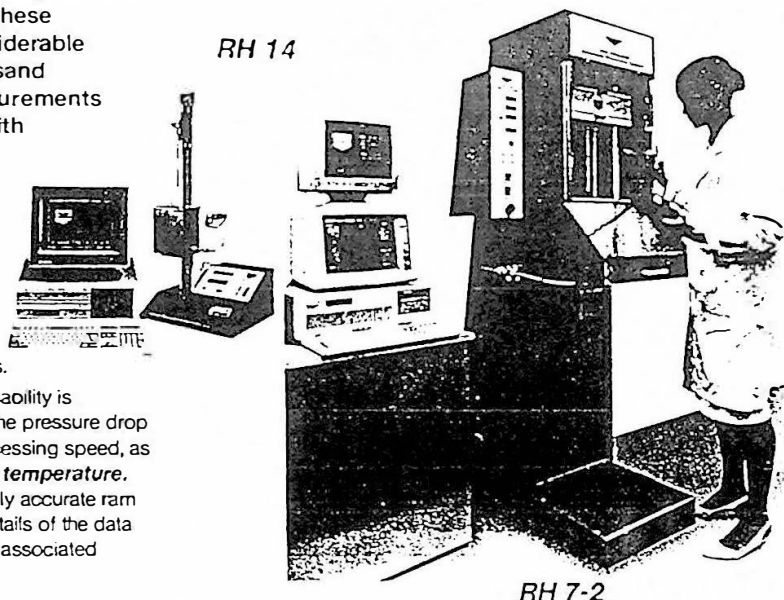


Rosand Rheometers Technical Specification and Selection Guide

High-speed mass production requires the prediction of material processability. Historically, these measurements required time and considerable expertise. With the evolution of the Rosand computerised rheometers, these measurements can be achieved very accurately and with advanced automation with minimal resource (time, people, money).

The entire range of well-proven Rosand rheometer systems have the rare combination of very high accuracy with ease and speed of use. The wide variety of systems ensures that your specific requirements are ideally met. Rosand rheometers are ideally suited to both Research and Quality Control applications.

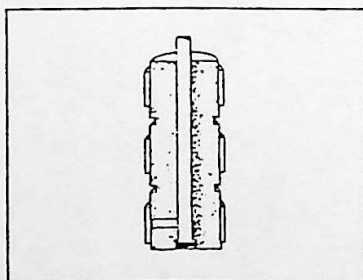
The primary measurement required for processability is **viscosity** (resistance to flow, as measured by the pressure drop through a die) as a function of **shear rate** (processing speed, as measured by the flow rate through the die) and **temperature**. Rosand rheometers can be considered as highly accurate ram extruders, in which the above is carried out. Details of the data obtained and its interpretation are described in associated Rosand Notes (RH-02 and RH-03).



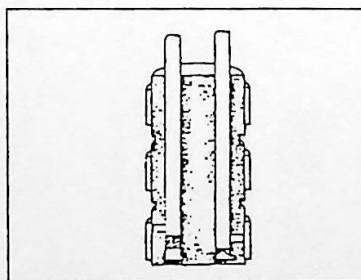
Systems

Systems are available with a range of benefits covering performance, versatility and speed-of-operation. Rosand offer twin-bore barrel systems, which provide more useful and precise information, more quickly and easily. For even greater throughput of samples, Rosand produce a system with TWO twin-bore barrels. One barrel is used for loading/pre-heating while the test is carried out in the other, on completion, the loaded barrel is tested... etc.

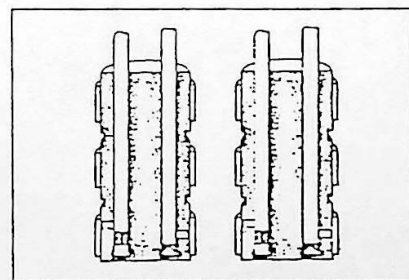
System Type	Number of Bores	Frame Type	Piston Force	Maximum Temperature °C
RH14A	1	Bench	3.5 kN	400 (500 Opt)
RH14B	1	Bench	10 kN	400 (500 Opt)
RH7-1	1	Floor	40 kN (100 kN Opt)	400
RH7-2	2	Floor	40 kN (100 kN Opt)	400
RH7-4	4	Floor	40 kN (100 kN Opt)	400
RH8-1	1	Floor	40 kN (100 kN Opt)	500
RH8-2	2	Floor	40 kN (100 kN Opt)	500
RH8-4	4	Floor	40 kN (100 kN Opt)	500



Single-Bore (7-1, 8-1, 14)



Twin-Bore (7-2, 8-2)



Double Twin-Bore (7-4, 8-4)

Figure 1 Barrel Layouts in Rosand Rheometers

Features

Benefits

Operational Advantages

Fully automatic cycle including pressure equilibrium determination and auto-speed-change	High throughput of tests Reduced operator time Rheology now available for the QC laboratory Increased Data with one sample
Computer Control and "Watch-Dog" system, with Advanced Graphical Display	Every step of every test Monitored/Stored Clear Representation of Data and Full System Control
Full interlocks for overload of piston force and pressure	Protects the system, even with cross-linking and other difficult materials
Integrated safety systems	Ensures safe operation.

Accuracy Advantages

Fully automatic cycle including pressure equilibrium determination	Repeatability of results Reduced variability between operators
Superior Temperature Control/Measurement (see below)	Better Data Integrity.
Pressure measured at die	No errors due to friction, compaction, filler-bridging or shear losses down the barrel.
Auto-zero and auto-calibration of all amplifiers with every run	Better Accuracy/Consistency of results

Versatility Advantages

Open frame with large range of hardware options	Allows easy access for cleaning and versatile use.
Large range of software options	Allows the most advanced characterisation.
Degradation Testing	Automatic determination of permissible residence time for molten polymers in real processes
Software sequence for zero-length die testing (RH14) (Bagley correction)	Provides the necessary data for convergent/divergent flow situations

Additional Features on RH7 and RH8 systems

Integrated Fume extraction (RH7/8)	Ensures safe, pleasant operation.
40,000 N or 100,000 N systems available (RH7/8) with 250,000 N frame strength	Strength suitable for all materials currently processed (or ever likely to be!), even at very high shear rates.
Unique Twin bore systems for zero-length testing (RH7/8) (Bagley correction)	Provides the necessary data for convergent/divergent flow situations
At three times the throughput of any other rheometer.	
Advanced Twin-Screen Graphical Display	Clear Representation of Data and Full System Control while making measurements

In brief, the Rosand Rheometers provide a lot of useful information with minimum effort/cost.

Shear Stresses and Rates

The calculation of these parameters is described in detail in our Data Sheet Number RH-02. Briefly, the only limitations on the Rosand rheometers are mainly those imposed by the maximum speed and pressure sensitivity.

Shear Rates As examples:

System	Die Dia. mm,	Barrel Dia. mm,	Max Shear Rate, s ⁻¹	Min Shear Rate, s ⁻¹
Standard	0.25	12	620,000	62
Standard	0.25	15	1,000,000	100
High Speed	0.25	15	2,300,000	230
High Speed	0.25	19	3,200,000	320
Standard	0.50	15	120,000	12
High Speed	0.50	15	300,000	30
Standard	1.00	15	15,000	1.5
High Speed	1.00	15	38,000	3.8
Standard	2.00	15	2,000	0.2
High Speed	2.00	15	4,800	0.5

In practice the lowest shear rate will be limited by the pressure transducer sensitivity, or the time to reach equilibrium exceeding the thermal degradation.

Shear Stresses

For any die size, these are defined by pressure sensitivity limitations. For illustration, if we assume that the most sensitive pressure transducer (500 psi) is reasonably accurate at 10% full-scale, and the die being used is 1 mm x 32mm long, then the minimum shear stress seen here is approx 0.005 MPa. If we assume that the most robust pressure transducer (30,000 psi) is in use, and the die being used is 1 mm diameter x 10mm long, then the maximum shear stress here is approx 10 MPa (Note: most fluids break down at about 1MPa).

Technical Specifications

The *Capacity and Accuracy* of a *Test System* are defined by:

- Barrel - construction, mechanical accuracy and hardness.
- Piston Drive - capacity, speed range and accuracy.
- Pressure measurement - range and accuracy.
- Temperature - accuracy of measurement and control.
- Die - construction, mechanical accuracy and hardness.

Barrels

	RH14	RH7, RH8
--	------	----------

Precision Bored, Honed and polished in Nitrided Steel (*)		
Supported on rigid strong frame,		
Strength, kN	20	250
Options	Single bore only	Single or Twin Bores
Diameters available, mm	12 only	12, 15 or 19 (**)
Barrel Length mm	230	280

(*) Barrels can be manufactured in other materials, e.g.
Hastelloy - for use with PEEK, PES etc which adhere to steel
Stainless Steel - for use with food, pharmaceutical products etc.

(**) The choice of barrel diameter is defined by a compromise where Larger Diameters have:
Better strength (buckling strength of piston)
Better capacity (more experiments)
Higher Shear Rate capability
Easier loading (especially for rubbers, coarse-cut plastics etc)

BUT they need...
Longer time to reach temperature equilibrium
More material for a measurement

In general therefore, Rosand do not recommend the small 9.5mm barrel frequently offered. The 12mm barrel is appropriate to the 10kN drives of the RH14. Usually the RH7 and RH8 are supplied with 15mm diameter barrels, being a good compromise. 19mm should be chosen when the extra test volume is useful, 12mm when materials are likely to degrade.

Drive and Frame

	RH14	RH7, RH8
--	------	----------

Precision screw drive (d.c. servo-drive motor) for crosshead/pistons, with options:		
Standard system drive: Max force kN	3.5	40
Motor Power, standard system, W	100	1,200
High-Force (HF) system capacity kN	10	100
Motor Power, (HF) system, W	300	1,800
Maximum Speeds, mm/min		
standard and HF systems	500	500
Optional High-Speed (HS) system:	not available	1,200 mm/min, 40kN
Speed Range	10,000:1	50,000:1
Position Encoder Resolution	0.00125mm	0.0004mm

Pressure Transducers.

These are high-precision high-temperature units, supplied to suit the maximum temperature available to your unit. They are mounted 9.0mm above the die surface (independent of die length) using special Rosand mounting technology which makes transducer changes faster and easier.

Accuracy 0.5% . Temperature stability 0.02%/°C

Temperature

Rosand offer two temperature ranges:

	40 deg C - 400 deg C	Standard
	40 deg C - 500 deg C	Optional
Barrel temperature accuracy	+/- 0.3 deg C	
Temperature uniformity	+/- 0.7 deg C	

Heaters:

	RH14	RH7, RH8
--	------	----------

Ceramic-stainless steel units for longevity		
Top zone of barrel, W	900	1,000
Centre zone of barrel, W	120	600
Die zone, W	600	900

Note.

Temperature uniformity, control and accuracy are of paramount importance in these measurements. The above are controlled by the unique Rosand "intelligent" multi-zone self-calibrating system with three high-precision sensors (platinum resistance thermometers manufactured to better than 10 times DIN standard accuracy).

This system effectively eliminates the need for periodic recalibration, as it incorporates two reference bridges which emulate the pt's at 0°C and 400°C. These reference bridges have very high accuracy (0.01%) and high stability (0.0003 %/°C, 0.001%/year). This automatic self-calibration is carried out with every test run, unseen to the operator.

Dies.

Two dies are supplied as standard. These are manufactured from Tungsten Carbide (high wear resistance) to very fine tolerances and finishes. They are supplied with special retainers to withstand the high loads capable of being exerted on the Rosand systems, but which are...

- Quick and Easy to remove
- Fitted with special bolster to ensure that the distance from the die to the pressure transducer is constant

Standard Dimensions

	Bore mm	Length
"Long" die	1.000mm +/- 0.005	Length 16.0
"Orifice" die	1.000mm +/- 0.005	Length 0.25

Many other die sizes, with or without conical entry angles are available.



Standard Equipment List

Rosand Rheometer systems are supplied complete with an enhanced equipment list which includes a good-quality IBM-AT compatible computer, all tools, dies and even a die reference gauge.

Rosand Rheometer Frame/Drive/Barrel system Control Data System

- 12 MHz good quality IBM-AT compatible computer
- Enhanced keyboard
- 40 MByte hard disc drive
- EGA card and high-resolution colour monitor
- DOS system
- High-quality 24-pin dot-matrix printer
- 1 MByte internal RAM
- 1.2 MByte floppy disc drive
- All interfaces for RH14-'s

Two Tungsten Carbide dies with precision "Go/NoGo" gauge and retainers.

Pressure Transducer - 10,000psi (70 MPa) as standard -many others available.

Tool set, with the following :-

- | | |
|----------------|------------------|
| Charging tool, | Die ejector, |
| Cleaning tool, | Cleaning brush, |
| Cut-off knife, | Die broach, |
| Hexagon key, | Cleaning patches |

RH7-2, 7-2, 8-1, 8-2 have the following additional items

- Second high-resolution monochrome monitor for twin-screen display/control system
- Second pressure transducer (1,500 psi, 10.5 MPa as standard) with amplifier/interface etc

RH7-4 and 8-4 have the following additional items

- Two complete frame/drive/barrel systems in single integrated unit
- Two added pressure transducers with amplifiers/interfaces etc
- Two extra dies

Dimensions and Power requirements

System	N. of Bores	Frame Type	Width cm	Depth cm	Ht. cm	Wght kg	Power(*) V, A
RH14A	1	Bench	70	49	112	56	208/220/240V, 9A
RH14B	1	Bench	70	49	122	63	208/220/240V, 10A
RH7-1, 7-2, 8-1, 8-2	1, 2	Floor	63	105	234	350	208/220/240V, 20A OR 3-phase 3 N, 16A/phase
RH7-4, 8-4	4	Floor	126	105	234	650	3-phase 3 N only 208/380/415V, 16A/phase

(*) Power input can be configured to suit any country.

Optional non-standard Equipment (Full Technical Data in Data Sheet RH-05)

OPTION For use with rheometers

RH	001	002	003	004	005
Spares Kit	✓	✓	✓	✓	✓
Extra High Force (100kN)	X	X	✓	✓	✓
OR Extra High Speed (1000mm/min)	X	X	✓	✓	✓
Hastelloy Barrel	✓	✓	✓	✓	✓
Extra High-Temp (500°C)	✓	✓	X	X	Inc. Inc.

Pressure Transducer Calibration Kits

Pressure	Kit	010	011	012	013
0- 2,000 psi (0- 14MPa)	010	✓	✓	✓	✓
0- 5,000 psi (0- 35MPa)	011	✓	✓	✓	✓
0-10,000 psi (0- 70MPa)	012	X	✓	✓	✓
0-20,000 psi (0-140MPa)	013	X	✓	✓	✓

Additional /Spare Pressure Transducers

Complete with Rosand retention and location system:

Pressure	Kit	014	015	016	017	018	019
500 psi (0.35MPa)	014	✓	✓	✓	✓	✓	✓
1,500 psi (1.05MPa)	015	✓	✓	✓	✓	✓	✓
5,000 psi (3.5 MPa)	016	✓	✓	✓	✓	✓	✓
10,000 psi (0.35MPa)	017	✓	✓	✓	✓	✓	✓
20,000psi (0.35MPa)	018	X	✓	✓	✓	✓	✓
30,000 psi (0.35 MPa)	019	X	X	✓	✓	✓	✓

Spares for the Rosand pressure transducer retention and location system:

Item	Kit	020	021	022
Complete system	020	✓	✓	✓
Retention Nut	021	✓	✓	✓
Copper seal and location washers Per pack 5	022	✓	✓	✓

Melt Strength Evaluation:

Medium Speed (0 - 70 m/min) for Assessment of Extrusion Blow Moulding Processability

Type	Kit	031	032	033	034
Type A: Standard Sensitivity (Tragethon Technique)	031	X	X	✓	✓
Type B: High Sensitivity	032	X	X	✓	✓

High Speed for Assessment of Fibre Processability

Type	Kit	033	034
Type C: Standard Sensitivity	033	X	X
Type D: High Sensitivity (Tragethon Technique)	034	X	X

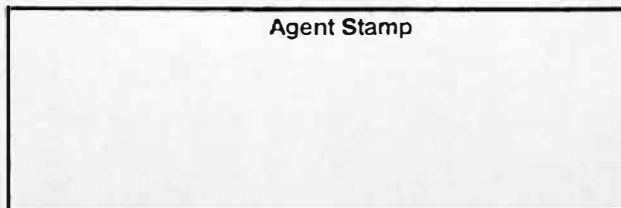
Temperature controlled Chamber for use with Melt Strength Evaluation Systems

Item	Kit	035	041	042	050
For use with 031 and 033 units	035	X	X	✓	✓
Diameter Gauge Options:					
Single Axis	041	✓	✓	✓	✓
Double Axis	042	X	X	✓	✓
Die Options:					
Slit Die (3-transducer)	050	X	X	✓	✓

All other dies available for all units, supplied complete with adaptor and retaining nut. State barrel diameter when ordering.

NOVEMBER '90

Rosand Precision Ltd
11 Little Ridge
Welwyn Garden City
Herts AL7 2BH
United Kingdom
Tel. (44) 0707 332231
Fax. (44) 0707 372170



Rosand Precision Inc
8580 Cinderbed Rd
Suite 1400
Newington VA 22122
United States of America
Tel. (1) 703 339 1097
Fax. (1) 703 339 1099

Appendix C Experimental Test Procedures

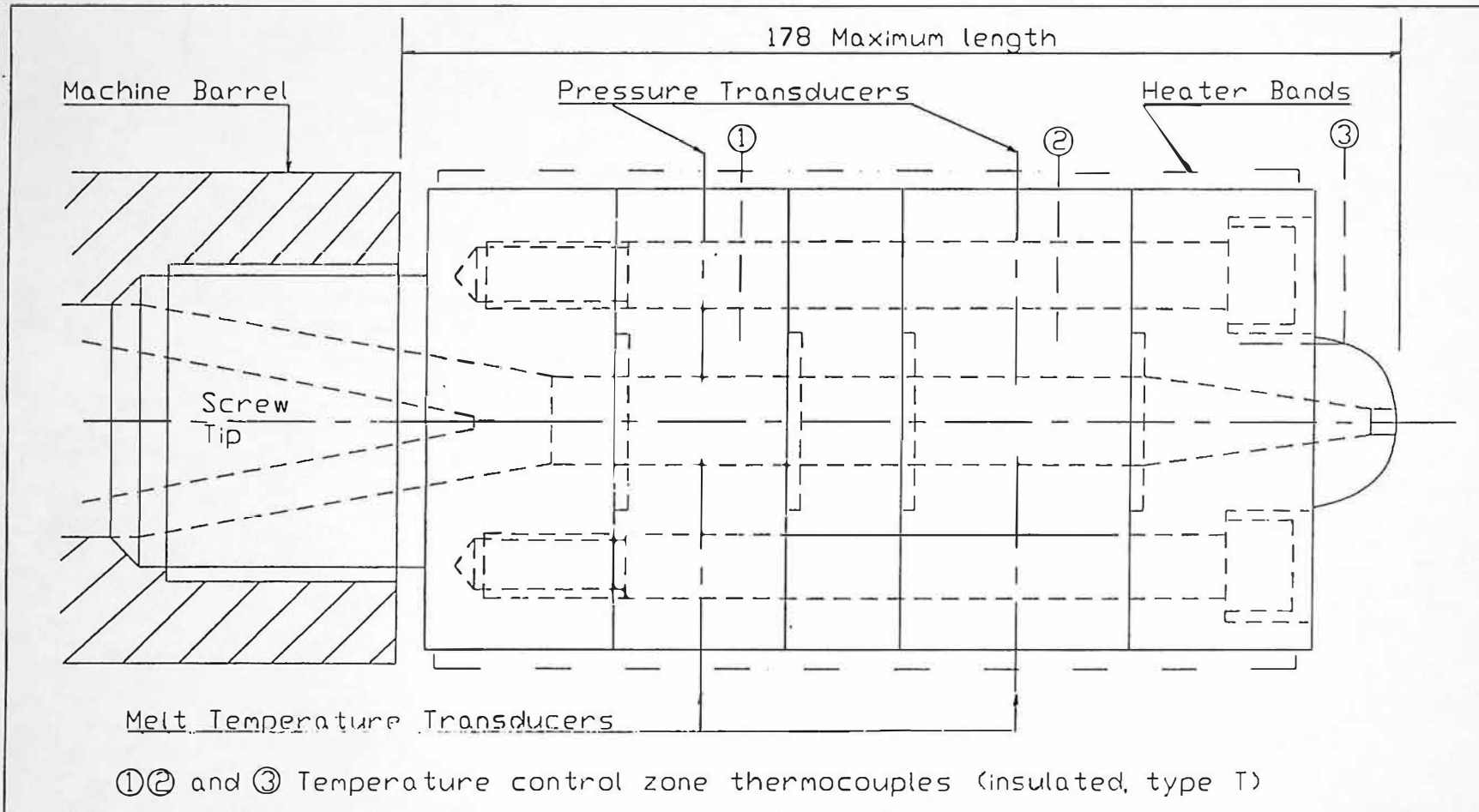
(i) Off-line capillary rheometry

1. Select rheometer control program 'A'.
2. The required barrel temperature was set.
3. Insert floppy disc into disc drive.
4. Check the rheometer bores, pistons and dies are clean.
5. Place pistons on the rheometer to warm.
6. Fit long and short dies, use anti seize compound.
7. Enter the test sequence, it is desirable to enter shear rates.
9. Calibrate and zero the pressure transducers, at the desired operating temperature.
10. Fill the bore with polymer, packing if necessary.
11. Fit the pistons, being careful to fit the correct pistons, for the long and short dies.
12. Run the normal test.
13. Check that the raw and calculated data has been saved correctly on the floppy disc.
14. Print a standard record of the test.
15. Thoroughly clean the rheometer bores and dies.

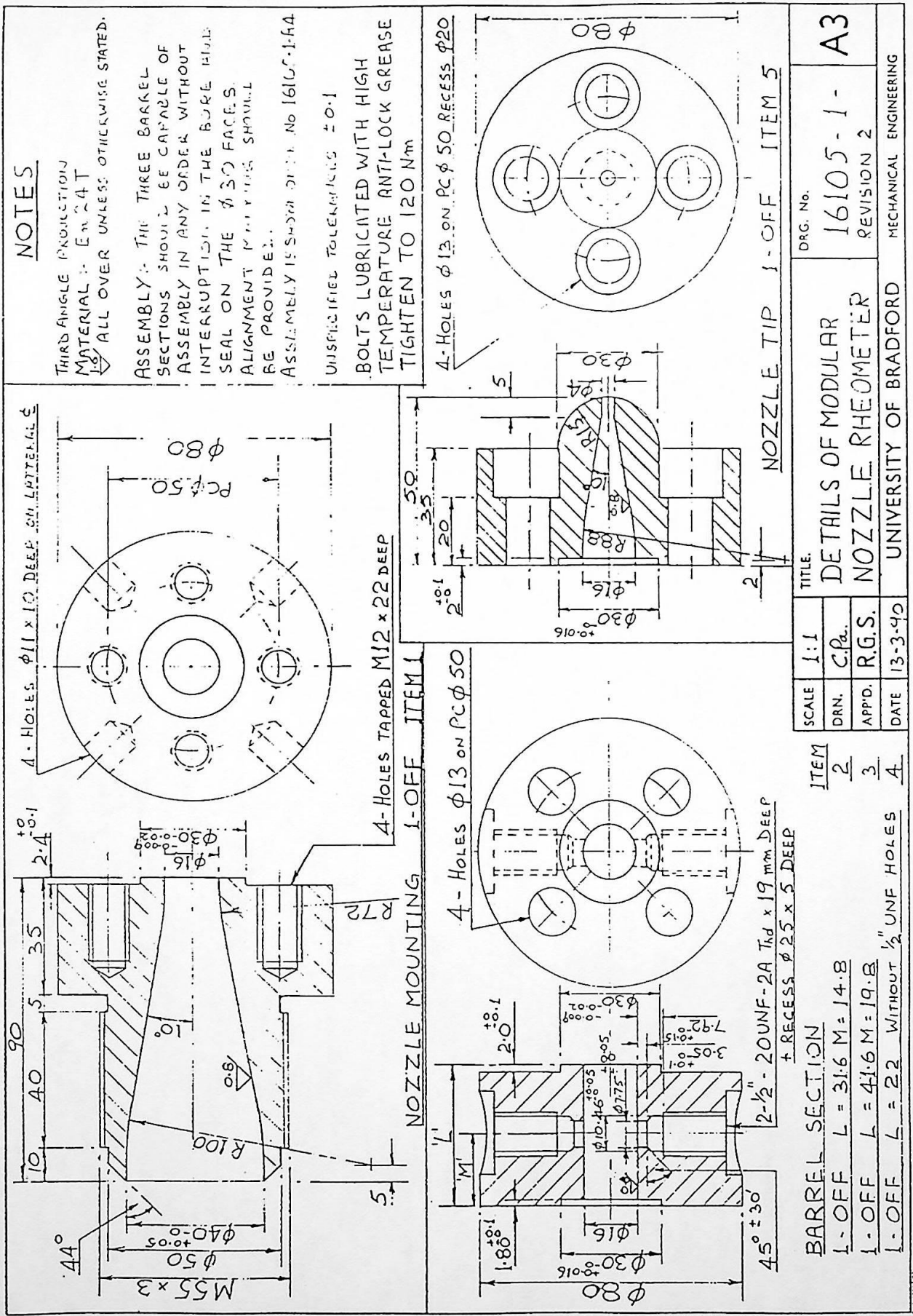
(ii) **In-line capillary rheometry and experimental moulding tests**

1. Raw materials were conditioned prior to being processed, where necessary. Material was used directly from the bag when conditions allowed.
2. Machine Selec controller and instrumentation circuits were 'switched on' to allow adequate time for the electronic circuits to stabilise. Whenever possible the Selec controller and instrumentation circuits remained 'switched on', for the duration of a complete set of tests.
3. Water supply to the machine and tool temperature controllers was 'turned on'. The machine requires water to cool the hydraulic oil during machine operation and cool the material feed zone, at the rear of the barrel.
4. Machine hydraulic power was 'switched on' to allow the oil temperature to stabilise. Normal operating temperatures are between 40 to 50C, typically reached within 1 hour.
5. Machine lubrication was initiated, this operation was then repeated automatically every 100 machine cycles.
6. Fume extraction was 'switched on' to remove any hazardous fumes from the machine nozzle.
7. The required machine parameters were set.
8. Nozzle, hot-tip (when installed) and tool temperature controllers were 'switched on'. When the nozzle was approximately at the desired temperature the barrel temperature controllers were 'switched on'. This procedure was necessary to maintain a positive temperature gradient along the injection unit.
9. When the desired nozzle and barrel temperatures were reached, material was purged through the injection unit and hot-tip. The purge material was either polyethylene or polypropylene, i.e. well behaved material. The material to be processed was then introduced and purged through the injection unit and hot-tip.

10. Machine was then cycled for approximately one hour to allow steady processing conditions to be achieved. Machine parameter settings were adjusted if necessary to achieve a good quality moulding.
11. One cycle was monitored, plasticisation and Injection phases, to check that the instrumentation was functioning correctly.
12. The selected number of cycles were monitored, at a specified data storage interval. The plasticisation phase was initially monitored, followed by the injection phase.
13. The injection unit was then purged through with a well behaved material, if necessary.
14. Machine nozzle and hot-tip were cleaned, the carriage was fully retracted and the tool closed. The machine hydraulic power was then 'switched off'.
15. The tool, barrel and hot-tip temperature controllers were 'switched off'. When the barrel temperature had reduced significantly, the nozzle temperature controllers were 'switched off'. Again this procedure was to maintain a positive temperature gradient.
16. Water supply to the machine and tool temperature controllers were 'turned off'.
17. Machine Selec controller and instrumentation were 'switched off'.



Scale	Full size	Title	Drg. No.
Drn	C Parminter		
App'd	RG Speight		
Date	21-03-90		
		MODULAR NOZZLE RHEOMETER ASSEMBLY	16105-1-A4



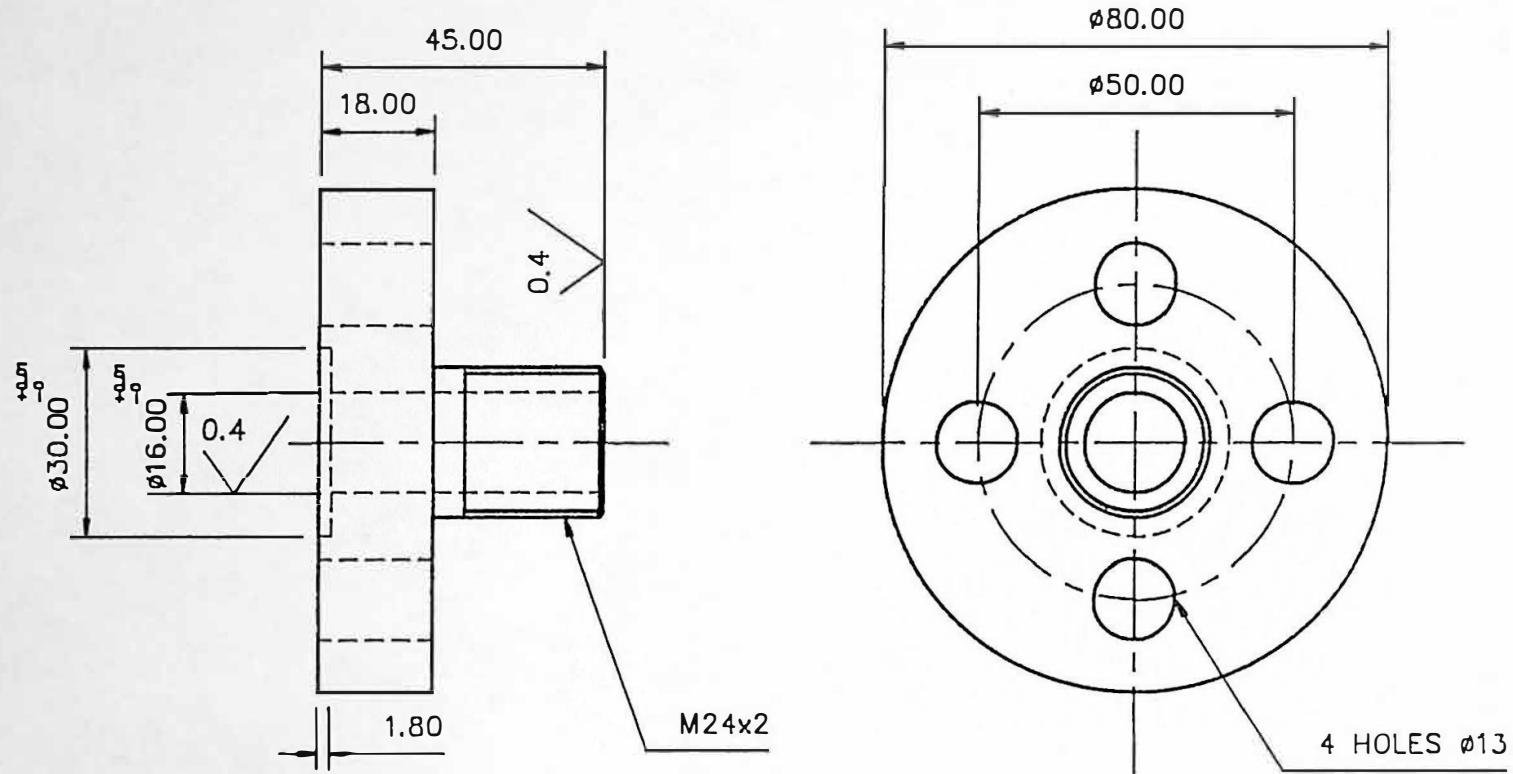
DO NOT SCALE

IF IN DOUBT ASK

ALL DIMENSIONS IN MILLIMETRES

FINISH $\sqrt{1.6}$

ALL UNTOLERANCED DIMS ± 0.1



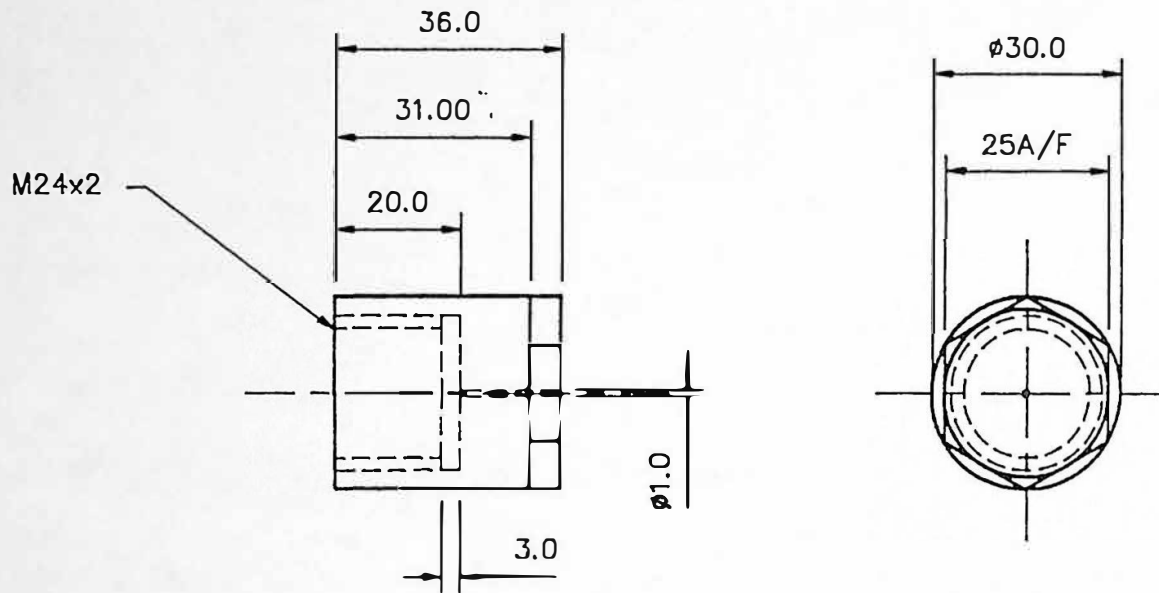
SCALE	1:1	TITLE	NOZZLE ATTACHMENT		DRG.No.	16132/1	A4
DRN	MF	(MATRL: EN24T)					
APP'D	R.G.S.	UNIVERSITY OF BRADFORD		I.R.C.			
DATE	28/2/92						

DO NOT SCALE

IF IN DOUBT ASK

ALL DIMENSIONS IN MILLIMETRES
ALL UNTOLERANCED DIMS ± 0.1

FINISH $\sqrt{1.6}$



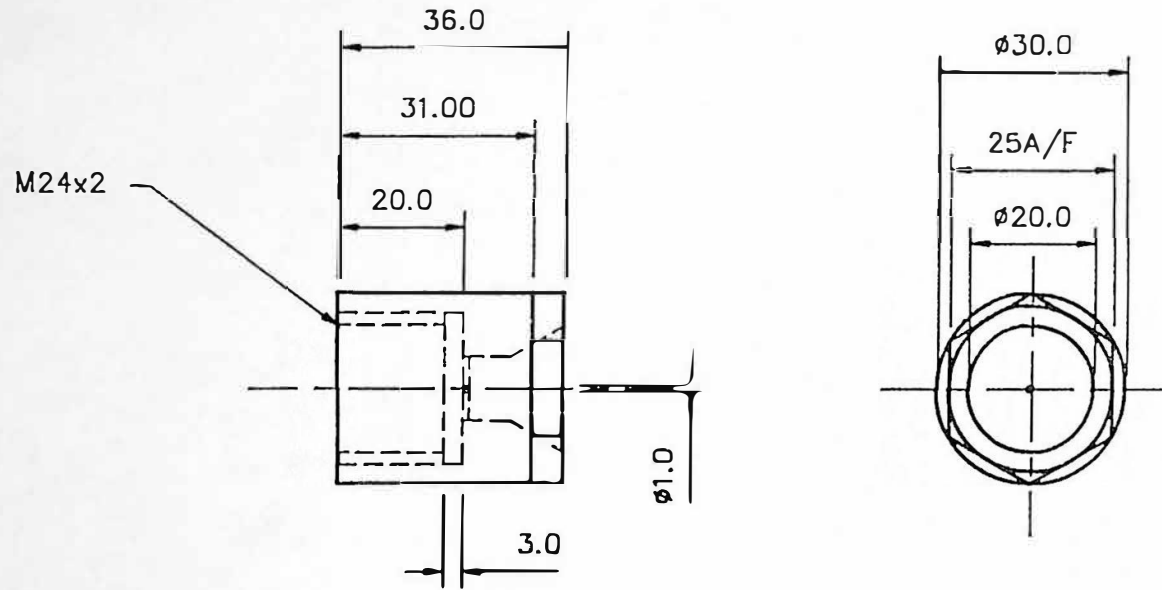
SCALE	1:1	TITLE. NOZZLE TIP (MATRL: EN24T)	DRG.No. 16132/2	A4
DRN	MF			
APP'D	R.G.S.			
DATE	2/3/92			
UNIVERSITY OF BRADFORD		I.R.C.		

DO NOT SCALE

IF IN DOUBT ASK

ALL DIMENSIONS IN MILLIMETRES
ALL UNTOLERANCED DIMS $\begin{matrix} +0.1 \\ -0.1 \end{matrix}$

FINISH $\sqrt{1.6}$



SCALE	1:1	TITLE. NOZZLE TIP (MATRL: EN24T)	DRG.No. 16132/3	A4
DRN	MF			
APP'D	R.G.S.			
DATE	2/3/92			
UNIVERSITY OF BRADFORD		I.R.C.		

Appendix E Temperature Zone Controllers**(i) Nozzle temperature**

Eurotherm Temperature Controller Type 070, 071

Technical Specification:

Operating Temperature Range:	0 to 400C
Type:	Internal Thyristor
Control Type:	Proportional (Proportional Band X_p) Manual Control of Output Power
Thermocouple:	Copper Constantan (Type T)

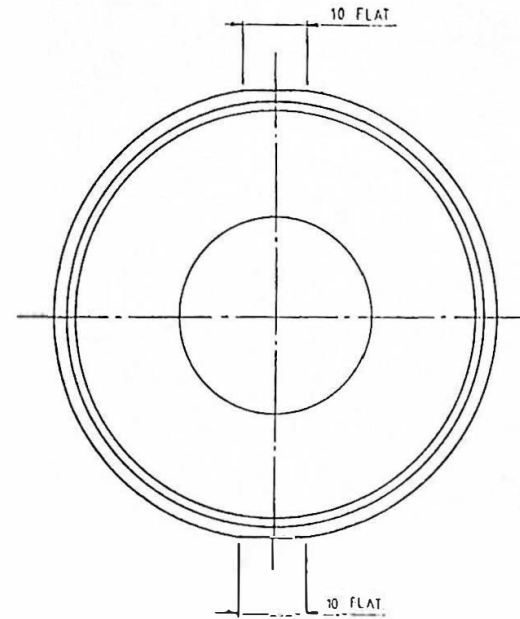
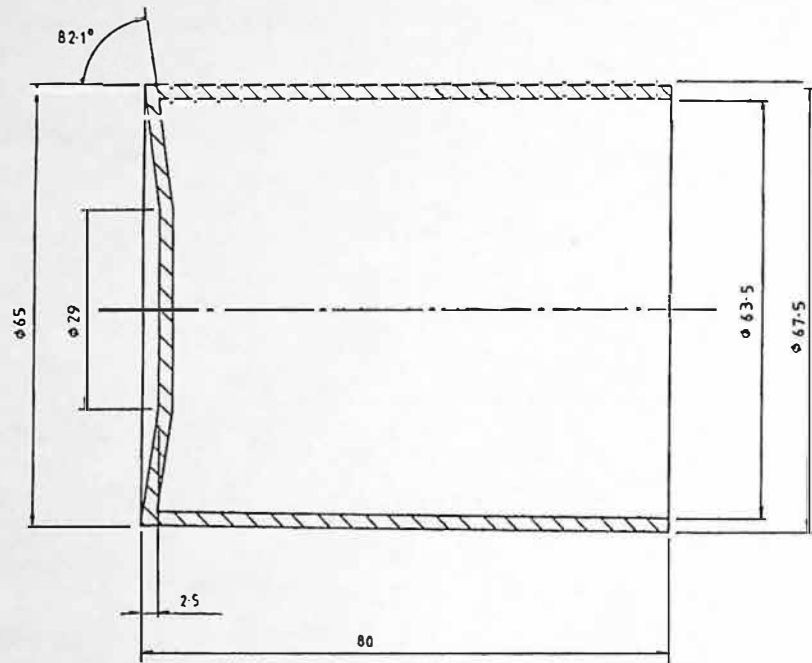
(ii) Tool temperature

Conair Churchill Tool Temperature Controller Junior SW/140

Technical Specification:

Operating Temperature Range:	20 to 140C
Heating Capacity:	3 kW
Circulation Medium:	Water
Cooling Capacity:	9000 kcal/ h at 120C (36000 kJ/ h at 120C)
Type of Cooling:	Indirect with water
Pumping Capacity:	18 l/ min (Maximum)
Pumping Pressure:	3.5 bar (Maximum)
Mains Water Pressure:	2.6 to 6.3 bar

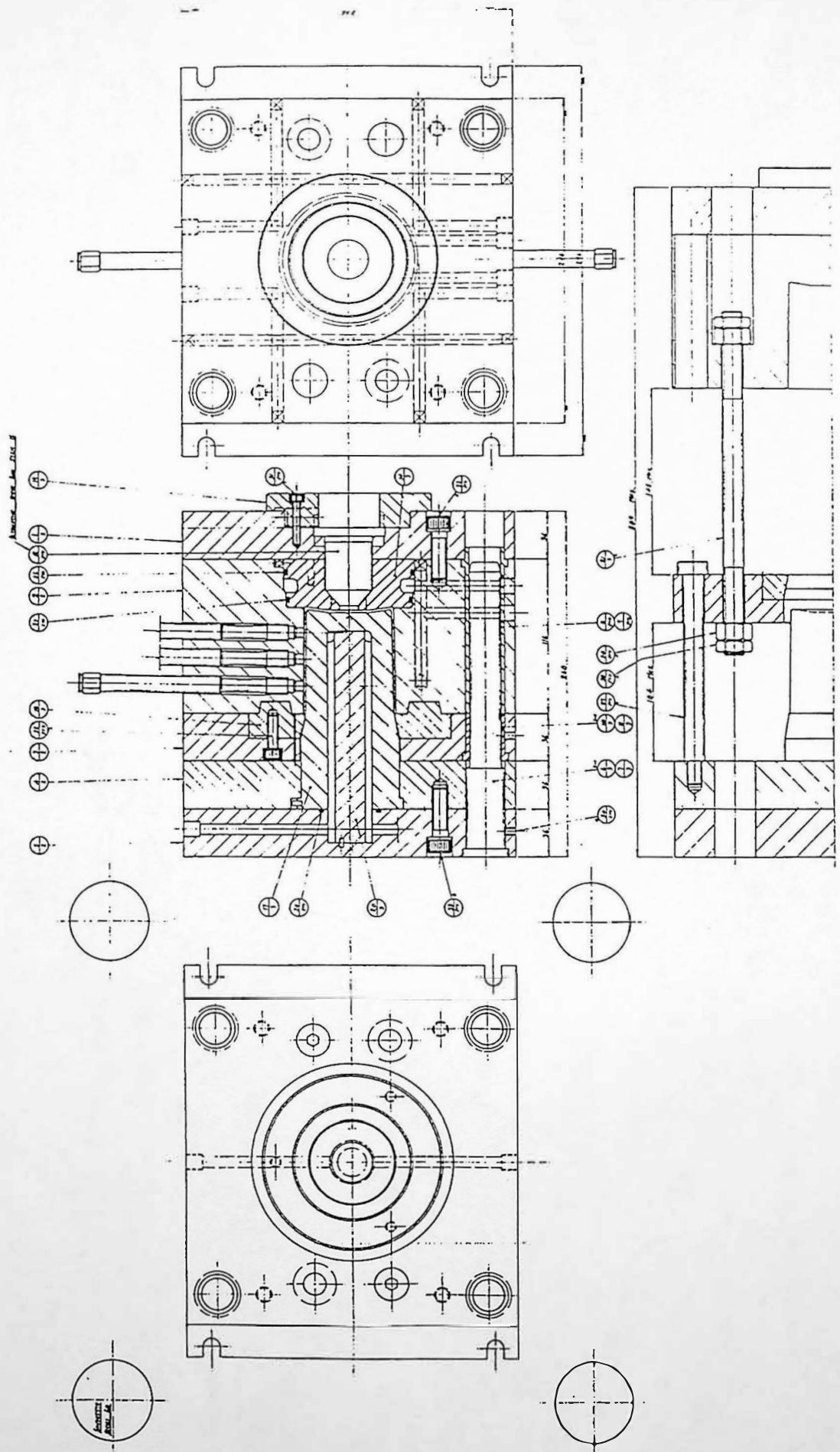
DO NOT SCALE IF IN DOUBT ASK BREAK SHARP EDGES



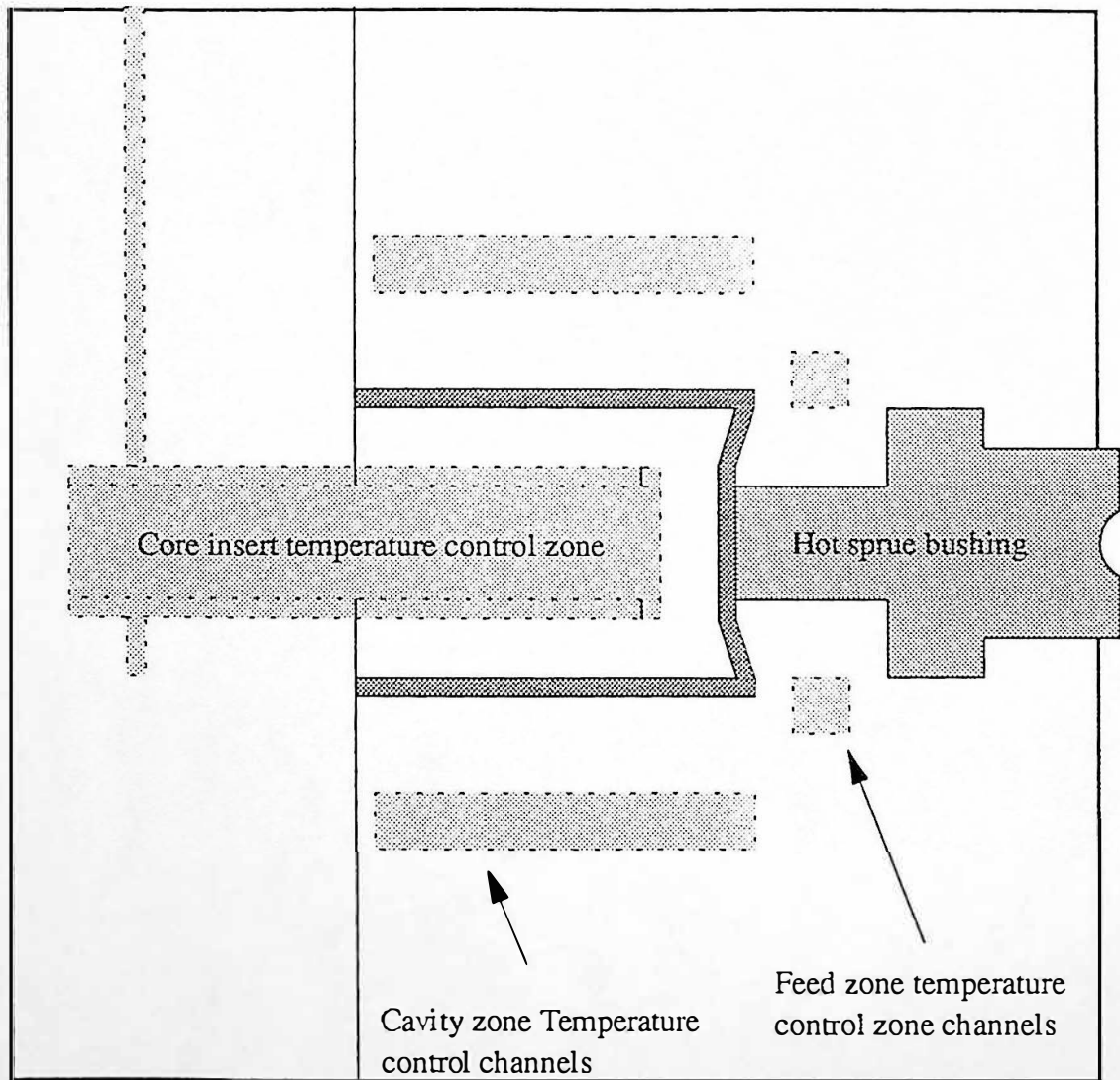
NOTE SHARP EDGES TO BE GIVEN APPROPRIATE RADI


ALL DIMENSIONS IN mm

	SCALE	2:1	TITLE	ORG NO	A2
	DRN	MW	SINGLE IMPRESSION BEAKER DESIGN	1614.2.1.A2	
	APP'D	RG S			
	DATE	14.6.91	UNIVERSITY OF BRADFORD	MECHANICAL ENGINEERING	



Beaker tool general assembly (Complexa Tools, drawing number 0557)




Temperature control
zone channels

Beaker tool temperature control zones

(iv) Hot sprue bushing ('hot tip')

Kona Bushing Series 25

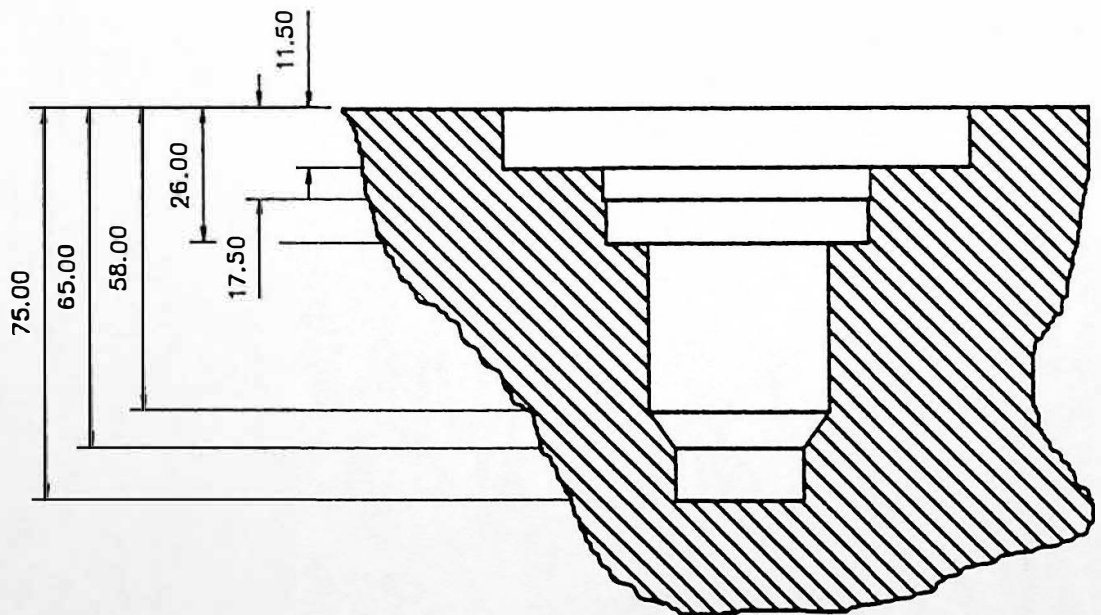
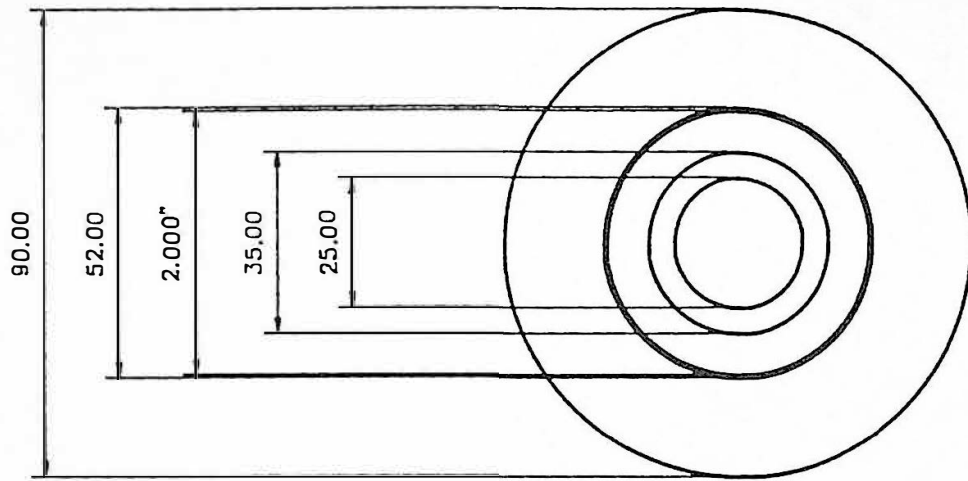
Technical Specification:

Type:	Heat pipe
Model:	25-1020-11
Shot Capacity:	5 to 600 grams
Maximum Operating Temperature	650F
Orifice Diameter	0.122 Inch
Overall Length:	5.24 Inch
Nozzle Consent Spherical Radius:	0.75 Inch
Tip Style:	Gate - Cone CV (Controlled Vestige)-11 Vespel Insert
Material:	420 Stainless Steel

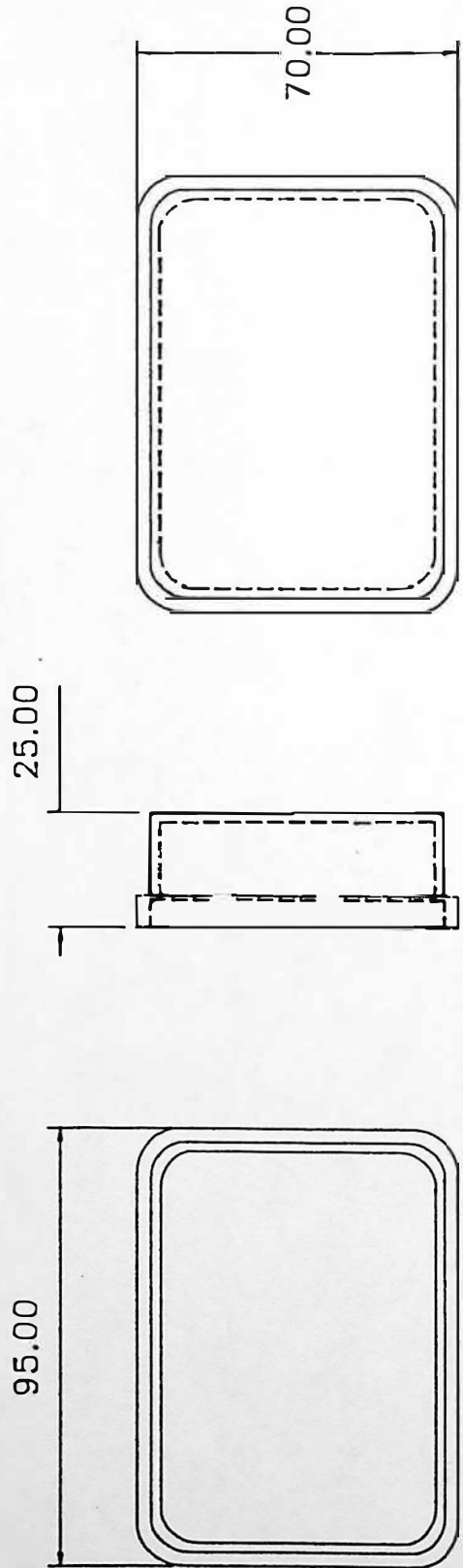
Heat pipes transfer heat across long distances with little or no temperature loss, unlike conductive heat which relies on temperature differences (loss) to move heat, Kona Corporation (1990).

For processing Polyoxymethylene a Vespel insert is used to prevent residual material to accumulate and degrade. For processing glass filled nylon an abrasion resistant cone point is used (D2 insert), to prolong tip life.

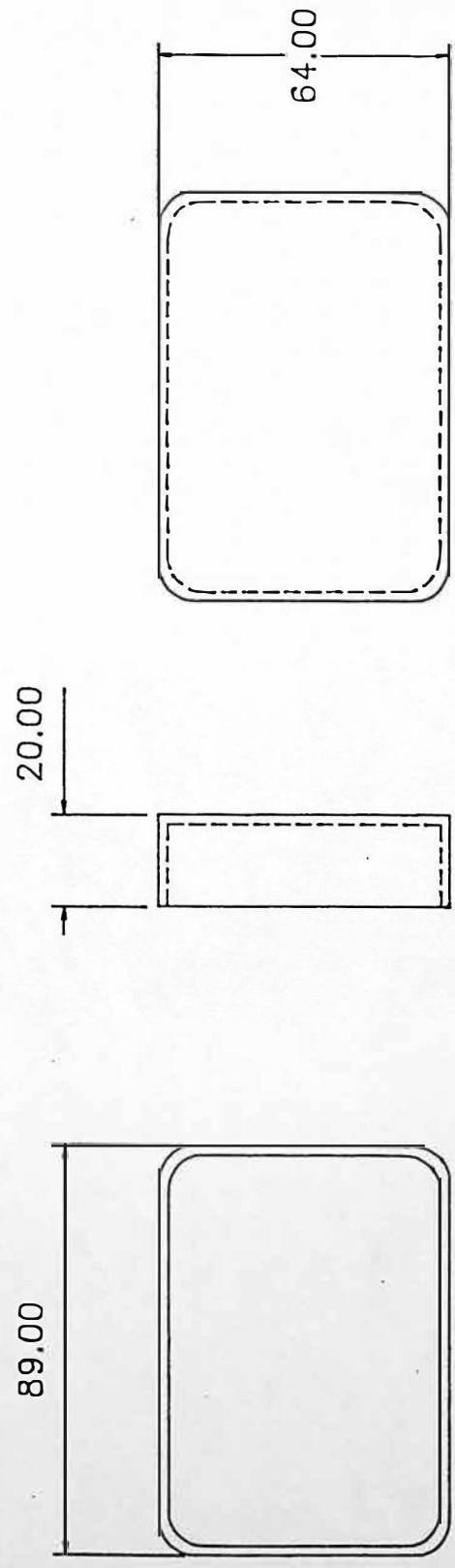
For processing PVC or other corrosive materials stainless steel prevents corrosion of the hot tip.



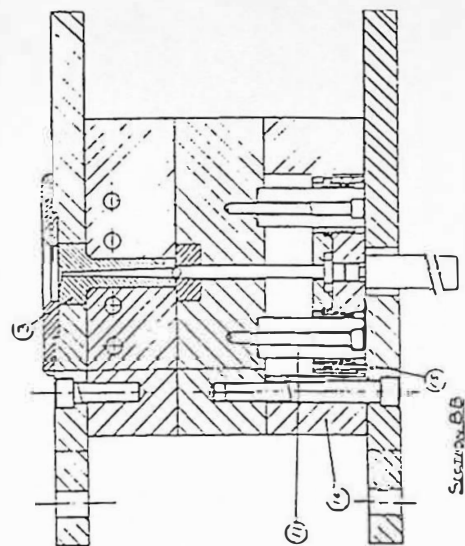
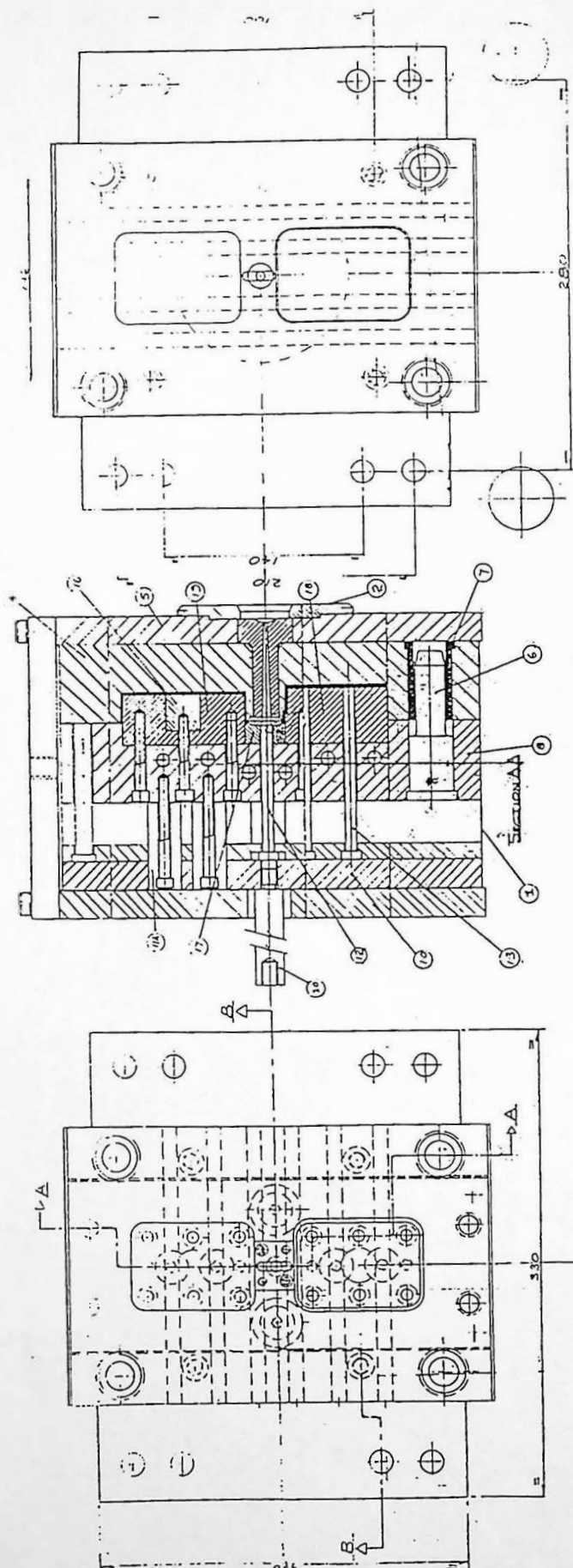
Hot sprue bushing ('hot tip') mounting



FEMALE MOULDING.

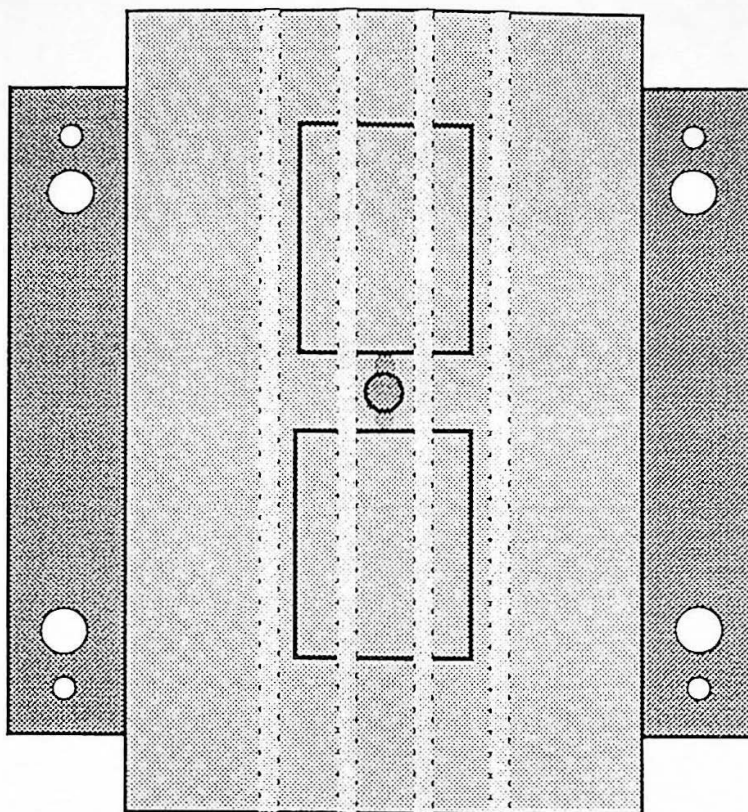


MALE MOULDING

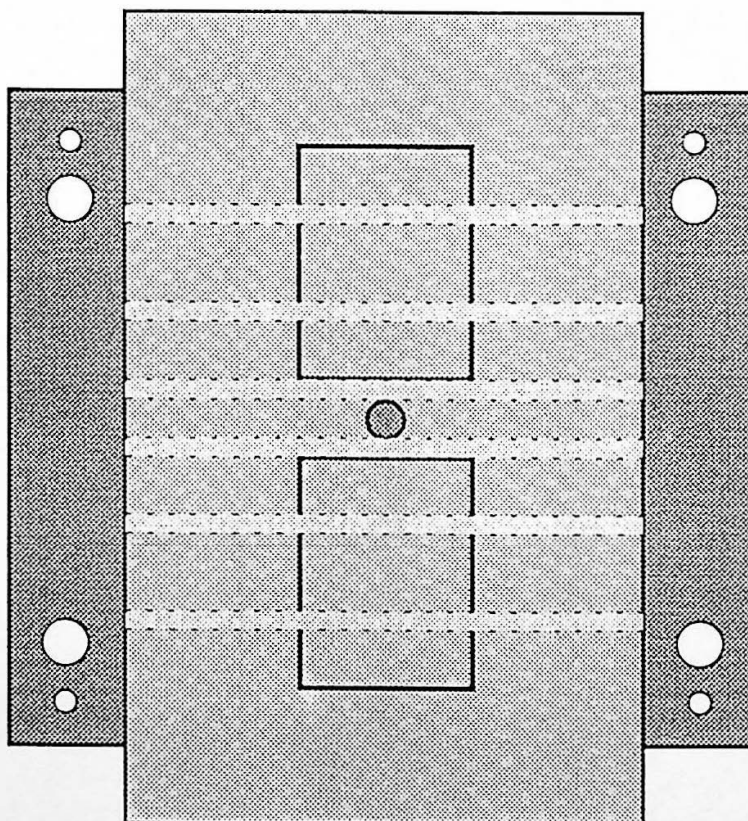


Part No.	Description	Quantity	Material	Notes
1/10	BRASS END	1	BRASS	
1/11	BRASS (20)	1	BRASS	
1/12	BRASS (20)	1	BRASS	
1/13	BRASS (20)	1	BRASS	
1/14	BRASS (20)	1	BRASS	
1/15	BRASS (20)	1	BRASS	
1/16	BRASS (20)	1	BRASS	
1/17	BRASS (20)	1	BRASS	
1/18	BRASS (20)	1	BRASS	
1/19	BRASS (20)	1	BRASS	
1/20	BRASS (20)	1	BRASS	
1/21	BRASS (20)	1	BRASS	
1/22	BRASS (20)	1	BRASS	
1/23	BRASS (20)	1	BRASS	
1/24	BRASS (20)	1	BRASS	
1/25	BRASS (20)	1	BRASS	
1/26	BRASS (20)	1	BRASS	
1/27	BRASS (20)	1	BRASS	
1/28	BRASS (20)	1	BRASS	
1/29	BRASS (20)	1	BRASS	
1/30	BRASS (20)	1	BRASS	

Container tool general assembly



Core Plate - Moving Platen



Cavity Plate - Fixed Platen



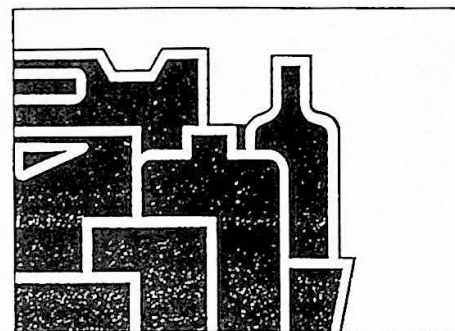
Temperature control zone channels

Impression corners are shown square for convenience
Impression (corners are radii of 10 mm)
Water Cooling Manifold is not shown

Container tool temperature control zones

Rigidex

high density
polyethylene



TECHNIGRAM

RIGIDEX HD5226EA

Rigidex HD5226EA is an easy flow high density polyethylene copolymer grade with a narrow molecular weight distribution, suitable for thin wall injection moulding applications.

Rigidex HD5226EA has the following characteristics:

- high flow
- high warpage resistance
- suitable for fast cycling applications

APPLICATIONS

- housewares
- thin walled containers
- PET bottle bases

TYPICAL PROPERTIES

Property	Value	Units	Test References
Melt flow rate (2.16 kg load)	26	g/10 min	ISO 1133-1981 : Condition 4
Density (annealed)	953	kg/m ³	ISO 1872/1-1986
Tensile strength at yield	26	MPa	ISO/R527-1966 : Type 2 Speed D
Elongation at break	>200	%	ISO/R527-1966 : Type 2 Speed D
Flexural modulus	1100	MPa	BS 2782 : 1976 : Method 335 A ISO 178-1975
Impact strength (Charpy)	3	kJ/m ²	BS 2782 : 1984 : Method 359 ISO 179-1982 Condition 2 C
Melting point	130	°C	ASTM D 2117
Vicat softening point (1 kg load)	123	°C	BS 2782 : 1976 : Method 102 D ISO 306
Thermal conductivity	0.48	W/m°C	BS 874 : 1973 ASTM C 177
Specific heat	2300	J/kg°C	
Coefficient of linear expansion	2 × 10 ⁻⁴	/°C	ASTM D 696

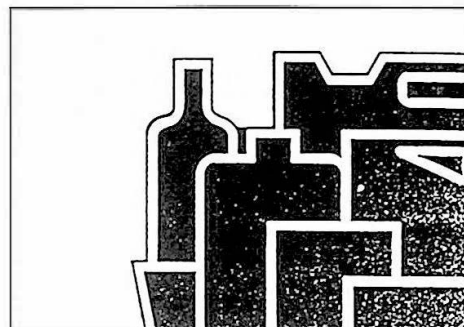
The physical properties shown are typical values obtained by averaging a number of test results and small divergencies from the quoted figures may occur.



BP CHEMICALS

Rigidex

high density
polyethylene



TECHNIGRAM

RIGIDEX HD5050EA

Rigidex HD5050EA is a high density polyethylene copolymer grade with a narrow molecular weight distribution, specially developed for injection moulding applications where a good resistance to environmental stress cracking is required.

Rigidex HD5050EA has the following characteristics:

- good environmental stress cracking resistance
- good impact strength
- good warpage resistance

Applications

- caps and closures
- technical mouldings
- crates, boxes, household items

TYPICAL PROPERTIES

Property	Value	Units	Method of test
Melt flow rate (2.16 kg load)	4	g/10 min	ISO 1133-1981: Condition 4
Density	950	kg/m ³	ISO 1872-1972
Water absorption	<0.03	%	ISO 62
Tensile strength at yield	25	MPa	ISO/R527-1966: Type 2 Speed D
Elongation at break	>200	%	ISO/R527-1966: Type 2 Speed D
Flexural modulus	800	MPa	BS 2782: 1976: Method 335 A ISO 178-1975
Impact strength (Charpy)	15	kJ/m ²	BS 2782: 1984: Method 359 ISO 179-1982 Condition 2 C
Hardness (Shore D)	64		ISO/R868-1968 Type D
Melting point	130	°C	ASTM D 2117
Vicat softening point (1 kg load)	121	°C	BS 2782: 1976: Method 102 D ISO 306
Thermal conductivity	0.48	W/m°C	BS 874: 1973 ASTM C 177
Specific heat	2300	J/kg°C	
Coefficient of linear expansion	2×10^{-4}	/°C	ASTM D 696
Dielectric constant (10 ⁶ Hz)	2.3		ASTM D 150
Dissipation (power factor) (10 ⁶ Hz)	2×10^{-4}		ASTM D 150
Dielectric strength	$>4 \times 10^4$	kV/m	
Volume resistivity	10^{16}	Ωm	BS 2782: 1982: Method 230 A

The properties shown are typical values obtained by averaging a number of test results and small divergencies from the quoted figures may occur.



BP CHEMICALS

DELTRIN* II

Acetal resin

Processing Guide

New developments in stabilisation technology have made possible a new generation of easy-to-mould acetal resins from Du Pont.

DELTRIN II acetal resin retains all the superior end use properties you have always depended upon with DELTRIN.

It is fast cycling, reduces sensitivity to gassing, discolouration and has almost no odour.

Typical Processing Conditions

Suggested processing conditions for DELTRIN II are virtually identical to those for DELTRIN.

DELTRIN II has a wider range of processing temperatures, allowing higher productivity to be more easily achieved.

Otherwise, the same conditions outlined in the DELTRIN Moulding Guide (E-15489) should be followed.

As with DELTRIN, drying is not necessary for DELTRIN II.

Converting to DELTRIN II from DELTRIN or other homopolymer

It will not be necessary to make any changes in moulding conditions.

First, allow your hopper to run dry. Then pour in a bag of DELTRIN II, preferably without interrupting cycle. You should note very minimal changes in moulding performance.

If you see a minor change in dimension, as might occur over a period of time in any moulding run, adjustments should be made as you would make in normal production (see Table below).

Converting to DELTRIN II from copolymer acetal resins

Let the hopper run empty on cycle and introduce DELTRIN II.

In many cases, the conversion from copolymer to DELTRIN II will usually require changes in moulding conditions, mainly in the setting of the barrel's temperature due to the difference in the melting point of DELTRIN II and copolymer. If after the DELTRIN II is introduced, evidence of low temperature appears (unmelted particles, poor surface), your settings should be increased in order to get the right melt temperature.

Also, when beginning to use a copolymer mould, conditions may need to be adjusted as in any normal production to achieve correct dimensions.

Once satisfactory moulding conditions have been achieved, you may find that DELTRIN II, a homopolymer, will allow you to reduce the cooling time of the cycle, since it sets up faster than copolymer and can be ejected at higher temperatures.

This translates into faster cycle times and higher yields.

Moulding variables affecting dimensions

	Injection hold pressure	Mould temperature
Increase part dimension	Increase	Decrease
Decrease part dimension	Decrease	Increase

These variables are often used to make fine adjustments to dimensions. Optimum moulding conditions that produce stable dimensions to the desired tolerances at minimum cycle must come from a mould cavity sized to produce parts under those conditions. Decreasing mould temperature may lead to greater post-mould shrinkage. Increasing injection pressures may be limited by tendencies to overcome the locking force.

**Start
with
Du Pont**

Engineering Polymers



Typical processing conditions for DELRIN* II

Resin description	High viscosity	General purpose	Low viscosity - high flow	Very low viscosity - very high flow		
Code	DELRIN II 100	DELRIN II 500	DELRIN II 900	DELRIN II 1700		
Suggested temperature profile	Nozzle 180°C - 190°C Front 200°C - 220°C Centre 195°C - 215°C Rear 190°C - 215°C					
Melt temperature	215°C ± 5°C					
Mould temperature	90°C ± 5°C					
Injection pressure	1000 bars	900 bars	900 bars	900 bars		
Fill speed	Slow to moderate	Moderate to fast	Moderate to fast	Moderate to fast		
Screw speed	0,15 m/s	0,2 m/s	0,2 m/s	0,2 m/s		
Back pressure	Increasing back pressure increases the work done by the screw on the melt. This has the following advantages and disadvantages: <table style="width: 100%; border: none;"> <tr> <td style="width: 50%; border: none;"> Advantages - Increase melt temperature and uniformity. - Can be used to minimise unmelted particles. - Improves colour mixing when colour concentrates are used. </td> <td style="width: 50%; border: none;"> Disadvantages - Decrease output of screw. - Increases drool (nozzle). </td> </tr> </table>				Advantages - Increase melt temperature and uniformity. - Can be used to minimise unmelted particles. - Improves colour mixing when colour concentrates are used.	Disadvantages - Decrease output of screw. - Increases drool (nozzle).
Advantages - Increase melt temperature and uniformity. - Can be used to minimise unmelted particles. - Improves colour mixing when colour concentrates are used.	Disadvantages - Decrease output of screw. - Increases drool (nozzle).					

Comments

PRECAUTION : DELRIN II has good thermal stability for normal processing.

But degradation can occur under improper processing conditions, such as :

- Excessive hold up times and/or high melt temperature.
- Contaminants and impurities from acid-generating resins such as PVC, flame retardant resins, etc..

- Contact of the melt with copper, copper alloys or thread lubricants containing copper.

Please refer to moulding manual on DELRIN for details and safety instructions.

Du Pont de Nemours International S.A.
 Polymer Products Department
 ENGINEERING POLYMERS
 P.O.B 50
 CH-1218 Le Grand-Saconnex, Switzerland
 Tel. (022) 717 5111. Telex 422 512

Du Pont (U.K.) Limited
 Polymer Products Department
 ENGINEERING POLYMERS
 Maylands Avenue
 Hemel Hempstead, Herts. HP2 7DP
 Tel. 0442 21 85 00. Telex 825 713

We believe this information is the best currently available on the subject. It is offered as a possible helpful suggestion in experimentation you may care to undertake along these lines. It is subject to revision as additional knowledge and experience are gained. Du Pont makes no guarantee of results and assumes no obligation or liability whatsoever in connection with this information. This publication is not a licence to operate under, or intended to suggest infringement of any existing patents.

ARYLON

Polyarylate resins

MINLON*

Engineering thermoplastic resins

DELRIN*

Acetal resins

RYNITE*

Thermoplastic polyester resins

HYTREL*

Engineering thermoplastic elastomers

ZYTEL*

Nylon resins

DU PONT

Appendix I Experimental Moulding Tests

(i) Sandretto series seven 60 tonne - experimental test results

Date:	Test Name	Manufacturer: Material:	Material:	Grade:	No. of Cycles:
17-4-91	1-D100	DuPont POM	Delrin II	100 NC-010 LOT 085010L010	10
17-4-91	2-D100	DuPont POM	Delrin II	100 NC-010 LOT 085010L010	50
17-4-91	3-D500	DuPont POM	Delrin II	500 NC-010 LOT 347008K011	50
17-4-91	4-D900	DuPont POM	Delrin II	900F NC-010 LOT 262007K022	50
22-8-91	A-TESTP	BP HDPE	Rigidex	HD 5050 EA 0F536	25
22-8-91	B-TESTP	BP HDPE	Rigidex	HD 5050 EA 0F536	25
23-8-91	C-5050B1	BP HDPE	Rigidex	HD 5050 EA 0F536	25
23-8-91	D-5050B2	BP HDPE	Rigidex	HD 5050 EA 0F536	25
27-8-91	E-5050B2	BP HDPE	Rigidex	HD 5050 EA 0F536	25
27-8-91	F-5050B1	BP HDPE	Rigidex	HD 5050 EA 0F536	25
28-8-91	G-5050B2	BP HDPE	Rigidex	HD 5050 EA 0F536	25
28-8-91	H-5050B2	BP HDPE	Rigidex	HD 5050 EA 0F536	25
28-8-91	I-5050B2	BP HDPE	Rigidex	HD 5050 EA 0F536	25
11-9-91	J-5050B2	BP HDPE	Rigidex	HD 5050 EA 0F536	25
11-9-91	K-5050B2	BP HDPE	Rigidex	HD 5050 EA 0F536	25
12-9-91	M-5050B3	BP HDPE	Rigidex	HD 5050 EA 0F536	25
13-9-91	L-D500B1	DuPont POM	Delrin II	500 NC-010 LOT 347008K011	10
13-9-91	O-D500B1	DuPont POM	Delrin II	500 NC-010 LOT 347008K011	10
13-9-91	N-D500B2	DuPont POM	Delrin II	500 NC-010 LOT 258104K008	10
13-9-91	P-D500B2	DuPont POM	Delrin II	500 NC-010 LOT 258104K008	10
10-10-91	Q-D500B2	DuPont POM	Delrin II	500 NC-010 LOT 258104K008	10
8-9-92	A-30%5B	BP HDPE	Rigidex	HD 5050 EA 403 012 127	25
8-9-92	B-30%3B	BP HDPE	Rigidex	HD 5050 EA 403 012 127	25
8-9-92	C-20%3B	BP HDPE	Rigidex	HD 5050 EA 403 012 127	25
8-9-92	D-20%5B	BP HDPE	Rigidex	HD 5050 EA 403 012 127	25
15-9-92	E3%2B	BP HDPE	Rigidex	HD 5050 EA 4B0 012 127	25
15-9-92	F3%3B	BP HDPE	Rigidex	HD 5050 EA 4B0 012 127	25
15-9-92	G4%2B	BP HDPE	Rigidex	HD 5050 EA 4B0 012 127	25
15-9-92	H4%3B	BP HDPE	Rigidex	HD 5050 EA 4B0 012 127	25
16-9-92	I4%2B	BP HDPE	Rigidex	HD 5226 EA 4.164.179	10
16-9-92	J4%2B	BP HDPE	Rigidex	HD 5226 EA 4.164.179	25
16-9-92	K4%15B	BP HDPE	Rigidex	HD 5226 EA 4.164.179	25

17-9-92	L4%2B	BP HDPE	Rigidex	HD 5226 EA 4.164.179	10
17-9-92	M4%X%	BP HDPE	Rigidex	HD 5226 EA 4.164.179	30
17-9-92	NX%2B	BP HDPE	Rigidex	HD 5226 EA 4.164.179	15
17-9-92	OX%2B	BP HDPE	Rigidex	HD 5226 EA 4.164.179	15
18-9-92	P3%2B	DuPont POM	Delrin II	500 NC-010 LOT 276108L003	25
18-9-92	Q3%2B	DuPont POM	Delrin II	500 NC-010 LOT 276108L003	25
18-9-92	R3%2B	DuPont POM	Delrin II	500 NC-010 LOT 048110L007	25
18-9-92	S3%2B	DuPont POM	Delrin II	500 NC-010 LOT 048110L007	25
21-9-92	T3%2B	DuPont POM	Delrin II	500 NC-010 LOT 276108L003	25
28-9-92	UX%NOZ	BP HDPE	Rigidex	HD 5226 EA 4.164.179	7
28-9-92	VX%NT	BP HDPE	Rigidex	HD 5226 EA 4.164.179	7
5-10-92	W30%20B	DuPont POM	Delrin II	500 NC-010 LOT 276108L003	25
5-10-92	X30%20BX	DuPont POM	Delrin II	500 NC-010 LOT 276108L003	25
5-10-92	Y30%20B	DuPont POM	Delrin II	500 NC-010 LOT 048110L007	25
5-10-92	Z30%20B	DuPont POM	Delrin II	500 NC-010 LOT 048110L007	25
16-10-92	AA-3%2B	DuPont POM	Delrin II	500 NC-010 LOT 048110L007	15
16-10-92	AB-3%2B	DuPont POM	Delrin II	500 NC-010 LOT 048110L007	15
16-10-92	AC-3%2B	DuPont POM	Delrin II	500 NC-010 LOT 276108L003	15
16-10-92	AD-3%2B	DuPont POM	Delrin II	500 NC-010 LOT 276108L003	15
16-10-92	AE-3%2B	DuPont POM	Delrin II	500 NC-010 LOT 276108L003	15
17-10-92	AF-3%2B	DuPont POM	Delrin II	500 NC-010 LOT 276108L003	15
17-10-92	AG-3%2B	DuPont POM	Delrin II	500 NC-010 LOT 048110L007	15
17-10-92	AH-3%2B	DuPont POM	Delrin II	500 NC-010 LOT 048110L007	15
19-10-92	AI-3%2B	DuPont POM	Delrin II	900F NC-010 LOT 009109K017	15
19-10-92	AJ-3%2B	DuPont POM	Delrin II	900F NC-010 LOT 261003K020	15
19-10-92	AK-3%2B	DuPont POM	Delrin II	900F NC-010 LOT 261003K020	15
19-10-92	AL-3%2B	DuPont POM	Delrin II	900F NC-010 LOT 009109K017	15
20-10-92	AM-3%2B	DuPont POM	Delrin II	900F NC-010 LOT 261003K020	15
20-19-92	AN-3%2B	DuPont POM	Delrin II	900F NC-010 LOT 009109K017	15
21-10-92	AO-3%2B	DuPont POM	Delrin II	900F NC-010 LOT 261003K020	12
21-10-92	AP-3%2B	DuPont POM	Delrin II	900F NC-010 LOT 261003K020	9
21-10-92	AQ-3%2B	DuPont POM	Delrin II	900F NC-010 LOT 261003K020	4
21-10-92	AR-3%2B	DuPont POM	Delrin II	900F NC-010 LOT 261003K020	12
21-10-92	AS-3%2B	DuPont POM	Delrin II	900F NC-010 LOT 261003K020	12
21-10-92	AT-3%2B	DuPont POM	Delrin II	900F NC-010 LOT 009109K017	12
21-10-92	AU-3%2B	DuPont POM	Delrin II	900F NC-010 LOT 009109K017	12
21-10-92	AV-3%2B	DuPont POM	Delrin II	900F NC-010 LOT 009109K017	12
21-10-92	AW-3%2B	DuPont POM	Delrin II	900F NC-010 LOT 009109K017	12

22-10-92	AX-3%2B	DuPont POM	Delrin II	100 NC-010 LOT 658105L029	15
22-10-92	AY-3%2B	DuPont POM	Delrin II	100 NC-010 LOT 658105L029	15
22-10-92	AZ-3%2B	DuPont POM	Delrin II	100 NC-010 LOT 658105L029	15
23-10-92	BA-3%4B	DuPont POM	Delrin II	100 NC-010 LOT 658105L029-90% 900F NC-010 LOT 325012K003-10%	15
23-10-92	BB-3%4B	DuPont POM	Delrin II	100 NC-010 LOT 658105L029-90% 900F NC-010 LOT 325012K003-10%	15
23-10-92	BC-3%4B	DuPont POM	Delrin II	100 NC-010 LOT 658105L029-90% 900F NC-010 LOT 325012K003-10%	15
23-10-92	BD-3%4B	DuPont POM	Delrin II	100 NC-010 LOT 211104H019	15
23-10-92	BE-3%4B	DuPont POM	Delrin II	100 NC-010 LOT 211104H019	15
23-10-92	BF-3%4B	DuPont POM	Delrin II	100 NC-010 LOT 211104H019	15
1-12-92	PP10%	ICI PP	Propathene	GWM213 ICI Reference Grade	5
1-12-92	PP20%	ICI PP	Propathene	GWM213 ICI Reference Grade	5
1-12-92	PP30%	ICI PP	Propathene	GWM213 ICI Reference Grade	5
1-12-92	PP40%	ICI PP	Propathene	GWM213 ICI Reference Grade	5
1-12-92	PP50%	ICI PP	Propathene	GWM213 ICI Reference Grade	5
1-12-92	PP60%	ICI PP	Propathene	GWM213 ICI Reference Grade	5

(ii) Stork 440 tonne- experimental test results

Date	Test Name	Manufacturer: Material:	Material:	Grade:	Num. of Cycles
1-10-92	A11-0902	BASF ABS	Terluran	968SM Black	12
25-11-92	A11-2511	BASF ABS	Terluran	968SM Black	25
8-12-92	A11-0812	BASF ABS	Terluran	968SM Black	50

(iii) Cincinnati Milacron ACT30 30 tonne- experimental test results

Date	Test Name	Manufacturer: Material:	Material:	Grade:	Num. of Cycles
12-1-92	A-ACT	BP LLDPE	Innovex	LL 0640 AA	10
12-1-92	B-ACT	BP LLDPE	Innovex	LL 0640 AA	10
15-1-92	C-ACT	BP LLDPE	Innovex	LL 0640 AA	25
19-1-92	D-ACT	BP LLDPE	Innovex	LL 0640 AA	25

Appendix J Statistical Analysis

The following definitions of statistical analysis techniques are referenced from, Cooper (1969), Neville and Kennedy (1964) and Rees (1989).

1. Arithmetic mean

This parameter is often referred to as 'average' or 'mean'. The sum of the measurements from it are zero, therefore the mean is the sum of the observations divided by their number.

$$\bar{x} = \frac{1}{n} \sum_{i=1}^n x_i$$

where x_i = an observation or measurement

n = total number of observations

\bar{x} = mean

2. Variance

This parameter is a fundamental measure of dispersion. For a set of n observations x_i , whose mean is μ , for each measurement the deviation can be calculated $(x_i - \mu)$.

The mean square deviation is known as the variance σ^2 .

$$\sigma^2 = \frac{\sum_{i=1}^n (x_i - \mu)^2}{n}$$

3. Standard deviation

Variance is a fundamental measure of dispersion, but is not a convenient measure, as its units are the square of the variants unit. For this reason distributions are expressed as the square root the variance i.e. the standard deviation σ .

$$\sigma = \sqrt{\frac{\sum_{i=1}^n (x_i - \mu)^2}{n}}$$

4. Coefficient of variation

Standard deviation is expressed in the same units as the original variant x_i . It is often convenient to express the dispersion as a percentage, i.e. in relative terms rather than absolute terms. The coefficient of variation is a dimensionless unit.

$$v = \frac{\sigma}{\bar{x}} \times 100$$

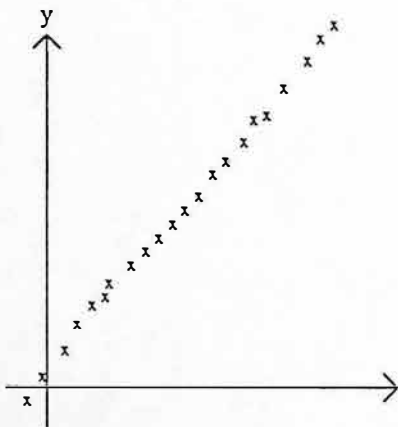
5. Coefficient of correlation

Coefficient of correlation (r) is used to determine if a relationship exists between two data sets x and y . Data is analysed for n pairs of observations (x_i, y_i) .

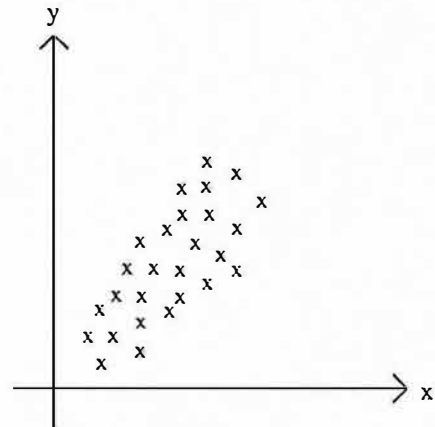
$$r = \frac{\sum_{i=1}^n (x_i - \bar{x})(y_i - \bar{y})}{\sqrt{\sum_{i=1}^n (x_i - \bar{x})^2 \sum_{i=1}^n (y_i - \bar{y})^2}}$$

where \bar{x} and \bar{y} denote the means of data sets x and y .

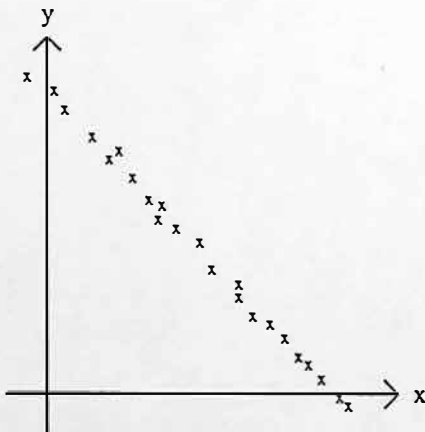
If there is no correlation between two sets of data x and y , that is x is independent of y , the coefficient of correlation = 0. Conversely, when there is perfect correlation, i.e. all points exactly coincide, the coefficient of correlation = 1. The relationship between two sets of data x and y , may be proportional (positive) or inversely proportional (negative), as shown below.



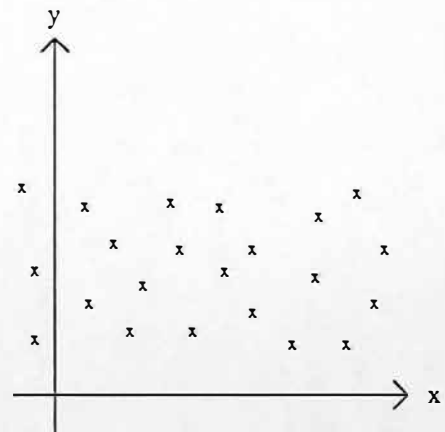
High Positive Correlation



Low Positive Correlation



High Negative Correlation



None (the variables are independent)

Appendix K Design for Nozzle Thermocouple Mounting

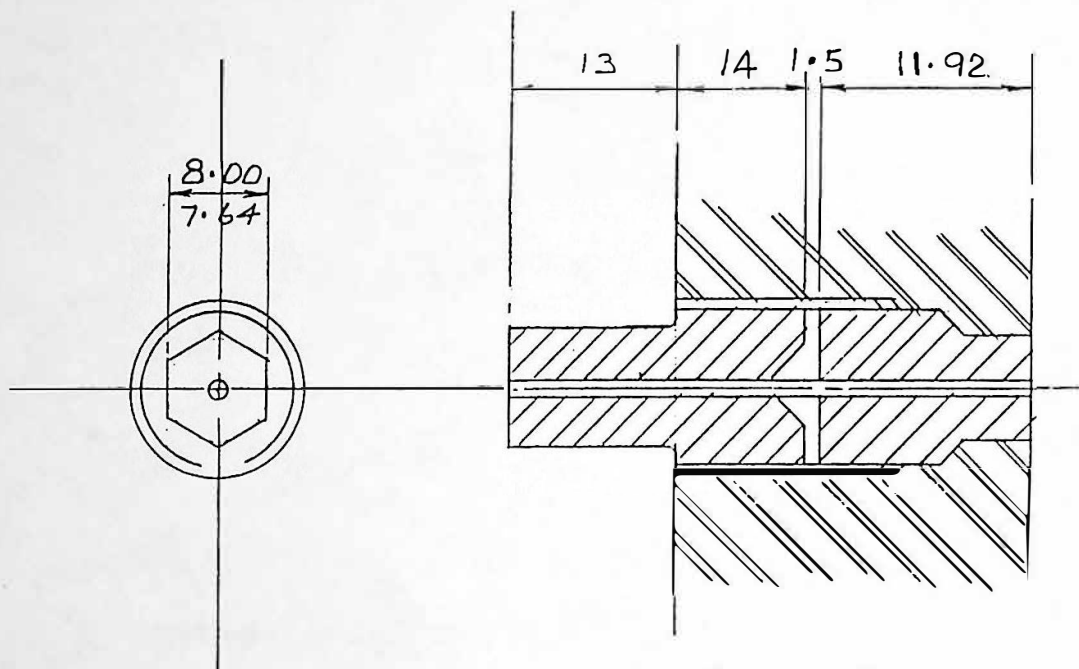
Typical nozzle thermocouples have response times of 2.30 seconds (see chapter 5.5.3), such devices are too slow in response for the injection moulding process and reflect bulk nozzle temperature, and not polymer melt temperature. The mounting was designed to use 1 mm thermocouples, response time 0.21 seconds (see chapter 5.3.3), using a machineable glass ceramic (McGeoch, Macor Code 9658).

The design uses the same mounting as a typical melt pressure transducer. The maximum nozzle melt pressure possible is 1409 bar, therefore bulky slow response thermocouples have previously been used.

Load considerations for 1 mm diameter thermocouple:

$$\text{Load on Thermocouple Tip} = (1409 \times 10^5) \times \left(\frac{\pi \times (0.001)^2}{4} \right) = 110.7 \text{ N}$$

The previous calculations show the maximum load on the 1 mm diameter thermocouple (110.7 N). The design uses the load on the glass ceramic for its advantage, i.e. the greater the load the greater the sealing and gripping of the thermocouple by the copper washer.



DESIGN E

SCALE	TWICE SIZE	TITLE.	DRG. No.
DRN.	<i>SP.</i>	DESIGN FOR	16107-3-A4
APP'D.		THERMOCOUPLE MOUNTING	
DATE	14-6-90	UNIVERSITY OF BRADFORD	MECHANICAL ENGINEERING